FACULTAD DE CIENCIAS

DEPARTAMENTO DE BIOLOGÍA MOLECULAR

METABOLISMO ENERGÉTICO EN PATOLOGÍA Y SU TRASLACIÓN A LA CLÍNICA

TESIS DOCTORAL

FULVIO SANTACATTERINA

Madrid, 2016

Universidad Autónoma de Madrid

Facultad de Ciencias

Departamento de Biología Molecular

Centro de Biología Molecular "Severo Ochoa" (CSIC-UAM)

METABOLISMO ENERGÉTICO EN PATOLOGÍA Y SU TRASLACIÓN A LA CLÍNICA

Memoria presentada por el licenciado

Fulvio Santacatterina

para optar al grado de Doctor en Biología Molecular

por la Universidad Autónoma de Madrid

Director de Tesis: **Dr. José Manuel Cuezva Marcos**

Madrid, 2016

Este trabajo ha sido realizado en el laboratorio 326 del Centro de Biología Molecular "Severo Ochoa" (CSIC-UAM) que dirige el profesor José Manuel Cuezva Marcos, Catedrático de Biología Molecular de la Universidad Autónoma de Madrid (Agosto 2010-Julio 2016). Durante este periodo, el licenciado Fulvio Santacatterina ha disfrutado de una Beca predoctoral Bancaja-CIBER de Enfermedades Raras (Agosto 2010-Julio 2011), de una beca (Octubre 2011-Septiembre 2013)/contrato (Octubre 2013-Septiembre 2015) predoctoral del Programa de Formación de Personal Investigador de la Universidad Autónoma de Madrid (FPI-UAM) y de un contrato (Diciembre 2015-Julio 2016) de personal investigador de la Fundación de la Universidad Autónoma de Madrid (FUAM).

Alla mia famiglia

Per aspera ad astra

Agradecimientos

Finalmente ha llegado el fatídico momento que, como la cereza sobre el helado, corona mi experiencia científica de los últimos seis años.

Quizá sea la mejor experiencia de mi vida, puesto que los sacrificios que supone un doctorado en ciencias, en un país lejano de mis afectos familiares, ha sido compensado por los momentos felices que me ha regalado toda la gente que conocí aquí en España acogiéndome y acompañándome en estos años. Por todo eso, debo mi más profundo agradecimiento a muchas personas que me han empujado hacia esta línea de meta profesional que al mismo tiempo me ha permitido crecer y mejorarme como persona.

Todavía recuerdo las sabias palabras de Pepe Cuezva, mi director de tesis, quien en mi primera semana en el laboratorio me dijo: "nadie es imprescindible". Sin embargo, hoy me atrevo a rebatirlo, ya que en este largo camino, importantes presencias han desempeñado un papel fundamental para rechazar dicha teoría, en especial su propio autor. Aunque resulte particularmente difícil hablar de tu director de tesis sin caer en los típicos clichés, haré mi mejor intento. En primer lugar, quisiera agradecerle por haberme brindado la posibilidad de desarrollar esta tesis bajo su guía, así como de haber podido experimentar una inagotable trayectoria de aprendizaje en su laboratorio. Y no menos importante es la gratitud que siento por mostrarme una y otra vez su lado más humano cuando más necesitaba apoyo y comprensión, tanto para superar las dificultades científicas como las de la vida personal. Su confianza me ha animado a empezar, a levantarme tras las caídas y a seguir con más ganas en esta profesión.

Asimismo, me gustaría agradecer al magnífico equipo del laboratorio, que ha sido una segunda familia, con quienes he compartido desde el desayuno hasta las más apasionantes discusiones científicas.

Agradezco a María por sus enseñanzas, consejos, ayudas hasta el final y por supuesto por su amistad; a Marga, fuente infinita de anticuerpos, por acogerme con cariño como al niño nuevo del labo, por presentarme mi primera pipeta y por dar color a nuestras navidades; a Formen, por ser la mejor compañera de escritorio y por entretenerme diariamente con sus cuentos, digna rival de Agata Cristhie; a Marcos, por introducirme al maravilloso mundo del *Array*; a la prima Cristina por su ayuda, nuestras juergas, confesiones y por mantenernos al día como *gazzettino* oficial del labo; a Laura Sánchez, por su amistad y por abrirme la puerta del animalario enseñándome a tratar éticamente a los ratoncitos; a Inma por su amabilidad, dulzura y simpatía; a Javi, por sus dosis de realismo; a Álvaro, por acogerme dentro y fuera del labo y además de ciencia, enseñarme el mundo del flamenco; a Cristina Yolanda, Pau, Beatriz, Laura Torresano, Lucía y miniSolde, por traer frescura al labo, por ser mis diccionarios vivientes, por su ayuda y paciencia, y por soportarme en esta fase *pretésica*. Gracias también a Imke, Carmen, Estefanía, Estela, Marta, Noelia, Santi, Juan Manuel, María Morán, Jon Fredi, Marek, Piccolino, David, Irene, Joana, Mariví y a la recién llegada Lucía, todos han sido buenos compañeros, con quienes he compartido momentos buenos y a veces difíciles de estos años.

No olvidaría jamás agradecer a los afiliados del labo, en primer lugar a Enrique, por sus consejos técnicos, su simpatía y sus visitas diarias; los primos del 321, por su espíritu de colaboración, teniendo siempre lo que nos falta en el 326 completándonos simbióticamente. Asimismo quiero agradecer a la pandilla del 320 por su disponibilidad y colaboración; a Marta Pereira, por su ayuda con la Inmunohistoquimica; a Anabel y todo el laboratorio de proteómica, por su servicio científico y su compañía durante la comida/merienda y el vapeo; Paco, de instrumentación, por su genio, por las ya no sé cuántas veces que ha salvado nuestras máquinas *en extremis* y con ellas la presente tesis; a los del grupo de informática, de microscopía óptica confocal y electrónica, por haber sido siempre amables y disponibles y por todo lo que me han enseñado.

Mis gracias van también a la fundación del CIBER de Enfermedades Raras y especialmente a las personas con quienes hemos colaborado.

Un agradecimiento especial a algunas piezas importantes: nuestro Dire del CBMSO José Felix de Celis, por nuestra empatía, su disponibilidad, por nuestras charlas y sus consejos preciosos al aproximarme a la fase de escritura; a Mada, por ser tan maja y amable y llevar de la mano a los tesistas hasta la entrega.

Estos años no hubieran sido tan especiales sin un grupillo de gente al que el Walter White de bioinformática ha pintorescamente definido "la crema del CBM". Muchas son las personas de este grupo que merecen mis gracias por haber alegrado mi estancia madrileña, así que no los nombraré uno por uno, confiando en que los lectores son buenos entendedores.

Como no sólo de ciencia vive el hombre, debo mis gracias a muchas personas que me han sostenido fuera del ámbito profesional, empezando por Teresa. A esta flor, que en este último año ha tenido que aguantarme cuidando de mí con amor y dándome fuerza día tras día. A mi amiga eterna Dafne, que ha convertido las nubes de mi vida en un sol cálido, creando conmigo lo que no sé cómo llamar sino familia. Gracias desde lo más profundo de mi corazón a mis fieles amig@s Luza y Luis, a Salvina y Luis, a Clhoe y Andrés, a todos los compis del Castillo Caracas, a Armandiño el Maradona de la barra, al *Captain* Stefano Benvenú y al grupo del voley, a los hermasmus Stefano y Manuel con quien empezó todo esto, y por supuesto a Marco y a la familia del Grazie mille.

Mientras alcanzo este objetivo no puedo olvidar agradecerle a Dios la fuerza que me ha concedido y el don que me ha dado, poniendo en mi camino a todas estas personas y, especialmente en conexión con él, a Don José Antúnez Cid, a mi compadre Juan Quiroga y a todo el grupo de la iglesia de santa Teresa y Santa Isabel, que agradezco por haber sido mi guía espiritual en estos años.

Aunque me haya adaptado muy bien, no hay día que no recuerde mi origen, mis familiares y mis amigos italianos que, aunque los ojos no vean, el corazón siente. Para agradecerles por haber creído en mí, sostenido y dado la posibilidad de llegar a este punto, me despido de Cervantes para ir a charlar con mi querido Dante.

Sulla soglia di un traguardo importante non posso fare a meno di voltarmi indietro e rivedere il mio tragitto con tutti i volti di coloro che sono stati al mio fianco. Neanche una lontananza di sei anni riesce minimamente a scalfire l'unione degli *amicipersempre* che di fatto mi hanno incoraggiato, sostenuto e mantenuto nei loro pensieri. Per questo ci tengo a ringraziare di cuore i miei amici più cari: Danilo, Samuele, Emanuela, Sandro, Cannata, Giovanni, Domenico, Massimo e molti altri ancora che sanno di fare parte della mia storia. Un ringraziamento particolare alla Prof. Caterina Faggio, per essere stata presente e per incoraggiarmi fino a oggi dopo sei anni. Ad Agnese, grazie per aver sopportato una buona parte di questa tesi e per essere riuscita a migliorarmi anche a distanza.

Per ultimo ma non con meno importanza, non riuscirò mai a ringraziare abbastanza la mia famiglia. Ai miei genitori per avermi insegnato i valori che danno la vera ricchezza, spronato a puntare in alto ed essere riusciti a farmi ritornare sui binari giusti nei momenti di debolezza, per aver creduto in me, sempre. Ai miei fratelli Carmen e Carlo due fari nel mio cammino, grazie per avermi sempre protetto e per essere stati due modelli diversi ed ugualmente belli da cui attingere. Ai miei Nonni defunti per essere stati un esempio di dedizione, altruismo e sacrificio. A tutti i miei zii per il loro affetto e sostegno. Ancora grazie in particolare a mio fratellone per le sue consulenze informatiche durante tutti questi anni.

Ogni mio successo è merito vostro.

Abreviaturas

(R)-2HG	(R)-2-hidroxiglutarato
3BP	3-bromopiruvato
ADP	Adenosín difosfato
AEBSF	4-(2-aminoetil)-benceno sulfonilo fluoruro cloridrato
AKAP	*A-kinase anchor protein*, proteína de anclaje de quinasa A
AMP/ADP/ATP	Adenosín 5’ mono/di/trifosfato
AMPK	*AMP-activated protein kinase*, proteína quinasa activada por AMP
APAP	N-Acetil-p-Aminophenol o Acetaminofeno
APTES	Aminosilano, aminopropil-trimetoxysilano
Bcl-2	B cell lymphoma gene-2, linfoma de linfocitos B del gen-2
Bcl-xL	B-cell lymphoma-extra large
BEC	Índice Bioenergético Celular
BH3	Bcl-2 homology domain 3, dominios de homología con Bcl-2 3
BMD	Distrofia muscular tipo Becker
BN-PAGE	Electroforesis azul nativa en geles de poliacrilamida
Ca2+	Calcio
CaM	Calmodulina
CAmK	Calcio-calmodulina quinasa
cAMP	AMP cíclico
CD8	*Cluster of differentation 8*, Cúmulo de diferenciación 8
Cit c	Citocromo c
CIV	Complejo mitocondrial IV
CN-PAGE	Electroforesis clara nativa en geles de poliacrilamida
CO2	Dióxido de carbono
CoC12	Cloruro de cobalto
CoA	Coenzima A
COX	Citocromo Oxidasa
CPK	Creatina fosfoquinasa
CS	Citrato sintasa
CsA	Ciclosporina A
CTD	*Connective tissue disease*, enfermedad del tejido conectivo
CTE	Cadena de transporte de electrones
CV	Complejo mitocondrial V
DAPC	Complejo de proteínas asociadas a la distrofina

DAPIT	Proteína asociada a diabetes en tejidos sensibles de insulina
Db-cAMP	Dibutiril-AMP cíclico
DCA	Dicloroacetato
DEN	N-dimetilnitrosamina
DM	Dermatomiositis
DMD	Distrofia muscular tipo Duchenne
Dox	Doxiciclina
Drp1	*Dynamin-related protein 1*, proteína relacionada con la dinamina-1
EM	Espacio intermembrana
EMT	Transición epitelio-mesénquima
ER	Retículo endoplásmico o Enfermedades Raras
ERMES	Estructura de encuentro retículo endoplasmatico-mitocondria
FADH2	Flavín adenín dinucleótido reducido
FCCP	Cianuro de p-trifluorometoxifenilhidrazona
FH	Fumarato hidratasa
FPPA	*Forward Phase Protein Microarray*, microarray de proteínas en fase directa
GAPDH	Gliceraldehído-3-fosfato deshidrogenasa
GCL-C	Subunidad catalítica de la glutamato-cisteína ligasa
GCL-M	Subunidad reguladora de la glutamato-cisteína ligasa
GLDH	Inhibidores de la glutamato deshidrogenasa
GLS1	Glutaminasa 1
GLUT1	Transportador de glucosa 1
GLyc-V	Glucogenosis de tipo V
GPD1	Glicerol-3-fosfato deshidrogenasa
GPx	Glutatión peroxidasa
GR	Glutatión reductasa
H2O2	Peróxido de hidrógeno
H49K	Mutante de IF1 (con sustitución de histidina por lisina en posición 49)
HCC	Carcinoma Hepatocelular
HIF-1α	Factor inducible por hipoxia 1
HK-II	Hexoquinasa II
hMSC	*Human Mesenchymal Stem Cells*, células mesenquimáticas humanas
HO-1	Hemo oxigenasa 1
Hsp60	*Heat-shock protein 60*, proteína de estrés térmico 60
ICU	Unidad de cuidado intensivo
IDH	Isocitrado deshidrogenasa

IER3	*Immediate early response gene 3*, gen de respuesta temprana inmediata 3
IEX-1	*Immediate Early Gene X1*, gen de respuesta temprana inmediata X1
IF1	*Inhibitory Factor 1*, factor inhibitorio 1
IHQ	Inmunohistoquímica
IKBα	Inhibidor de NFκB α
IMs	Miopatías Inflamatorias idiopáticas
IVD	Diagnóstico in vitro
LAP	*Liver Activated Protein*, proteína hepática activada
LDH	Lactato deshidrogenasa
LGMD2C	Distrofia muscular de cinturas autosómica recesiva tipo 2C
LOD	*Limit of detection*, límite de detección
LRPPRC	*Leucine-rich PPR motif-containing protein*, proteína con motive PPR rico en leucina
LSD	Trastornos del almacenamiento lisosomal
Mcl-1	Proteína inductora de la diferenciación celulas mieloides
MCT	Transportadores lactato monocarboxilato
MDLC	Cromatografía Liquida Multidimensional
Mfn	Mitofusina
Mg2+	Magnesio
MICOS	Sistema de organización de las crestas y sitios de contacto mitocondrial
MITO	Miopatía metabólica con defectos del complejo I
MME	Membrana mitocondrial externa
MMI	Membrana mitocondrial interna
MnSOD	Superóxido dismutasa 2 dependiente de manganeso
MOMP	Permeabilización de la membrana externa mitocondrial
MPC	Transportador mitocondrial del piruvato
MPTS	3-mercaptopropil trimetóxisilano
mRNA	RNA mensajero
mtAC	Adenilato ciclasa transmembrana
mtDNA	DNA mitocondrial
mTOR	*Mammalian target of rapamycin,* Diana en mamíferos de la rapamicina
NAD+/NADH	Nicotidamida-adenina dinucleótido oxidado/reducido
NADPH	Nicotidamida-adenina dinucleótido fosfato reducido
NC	Nitrocelulosa
NCL	Lipofuscinosis neuronal ceroide
nDNA	DNA nuclear
NF-YA	*Nuclear transcription factor Y subunit alpha,* factor de transcripción Y subunidad alfa

NF-YB	*Nuclear transcription factor Y subunit beta*, factor de transcripción Y subunidad beta
NFκB	*Nuclear Factor-kappaB*, factor nuclear kappaB
NGS	*Next-generation sequencing*, secuenciación de nueva generación
Nrf	*Nuclear respiratory factor*, factor respiratorio nuclear
O2•-	Anión superóxido
OGDH	α-cetoglutarato deshidrogenasa
Opa1	proteína homóloga de atrofia óptica
OSCP	proteína que confiere sensibilidad a oligomicina
OXPHOS	*OXidative PHOSphorilation*, fosforilación oxidativa
P13K/Akt	Fosfatidilinositol-3-quinasa/Proteína quinasa B
p38MAPK	*p38 Mitogen activated protein kinase, proteina quinasa p38* activada por mitógenos
PDH	Piruvato deshidrogenasa
PDK1	Piruvato deshidrogenasa 1 quinasa
PET	*Positron Emission Tomography*, tomografía de emisión de positrones
PFK	Fosfofrutoquinasa
PFKFB3	6-fosfofruto-2-quinasa/fructosa-2,6-bifosfatasa 3
PGC1α	*Peroxisome proliferator-activated receptor gamma coactivator 1-alpha*
Pi	Fosfato inorgánico
PI	Punto Isoeléctrico
PiC	Trasportador de fosfato
PK	Piruvato quinasa
pKa	Constante de disociación ácida
PKM	Piruvato quinasa isoforma M
PM	Polimiositis
PL	Poly-L-lisina
PPP	Vía de las pentosas fosfato
PTEN	*Phosphatase and tensin homolog*
PTP	*Permeability Transition Pore*, poro de transición de permeabilidad mitocondrial
PYGM	Glucógeno fosforilasa muscular
ROS	*Reactive Oxygen Species*, especies reactivas de oxígeno
RP-LC-MS/MS	Cromatografía líquida en fase reversa acoplada a espectrometría de masa
RPPA o RPMA	*Reverse Phase Protein Microarray*, Microarray de proteínas en fase reversa
rRNA	RNA ribosómico
S/N	*Signal-to-noise ratio*, fluorescencia de fondo
sAC	adenilato ciclasa mitocondrial
SC	Supercomplejo

SDH	Succinato deshidrogenasa
shRNA	*short hairpin RNA*, RNA de horquilla corta
sIBM	Miositis esporádica por cuerpos de inclusión
siRNA	RNA de silenciamiento
SIRT	Sirtuina
SOD-2	Superóxido Dismutasa-2
T/H	Ratón doble transgénico para el transactivador y para H49K tumorales del hígado
TCA	Ciclo de los ácidos tricarboxílicos
Tet	Tetraciclina
TIM	Traslocasa de la membrana interna
TOM	Traslocasa de la membrana externa
TRE	*Tetracycline Responsive Element*, elemento de repuesta a tetraciclinas
tRNA	RNA de transferencia
tTa	Transactivador
UCI	Unidad de cuidados intensivos
UPRmt	*Mitochondrial unfolded protein response*, Respuesta a proteínas desplegadas mitocondrial
VDAC	Canal aniónico voltaje dependiente
ΔΨm	Potencial de membrana mitocondrial

ÍNDICE

RESUMEN

Resumen

El estudio del metabolismo energético ha experimentado un gran auge en los últimos tiempos después de haber pasado una época de relativo ostracismo. Así, hoy se reconoce su implicación en la génesis y progresión de patologías humanas de gran prevalencia como son el cáncer, el síndrome metabólico, la obesidad, diabetes etc. En este sentido, la metabolómica se ha incorporado junto con la genómica, transcriptómica y proteómica como una "nueva" ómica en biomedicina.

En esta tesis se resume la actividad que he desarrollado en el ámbito del metabolismo energético en dos vertientes diferenciadas: una es más básica y está relacionada con la implicación del metabolismo energético en la biología de la célula (**Artículos #1-4**) y en un segundo apartado, mas aplicado, relacionado con el desarrollo de una técnica proteómica de alto rendimiento que permite la traslación del metabolismo energético al ámbito de la clínica y en concreto al ámbito de las Enfermedades Raras (**Artículo #5 y #6**).

La mitocondria es el orgánulo responsable de producir la mayoría del ATP celular en un proceso que se conoce como fosforilación oxidativa. El cuello de botella de esta actividad constituye el motor molecular giratorio de la membrana interna mitocondrial denominado complejo V o ATP sintasa. La ATP sintasa está regulada por diversos mecanismos y fundamentalmente por la actividad de la cadena de transporte de electrones (CTE) así como por una proteína inhibidora que se denomina IF1, Factor Inhibidor 1 de la ATPasa. Estudios recientes de nuestro laboratorio han demostrado que IF1 es una proteína regulada por fosforilación. Únicamente cuando IF1 está defosforilado se une a la H^+ATP sintasa y bloquea la actividad sintética e hidrolítica de ATP (Garcia-Bermudez *et al.*, 2015). La sobreexpresión de IF1 promueve la inhibición de la ATP sintasa, lo que genera un aumento de la glucolisis aerobia de la célula así como la generación de una señal de especies reactivas de oxígeno (ROS) que desencadena mecanismos de supervivencias celular (**Artículo #1-4**). Mi contribución en estos cuatros artículos que componen parte de mi tesis correspondiente a los aspectos más básicos del metabolismo energético, se ha centrado en demostrar la implicación de IF1 en la regulación de la bioenergética mitocondrial por su posible participación en el ensamblaje/desensamblaje de complejos respiratorios así como por su función oncogénica en hepatocarcinogénesis.

Por la implicación evidente del metabolismo energético en biomedicina hemos desarrollado e implementado una plataforma de array de fase reversa de alto rendimiento que permite el análisis cuantitativo de la expresión de proteínas del metabolismo (**Artículos #5 y #6**). Esta plataforma de array de proteínas de fase reversa evalúa la expresión de estas proteínas en condiciones normales y patológicas, lo que permite su aplicación en el ámbito de la clínica con el propósito de encontrar nuevos marcadores moleculares de la enfermedad. La plataforma la hemos validado en el estudio de Enfermedades Raras con afectación muscular.

SUMMARY

Summary

After a period of relative ostracism, the study of energy metabolism has experienced a sharp increase in recent years. Today, the implication of metabolism is recognized of high prevalence in the genesis and progression of human pathologies such as cancer, metabolic syndrome, obesity, diabetes etc… and metabolomics has been incorporated as a "new" omic in biomedicine together with genomics, transcriptomics and proteomics.

This thesis will summarize the activity that I have developed in the field of energy metabolism in two different aspects: a more basic one, that deals with the implication of energy metabolism in cell biology (**Articles #1-4**) and another aspect, more applied, aimed to the development and implementation of a high-throughput proteomic technique that could allow the translation of energy metabolism in the clinical setting and specifically within the field of Rare Diseases (**Articles #5-6**).
Mitochondria are the organelles responsible for the production of the majority of cellular ATP in a process known as oxidative phosphorylation. The bottleneck of this activity is the molecular rotatory engine of the inner mitochondrial membrane called complex V or ATP synthase. The ATP synthase is regulated by a variety of mechanisms and mainly by the activity of the electron transport chain (ETC) as well as by an inhibitory protein named IF1, ATPase inhibitory factor 1. Recent studies from our lab have demonstrated that IF1 is a protein regulated by phosphorylation. Only when IF1 is dephosphorylated it is able to bind the ATP synthase blocking both the synthetic and hydrolytic activity of ATP (Garcia-Bermudez *et al.*, 2015). The overexpression of IF1 promotes the inhibition of the ATP synthase, which generates an increase in aerobic glycolysis, as well as the generation of a reactive oxygen species signal (ROS) that triggers mechanisms of cell survival (**Articles #1-4**). My contribution in these four articles correspond to the basic aspects that I have studied regarding energy metabolism focused in the analysis of the implication of IF1 in the regulation of the assembly/disassembly of respiratory complexes and on its potential oncogenic role in hepatocarcinogenesis.

Because of the relevance of energy metabolism in biomedicine, we have developed and implemented a reverse phase protein microarray high-throughput platform that could allow a quantitative analysis of the expression of proteins of energy metabolism in normal and pathological condition. This platform has the obvious aim of identifying new molecular biomarkers of disease. The platform has been validated by the study of patient affected with Rare Neuromuscular diseases. (**Articles #5 y #6**).

INTRODUCCIÓN

1 Introducción

"Ex nihilo nihil fit" nada surge de la nada y nada puede transformarse en nada (Empédocles, Agrigento, Sicilia, 490-430 a.c.). En el mismo sentido, el primer principio de la termodinámica establece que la energía ni se crea ni se destruye, sólo se transforma. El proceso de transformación de la energía en los organismos vivos es lo que denominamos Metabolismo. El metabolismo energético es el proceso de generación de energía biológica a partir de nutrientes mediante una serie de rutas bioquímicas interconectadas que pueden ocurrir tanto en presencia (aeróbico) como en ausencia de oxígeno (anaeróbico). La vía glucolítica, es la única vía de provisión de energía que puede producir ATP en ausencia de oxígeno. Además, la glucolisis es responsable de la generación de los metabolitos intermediarios requeridos para la producción de ácidos nucleicos, aminoácidos y lípidos, es decir, proporciona la materia prima para la producción de biomasa. Las adaptaciones metabólicas, en respuesta al microambiente y/o a condiciones fisiopatológicas, son simples soluciones lógicas debidas a la presión selectiva y a los vínculos impuestos por la evolución (Bar-Even *et al.*, 2012). Por contra, en la célula en presencia de oxígeno, el metabolismo de la glucosa tiene un rendimiento energético mucho mayor y necesita de la participación de rutas metabólicas localizadas en la mitocondria, como son el ciclo de Krebs, la cadena de trasporte de los electrones y la fosforilación oxidativa (OXPHOS) entre otros.

1.1 La mitocondria

1.1.1 Estructura

La mitocondria es un orgánulo de doble membrana extremadamente dinámico presente en la mayoría de las células eucarióticas que juega un papel fundamental tanto en la fisiología como en la adaptación patológica ya que su función principal es la producción de energía (Mitchell, 1961) y el control de la señalización intracelular que deviene en el destino final de la célula (Sanchez-Arago *et al.*, 2013). Tanto el número, la disposición, la estructura, como el perfil proteómico y la función de este orgánulo están estrechamente relacionados. Esta relación se regula en función del tipo celular, del estado fisiológico del desarrollo o del estado patológico que tienen requerimientos energéticos y metabólicos distintos (Forner *et al.*, 2009; Izquierdo *et al.*, 1995; Mootha *et al.*, 2003; Pagliarini *et al.*, 2008). La morfología de la mitocondria es variada, distinguiéndose orgánulos esféricos, filamentoso, ramificados y de forma especializada como de discos o copas (Munn, 1974) (Figura 1). El tamaño oscila entre 0,5 y 1 μm de diámetro y hasta 7 μm de longitud. La mitocondria está en contacto directo y permanente con el citoesqueleto, lo que le confiere motilidad (Hollenbeck and Saxton, 2005) y con el retículo endoplásmico (ER) a través de los complejos proteicos ERMES, lo que contribuye al mantenimiento de la homeostasis del calcio y la biogénesis de lípidos (Hayashi *et al.*, 2009; Kornmann and Walter, 2010). Existen diferentes enfermedades metabólicas que cursan con disfunciones mitocondriales debido tanto a alteraciones genéticas como epigenéticas. La diversidad patológica es

un reflejo de la organización fisiológica que es específica de cada tipo celular y tejido, y que hace referencia a la distribución, la composición, la estructura e incluso la función de las mitocondrias (Pagliarini *et al.*, 2008).

La mitocondria contiene su propio genoma de 16,569bp, sin intrones y localizado en la matriz mitocondrial: el mtDNA. De los 37 genes codificados en su genoma, 13 codifican proteínas hidrofóbicas de la OXPHOS. Para permitir la síntesis de estas proteínas, el mtDNA también codifica por 22 tRNA y 2 rRNA (Anderson *et al.*, 1981; Calvo and Mootha, 2010). El mtDNA se encuentra en múltiples copias en cantidades que dependen del tipo celular (Shoubridge and Wai, 2007). Una célula se denomina heteroplásmica cuando en ella coexisten diferentes genomas mitocondriales debidos a polimorfismos o a variaciones patogénicas (mutaciones) del mtDNA, por lo contrario se denomina homoplásmica cuando todas las moléculas de mtDNA son iguales. El nivel de heteroplasmia define el porcentaje de moléculas mutadas en relación a la secuencia "wild type". El genoma mitocondrial se encuentra empaquetado en complejos de nucleoproteínas denominados nucleoides, que contienen proteínas esenciales para la maquinaria de replicación y trascripción del mtDNA: el factor de trascripción mitocondrial A, la proteína de unión a DNA de cadena simple y la helicasa "twinkle" (Brown *et al.*, 2011; Wang and Bogenhagen, 2006).

Estructuralmente, las mitocondrias poseen dos membranas lipídicas, muy distintas en composición y función: la membrana mitocondrial externa (MME), que está en contacto con el citoplasma y es permeable a los protones, y la membrana mitocondrial interna (MMI), impermeable a los protones que posee unas invaginaciones o crestas mitocondriales que principalmente sirven para aumentar la superficie total de la membrana en la que tiene lugar la fosforilación oxidativa (Figura 1). La MMI se une a la MME, en las zonas periféricas de las crestas adyacentes a la MME, por estructuras tubulares llamadas "*crista junctions"* (Mannella, 2000; Perkins and Frey, 2000) (Figura1). Esta organización de doble membrana separa tres compartimentos necesarios para el correcto funcionamiento del orgánulo: el citosol, el espacio intermembrana (EM) y la matriz mitocondrial (Figura 1). Recientemente, se ha

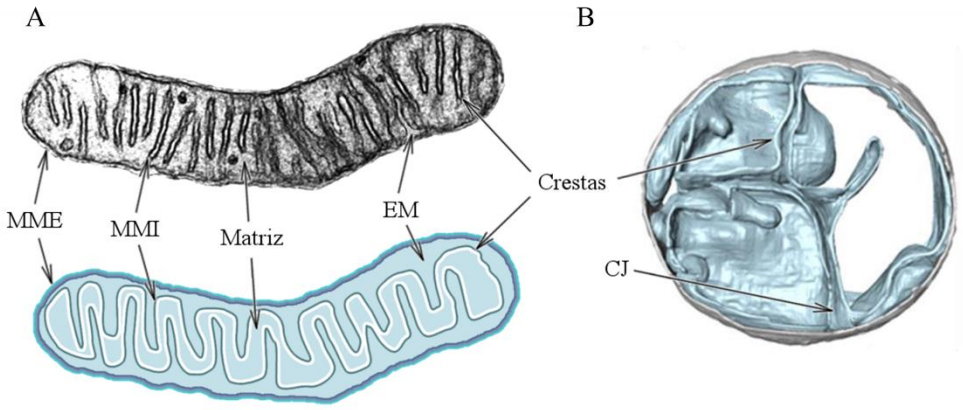

Figura 1. Esquema de la estructura y compartimentación mitocondrial. (A), Se representa la membrana mitocondrial externa (MME), interna (MMI) y el espacio intermembrana (ME) en la imagen por microscopía electrónica de trasmisión (TEM). (B), se indican las "cristae junction" (CJ) en una micrografia ecotomográfica electrónica a transmisión de una sección de mitocondria de levadura. La matriz y las crestas mitocondriales están indicadas en (A) y (B), (modificado de (Davies *et al.*, 2014)).

descrito un complejo proteico implicado en la organización y plegamiento de la membrana interna (MICOS) (Barbot *et al.*, 2015; Harner *et al.*, 2011), siendo varios los elementos que participan en este proceso (Zick *et al.*, 2009). En este contexto, se atribuye un papel importante a la composición de la membrana interna rica en cardiolipina y fosfatidiletanolamina (Osman *et al.*, 2011). Además, la MMI contiene todos los complejos proteicos que forman la cadena transportadora de electrones (CTE) (Wittig and Schagger, 2008) así como a la ATP sintasa, cuya agrupación oligomérica de dímeros en bandas (*ribbons*) en forma de "v", son responsables de la curvatura de la MMI que forma la cresta mitocondrial (Arnold *et al.*, 1998; Davies *et al.*, 2012a; Davies *et al.*, 2012b; Paumard *et al.*, 2002; Strauss *et al.*, 2008).

Puesto que la mayoría de las proteínas mitocondriales se producen en el citosol, existe un sistema de transporte dedicado al tráfico de proteínas por el sistema de membranas mitocondriales; TOM es la translocasa de la MME y TIM de la MMI. Estos complejos de múltiples subunidades reconocen secuencias dianas situadas principalmente en el extremo N-terminal de la proteína, permitiendo su ingreso en la matriz y una vez en el interior la secuencia es cortada por una peptidasa de matriz (Schmidt *et al.*, 2010).

Las mitocondrias, tanto en su organización interna como en su disposición y número en la célula, están sujetas a un constante remodelado gracias a su capacidad de fusionarse por la actividad de mitofusinas Mfn1/Mfn2 y Opa1/Mgm1, o fisionarse por acción de las proteínas Drp1/Dnm1 y FIS1 (Twig *et al.*, 2008). La dinámica mitocondrial permite una adaptación estructural y funcional en respuesta a distintas condiciones celulares como la demanda metabólica (Liesa and Shirihai, 2013; Mannella, 2006), estimulación apoptótica (Frezza *et al.*, 2006; Olichon *et al.*, 2003; Santamaria *et al.*, 2006; Song *et al.*, 2007), división celular (Martinez-Diez *et al.*, 2006), autofagia (Gomes *et al.*, 2011; Twig *et al.*, 2008) y supervivencia (Takuma *et al.*, 2009).

1.1.2 Papel fisiológico

La glucosa es el sustrato metabólico preferido de la mayoría de las células, su esqueleto carbonado es oxidado en el citoplasma y/o en la mitocondria proporcionando energía e intermediarios metabólicos para el mantenimiento, el crecimiento y/o proliferación. La parcial oxidación de un mol de glucosa por la glucolisis en el citoplasma produce dos moles de piruvato, ATP y NADH. Una limitación de oxígeno o un trastorno genético que impida la oxidación del piruvato en la mitocondria provoca su reducción a lactato en el citoplasma por la lactato deshidrogenasa (LDH), con objeto de regenerar NAD^+ necesario para la glucolisis (Figura 2). En condiciones de normoxia todo el piruvato se oxida a CO_2 en la mitocondria por la piruvato deshidrogenasa (PDH) y por el ciclo de los ácidos tricarboxílicos (TCA) (Figura 2). Los electrones obtenidos por la oxidación de la glucosa en el citoplasma y en la mitocondria son trasportados por los complejos de la cadena respiratoria para generar un gradiente electroquímico de protones a través de la MMI (Figura 2). El retorno de los protones a la matriz mitocondrial a través del canal de H+ de la ATP sintasa se utiliza para la síntesis

de ATP a partir de ADP y Pi (Figura 2). El piruvato, totalmente oxidado, proporciona una cantidad de ATP casi 20 veces mayor a la que se produce por la glucolisis (Figura 2). El TCA, también participa en los procesos anabólicos proporcionando metabolitos utilizados como precursores en otras rutas biosintéticas. En este contexto, el oxalacetato y el α-cetoglutarato son precursores del aspartato y glutamato respectivamente, los cuales son utilizados en la síntesis de los aminoácidos y de las bases púricas y pirimidínicas. Asimismo, el succinil-CoA sirve como precursor de las porfirinas y del grupo hemo (Figura 2). El citrato es fuente de acetil-CoA requerido para la síntesis de los ácidos grasos y esteroles (Figura 2), rutas particularmente activas en las células proliferativas (DeBerardinis *et al.*,

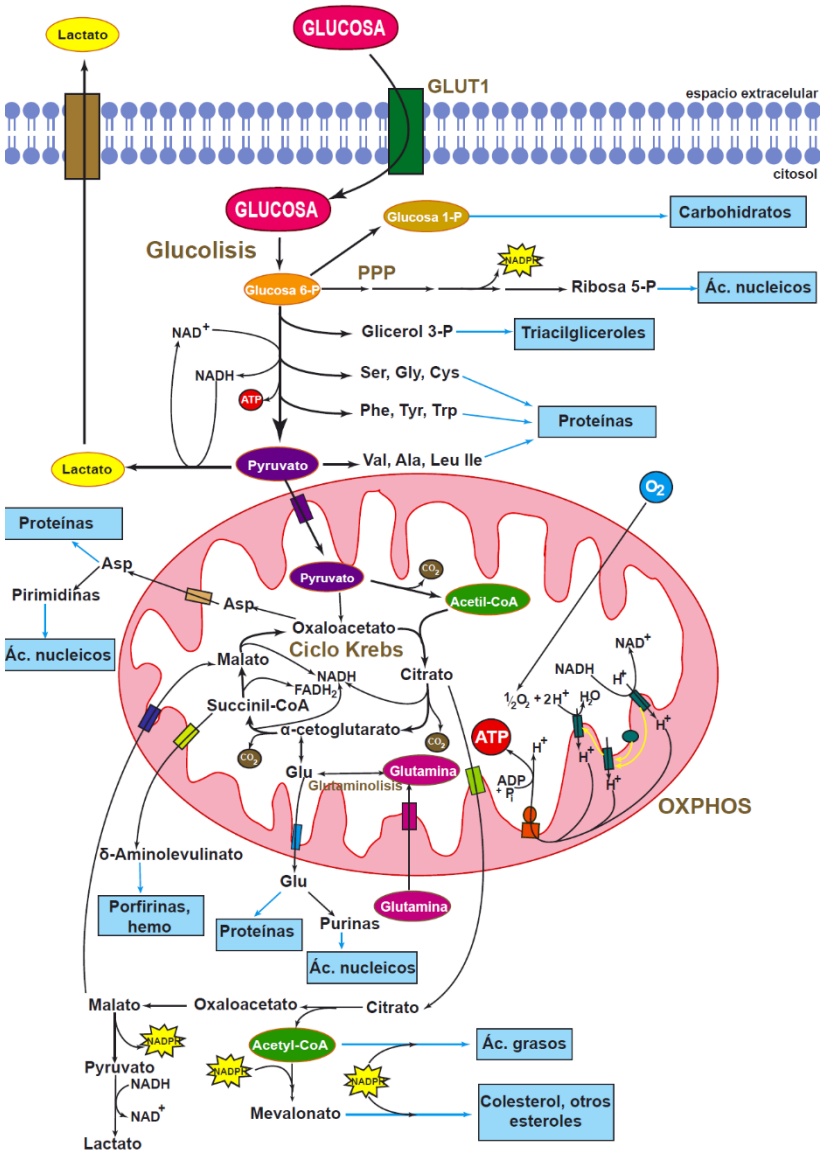

Figura 2: Esquema del metabolismo glucolítico y mitocondrial. Tras el ingreso en la célula por su trasportador especifico (GLUT1), la glucosa puede ser (i) catabolizada por la ruta de las pentosas fosfatos (PPP), proporcionando poder reductor en forma de NADPH, (ii) utilizada para la síntesis de carbohidratos o (iii) oxidada a piruvato en la glucolisis generando intermediarios metabólicos que pueden ser utilizados en procesos anabólicos (rectángulos azules). En el citoplasma, el piruvato puede ser reducido a lactato y sucesivamente exportado al exterior de la célula u oxidado a acetil-CoA en la mitocondria para su oxidación completa a CO_2 en ciclo de Krebs. Algunos intermediarios son sustraídos a la mitocondria para ciertas rutas biosintéticas y/o anapleróticas. Las líneas amarillas representan los electrones obtenidos en las oxidaciones ($NADH/FADH_2$) y transferidos al oxígeno por los complejos de la cadena respiratoria (en verde) en la fosforilación oxidativa (OXPHOS). La ATP sintasa (en naranja) utiliza el gradiente protónico generado en la OXPHOS para sintetizar ATP, (modificado de (Ortega *et al.*, 2009)).

2008; Green *et al.*, 2014). Los intermediarios del TCA, utilizados por necesidades biosintéticas, tienen que ser restaurados por otras rutas anapleróticas para garantizar el flujo continuo de sustratos. El catabolismo de la glutamina tiene una doble funcionalidad: por un lado sirve para proporcionar grupos amino para la síntesis de aminoácidos y bases, y por otro proporciona esqueletos carbonados (DeBerardinis *et al.*, 2008; Green *et al.*, 2014). La actividad de estas vías está regulada por la disponibilidad de nucleótidos de adenina, NADH y/o algunos intermediarios clave como el citrato (Ortega *et al.*, 2009). En este contexto, enzimas reguladoras son: la fosfofrutoquinasa (PFK) y piruvato quinasa (PK) en la glucolisis, la piruvato deshidrogenasa (PDH), citrato sintasa (CS), isocitrado deshidrogenasa (IDH) y α-cetoglutarato deshidrogenasa (OGDH) en la mitocondria y la citocromo c oxidasa (CIV) y la ATP sintasa en la OXPHOS (Ortega *et al.*, 2009). Como consecuencia del flujo electrónico por la CTE se generan, especies reactivas de oxígeno (ROS) fundamentalmente en los complejos I y III. En particular, el anión superóxido ($O_2^{\bullet-}$) y su derivado el peróxido de hidrógeno (H_2O_2) difunden a través de las membranas y modifican toda clase de moléculas que pueden provocar fallos que desembocan en diversas patologías (revisado en (Valko *et al.*, 2007)) o, según la intensidad de la señal, pueden señalizar al núcleo activando un determinado programa celular (D'Autreaux and Toledano, 2007; Mittal and Murad, 1977; Yun and Finkel, 2014). En este contexto, es interesante resaltar cómo la misma clase de moléculas puede desencadenar procesos fisiológicos tan diferentes como la inducción de la apoptosis, necrosis, autofagia y mitofagia o proliferación y supervivencia celular en función de la concentración producida (Formentini *et al.*, 2012; Hamanaka and Chandel, 2010; Orrenius *et al.*, 2007; Ristow, 2014) (**Artículo #2**). El sistema de detoxificación se atribuye a enzimas principalmente mitocondriales como la superóxido dismutasa (SOD2 o MnSOD) que detoxifica $O_2^{\bullet-}$ y la catalasa y glutatión peroxidasa (GPx) que detoxifican H_2O_2.

Además de la producción de ATP y de la señalización por ROS la mitocondria está implicada en la ejecución de la muerte celular (Green *et al.*, 2014), la homeostasis del calcio (Rizzuto *et al.*, 2012; Satrustegui *et al.*, 2007), el metabolismo de los ácidos grasos, la síntesis del grupo hemo y el metabolismo de los aminoácidos (Nelson and Cox, 2004). Las funciones mitocondriales están reguladas por el núcleo así como funciones nucleares pueden estar reguladas por la mitocondria a través de una robusta red de moléculas señalizadoras que, en sentido bidireccional, regulan la homeostasis celular, proceso al que se le ha denominado recientemente comunicación mitonuclear (Quiros *et al.*, 2016).

1.1.3 Organización estructural de la CTE

Por muchos años el modelo de colisión casual o modelo "fluido" se ha considerado el más acertado para describir la organización estructural de la CTE (Hackenbrock *et al.*, 1986). Sin embargo, el modelo "sólido", con los complejos respiratorios ordenados en secuencias I-IV (Chance and Williams, 1955), nunca ha sido abandonado, especialmente por los estudios llevados a cabo por Hatefi y Fowler (revisado en (Rich, 1984)). Este modelo ha cobrado más importancia en las últimas décadas debido a

las evidencias de agregación de complejos en supercomplejos, demostrables gracias a la introducción de Schägger de los geles electroforéticos en condiciones nativas (BN-PAGE) (Schagger *et al.*, 1994). Schägger describió nuevas evidencias de ensamblajes estequiométricos preferenciales, tanto en levadura como en mamíferos, sugiriendo un modelo de CTE (el respirasoma) basado en el direccionamiento "channeling" de los electrones entre complejos en lugar de la colisión casual (Genova *et al.*, 2008; Schagger and Pfeiffer, 2000). Esta agregación, además de estabilizar los propios complejos, mejoraría el flujo electrónico por efecto del direccionamiento del substrato ("substrate channeling"), o de los intermedios de reacción, enviados directamente al enzima específico, minimizando la generación de ROS (Boekema and Braun, 2007; Boumans *et al.*, 1998; Schagger, 2001) (Figura 3A). La agregación entre el complejo III y IV, estabilizada por la cardiolipina (un glicerofosfolipido de membrana cargado negativamente), parece ser la más frecuente, tanto es así que en levadura no se ha identificado el complejo IV libre incluso en mutantes de *S. Cerevisiae* que no poseen este glicerofosfolipido (Pfeiffer *et al.*, 2003).

Se han descrito diferentes estequiometrias entre los complejos, la agregación I-III forma el supercomplejo I_1-III_2 pero también se ha observado en combinación con varias copias del complejo IV (I_1-III_2-IV_2 y I_1-III_2-IV_4) mientras que raramente el complejo I se encuentra en su forma libre (Schagger, 2001; Wittig and Schagger, 2009) (Figura 3B). En un modelo 3D se indica cómo los sitios de unión entre complejos corresponden, aunque solo en parte, con sitios de interacción de los

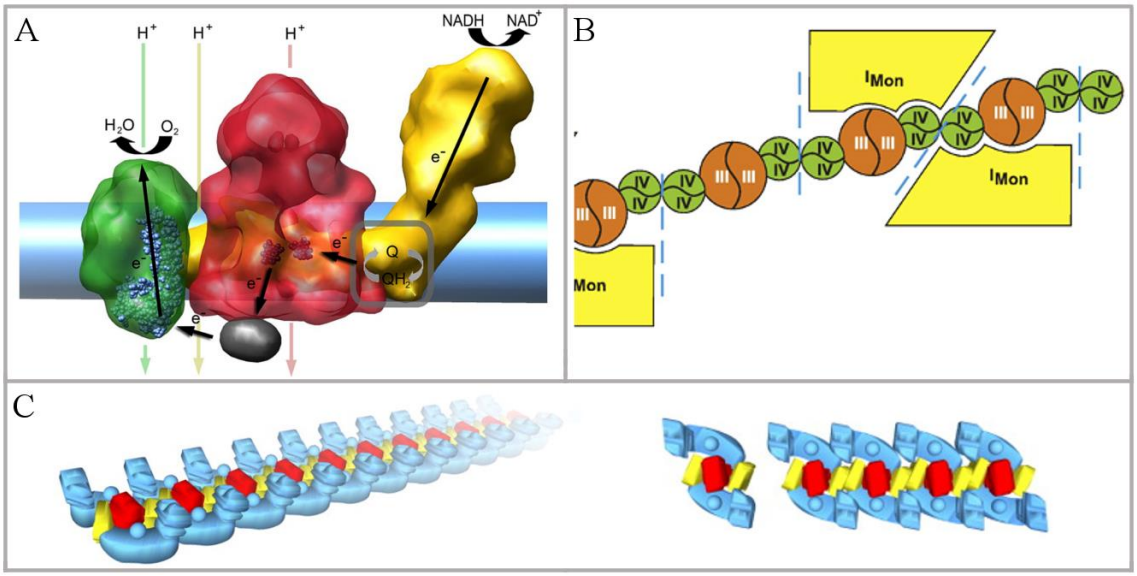

Figura 3. **Modelos de agregaciones supramoleculares.** (A) Flujo electrónico hipotético en el supercomplejo I-III_2-IV: el complejo I se muestra en amarillo, el complejo III en rojo, el complejo IV en verde. El NADH se oxida a NAD+ y los electrones pasan, por el complejo I, a la Ubiquinona. Su sitio de unión localizado entre el complejo I y el complejo III_2, indicado con un rectángulo en gris. Desde el complejo III_2, un electrón por vez reduce el citocromo c (en negro) localizado en proximidad del complejo IV, que cuando posee 4 electrones reduce el oxígeno molecular a agua (tomado de (Vonck and Schafer, 2009)). (B) Modelo de asociación de complejos respiratorios mitocondriales de mamífero. Las separaciones por las líneas discontinuas azules distinguen un elemento básico constituido por un dímero del complejo III intercalado en el tetrámero del complejo IV y un agregado mayor que además incluye el complejo I. El complejo I se muestra en amarillo, el complejo III en naranja y el complejo IV en verde (modificado de (Wittig and Schagger, 2009)). (C) Reconstrucción esquemática de la organización supramolecular en megacomplejos cuya unidad básica está constituida por dos copias del complejo I, una copia del complejo III_2 y dos copias del complejo IV. Vista lateral (izquierda), vista de arriba (derecha). El complejo I está indicado en azul, el complejo III en rojo y el complejo IV en amarillo (modificado de (Bultema *et al.*, 2009)).

transportadores móviles (CoQ y cit c) favoreciendo el "channeling" (Vonck and Schafer, 2009) (Figura 3A). Esta teoría ha sido muy debatida ya que otros autores, tras estudios de microscopía electrónica de alta resolución (18 Å), sostienen que es improbable un mecanismo de channeling de la ubiquinona en el interior del supercomplejo. Sin embargo, esta organización permitiría una velocidad de difusión electrónica más alta que la del modelo fluido (Dudkina *et al.*, 2005). Por otro lado, estudios mediante análisis de control de flujo siguen apoyando la teoría del channeling (Bianchi *et al.*, 2004), mientras que por microscopía electrónica de alta resolución, se ha observado la asociación de supercomplejos en forma de largas colas de unidades I_2+III_2+IV_2 llamados megacomplejos (Bultema *et al.*, 2009; Wittig *et al.*, 2006) (Figura 3C). Recientemente, entre el modelo fluido y el modelo sólido se ha sugerido un tercer modelo definido "plástico", en el que coexistirían ambos modelos, justificando las distintas demandas funcionales y estructurales de la célula (Acin-Perez and Enriquez, 2014; Cogliati *et al.*, 2016; Enriquez, 2016; Lapuente-Brun *et al.*, 2013).

Con respecto al complejo V, se ha especulado durante mucho tiempo que la proximidad entre monómeros de ATP sintasa se debía a la abundancia de esta proteína en las crestas mitocondriales, hasta que en 1989 Richard Allen, observando por crio-microscopía electrónica membranas mitocondriales de *Paramecium multimicronucleatum*, describió agregaciones diméricas y oligoméricas sugiriendo que las primeras fuesen las unidades básicas de las segundas. Esta teoría se demostró definitivamente con la puesta a punto de los geles en condiciones nativas "*clear native gel*" (CN-PAGE) que utilizando bajas concentraciones de un detergente como la digitonina y sin el marcaje con coomassie G250, permite aislar agregaciones múltiples de dímeros (como tetrámeros, hexámeros y octámeros) y también estudiar la actividad hidrolítica de la ATP sintasa en gel (Krause *et al.*, 2005; Wittig and Schagger, 2005, 2009).

1.2 La ATP sintasa

1.2.1 Estructura y función

La ATP sintasa es un complejo multiproteico muy conservado durante la evolución, que realiza la reacción enzimática de la producción de ATP (Yoshida *et al.*, 2001). Es un complejo de 650kDa que se compone por 16 subunidades organizadas en dos dominios principales: i) el dominio liposoluble embebido en la MMI, F_O ($c_{8\text{-}10}a_1$), y ii) el dominio hidrosoluble F_1 ($\alpha_3\beta_3\gamma_1\delta_1\varepsilon_1$) orientado hacia la matriz y unido al F_O un eje lateral ($b_1F6_1d_1A6L_1OSCP_1$) (Walker, 2013) (Figura 4). También se han descrito otras subunidades como la *e, f, g,* DAPIT y el proteolípido de 8kDa no conservadas en todas las especies y que contribuirían tanto a la estructura como a la función y organización supramolecular de la ATP sintasa (Walker, 2013) (Figura 4).

La ATP sintasa es el motor reversible de la OXPHOS capaz de sintetizar o hidrolizar ATP, en función de las condiciones fisiológicas y es por tanto un importante regulador del metabolismo energético. Además de jugar este papel central, es protagonista de funciones celulares muy destacables.

Entre ellas, es responsable de generar la estructura de las crestas, la regulación de la apoptosis y su posible participación en la generación del poro de permeabilidad transitoria (PTP) así como su posible papel en la señalización intracelular (Bernardi, 2013; Bonora *et al.*, 2013; Carraro *et al.*, 2014; Giorgio *et al.*, 2013; von Stockum *et al.*, 2015). A la vista de su relevancia no sorprende que la ATP sintasa esté también implicada en el proceso de envejecimiento (Chin *et al.*, 2014).

La subunidad γ, proporcionando un eje central asimétrico, juega un papel funcional importante en el dominio F_1 (Figura 4). Su rotación repercute sobre la conformación de las subunidades β catalíticas, determinando cuatro cambios conformacionales en cada subunidad por cada giro de 360º. Dos conformaciones permiten la unión con el ADP + Mg^{2+} o ATP + Mg^{2+}, β_{DP} y β_{TP} respectivamente,

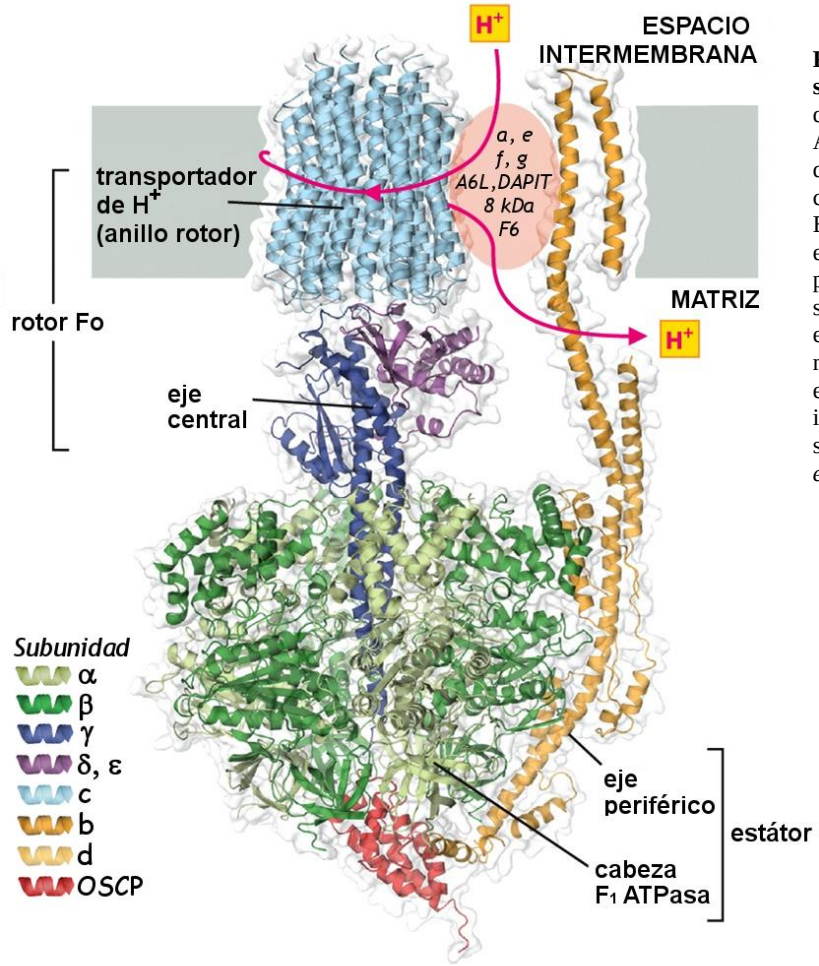

Figura 4. Estructura de la ATP sintasa. Representación esquemática de la organización estructural de la ATP sintasa con sus subunidades. El dominio globular hidrosoluble está constituido por la cabeza F_1 ATPasa. El rotor de la turbina se compone por el dominio liposoluble F_O, formado por el anillo oligomérico de las 8 subunidades c, por la subunidad *b* del eje periférico y por otras subunidades menores (*a*, *e*, *f*, *g*, *A6L*, *DAPIT*, *F6* y el péptido de *8 kDa*). La leyenda indica el color de las respectivas subunidades (modificado de (Alberts *et al.*, 2013)).

mientras que la tercera conformación denominada β_E resulta en un estado de baja afinidad por nucleótidos y la cuarta, β_{HC}, en un estadio parcialmente avanzado de β_E parcialmente cerrado (Mao and Weber, 2007). Contrariamente, la subunidad α no sufre cambios conformacionales (Walker, 2013). Para una rotación completa ocho H^+, uno por cada subunidad c del F_O, son translocados a la matriz cuando la ATP sintasa opera en modalidad sintética (directa), produciendo ATP. El mecanismo rotacional puede operar también en modalidad "reversa", hidrolizando ATP y bombeando protones hacia el EM, para restaurar el $\Delta\Psi_m$ en casos de despolarización como por ejemplo en hipoxia (Adachi *et al.*, 2007) o durante la apertura del PTP. Cada 11 protones se realiza una vuelta completa del rotor

con producción de tres ATP, es decir 3.7 protones / molécula de ATP, si contamos los que se necesitan para translocar una molécula de ATP al EM por una de ADP a la matriz (Watt *et al.*, 2010).

1.2.2 Ensamblaje

Para el ensamblaje de la ATP sintasa se han identificados chaperonas, en *Saccharomyces cerevisiae*, implicadas tanto para el dominio F_1 (Ackermann and Geering, 1990), como para el F_O (Ruhle and Leister, 2015). Asimismo, se ha descrito el complejo de ensamblaje de la membrana interna "INA" que sería responsable de los pases finales del proceso (Lytovchenko *et al.*, 2014). Con respecto a la formación del dímero de ATP sintasa se ha descrito que aunque el ángulo entre dos monómeros de un mismo dímero dependa de las especies analizadas, en muchos casos es mayor de 70º, excluyendo así una interacción directa entre los sectores hidrosolubles F_1 (Dudkina *et al.*, 2005; Dudkina *et al.*, 2006; Thomas *et al.*, 2008; Vonck and Schafer, 2009; Wittig and Schagger, 2009) (Figura 5A). La subunidad a del sector liposoluble F_O, se ha descrito implicada en la dimerización, tanto por la proximidad como por la identificación de un dímero de la subunidad a asociado a dos anillos c del sector liposoluble F_O (c_{10}- a_2-c_{10}) aislado de dímeros de ATP sintasa (Wittig and Schagger, 2008). Sin embargo, otros autores atribuyen este papel a las subunidades *e* y *g* describiendo la formación de un heterodímero *e-g* responsable de la dimerización (Bustos and Velours, 2005; Ruhle and Leister, 2015; Walker, 2013). Dímeros de ATP sintasa organizados en lazos se han descrito en estudios por crio-tomografia electrónica en mitocondrias de bovino y rata (Davies *et al.*, 2011; Strauss *et al.*, 2008), y también por microscopio de fuerza atómica en levadura (Buzhynskyy *et al.*, 2007), reforzando la teoría del papel modelador de los oligómeros con respecto a las crestas (Figura 5B y C).

La agregación de dímeros en oligómeros de ATP sintasa sigue siendo un debate abierto, aunque entre otras, son tres las teorías más acreditadas. La primera, indica como responsables las subunidades *e* y *g*, ya que se ha descrito la existencia de puentes disulfuros *e-e* y *g-g* en homodímeros de ATP sintasa tras la oxidación de la MMI (Arselin *et al.*, 2003; Bustos and Velours, 2005; Fronzes *et al.*, 2006; Gavin *et al.*, 2005; Wittig and Schagger, 2009) (Figura 5B). La segunda, indica la subunidad *b* en el brazo periférico como estabilizadora de la estructura oligomérica (Weimann *et al.*, 2008) y, la tercera, describe como responsable de la unión entre dímeros el inhibidor fisiológico de la ATP sintasa IF1 (Campanella *et al.*, 2008; Wittig and Schagger, 2008) (Figura 5A). Otros candidatos implicados en la oligomerización son: el llamado factor B, que se ha descrito como parte integrante de la ATP sintasa, implicado en la oligomerización y regulador positivo de la actividad (Belogrudov, 2009), la subunidad *f*, la subunidad *8* y el trasportador de nucleótidos y de fosfato inorgánico (P_i). Esta asociación ha sido descrita como un ATP sintasoma (Acin-Perez *et al.*, 2008; Chen *et al.*, 2004a; Ko *et al.*, 2003). Otras proteínas implicada en el mantenimiento de un correcto ensamblaje son la proteína de fusión mitocondrial OPA1 (Patten *et al.*, 2014), LRPPRC cuya inactivación provocaría el desensamblaje del ATP sintasa (Mourier *et al.*, 2014), la ciclofilina D que por interacción con el brazo lateral produce el desensamblaje de los dímeros durante el envejecimiento (Daum *et al.*, 2013; Giorgio *et al.*, 2009) o

disminuye la velocidad tanto de la síntesis como de la hidrolisis de ATP (Chinopoulos, 2011) y la subunidad DAPIT que además de haber sido relacionada con la cantidad de ATP sintasa (Ohsakaya *et al.*, 2011) parece estar implicada en la adaptación metabólica de algunas patologías como la diabetes (Ohsakaya *et al.*, 2011; Paivarinne and Kainulainen, 2001) y el cáncer (Kontro *et al.*, 2015).

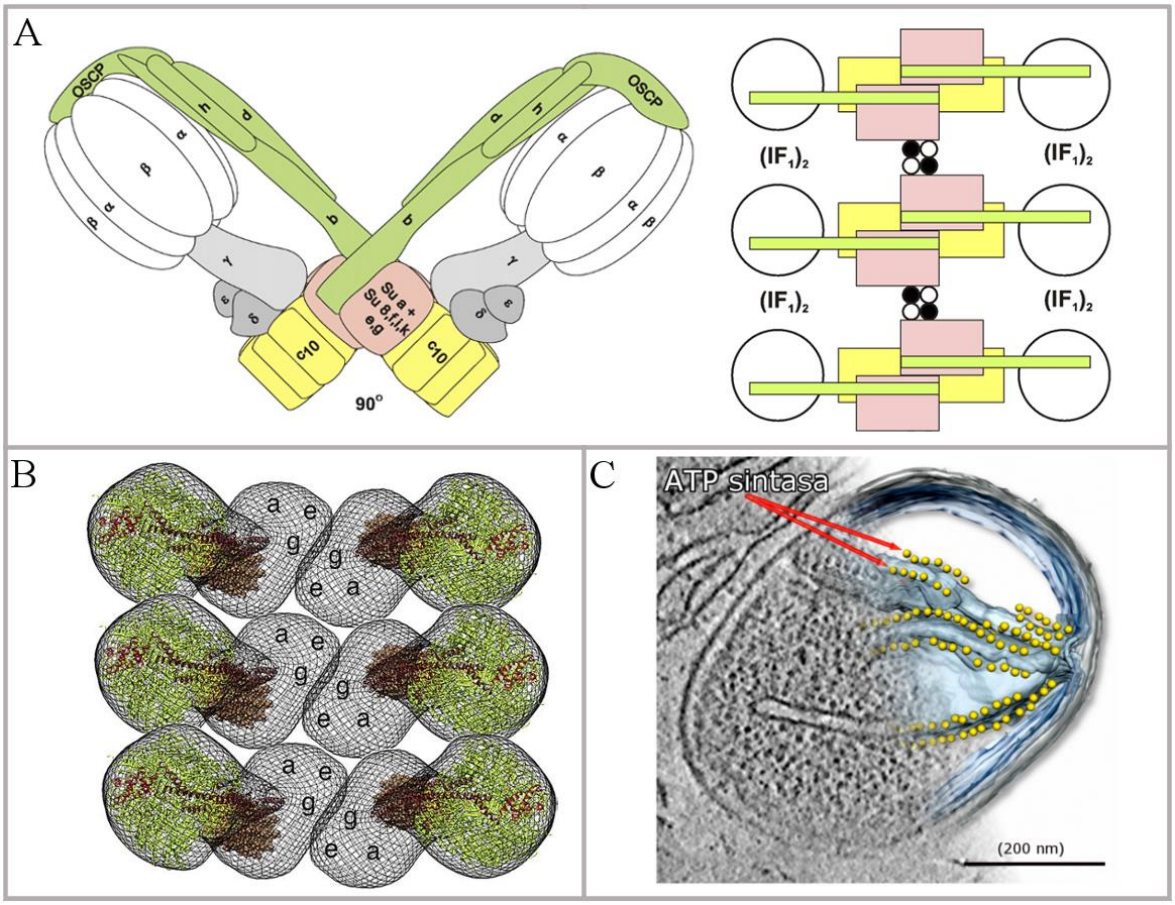

Figura 5: Modelo de la organización estructural de la ATP sintasa dimérica. (A) El modelo se basa en la dimerización de dos elementos monoméricos por interacción de las subunidades ɑ (a la izquierda) y en la asociación adicional de las unidades diméricas en estructuras oligoméricas por interacción de las subunidades e y g (círculos blancos y negros) y por el dímero del factor inhibitorio de la ATP sintasa 1 ($IF1_2$) visto desde la matriz hacia la MMI (a la derecha) (modificado de (Wittig and Schagger, 2009)). (B) Modelo hipotético de la organización supramolecular de la ATP sintasa en lazos de dímeros visto perpendicularmente a la MMI (modificado de (Vonck and Schafer, 2009)). (C) Reconstrucción de imagen por crio-tomografía electrónica de una mitocondria del hongo filamentoso *P. anserina*. Lazos de dímeros de ATP sintasa (en amarillo) se localizan por encima de la MMI en sitios de alta curvatura de las crestas. Barra de escala representa 200 nm (modificado de (Davies *et al.*, 2014)).

1.2.3 Papel en muerte celular

Los sensores intracelulares de los estímulos apoptóticos son un subgrupo de la familia Bcl-2 que contienen el dominio de homología 3 con Bcl-2 (BH3) conservado, por tanto se le ha nombrado *BH3-only proteins* (Bender and Martinou, 2013; Czabotar *et al.*, 2014). Estas proteínas, en concreto Bid, Bim, Bad, Noxa y Puma, responden a estímulos, como daño al DNA o estrés del ER, activándose y uniéndose a la MME mitocondrial, donde pueden unir proteínas Bcl-2 anti-apoptóticas como Bcl-X_L y Mcl-1 o activar las pro-apoptóticas Bax o Bak. La oligomerización de Bax o Bak activadas lleva a la permeabilización de la membrana. En todos casos, el destino de la célula se debe al control de las proteínas de la familia Bcl-2 y al equilibrio entre los miembros pro- y anti-apoptóticos en la MME.

Otro fenómeno que ocurre conjuntamente a la permeabilización de la membrana externa mitocondrial (MOMP) es la apertura del poro de transición de permeabilidad (PTP). La apertura sostenida de este megacanal permite el paso de solutos de bajo peso molecular y con ello una cascada de eventos como la despolarización mitocondrial, la generación de ROS, la liberación del Ca^{2+} de la matriz mitocondrial con el consiguiente hinchamiento osmótico (*swelling*), ruptura y liberación de proteínas con función pro-apoptótica (Bernardi, 2013; Bernardi *et al.*, 1999; Di Lisa *et al.*, 2011; Galluzzi *et al.*, 2009). El PTP responde a varios estímulos entre los cuales la acumulación patológica de calcio en el citosol, el fosfato inorgánico (Pi) (Hunter and Haworth, 1979) y ROS (Crompton *et al.*, 1987) inducen la abertura del mismo, mientras que el ATP (Duchen *et al.*, 1993) y la ciclosporina A (Crompton and Costi, 1988; McGuinness *et al.*, 1990) muestran un efecto inhibitorio. Sobre su composición molecular, la teoría más tradicional describe un complejo multimérico formado por proteínas localizadas tanto en la MME (el canal aniónico dependiente de voltaje VDAC) y MMI (el translocador de nucleótido de adenina ANT), como en la matriz (Ciclofilina D) (Rasola and Bernardi, 2011). Otros autores han propuesto que la ATP sintasa en su forma dimérica (Carraro *et al.*, 2014; Giorgio *et al.*, 2013; von Stockum *et al.*, 2015), o solo los anillos de las subunidades c, formarían parte del PTP (Alavian *et al.*, 2014; Bonora *et al.*, 2013).

Además, no se excluye la implicación de proteínas como la ciclofilina D que, junto con el trasportador de fosfato (PiC), regula la actividad del PTP (Leung *et al.*, 2008) y también interacciona y regula la actividad de la ATP sintasa (Giorgio *et al.*, 2009) (**Artículo #3**). La misma ATP sintasa es capaz de inclinar la balanza según interaccione con Bcl-X_L, optimizando su actividad anti-apoptótica en cerebro, hígado y en células cancerígenas (Alavian *et al.*, 2011; Formentini *et al.*, 2012) (ver discusión **Artículo #1, #2** y **#3**), o desencadenando la muerte por Bax y otros agentes pro-apoptóticos (Matsuyama *et al.*, 1998; Sanchez-Arago *et al.*, 2013; Santamaria *et al.*, 2006), recientemente demostrado *in vivo* en neuronas de ratón y en cultivo primario (**Artículo #3**).

1.3 El factor inhibidor de la ATP sintasa: IF1

1.3.1 Estructura de IF1 e interacciones con la ATP sintasa

IF1, el factor inhibidor de la ATPasa, es una pequeña proteína descrita por primera vez en músculo cardíaco bovino en los años 60 (Pullman and Monroy, 1963). IF1 está codificado en el DNA nuclear por el gen *ATPIF1* (*Gene ID*: 93974) del cromosoma 1 en *Homo sapiens* y por el gen *Atpif1* (*Gene ID*: 11983) en el cromosoma 4 en *Mus musculus*. El gen humano da lugar a 3 mRNAs distintos por *splicing* alternativo del pre-mRNA (Garcia-Bermudez and Cuezva, 2016). Algunos autores han descrito *in vitro* que IF1 interacciona a través del dominio N-terminal, con el dominio C-terminal de la calmodulina (CaM) de forma Ca^{2+} y pH dependiente. La interacción con la CaM, proteína exclusivamente citosólica, sugiere que podría ser la responsable de la importación de IF1 a la mitocondria (Contessi *et al.*, 2007; Contessi *et al.*, 2005; Pagnozzi *et al.*, 2010; Pedersen and Hullihen, 1984). IF1 se ha descrito en otros mamíferos (Cintron and Pedersen, 1979; Rouslin and Pullman, 1987), en *Caenorhabditis*

elegans (Ichikawa *et al.*, 2006), en el artrópodo *Litopenaeus vannamei* (Chimeo *et al.*, 2015), *Saccharomyces cerevisiae* (Hashimoto *et al.*, 1981) y en mitocondrias de plantas, pero no en cloroplastos (Norling *et al.*, 1990). En las distintas especies IF1 tiene un alto grado de homología, especialmente de la región que se une al dominio F1-ATPasa, lo que explica su capacidad de inhibir la ATP sintasa de otras especies, incluso para el homólogo Inh1 de levadura, que presenta menor conservación de secuencia (Cabezon *et al.*, 2002; Hashimoto *et al.*, 1984).

IF1 es una pequeña proteína básica que tiene en solución una estructura intrínsecamente desordenada en el N-terminal y una estructura en forma de α-hélice en C-terminal (Cabezon *et al.*, 2000a; Gordon-Smith *et al.*, 2001) (Figura 6A). La estructura cristalográfica del dominio F1 de la ATP sintasa inhibida por una forma truncada de IF1 de bovino (I1-60His), ha proporcionado datos importantes acerca de los residuos clave y los cambios conformacionales que ocurren durante el proceso de inhibición (Bason *et al.*, 2014; Cabezon *et al.*, 2003; Cabezon *et al.*, 2001; Gledhill *et al.*, 2007) (Figura 6B). El pH bajo estabiliza las interacciones hidrofóbicas entre residuos de histidina, leucina e isoleucina de la región 49-81, favoreciendo la dimerización de dos moléculas de IF1 por sus extremos C-terminales en forma de doble-hélices antiparalelas (Cabezon *et al.*, 2000a; Gordon-Smith *et al.*, 2001) (Figura 6A).

El homodímero de IF1 representa la forma activa del inhibidor, que se une con un óptimo de actividad en el rango de pH 5.8-7 (Cabezon *et al.*, 2000b; Panchenko and Vinogradov, 1985; Pullman

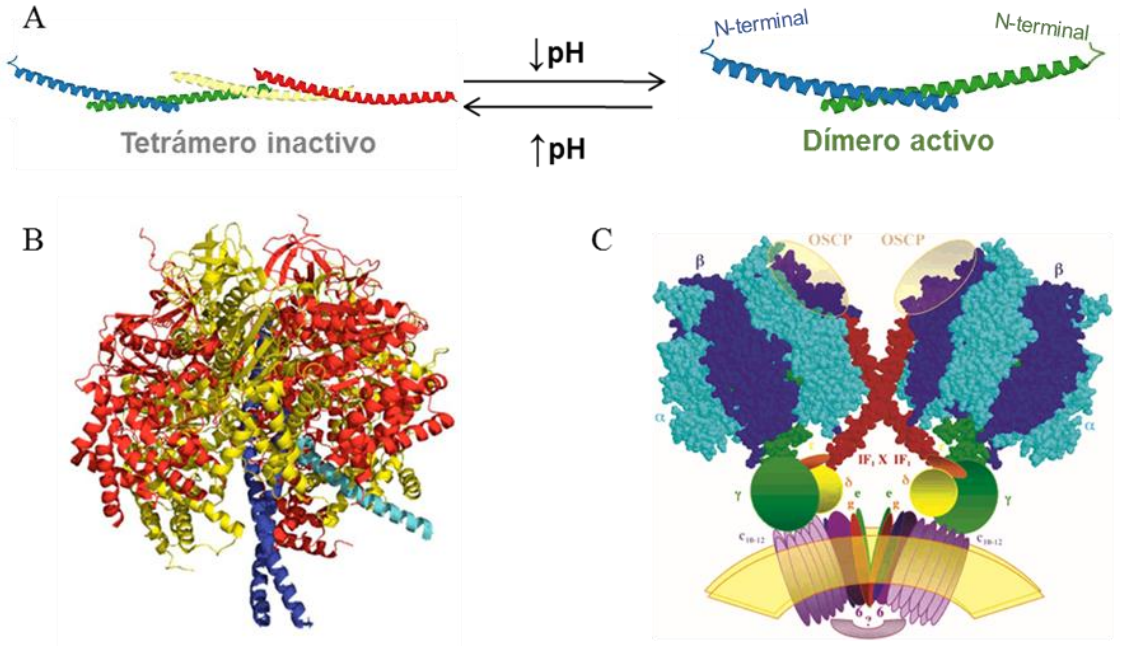

Figura 6. Esquema de la regulación por pH de IF1 e interacción con la ATPasa. (A) Regulación por pH. Una disminución del pH en el interior de la matriz induce la ATP sintasa a funcionar en modalidad reversa para restablecer el potencial de membrana. A pH bajo (<6.7) IF1 se encuentra en su forma dimérica activa capaz de unir e inhibir la ATPasa. El aumento de pH (>6.7) favorece la oligomerización entre dímeros por el extremo N-terminal formando así tetrámeros inactivos. (B) Estructura cristalográfica representativa del dominio F_1 de la ATP sintasa bovina unido al péptido de IF1 bovino truncado I1-60. Se muestran las subunidades α (amarillo), β (rojo), γ (azul) e IF1 (azul claro), (modificado de (Bason *et al.*, 2014)). (C) Representación del dímero de ATP sintasa estabilizado por el dímero de IF1 según el modelo propuesto por J. García. Se muestra como cada monómero de IF1 toma contacto con la subunidad OSCP de un dominio F_1 por su extremo C-terminal y con la interfase α/β hasta la subunidades γ y ε de otra molécula de ATPasa por su extremo N-terminal, (tomado de (Garcia *et al.*, 2006)).

and Monroy, 1963; Sah *et al.*, 1993). El aumento del pH promueve la agregación de los dímeros de IF1 en tetrámeros por interacción entre sus extremos N-terminales libres, produciendo, por tanto, su inactivación (Cabezon *et al.*, 2000b; Cabezon *et al.*, 2001; Gordon-Smith *et al.*, 2001) (Figura 6A). El efecto regulador del pH sobre la actividad y la estructura de IF1 es debido a la protonación/desprotonación de 5 histidinas altamente conservadas estando sus valores de pKa en el mismo rango de regulación por pH de la proteína (pH 5.8-7). Para algunos autores el remplazo de cada una o incluso de todas las histidinas en el péptido inhibitorio mínimo provoca la pérdida de la capacidad reguladora por pH y una concomitante disminución de la actividad (Papa *et al.*, 1996; Zanotti *et al.*, 2000). Otros estudios de mutagénesis dirigida demuestran que el mutante H49K, resulta en una actividad inhibidora independiente del pH (IF1 sigue activo incluso a pH>6.7) (Cabezon *et al.*, 2000b; Schnizer *et al.*, 1996).

Se ha descrito que la estequiometria de unión es de un mol de IF1 por mol de ATP sintasa (Hashimoto *et al.*, 1981; Hekman *et al.*, 1991; Klein *et al.*, 1981; Klein *et al.*, 1980). Puesto que la forma activa de IF1 es un dímero con los dos extremos N-terminales libres en lados opuestos, es lógico pensar que cada dímero se una a dos complejos de ATP sintasa con un estequiometria 1:1 (Cabezon *et al.*, 2000b; Garcia *et al.*, 2006). De hecho, se ha descrito por cromatografía, ultracentrifugación, microscopía electrónica y cristalografía (Cabezon *et al.*, 2000a; Cabezon *et al.*, 2003), así como por electroforesis en condiciones nativas (Garcia *et al.*, 2006) (Bisetto *et al.*, 2013; Campanella *et al.*, 2008), como la cantidad de dímeros está relacionada con el nivel de IF1 en hígado, en corazón de rata y en sincitiotrofoblasto de placenta humana (De los Rios Castillo *et al.*, 2011). Sin embargo, otros autores describen que IF1 se une indistintamente a monómeros y dímeros de ATP sintasa en corazón bovino (Tomasetig *et al.*, 2002) o que la ausencia de IF1 no produce alteraciones estructurales en la mitocondria ni diferencias en la formación de dímeros en células HeLa silenciadas estables (Fujikawa *et al.*, 2012) y tampoco en levadura (Dienhart *et al.*, 2002).

Por otra parte, un estudio confirma la participación de IF1 en la formación de dímeros de ATP sintasa y le atribuye un papel de puente estabilizador entre los dominios F1 argumentando que las interacciones responsables de la dimerización se dan a nivel del dominio Fo (las subunidades *e*, *g* y *b*) (Minauro-Sanmiguel *et al.*, 2005). Por último, estudios de entrecruzamiento (*crosslinking*) describen una interacción del extremo C-terminal de IF1 con la OSCP (Zanotti *et al.*, 2004; Zanotti *et al.*, 2000), apoyando la hipótesis de García según la cual los extremos N-terminales del dímero de IF1 tomarían contacto con las subunidades γ y ε, y con la interfase α/β, mientras el extremo C-terminal interaccionaría con la OSCP de otra molécula de ATP sintasa (Garcia *et al.*, 2006) (Figura 6C).

Otro aspecto controvertido de la dimerización de la ATP sintasa por IF1 es cómo influye éste inhibidor sobre la actividad del dímero. Algunos autores sugieren que la estabilización del dímero llevaría a una mayor actividad (Campanella *et al.*, 2008; Strauss *et al.*, 2008) mientras que otros afirman que no hay evidencias de cambios en la misma (Wittig and Schagger, 2009).

1.3.2 Papel de IF1 en patolgía

La inhibición de la ATP sintasa por la unión de IF1 ha sido atribuida por mucho tiempo únicamente a su actividad reversa, la hidrólisis de ATP. Este proceso se manifiesta en condiciones de hipoxia, cuando, tras una disminución de la respiración, el potencial de membrana mitocondrial ($\Delta\psi m$) colapsa y la ATP sintasa hidroliza ATP translocando H^+ al espacio intermembrana para restablecer la fuerza protón-motriz. En este escenario, el colapso del $\Delta\psi m$, la consiguiente bajada del pH y la importación de ATP glucolítico por la ANT (Zanotti *et al.*, 1987) favorecen su unión e inhibición de la actividad hidrolítica (Cabezon *et al.*, 2000b; Hashimoto *et al.*, 1990). Este papel, ha sido demostrado en células en hipoxia tratadas con un desacoplante (FCCP) silenciando y sobreexpresando IF1 (Campanella *et al.*, 2008).

En isquemia cardiaca el daño necrótico es determinado por la velocidad del consumo de ATP. Por tanto, factores inhibidores de la ATP sintasa pueden reducir el daño necrótico (Grover *et al.*, 2004; Jennings *et al.*, 1991). Rouslin ha estudiado el efecto de IF1 en isquemia en cuanto inhibidor de la hidrólisis de ATP, describiendo cómo la diferencia de sus niveles y actividad entre especies es un índice de susceptibilidad a la isquemia (Rouslin and Broge, 1996; Rouslin *et al.*, 1995). Además, se ha descrito cómo los tejidos que han sufrido un episodio isquémico sobre-regulan los niveles basales de IF1, resultando más protegidos frente a un posterior evento isquémico (Di Pancrazio *et al.*, 2004; Vuorinen *et al.*, 1995). De hecho, el fármaco cardioprotector que se suministra en caso de infarto, el diazóxido, favorece la inhibición de la ATP sintasa y la unión de IF1 (Contessi *et al.*, 2004).

Se han estudiado defectos en la actividad de IF1 que promueven el malfuncionamiento de otras enzimas como en el caso de la ferrocatalasa, enzima responsable de la inserción del Fe^{2+} en el anillo de protoporfirina IX durante la síntesis del grupo hemo, causando de tal manera una anemia en los modelos animales estudiados (Shah *et al.*, 2012). En otros casos, un defecto en IF1 puede resultar ventajoso en ciertas situaciones patológicas. En un *screening* genético en el que se reprodujo una disfunción en la CTE mediante tratamiento con antimicina A, se ha descrito una mayor viabilidad celular tras la pérdida de IF1 por la regeneración del $\Delta\psi m$, indicando IF1 como una posible diana terapéutica en enfermedades mitocondriales (Chen *et al.*, 2014).

Sin embargo, resultados recientes de nuestro laboratorio indican que IF1 tiene actividad inhibitoria sobre la actividad sintética de la ATP sintasa (revisado en (Garcia-Bermudez and Cuezva, 2016)). En este sentido, hemos demostrado la inhibición de la síntesis de ATP mediada por la sobreexpresión de IF1 o por el dominante activo H49K tanto en modelos celulares (Formentini *et al.*, 2012; Sanchez-Cenizo *et al.*, 2010) así como en células madre y en modelos animales de sobreexpresión de IF1-H49K en cerebro y en hígado, como se detalla más adelante (ver apartado Discusión) **Artículos #1, #4, #3 y #2** respectivamente.

1.3.3 Regulación de IF1

Por su implicación en procesos de gran importancia en la patología y fisiología celular, no sorprende que la regulación de IF1 sea un mecanismo complejo que ocurre a diferentes niveles, básicamente a nivel de la expresión y de la actividad. La elevada expresión de IF1 en los tumores humanos más prevalentes como mama, ovario, colon y pulmón, ha llevado nuestro laboratorio a determinar los factores transcripcionales implicados en la regulación de su expresión (**Artículo #1**). Tras el análisis de datos públicos de ChIP-seq se ha observado que varios factores de trascripción implicados en el ciclo celular (NF-YA, NF-YB, Ini1, TAF1), inflamación y muerte (NFκB), proliferación (c-MYC, c-FOS, Sp1) y biogénesis mitocondrial (NRF1) interaccionan con la región promotora del gen *ATPIF1* (**Artículo #1**). Sin embargo, la elevada expresión de IF1 no se refleja en los niveles de mRNA de estos tumores, sugiriendo que su acumulación está más bien regulada a nivel post-transcripcional (Sanchez-Cenizo *et al.*, 2010) (**Artículo #1**). En este contexto, se ha descrito que la interacción de la proteína IER3 en humanos (o su homólogo IEX-1 en ratón) con el dominio C-terminal de IF1 desestabiliza la proteína y media su degradación por proteasas independientes del proteasoma (Shen *et al.*, 2009). Sin embargo, el silenciamiento de IER3 en células cancerígenas de colon no produce variaciones en la expresión de IF1 (**Artículo #1**). Además, a pesar de haberse descrito un papel pro-apoptótico y supresor de tumores para IER3 (Sebens Muerkoster *et al.*, 2008; Wu, 2003), su expresión, como también la de IF1, está altamente inducida en tejidos tumorales de colon, mama y pulmón en relación a los respectivos tejidos normales (**Artículo #1**). Desafortunadamente, el *screening* para identificar la posible proteasa implicada en la degradación de IF1 no ha dado resultados en hMSC ni en células tumorales (**Artículo #4**).

Tras la observación de que IF1 tiene una vida media muy corta (~ 2 y 4 horas), nuestro laboratorio ha demostrado que su degradación es debida a la acción proteolítica de serín-proteasas puesto que, en células de cáncer de colon (**Artículo #1**) y en hMSC (**Artículo #4**), el tratamiento con un inhibidor de serín-proteasas (AEBSF) produce la acumulación de IF1. Sin embargo, parece que la degradación proteolítica de IF1 implique a más de una proteasa. En este sentido, se ha descrito que el tratamiento con un inhibidor específico de metaloproteasas, la o-fenantrolina (Shen *et al.*, 2009), o en el modelo de levadura *knockout* para el gen codificante una metalo-proteasa mitocondrial, YME1 (YME1L en mamíferos) (Kominsky *et al.*, 2002; Rainbolt *et al.*, 2013), producen la acumulación de IF1.

Un posible candidato para la regulación transcripcional de IF1 por su papel en hipoxia es HIF-1α. Se ha descrito que la inducción de su expresión por tratamiento con $CoCl_2$, correlaciona con un aumento de la expresión de IF1 en hígado de rata e *in vitro* (Huang *et al.*, 2011). Sin embargo, el tratamiento a corto plazo con $CoCl_2$ en líneas celulares de cáncer de colon, mama, ovario y pulmón no produce un aumento en la cantidad de IF1, a pesar de la evidente sobreexpresión de HIF-1α (**Artículo #1**). Todas estas observaciones sugieren que la regulación de IF1, tanto a nivel transcripcional como post-transcripcional, implican la participación de varios factores, ninguno de forma exclusiva,

probablemente cooperando en un sistema complejo y configurable según el tipo celular y su estado patológico (**Artículo #1**).

Más recientemente, nuestro laboratorio ha puesto de manifiesto que la actividad inhibidora de IF1 se regula por modificación covalente (Garcia-Bermudez *et al.*, 2015). En este estudio se ha demostrado tanto en células como *in vivo*, que IF1 se fosforila en su residuo S39, por una quinasa mitocondrial dependiente de AMP cíclico (PKA), lo que impide su unión con la ATPasa y por consiguiente previene su actividad como inhibidor (Garcia-Bermudez *et al.*, 2015). En el mismo trabajo se ha demostrado que IF1 defosforilado es la forma molecular que interacciona con la ATP sintasa y es en esta condición cuando promueve la inhibición de la síntesis o hidrolisis de ATP (Garcia-Bermudez *et al.*, 2015).

En un ensayo de quinasa *in vitro* se ha observado que la PKA no es capaz de fosforilar IF1 probablemente debido a la falta de algún complejo proteico de anclaje (AKAPs) (Garcia-Bermudez *et al.*, 2015). En condiciones de hipoxia, en la fase G2/M del ciclo celular, y en diferentes carcinomas humanos se ha descrito que IF1 está totalmente defosforilado (Garcia-Bermudez *et al.*, 2015). Por contra, en fase G1 del ciclo y en respuesta a demanda energética *in vivo* IF1 se encuentra fosforilado para impedir su unión a la ATP sintasa y promover la síntesis de ATP (Garcia-Bermudez *et al.*, 2015). Dado que cAMP no puede difundir las membranas mitocondriales, la fosforilación de IF1 depende exclusivamente de los niveles de cAMP mitocondrial (Di Benedetto *et al.*, 2013; Lefkimmiatis and Zaccolo, 2014). De hecho, tratando las mitocondria aisladas con el análogo permeable a las membranas dibutiril-cAMP (db-cAMP), IF1 es rápidamente fosforilado (Garcia-Bermudez *et al.*, 2015). El incremento del cAMP en la mitocondria depende de una clase de adenilato ciclasas mitocondriales solubles (sAC) activadas por Ca^{2+} (Di Benedetto *et al.*, 2013) y bicarbonato (Acin-Perez *et al.*, 2009). Además, la activación por vía hormonal, con forskolina y norepinefrina (Di Benedetto *et al.*, 2013) de una adenilado ciclasa transmembrana (mtAC), remarca la importancia del calcio en el incremento de cAMP intramitocondrial (Di Benedetto *et al.*, 2014; Di Benedetto *et al.*, 2013). En línea con estas observaciones, la administración de clenbuterol, un agonista β-adrenérgico, promueve la fosforilación de IF1 en el corazón de ratones y la consiguiente activación de la ATP sintasa (Garcia-Bermudez *et al.*, 2015). No se conoce si existe un mecanismo de defosforilación específico por IF1 (Garcia-Bermudez and Cuezva, 2016).

1.4 Metabolismo y cáncer

1.4.1 El fenotipo glucolítico de la célula proliferativa

Hoy en día el consenso general en el campo coincide con que el fenotipo metabólico del cáncer puede ocurrir anteriormente a, como resultado de, o en combinación con, las alteraciones genéticas que conducen a la patología por ser necesario para soportar el crecimiento y la supervivencia tumoral (Seyfried *et al.*, 2014; Thompson, 2009).

De hecho, se ha demostrado que tanto las células proliferativas (Sanchez-Arago *et al.*, 2013) como las embrionarias (Cuezva *et al.*, 2007; Kondoh *et al.*, 2007) (**Artículo #4**) están caracterizadas por un

drástico aumento del flujo glucolítico, puesto que requieren biomoléculas precursoras y potencial reductor en forma de NADPH para sintetizar biomasa (Cuezva *et al.*, 2009). En este contexto, la alta demanda de glucosa y la intensa actividad enzimática de la glucolisis vienen satisfechas a través de una elevada expresión del transportador GLUT1 y de varias enzimas de la glucolisis (DeBerardinis *et al.*, 2008; Hsu and Sabatini, 2008) (Figura 7). El fenotipo glucolítico proporciona varias ventajas a las células proliferativas sean estas normales o tumorales. A pesar de la menor eficiencia de la glucolisis en generar ATP, con respecto a la OXPHOS, ésta es la vía que proporciona la mayoría de los intermediarios metabólicos especialmente necesarios durante la proliferación celular (Cuezva *et al.*, 2009; Formentini *et al.*, 2010; Lunt and Vander Heiden, 2011). Además, la acidificación del medio por un aumento de la producción y extrusión de lactato y la menor dependencia de oxígeno por una OXPHOS parcialmente reprimida confieren una mayor capacidad invasiva a la célula especialmente en condiciones de hipoxia, típica de las masas tumorales (de Groof *et al.*, 2009; Fukumura *et al.*, 2001; Funes *et al.*, 2007; Gillies and Gatenby, 2007).

Los intermediarios glucolíticos no son los únicos requeridos para la producción de biomasa celular. El aspartato y el citrato para la síntesis de nucleótidos y de lípidos respectivamente, son un ejemplo de intermediarios del TCA que pueden ser sustraídos y remplazados por el catabolismo de la glutamina, notoriamente involucrada en el flujo anaplerótico que es necesario para cubrir las necesidades metabólicas de muchos tipos de células cancerígenas (DeBerardinis *et al.*, 2007; Ortega *et al.*, 2009; Wise *et al.*, 2008; Yuneva *et al.*, 2007) (Figura 7). La mitigación de la OXPHOS tiene además la ventaja de limitar la producción de ROS que, especialmente en fase de división celular, pueden producir daños en el DNA y activar el programa de muerte celular (Chen and McKnight, 2007). Asimismo, se ha descrito cómo las células cancerígenas responden de forma diferente a la quimioterapia según su capacidad OXPHOS, siendo tanto más sensible al tratamiento cuanto más activa sea la OXPHOS (Sanchez-Arago *et al.*, 2013; Santamaria *et al.*, 2006), confiriendo por tanto a la actividad mitocondrial un valor de indicador pronóstico y de respuesta a terapia de la enfermedad (Sheffer *et al.*, 2009). En este contexto, PGC1α, un co-activador transcripcional que activa la biogénesis y la función mitocondrial, previene/minimiza la carcinogénesis por inducir la actividad mitocondrial con la consiguiente elevada producción de ROS y estimulación de la apoptosis (D'Errico *et al.*, 2011). Tanto PGC1α como la sirtuina SIRT3, esta última descrita como estabilizadora de la integridad y actividad mitocondrial (Kim *et al.*, 2010), han sido consideradas como dianas para eventuales estrategias terapéuticas basadas en la activación de la función mitocondrial (Barbosa *et al.*, 2012; Tennant *et al.*, 2010), puesto que un estudio previo había demostrado el poder del resveratrol en la activación de PGC1α y SIRT1 (Lagouge *et al.*, 2006).

1.4.2 La señalización y aproximación terapéutica del metabolismo del cáncer

Una de las vías de señalización más comunes en cáncer son la activación de la PI3K con posterior activación de Akt (Jiang *et al.*, 2001) y de mTOR (Wouters and Koritzinsky, 2008) que inducen un estado pseudo-hipóxico (independiente del oxígeno), estabilizando Hif1α que a su vez estimula la glucolisis por inducción de la expresión de enzimas glucolíticas y del transportador GLUT1 de glucosa (Semenza *et al.*, 1994) (Figura 7). El oncogén Akt también puede ser activado por un mecanismo redox, por ejemplo generado por la mitocondria en situación de estrés hipóxico, que lleva a la inactivación de PTEN (Pelicano *et al.*, 2006). Otro oncogén que controla en primera línea el cambio metabólico exigido para la trasformación celular es *c-myc*. Éste último actúa como regulador de la expresión de enzimas tanto de la glucolisis (Osthus *et al.*, 2000) así como de la biogénesis mitocondrial (Kim *et al.*, 2008). La estabilización de Hif1α determina el papel de c-myc. Por un lado, Hif1α inhibe la actividad transcripcional de c-myc relativa a los genes implicados en la biosíntesis mitocondrial activando MXL1 (Zhang *et al.*, 2007). Por otro lado, en cooperación con *c-myc*, promueve la expresión de muchas enzimas glucolíticas como el trasportador GLUT1, la hexoquinasa II (HK-II), la lactado deshidrogenasa A (LDHA), y la piruvato deshidrogenasa 1 quinasa (PDK1), que inactiva el complejo de la piruvato deshidrogenasa (PDH) (Kim *et al.*, 2007) favoreciendo el consumo de glucosa y la

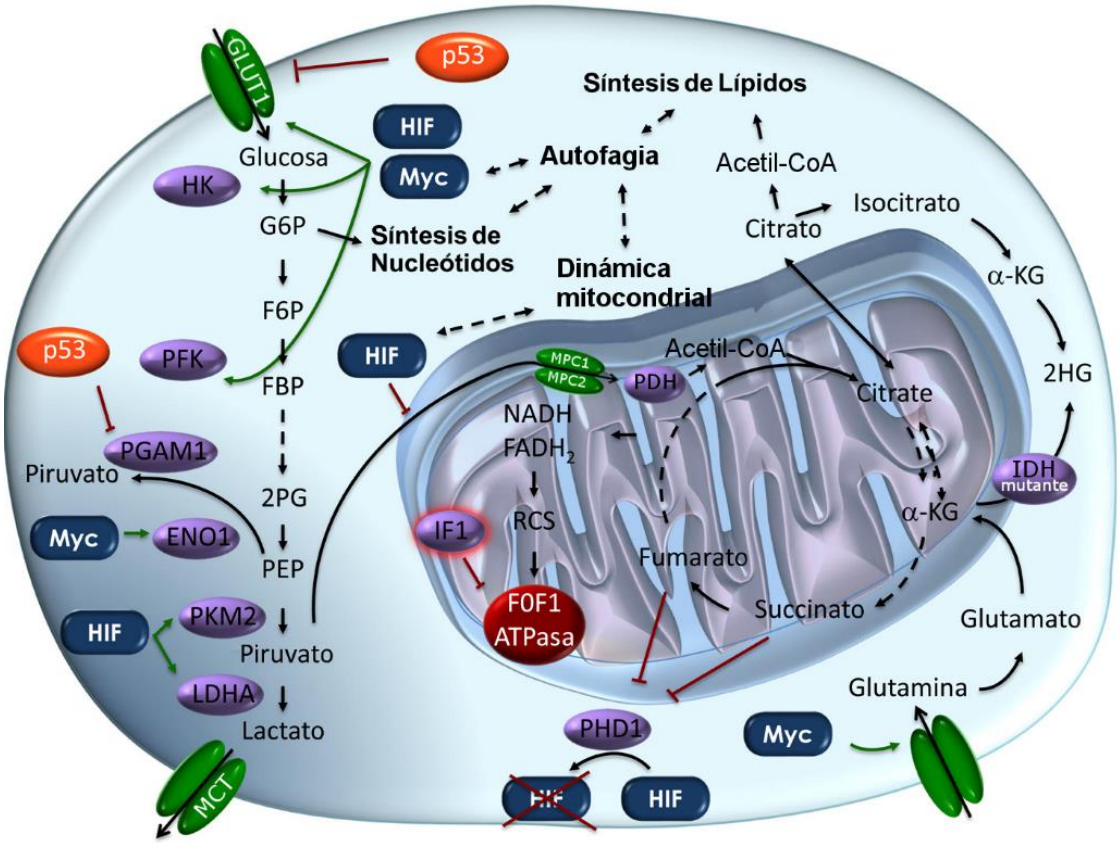

Figura 7: Representación esquemática de las rutas metabólicas alteradas en cáncer. Esquema de las rutas metabólicas controlada por los principales oncogenes y genes oncosupresores. Se muestran los eventos clave que promueven el "efecto Warburg" en las células cancerígenas. En azul se representan las onco-proteinas mientras que en naranja las proteínas oncosupresoras. Las proteínas que son dianas directas de las onco-proteínas están representadas en morado. Las líneas discontinuas representas las interacciones bidireccionales, modificado de (Corrado *et al.*, 2016).

producción de lactato (Figura 7). Además, se ha descrito que Hif1α estaría implicado en la expresión diferencial de la isoforma de la citocromo c oxidasa COX4-2 que trasfiere de forma más eficiente los electrones, reduciendo así la formación de ROS en estado de hipoxia (Fukuda *et al.*, 2007). Otro papel relevante de c-myc en el contexto tumoral es la inducción de las proteínas de unión a RNA (David *et al.*, 2010). Estas proteínas son responsable del "splicing" alternativo que a partir del gen que codifica por la piruvato kinasa M1 (*PKM*), isoforma expresada en musculo esquelético, genera la isoforma M2, exclusivamente expresada en tejidos embrionarios y proliferativos (Christofk *et al.*, 2008) (Figura 7).

PKM2 es la única isoforma de la PK regulada alostericamente por su capacidad de pasar de la forma monomérica o dimérica de baja actividad a la tetramérica 50 veces más activa (Anastasiou *et al.*, 2012; DeLaBarre *et al.*, 2014; Mazurek, 2011). Siendo el piruvato el pivote entre la glucolisis y la OXPHOS, la PKM2 puede en su forma dimérica promover la glucolisis aerobia favoreciendo la progresión del cáncer (Hitosugi *et al.*, 2009), o por el contrario, en su forma tetramérica forzar el cáncer en un estado metabólico de menor proliferación (DeLaBarre *et al.*, 2014). Además, la PKM2 en su forma dimérica tiene un papel "no-metabólico" en la tumorogenesis. Varios autores describen cómo en la forma dimérica PKM2 pueda translocar al núcleo y actuar como co-activador de varios factores transcripcionales, entre los cuales están β-catenina o Hif1α activando la transcripción de *c-myc* y de otros genes implicados en la reprogramación metabólica, proliferación celular y carcinogénesis, incluyendo al mismo gen de PKM y de las proteínas de unión a RNA (Iqbal *et al.*, 2014; Luo *et al.*, 2011; Yang *et al.*, 2012) (Figura 7). La conexión entre su papel en el metabolismo glucolítico y la trasformación metabólica se debe a la capacidad del dímero de actuar como proteína quinasa regulando así la transcripción génica (Iqbal *et al.*, 2014; Luo *et al.*, 2011; Wang *et al.*, 2014; Yang *et al.*, 2011; Yang *et al.*, 2012). Recientemente, algunos autores sostienen que PKM2, aunque se encuentre altamente expresado en varios tipos de tumores, no es necesario para el mantenimiento del estado oncogénico dado que su supresión por shRNA no afecta la proliferación (Cortes-Cros *et al.*, 2013). Otros autores afirman que la isoforma M2 se expresa en tejidos normales y que el cambio de M1 a M2 se debe a una regulación epigenética por metilación del intrón 1 del gen *PKM* aunque solo se manifieste en glioblastomas sobre dieciséis tumores analizados (Desai *et al.*, 2014). Sin embargo, todos los autores coinciden en que la actividad de la PK constitutiva es perjudicial a efectos de la proliferación celular. Efectivamente algunas aproximaciones terapéutica actuales están dirigidas a promover la actividad de la PKM2 estabilizando su forma tetramérica de elevada actividad metabólica (Hirschey *et al.*, 2015).

El piruvato tiene un papel central en la reprogramación metabólica y adquisición del fenotipo glucolítico (efecto Warburg), estando su oxidación disminuida en las células cancerígenas. Así, en la actualidad, otras aproximaciones apuntan a la regulación de los niveles de este "onco-metabolito" y a su localización (Olson *et al.*, 2016). Su destino está controlado por dos enzimas: la LDHA, que convierte el piruvato en lactado en el citoplasma, y el complejo de la PDH que lo convierte en acetil-CoA en la mitocondria (Schell *et al.*, 2014) (Figura 7). Los niveles de lactato, recientemente

reconocido como metabolito que juega un papel clave en la progresión del cáncer (Kroemer and Pouyssegur, 2008), pueden ser modulados por varias vías. Entre estas, se destaca la inhibición de la actividad de la LDHA por inhibidores farmacológicos o de su expresión por shRNA o siRNA (Fantin *et al.*, 2006; Le *et al.*, 2010). En el mismo contexto, una estrategia terapéutica apunta a la inhibición de la activad y/o de la expresión de la familia de transportadores lactato monocarboxilato (MCT) (Miranda-Goncalves *et al.*, 2013) (Figura 7). Por otro lado, el complejo de la PDH puede ser inactivado mediante fosforilación por la PDK1, frecuentemente inducida en células cancerígenas (Kim *et al.*, 2006). De hecho, en los últimos años varios estudios han descrito la eficacia del dicloroacetato (DCA), una droga capaz de inhibir las PDKs y revertir el fenotipo glucolítico favoreciendo la oxidación del piruvato y disminuyendo la proliferación tumoral (Bonnet *et al.*, 2007; Michelakis *et al.*, 2010; Sanchez-Arago *et al.*, 2010). Además de los niveles de piruvato, su regulación depende de la localización celular. Así, un estudio muy reciente ha descrito que el complejo multimérico del transportador mitocondrial del piruvato (MPC) es esencial en la determinación del destino final del mismo en las células cancerígenas (Figura 7). En efecto, la expresión de MPC es necesaria para la provisión del piruvato a la mitocondria, de manera independiente a la actividad de otras enzimas implicadas en la oxidación del mismo (PK, LDHA, PDH) y de sus reguladores (Schell *et al.*, 2014). Este hecho puede justificar el fallo clínico en algunas estratégicas terapéuticas, como es el caso del DCA, cuyo efecto es prácticamente irrelevante en pacientes que presentan una mutación en el transportador MPC impidiendo la entrada del piruvato mitocondrial (Schell *et al.*, 2014). Estos resultados demuestran que en el abordaje de los tratamientos anti-cancerígenos es esencial un estudio previo que defina el perfil metabólico del tumor (Olson *et al.*, 2016).

Muchas otras proteínas clave en la regulación metabólica, así como moléculas activadoras/inhibidoras de las mismas, se están utilizando como "agentes anti-tumorales" en combinación con terapias citotóxicas que generan estrés oxidativo. En este contexto cabe destacar al 3-bromopiruvato (3BP) inhibidor de la HK II (Mathupala *et al.*, 2009), el 3PO inhibidor de la 6-fosfofruto-2-quinasa/fructosa-2,6-bifosfatasa 3 (PFKFB3) y su derivado PFK15 (Clem *et al.*, 2013; Reddy *et al.*, 2012), el BPTES inhibidor de la glutaminasa 1 (GLS1) (Robinson *et al.*, 2007) o los polifenoles del té verde como inhibidores de la glutamato deshidrogenasa (GLDH) (Yang *et al.*, 2009) y agentes limitantes el metabolismo de los ácidos grasos (Fas) como estrategia quimioterapéutica (Currie *et al.*, 2013) (Figura 7). Algunas estrategias terapéuticas prometedoras apuntan a la utilización de moléculas inhibidoras de las formas mutantes de la isocitrato deshidrogenasa 1 y 2 (IDH1/2) responsables de la producción del oncometabolito hidroxiglutarato ((R)-2HG) implicado en el silenciamiento de genes de la diferenciación celular por hipermetilación de DNA (Dang *et al.*, 2009; Rohle *et al.*, 2013; Wang *et al.*, 2013) (Figura 7). El (R)-2HG también se ha descrito útil como marcador diagnóstico y pronóstico en pacientes con cáncer que presentan dichas formas mutantes de la IDH, tanto por niveles en suero como por espectroscopia de resonancia magnética (Choi *et al.*, 2012; DiNardo *et al.*, 2013).

Otras moléculas capaces de actuar de oncometabolitos son el fumarato y el succinato cuya acumulación, debida a mutaciones con pérdida de función de la fumarato hidratasa (FH) y succinato deshidrogenasa (SDH), respectivamente, les confiere un papel de protagonista en tipos de tumores específicos con un mecanismo similar del (R)-2HG (Killian *et al.*, 2013; Letouze *et al.*, 2013; Xiao *et al.*, 2012).

1.4.3 La huella bioenergética del cáncer

La mitocondria, además de su función principal en la producción de energía, juega un papel central en muchos procesos fisiológicos vitales entre los cuales se destacan la homeostasis del calcio, la señalización por ROS y la ejecución y regulación de la apoptosis. De hecho, la disfunción mitocondrial ocurre en muchas patologías como diabetes, Parkinson, Alzheimer y por supuesto el cáncer. En efecto, la reprogramación metabólica de la célula tumoral a una activa glucolisis aerobia es una característica esencial enunciada por vez primera en 1924 por Otto Warburg (Cuezva *et al.*, 2009; Hanahan and Weinberg, 2011; Hirschey *et al.*, 2015; Vander Heiden *et al.*, 2009). En este contexto, nuestro laboratorio ha ideado una aproximación proteómica con la intención de trasladar esta particularidad metabólica del cáncer al ámbito de la investigación clínica. Una de las principales alteraciones encontrada en carcinomas humanos es el aumento de la expresión de enzimas de la glucolisis (Cuezva *et al.*, 2002; Chen *et al.*, 2003; Isidoro *et al.*, 2005). En nuestro laboratorio se ha descrito cómo la inducción de la expresión de la gliceraldhéido-3-fosfato-deshidrogenasa (GAPDH), se acompaña, en la mayoría de los tumores estudiados (>97%), por una disminución de la expresión de la subunidad catalítica de la ATP sintasa la β-F1-ATPasa. La razón de la expresión entre estas proteínas es lo que se ha venido en llamar *huella bionergética del cáncer* (Cuezva *et al.*, 2002; Cuezva *et al.*, 2009; Sanchez-Arago *et al.*, 2010). El análisis de la expresión de estas enzimas, conjuntamente con la expresión de una proteína que nos indica la masa mitocondrial como es la chaperona "heat shock protein 60" (Hsp60) nos ha permitido evaluar tanto la competencia bioenergética del orgánulo (razón β-F1-ATPasa/Hsp60) como el potencial mitocondrial total de la célula (razón β-F1-ATPasa/GAPDH) y el indicado índice bioenergético celular (BEC) (Cuezva *et al.*, 2002; Cuezva *et al.*, 2009). El índice BEC proporciona un biomarcador útil que informa sobre la actividad de las rutas de provisión de energía en cáncer (revisado en (Cuezva *et al.*, 2009)) habiendo sido corroborado en otros tumores por otros laboratorios (Bi *et al.*, 2006; Chen *et al.*, 2004b; He *et al.*, 2004; Li *et al.*, 2010; Lin *et al.*, 2008; Unwin *et al.*, 2003; Yizhak *et al.*, 2014). De hecho, correlaciona con las pruebas no-invasivas de diagnóstico y pronóstico basadas en la visualización de la captación de glucosa por tomografía de emisión de positrones (PET) (Lopez-Rios *et al.*, 2007; Plathow and Weber, 2008). Además, proporciona un marcador de prognosis de la enfermedad (Aldea *et al.*, 2011; Cuezva *et al.*, 2004; Cuezva *et al.*, 2002; Isidoro *et al.*, 2005; Lin *et al.*, 2008; Lopez-Rios *et al.*, 2007) como un marcador de respuesta a la intervención terapéutica en cáncer de colon y ovario (Aldea *et al.*, 2011; Hernlund *et al.*, 2009; Lin *et al.*, 2008; Sanchez-Arago and Cuezva, 2011).

1.5 Microarray de proteínas

1.5.1 Reseña histórica

Desde la segunda mitad del siglo XX, los ensayos inmunológicos han sido los más utilizados por sus alta sensibilidad, robustez y fiabilidad (Ekins, 1998; Yalow and Berson, 1960). A principio de los años 60 la estandarización, automatización y miniaturización de estos métodos ha permitido su aplicación no sólo en el campo de la investigación sino también como técnica diagnóstica en la práctica clínica (Feinberg, 1961; Feinberg and Wheeler, 1963), y son cientos los ensayos disponibles en el mercado. En el año 1961 en el laboratorio de Feinberg se realizó el primer ensayo antígeno-anticuerpo, en forma de "microspot", utilizando una membrana de acetato de celulosa que permitió la eliminación de las limitaciones relacionadas con el uso de agar donde se realizaba dicha técnica (Feinberg, 1962) (Figura 8). Aunque los autores describieron las ventajas del ensayo en microspot, como su fácil manejo rutinario, la sensibilidad, la rapidez del proceso, la pequeña cantidad de muestras biológicas necesarias y la facilidad de lectura y de archivar los datos, la técnica no alcanzó su merecida difusión en aquellos años. Tuvieron que pasar dos décadas hasta que Ekins explicó y desarrolló el fundamento que permite la obtención de una alta sensibilidad de los ensayos inmunológicos miniaturizados (Ekins, 1989), lo que confirió a esta metodología un enorme potencial aplicativo en el campo diagnóstico. Su ensayo en formato "microspot" se puede considerar el ancestro de los actuales microarrays de proteínas.

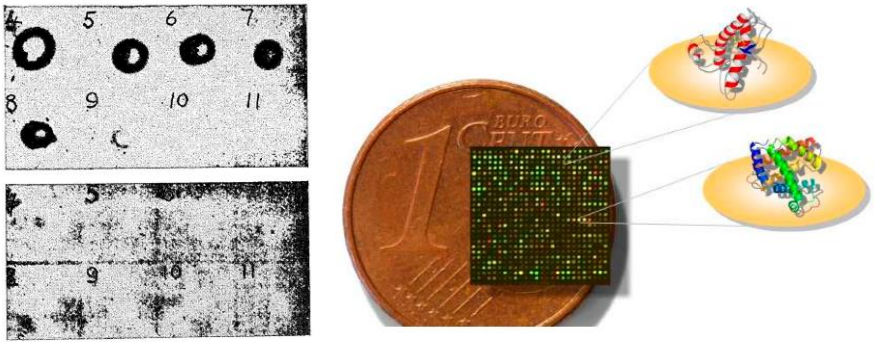

Figura 8. Imagen del primer ensayo en forma de microspot publicado (Feinberg *et al.*, 1962) (izquierda). Imagen representativa de las dimensiones de un microarray de proteínas actual (derecha).

1.5.2 Desde la genómica a la proteómica

A pesar del gran potencial de los Microarrays de proteínas para aplicaciones diagnósticas, fue en el campo de la Genómica donde se desarrolló en mayor medida este tipo de tecnología. Muchas tecnologías de alto rendimiento se han desarrollado para definir exhaustivamente el perfil del genoma y transcriptoma de fenotipos particulares.

Sin embargo, las proteínas son las reales protagonistas de la regulación de las funciones celulares. El análisis del DNA y RNA no siempre permite realizar asociaciones con patologías específicas, ya que debido a determinados procesos de regulación post-transcripcional (Sereni *et al.*, 2013) los niveles de mRNA no siempre se relacionan cuantitativamente con la expresión de las proteínas a las que da

lugar ni tienen en cuenta del estado funcional de las mismas (Gygi *et al.*, 1999). El Microarray de proteínas es una tecnología de alto rendimiento que se ha aceptado ampliamente debido a su capacidad para obtener un perfil proteómico del estado funcional de la célula así como por su utilidad en la validación de datos obtenidos mediante otras técnicas y no menos importante, por su aplicación en la identificación de biomarcadores fundamentales para el diagnóstico, pronóstico y predicción de respuesta a tratamiento en múltiples patologías (Aldea *et al.*, 2011; Ledford, 2014; Mueller *et al.*, 2010; Sereni *et al.*, 2013). Así, la tecnología del Microarray de proteínas ha sido recientemente aprobada como implementación en el desarrollo de algunos ensayos clínicos (Mueller *et al.*, 2010), confirmando lo que Ekins predijo.

A las aproximaciones proteómicas se adscriben las tecnologías de análisis de proteínas cuya finalidad es la separación, cuantificación y caracterización de las proteínas que se expresan diferencialmente. Aunque las técnicas clásicas como la Espectrometría de Masas en combinación con técnicas de separación como electroforesis en geles de dos dimensiones (2D) y con Cromatografía Liquida Multidimensional (MDLC, *Multi-dimensional liquid chromatography*) proporcionan una poderosa herramientas para el análisis en paralelo de cientos de proteínas y péptidos, todavía son técnicas de bajo rendimiento, requiriendo un alto grado de experiencia en el manejo de la técnica. Además, son técnicas con limitaciones destacables como son la falta de sensibilidad y de rango dinámico para detectar proteínas cuya expresión es muy baja pero determinante en muestras biológicas complejas (Sydor and Nock, 2003). Este es el caso de los fluidos corporales, como el suero o el plasma, que presentan una especial dificultad de análisis a la hora de cuantificar múltiples proteínas con un rango dinámico de concentración muy amplio, puesto que puede alcanzar una diferencia en un orden de magnitud superior a diez veces (Liotta and Kohn, 2003). Las limitaciones de estas tecnologías proteómicas han impulsado el desarrollo de nuevas herramientas tecnológicas como los arrays de proteínas (Kodadek, 2001; Templin *et al.*, 2002; Wilson and Nock, 2003; Zhu and Snyder, 2001) que han sido desarrollados como una extensión del Microarray de DNA (Schena *et al.*, 1995), donde en lugar de la expresión del mRNA se estudia la expresión de las proteínas (Templin *et al.*, 2004). Entre las varias ventajas, con respecto a las técnicas tradicionales de separación/identificación de proteínas como el ELISA y el Western blot, se destacan la escalabilidad, la idoneidad a la automatización, la pequeña cantidad de volúmenes para la obtención de un alto grado de sensibilidad y un amplio rango dinámico. De hecho, la técnica permite analizar a la vez diferentes proteínas dianas cuya concentración, en una muestra compleja, puede ser entre ellas muy diferente, manteniendo una buena linealidad, entre 2 y 3 órdenes de magnitud (Hsu *et al.*, 2008). Los arrays de proteínas tienen un amplio rango de aplicaciones potenciales puesto que pueden adscribirse a los ensayos de alto rendimiento para el estudio de proteínas diana asociadas con procesos patológicos o intervenciones terapéuticas. Esta herramienta está revolucionando el campo del descubrimiento de biomarcadores, de validación y monitorización de marcadores tempranos y progresivos de enfermedad, así como el estudio de la eficacia de tratamientos y su toxicidad.

1.5.3 Tecnología del Microarray de proteínas basadas en el "microspot"

La tecnología del Microarray de proteínas se basa en el acoplamiento de moléculas como son los anticuerpos y antígenos en un soporte estandarizado para análisis multiplexada. Al igual que los arrays de DNA, la fluorescencia revelada por un escáner confocal es la modalidad estándar de detección de los arrays de proteínas, ya que garantiza un elevado límite de detección "*Limit of detection*" (LOD). En las últimas décadas se han desarrollado muchas mejoras en la tecnología de array de proteínas, especialmente en el aporte de alternativas que permiten modelar la plataforma dando lugar a una gran multitud de formatos para muchas aplicaciones.

Las plataformas de array de proteínas se pueden diferenciar según el tipo de soporte y la química de superficie de los soportes, los reactivos de captura, la aproximación de detección o la metodología de impresión (Huang, 2003). Utilizando anticuerpos como moléculas de capturas existen varios tipos de plataformas de array que difieren fundamentalmente en el tipo de soporte, y por ello se destinan a diferentes aplicaciones. En el desarrollo de esta tesis doctoral se ha utilizado únicamente la plataforma de array basada en el microspot, en la que se imprimen directamente las muestras biológicas o las moléculas de captura en un soporte sólido de superficie plana. Los arrays en fase sólida utilizan mayoritariamente tres tipos de soportes: portaobjetos de cristal o plástico tratados con varias superficies químicas, membranas y placas. Los portaobjetos de cristal son los soportes más utilizados debido a los bajos niveles de fluorescencia de fondo "*signal-to-noise ratio*" (S/N), uno de los problemas principales de esta técnica. Al igual que los establecidos array de DNA, los arrays de proteínas en soporte sólido son sistemas de ensayos altamente miniaturizados que utilizan un gran número de moléculas de captura diferentes o de proteínas dianas inmovilizadas en forma de microspot con un diámetro <360 μm y con una densidad entre cientos y miles de "spots" por centímetro cuadrado (Figura 8). El talón de Aquiles de los soportes de cristal es la reducida capacidad de unión a las proteínas mediante la utilización de una química de superficie que mantenga bajo el nivel de fluorescencia de fondo. Asimismo, otros criterios no menos relevantes que debe poseer un soporte sólido son tanto el mantenimiento de la funcionalidad de las moléculas de captura como la accesibilidad a sus moléculas diana y la capacidad de proveer puntos (spots) con una morfología compacta y uniforme.

En las últimas décadas se han comercializado soportes de cristal revestidos con varias superficies químicas que pueden distinguirse según el tipo de unión con las proteínas. Así podemos diferenciar dos grupos: 1) de unión por absorción física y 2) de unión covalente. La absorción física es el método de inmovilización más sencillo, basado en la interacción iónica entre los grupos con cargas negativas presentes en las proteínas y las cargas positivas que recubren la superficie del soporte. El resultado es una inmovilización heterogénea con orientación al azar en la superficie como consecuencia de los diferentes sitios de unión de cada proteína y de las interacciones repulsivas con el substrato y/o con las proteínas previamente absorbidas. Entre los más difundidos que se adscriben a este grupo son los soportes que utilizan como substrato Poly-L-lisina (PL), aminosilano, aminopropil-trimetoxysilano

(APTES), nitrocelulosa (NC) (Kusnezow *et al.*, 2003) o superficie de polistireno, que adsorben las proteínas por las fuerzas de Van der Waals, interacciones electrostáticas e hidrofóbicas (Espina *et al.*, 2004).

Al segundo grupo se adscriben los soportes de cristal con superficie funcionalizada o activada con un polímero que reacciona con las proteínas (por ejemplo con grupo amínico o sulfidrico) estableciendo una unión covalente. Los soportes comercializados más utilizados para este grupo son polímeros activados con un grupo aldehído, epoxylo, maleimido… o bien entrecruzados con otro substrato como el caso del APTES o el MPTS entrecruzados con maleimido-R-*N*- succinimidil ester que es un grupo heterobifuncional (Kusnezow *et al.*, 2003). Con el objetivo de aumentar la densidad de superficie de los ligandos se han introducidos soportes tratados con dos o más polímeros individuales con distintas funciones: un polímero para crear una red estructural 3D y otro que lleva grupos funcionales para unir el compuesto entero a la superficie de cristal y a las proteínas. Con este tipo de arquitectura, denominada *Hydrogel*, se han comercializado varios soportes como los de Perkin Elmer y Schott Nexterion H basados en la formación de un hidrogel compuesto por poliacrilamida y con grupos amínicos como grupos funcionales. Este tipo de soporte permite obtener una ratio señal/ruido seis veces mayor a otros tipos de soportes (Miller *et al.*, 2003) gracias a la baja dispersión de luz de la capa de gel transparente y a la alta sensibilidad debida a la mayor capacidad de unión de la red polimérica 3D. A pesar de todas sus ventajas, el Hydrogel no es apto para todas las aplicaciones ya que su capacidad de absorción es sólo 1.5 – 2 veces más alta que las superficies planas 2D convencionales (Angenendt *et al.*, 2002).

Independientemente del tipo de unión de las proteínas a la superficie (interacción no específica o covalente), o el tipo de superficie (2D o 3D) el objetivo principal es obtener la máxima capacidad de unión y la mayor señal/ruido. En este sentido, es importante bloquear los sitios inespecíficos de la superficie remanente antes del ensayo, para minimizar la unión inespecífica de la molécula diana, o de captura, con el substrato. Así puede obtenerse una mayor ratio señal/ruido, lo que lleva a una mejor sensibilidad (Angenendt *et al.*, 2003; Seurynck-Servoss *et al.*, 2007). Todos los soportes comercializados tienen alguna ventaja, ya sea una alta capacidad de unión, la salvaguarda de la estructura, funcionalidad y capacidad de unión de las proteínas y/o mantener un bajo nivel de fluorescencia de fondo. Sin embargo, actualmente los soportes recubiertos de nitrocelulosa siguen siendo los substratos más utilizados por su alta capacidad de absorción (75 – 150 µg/cm^2 en un volumen de 0.3-2 nl/spot (Mueller *et al.*, 2010) y por mantener las proteínas en su estado conformacional nativo, lo que se refleja en un bajo LOD, criterio fundamental para la detección de proteínas en muestras complejas poco concentradas.

1.5.4 Formatos de ensayos

Existen dos formatos generales de array, en fase directa, *Forward Phase Protein Microarray* (FPPA), y en fase reversa, *Reverse Phase Protein Microarray (RPPA)* (Figura 9). El FPPA consiste

en la impresión de las moléculas de captura permitiendo el análisis de la expresión de muchas proteínas en una muestra biológica (e.j. lisados celulares, de tejido, plasma etc.) (Figura 9). Por otro lado, el formato RPPA consiste en la impresión de un elevado número de muestras biológicas en las cuales se analiza la expresión de la proteína mediante la incubación con una sola molécula de captura (Figura 9). El RPPA o RPMA, formato utilizado en el marco de esta tesis doctoral, es ideal para análisis en grandes cohortes de muestras biológica ya que permite cuantificar proteínas poco abundantes y diferentemente reguladas en tejidos, fluidos corporales o muestras celulares en diferentes condiciones (Figura 9). Con esta técnica pueden identificarse biomarcadores específicos de múltiples enfermedades con aplicación en el diagnóstico, pronóstico y en predicción de la respuesta a tratamientos siendo por lo tanto indicada como técnica para el desarrollo de terapias personalizadas (Kononen *et al.*, 1998; Masuda and Yamada, 2015; Nishizuka and Mills, 2016; Speer *et al.*, 2007).

Los arrays de proteínas se encajan como una herramienta válida en el mundo de la investigación básica y clínica gracias a su alta densidad de datos partiendo de pequeñas cantidades de muestras y reactivos. Sin embargo, el camino para ser ampliamente aceptado como sistema de diagnóstico *in vitro* (IVD) es aún largo, ya que en la actualidad, sería necesario mejorar los sistemas de fabricación de los microarrays, la automatización, la reducción del tiempo de los ensayos, la adquisición y el análisis de datos, así como la fiabilidad y reproducibilidad.

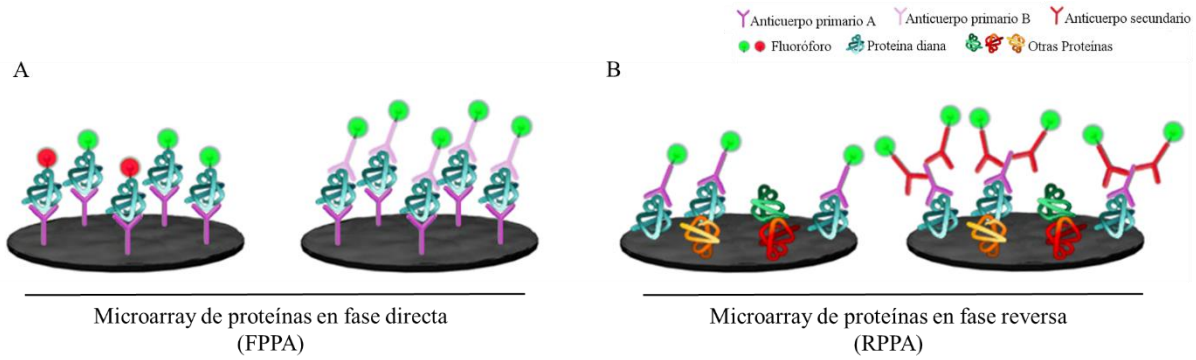

Figure 9. Esquema de formatos de array. Ejemplos de formatos de arrays de proteínas en fase directa y reversa. (A) En el array de fase directa (FPPA) se inmovilizan anticuerpos que capturan un analito específico en una muestra compleja. El analito se detecta por marcaje directo generalmente con un fluoróforo (izquierda) o por otro anticuerpo primario marcado que reconoce otro antígeno del mismo analito, método conocido como *sándwich* (derecha). (B) En el array en fase reversa (RPPA) se inmovilizan los analitos de la muestra en el soporte sólido. El analito se detecta aplicando un anticuerpo específico contra el analito (primario) directamente marcado (izquierda) o bien aplicando un anticuerpo adicional (secundario) específico contra el anticuerpo primario (derecha).

1.6 Aplicación del RPPA

1.6.1 Análisis del metabolismo energético en Enfermedades Raras

Las alteraciones genéticas que dan lugar a las disfunciones celulares frecuentemente se acompañan por cambios en la expresión de proteínas del metabolismo energético. En este contexto, un ejemplo apropiado es el dado por las múltiples mutaciones genéticas que promueven el cáncer y que desembocan en la reprogramación del metabolismo energético (Cuezva *et al.*, 2009; Vander Heiden *et*

al., 2009; Willers and Cuezva, 2011), que han demostrado aportar marcadores moleculares de prognosis y de respuesta a terapia.

En este apartado de mi tesis he desarrollado e implementado una plataforma de alto rendimiento como el RPPA para la identificación de biomarcadores que se pueden producir por los cambios metabólicos que acompañan a enfermedades pobremente exploradas como son las Enfermedades Raras (ER).

Las ER son un grupo de trastornos de amplia variabilidad fenotípica, de difícil diagnóstico, pronóstico y sin tratamiento efectivo en la mayoría los casos. En su conjunto, representan un problema socio-sanitario de primera magnitud, estimándose su incidencia en 1:2000 y siendo su prevalencia mínima global alrededor de 1:10.000. Consecuentemente, el esclarecimiento de los mecanismos moleculares y celulares que dan lugar a las alteraciones celulares y tisulares, y por ende, al fenotipo particular de cada una de estas patologías, es el primer paso para identificar posibles dianas y diseñar estrategias terapéuticas.

La plataforma RPPA, consolidada por anticuerpos monoclonales producidos y/o validados en nuestro laboratorio, es de gran utilidad en patología, y especialmente en las mitocondriales, ya que permite un análisis cuantitativo rápido y fiable de los marcadores metabólicos asociados a la función y estructura de la mitocondria y de algunas vías metabólicas como la glucolisis, ciclo de Krebs, CTE, OXPHOS, β-oxidación, glucogenolisis, respuesta antioxidante y ciclo de pentosas fosfatos en un elevado número de pacientes. Para la realización de la presente tesis se ha aplicado la plataforma anteriormente citada en dos casos particulares.

1.6.2 Enfermedades Neuromusculares Genéticas

En este caso se ha estudiado la expresión de diecinueve proteínas del metabolismo energético en una cohorte de 73 biopsias musculares incluyendo individuos sanos donadores (controles, n = 20) y pacientes afectados por algunas ERs con afectación muscular. La mayoría de ellas procedentes del grupo de Enfermedades Neuromusculares Genéticas con defectos en la distrofina como la distrofia muscular de Duchenne (DMD, n = 6) y Becker (BMD, n = 6), forma sintomática de la DMD en mujeres portadoras (Portadoras Xp21, n = 4), distrofia muscular de cinturas autosómica recesiva tipo 2C o gamma-sarcoglicanopatía (LGMD-2C, n = 6) y una neuromuscular no distrófica como la glucogénosis de tipo V (síndrome de Mc Ardle, n = 7), la Lipofuscinosis neuronal ceroide que es una enfermedad del grupo de Epilepsias mioclónicas progresivas (NCL, n = 6), una enfermedad metabólica mitocondrial con defecto del complejo I (n = 12) y miopatías de pacientes hospitalizados en la unidad de cuidados intensivos (UCI, n = 6).

Las distrofias musculares son un grupo de Enfermedades Neuromusculares debidas a defectos de algunas proteínas, ya sean estructurales o funcionales, que forman la fibra muscular. A este grupo se adscriben las enfermedades debidas a anomalías moleculares de la distrofina, por tanto denominadas Distrofinopatias. La DMD, que afecta 1 de cada 3.500 varones, es una distrofinopatia caracterizada

por atrofia y debilidad musculares progresivas, como consecuencia de la degeneración de los músculos esqueléticos, lisos y cardíacos que lleva a la muerte prematura sobre los 20 años de edad (Emery, 1998). Las mujeres son habitualmente asintomáticas, pero un porcentaje pequeño de mujeres portadoras presenta formas moderadas de la enfermedad (Portadoras Xp21). Ambas distrofias son enfermedades recesivas ligadas al cromosoma X y están provocadas por anomalías en el gen *DMD* (Xp21.2), uno de los genes más grande del genoma humano, que conducen a la completa deficiencia de distrofina en el tipo Duchenne y en una deficiencia más leve en el tipo Becker (Burghes *et al.*, 1987; Emery, 1998). De hecho la BMD es menos frecuente, más tardía y de menor gravedad que la DMD. La distrofina interactúa con varias proteínas formando el complejo de proteínas asociadas a la distrofina (DAPC), un complejo que atraviesa el sarcolema del músculo esquelético y cardíaco. Un componente principal del DAPC es el distroglicano cuya insuficiente glicosilación es responsable de las sarcoglicanopatias, un grupo de distrofias musculares congénitas heterogéneas clínicamente muy parecida a la DMD (Emery, 1998). Mutaciones con pérdida de función en genes codificantes por las cuatro subunidades del complejo del sarcoglicano causan, por disociación del complejo DAPC, las sarcoglicanopatias (Yoshida *et al.*, 1994), un subtipo de distrofias musculares de cintura "*Limb-girdle muscular dystrophies*" (LGMD) recesivo hereditario, al cual se le denomina LGMD2D, 2E, 2C y 2F según la mutación afecte a la subunidad α, β, γ and δ respectivamente (Nigro and Savarese, 2014). Dentro del gran grupo de enfermedades neuromusculares, otra enfermedad estudiada ha sido una enfermedad metabólica de almacenamiento de glucógeno, también conocida como síndrome de Mc Ardle o Glucogenosis de tipo V. Esta enfermedad es un trastorno autosómico recesivo causado por mutaciones en el gen *PYGM* (11q13) (Lebo *et al.*, 1984), el cual codifica por la isoforma muscular de la glucógeno fosforilasa o miofosforilasa. Esta enzima cataliza la primera reacción del catabolismo del glucógeno (Cori and Larner, 1951) y su actividad está ausente en estos pacientes. Los pacientes presentan un síndrome de intolerancia al ejercicio muscular con mialgia, calambres, fatiga y debilidad muscular. A diferencia de las anteriores la Lipofuscinosis Neuronal Ceroide está adscrita a las Enfermedades Neurológicas y Neurodegenerativas. Los trastornos del almacenamiento lisosomal (LSDs) son un grupo de patologías que afectan a 1 individuo de cada 7.500 nacidos (Meikle *et al.*, 1999; Wang *et al.*, 2011). Las Lipofuscinosis Neuronal Ceroideas (NCLs), también conocida como síndrome de Batten, representan un subgrupo de las LSDs causadas por mutaciones genéticas en 14 genes diferentes (Williams and Mole, 2012). Características patológicas de las NCLs son la acumulación de material ceroide en los lisosomas, degeneración neuronal progresiva y activación glial masiva que resultan en la muerte de los afectados (Geraets *et al.*, 2016). En este estudio también se ha incluido un grupo de ER mitocondriales con defectos en el complejo I. Las alteraciones en los complejos de la CTE pueden ser causadas por mutaciones en el mtDNA, aunque el 80% de las enfermedades mitocondriales se deben a mutaciones en el DNA nuclear. En todos casos, debido a la enorme heterogeneidad de este grupo, estas patologías están muy poco caracterizadas. Por último, se ha incorporado en el estudio un grupo de biopsias procedente de pacientes con diferentes patologías

para estudiar las alteraciones metabólicas debidas al factor epigenético de las miopatías, en este caso desencadenado por la hospitalización e inmovilidad prologada en la unidad de cuidados intensivos (UCI).

1.6.3 Miopatías Inflamatorias

Un segundo estudio de menor densidad de datos por RPPA se ha llevado a cabo interrogando la expresión de nueve proteínas para la caracterización metabólica de un grupo de Enfermedades Neuromusculares Inflamatorias, las Miopatías Inflamatorias idiopáticas (IMs). Este es, un grupo de enfermedades heterogéneas caracterizadas por debilidad muscular e infiltrados inflamatorios en musculo esquelético. Debido a su similar patogenicidad, la Polimiositis (PM), Dermatomiositis (DM) y la Miositis esporádica por cuerpos de inclusión (sIBM) son los tres principales subtipos adscritos al grupo de IMs (Dalakas and Hohlfeld, 2003). Las IMs se consideran enfermedades raras debido a su incidencia entre 2.1 y 7.7 nuevos casos por millón de habitantes/año. La DM y PM son enfermedades adquiridas, aunque puede existir un fondo genético de predisposición, caracterizadas clínicamente por debilidad muscular e inflamación del músculo faríngeo causando alteraciones de la deglución, y requiriendo hospitalización de emergencia en unidades especializadas. Un síntoma característico de la DM es el eritroedema fotosensible sobre áreas expuestas. La sIBM fue descrita por primera vez en 1971 por Yunis y Samaha, que definieron una entidad clínicamente similar a una PM crónica, caracterizada anatomopatológicamente por la presencia de inclusiones vacuolares con productos de degradación citoplasmáticos (Yunis and Samaha, 1971). La sIBM es la IM más comúnmente adquirida en pacientes a partir de los cincuenta años de edad (Catalan *et al.*, 2014; Mastaglia and Phillips, 2002). Aunque DM y sIBM están casi definidas, el diagnostico de PM se asigna frecuentemente por criterios de exclusión (Dalakas and Hohlfeld, 2003). Los criterios para el diagnóstico incluyen las manifestaciones clínicas, aumento en suero de enzimas musculares como creatina fosfoquinasa (CPK) y aldolasas, electromiogramas, y principalmente los resultados de la biopsia muscular (necrosis muscular, regeneración de fibras, infiltrado de linfocitos CD8+ T difuso) (Dalakas, 2015). Es necesaria una biopsia para distinguir una miositis de otra a excepción de la DM cuando ésta presenta su típica erupción cutánea. Además, a menudo es necesaria una biopsia adicional procedente de otra faja muscular debido a su típico perfil de inflamación a manchas y/o a los tratamientos esteroideos que pueden minimizar la inflamación dando por tanto un resultado negativo (Selva O'Callaghan and Trallero Araguas, 2008).

El propósito de ambos estudios ha sido la traslación de la "firma" del metabolismo energético a la práctica clínica, indicando que las enzimas del metabolismo pueden proveer biomarcadores relevantes que pueden ayudar a la comprensión de la biología de las enfermedades raras y, eventualmente, el seguimiento de estos pacientes.

INTRODUCCIÓN DE LOS ARTÍCULOS PRESENTADOS Y CONTRIBUCIÓN ORIGINAL DEL AUTOR

Introducción de los artículos presentados y contribución original del autor

En el **Artículo #1** hemos estudiado la reprogramación metabólica en carcinomas humanos demostrando cómo IF1, además de promover la glucolisis aerobia, desencadena una señal mediada por especies reactivas del oxígeno (ROS) que induce un estado proliferativo y de supervivencia celular. Se ha contribuido a la caracterización de los mecanismos de regulación de la expresión de IF1 así como de su potencial impacto clínico en algunos de los tumores humanos más prevalentes como colon, mama, pulmón y ovario. Además, hemos puesto de manifiesto su validez como marcador pronóstico en cáncer de colon y mama.

Artículo #2. Estudios recientes han demostrado *in vivo* cómo la activación de la OXPHOS proporciona un estado metabólico que favorece la supresión tumoral (Garcia-Cao *et al.*, 2012; Serrano and Blasco, 2007). Sin embargo, no se había demostrado como la inhibición parcial de la OXPHOS puede jugar un papel en la génesis y progresión del cáncer. En este estudio, en un modelo de ratón transgénico que expresa IF1 activo (H49K) en hígado, se demuestra el papel en reprogramación metabólica que ejerce esta proteína así como se confirma que el precondicionamiento mediado por IF1 protege frente a muerte celular por estrés oxidativo provocado por la inyección de acetaminofeno (APAP). Además, y como objetivo destacado del estudio, se demuestra por primera vez cómo la inhibición de la OXPHOS mediada por IF1 *in vivo* produce un fenotipo metabólico que favorece el desarrollo y la progresión del cáncer empleando un modelo de carcinogénesis inducida por dietilnitrosoamina (DEN).

Artículo #3. En este estudio hemos generado un modelo de ratón transgénico que expresa una forma mutante activa de IF1 (H49K) en neurona, para determinar el papel de la ATP sintasa en la muerte celular *in vivo*. La sobreexpresión de IF1 en neuronas induce un estado de precondicionamiento que protege de la muerte neuronal en respuesta a un daño excitotóxico inducido por inyección estereotáxica de ácido quinolínico. En este contexto, se produce una pérdida de actividad del complejo IV que se pone de manifiesto por el desensamblaje de los supercomplejos que contienen al CIV indicando una regulación de la cadena respiratoria por la actividad del complejo V. Estos resultados proporcionan, por primera vez *in vivo*, la relevancia de la ATP sintasa como reguladora de la muerte neuronal y su valor potencial como diana terapéutica en neurodegeneración.

Artículo #4. Las células madre mesenquimales (hMSCs) están caracterizadas por una exigua actividad de la OXPHOS y por utilizar preferencialmente la glucolisis aerobia como vía de aprovisionamiento energético. Los mecanismos que promueven el cambio metabólico de las células madre hacia una OXPHOS activa y por tanto, hacia el inicio del programa de diferenciación celular no se conocen. En este estudio se ha descrito cómo la perdida de expresión de IF1, inhibidor fisiológico de la ATP sintasa, induce la activación de la OXPHOS en ausencia de cambios relevantes en la

formación de complejos respiratorios y pone de manifiesto a IF1 como un marcador del estado de quiescencia de células madre.

Artículo #5. El estudio del metabolismo aporta biomarcadores potenciales que pueden contribuir al entendimiento de los principios biológicos de las enfermedades raras, así como al diagnóstico y/o seguimiento de los pacientes. En este artículo se evalúa la expresión de proteínas claves del metabolismo, mediante una técnica proteómica cuantitativa y de alto rendimiento denominada microarrays de proteínas en fase reversa (RPPA), en una cohorte de 73 biopsias musculares de pacientes afectados por distintas Enfermedades Raras Neuromusculares. A través del desarrollo de una batería de anticuerpos altamente específicos, en su mayoría desarrollados en nuestro laboratorio, aplicados al análisis por RPPA hemos identificado marcadores metabólicos que pueden facilitar el diagnóstico, así como el manejo clínico y eventualmente la terapia de pacientes con alguna de estas enfermedades.

Artículo #6. Al igual que en el **Artículo #5,** en este trabajo hemos definido la firma metabólica en otro grupo de enfermedades raras como las Miopatías Inflamatorias (IMs) del músculo estriado (Polimiositis (PM), Dermatomiositis (DM) y Miositis esporádica con cuerpos de inclusión (sIBM) mediante la aplicación de la plataforma RPPA. Describimos nuevos marcadores con un importante potencial diagnóstico ya que permiten discriminar un paciente afecto por una IM de un sujeto sano con una alta sensibilidad y especificidad. De forma congruente con la información clínica existente que indica que los pacientes afectos de DM tienen una alta incidencia de cáncer, demostramos cómo dos proteínas implicadas en la reprogramación metabólica del cáncer y en su progresión, como son la piruvato quinasa isoforma M2, (PKM2), y la proteína inhibidora de la ATP sintasa, (IF1), están altamente inducidas en estos pacientes.

Resumen de la contribución original del autor en los artículos presentados

- IF1 presenta niveles de expresión variables según el tipo de tejido, manteniendo una elevada expresión en todos los tumores estudiados. IF1 se define como un marcador de buen pronóstico en cáncer de colon. (He contribuido en la realización del estudio). **Artículo #1**

- La sobreexpresión hepática de H49K en ratón promueve la dimerización del complejo V e inhibe su actividad. Esta inhibición, provoca la desestabilización del complejo IV y de sus supercomplejos resultando en una disminución de su actividad. Además, la sobreexpresión de H49K favorece la formación de tumores mediante la inducción de la proliferación y de la resistencia a muerte celular en un modelo de hepatocarcinogénesis inducida. **Artículo #2**

- Como consecuencia de la inhibición de la ATP sintasa por la sobreexpresión de IF1 en cerebro de ratón se produce el desensamblaje de las estructuras supramoleculares que contienen el complejo IV y la disminución de su actividad. (He contribuido en la realización del estudio). **Artículo #3**

- La diferenciación de las hMSCs a osteocitos maduros cursa con una inducción de la expresión de las proteínas de la CTE. Sin embargo, el incremento de expresión descrito no se acompaña por cambios significativos en la organización estructural de los complejos de la CTE. (He contribuido en la realización del estudio). **Artículo #4**

- Se describen marcadores metabólicos para el diagnóstico de algunas Enfermedades Raras con afectación muscular mediante análisis de array de proteínas en fase reversa RPPA. **Artículo #5**

- Se describen marcadores metabólicos de utilidad para el diagnóstico diferencial y eventualmente para la prognosis del riesgo de cáncer en Miopatías Inflamatorias por RPPA. **Artículo #6**

Referencias bibliográficas de los artículos presentados

Artículo #1

Sánchez-Aragó, M., Formentini, L., Martínez-Reyes, I., García-Bermudez, J., **Santacatterina, F.**, Sánchez-Cenizo, L., Willers, I.M., Aldea, M., Nájera, L., Juarránz, A., López, E.C., Clofent, J., Navarro, C., Espinosa, E., Cuezva, J.M. (2013). Expression, regulation and clinical relevance of the ATPase inhibitory factor 1 in human cancers. *Oncogenesis* 22;2:e46.

Artículo #2

Santacatterina, F., Sánchez-Cenizo, L., Formentini, L., Mobasher, M.A., Casas, E., Rueda, C.B., Martínez-Reyes, I., Núñez de Arenas, C., García-Bermúdez, J., Zapata, J.M., Sánchez-Aragó, M., Satrústegui, J., Valverde, Á.M., Cuezva, J.M. (2016) Down-regulation of oxidative phosphorylation in the liver by expression of the ATPase inhibitory factor 1 induces a tumor-promoter metabolic state. *Oncotarget.* 5;7(1):490-508.

Artículo #3

Formentini, L., Pereira, M.P., Sánchez-Cenizo, L., **Santacatterina, F.**, Lucas, J.J., Navarro, C., Martínez-Serrano, A., Cuezva, J.M. (2014). In vivo inhibition of the mitochondrial H+-ATP synthase in neurons promotes metabolic preconditioning. *EMBO J.* 1;33(7):762-78

Artículo #4

Sánchez-Aragó, M., García-Bermúdez, J., Martínez-Reyes, I., **Santacatterina, F.**, Cuezva, J.M. (2013). Degradation of IF1 controls energy metabolism during osteogenic differentiation of stem cells. *EMBO Rep.* 14(7):638-44.

Artículo #5

Santacatterina, F., Chamorro, M., de Arenas, C.N., Navarro, C., Martín, M.A., Cuezva, J.M., Sánchez-Aragó, M. (2015). Quantitative analysis of proteins of metabolism by reverse phase protein microarrays identifies potential biomarkers of rare neuromuscular diseases. *J Transl Med.* 18;13:65.

Artículo #6

Santacatterina, F., Sánchez-Aragóa,M., de Arenas, C.N., Catalán, M., Garraboud, G., Cardellach, F., Cuezva, J.M. PKM2 and IF1 provide novel biomarkers of dermatomyositis: A metabolic link to oncogenesis.

Artículo #1

Sánchez-Aragó, M., Formentini, L., Martínez-Reyes, I., García-Bermudez, J., **Santacatterina, F.**, Sánchez-Cenizo, L., Willers, I.M., Aldea, M., Nájera, L., Juarránz, A., López, E.C., Clofent, J., Navarro, C., Espinosa, E., Cuezva, J.M. (2013). Expression, regulation and clinical relevance of the ATPase inhibitory factor 1 in human cancers. *Oncogenesis* 22;2:e46.

OPEN

Citation: Oncogenesis (2013) **2**, e46; doi:10.1038/oncsis.2013.9

www.nature.com/oncsis

ORIGINAL ARTICLE

Expression, regulation and clinical relevance of the ATPase inhibitory factor 1 in human cancers

M Sánchez-Aragó[1,6], L Formentini[1,6], I Martínez-Reyes[1], J García-Bermudez[1], F Santacatterina[1], L Sánchez-Cenizo[1], IM Willers[1], M Aldea[1], L Nájera[2], Á Juarránz[3], EC López[1], J Clofent[4], C Navarro[4], E Espinosa[5] and JM Cuezva[1]

Recent findings in colon cancer cells indicate that inhibition of the mitochondrial H^+-adenosine triphosphate (ATP) synthase by the ATPase inhibitory factor 1 (IF1) promotes aerobic glycolysis and a reactive oxygen species (ROS)-mediated signal that enhances proliferation and cell survival. Herein, we have studied the expression, biological relevance, mechanism of regulation and potential clinical impact of IF1 in some prevalent human carcinomas. We show that IF1 is highly overexpressed in most (>90%) of the colon ($n=64$), lung ($n=30$), breast ($n=129$) and ovarian ($n=10$) carcinomas studied as assessed by different approaches in independent cohorts of cancer patients. The expression of IF1 in the corresponding normal tissues is negligible. By contrast, the endometrium, stomach and kidney show high expression of IF1 in the normal tissue revealing subtle differences by carcinogenesis. The overexpression of IF1 also promotes the activation of aerobic glycolysis and a concurrent ROS signal in mitochondria of the lung, breast and ovarian cancer cells mimicking the activity of oligomycin. IF1-mediated ROS signaling activates cell-type specific adaptive responses aimed at preventing death in these cell lines. Remarkably, regulation of IF1 expression in the colon, lung, breast and ovarian carcinomas is exerted at post-transcriptional levels. We demonstrate that IF1 is a short-lived protein ($t_{1/2} \sim 100$ min) strongly implicating translation and/or protein stabilization as main drivers of metabolic reprogramming and cell survival in these human cancers. Analysis of tumor expression of IF1 in cohorts of breast and colon cancer patients revealed its relevance as a predictive marker for clinical outcome, emphasizing the high potential of IF1 as therapeutic target.

Oncogenesis (2013) **2,** e46; doi:10.1038/oncsis.2013.9; published online 22 April 2013

Subject Categories: cancer metabolism

Keywords: H^+-ATP synthase; ATPase inhibitory factor 1; energy metabolism; mitochondria; cancer prognosis; ROS signaling

INTRODUCTION

Downregulation of oxidative phosphorylation and concurrent activation of aerobic glycolysis is a hallmark feature of proliferating cells and of many different human carcinomas.[1–3] An enhanced aerobic glycolysis provides the metabolic intermediates required to sustain proliferation.[1,4] Several genetically-driven mechanisms directly promoting glycolysis, the inhibition of mitochondrial function or both have been proposed in order to explain energy metabolism in cancer cells and tumors (for review see Cuezva *et al.*[1] and Cairns *et al.*[5]). Moreover, it has been suggested that the APC/C–Cdh1 complex that controls the levels of PFKFB3, and hence, the rate of glucose consumption might participate in sustaining glycolysis in some types of human carcinomas.[6] However, epigenetic mechanisms[7,8] and the tumor microenvironment[5,9] also have relevant roles in cancer development and progression by regulating the bioenergetic phenotype of cancer cells.[10]

The H^+-adenosine triphosphate (ATP) synthase is a master regulator of energy metabolism and cell fate. It is the mitochondrial protein complex of oxidative phosphorylation that catalyzes the synthesis of ATP using as driving force the proton gradient generated by the respiratory chain.[11] The H^+-ATP synthase is also required for efficient execution of cell death.[12,13] In fact, cells that are unable to perform oxidative phosphorylation have an apoptotic-resistant phenotype.[13–15] Conversely, activation of the bioenergetic function of mitochondria prevents tumor development.[16,17]

A compromized bioenergetic activity of mitochondria, as assessed by genomic,[18] transcriptomic,[10] proteomic[1,19] and functional studies,[20] is involved in tumor progression and in chemotherapeutic resistance.[21–24] Specifically, it has been described: (i) the downregulation of the cellular abundance of the mRNAs that encode rate-limiting subunits of the H^+-ATP synthase by either promoter hypermethylation of the *ATP5B* gene[23] or by genetic deletion of *ATP5A1*[18]; (ii) the masking of the translation of β-F1-ATPase mRNA[25,26] through the binding of repressor proteins[27] that impede ribosome recruitment and translation and (iii) the overexpression in cancer cells and tumors of the ATPase inhibitory factor 1 (IF1) that inhibits the activity of the mitochondrial H^+-ATP synthase.[28] Furthermore,

[1]Departamento de Biología Molecular, Centro de Biología Molecular Severo Ochoa, Consejo Superior de Investigaciones Científicas-Universidad Autónoma de Madrid (CSIC-UAM), Centro de Investigación Biomédica en Red de Enfermedades Raras (CIBERER), ISCIII, Instituto de Investigación Hospital 12 de Octubre, Universidad Autónoma de Madrid, Madrid, Spain; [2]Servicio de Anatomía Patológica, Hospital de Fuenlabrada, Madrid, Spain; [3]Departamento de Biología, Universidad Autónoma de Madrid, Madrid, Spain; [4]Departamento de Patología y Neuropatología, Hospital Universitario de Vigo, Instituto de Investigación Biomédica de Vigo (IBIV), Vigo, Spain and [5]Servicio de Oncología Médica, Hospital Universitario La Paz, Madrid, Spain. Correspondence: Professor JM Cuezva, Departamento de Biología Molecular, Centro de Biología Molecular Severo Ochoa, Universidad Autónoma de Madrid, 28049 Madrid, Spain.
E-mail: jmcuezva@cbm.uam.es
[6]These authors contributed equally to this work.
Received 17 October 2012; revised 26 January 2013; accepted 9 March 2013

recent findings indicate that IF1 has additional functions in colon cancer cells by promoting a reactive oxygen species (ROS)-mediated adaptive cellular response that triggers proliferation and resistance to cell death.[29]

In this investigation, we have addressed (i) the study of the expression level of IF1 in different prevalent human carcinomas, (ii) the metabolic and signaling events that mediate IF1 overexpression in the lung, breast and ovarian cancer cells, (iii) the mechanisms that mediate IF1 overexpression in tumors and (iv) its relevance as a prognostic marker in breast and colon cancer patients. Overall, the results indicate that IF1 has a very short half-life being highly overexpressed in the colon, lung, breast and ovarian carcinomas by mechanisms that are regulated at post-transcriptional levels. In contrast, normal tissues that overexpress IF1, such as endometrium and kidney, reveal no relevant changes in IF1 triggered by carcinogenesis. The overexpression of IF1 promotes the activation of aerobic glycolysis and concurrently confers a ROS-mediated resistance to staurosporine (STS)-induced cell death to the lung, breast and ovarian cancer cells. Moreover, the tumor expression of IF1 is a predictive marker for clinical outcome in breast and colon cancer patients. As IF1 masters the reprogramming of energy metabolism and signals cell-death resistance in cancer cells, we suggest that IF1 offers a relevant molecule with high potential as a new therapeutic target for treatment of prevalent human carcinomas.

RESULTS

IF1 is overexpressed in most prevalent human carcinomas

Western blots in Figure 1 illustrate that the monoclonal antibody[28] recognizes the recombinant, as well as the two major isoforms (~12 and ~8 kDa) of native IF1 in normal human liver and stomach extracts (Figure 1). The expression of IF1 is negligible in the normal breast, colon and lung (Figure 1), but sharply increases in their corresponding carcinomas (Figure 1). Colon carcinomas also express the short ~8 kDa IF1 isoform (Figure 1). Interestingly, normal stomach shows a high expression of IF1 and revealed no relevant changes by carcinogenesis (Figure 1). It should be noted that heart (not shown) and liver (Figure 1) are the normal human tissues with highest expression of IF1.

The expression of IF1 was also assessed by immunohistochemistry in a different cohort of normal human tissues and carcinomas (Figure 2). Consistent with western blot data (Figure 1), immunohistochemistry of cancer tissue microarrays confirmed that the expression of IF1 is negligible in the normal colon, lung, breast and ovary (Figure 2). In contrast, carcinomas in these tissues showed a highly significant increase in the granular cytoplasmic immunostaining of IF1 (Figure 2). Contrary to these findings, the expression of IF1 in normal epithelial cells of the endometrium and kidney was very high (Figure 2) and its content did not show significant changes by carcinogenesis (Figure 2).

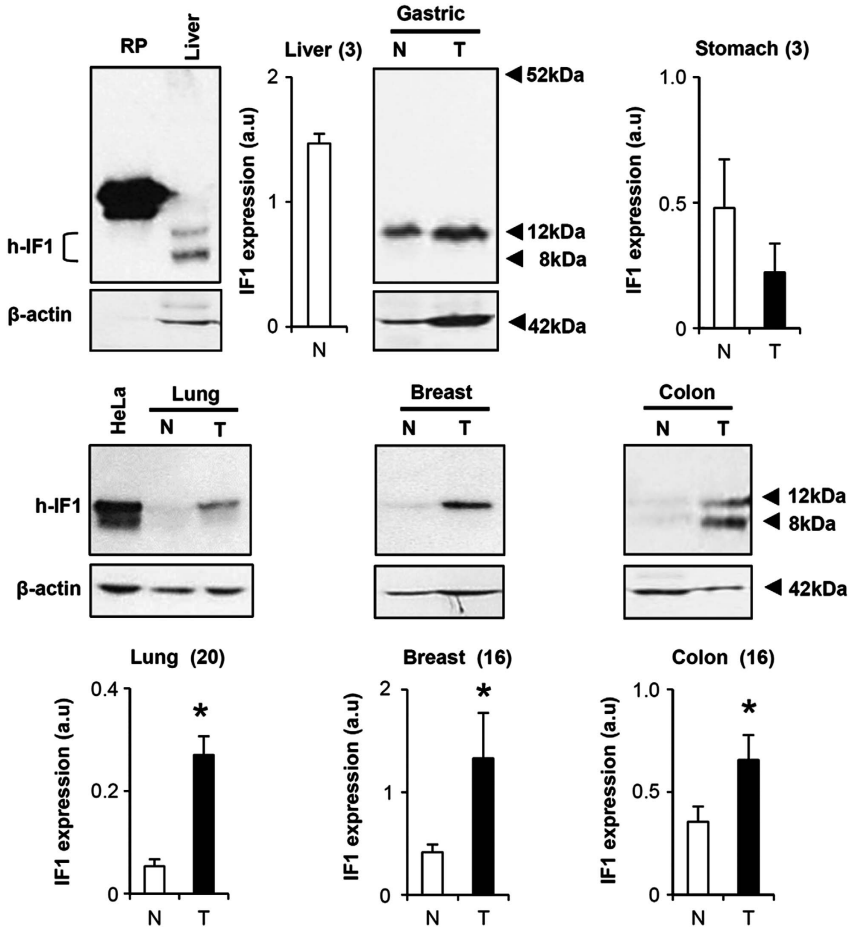

Figure 1. Expression of human IF1 in normal and tumor tissues. Western blots reveal the expression of IF1 (h-IF1) in SDS–polyacrylamide gel electrophoresis fractionated proteins from normal (N) and tumor (T) biopsies of different human tissues. The antibody recognizes the recombinant protein, as well as the two major 12- and 8-kDa protein isoforms of IF1. β-actin expression is shown as loading control. For comparison purposes, the expression level of IF1 in human tissues (histograms) is normalized relative to its expression in HeLa cells (a.u., arbitrary unit) assayed in the same blot. The number of paired normal and tumor biopsies analyzed is indicated in parenthesis.

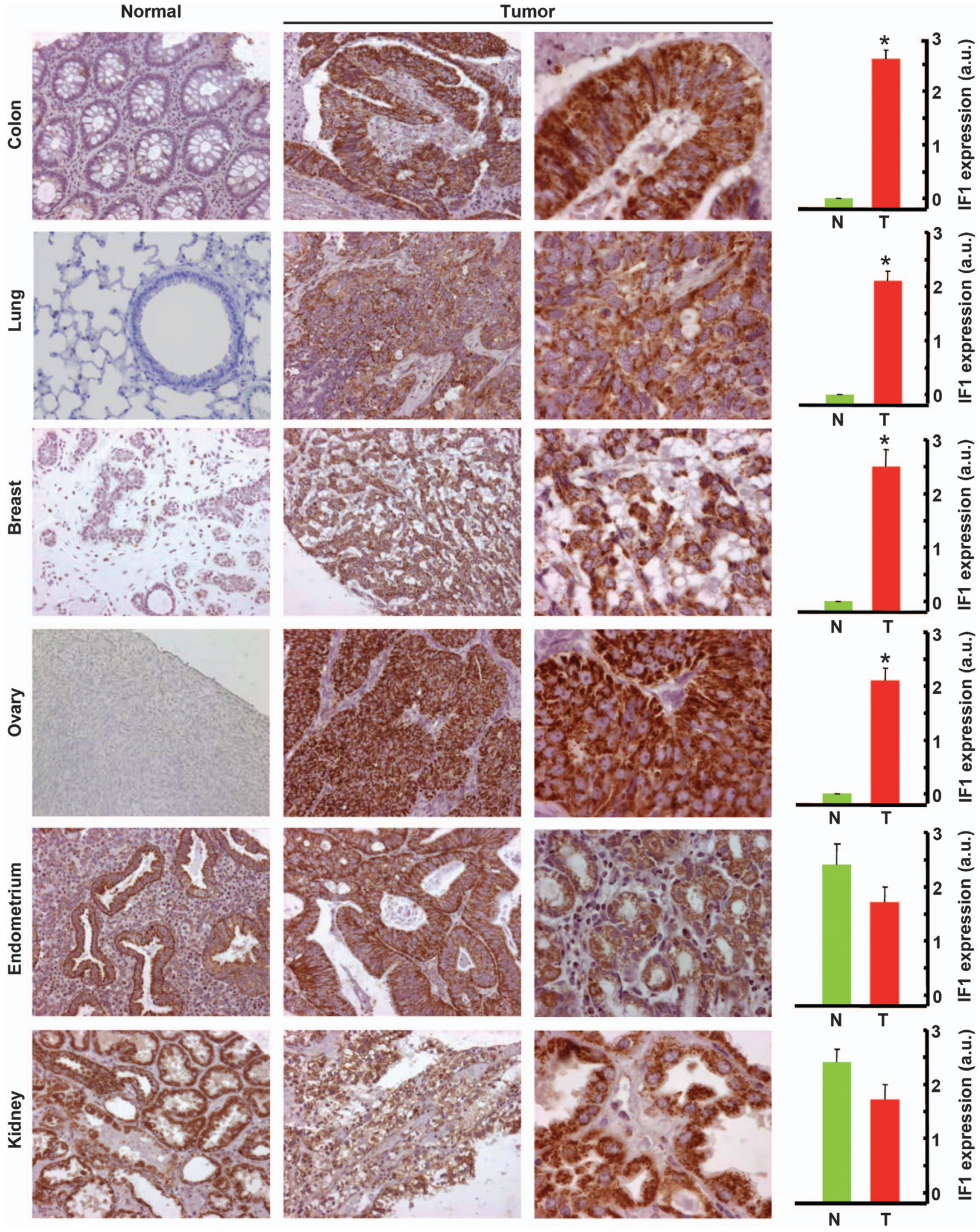

Figure 2. IF1 is upregulated in some prevalent human carcinomas. Representative immunohistochemistries of IF1 expression in normal and tumor tissue of the colon, lung, breast, ovary, endometrium and kidney. Magnification $\times 20$, $\times 40$ and $\times 63$. Histograms to the right of the pictures show the quantification of IF1 expression in normal (N, green, $n = 5$) and tumor (T, red, $n = 10$) specimens expressed as arbitrary units (a.u.). The results shown are the mean ± s.e.m. $^*P < 0.05$ when compared with normal by Student's *t*-test. Note that whereas normal epithelial cells from the colon, lung, breast and ovary show low or negligible expression of IF1, endometrial and kidney cells have very-high expression of IF1.

Post-transcriptional regulation of IF1 expression in cancer

Details on the analysis of the promoter region of the human IF1 gene (*ATPIF1*) and its possible relationship with the expression of hypoxia-inducible factor-1α[30] are provided in Supplementary Figure S1 and Supplementary Figure S2, respectively. In any case, the cellular availability of IF1 mRNA was not significantly different in the colon, lung and breast carcinomas when compared with that in the corresponding normal tissues (Figure 3a). Moreover, IF1 mRNA was significantly reduced in ovarian carcinomas (Figure 3a).

The immediate early response gene (*IER3*) has been shown to target IF1 for degradation by a mitochondrial protease.[31] Studies aimed at characterizing the relevance of protein stability in the expression of IF1 in colon cancer cells revealed a very rapid accumulation of the protein in response to the serine-protease inhibitor 4-(2-aminoethyl) benzenosulfonyl fluoride hydrochloride (Figure 3b), suggesting the participation of either the ATP-dependent Lon protease or ClpXP[32] in the degradation of IF1. The short half-life of IF1 was further demonstrated by pulse-chase experiments (Figure 3c) that indicated a t1/2 for the protein of ~100 min. Overall, these findings indicate the relevance of translational and post-translational regulatory mechanisms for the expression of IF1 in cancer.

Analysis of the expression of IER3 in the lung, breast and colon carcinomas revealed that it is overexpressed in 16 out of the 18 carcinomas analyzed (Supplementary Figure S3A). Moreover, partial silencing of the protein in colon cancer cells revealed no relevant effect on the expression of IF1 (Supplementary Figure S3B), what suggests that degradation of IF1 is a complex process.

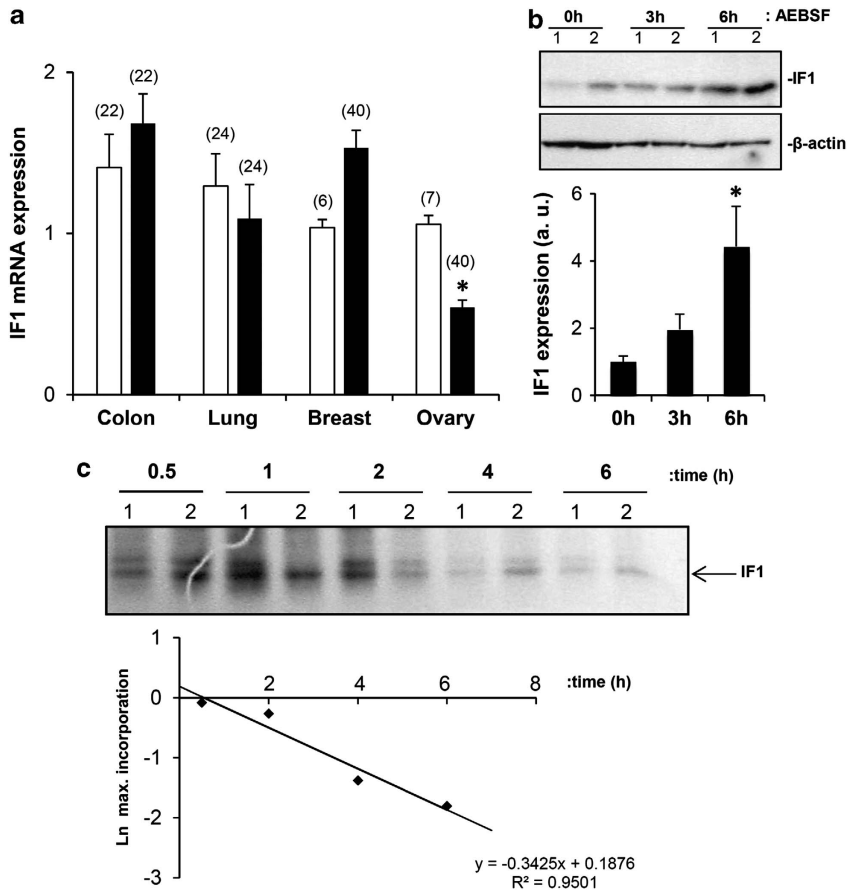

Figure 3. IF1 expression is regulated at post-transcriptional levels. (**a**) The colon (HCRT103), lung (HLRT104), breast (BCRT101) and ovarian (HORT102) TissueScan Tissue quantitative PCR Arrays were used to determine the expression of IF1 mRNA in different normal (open bars) and tumor (closed bars) tissue specimens. The number of studied patients is indicated in brackets. The results shown are the mean ± s.e.m. $^*P<0.001$ when compared with normal by Student's *t*-test. (**b**) HCT116 cells were treated with 400 μM of the serine-proteases inhibitor 4-(2-aminoethyl) benzenosulfonyl fluoride hydrochloride for the indicated time and the expression of IF1 and β-actin (loading control) analyzed by western blot. Lanes 1 and 2, show different experiments of the same condition. Bars are the mean ± s.e.m. of four experiments. $^*P<0.05$ when compared with 0 h by Student's *t*-test. (**c**) After metabolic labeling with ^{35}S-methionine IF1 was immunoprecipitated from HCT116 cells at the indicated time. Lanes 1 and 2, show different experiments of the same condition of the chase. The fluorogram reveals the migration of both the precursor and mature IF1 (arrow) ^{35}S-labeled immunoprecipitated proteins. The plot shows the first order rate kinetics of the decay of IF1. The t1/2 for IF1 is in the 105–120 min range.

IF1 regulates energy metabolism in the lung, breast and ovarian cancer cells

Consistent with previous reports in colon cancer cells,[29] the overexpression of IF1 in the lung, breast and ovarian cancer cells promoted a significant increase in the rates of aerobic glycolysis (Figure 4a). The increase in glycolysis was similar to that exerted by incubation of the cells with oligomycin, a pharmacological inhibitor of the H^+-ATP synthase (Figure 4a). Conversely, small interfering RNA-mediated silencing of IF1 promoted a significant reduction in the rates of glycolysis in most cancer cells except in HOP62 (Figure 4a). The expression of IF1 varies largely between cancer cells (Figure 4b), whereas the basal rates of aerobic glycolysis were found to be quite similar (Figure 4a), indicating that glycolysis is regulated by other factors in addition to the expression level of IF1.[33]

IF1 overexpression generates a mitochondrial ROS signal in the lung, breast and ovarian cancer cells

The overexpression of IF1 in the lung, breast and ovarian cancer cells promoted a significant increase in the production of superoxide radical (Figure 5). The mitochondrial scavenger MitoQ (MQ)[34] was able to quench the production of superoxide in all cell lines studied (Figure 5), supporting the role of IF1 as a general ROS-mediating signaling molecule in mitochondria.[29] We should mention that the IF1-mediated ROS signal generated in mitochondria is of mild intensity because neither the cellular hydrogen peroxide levels nor the GSH/GSSG ratio have been found to be altered by IF1 overexpression.[29]

In sharp contrast with the findings in colon cancer cells,[29] the IF1-mediated ROS signal was unable to stimulate cellular proliferation as assessed by the incorporation of 5-ethynyl-2′-deoxyuridine (EdU) into cellular DNA in the lung, breast and ovarian cancer cells (Supplementary Figure S4).

Mitochondrial ROS protect the lung, breast and ovarian carcinomas from STS-induced cell death

The IF1-mediated ROS signal was able to protect the lung, breast and ovarian cancer cells from STS-induced cell death (Figure 6). Quenching the ROS signal with MQ prevented protection against STS-induced cell death (Figure 6). Interestingly, we observed that the intensity of the ROS-mediated response to IF1 overexpression (Figure 5) correlated with the degree of protection against

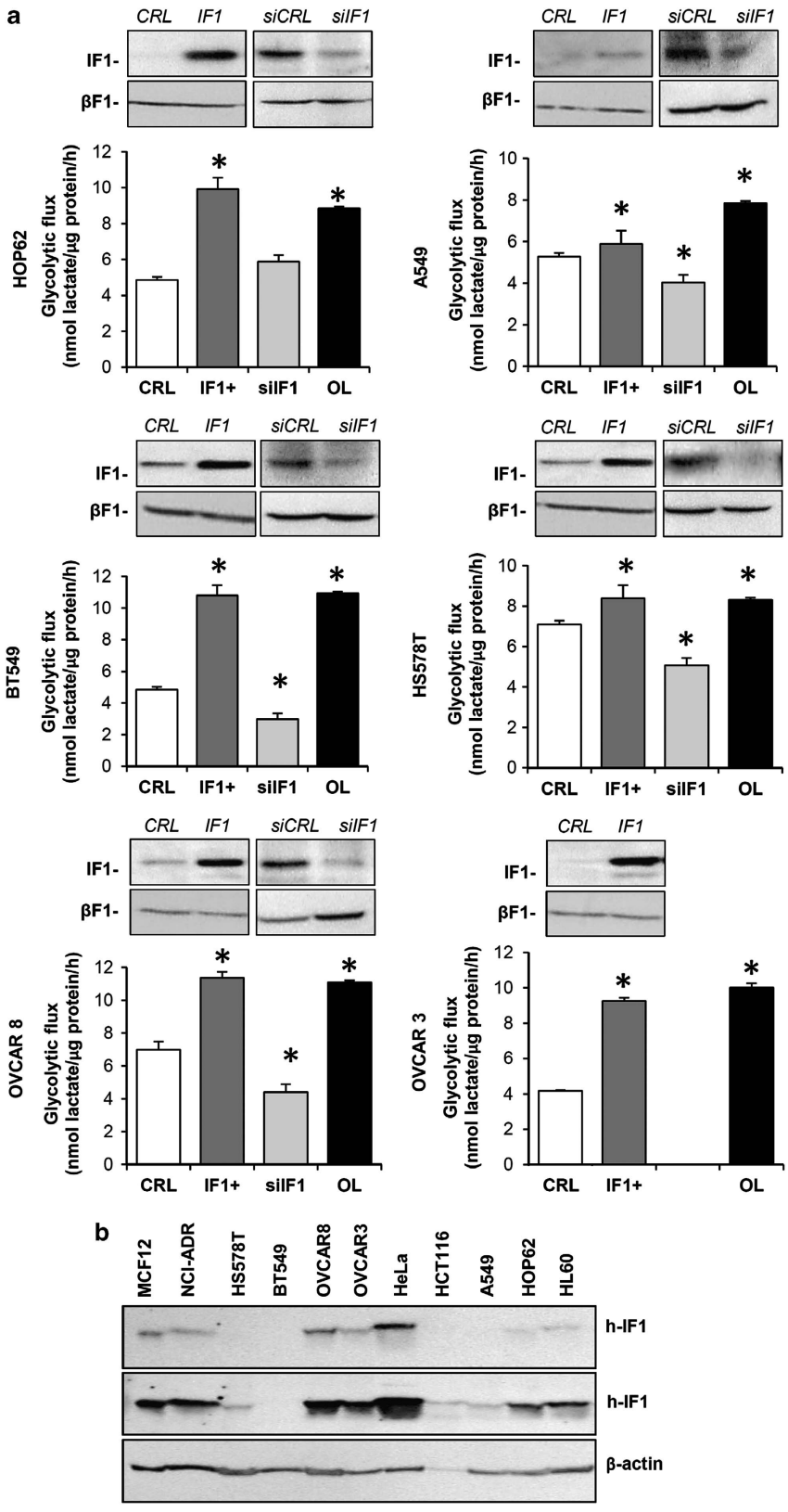

Figure 4. IF1 regulates the activity of aerobic glycolysis in the lung (HOP62, A549), breast (BT549, HS578T) and ovarian (OVCAR8, OVCAR3) cancer cells. (**a**) Cells transfected with CDL-GFP-β-3′UTR were co-transfected with control (CRL and siCRL, open bars), IF1 plasmid (IF1 +, dark gray bars) or siIF1 small interfering RNA (siIF1, light gray bars) to regulate the expression of IF1 for the determination of the rates of aerobic glycolysis. The effect of 6 μM oligomycin (OL, closed bars) is shown. Representative blots of IF1 and β-F1-ATPase (β-F1) expression. Bars are the mean ± s.e.m. of six different samples. *$P < 0.05$ when compared with CRL by Student's *t*-test. (**b**) IF1 (h-IF1) expression in 20 μg of protein from different human cell lines. Two different exposures of the IF1 film are presented. β-actin expression is shown as loading control.

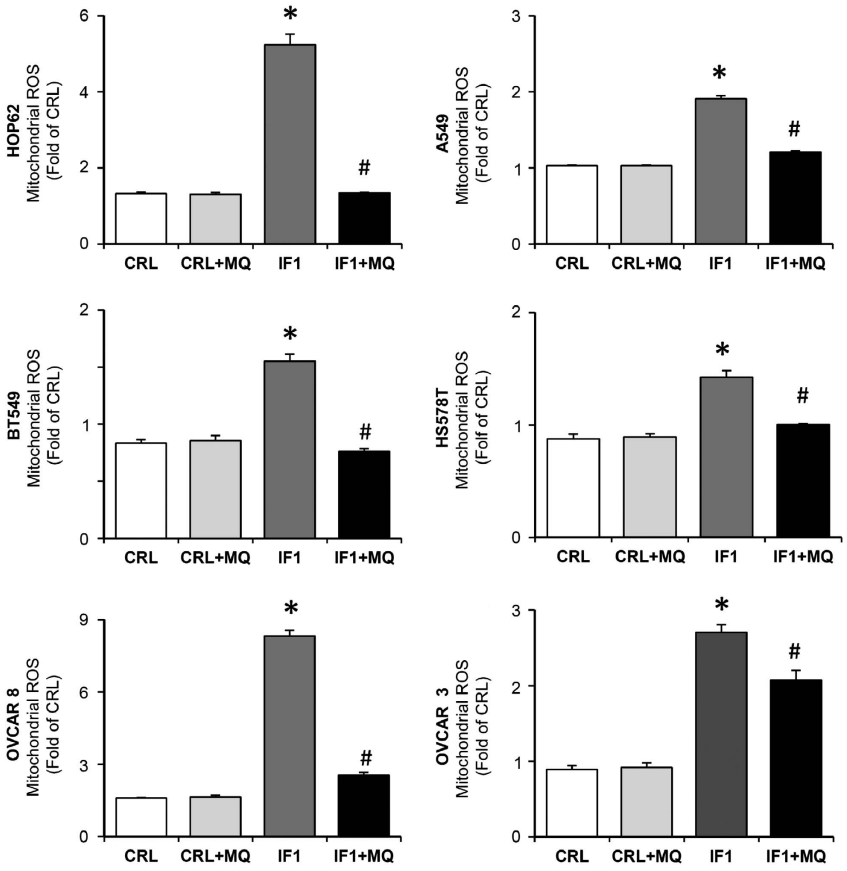

Figure 5. IF1 regulates mitochondrial ROS production in the lung (HOP62, A549), breast (BT549, HS578T) and ovarian (OVCAR8, OVCAR3) cancer cells. Cells transfected with CDL-GFP-β-3′UTR were co-transfected with control (CRL, open and light gray bars) or IF1 plasmid (IF1, dark gray and closed bars) in the absence or presence (+MQ) of 5 nM of the mitochondrial ROS scavenger MitoQ (MQ). The superoxide radical was determined by fluorescence-activated cell sorting analysis using MitoSox. The data shown are mean ± s.e.m. of 12 different samples. $^{*}P<0.05$ and $^{\#}P<0.05$ when compared with CRL or IF1 by Student's *t*-test, respectively.

STS-induced cell death (plot in Figure 6), suggesting a relevant role for mitochondrial ROS signaling in promoting survival pathways in all cancer cells.

For instance, and in support of this idea, transcriptional activity of the nuclear factor kappa-light-chain-enhancer of activated B cells (NFκB) promoter in the lung, breast and ovarian carcinomas was greatly enhanced by IF1 overexpression (Figure 7a) and partially quenched by the mitochondrial ROS scavenger MQ (Figure 7a). The ROS-mediated activation of the NFκB pathway in HOP62 lung cancer cells is supported by a reduction in the expression of the NFκB repressor IκBα (nuclear factor of kappa light polypeptide gene enhancer in B-cells inhibitor, alpha) and the concurrent increase in the expression of the antiapoptotic Bcl-xL (Figure 7b). These changes were partially reversed by the mitochondrial ROS scavenger MQ (Figure 7b). However, the same studies in breast (BT549, HS578T) and ovarian (OVCAR8) cancer cells did not provided similar findings (data not shown) emphasizing the complexity of the survival pathways that are activated in cancer cells in response to mitochondrial ROS signaling.

Clinical relevance of IF1 in breast cancer

A next question was to assess the potential relevance of IF1 in the clinics. We determine the expression level of IF1 in a cohort of tumors of breast cancer patients operated from invasive carcinomas for which the bioenergetic signature or bioenergetic cellular index (β-F1-ATPase/Hsp60/GAPDH ratio) and follow-up information is available.[35,36] The results in Supplementary Table S1 summarize the clinicopathological characteristics of the cohort of patients studied and the expression level of IF1 in the carcinomas according to the clinical information. It should be noted that the expression of IF1 in normal breast biopsies was negligible (Figures 1 and 2). Although the tumor expression of IF1 did not show significant differences between patients with clinical-pathological markers relevant for tumor progression, such as nodal involvement, tumor size and histological grade (Supplementary Table S1), it was significantly diminished in the poor prognosis groups of lobular and hormone receptor negative carcinomas when compared with ductal and hormone receptor positive carcinomas, respectively (Supplementary Table S1).

From the molecular point of view, the expression of IF1 inversely correlated with the bioenergetic cellular index[35] of the tumors ($R=-0.437$; $P=0.0001$), suggesting that the increased expression of IF1 parallels the program of repression of the bioenergetic activity of mitochondria in cancer cells. Surprisingly, Kaplan–Meier survival analysis revealed that a low tumor expression of IF1 predicted a higher rate for disease-recurrence in breast cancer patients (Figure 8a).

Clinical relevance of IF1 in colon cancer

Next, we determine the quantity of IF1 in normal and tumor biopsies in a cohort of colon cancer patients in which the markers of energy metabolism have been previously quantified.[37] The amount of IF1 was determined using reverse phase

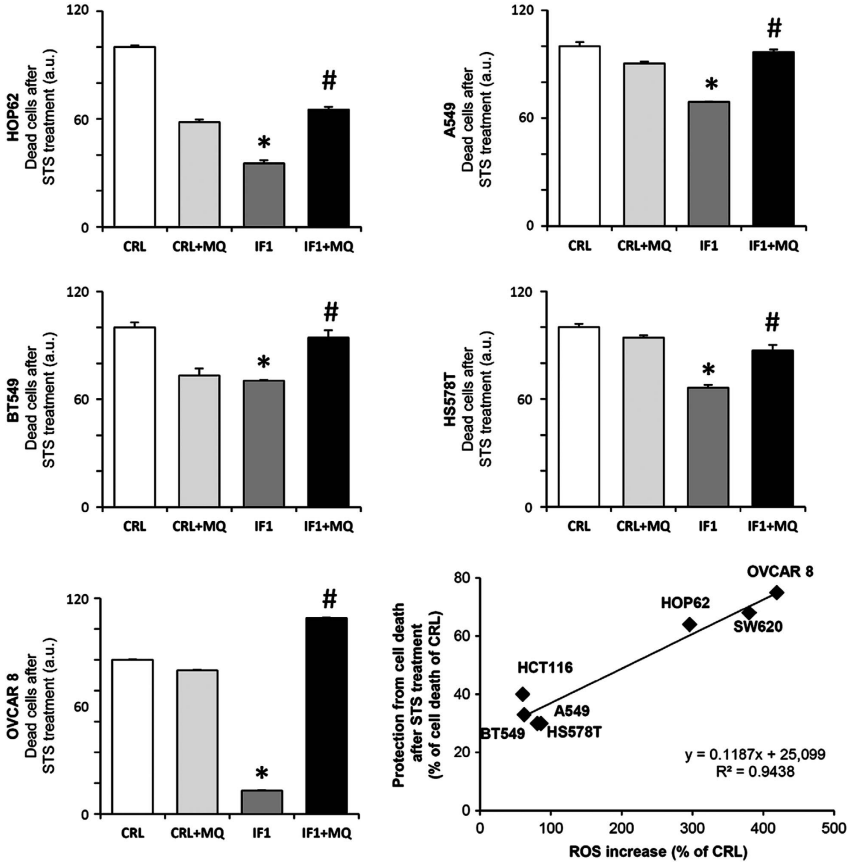

Figure 6. IF1 regulates the cell-death response in the lung (HOP62, A549), breast (BT549, HS578T) and ovarian (OVCAR8) cancer cells. Cells transfected with CDL-GFP-β-3′UTR were co-transfected with control (CRL, open and light gray bars) or IF1 plasmid (IF1, dark gray and closed bars) in the absence or presence (+MQ) of 5 nM of the mitochondrial ROS scavenger MitoQ (MQ). Twenty-four hours after transfection, the cells were treated with 1 μM STS and 24 h later the cells were stained with propidium iodide and the green population of cells was analyzed by flow cytometry to evaluate the percentage of sub-G0 cells. The data shown are mean ± s.e.m. of six–nine different samples. $^{*}P<0.05$ and $^{\#}P<0.05$ when compared with CRL or IF1 by Student's *t*-test, respectively. The plot shows the linear correlation that exists between the IF1-mediated ROS-response and the observed cell death.

protein microarrays (Supplementary Figure S5).[37] The results in Supplementary Table S2 summarize the clinicopathological characteristics of the cohort of patients studied and the quantity of IF1 in the carcinomas according to the clinical information. Colon carcinomas showed a significant twofold increase in the amount of IF1 when compared to normal colon biopsies (Supplementary Table S2). The tumor content of IF1 did not show significant differences between patients with clinical-pathological markers relevant for tumor progression (Supplementary Table S2).

In colon cancer, the expression of IF1 also inversely correlated with the bioenergetic cellular index[37] of the tumors ($R=-0.526$; $P=0.001$), once again suggesting that the increased expression of IF1 in colon cancer cells parallels the program of metabolic reprogramming experienced by these carcinomas. Kaplan–Meier survival analysis also revealed that a low tumor expression of IF1 predicted a worst overall prognosis for colon cancer patients (Figure 8b).

DISCUSSION

We show that IF1 is highly overexpressed in all human carcinomas of the colon, lung, breast and ovary showing negligible expression in their corresponding normal tissues. IF1 promotes the activation of aerobic glycolysis and generates a concurrent ROS signal in mitochondria that activates cell-type specific adaptive responses aimed at preventing death in the lung, breast and ovarian cancer cells. Mechanistically, IF1 mimics the effects of oligomycin, an inhibitor of the H^+-ATP synthase.[13,29] Remarkably, we show that the regulation of the expression of IF1 in carcinomas of the colon, lung, breast and ovary is exerted at post-transcriptional levels. In fact, we demonstrate that IF1 is a short-lived protein that is degraded by mitochondrial serine-proteases. Overall, we provide the first demonstration supporting that regulation of the synthesis and/or degradation of a mitochondrial protein involved in the control of oxidative phosphorylation has a master role in metabolic rewiring and in signaling cell-death resistance in prevalent human carcinomas. Moreover, we show that IF1 expression has relevance as a predictive marker for clinical outcome in breast and colon cancer patients.

The expression level of IF1 varies greatly within normal human tissues. Consistent with the role of IF1 as inhibitor of the H^+-ATP synthase,[28,29] a high expression of IF1 in normal tissues such as heart, liver and kidney would imply the partial mass-action-mediated inhibition of oxidative phosphorylation and thus a limitation in cellular ATP availability. This situation is obviously not possible because these tissues have a very-high metabolic demand. Thus, our findings suggest that in addition to the well characterized pH regulated binding of IF1 to the H^+-ATP synthase,[38] a mechanism should exist in tissues with high metabolic demand to promote the mass-action-mediated inhibition of IF1 on the H^+-ATP synthase activity.[28] In this

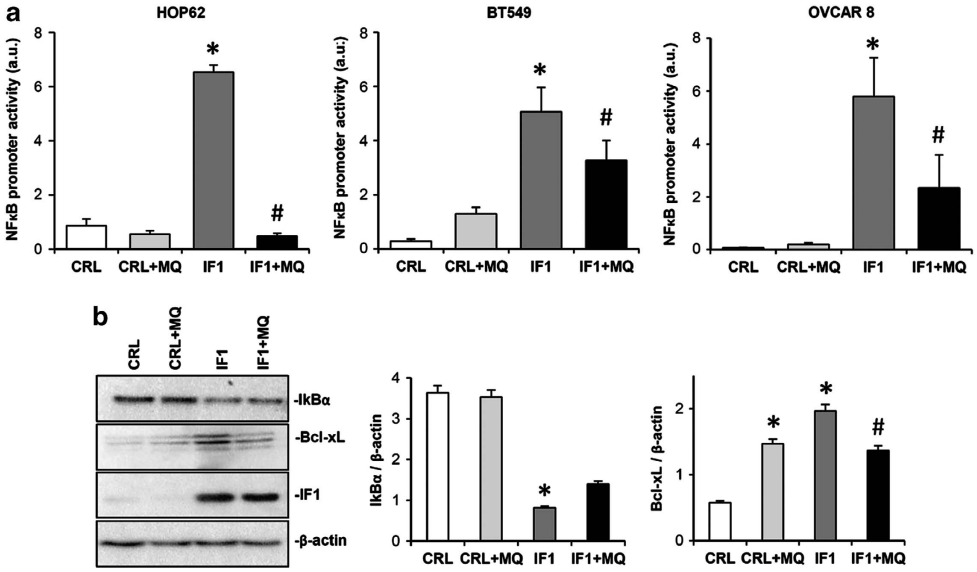

Figure 7. IF1 triggers transcriptional activation of the NFκB promoter in the lung (HOP62), breast (BT549) and ovarian (OVCAR8) cancer cells. Cells transfected with CDL-GFP-β-3′UTR were co-transfected with control (CRL, open and light gray bars) or IF1 (IF1, dark gray or closed bars) plasmid in the absence or presence (+MQ) of 5 nM of the mitochondrial ROS scavenger MitoQ (MQ). (**a**) A luciferase reporter plasmid of the NKκB promoter was co-transfected and the luciferase activity was determined in cellular extracts after 24-h transfection. The data shown are mean ± s.e.m. of 10 samples. $^{*}P<0.05$ and $^{\#}P<0.05$ when compared with CRL or IF1 by Student's *t*-test, respectively. (**b**) Cellular proteins of HOP62 were fractionated on SDS–polyacrylamide gel electrophoresis and processed for western blotting with the indicated primary antibodies. Representative blots are shown. The results are mean ± s.e.m. of three experiments. $^{*}P<0.05$ and $^{\#}P<0.05$ when compared with CRL or IF1 by Student's *t*-test, respectively.

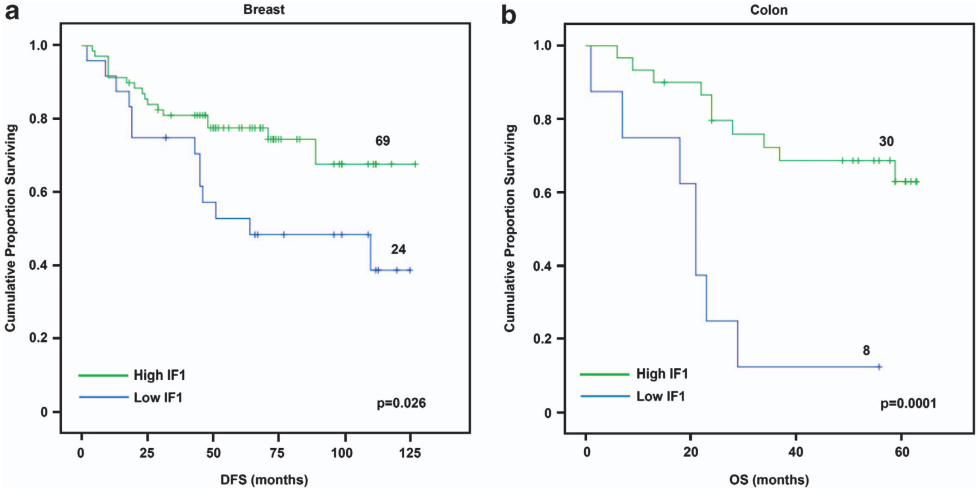

Figure 8. Kaplan–Meier survival analyses reveal the clinical relevance of IF1. (**a**) Protein samples from breast tumor biopsies were analyzed by western blot for the expression level of IF1. Kaplan–Meier disease-free survival analysis for 93 breast cancer patients stratified by the tumor expression level of IF1. The plot shows a significant association of low IF1 expression with a poor outcome for the patients. The log-rank test *P*-value is shown. (**b**) Protein samples from normal and tumor biopsies from a cohort of patients with colorectal cancer were analyzed by reverse phase protein microarrays to quantify IF1 (see Supplementary Figure S4). Kaplan–Meier overall survival analysis for 38 colon cancer patients stratified by the tumor quantity of IF1. The plot shows a significant association of low IF1 expression with a poor outcome for the patients. The log-rank test *P*-value is shown.

regard, it has been described that IF1 also binds other membrane proteins of mitochondria in a pH and $\Delta\Psi$m independent manner[39,40] hampering its activity as an inhibitor of the ATPase.[40] Alternatively, potential tissue-specific post-translational modifications of IF1 could explain the differential activity exerted by IF1 in different human tissues.

At variance with other mitochondrial proteins[41] we show that IF1 is a short-lived protein with a turnover in the range of minutes. This finding is of utmost importance to understand the bioenergetic activity of mitochondria. In fact, a rapid turnover of the protein would allow cells to quickly adapt the output of ATP by oxidative phosphorylation to changing physiological cues. One can speculate that mutations in cancer genes or other epigenetic events of the tumor microenvironment switch-on the mechanisms that promote a high expression of IF1 in the tumor. We suggest that an increase in translation of IF1 mRNA and/or in the stability of the protein should occur in human carcinomas to provoke the overwhelming expression of IF1 observed in these tumors. The

control of IF1 translation is presently unknown and it might involve regulatory proteins and microRNAs as we have shown for β-F1-ATPase mRNA.[27,42,43]

IER3 gene has been shown to suppress ROS production and to render IF1 prone to proteolytic digestion.[31] Paradoxically, and in contrast with findings in ovarian[44] and pancreatic[45] cancer our results indicate that IER3 is overexpressed in the lung, breast and colon cancer. Moreover, we found no correlation between IER3 and IF1 expression suggesting that the control of the degradation of IF1 is more complex than originally anticipated and that the participation of IER3 might depend on the cell-type analyzed. An alternative explanation for the accumulation of IF1 in carcinomas could be the partial inactivation of the mitochondrial serine-protease involved in its turnover. In this regard, the Lon protease has been reported to diminish its activity during ageing.[46] Moreover, cancer cells exhibit high basal levels of oxidative stress[5] and the Lon protease is particularly vulnerable to inactivation by ROS.[47] The implication of ClpXP in human pathology is scant despite its relevance in the degradation of proteins involved in metabolic reprogramming.[48] As previously discussed, potential oncogene- and/or metabolic-driven post-translational modifications of IF1 could also explain its accumulation in carcinomas if such changes hamper the mitochondrial pathway of IF1-degradation.

Despite the large structural and molecular differences of mitochondria in mammalian cells,[49] but consistent with previous findings in colon cancer,[29] we show that the IF1-mediated inhibition of the H^+-ATP synthase switches on aerobic glycolysis and generates a mitochondrial ROS signal in all cancer cells studied. Mitochondrial ROS signaling represents a pathway of retrograde communication to the nucleus of the cell that influences adaptive cellular responses.[50] The results herein indicate that whereas mitochondrial ROS signaling triggers protection against cell death in all cellular types studied, it is unable to stimulate proliferation in the lung, breast and ovarian carcinomas, what is at variance with colon cancer cells.[29] These findings indicate the existence of common and cell-type specific programs of nuclear response to mitochondrial ROS signaling. The effect of ROS on the cellular response depends on the level[51] and site[52] at which they are being produced. Moreover, ROS interact with diverse signaling pathways being transcription factor NFκB, a crucial regulator of adaptive responses related with survival.[53,54] In colon cancer cells, IF1 mediated the activation of the canonical NFκB pathway of survival.[29] The results herein support that although IF1 is able to trigger the ROS-mediated transcriptional activation of the NFκB promoter as a common response to the lung, breast and ovarian cancer cells, only lung carcinomas seem to activate the same NFκB-mediated survival pathway. These results emphasize the critical function that NFκB has in signaling lung tumor development, in agreement with previous findings in a mouse model of lung carcinogenesis,[55] and highlight the need of specific studies aimed at unveiling the IF1-mediated pathways of survival that are activated in breast and ovarian cancer cells.

Redox regulation has an essential role in malignancies[29,56,57] but the mechanisms of its actions and its impact in tumor prognosis remain unclear. Contrary to what would be expected for an oncogenic protein,[58] we found that breast and colon cancer patients with high tumor expression of IF1 have a better prognosis. There are other examples in the literature illustrating similar paradoxes. For instance, miR-200s that modulate the oxidative stress response increase tumor growth in mouse models.[59] However, a high expression of miR-200s is linked to a favorable prognosis,[60] whereas downregulation of miR-200s is associated with relapse in patients with ovarian cancer.[61] Similarly, isocitrate dehydrogenase mutations are paradoxically associated with better survival in glioma patients.[62] As a low expression of IF1 in carcinomas predicts a shorter time for relapse or death of the patient, we suggest that cells with low expression of IF1 are more likely to metastasize. In this regard, it is possible that cells with high expression of IF1, which have a low bioenergetic signature become more vulnerable to metabolic or other forms of stress during detachment and/or become more easily recognized by the immune system.[2] Indeed, cells with a low bioenergetic signature are addicted to glucose and are more sensitive to glucose deprivation and the inhibition of glycolysis.[24,63]

Overall, we document that the short-lived inhibitor of the mitochondrial H^+-ATP synthase is overexpressed in the colon, lung, breast and ovarian cancer mastering the reprogramming of energy metabolism and signaling a cell-death resistance phenotype. Moreover, we support its potential as a marker of clinical outcome in breast and colon cancer patients. We stress that specific studies and animals models are needed to unveil the molecular and cellular biology of IF1 in the different cell types of mammals.

MATERIALS AND METHODS

Patient specimens and protein extraction

Frozen tissue obtained from surgical specimens of untreated cancer patients with primary adenocarcinomas of the breast, colon, stomach, kidney and lung were obtained from the Banco de Tejidos y Tumores, IDIBAPS (Instituto de Investigaciones Biomédicas Pi y Suñer), Hospital Clinic, Barcelona, Spain.[64] A collection of frozen tissue sections obtained from surgical specimens of (i) ninety-three patients who had an operation for invasive breast carcinoma at the Hospital Universitario La Paz between 1991 and 2000[35,36] and (ii) of untreated cancer patients with primary colorectal adenocarcinomas enrolled in the incident Spanish CRC Epicolon Study and prospectively followed during 5 years[37,65] obtained from the Banco de Tejidos y Tumores, Hospital Meixoeiro, Vigo, Spain were also used (see Supplementary Information for Bioethic details).

Cell cultures, treatments, transfections and small interfering RNA silencing

The Human cervical (HeLa), breast (HS578T, NCI-ADR-RES, BT549, MCF12), lung (A549, HOP62), colon (KM12, HCT116) and ovarian (OVCAR8, OVCAR 3) cells were grown following the supplierś instructions. When needed, cells were left untreated or treated with 200 μM $CoCl_2$ (Sigma-Aldrich, St Louise, MO, USA) for 6 h. For inhibition of mitochondrial serine-proteases HCT116 cells were treated with 400 μM of 4-(2-aminoethyl) benzenosulfonyl fluoride hydrochloride for the indicated time. Transfection and silencing experiments were performed as recently described.[29]

Protein fractionation and western blots

Cell lysis and protein fractionation were carried out as described.[27] The primary antibodies used were: anti-β-actin (Sigma-Aldrich, 1:20000), anti-β-F1-ATPase (Acebo *et al.*[66] 1:20000), anti-IkBα and anti-Bcl-xL (Cell Signaling Technology, Inc., Danvers, MA, USA, 1:1000), anti-hypoxia-inducible factor-1α (Santa Cruz Biotechnology Inc., Dallas, TX, USA, 1:150) and anti-IF1 (Sanchez-Cenizo *et al.*[28] 1:200).

Immunohistochemistry

Cancer Survey Tissue Microarrays (OriGene (Rockville, MD, USA)) containing 5 μm sections of formalin-fixed normal and tumor specimens of the breast, colon, lung, kidney, ovarian and endometrial tissues were immunostained using the monoclonal anti-IF1 (1:200) antibody as previously described.[19] Sections were counterstained with hematoxylin.

Quantification of mRNA expression

Human β-F1-ATPase and IF1 mRNA levels in normal and tumor tissues were carried out by quantitative PCR using the breast (BCRT101), ovarian (HORT102), colon (HCRT103) and lung (HLRT104) TissueScan Tissue quantitative PCR Arrays from OriGene Technologies, Inc. For detailed pathological information of these patients see Supplementary Table S3. Real-time quantitative PCR was performed as described.[27] The following forward (F) and reverse (R) primers were used to amplify human β-F1-ATPase and IF1 cDNAs: F: 5′- CAGCAGATTTTGGCAGGTG-3′, R: 5′-CTTCAATG GGTCCCACCATA-3′; F: 5′-GGGCCTTCGGAAAGAGAG-3′ and R: 5′-TTCAAAGC TGCCAGTTGTTC-3′, respectively.

Metabolic labeling and immunoprecipitation

Metabolic labeling was initiated by addition to the culture medium 0.65 mCi of [^{35}S]-methionine/ml. Duration of the pulse was 1 h. At the indicated time-points IF1 was immunoprecipitated from cellular lysates using G-sepharose precoated with 12 μg of anti-IF1 IgGs.[67]

Quantification of IF1 in colorectal adenocarcinoma biopsies using reverse phase protein microarrays

IF1 was expressed and purified as detailed.[28] Samples from colorectal adenocarcinoma patients were diluted in PBS to a final protein concentration of 1 μg/μl before printing onto nitrocellulose-coated glass slides (FAST Slides, Scheleicher & Schuell BioScience, Inc.) using a BioOdyssey Calligrapher MiniArrayer printer (Bio-Rad Laboratories, Inc., Keene, NH, USA) as recently described.[37] Arrays were incubated with anti-IF1 (1 μg/ml) followed by incubation with a donkey anti-mouse conjugated with alexa-488 (Life Technologies, Grand Island, NY, USA). Microarrays were scanned using a Typhoon 9410 scanner (GE Healthcare Bio-Sciences Corp., Piscataway, NJ, USA). The mean fluorescent intensity of the spots was quantified using Image J software (N.I.H., USA) and converted into pg of protein/ng of total protein using the fluorescent intensity units obtained in the respective standard curve of recombinant protein.[37]

Bioinformatic Search of the *ATPIF1* gene

UCSC Genome Browser (http://genome.ucsc.edu/) was used. Chip-sep data was obtained from ENCODE database.

Determination of reactive oxygen species

Where indicated, $\sim 2 \times 10^5$ cells were incubated overnight with 10–20 nM of MQ. The intracellular production of superoxide radical was monitored by flow cytometry using 5 μM MitoSOX (Invitrogen) incubated 15 min at 37 °C.[29] Cells were analyzed in a FACScan. For each analysis 10 000 events were recorded.

Other methods

Details for the determination of aerobic glycolysis, proliferation, cell death and NFκB promoter activity have been recently provided.[29] Where indicated 5 nM of MQ was added to the incubation.

Statistical analysis

Distribution of molecular markers and other categorical variables were compared by χ^2 and Student's *t*-test. The statistical significance of linear regressions was assessed by Pearson's correlation *t*-test. To determine the association between the expression level of IF1 with disease-free survival and overall survival the cutoff point used to define high- and low-risk groups was the mean value of protein expression in normal breast or colon samples. Survival curves were derived from Kaplan–Meier estimates and compared by log-rank test. Statistical test were two-side at the 5% level of significance. All computations were carried out using SPSS, version 17.0 (IBM Corporation, Armonk, NY, USA).

CONFLICT OF INTEREST

The authors declare no conflict of interest.

ACKNOWLEDGEMENTS

We are indebted to Professor Manuel González-Barón and other members of the Oncopaz group for support and encouragement. We thank Mrs. Margarita Chamorro, Cristina Núñez de Arenas and Irma Joyce Diaz de Almeida for expert technical assistance. IMR, JGB, FS, IMW and LSC and were supported by predoctoral fellowships from JAE-CSIC (IMR), FPI-MEC (JGB, LSC), FPI-UAM (FS), FPU-MEC (IMW), Spain. LF is supported by a Juan de la Cierva Grant (JCI2009-03918) and Fundación Asociación Española Contra el Cáncer. This work was supported by grants from the Ministerio de Educación y Ciencia (BFU2010-18903), the Centro de Investigación Biomédica en Red de Enfermedades Raras (CIBERER), ISCIII, Madrid and Comunidad de Madrid (S2011/BMD-2402), Spain. The CBMSO receives an institutional grant from the Fundación Ramón Areces.

REFERENCES

1 Cuezva JM, Ortega AD, Willers I, Sanchez-Cenizo L, Aldea M, Sanchez-Arago M. The tumor suppressor function of mitochondria: translation into the clinics. *Biochim Biophys Acta* 2009; **1792**: 1145–1158.
2 Hanahan D, Weinberg RA. Hallmarks of cancer: the next generation. *Cell* 2011; **144**: 646–674.
3 Kroemer G, Pouyssegur J. Tumor cell metabolism: cancer's Achilles' heel. *Cancer Cell* 2008; **13**: 472–482.
4 Vander Heiden MG, Cantley LC, Thompson CB. Understanding the Warburg effect: the metabolic requirements of cell proliferation. *Science* 2009; **324**: 1029–1033.
5 Cairns RA, Harris IS, Mak TW. Regulation of cancer cell metabolism. *Nat Rev Cancer* 2011; **11**: 85–95.
6 Almeida A, Bolanos JP, Moncada S. E3 ubiquitin ligase APC/C-Cdh1 accounts for the Warburg effect by linking glycolysis to cell proliferation. *Proc Natl Acad Sci USA* 2010; **107**: 738–741.
7 Rodriguez-Paredes M, Esteller M. Cancer epigenetics reaches mainstream oncology. *Nat Med* 2011; **17**: 330–339.
8 Sharma SV, Lee DY, Li B, Quinlan MP, Takahashi F, Maheswaran S *et al.* A chromatin-mediated reversible drug-tolerant state in cancer cell subpopulations. *Cell* 2010; **141**: 69–80.
9 Bissell MJ, Hines WC. Why don't we get more cancer? A proposed role of the microenvironment in restraining cancer progression. *Nat Med* 2011; **17**: 320–329.
10 Sanchez-Arago M, Chamorro M, Cuezva JM. Selection of cancer cells with repressed mitochondria triggers colon cancer progression. *Carcinogenesis* 2010; **31**: 567–576.
11 Boyer PD. The ATP synthase. A splendid molecular machine. *Annu Rev Biochem* 1997; **66**: 717–749.
12 Matsuyama S, Xu Q, Velours J, Reed JC. The mitochondrial F0F1-ATPase proton pump is required for function of the proapoptotic protein Bax in yeast and mammalian cells. *Mol Cell* 1998; **1**: 327–336.
13 Santamaria G, Martinez-Diez M, Fabregat I, Cuezva JM. Efficient execution of cell death in non-glycolytic cells requires the generation of ROS controlled by the activity of mitochondrial H + -ATP synthase. *Carcinogenesis* 2006; **27**: 925–935.
14 Dey R, Moraes CT. Lack of oxidative phosphorylation and low mitochondrial membrane potential decrease susceptibility to apoptosis and do not modulate the protective effect of Bcl-x(L) in osteosarcoma cells. *J Biol Chem* 2000; **275**: 7087–7094.
15 Tomiyama A, Serizawa S, Tachibana K, Sakurada K, Samejima H, Kuchino Y *et al.* Critical role for mitochondrial oxidative phosphorylation in the activation of tumor suppressors Bax and Bak. *J Natl Cancer Inst* 2006; **98**: 1462–1473.
16 Schulz TJ, Thierbach R, Voigt A, Drewes G, Mietzner B, Steinberg P *et al.* Induction of oxidative metabolism by mitochondrial frataxin inhibits cancer growth: Otto Warburg revisited. *J Biol Chem* 2006; **281**: 977–981.
17 D'Errico I, Salvatore L, Murzilli S, Lo Sasso G, Latorre D, Martelli N *et al.* Peroxisome proliferator-activated receptor-gamma coactivator 1-alpha (PGC1alpha) is a metabolic regulator of intestinal epithelial cell fate. *Proc Natl Acad Sci USA* 2011; **108**: 6603–6608.
18 Sheffer M, Bacolod MD, Zuk O, Giardina SF, Pincas H, Barany F *et al.* Association of survival and disease progression with chromosomal instability: a genomic exploration of colorectal cancer. *Proc Natl Acad Sci USA* 2009; **106**: 7131–7136.
19 Cuezva JM, Krajewska M, de Heredia ML, Krajewski S, Santamaria G, Kim H *et al.* The bioenergetic signature of cancer: a marker of tumor progression. *Cancer Res* 2002; **62**: 6674–6681.
20 Lopez-Rios F, Sanchez-Arago M, Garcia-Garcia E, Ortega AD, Berrendero JR, Pozo-Rodriguez F *et al.* Loss of the mitochondrial bioenergetic capacity underlies the glucose avidity of carcinomas. *Cancer Res* 2007; **67**: 9013–9017.
21 Shin YK, Yoo BC, Chang HJ, Jeon E, Hong SH, Jung MS *et al.* Down-regulation of mitochondrial F1F0-ATP synthase in human colon cancer cells with induced 5-fluorouracil resistance. *Cancer Res* 2005; **65**: 3162–3170.
22 Hernlund E, Hjerpe E, Avall-Lundqvist E, Shoshan M. Ovarian carcinoma cells with low levels of beta-F1-ATPase are sensitive to combined platinum and 2-deoxy-D-glucose treatment. *Mol Cancer Ther* 2009; **8**: 1916–1923.
23 Li RJ, Zhang GS, Chen YH, Zhu JF, Lu QJ, Gong FJ *et al.* Down-regulation of mitochondrial ATPase by hypermethylation mechanism in chronic myeloid leukemia is associated with multidrug resistance. *Ann Oncol* 2010; **7**: 1506–1514.
24 Sanchez-Arago M, Cuezva JM. The bioenergetic signature of isogenic colon cancer cells predicts the cell death response to treatment with 3-bromopyruvate, iodoacetate or 5-fluorouracil. *J Transl Med* 2011; **9**: 19.
25 de Heredia ML, Izquierdo JM, Cuezva JM. A conserved mechanism for controlling the translation of beta-F1-ATPase mRNA between the fetal liver and cancer cells. *J Biol Chem* 2000; **275**: 7430–7437.
26 Willers IM, Isidoro A, Ortega AD, Fernandez PL, Cuezva JM. Selective inhibition of beta-F1-ATPase mRNA translation in human tumours. *Biochem J* 2010; **426**: 319–326.
27 Ortega AD, Willers IM, Sala S, Cuezva JM. Human G3BP1 interacts with beta-F1-ATPase mRNA and inhibits its translation. *J Cell Sci* 2010; **123**: 2685–2696.
28 Sanchez-Cenizo L, Formentini L, Aldea M, Ortega AD, Garcia-Huerta P, Sanchez-Arago M *et al.* Up-regulation of the ATPase inhibitory factor 1 (IF1) of the

mitochondrial H + -ATP synthase in human tumors mediates the metabolic shift of cancer cells to a Warburg phenotype. *J Biol Chem* 2010; **285**: 25308–25313.
29 Formentini L, Sánchez-Aragó M, Sánchez-Cenizo L, Cuezva JM. The mitochondrial ATPase Inhibitory Factor 1 (IF1) triggers a ROS-mediated retrograde pro-survival and proliferative response. *Mol Cell* 2012; **45**: 731–742.
30 Huang LJ, Chuang IC, Dong HP, Yang RC. Hypoxia-inducible factor 1alpha regulates the expression of the mitochondrial ATPase inhibitor protein (IF1) in rat liver. *Shock* 2011; **36**: 90–96.
31 Shen L, Zhi L, Hu W, Wu MX. IEX-1 targets mitochondrial F1Fo-ATPase inhibitor for degradation. *Cell Death Differ* 2009; **16**: 603–612.
32 Koppen M, Langer T. Protein degradation within mitochondria: versatile activities of AAA proteases and other peptidases. *Crit Rev Biochem Mol Biol* 2007; **42**: 221–242.
33 Formentini L, Martinez-Reyes I, Cuezva JM. The mitochondrial bioenergetic capacity of carcinomas. *IUBMB Life* 2010; **62**: 554–560.
34 Kelso GF, Porteous CM, Coulter CV, Hughes G, Porteous WK, Ledgerwood EC *et al.* Selective targeting of a redox-active ubiquinone to mitochondria within cells: antioxidant and antiapoptotic properties. *J Biol Chem* 2001; **276**: 4588–4596.
35 Isidoro A, Casado E, Redondo A, Acebo P, Espinosa E, Alonso AM *et al.* Breast carcinomas fulfill the Warburg hypothesis and provide metabolic markers of cancer prognosis. *Carcinogenesis* 2005; **26**: 2095–2104.
36 Ortega AD, Sala S, Espinosa E, Gonzalez-Baron M, Cuezva JM. HuR and the bioenergetic signature of breast cancer: a low tumor expression of the RNA-binding protein predicts a higher risk of disease recurrence. *Carcinogenesis* 2008; **29**: 2053–2061.
37 Aldea M, Clofent J, Nunez de Arenas C, Chamorro M, Velasco M, Berrendero JR *et al.* Reverse phase protein microarrays quantify and validate the bioenergetic signature as biomarker in colorectal cancer. *Cancer Lett* 2011; **311**: 210–218.
38 Cabezon E, Montgomery MG, Leslie AG, Walker JE. The structure of bovine F1-ATPase in complex with its regulatory protein IF1. *Nat Struct Biol* 2003; **10**: 744–750.
39 Ichikawa N, Nakabayashi K, Hashimoto T. A yeast mitochondrial ATPase inhibitor interacts with three proteins that are easy to dissociate from the mitochondrial inner membrane. *J Biochem* 2002; **132**: 649–654.
40 Lopez-Mediavilla C, Vigny H, Godinot C. Docking the mitochondrial inhibitor protein IF1 to a membrane receptor different from the F1-ATPase beta subunit. *Eur J Biochem* 1993; **215**: 487–496.
41 Grisolía S, Hernandez-Yago J, Knecht E. Regulation of mitochondrial protein concentration: a plausible model which may permit assessing protein turnover. *Curr Top Cell Regul* 1985; **27**: 387–396.
42 Izquierdo JM, Cuezva JM. Control of the translational efficiency of beta-F1-ATPase mRNA depends on the regulation of a protein that binds the 3′ untranslated region of the mRNA. *Mol Cell Biol* 1997; **17**: 5255–5268.
43 Willers IM, Martínez-Reyes I, Martínez-Diez M, Cuezva J. miR-127-5p targets the 3′UTR of human β-F1-ATPase mRNA and inhibits its translation. *Biochim Biophys Acta-Bioenergetics* 2012; **1817**: 838–848.
44 Han L, Geng L, Liu X, Shi H, He W, Wu MX. Clinical significance of IEX-1 expression in ovarian carcinoma. *Ultrastruct Pathol* 2011; **35**: 260–266.
45 Sasada T, Azuma K, Hirai T, Hashida H, Kanai M, Yanagawa T *et al.* Prognostic significance of the immediate early response gene X-1 (IEX-1) expression in pancreatic cancer. *Ann Surg Oncol* 2008; **15**: 609–617.
46 Bakala H, Delaval E, Hamelin M, Bismuth J, Borot-Laloi C, Corman B *et al.* Changes in rat liver mitochondria with aging. Lon protease-like reactivity and N(epsilon)-carboxymethyllysine accumulation in the matrix. *Eur J Biochem* 2003; **270**: 2295–2302.
47 Stanyer L, Jorgensen W, Hori O, Clark JB, Heales SJ. Inactivation of brain mitochondrial Lon protease by peroxynitrite precedes electron transport chain dysfunction. *Neurochem Int* 2008; **53**: 95–101.
48 Flynn JM, Neher SB, Kim YI, Sauer RT, Baker TA. Proteomic discovery of cellular substrates of the ClpXP protease reveals five classes of ClpX-recognition signals. *Mol Cell* 2003; **11**: 671–683.
49 Mootha VK, Bunkenborg J, Olsen JV, Hjerrild M, Wisniewski JR, Stahl E *et al.* Integrated analysis of protein composition, tissue diversity, and gene regulation in mouse mitochondria. *Cell* 2003; **115**: 629–640.
50 Butow RA, Avadhani NG. Mitochondrial signaling: the retrograde response. *Mol Cell* 2004; **14**: 1–15.
51 Hamanaka RB, Chandel NS. Mitochondrial reactive oxygen species regulate cellular signaling and dictate biological outcomes. *Trends Biochem Sci* 2010; **35**: 505–513.
52 Finkel T. Signal transduction by reactive oxygen species. *J Cell Biol* 2011; **194**: 7–15.
53 Karin M. Nuclear factor-kappaB in cancer development and progression. *Nature* 2006; **441**: 431–436.
54 Morgan MJ, Liu ZG. Crosstalk of reactive oxygen species and NF-kappaB signaling. *Cell Res* 2011; **21**: 103–115.
55 Meylan E, Dooley AL, Feldser DM, Shen L, Turk E, Ouyang C *et al.* Requirement for NF-kappaB signalling in a mouse model of lung adenocarcinoma. *Nature* 2009; **462**: 104–107.
56 Ishikawa K, Takenaga K, Akimoto M, Koshikawa N, Yamaguchi A, Imanishi H *et al.* ROS-generating mitochondrial DNA mutations can regulate tumor cell metastasis. *Science* 2008; **320**: 661–664.
57 Weinberg F, Hamanaka R, Wheaton WW, Weinberg S, Joseph J, Lopez M *et al.* Mitochondrial metabolism and ROS generation are essential for Kras-mediated tumorigenicity. *Proc Natl Acad Sci USA* 2010; **107**: 8788–8793.
58 Sanchez-Arago M, Formentini L, Garcia-Bermudez J, Cuezva JM. IF1 reprograms energy metabolism and signals the oncogenic phenotype in cancer. *Cell Cycle* 2012; **11**: 2963–2964.
59 Mateescu B, Batista L, Cardon M, Gruosso T, de Feraudy Y, Mariani O *et al.* miR-141 and miR-200a act on ovarian tumorigenesis by controlling oxidative stress response. *Nat Med* 2011; **17**: 1627–1635.
60 Hu X, Macdonald DM, Huettner PC, Feng Z, El Naqa IM, Schwarz JK *et al.* A miR-200 microRNA cluster as prognostic marker in advanced ovarian cancer. *Gynecol Oncol* 2009; **114**: 457–464.
61 Marchini S, Cavalieri D, Fruscio R, Calura E, Garavaglia D, Nerini I *et al.* Association between miR-200c and the survival of patients with stage I epithelial ovarian cancer: a retrospective study of two independent tumour tissue collections. *Lancet Oncology* 2011; **12**: 273–285.
62 Parsons DW, Jones S, Zhang X, Lin JC, Leary RJ, Angenendt P *et al.* An integrated genomic analysis of human glioblastoma multiforme. *Science* 2008; **321**: 1807–1812.
63 Pelicano H, Martin DS, Xu RH, Huang P. Glycolysis inhibition for anticancer treatment. *Oncogene* 2006; **25**: 4633–4646.
64 Isidoro A, Martinez M, Fernandez PL, Ortega AD, Santamaria G, Chamorro M *et al.* Alteration of the bioenergetic phenotype of mitochondria is a hallmark of breast, gastric, lung and oesophageal cancer. *Biochem J* 2004; **378**: 17–20.
65 Jover R, Zapater P, Castells A, Llor X, Andreu M, Cubiella J *et al.* The efficacy of adjuvant chemotherapy with 5-fluorouracil in colorectal cancer depends on the mismatch repair status. *Eur J Cancer* 2009; **45**: 365–373.
66 Acebo P, Giner D, Calvo P, Blanco-Rivero A, Ortega AD, Fernandez PL *et al.* Cancer abolishes the tissue type-specific differences in the phenotype of energetic metabolism. *Transl Oncol* 2009; **2**: 138–145.
67 Martinez-Reyes I, Sanchez-Arago M, Cuezva JM. AMPK and GCN2-ATF4 signal the repression of mitochondria in colon cancer cells. *Biochem J* 2012; **444**: 249–259.

Supplementary Information accompanies this paper on the Oncogenesis website (http://www.nature.com/oncsis).

Supplemental Material

Title: Expression, regulation and clinical relevance of the ATPase Inhibitory Factor 1 (IF1) in human cancers.

Authors: María Sánchez-Aragó, Laura Formentini, Inmaculada Martínez-Reyes, Javier García-Bermudez, Fulvio Santacatterina, Laura Sánchez-Cenizo, Imke M. Willers, Marcos Aldea**,** Laura Nájera, Ángeles Juarránz, Estela C. López, Juan Clofent, Carmen Navarro, Enrique Espinosa and José M. Cuezva

Bioethics. Patients' medical records were reviewed and identifiers coded to protect patient confidentiality. Anonymized and coded normal and tumor samples supplied by (i) the Banco de Tejidos y Tumores of the IDIBAPS (Instituto de Investigaciones Biomédicas Pi y Suñer), Hospital Clinic, Barcelona, (ii) the Hospital Universitario La Paz, Madrid and (iii) Banco de Tejidos y Tumores, Hospital Meixoeiro, Vigo, Spain were provided with informed consent from the patients and obtained after approval of the corresponding Institutional Review Board. The overall project was approved by the Ethical Committee of the Universidad Autónoma de Madrid (CEI-24-571).

Supplemental Results and Discussion

The very large increase of IF1 observed in prevalent human carcinomas posed the question of the mechanism(s) that might control the expression of this gene in cancer. *In silico* analysis of the promoter region of the human IF1 gene (ATPIF1) revealed the existence of potential *cis*-acting responsive elements for transcription factors involved in cancer. Data from high-throughput ChiP-sequencing confirmed the binding of several transcription factors involved in the regulation of cell cycle (NF-YB, NF-YA, Ini1, TAF1), proliferation (c-FOS, Sp1, c-MYC), inflammation and cell death (NFκB) in the proximal promoter region of ATPIF1 gene (Supplemental Fig. S1). Consistent with the mitochondrial location of IF1 (1) its promoter also binds NRF1 (Supplemental Fig. S1); a transcription factor that controls the expression of nuclear genes required for mitochondrial biogenesis and function (2). However, and despite the

binding of relevant transcription factors involved in proliferation and cancer progression in the proximal promoter region of the ATPIF1 gene the regulation of IF1 expression in colon, lung, breast and ovarian carcinomas is not exerted at the transcriptional and/or mRNA levels as revealed by the lack of changes in the availability of IF1 mRNA observed in these tumors (see Fig. 3A in main paper).

To explore the possible connection between HIF-1α, a main driver in tumor hypoxia and a suggested regulator of IF1 expression (3), we studied the effect of treatment of different cancer cells with the hypoxic mimetic $CoCl_2$ (Supplemental Fig. S2). Consistent with previous findings by others we observed the rapid induction of HIF-1α in all cancer cells studied in response to $CoCl_2$ treatment (Supplemental Fig. S2). However, the expression of IF1 was not affected (Supplemental Fig. S2) suggesting the unlikely association of hypoxia with IF1 expression.

References

1. Sanchez-Cenizo L, Formentini L, Aldea M, Ortega AD, Garcia-Huerta P, Sanchez-Arago M *et al.* Up-regulation of the ATPase inhibitory factor 1 (IF1) of the mitochondrial H+-ATP synthase in human tumors mediates the metabolic shift of cancer cells to a Warburg phenotype. *J Biol Chem* 2010; **285**: 25308-25313.

2. Scarpulla RC. Transcriptional paradigms in mammalian mitochondrial biogenesis and function. *Physiol Rev* 2008; **88**: 611-638.

3. Huang LJ, Chuang IC, Dong HP and Yang RC. Hypoxia-inducible factor 1alpha regulates the expression of the mitochondrial ATPase inhibitor protein (IF1) in rat liver. *Shock* 2011; **36**: 90-96.

Supplemental Table S1. Summary of the clinical-pathological characteristics and IF1 expression level in tumors of breast cancer patients. No. indicates the number of biopsies in each group. Others, mostly mixed invasive and lobular carcinomas. The expression level of IF1 is expressed in arbitrary units as the mean ± SEM. In normal biopsies IF1 expression was below 0.06 arbitrary units. *, $P<0.05$ when compared to ductal histology and negative hormone receptor as assessed by Student's t test.

Characteristics	No.	IF1		
Age				
<50	33	0.77	±	0.19
≥50	60	0.83	±	0.15
Histology				
Ductal	79	0.88	±	0.13
Lobular	9	0.19	±	0.06*
Others	5	0.78	±	0.39
No. Nodes				
0	45	0.88	±	0.19
1-3	30	0.73	±	0.19
>3	18	0.75	±	0.22
Size				
<20mm	29	1.07	±	0.27
≥20mm	64	0.69	±	0.12
Stage				
I	17	1.28	±	0.36
II	54	0.72	±	0.15
III	22	0.68	±	0.18
Grade				
N/A	14	0.25	±	0.07
1	8	1.24	±	0.56
2	28	0.91	±	0.26
3	43	0.85	±	0.16
Hormonal Receptor				
Negative	18	0.38	±	0.09
Positive	75	0.91	±	0.14*

Supplemental Table S2. Summary of the clinicopathological characteristics and IF1 expression in normal and tumor biopsies of colon cancer patients. The expression of IF1 was determined as indicated in Supplemental Fig. S3 and is expressed in pg/ng protein in the biopsy. The results shown are mean ± S.E.M. *, $p < 0.05$ by Student's t-test when compared with normal.

Characteristics		No.	IF1 (pg/ng protein)
Normal		36	2.21 ± 0.12
Tumor		38	3.59 ± 0.36*
Sex			
	female	13	3.31 ± 0.60
	male	25	3.71 ± 0.46
Age			
	< 70	15	3.00 ± 0.24
	≥ 70	23	3.97 ± 0.57
Histology			
	colon	27	3.17 ± 0.30
	rectum	11	4.60 ± 0.98
Nodes			
	no	17	3.71 ± 0.61
	yes	21	3.48 ± 0.44
Stage			
	I	4	3.96 ± 1.57
	II	10	3.29 ± 0.75
	III	16	4.19 ± 0.58
	IV	8	2.56 ± 0.38
Grade			
	1	6	2.79 ± 0.35
	2	27	3.89 ± 0.50
	3	5	2.89 ± 0.72

Supplemental Table S3: Summary of the clinicopathological characteristics of the cohort of breast, lung, colon and ovarian cancer patients studied for analysis of the expression of IF1 mRNA. IDC, infiltrating ductal carcinoma; AC, adenocarcinoma; SCC, squamous cell carcinoma; LC, large cell carcinoma.

Breast		**Lung**		**Colon**		**Ovarian**	
Histology	**No.**	**Histology**	**No.**	**Histology**	**No.**	**Histology**	**No.**
Normal	6	Normal	24	Normal	22	Normal	8
IDC	40	AC	11	AC	22	AC	40
		SCC	7				
		LC	6				
Stage	**No.**	**Stage**	**No.**	**Stage**	**No.**	**Stage**	**No.**
I	10	IA	4	I	4	IA, IB, IC	8
IIA	13	IB	4	IIA	5	IIA, IIB, IIC	9
IIB	6	IIA	2	III	1	III	3
IIIA	7	IIB	8	IIIA	1	IIIA	4
IIIB	1	IIIA	3	IIIB	5	IIIB	4
IIIC	3	IIIB	3	IIIC	2	IIIC	6
				IV	4	IV	6
Grade	**No.**	**Grade**	**No.**	**Grade**	**No.**	**Grade**	**No.**
1	1	1	2	1	6	1	1
2	12	2	8	2	13	2	13
3	20	3	12	3	1	3	22
N/R	7	N/R	2	N/R	2	N/R	4
Node metastasis	**No.**	**Node metastasis**	**No.**	**Node metastasis**	**No.**	**Node metastasis**	**No.**
NO	18	NO	7	NO	11	NO	4
YES	17	YES	14	YES	9	YES	7
N/R	5	N/R	3	N/R	2	N/R	29

Supplemental Figure Legends

Supplemental Figure S1. Summary of Chip-seq analysis of the ATPIF1 gene promoter. Schematic of the binding site and affinities (1 to 3 stars = low to high) of the transcription factors that interact with the proximal promoter of the ATPIF1 gene. Data used was obtained from Chip-seq experiments taken from ENCODE whole genome data compiled in the UCSC Genome Browser.

Supplemental Figure S2. Colon (HCT116), ovarian (OVCAR8), lung (HOP62) and breast (BT549) cancer cells were treated (+) with 200 μM of the hypoxia mimetic $CoCl_2$ or left untreated (-, CRL) and the expression of HIF-1α and IF1 analyzed by western blot. Lanes 1 and 2, show different experiments of the same condition. β-actin expression is shown as loading control. The histograms illustrate the expression of HIF-1α and IF1 relative to the expression of β-actin. The results shown are the mean±S.E.M. *, $P<0.05$ when compared to CRL by Student's t test. Note that the induction of HIF-1α is not accompanied by relevant changes in IF1 expression in any of the cell lines studied.

Supplemental Figure S3. IER3 is overexpressed in human carcinomas. A, Representative western blots of the expression of IER3 using rabbit anti IER3 antibody (Sigma) and β-F1-ATPase in paired normal (N, closed bars) and tumor (T, open bars) biopsies of breast, colon and lung cancer patients. The number of patients analyzed is indicated (n). IER3 expression in tumors is normalized relative to the expression in normal tissues. * $p<0.05$ when compared to normal samples. **B**, HCT116 cells were transfected with 100 nM control siCRL or siIER3 siRNA (Ambion, s16940). The expression of IER3, IF1 and β-actin was analyzed by western blot. Histograms show the relative expression of IER3 and IF1. Bars are the mean ± SEM of 4 independent determinations.

Supplemental Figure S4. Cell-type specific regulation of cellular proliferation by IF1. Colon (HCT116, SW620), lung (HOP62, A549), breast (BT549) and ovarian (OVCAR8) cancer

cells transfected with CDL-GFP-β-3'UTR and co-transfected with control (CRL, open and light grey bars) or IF1 plasmid (IF1, dark grey and closed bars) in the absence or presence (+MQ) of 5 nM of the mitochondrial ROS scavenger MitoQ (MQ). Cellular proliferation was assessed by the incorporation of EdU into cellular DNA. The data shown are mean±S.E.M. of six-twelve samples. *, $P<0.05$ and $^{\#}$, $P<0.05$ when compared to CRL or IF1 by Student's t test, respectively.

Supplemental Figure S5. Quantification of IF1 in normal and tumor biopsies of CRC patients. Paired normal (N, black boxed) and tumor (T, red boxed) biopsies of each CRC patient (P1 to P40) were spotted in duplicate. Increasing amounts of BSA (0-1 μg/μl), extracts from HCT116 cells (0-1 μg/μl) and of the recombinant IF1 (r-IF1) protein (0-10 ng/μl) were also spotted in the same array. A representative *Reverse Phase Protein Microarray* of IF1 is shown. Highly significant linear correlations exist between the fluorescence intensity (arbitrary units) of the spots and the amount of recombinant protein or native protein in HCT116 lysates. Protein concentration in the biopsies (see Supplemental Table S2) was calculated according to the fluorescence intensity obtained in r-IF1 plot.

Supplementary Figure S1

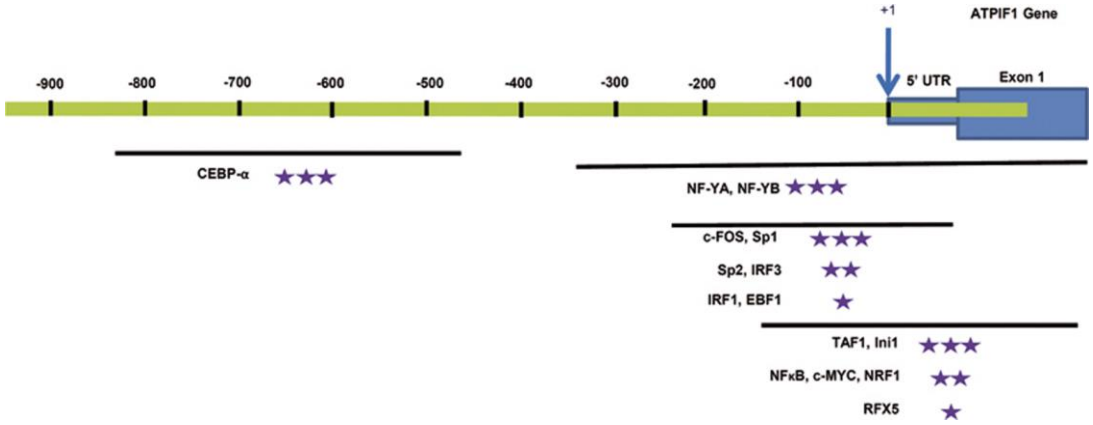

Supplementary Figure S2

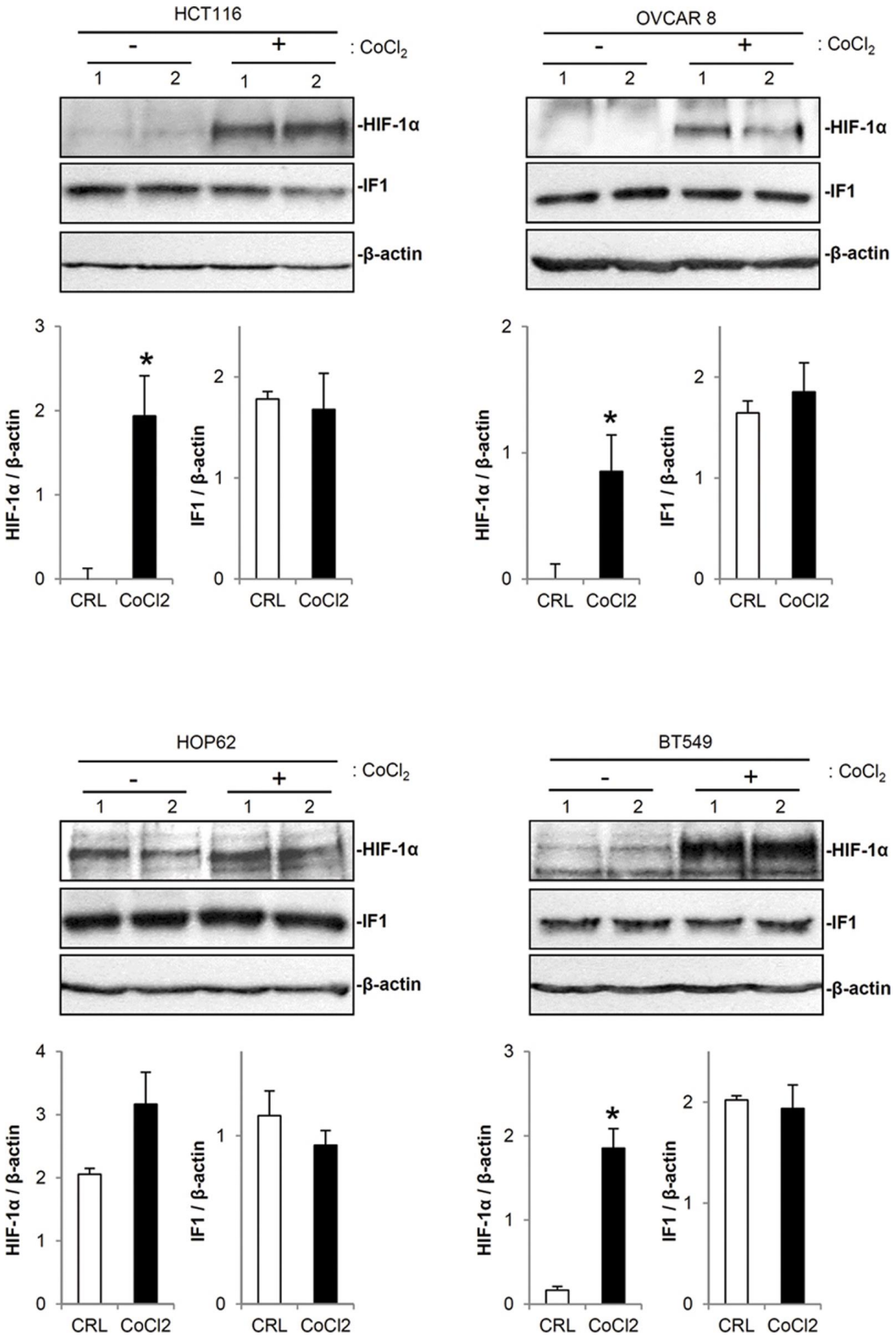

Supplementary Figure S3

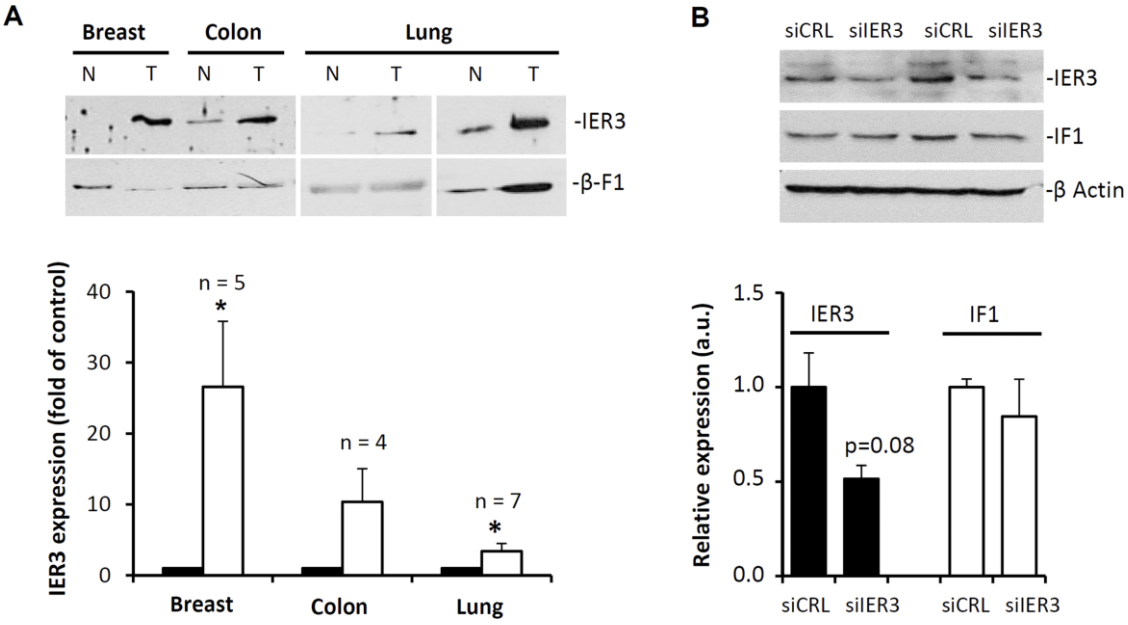

Supplementary Figure S4

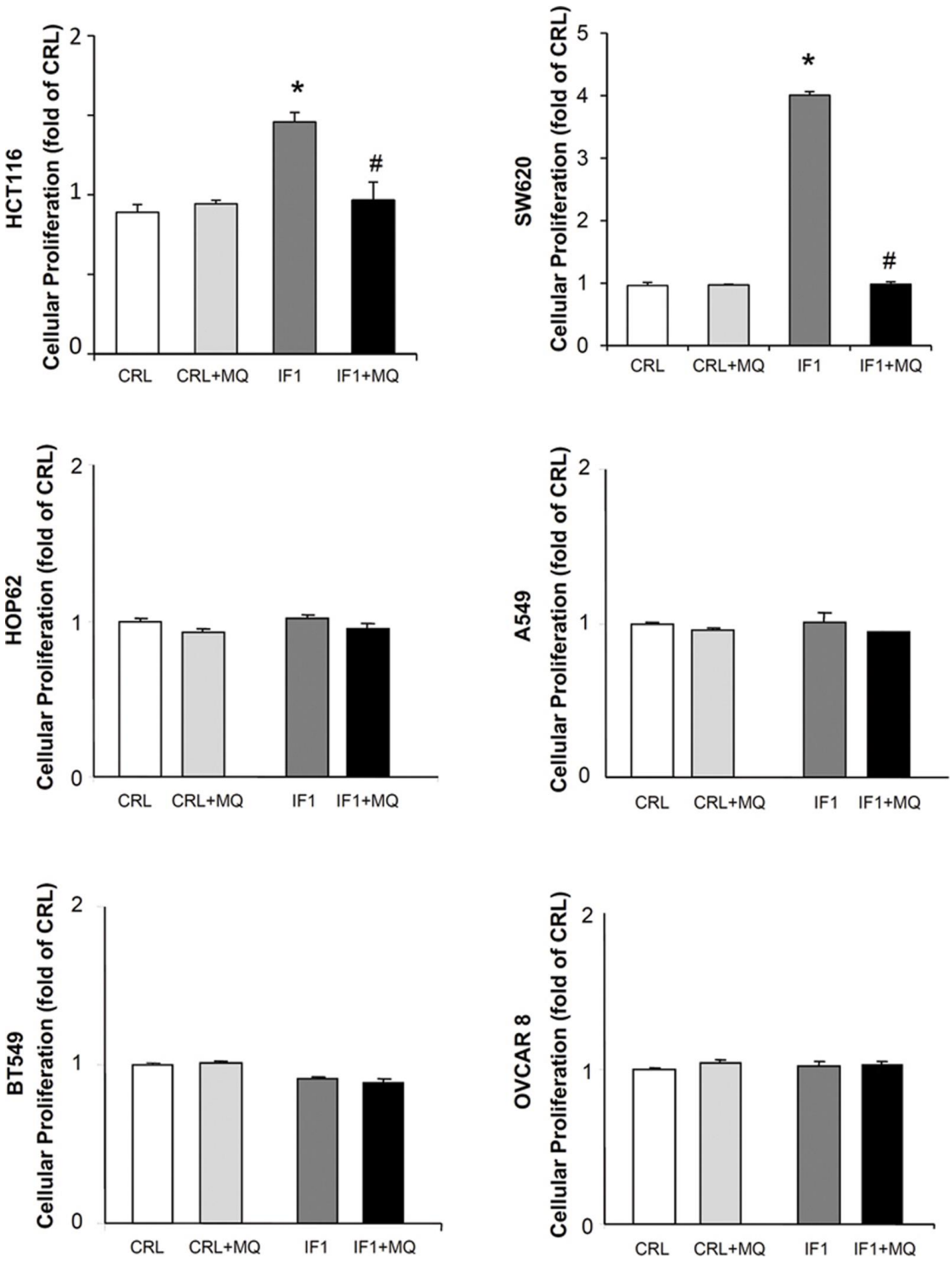

Supplementary Figure S5

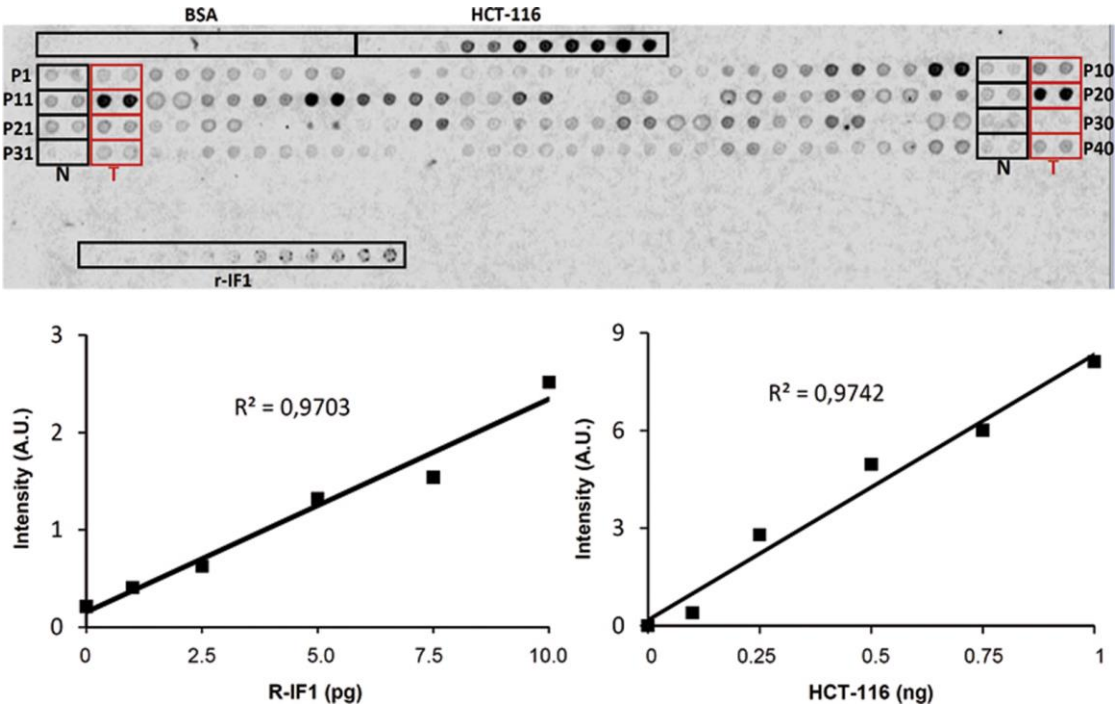

Artículo #2

Santacatterina, F., Sánchez-Cenizo, L., Formentini, L., Mobasher, M.A., Casas, E., Rueda, C.B., Martínez-Reyes, I., Núñez de Arenas, C., García-Bermúdez, J., Zapata, J.M., Sánchez-Aragó, M., Satrústegui, J., Valverde, Á.M., Cuezva, J.M. (2016) Down-regulation of oxidative phosphorylation in the liver by expression of the ATPase inhibitory factor 1 induces a tumor-promoter metabolic state. *Oncotarget.* 5;7(1):490-508.

Down-regulation of oxidative phosphorylation in the liver by expression of the ATPase inhibitory factor 1 induces a tumor-promoter metabolic state

Fulvio Santacatterina[1,2,3,*], Laura Sánchez-Cenizo[1,2,3,*], Laura Formentini[1,2,3,*], Maysa A. Mobasher[4,5], Estela Casas[1,2,3], Carlos B. Rueda[1,2,6], Inmaculada Martínez-Reyes[1,2,3], Cristina Núñez de Arenas[1,2], Javier García-Bermúdez[1,2,3], Juan M. Zapata[4], María Sánchez-Aragó[1,2,3], Jorgina Satrústegui[1,2,6], Ángela M. Valverde[4,5] and José M. Cuezva[1,2,3]

[1] Departamento de Biología Molecular, Centro de Biología Molecular Severo Ochoa, CSIC-UAM, Madrid, Spain

[2] Centro de Investigación Biomédica en Red de Enfermedades Raras (CIBERER), Madrid, Spain

[3] Centro de Investigación Hospital 12 de Octubre, ISCIII, Madrid, Spain

[4] Instituto de Investigaciones Biomédicas Alberto Sols, CSIC-UAM, Madrid, Spain

[5] Centro de Investigación Biomédica en Red de Diabetes y Enfermedades Metabólicas Asociadas (CIBERDEM), Madrid, Spain

[6] Instituto de Investigación Sanitaria Fundación Jiménez Díaz (IIS-FJD), Madrid, Spain

[*] These authors have equally contributed to this work

***Correspondence to**: José M. Cuezva, **email**: jmcuezva@cbm.csic.es*

Keywords: ATPase inhibitory factor 1, cancer, energy metabolism, mitochondria, reactive oxygen species

***Received**: June 30, 2015* ***Accepted**: November 14, 2015* ***Published**: November 22, 2015*

ABSTRACT

The ATPase Inhibitory Factor 1 (IF1) is an inhibitor of the mitochondrial H^+-ATP synthase that regulates the activity of both oxidative phosphorylation (OXPHOS) and cell death. Here, we have developed transgenic Tet-On and Tet-Off mice that express a mutant active form of hIF1 in the hepatocytes to restrain OXPHOS in the liver to investigate the relevance of mitochondrial activity in hepatocarcinogenesis. The expression of hIF1 promotes the inhibition of OXPHOS in both Tet-On and Tet-Off mouse models and induces a state of metabolic preconditioning guided by the activation of the stress kinases AMPK and p38 MAPK. Expression of the transgene significantly augmented proliferation and apoptotic resistance of carcinoma cells, which contributed to an enhanced diethylnitrosamine-induced liver carcinogenesis. Moreover, the expression of hIF1 also diminished acetaminophen-induced apoptosis, which is unrelated to differences in permeability transition pore opening. Mechanistically, cell survival in hIF1-preconditioned hepatocytes results from a nuclear factor-erythroid 2-related factor (Nrf2)-guided antioxidant response. The results emphasize *in vivo* that a metabolic phenotype with a restrained OXPHOS in the liver is prone to the development of cancer.

INTRODUCTION

Mitochondria play key roles in cell metabolism and bioenergetics, mediate intracellular signaling by calcium and reactive oxygen species (ROS) and regulate the execution of cell-death [1]. Most of the ATP that is required to maintain cellular activities is synthesized by the mitochondrial H^+-ATP synthase [2]. Down-regulation of oxidative phosphorylation (OXPHOS) and the concurrent activation of aerobic glycolysis is a hallmark of proliferating cancer cells [1, 3] whereas an increase in oxidative metabolism halts cellular proliferation and tumor progression [1, 4, 5]. The activity of OXPHOS is required for the execution of cell death [1, 6] and in particular, the ATP synthase is needed for the execution of apoptosis [7] as recently demonstrated in neurons *in vivo*

[8]. In fact, the ATP synthase is a critical component in the permeabilization of the inner mitochondrial membrane to low molecular weight solutes, i.e., in the opening of the permeability transition pore (PTP) [9-11]. Not surprisingly, inhibition of the ATP synthase is involved in lifespan extension [12, 13] illustrating the relevance of this protein complex in aging and age-related diseases.

In mitochondria, futile ATP hydrolysis by the ATP synthase is inhibited by the ATPase Inhibitory Factor 1 (IF1) a small nuclear-encoded protein that reversibly binds to the enzyme [2]. Data obtained in cancer [14, 15], in stem cells [16], and in a mouse model over-expressing an active form of IF1 in neurons[8], support that *in vivo* IF1 also inhibits the synthase activity of the ATP synthase. The IF1-mediated inhibition of the ATP synthase prevents cell death [8, 14, 17]. Remarkably, IF1 is highly over-expressed in human carcinomas [14, 15, 18]. In hepatocarcinomas the over-expression of IF1 favors angiogenesis and metastasis [19].

Herein, we have questioned: What is the relevance of a metabolic phenotype with a restrained OXPHOS in cancer onset and progression *in vivo?* To that aim we have generated transgenic mice that express a mutant active form of human IF1 (hIF1) under a tetracycline regulated promoter in hepatocytes. We show that expression of the transgene promotes inhibition of OXPHOS and a higher susceptibility to diethyl-nitrosamine (DEN)-induced carcinogenesis. Mechanistically, an enhanced carcinogenesis in hepatocytes of hIF1 expressing mice involves an enhanced proliferation and the down-regulation of the potential to execute cell death as further illustrated *in vivo* in a model of acetaminophen (APAP)-induced hepatotoxic damage. Cell survival in hIF1 expressing hepatocytes is not mediated by differential regulation of PTP opening in response to APAP treatment but by the induction of a nuclear factor-erythroid 2-related factor (Nrf2)-guided antioxidant response. These findings emphasize that metabolic preconditioning by restraining OXPHOS is deleterious in the context of liver cancer because it limits cell death favoring the progression of oncogenic events.

RESULTS

In vivo IF1-mediated inhibition of OXPHOS in the liver of Tet-Off mice

Breeding of mice expressing the tTA transactivator in liver with transgenic mice containing the human IF1-H49K transgene (hIF1) resulted in double transgenic mice (T/H). The double transgenic animals (T/H) expressed hIF1 in the absence of Doxycycline (Dox) administration as revealed by the presence of hIF1 mRNA and protein levels in their livers (Figure 1A). Expression of hIF1 is restricted to mitochondria of hepatocytes (Figure 1B) and negatively regulated by the administration of Dox as revealed by qPCR and western blotting (Figure 1A), confocal microscopy (Figure 1B, panels to the left) and immunohistochemistry (Figure 1B, panels to the right). The expression of hIF1 had no impact on the expression level of relevant mitochondrial proteins of different OXPHOS complexes (Figure 1C). Isolated liver mitochondria from adult T/H mice revealed that both the ADP-stimulated respiration and the maximum respiratory rates were significantly reduced when compared to littermate controls (Figure 1D). In addition, liver ATP concentrations were diminished in T/H mice (Figure 1E). An overnight fast of adult Tet-Off T/H mice promoted a significant reduction in blood glucose and lactate concentrations (Figure 1F).

In vivo IF1-mediated inhibition of OXPHOS in the liver of Tet-On mice

Breeding of mice expressing the rtTA-Adv transactivator in liver with transgenic mice containing the human IF1-H49K transgene (hIF1) (Supplemental Figure S1A) resulted in double transgenic mice (T/H) (Supplemental Figure S1B) able to express hIF1 in the liver only in response to the administration of doxycycline (Dox) (Supplemental Figure S1B). The expression level of hIF1 varied among different T/H mice (Supplemental Figure S1B) and was higher than that of the endogenous IF1 present in mouse liver of control littermates (Supplemental Figure S1C). Expression of hIF1 was preferentially concentrated in perivenous hepatocytes (Supplemental Figure S1D) and had no impact on the expression level of relevant mitochondrial proteins of different OXPHOS complexes (Supplemental Figure S1E). T/H mice showed no differences in weight, life span and cage behavior when compared to controls after one year of follow up. However, and consistent with the inhibitory role of IF1 on the activity of the H^+-ATP synthase we observed that both the basal and the ADP-stimulated respiration in isolated mitochondria from adult livers of T/H mice was significantly reduced when compared to controls (Supplemental Figure S1F). A significant decrease in the maximum respiratory rate was also noted in mitochondria of T/H mice (Supplemental Figure S1F). Overall, these findings indicate that expression of hIF1 is partially arresting both respiration and ADP phosphorylation in liver mitochondria.

In agreement with a partial energy deficit in the liver of T/H mice we observed: (i) reduced ATP and increased AMP contents in their livers (Supplemental Figure S2A), (ii) a significant increase in the AMP/ATP ratio (Supplemental Figure S2A) and (iii) the activation by phosphorylation of the metabolic stress kinase AMPK (Supplemental Figure S2B), when compared to liver of controls. The pyruvate content was also diminished

in the liver of T/H mice (Supplemental Figure S2C). Other liver organic acids showed no relevant differences (Supplemental Figure S2C). Blood glucose and lactate concentrations were not significantly different between fed T/H and control mice (Supplemental Figure S2D). However, an overnight fast promoted a marked hypoglycaemia (Supplemental Figure S2E) and hypolactatemia (Supplemental Figure S2E) in T/H mice. The liver of 15 day-old T/H neonates revealed a significant induction of mitochondrial superoxide dismutase (SOD2) (Supplemental Figure S2F). Functionally, induction of SOD2 in liver of T/H mice was expressed by less carbonylation of some cellular proteins when compared to livers of control mice (Supplemental Figure S2G). These results suggest that a limited OXPHOS by the expression of hIF1 in the liver of T/H mice compromises the energy supply needed for normal activity of gluconeogenesis and eventually favors the utilization of lactate for oxidative purposes in extrahepatic tissues during fasting. Overall, using two different experimental systems to regulate the expression of hIF1 in mouse liver we show that its expression triggers an energy deficit in the hepatocytes by inhibiting the activity of OXPHOS. Dox is known to induce the arrest of mitochondrial protein translation [20, 21], and eventually, to promote the unfolded protein response in mitochondria (UPRmt) [22]. Since we obtained similar findings with a Tef-Off mouse model (Figure 1), we ruled out any role for Dox in triggering metabolic adaptation by unleashing the UPRmt.

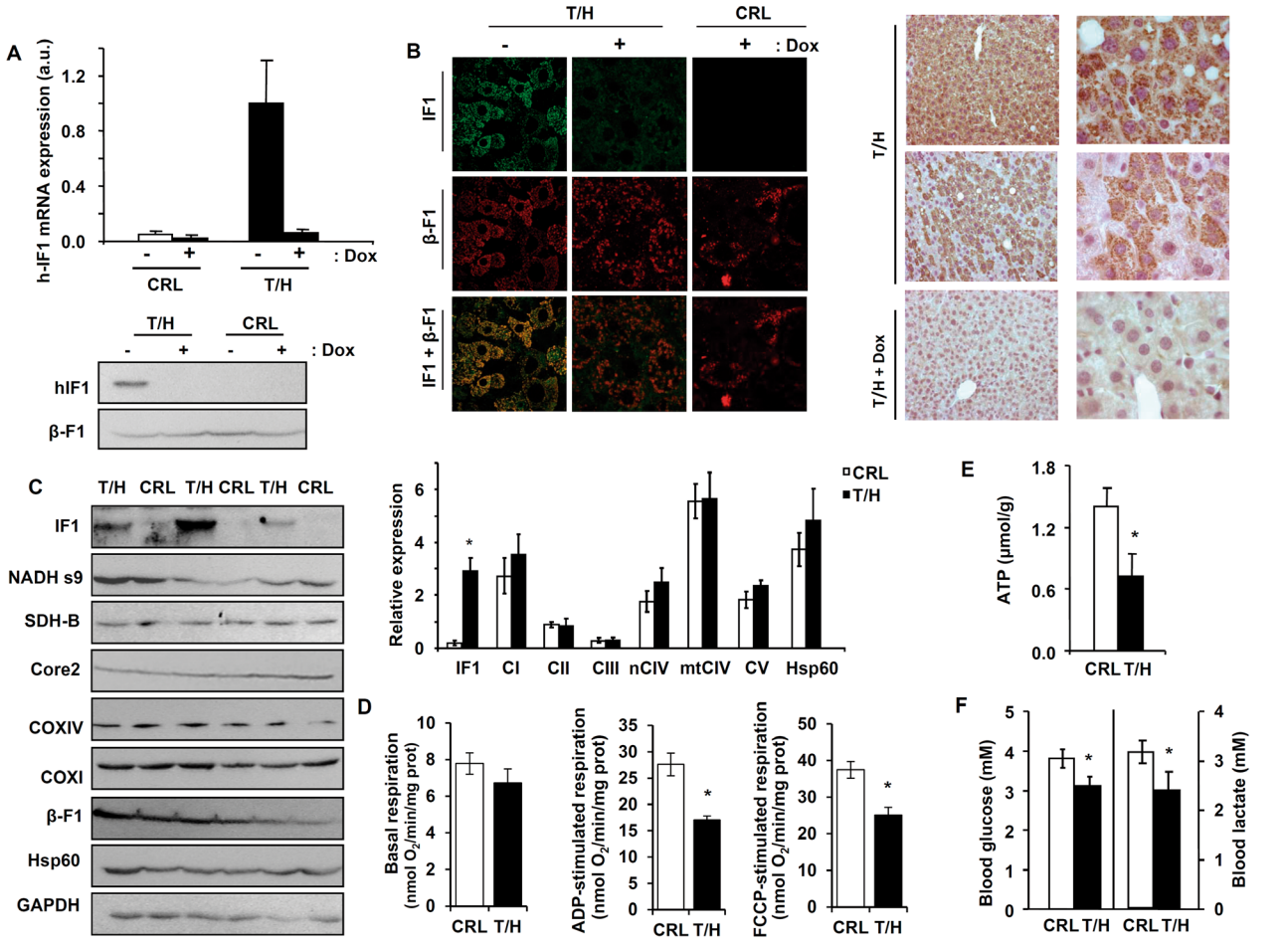

Figure 1: OXPHOS is inhibited in the liver of mice expressing hIF1. Only the double transgenic animals (T/H) expressed hIF1 in the absence of Doxycycline (Dox) administration. **A**. hIF1 mRNA expression in the liver of control (CRL) and T/H mice. Blot of hIF1 (12 kDa) and β-F1-ATPase (β-F1) in T/H and CRL mice. **B**. Double-immunofluorescence microscopy (63X) of liver from CRL and T/H mice stained with IF1 (green) and β-F1-ATPase (red) antibodies. Merged images (IF1+β-F1). Immunohistochemistry for hIF1 in the liver of T/H mice at 20X and 63X magnification. **C**. Blots of hIF1, complex I (NADH s9), complex II (SDH-B), complex III (Core2), complex IV (COXI and COX IV) and complex V (β-F1), Hsp60 and GAPDH in liver extracts of CRL and T/H mice. Histograms to the right show the relative expression of each protein normalized to GAPDH expression. **D**. Polarographic determination of basal, ADP-stimulated and FCCP-stimulated respiration in isolated liver mitochondria of CRL and T/H mice. The results are the mean ± SEM of 8 mice per group. **E**. ATP concentration in liver extracts of CRL and T/H mice. The results shown are the mean ± SEM of 5 mice per group. **F**. Blood glucose and lactate concentrations of fasted CRL and T/H mice. Histograms are the mean ± SEM of 12-14 mice per group. (C-F) *, $p < 0.05$ when compared to control by Student's t test. See also Figures S1 and S2.

Expression of hIF1 affects the activity and assembly of Complex IV and Complex V

Isolated liver mitochondria from both the hIF1 expressing Tet-On and Tet-Off mice revealed reduced activities of Complex IV and V when compared to controls (Figure 2A). In contrast, the activities of Complex I and II+III were not significantly affected by the expression of hIF1 (Figure 2A). Interestingly, a significant correlation between the inhibition of Complex V and Complex IV activities was observed (Figure 2A). In-gel activity of complexes I and IV revealed that whereas the activity of Complex I was not modified in hIF1 expressing Tet-Off mice, the activity of Complex IV and its super-complexes were very much reduced (Figure 2B). A similar study to assess the oligomycin (OL)-sensitive ATP hydrolase activity in super-complexes confirmed that hIF1 expressing mice had reduced ATPase activity despite essentially containing the same amount of the β-catalytic subunit of the complex in ATPase oligomers (Figure 2C).

Western blotting of BN-gels appears to confirm that the assembly of Complex IV was reduced in both mouse models of hIF1 expressing mice because its monomeric form was diminished when compared to that of controls (Figure 2D), what is in agreement with the reduced Complex IV activity observed in these animals (Figure 2A, 2B). Likewise, the expression of hIF1 in the liver of both Tet-On and Tet-Off mice promoted the assembly of a low migrating super-complex that contained complex V and might represent dimers of the ATP synthase ($(CV)_2$ in Figure 2D). Trypsin digestion and mass spectrometric analysis of the three upper bands recognized by anti-β-F1-ATPase antibody supported these results and revealed that the major component of the SC band in Figure 2D is Complex I (see Supplemental Table SI).

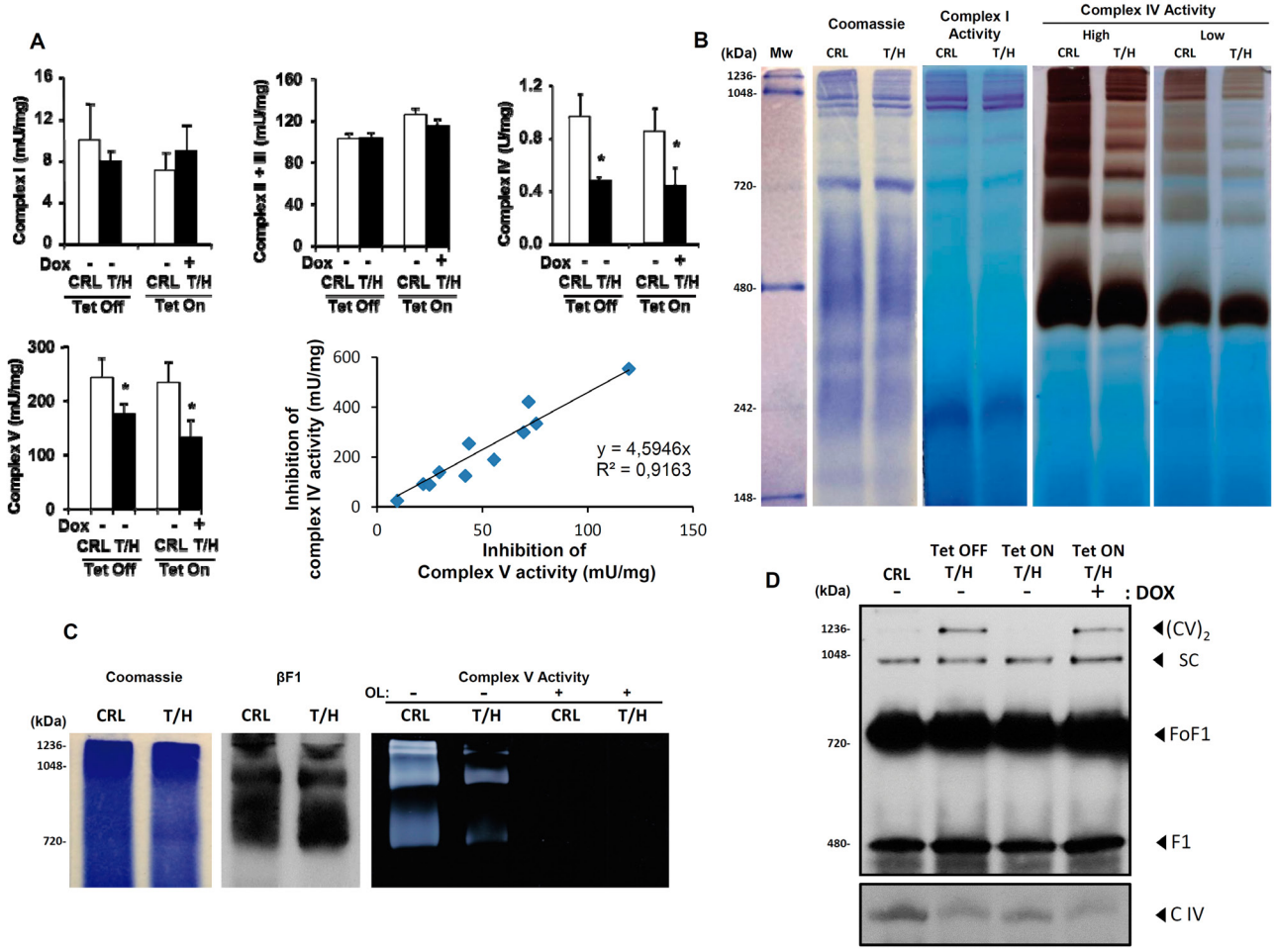

Figure 2: Activities and assembly of OXPHOS complexes in the liver of hIF1 mice. A. Enzymatic activities of complex I, II+III, IV and V in isolated liver mitochondria of CRL and T/H mice. Histograms are the mean ± SEM of 3 experiments. *, $p<0.05$ when compared to control by Student's t test. Linear correlation between the inhibition of Complex V activity by hIF1 and the inhibition of Complex IV activity. **B**. BN-PAGE-in-gel-activities of Complex I and Complex IV (low and high exposures). **C**. CN-PAGE immunoblot analysis of β-F1-ATPase (βF1) and CN-PAGE-in-gel-activity of complex V in the presence (+) or absence (-) of oligomycin (OL). **D**. BN-PAGE immunoblot analysis of mitochondrial complexes IV (COX IV) and V (β-F1-ATPase). The migration of dimers of ATP synthase $(CV)_2$, supercomplex (SC), ATP synthase (FoF1), F1-ATPase (F1) and complex IV (C IV) is indicated. See also Supplemental Table S1.

A diminished activity of OXPHOS favors hepatocarcinogenesis

A preliminary experiment of DEN-induced hepatocarcinogenesis by single injection of DEN [23] was initially done in a small number of mice (Supplemental Figure S3). Hepatocarcinogenesis was further studied with the long-term DEN administration protocol [24] (Figure 3) because it leads to a higher tumor incidence in a shorter time span [25]. Both protocols provided the same findings (Figure 3 and Supplemental Figure S3). Dox administration slightly reduced the body weight of the animals (Figure 3A). In contrast, the liver weight of DEN-treated mice and especially of those expressing hIF1 was significantly augmented when compared to the rest of the animals (T/H minus Dox in Figure 3B). The increase in liver weight of mice expressing hIF1 was accompanied by a significant progressive increase in blood glutamate-pyruvate transaminase (GPT) activity towards the end of the study (Figure 3C and see Supplemental Figures S3C and S4). Consistent with these observations both the number of tumors and total tumor volume were significantly increased in hIF1 expressing mice (Figure 3D). Dox administration reduced the number of tumors and total tumor volume both in control and hIF1 silenced T/H mice (Figure 3D). The higher tumor burden of mice expressing the transgene resulted from increased rates of proliferation (Figure 4A) and diminished apoptosis (Figure 4B, 4C) as assessed by immunohistochemical analysis of the carcinomas. Overall, these findings indicate *in vivo* the oncogenic role of IF1 and that limiting the activity of OXPHOS in the liver favors cancer onset and progression.

The mitochondrial phenotype in hepatocarcinogenesis

Immunohistochemical, electron microscopy and molecular analysis of the livers revealed that long-term DEN-induced hepatocarcinogenesis in mice largely reproduced the findings on the mitochondrial phenotype previously reported in human hepatocarcinomas [26]. In fact, it was observed that tumor areas in both T/H

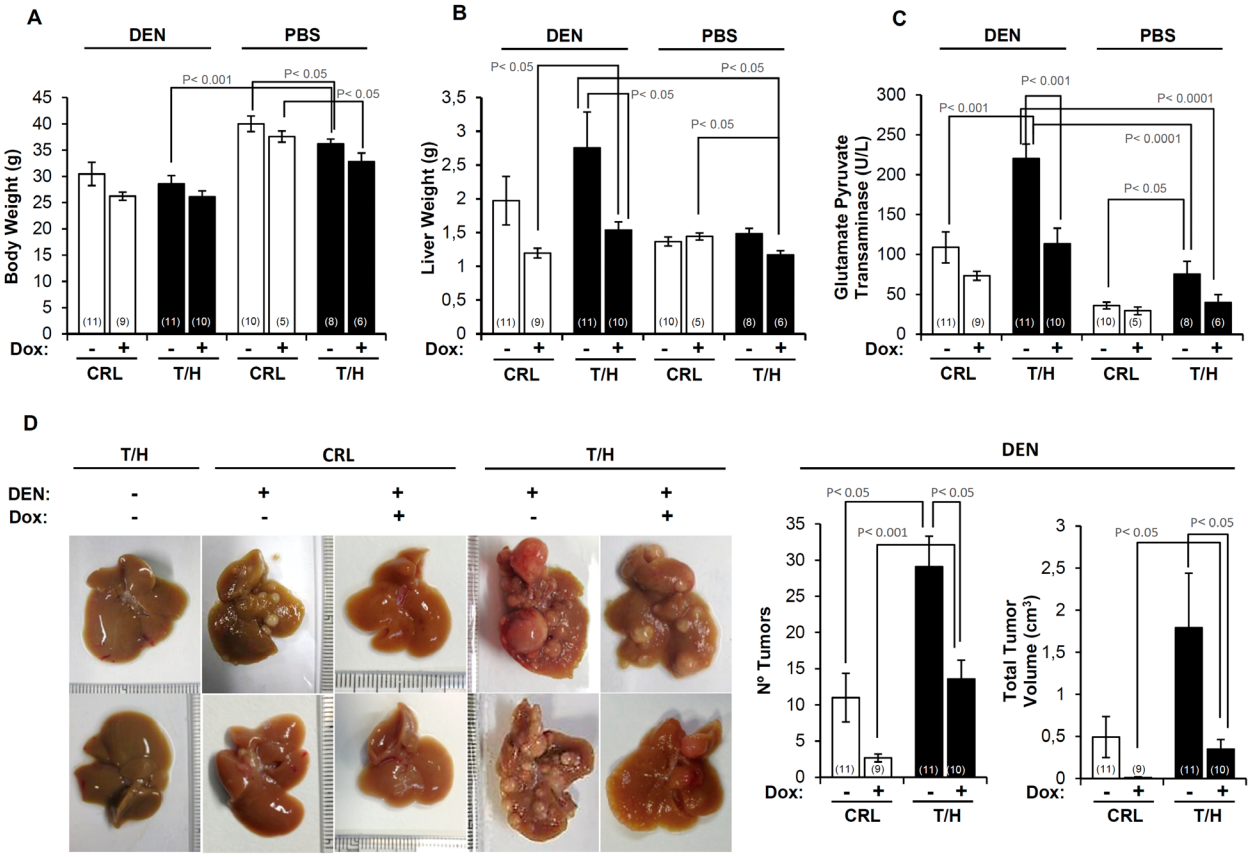

Figure 3: The expression of hIF1 increased DEN-induced hepatocarcinogenesis (HCC). A.-C. Changes in body weight (A), liver weight (B) and blood GPT (C) in PBS or DEN-treated CRL (open bars) and hIF1 Tet-Off T/H (closed bars) mice, treated in presence (+) or absence (-) of Dox. **D**. CRL and T/H livers of mice treated (+) or not treated (-) with DEN. The effect of Dox administration (+) or not (-) is also shown. The number of tumors and the total tumor volume in DEN-treated CRL (open bars) and T/H (closed bars) mouse livers treated (+) or not (-) with Dox. The number of mice is indicated in parenthesis. Results are means ± SEM. P values by Student's t test are indicated.

(Figure 5A) and CRL (Supplemental Figure S5A) were largely devoid of immunostaining for mitochondrial proteins such as β-F1-ATPase, Hsp60 and IF1, suggesting that progression of liver cancer is concurrent with the repression of mitochondrial biogenesis [26]. We observed no relevant differences in the expression of the glycolytic markers GAPDH and LDHA as assessed by inmmunohistochemical (IHC) (Figure 5A and Supplemental Figure S5A). However, since IHC is a qualitative technique we assessed protein expression by western blotting normal and tumor tissue of CRL and T/H mice (Supplemental Figure S5B). The results obtained indicate that carcinogenesis promoted the down-regulation of β-F1-ATPase expression concurrently with the upregulation of GAPDH in the absence of relevant changes in the expression of Hsp60 and LDHA (Supplemental Figure S5C). As a result the bioenergetic signature of the tumors, as assessed by the β-F1-ATPase/GAPDH ratio [26, 27] was significantly diminished when compared to the signature in normal tissues (Supplemental Figure S5C). Overall, we should mention that we did not observe differences in protein expression in the analysis of focal hepatic lesions between control and transgenic animals (Figure 5A and Supplemental Figure S5A).

Determination of mtDNA content in T/H mice revealed a very large reduction of mtDNA in liver tumors when compared to the normal tissue of the same liver (Figure 5B). This finding was further confirmed by assessing the lower cellular content and alteration of mitochondrial structure in these carcinomas by electron microscopy (Figure 5C), confirming the repression of mitochondrial biogenesis in hepatocarcinogenesis [26]. Consistent with the above findings, the expression of the transcriptional co-activator required in mitochondrial biogenesis PGC1α was significantly reduced in mouse carcinomas when compared to normal liver samples (Figure 5D).

Moreover, since DEN-induced hepatocarcinogenesis is an example of inflammation-driven tumorigenesis we also analyzed macrophage recruitment to focal hepatic lesions in CRL and T/H mice using the F4/80 antibody. The results reveal that there are no differences in macrophage recruitment to the tumor areas between control and T/H mice (Supplemental Figure S6).

Limiting OXPHOS minimizes apoptotic cell-death

To provide further mechanistic insight into the main pathway that might participate in the hIF1-mediated stimulation of liver cancer we studied the cell-death response of control and T/H mice to liver induced injury by APAP [28]. APAP overdose promoted a clear centrilobular hepatic cell death at 8h post-administration that was more evident in livers of control than of T/H mice (Figure 6A). Analysis of cell death by terminal deoxynucleotidyl transferase-mediated dUTP nick end labeling (TUNEL) (Figure 6B) and active caspase 3 (Figure 6C) revealed that

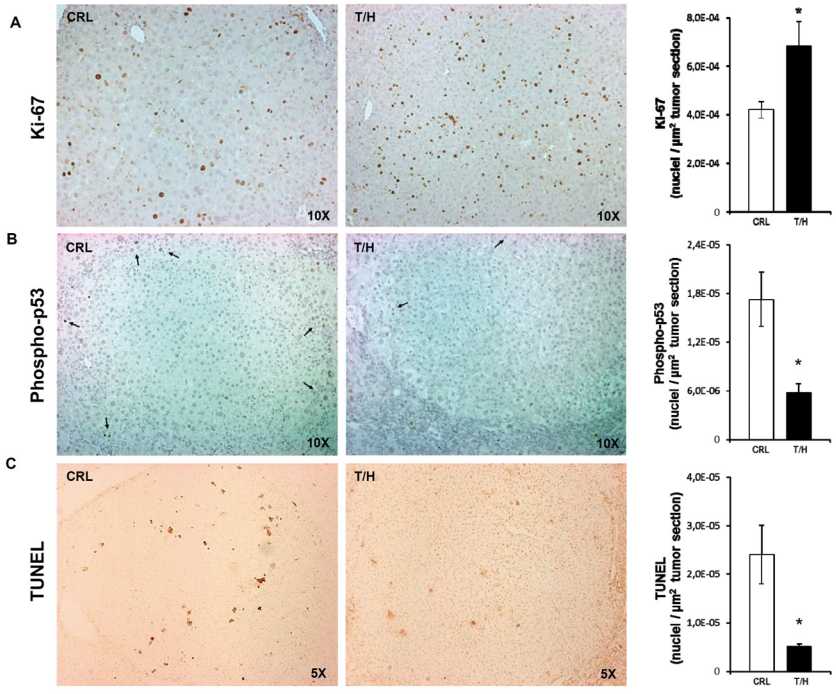

Figure 4: Expression of hIF1 promotes increased proliferation and apoptotic resistance of HCC. A.-C. Liver sections of DEN-treated CRL and hIF1 Tet-Off T/H mice were processed for immunohistochemistry to assess the rates of proliferation (A, Ki-67 staining) and apoptosis (B, phospho-p53 and C, TUNEL) in HCC. Magnification 5x-10x. Bars are the mean ± SEM of 6 mice per group. *, $p<0.05$ when compared to CRL by Student's *t* test.

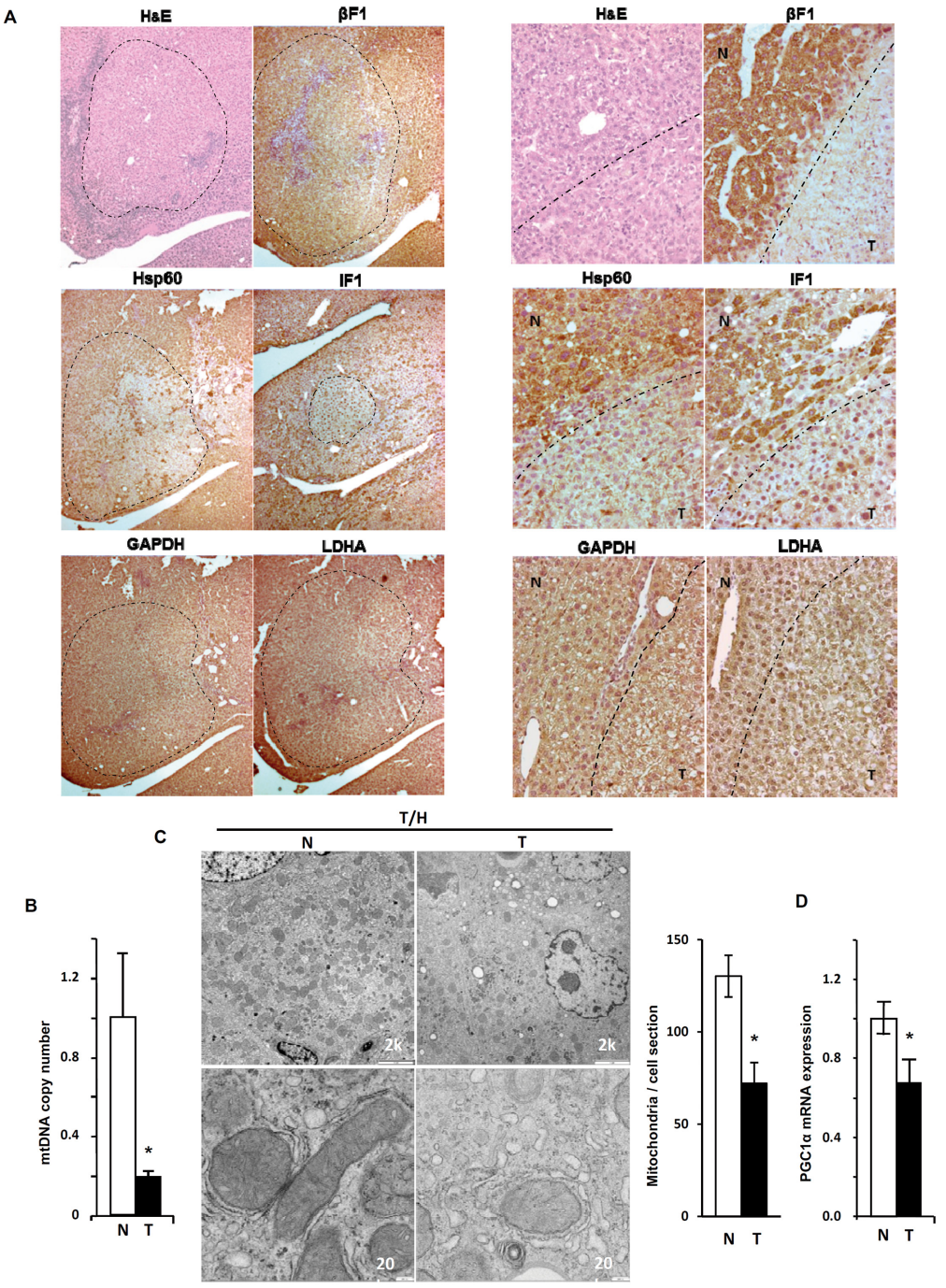

Figure 5: Repression of mitochondrial biogenesis in DEN-induced hepatocarcinogenesis (HCC). A. Focal hepatic lesions (magnification 5x) in long-term DEN-treated T/H mice identified by hematoxylin-eosin (H&E) and immunohistochemical staining with the antibodies against β-F1-ATPase (β-F1); Hsp60; hIF1; GAPDH and LDHA in the same localized tumor area (panels to the left). The same study in normal (N, upper left) and tumor (T, lower right) areas at 20X magnification (panels to the right). A dashed line marks the border between tumor and non-tumor areas. **B**. mtDNA copy number in DNA extracted from normal (N) and tumor (T) liver tissue of hIF1 expressing T/H mice. Results are means ± SEM for 6-7 animals. *P < 0.05 when compared with normal by Student's t test. **C**. Representative electron micrographs of normal (N) and tumor (T) tissue of the liver of hIF1 expressing T/H mice. Mitochondria of the hepatocytes in normal liver showed its characteristic high electron density and inner membrane cristae (left panels), whereas mitochondria are barely identifiable in the tumor tissue (right panels). Scale bars: 2k (upper panels); 20k (lower panels). Histograms show the number of mitochondria / cell section in normal (N) and tumor (T) tissue in T/H mice. Results are means ± SEM of five different sections from 3 animals. *$P < 0.05$ when compared with normal by Student's t test. **D**. Cellular mRNA expression of PGC1α in normal (N) and tumor (T) tissue of hIF1 expressing T/H mice. Results are means ± SEM of 6 experiments.*, $P < 0.05$ when compared with normal by Student's *t* test.

APAP promoted a higher increase in cell death in control than in T/H mice, strongly supporting that mice with a limited OXPHOS are partially protected from apoptotic cell death. Consistent with previous findings regarding the lower carbonylation observed in liver proteins of T/H mice in the Tet-On model (Supplemental Figure S2G), we noted that the oxidation of liver proteins both under basal conditions and in response to APAP treatment was less pronounced in adult Tet-Off T/H mice (Figure 6D).

The PTP is not involved in protection against death

Findings in different experimental settings support the role of OXPHOS [1, 6, 29] and of the H^+-ATP synthase [7, 30] in cell death. Moreover, it has been reported that the PTP is formed by the H^+-ATP synthase itself [9-11, 31, 32]. To verify the putative implication of the PTP

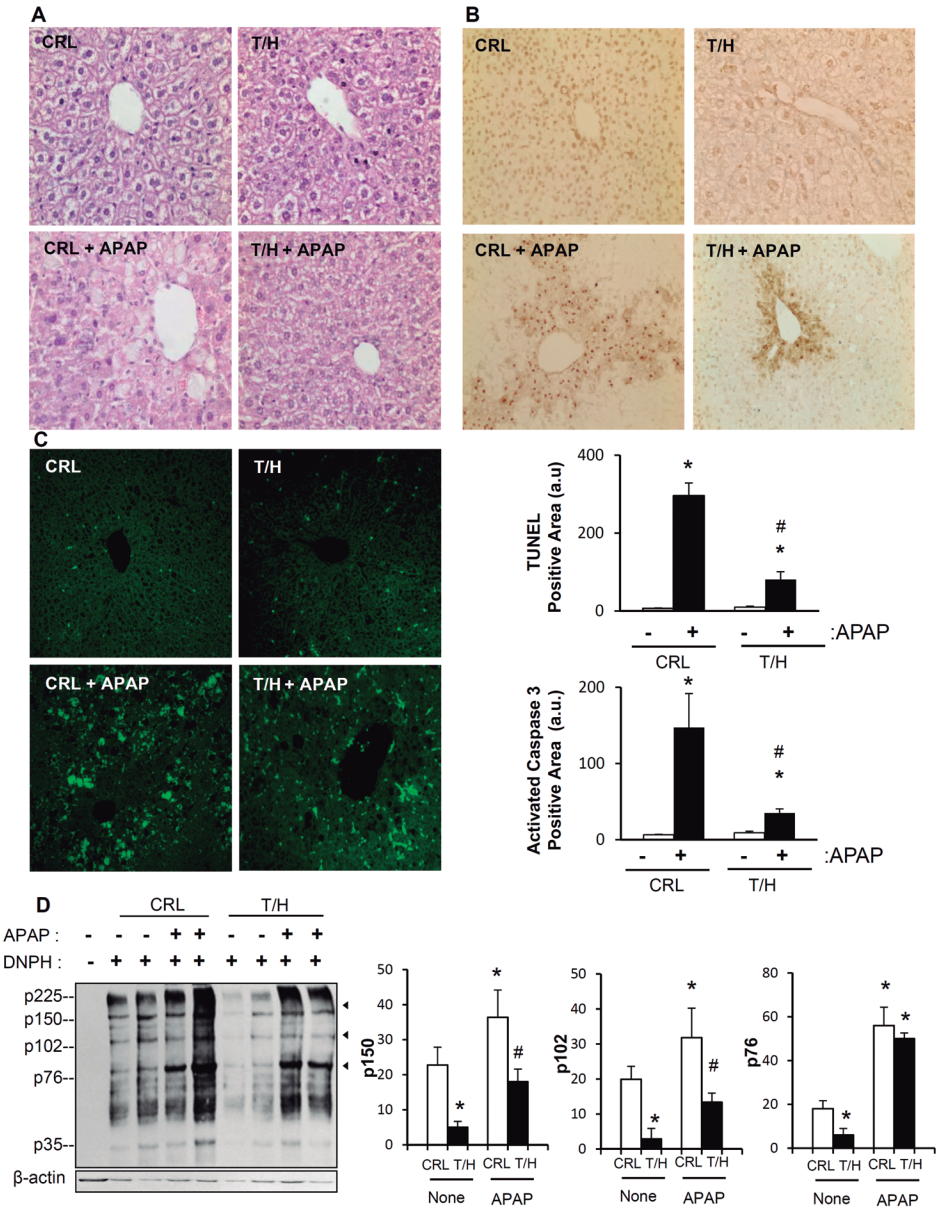

Figure 6: Restraining OXPHOS protects from APAP-induced cell death. Control (CRL) and hIF1 (T/H) mice were i.p. injected with APAP (+) or saline (-). Hematoxylin-eosin **A**., TUNEL **B**. and active caspase 3 **C**. staining in liver sections. Magnification 20x. Bars are the mean ± SEM of 6 mice per group. (B,C) *, p<0.05 when compared to non-treated (-) and #, p<0.05 when compared to CRL-APAP treated by Student's t test. **D**. Carbonylation of liver proteins from CRL and hIF1 (T/H) mice treated (+) or non-treated (-) with APAP is shown. The derivation of samples in the presence (+) or absence (-) of DNPH was used for the identification of protein carbonyls. Arrowheads (to the right) identify the migration of the three proteins used in quantification (histograms) of protein carbonylation. The results shown are the mean ± SEM of six CRL and eight T/H mice, respectively. *, $p < 0.05$ when compared to non-treated (-) and #, $p < 0.05$ when compared to CRL-APAP treated by Student's t test.

in the differential response to cell death between both mice phenotypes we studied the Ca^{2+}-retention capacity (Figure 7A-7C) and Ca^{2+}-induced swelling (Figure 7D-7F) of isolated mitochondria from livers of control and hIF1 expressing mice. No relevant differences were observed in any of these parameters between mitochondria of control and T/H mice (Figure 7A & 7D). Moreover, both cyclosporine A (CsA) (Figure 7B & 7E) and ATP-Mg (Figure 7C & 7F), which are known inhibitors of PTP opening [9], exerted the same regulation of the PTP in control and T/H mice. These findings support that inhibition of cell death by IF1 [8, 14, 17] is unrelated with PTP opening. Dimers of the ATP synthase have been shown to be required for PTP formation [11, 32]. Moreover, it has been suggested that IF1 regulates the oligomeric state of the ATP synthase increasing the formation of dimeric ATP synthase complexes and cristae density [33, 34]. Our observation that the expression of

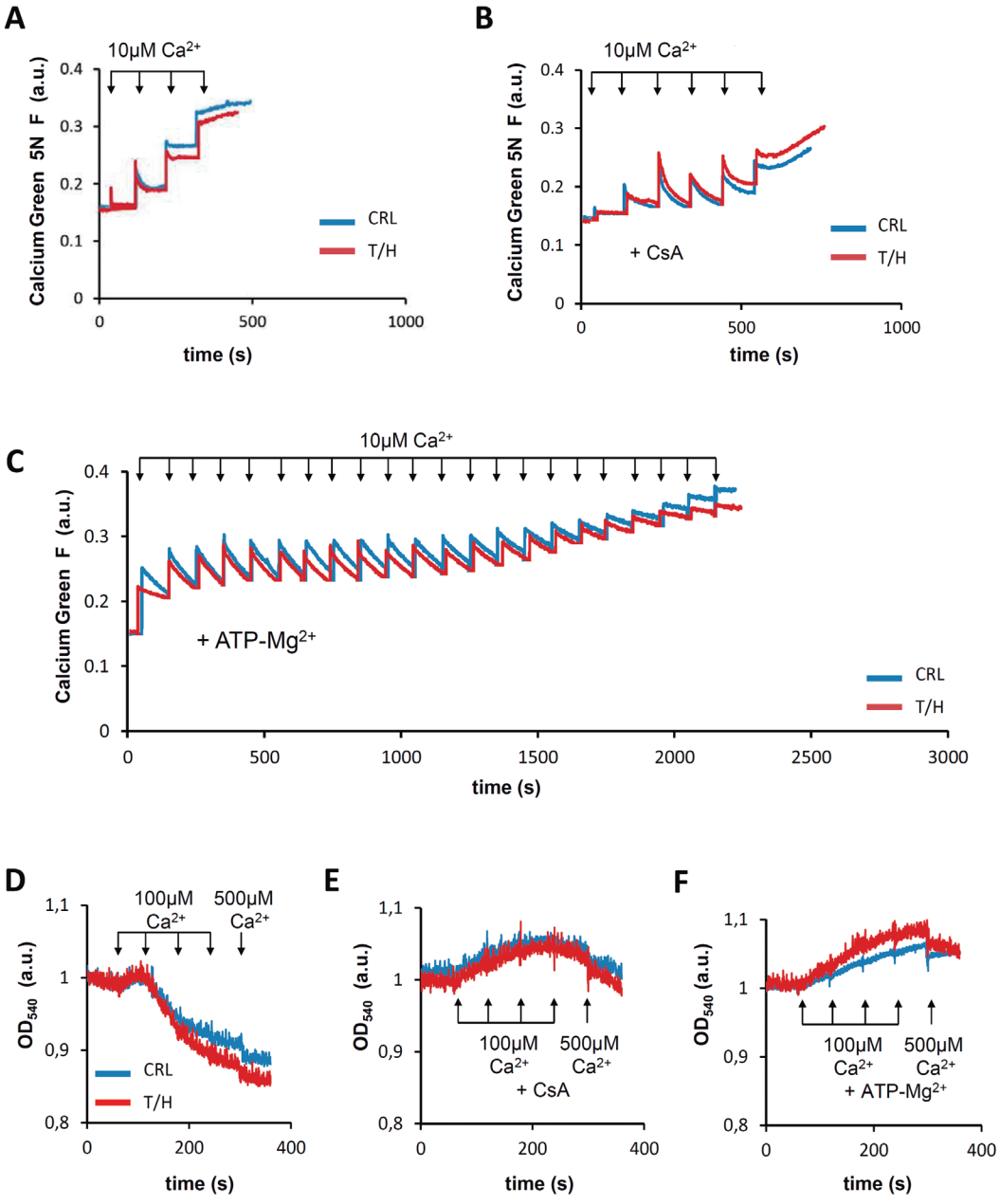

Figure 7: PTP opening and regulation is not affected by hIF1. A.-C. Calcium green 5N fluorescence in isolated liver mitochondria from control (blue traces) and hIF1 Tet-Off expressing (red traces) mice. Representative experiments show no differences between the calcium retention capacity of liver mitochondria from CRL and T/H mice after the addition of 10μM Ca^{2+} (arrows) in the absence (A) or presence of the PTP blockers 5 μM CsA (B) or 1mM ATP-Mg^{2+} (C). **D.-F.** Representative experiments show no differences in Ca^{2+} induced swelling between liver mitochondria derived from CRL and hIF1 expressing T/H mice after the addition of successive 100μM Ca^{2+} (arrows) except the last one which is 500μM Ca^{2+} in the absence (D) or presence of 5 μM CsA (E) or 1mM ATP-Mg^{2+} (F).

hIF1 in the liver of both the Tet-On and Tet-Off mice enhances the assembly of a Complex V super-complex (a putative ATPase dimer) is compatible with a role for IF1 in promoting the dimeric state of the ATP synthase *in vivo*, although in this situation, the IF1-mediated dimerization of the ATP synthase would argue against a role for dimeric ATP synthase as a major element of the PTP [11, 32]. However, we cannot exclude that additional mechanisms that are known to regulate the PTP [9] and the ATP synthase [12, 35, 36] could further participate in the hIF1-mediated inhibition of cell death. In any case, what is evident is that inhibition of the H^+-ATP synthase mediated either by oligomycin (OL) treatment [7] or by hIF1 expression [8, 14] protects from cell death, further supporting that the activity of the engine of OXPHOS is part of the machinery required for the execution of cell death *in vivo*.

hIF1 expressing mice are protected against oxidative stress

In livers of both mouse phenotypes, GSH levels (Figure 8A) and the basal expression of cytochrome P450 (Cyp2e1) (Figure 8B), both the catalytic and the modifier subunits of γ-glutamyl cysteine ligase (GCL-C and GCL-M) (Figure 8B) and basal glutathione reductase (GR) levels (Figure 8B) were comparable. APAP administration decreased both GCL-C and GCL-M (Figure 8B) and partially depleted GSH (Figure 8A) at 8 h, these effects being significantly ameliorated in T/H mice (Figure 8B and Figure 8A, respectively). Moreover, the induction of the detoxifying enzyme glutathione reductase (GR) in response to APAP challenge was more pronounced in hIF1 expressing mice (Figure 8B).

As intracellular redox state is chiefly regulated by the transcription factor Nrf2, we examined the expression level of total Nrf2. Although no differences were found at the basal state (Figure 8C), APAP administration significantly increased total Nrf2 degradation in wild-type mice whereas it was preserved in livers from T/H mice (Figure 8C). Likewise, the induction of Nrf2 target genes hemoxigenase-1 (HO-1) and superoxide dismutase 2 (SOD2) in response to APAP was significantly higher in mice expressing hIF1 (Figure 8D), consistent with the lower oxidative damage of liver proteins found in these animals (Figure 6D). Furthermore, we investigated the expression of Nrf2 and of redox-related genes (GCL-C, GCL-M, GR and SOD2) in normal and tumor tissue of control and T/H mice (Supplemental Figure S7). The results obtained reveal that tumors from T/H mice have higher expression of Nrf2, γ-glutamyl cysteine ligase (GCL-M) and mitochondrial superoxide dismutase (SOD2) than tumors originated in control animals further supporting a role for hIF1in counteracting an Nrf2-guided stress response.

It has been demonstrated that CO, the product of HO-1, is able to inhibit tumor necrosis factor alpha (TNFα)–induced apoptosis in endothelial cells through the activation of p38 MAPK [37]. In light of the low HO-1 induction upon APAP injection in wild-type mice, phosphorylated p38 MAPK was barely detected in these animals (Figure 9A). By contrast, the basal phosphorylated p38 MAPK was significantly increased in livers of T/H mice (Figure 9A), reinforcing the metabolic stress of the hepatocytes in hIF1 expressing mice (Figure 1 and Supplemental Figures S1 and S2). Moreover, and in contrast with wild type mice, T/H mice maintained phosphorylated p38 MAPK 8h after APAP injection (Figure 9A). The expression and phosphorylation of other stress kinases such as JNK and ERK 1/2 was not significantly different between control and T/H mice (Figure 9A). No differences were also found in survival signaling pathways mediated by IRS1/Akt between control and hIF1 expressing mice (Figure 9A). Remarkably, APAP-treated hIF1-expressing mice showed almost complete degradation of the NFκB repressor IκBα when compared to control treated mice (Figure 9A), supporting also the activation of this survival pathway [38]. Consistently, the anti-apoptotic Bcl-xL protein was increased at 8h post-APAP injection exclusively in T/H mice (Figure 9A).

DISCUSSION

Herein, we demonstrate *in vivo* that the expression of an active mutant of hIF1 in hepatocytes partially inhibits OXPHOS. The inhibition of OXPHOS results in a partial energy deficit in the liver, the activation of the metabolic stress kinase AMPK and a limited gluconeogenesis after a mild overnight fast of the animals. Inhibition of OXPHOS by hIF1 is exerted both by limiting the respiratory rate at the level of Complex IV and by inhibiting the activity of the ATP synthase. The inhibition of the activities of these complexes correlated with alterations in both the assembly and activities of super-complexes [39]. Within this background, a hIF1-limited activity of OXPHOS in the liver predisposes to cancer progression. Mechanistically, it appears that an enhanced cancer progression in hIF1-expressing mice is related to its pro-oncogenic activity that favors an increased proliferation and an increased resistance to execute apoptosis by the hepatocarcinomas. Inhibition of cell death seems to be unrelated to hIF1-mediated differences in PTP opening. Moreover, it appears that a restrained OXPHOS switches on a stress response that is most likely mediated by the cellular energy and redox states of the liver that triggers the basal activation of AMPK and p38 MAPK. This is particularly evident when the animals are challenged by an APAP overdose that induces a strong redox Nrf2 mediated response that involves the activation of the NFκB pathway and the overexpression of Bcl-xL favoring cell survival. It is

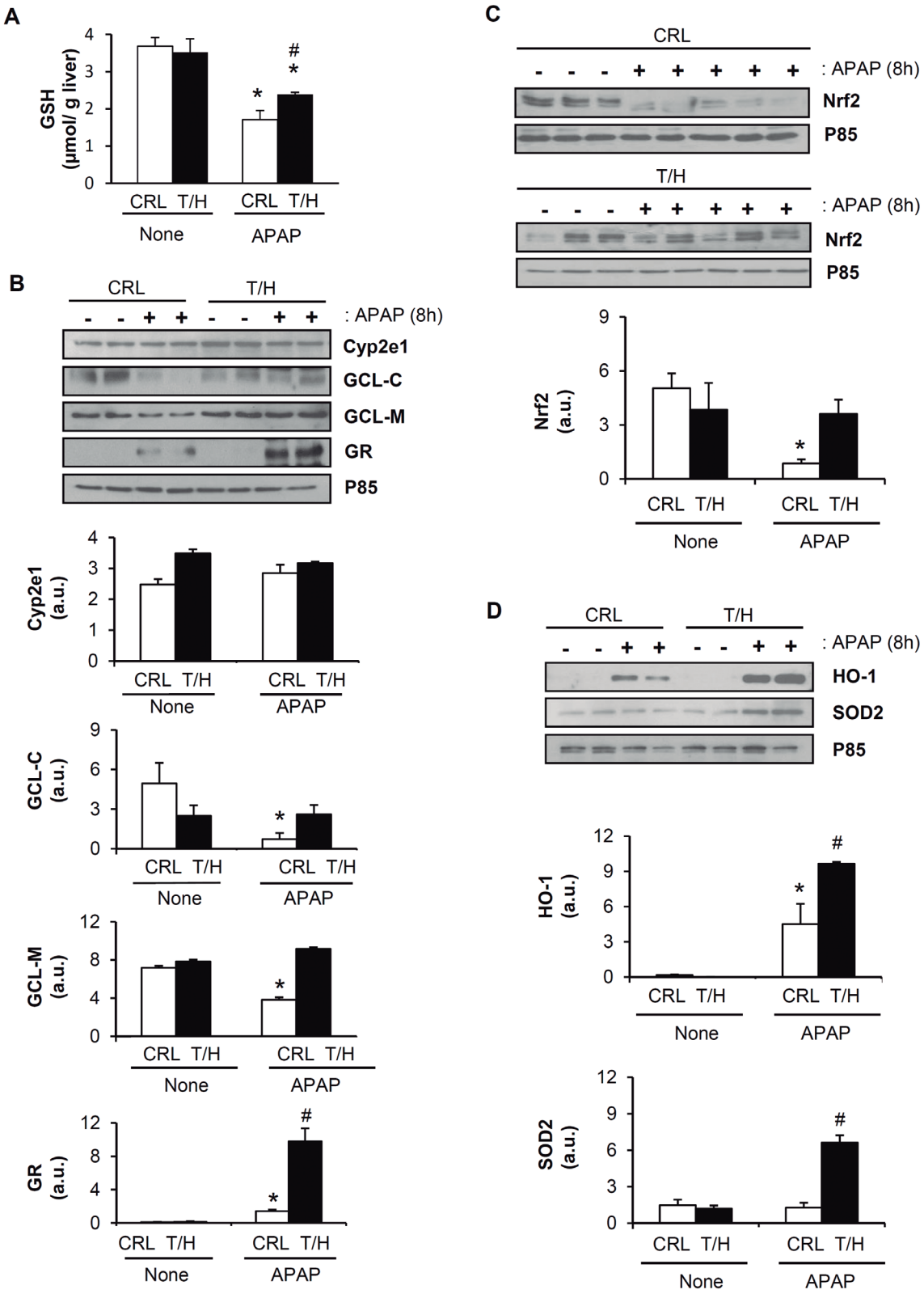

Figure 8: APAP treatment triggers a strong antioxidant response in the liver of hIF1 mice. Control (CRL) and Tet-Off (T/H) mice were treated (+) or not (-) with APAP. The results shown are the mean ± S.E.M of 6 mice per group. **A**. Liver GSH content. **B**.-**D**. Blots of Cyp2e1, GCL-C, GCL-M, GR, Nrf2, HO-1, SOD2 and P85 (used as loading control) in mice treated or not with APAP. Histograms show the quantification of the proteins normalized to p85 expression (arbitrary units, a.u.). *, $p < 0.05$ when compared to CRL non-treated (-) by Student's t test. #, $p < 0.05$ when compared to CRL-APAP treated by Student's *t* test.

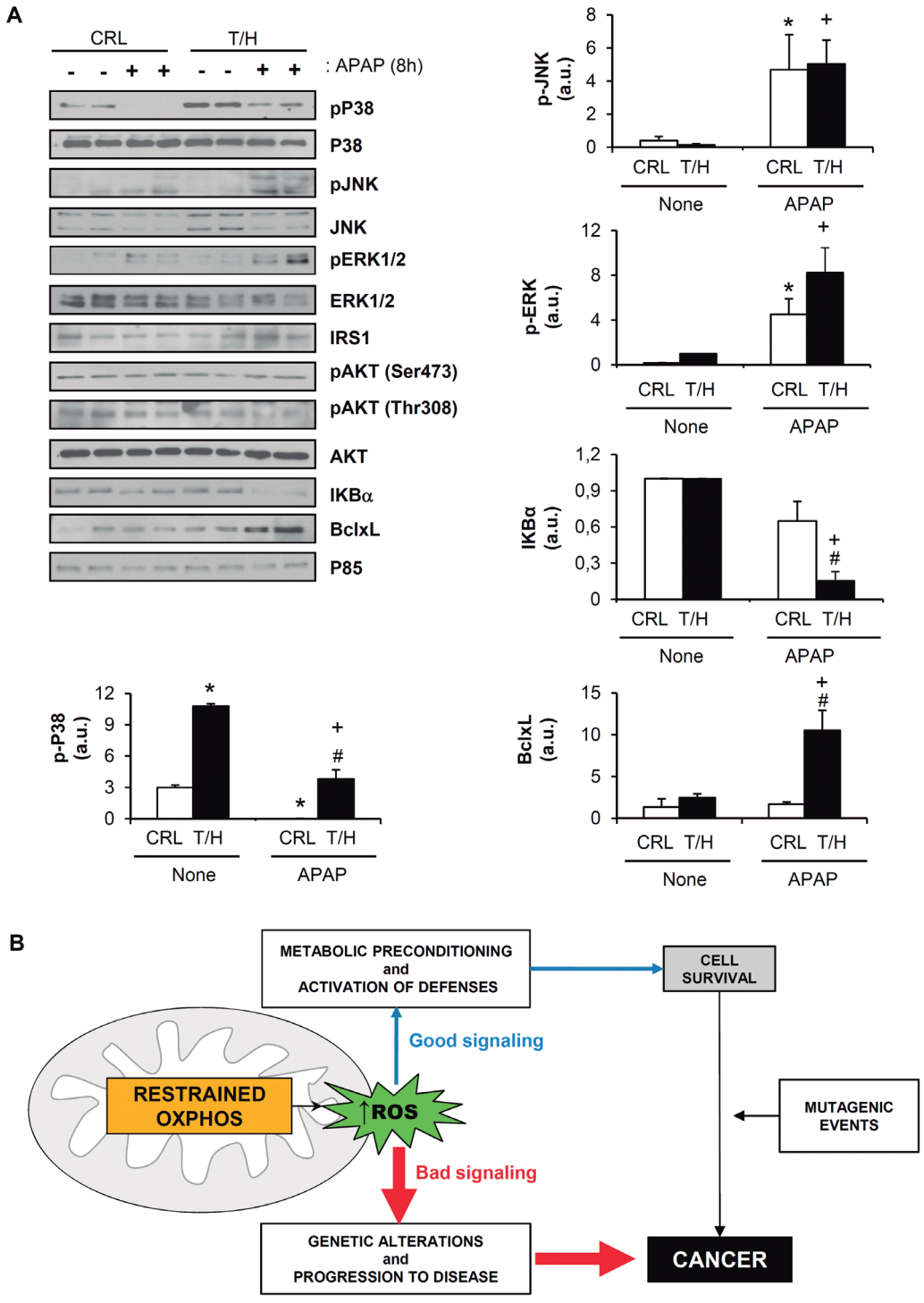

Figure 9: Signaling pathway in hIF1 expressing mice. Control (CRL) and Tet-Off (T/H) mice were treated (+) or not (-) with APAP. The results shown are the mean ± S.E.M of 6 mice per group. **A**. Blots of the serine-threonine protein kinases: pP38 MAPK / P38 MAPK; pJNK / JNK; pERK1/2 / ERK 1/2 and pAKT / AKT. Expression of the NFκB inhibitor IκBα, and Bcl-xL in livers is also shown. P85 is shown as loading control. Histograms show the quantification of the proteins normalized to p85 expression (arbitrary units, a.u.). *, $p < 0.05$ when compared to CRL non-treated (-); #, $p < 0.05$ when compared to CRL-APAP treated (+) and +, $p < 0.05$ when compared to T/H non-treated (-) by Student's t test. **B**. The bad and the good of mitochondrial ROS. Inhibition of OXPHOS could trigger a rise in the levels of ROS. Mild ROS levels (good, in blue) signal metabolic preconditioning and the activation of defenses (mitohormesis) [59] that result in cell survival. On the contrary, high ROS levels (bad, in red) cause intracellular damage, genetic alterations and progression to disease. Mitohormesis is beneficial for certain type of stressing stimuli, but it can be detrimental in the case of mutagenic events that lead to cancer.

within this metabolic background when genetic alterations that lead to carcinogenesis are able to progress because of a limited capacity to execute cell death by mitochondrial activity (Figure 9B), in agreement with recent suggestions [5] and the clinical observations that cancer recurrence is linked to the bioenergetic dysfunction of mitochondria (for review [1]).

Recent findings in *in vivo* mouse models indicate that the activation of mitochondrial OXPHOS provides a tumor-suppressive metabolic state [5, 40]. However, the role of the partial suppression of OXPHOS in cancer onset and progression has not been addressed so far. The availability of the Tet-Off T/H mice afforded a unique opportunity to verify *in vivo* the role of OXPHOS in carcinogenesis. Although T/H mice do not develop spontaneous tumors after more than one year follow up, perhaps because they overexpressed p38 MAPK which is a known tumor suppressor in the liver [41], they generated a three-fold higher number of carcinomas than control mice when exposed to DEN, supporting an oncogenic role for IF1 and a tumor-suppressive role for an enhanced activity of OXPHOS in the liver.

We have previously suggested a role for IF1 in carcinogenesis [14, 18]. Recent findings have stressed that a high expression level of IF1 is a bad predictor of survival and recurrence of the disease in liver, bladder and gastric cancer patients [19, 42, 43]. Moreover, IF1 promotes tumorigenesis and metastasis of human hepatocarcinomas and gastric cancer cells as assayed in mouse xenografts [19, 42]. In liver cancer, IF1 propitiates metastasis and angiogenesis through non-canonical signaling of the NFκB pathway to Snai1, which mediates epithelial mesenchymal transition, and to VEGF, that induces angiogenesis [19]. In bladder cancer, the oncogenic role of IF1 seems to be dependent on the stimulation of proliferation by cyclins and cyclin-dependent kinases related to the G1/S transition of the cell cycle [43]. In gastric cancer [42], similarly to what we observed in colon cancer [14], the oncogenic role of IF1 implicates an enhanced proliferation and cell-death resistant phenotype. Cell death resistance in colon and lung cancer is mediated by ROS-signaling to the canonical NFκB pathway [14, 18], whereas in breast and ovarian cancer the mechanism linking IF1 to the cell-death resistant phenotype remains to be investigated [18]. Hence, our findings in the Tet-Off T/H mice provide the first *in vivo* demonstration for the oncogenic role of IF1 that results from an enhanced proliferation and cell-death resistant phenotype of the hepatocyte, the latter attained by metabolic pre-conditioning of the anti-oxidant response of the liver.

It should be noted that carcinogenesis differentially affects the expression of IF1 in a tissue specific manner [18]. Moreover, the overexpression of IF1in the carcinomas not always correlate with a bad patient prognosis [19, 42, 43]. In fact, the overexpression of IF1 in breast and colon cancer predicts much better patient's prognosis [18]. These differences might stem from the different metabolic traits of the normal tissues as reveal by the large tissue-specific differences in the expression of IF1, which is very high in liver, kidney and stomach and almost negligible in breast, colon and lung [18]. At present time, we do not have a mechanistic explanation for the apparent tissue-specific differences in the oncogenic behavior of IF1. We speculate that mechanisms that involve a differential susceptibility of the different cell types to particular forms of stress and/or recognition by the immune system could be at the bases of these differences.

Interestingly, Dox administration that is used to silence the hIF1 transgene, and is also known to inhibit the growth of different cancer cells [20], promoted significant reductions in DEN-induced carcinogenesis both in the livers of control and hIF1 expressing mice, strongly supporting the use of this antibiotic as an anticancer agent [44, 45] and further emphasizing that targeting mitochondria translation offers an additional strategy to combat the disease.

Chronic liver injury is a major risk factor for the development of hepatocellular carcinomas. Interestingly, it has been recently demonstrated that dysfunction of mitochondrial oxidative phosphorylation ensues during the early stages of cirrhosis propitiating an enhanced rate of glycolysis [46] which is the metabolic pathway that chiefly provides the metabolic precursors that sustain proliferation of carcinomas [1]. In agreement with the role played by IF1 as inhibitor of OXPHOS and stimulator of both glycolysis [15, 18] and proliferation of cancer cells [14, 18, 19] we have observed that hIF1 expression in the liver mediates the rewiring of metabolism to an enhanced glycolysis that could support the elevated proliferation rate of the carcinomas. Moreover, the enhanced carcinogenesis observed in the liver of hIF1 expressing mice is also contributed by the reduced apoptosis observed in these tumors. Inhibition of the H^+-ATP synthase by hIF1 is known to generate a mild ROS signal that induces NFκB-guided nuclear programs of cell death evasion [8, 14, 18] and activate epithelial-mesenchymal transitions that favors metastasis [19]. This redox condition of the liver is consistent with the pathophysiological context for the development of hepatocellular carcinomas. Indeed, it has been previously suggested that increased intracellular ROS in chronic inflammatory states of the liver protect against cell death [47] and the increased basal ROS levels of cirrhotic hepatocytes seem to determine its increased apoptosis resistance [48]. Altogether, these findings reinforce the crucial role played by mitochondrial dysfunction during tumor transformation and suggest that the inhibition of the H^+-ATP synthase could represent a primary event in hepatic injury leading to the onset of carcinomas.

Energy limitation by a restrained activity of OXPHOS is known to induce the metabolic stress kinase AMPK [49] and to generate a mitochondrial ROS signal

of mild intensity [14]. This signal could also contribute to the induction of AMPK and of the stress p38 MAP kinase since it could modify the reduction state of thioredoxin which is known to halt the activation of both AMPK [50] and p38 MAPK [51]. The redox-mediated preconditioning is manifested when the animals are challenged with a ROS stressor such as APAP. Hence, we support that ROS-mediated signaling [8, 14] is the primary mechanism involved in evasion of cell-death mediated by IF1 in the liver. Indeed, the maintenance of total Nrf2 expression in the liver of T/H mice orchestrates a stress response that involves the overexpression of SOD2 and HO-1 as well as the detoxification of oxidized glutathione to provide protection against oxidative stress and cell death. Metabolic preconditioning and protection against death seems to be exerted by the basal activation of p38 MAPK and AMPK because other stress kinases such as JNK, ERK1/2 and Akt are not modified by the overexpression of hIF1 in the liver. The transcription factor NFκB is a crucial regulator of cell survival pathways [52]. The degradation of IKBα, which is the repressor of the NFκB pathway, and the concurrent accumulation of the anti-apoptotic Bcl-xL in the liver of T/H mice once again highlight the crosstalk between ROS and NFκB, and further implicate this pathway in hIF1-mediated cell survival after APAP treatment. Moreover, the transcriptional crosstalk between IF1 and the NFκB pathway has also been recently implicated in other hallmarks of liver cancer such as promoting angiogenesis and metastasis [19]. We cannot exclude that the maintenance of the phosphorylated state of p38 MAPK after APAP-induced cell death in T/H mice could contribute to cell survival because it has been shown to suppress ROS accumulation and cell death in hepatocytes [41]. Moreover, the activation of p38 MAPK has been reported to inhibit TNFα-induced apoptosis in endothelial cells [37]. In any case, the activation of different signaling pathways upon OXPHOS-mediated tissue preconditioning, p38 MAPK in the liver (this study) and PI3K/Akt in neurons [8], supports a large cell-type variability in mitochondrial signaling responses.

Overall, our data provide the first *in vivo* demonstration that the partial inhibition of OXPHOS generates a metabolic phenotype that is more prone to the development of cancer (Figure 9B), further indicating the pro-oncogenic nature of IF1. Hence, we conclude that the bioenergetic activity of mitochondria acts as a tumor-suppressor and guardian of cancer onset and progression.

MATERIALS AND METHODS

Transgenic animals

Transgenic mice containing the mutant H49K version of hIF1 (TRE-H49K-25, H) were obtained by pronuclear microinjection [8]. The commercially available B6.Cg-Tg(Lap-tTA)5Bjd/J mice (T) and B6.Cg-Tg(Cewbpb-rtTA2S*S2)1Bjd/Ibcm mice (rT), expressing respectively the transactivators tTA or rtTA in hepatocytes were used. The Tet-Off and Tet-On (T/H) double transgenic animals were obtained. To express hIF1, double transgenic T/H mice were administered (Tet-On) or not (Tet-Off) Dox (2mg/mL) in the drinking water. Animal experiments were carried out after approval of the Institutional Review Board (CEI-52-961) in compliance with animal policies and ethical guidelines of the European Community.

Determination of blood and liver metabolites

Adenine nucleotides and other liver metabolites were extracted from frozen liver powder with a 6% perchloric acid. The ATP concentration was determined using the ATP Bioluminescence Assay Kit CLS II (Roche). Liver GSH and GSSG concentrations were determined using the Glutathione Assay Kit (BioVision Inc.).

Western blotting, antibodies and protein carbonylation

The primary monoclonal antibodies developed in our lab and used in this study were: HSP60 (1:5,000), anti-NADH-9 (1:1,000), anti-β-F1-ATPase (1:20,000), anti-LDH-A (1:1,000) and anti-GAPDH (1:20,000) [53, 54]. The monoclonal antibody specifically recognizing the human [15] and mouse (Molecular Probes) IF1 proteins were used at 1:200 dilution. Other antibodies used were: anti-SDH-B (1:1000) from Life Technologies; anti-Complex III subunit Core 2 (1:1,000), anti-COXI (1:1,000), anti-COXIV (1:1,000) and anti-Cyp2e1 antibody (aB19140) from Abcam; anti-SOD2 (1:5,000), anti-JNK (sc-571; 1:1000), anti-phospho-Akt (Ser473) (sc-7985-R; 1:1000), anti-phospho-Akt (Thr308) (sc-16646-R; 1:1000) and anti-Nrf2 (C-20), (sc-722; 1:1000) from Santa Cruz Biotechnology, Inc.; anti-Bclx (610211; 1:1000) antibody from BD Biosciences; anti-IκBα (1:1,000), anti-phospho JNK (Thr183/Tyr185) (#4668, 1:1000), anti-phospho p38 MAPK (Thr180/Tyr182) (#9211; 1:1000), anti-p38 MAPK (#9212; 1:1000), anti-Phospho-p53(Ser15) (1:400) and anti-Akt (#9272; 1:1000) antibodies from Cell Signaling Technology Inc; anti-IRS1 (06-248; 1:1000), anti-p85 (06-195; 1:1000) and anti-HO1 (AB1284; 1:1000) antibodies from Upstate (Millipore); Anti-Ki-67 (SP6) (RM-9106-S1 1:200) from Fischer Scientific; Anti-F4/80 (123101; 1:200) from BioLegend; Anti-GCLc and GCLm antibodies were a gift from T Kavanagh (University of Washington, USA). Peroxidase-conjugated anti-mouse, anti-goat or anti-rabbit IgGs (Nordic Immunology; 1:3,000) and Biotin-SP anti-rat IgG (712-065-153; 1:500) from Jackson ImmunoResearch Inc.

were used as secondary antibodies. For the determination of protein carbonylation, the Oxyblot Oxidized Protein Detection kit (Chemicon International Inc.) was used. The blots were revealed using the ECL® reagent (Amersham Pharmacia Biotech). The intensity of the bands was quantified using a Kodak DC120 digital camera and the Kodak 1D Analysis Software.

Mitochondrial studies

Mitochondrial respiration was measured with the use of a Clark-type electrode [8]. The spectrophotometric determination of the activity of OXPHOS complexes was also carried out [55]. For Blue native (BN)-PAGE, Clear native (CN)-PAGE and In-gel activities, liver mitochondria were solubilized at the indicated digitonin/protein ratios [56].

Reverse phase-liquid chromatography RP-LC-MS/MS analysis (Dynamic Exclusion Mode)

After drying, gel bands from BN-PAGE were digested *in situ* with 12.5 ng/μl of trypsin (Promega) in 50 mM ammonium bicarbonate pH 8.8. Digestion was stopped by the addition of 1% trifluoracetic acid. Supernatants were dried down and then desalted onto ZipTip C18 Pipette tips (Millipore). The desalted protein digest was dried, resuspended in 10 μl of 0.1% formic acid and analyzed by RP-LC-MS/MS in an Easy-nLC II system coupled to an ion trap LTQ-Orbitrap-Velos-Pro mass spectrometer (Thermo Fischer Scientific, Bremen, Germany). The peptides were concentrated (on-line) by reverse phase chromatography using a 0.1mm×20 mm precolumn Acclaim PepMap C18, 5 μm, 100 A (Thermo Fischer Scientific), and then separated using a 0.075mm x 150 mm column Acclaim PepMap C18, 3 μm, 100 A (Thermo Fischer Scientific) operating at 0.3 μl/min. Peptides were eluted using a 90-min gradient from 5 to 40% solvent B (solvent A: 0.1% formic acid in water, solvent B: 0.1% formic acid, 80% acetonitrile in water). ESI ionization was done using a Nano-bore emitters Stainless Steel ID 30 μm (Proxeon) interface. The Orbitrap resolution was set at 30,000. Peptides were detected in survey scans from 400 to 1600 amu (1 μscan), followed by fifteen data dependent MS/MS scans (Top 15), using an isolation width of 2μ (in mass-to-charge ratio units), normalized collision energy of 35%, and dynamic exclusion applied during 30 seconds periods. Peptide identification from raw data was carried out using the SEQUEST algorithm (Proteome Discoverer 1.3, Thermo Scientific). Database search was performed against uniprot-mus.fasta. The following constraints were used for the searches: tryptic cleavage after Arg and Lys, up to two missed cleavage sites, and tolerances of 10 ppm for precursor ions and 0.8 Da for MS/MS fragment ions and the searches were performed allowing optional Met oxidation and Cys carbamidomethylation. Search against decoy database (integrated decoy approach) using false discovery rate (FDR) < 0.01.

Carcinogenesis

For an exploratory experiment of DEN-induced carcinogenesis two-week old control and Tet-Off T/H male mice received or not a single i.p. injection of DEN (25 mg/kg bw) [23] and the animals were sacrificed at week 44. In the main experiment, two-week old control (n=35) and Tet-Off T/H (n=35) mice received or not an i.p. injection of DEN (0.33 mmol/kg bw) once weekly for a total of 26 weeks [24]. Liver glutamate/pyruvate transaminase (GPT) was evaluated every 2 weeks using the Reflotron plus analyzer (Roche Diagnostics, Penzberg, Germany). Mice were sacrificed at week 29.

Hepatotoxicity

Six month old control (n=8) and Tet-Off T/H (n=8) mice were used to induce hepatotoxicity. The animals were fasted for 14 hours and then received a single i.p. injection of APAP (300 mg/kg; Sigma Aldrich). Eight hours after the injection mice were sacrificed.

Immunohistochemistry and immunofluorescence microscopy

The peroxidase based EnVisionTM FLEX Mini kit High pH (Dako Cytomation) and VECTASTAIN ABC kit (Vector Laboratories, Inc.) were used for immunohistochemistry using primary antibodies listed in Western blotting, antibodies and protein carbonylation section. The TUNEL kit (Roche) and anti-activated caspase 3 (1:250) were used to assess the rate of cell death. Secondary Cy-3/Cy-5-conjugated antibodies were used (Millipore Bioscience Research Reagents). Cellular fluorescence was analyzed by confocal microscopy.

Electron microscopy

Liver slices were fixed and embedded in Epon (TAAB 812 resin; TAAB Laboratories Equipment, Aldermaston, Berks, UK). Ultrathin sections were stained and processed for electron microscopy as described [26].

Quantitative RT-PCR analysis

RNA samples were extracted using the RNAeasy mini kit (QIAGEN). Reverse transcription (RT) reactions were performed using 1μg of total RNA

and the High Capacity Reverse Transcription Kit (Applied Biosystems) with random primers. Primers were designed with Probe Finder Software (Roche Applied Science). The primers used were: m-IF1-F: agaagctggtggagccttc, m-IF1-R: ggcagccagctgttctttag; m-β-F1-ATPase-F: ggcacaatgcaggaaagg, m-β-F1-ATPase-R: tcagcaggcacatagatagcc; m-Hsp60-F: tcttcaggttgtggcagtca, m-Hsp60-R: cccctcttctccaaacactg; m-GAPDH-F: agcttgtcatcaacgggaag, m-GAPDH-R: tttgatgttagtggggtctcg; m-PGC1α-F: gaaagggccaaacagagaga, m-PGC1α-R: gtaaatcacacggcgctctt; m-β-actin-F: ctaaggccaaccgtgaaaag, m-β-actin-R: accagaggcatacagggaca; h-IF1-F: gggccttcggaaagagag, h-IF1-R: ttcaaagctgccagttgttc. Real-time PCR was performed using Power Sybr Green PCR Master Mix (Bio-Rad) and an ABI PRISM 7900 SDS thermocycler (Applied Biosystems). The relative expression of the mRNAs was determined using the comparative ΔΔCt method with β-actin as control and relative to the normal tissues.

Determination of mitochondrial DNA (mtDNA) copy number

DNA (nDNA+mtDNA) was extracted using DNeasy Blood & Tissue Kit from Qiagen. Quantification of mtDNA (mtDNA/nDNA) was performed by qPCR in the ABI PRISM 7900HT SDS thermocycler (Applied Biosystems, Singapore) using 6 ng of DNA, 0.25 μM of primers and the Power Sybr Green PCR Master Mix (Bio-Rad). The nuclear ATPIF1 and the mitochondrial 12S rRNA encoded genes were chosen to determine the ratio of mtDNA to nDNA. The primers used were: m-12S-F: cctcttagggttggtaaatttcg, m-12S-R: cgaagataattagtttgggttaatcg; m-IF1-F: agaagctggtggagccttc, m-IF1-R: ggcagccagctgttctttag. The relative mtDNA copy number was calculated using the ΔΔCt method and the 12S/IF1 ratio used to compare the samples.

Swelling and Ca^{2+} uptake in isolated mitochondria

The calcium retention capacity (CRC) of isolated mitochondria was measured with the Ca^{2+}-sensitive fluorescent probe Calcium-Green 5N (0.1 μM, excitation 506 nm, emission 532 nm) as previously described [57], using an Aminco-Bowman II fluorimeter (SLM/Aminco, Urbana, IL, USA). Mitochondrial swelling was measured by monitoring the decrease in absorbance of the suspension at 540 nm [58], using a Nicolet Evolution 300 spectrophotometer (Thermo Scientific, Warrington, UK). All experiments were carried out at 37ºC in the presence of 1 mM $MgCl_2$, respiratory substrates (5 mM succinate + 2 μM rotenone) and in the presence or absence of 1 mM ATP-Mg or 5 μM CsA. After 3-5 min of incubation, mitochondria were challenged with subsequent 2.5-10 nmol $CaCl_2$ additions as indicated in the figure legends, and Ca^{2+} uptake into mitochondria was measured as a decrease in fluorescence. For swelling assays, the absorbance at 540 nm of mitochondria was monitored through sequential additions of 100-500 nmol $CaCl_2$.

Statistical analysis

Statistical analyses were performed using a two-tailed Student's t-test. ANOVA with post hoc Dunnett's test were used for multiple comparisons to the control, using the SPSS 17.0 software package. The results shown are means ± SEM. A $p < 0.05$ was considered statistically significant.

ACKNOWLEDGMENTS

We thank Margarita Chamorro for expert technical support. LSC and FS were supported by pre-doctoral fellowships from FPI-MEC and FPI-UAM, respectively. LF was supported from AECC and Ramon and Cajal Program, Spain.

FUNDING

This work was supported by Spanish grants from the MINECO (SAF2013-41945-R to JMC and SAF2012-33243 to AMV), CIBERER-ISCIII to JMC and CIBERDEM-ISCIII to AMV, Comunidad de Madrid (S2011/BMD-2402 to JMC and S2010/BMD-2423 to AMV), Fundación Ramón Areces (FRA) to JMC and EFSD and Amylin Paul Langerhans to AMV. The CBMSO receives an institutional grant from FRA, Spain.

CONFLICTS OF INTEREST

The authors declare no conflict of interest.

REFERENCES

1. Sanchez-Arago M, Formentini L and Cuezva JM. Mitochondria-mediated energy adaption in cancer: the H(+)-ATP synthase-geared switch of metabolism in human tumors. Antioxid Redox Signal. 2013; 19:285-298.
2. Walker JE. The ATP synthase: the understood, the uncertain and the unknown. Biochem Soc Trans. 2013; 41:1-16.
3. Vander Heiden MG, Cantley LC and Thompson CB. Understanding the Warburg effect: the metabolic requirements of cell proliferation. Science. 2009; 324:1029-1033.
4. Bonnet S, Archer SL, Allalunis-Turner J, Haromy A, Beaulieu C, Thompson R, Lee CT, Lopaschuk GD, Puttagunta L, Bonnet S, Harry G, Hashimoto K, Porter CJ, et al. A mitochondria-K+ channel axis is suppressed in cancer and its normalization promotes apoptosis and

inhibits cancer growth. Cancer Cell. 2007; 11:37-51.

5. Garcia-Cao I, Song MS, Hobbs RM, Laurent G, Giorgi C, de Boer VC, Anastasiou D, Ito K, Sasaki AT, Rameh L, Carracedo A, Vander Heiden MG, Cantley LC, et al. Systemic elevation of PTEN induces a tumor-suppressive metabolic state. Cell. 2012; 149:49-62.
6. D'Errico I, Salvatore L, Murzilli S, Lo Sasso G, Latorre D, Martelli N, Egorova AV, Polishuck R, Madeyski-Bengtson K, Lelliott C, Vidal-Puig AJ, Seibel P, Villani G, et al. Peroxisome proliferator-activated receptor-gamma coactivator 1-alpha (PGC1alpha) is a metabolic regulator of intestinal epithelial cell fate. Proc Natl Acad Sci U S A. 2011; 108:6603-6608.
7. Matsuyama S, Xu Q, Velours J and Reed JC. The Mitochondrial F0F1-ATPase proton pump is required for function of the proapoptotic protein Bax in yeast and mammalian cells. Mol Cell. 1998; 1:327-336.
8. Formentini L, Pereira MP, Sanchez-Cenizo L, Santacatterina F, Lucas JJ, Navarro C, Martinez-Serrano A and Cuezva JM. *In vivo* inhibition of the mitochondrial H+-ATP synthase in neurons promotes metabolic preconditioning. EMBO J. 2014; 33:762-778.
9. Bernardi P. The mitochondrial permeability transition pore: a mystery solved? Front Physiol. 2013; 4:95.
10. Alavian KN, Beutner G, Lazrove E, Sacchetti S, Park HA, Licznerski P, Li H, Nabili P, Hockensmith K, Graham M, Porter GA, Jr. and Jonas EA. An uncoupling channel within the c-subunit ring of the F1FO ATP synthase is the mitochondrial permeability transition pore. Proc Natl Acad Sci U S A. 2014; 111:10580-10585.
11. Giorgio V, von Stockum S, Antoniel M, Fabbro A, Fogolari F, Forte M, Glick GD, Petronilli V, Zoratti M, Szabo I, Lippe G and Bernardi P. Dimers of mitochondrial ATP synthase form the permeability transition pore. Proc Natl Acad Sci U S A. 2013; 110:5887-5892.
12. Chin RM, Fu X, Pai MY, Vergnes L, Hwang H, Deng G, Diep S, Lomenick B, Meli VS, Monsalve GC, Hu E, Whelan SA, Wang JX, et al. The metabolite alpha-ketoglutarate extends lifespan by inhibiting ATP synthase and TOR. Nature. 2014; 510:397-401.
13. Sun X, Wheeler CT, Yolitz J, Laslo M, Alberico T, Sun Y, Song Q and Zou S. A Mitochondrial ATP Synthase Subunit Interacts with TOR Signaling to Modulate Protein Homeostasis and Lifespan in Drosophila. Cell Rep. 2014; 8:1781-1792.
14. Formentini L, Sánchez-Aragó M, Sánchez-Cenizo L and Cuezva JM. The mitochondrial ATPase Inhibitory Factor 1 (IF1) triggers a ROS-mediated retrograde pro-survival and proliferative response. Mol Cell. 2012; 45:731-742.
15. Sanchez-Cenizo L, Formentini L, Aldea M, Ortega AD, Garcia-Huerta P, Sanchez-Arago M and Cuezva JM. Up-regulation of the ATPase inhibitory factor 1 (IF1) of the mitochondrial H+-ATP synthase in human tumors mediates the metabolic shift of cancer cells to a Warburg phenotype. J Biol Chem. 2010; 285:25308-25313.
16. Sanchez-Arago M, Garcia-Bermudez J, Martinez-Reyes I, Santacatterina F and Cuezva JM. Degradation of IF1 controls energy metabolism during osteogenic differentiation of stem cells. EMBO Rep. 2013; 14:638-644.
17. Faccenda D, Tan CH, Seraphim A, Duchen MR and Campanella M. IF1 limits the apoptotic-signalling cascade by preventing mitochondrial remodelling. Cell Death Differ. 2013; 20:686-697.
18. Sanchez-Arago M, Formentini L, Martinez-Reyes I, Garcia-Bermudez J, Santacatterina F, Sanchez-Cenizo L, Willers IM, Aldea M, Najera L, Juarranz A, Lopez EC, Clofent J, Navarro C, et al. Expression, regulation and clinical relevance of the ATPase inhibitory factor 1 in human cancers. Oncogenesis. 2013; 2:e46.
19. Song R, Song H, Liang Y, Yin D, Zhang H, Zheng T, Wang J, Lu Z, Song X, Pei T, Qin Y, Li Y, Xie C, et al. Reciprocal activation between ATPase inhibitory factor 1 and NF-kappaB drives hepatocellular carcinoma angiogenesis and metastasis. Hepatology. 2014; 60:1659-1673.
20. Onoda T, Ono T, Dhar DK, Yamanoi A, Fujii T and Nagasue N. Doxycycline inhibits cell proliferation and invasive potential: combination therapy with cyclooxygenase-2 inhibitor in human colorectal cancer cells. J Lab Clin Med. 2004; 143:207-216.
21. Son K, Fujioka S, Iida T, Furukawa K, Fujita T, Yamada H, Chiao PJ and Yanaga K. Doxycycline induces apoptosis in PANC-1 pancreatic cancer cells. Anticancer Res. 2009; 29:3995-4003.
22. Jovaisaite V, Mouchiroud L and Auwerx J. The mitochondrial unfolded protein response, a conserved stress response pathway with implications in health and disease. J Exp Biol. 2014; 217:137-143.
23. Chen B, Liu L, Castonguay A, Maronpot RR, Anderson MW and You M. Dose-dependent ras mutation spectra in N-nitrosodiethylamine induced mouse liver tumors and 4-(methylnitrosamino)-1-(3-pyridyl)-1-butanone induced mouse lung tumors. Carcinogenesis. 1993; 14:1603-1608.
24. Finnberg N, Stenius U and Hogberg J. Heterozygous p53-deficient (+/-) mice develop fewer p53-negative preneoplastic focal liver lesions in response to treatment with diethylnitrosamine than do wild-type (+/+) mice. Cancer Lett. 2004; 207:149-155.
25. Heindryckx F, Colle I and Van Vlierberghe H. Experimental mouse models for hepatocellular carcinoma research. Int J Exp Pathol. 2009; 90:367-386.
26. Cuezva JM, Krajewska M, de Heredia ML, Krajewski S, Santamaria G, Kim H, Zapata JM, Marusawa H, Chamorro M and Reed JC. The bioenergetic signature of cancer: a marker of tumor progression. Cancer Res. 2002; 62:6674-6681.
27. Cuezva JM, Ortega AD, Willers I, Sanchez-Cenizo L, Aldea M and Sanchez-Arago M. The tumor suppressor function of mitochondria: translation into the clinics. Biochim Biophys

Acta. 2009; 1792:1145-1158.

28. Mobasher MA, Gonzalez-Rodriguez A, Santamaria B, Ramos S, Martin MA, Goya L, Rada P, Letzig L, James LP, Cuadrado A, Martin-Perez J, Simpson KJ, Muntane J, et al. Protein tyrosine phosphatase 1B modulates GSK3beta/Nrf2 and IGFIR signaling pathways in acetaminophen-induced hepatotoxicity. Cell Death Dis. 2013; 4:e626.
29. Dey R and Moraes CT. Lack of oxidative phosphorylation and low mitochondrial membrane potential decrease susceptibility to apoptosis and do not modulate the protective effect of Bcl-x(L) in osteosarcoma cells. J Biol Chem. 2000; 275:7087-7094.
30. Harris MH, Vander Heiden MG, Kron SJ and Thompson CB. Role of oxidative phosphorylation in Bax toxicity. Mol Cell Biol. 2000; 20:3590-3596.
31. Bonora M, Bononi A, De Marchi E, Giorgi C, Lebiedzinska M, Marchi S, Patergnani S, Rimessi A, Suski JM, Wojtala A, Wieckowski MR, Kroemer G, Galluzzi L, et al. Role of the c subunit of the FO ATP synthase in mitochondrial permeability transition. Cell Cycle. 2013; 12:674-683.
32. Carraro M, Giorgio V, Sileikyte J, Sartori G, Forte M, Lippe G, Zoratti M, Szabo I and Bernardi P. Channel formation by yeast F-ATP synthase and the role of dimerization in the mitochondrial permeability transition. J Biol Chem. 2014; 289:15980-15985.
33. Minauro-Sanmiguel F, Wilkens S and Garcia JJ. Structure of dimeric mitochondrial ATP synthase: novel F0 bridging features and the structural basis of mitochondrial cristae biogenesis. Proc Natl Acad Sci U S A. 2005; 102:12356-12358.
34. Campanella M, Casswell E, Chong S, Farah Z, Wieckowski MR, Abramov AY, Tinker A and Duchen MR. Regulation of mitochondrial structure and function by the F1Fo-ATPase inhibitor protein, IF1. Cell Metab. 2008; 8:13-25.
35. Rahman M, Nirala NK, Singh A, Zhu LJ, Taguchi K, Bamba T, Fukusaki E, Shaw LM, Lambright DG, Acharya JK and Acharya UR. Drosophila Sirt2/mammalian SIRT3 deacetylates ATP synthase beta and regulates complex V activity. J Cell Biol. 2014; 206:289-305.
36. Vassilopoulos A, Pennington JD, Andresson T, Rees DM, Bosley AD, Fearnley IM, Ham A, Flynn CR, Hill S, Rose KL, Kim HS, Deng CX, Walker JE, et al. SIRT3 deacetylates ATP synthase F1 complex proteins in response to nutrient- and exercise-induced stress. Antioxid Redox Signal. 2014; 21:551-564.
37. Brouard S, Otterbein LE, Anrather J, Tobiasch E, Bach FH, Choi AM and Soares MP. Carbon monoxide generated by heme oxygenase 1 suppresses endothelial cell apoptosis. J Exp Med. 2000; 192:1015-1026.
38. Karin M and Greten FR. NF-kappaB: linking inflammation and immunity to cancer development and progression. Nat Rev Immunol. 2005; 5:749-759.
39. Lapuente-Brun E, Moreno-Loshuertos R, Acin-Perez R, Latorre-Pellicer A, Colas C, Balsa E, Perales-Clemente E, Quiros PM, Calvo E, Rodriguez-Hernandez MA, Navas P, Cruz R, Carracedo A, et al. Supercomplex assembly determines electron flux in the mitochondrial electron transport chain. Science. 2013; 340:1567-1570.
40. Serrano M and Blasco MA. Cancer and ageing: convergent and divergent mechanisms. Nat Rev Mol Cell Biol. 2007; 8:715-722.
41. Sakurai T, He G, Matsuzawa A, Yu GY, Maeda S, Hardiman G and Karin M. Hepatocyte necrosis induced by oxidative stress and IL-1 alpha release mediate carcinogen-induced compensatory proliferation and liver tumorigenesis. Cancer Cell. 2008; 14:156-165.
42. Yin T, Lu L, Xiong Z, Wei S and Cui D. ATPase inhibitory factor 1 is a prognostic marker and contributes to proliferation and invasion of human gastric cancer cells. Biomed Pharmacother. 2015; 70:90-96.
43. Wei S, Fukuhara H, Kawada C, Kurabayashi A, Furihata M, Ogura S, Inoue K and Shuin T. Silencing of ATPase Inhibitory Factor 1 inhibits cell growth via cell cycle arrest in bladder cancer. Pathobiology. 2015; 82:224-232.
44. Skrtic M, Sriskanthadevan S, Jhas B, Gebbia M, Wang X, Wang Z, Hurren R, Jitkova Y, Gronda M, Maclean N, Lai CK, Eberhard Y, Bartoszko J, et al. Inhibition of mitochondrial translation as a therapeutic strategy for human acute myeloid leukemia. Cancer Cell. 2011; 20:674-688.
45. Lamb R, Ozsvari B, Lisanti CL, Tanowitz HB, Howell A, Martinez-Outschoorn UE, Sotgia F and Lisanti MP. Antibiotics that target mitochondria effectively eradicate cancer stem cells, across multiple tumor types: treating cancer like an infectious disease. Oncotarget. 2015; 6:4569-4584. Doi: 10.18632/oncotarget.3174.
46. Nishikawa T, Bellance N, Damm A, Bing H, Zhu Z, Handa K, Yovchev MI, Sehgal V, Moss TJ, Oertel M, Ram PT, Pipinos, II, Soto-Gutierrez A, et al. A switch in the source of ATP production and a loss in capacity to perform glycolysis are hallmarks of hepatocyte failure in advance liver disease. J Hepatol. 2014; 60:1203-1211.
47. Black D, Bird MA, Samson CM, Lyman S, Lange PA, Schrum LW, Qian T, Lemasters JJ, Brenner DA, Rippe RA and Behrns KE. Primary cirrhotic hepatocytes resist TGFbeta-induced apoptosis through a ROS-dependent mechanism. J Hepatol. 2004; 40:942-951.
48. Raval J, Lyman S, Nitta T, Mohuczy D, Lemasters JJ, Kim JS and Behrns KE. Basal reactive oxygen species determine the susceptibility to apoptosis in cirrhotic hepatocytes. Free Radic Biol Med. 2006; 41:1645-1654.
49. Mihaylova MM and Shaw RJ. The AMPK signalling pathway coordinates cell growth, autophagy and metabolism. Nat Cell Biol. 2011; 13:1016-1023.
50. Shao D, Oka S, Liu T, Zhai P, Ago T, Sciarretta S, Li H and Sadoshima J. A redox-dependent mechanism for regulation of AMPK activation by Thioredoxin1 during energy starvation. Cell Metab. 2014; 19:232-245.

51. Dolado I, Swat A, Ajenjo N, De Vita G, Cuadrado A and Nebreda AR. p38alpha MAP kinase as a sensor of reactive oxygen species in tumorigenesis. Cancer Cell. 2007; 11:191-205.

52. Karin M. Nuclear factor-kappaB in cancer development and progression. Nature. 2006; 441:431-436.

53. Acebo P, Giner D, Calvo P, Blanco-Rivero A, Ortega AD, Fernandez PL, Roncador G, Fernandez-Malave E, Chamorro M and Cuezva JM. Cancer abolishes the tissue type-specific differences in the phenotype of energetic metabolism. Transl Oncol. 2009; 2:138-145.

54. Santacatterina F, Chamorro M, Nuñez de Arenas C, Navarro C, Martin MA, Cuezva JM and Sánchez-Aragó M. Quantitative analysis of proteins of metabolism by reverse phase protein microarrays identifies potential biomarkers of rare neuromuscular diseases. J Trans Med. 2015; 13:65.

55. Barrientos A, Fontanesi F and Diaz F. Evaluation of the mitochondrial respiratory chain and oxidative phosphorylation system using polarography and spectrophotometric enzyme assays. Curr Protoc Hum Genet. 2009; 19:13.

56. Wittig I, Carrozzo R, Santorelli FM and Schagger H. Functional assays in high-resolution clear native gels to quantify mitochondrial complexes in human biopsies and cell lines. Electrophoresis. 2007; 28:3811-3820.

57. Traba J, Del Arco A, Duchen MR, Szabadkai G and Satrustegui J. SCaMC-1 promotes cancer cell survival by desensitizing mitochondrial permeability transition via ATP/ADP-mediated matrix Ca(2+) buffering. Cell Death Differ. 2012; 19:650-660.

58. Amigo I, Traba J, Gonzalez-Barroso MM, Rueda CB, Fernandez M, Rial E, Sanchez A, Satrustegui J and Del Arco A. Glucagon regulation of oxidative phosphorylation requires an increase in matrix adenine nucleotide content through Ca2+ activation of the mitochondrial ATP-Mg/Pi carrier SCaMC-3. J Biol Chem. 2013; 288:7791-7802.

59. Yun J and Finkel T. Mitohormesis. Cell Metab. 2014; 19:757-766.

Down-regulation of oxidative phosphorylation in the liver by expression of the ATPase inhibitory factor 1 induces a tumor-promoter metabolic state

Supplemental Material

Supplemental Table S1, Related to Fig. 2. Protein bands labeled as $(CV)_2$, SC and FoF1 in BN-gels (see Fig. 2D) were trypsin digested and the peptides obtained analyzed by RP-LC-MS/MS. The known proteins of different respiratory complexes (CI to CV) are indicated. The number of proteins and peptides identified for each of the complexes in each band is shown. The percentage of proteins belonging to each complex is also indicated.

Band		C I		C II		C III		C IV		C V	
	Proteins	45		4		10		19		18	
		Number	%	Number	%	Number	%	Number	%	Number	%
$(CV)_2$	Proteins	11	24.4	--	--	2	20	1	5.3	6	33.3
	Peptides	38		--		10		3		20	
(SC)	Proteins	24	53.3	--	--	4	40	1	5.3	6	33.3
	Peptides	106		--		21		2		43	
(F_0F_1)	Proteins	--	--	--	--	1	10	3	15.8	10	52.6
	Peptides	--		--		4		7		79	

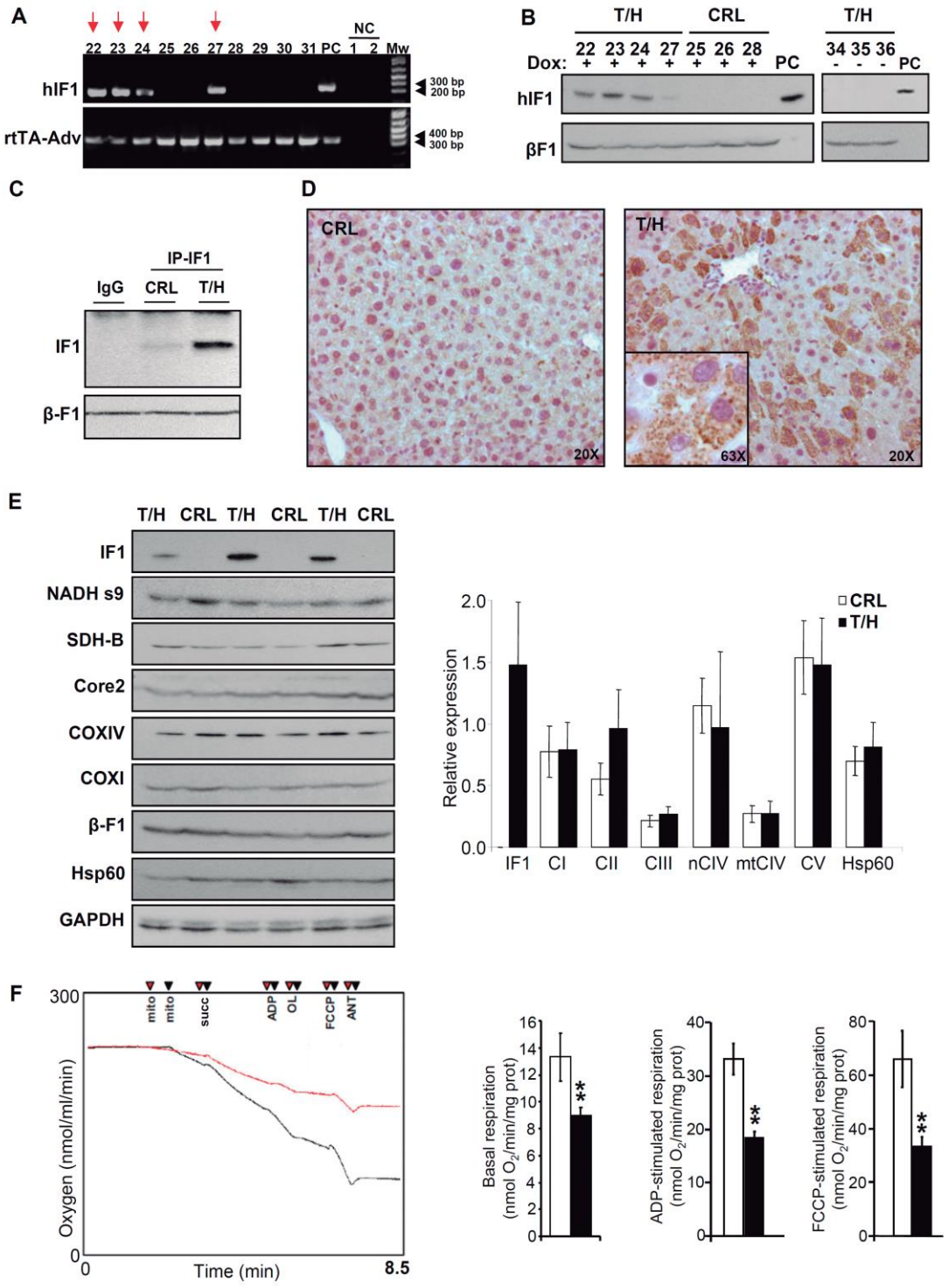

Figure S1, Related to Fig. 1. OXPHOS is inhibited in the liver of Tet-On mice expressing hIF1. (A) PCR analysis for the H49K variant of human IF1 (hIF1) and rtTA-Adv constructs. Red arrows indicate double-transgenic mice. (**B**) Western blots show the expression of hIF1 (12 kDa) in double transgenic (T/H) and control (CRL)

mice (identified by numbers) in the presence (+) or absence (-) of doxycycline (Dox). β-F1-ATPase (β-F1) expression is shown as a loading control. In **A** and **B**, PC and NC, positive and negative controls, respectively. (**C)** Liver extracts from CRL and T/H mice were subjected to immunoprecipitation (IP) using a monoclonal anti-IF1 antibody and subsequently analyzed by western blotting. Non-immune IgG is used as negative control. (**D**) Immunohistochemistry for hIF1 in the liver of CRL and T/H mice. Magnification 20X and 63X (inset). (**E**) Representative Western blots of the expression of hIF1, mitochondrial complex I (NADH s9), complex II (SDH-B), complex III (Core2), complex IV (COX I and COX IV) and complex V (β-F1), heat-shock protein 60 (Hsp60) and the glycolytic GAPDH in liver extracts of CRL and T/H mice. Three different mice per condition tested are shown. Histograms to the right show the relative expression of each protein in CRL and T/H mice. (**F**) Polarographic profiles of isolated mitochondria from CRL (black trace) and T/H mice (red trace). The effect of succinate, ADP, oligomycin (OL), FCCP, and antimycin A (ANT) is shown. Histograms show the basal, ADP-stimulated and FCCP-stimulated respiration in mitochondria of T/H mice (closed bars) when compared to CRL (open bars). Bars are the mean ± SEM of 5 CRL and 7 T/H animals. *, $p<0.05$ when compared to control mice by Student's t test.

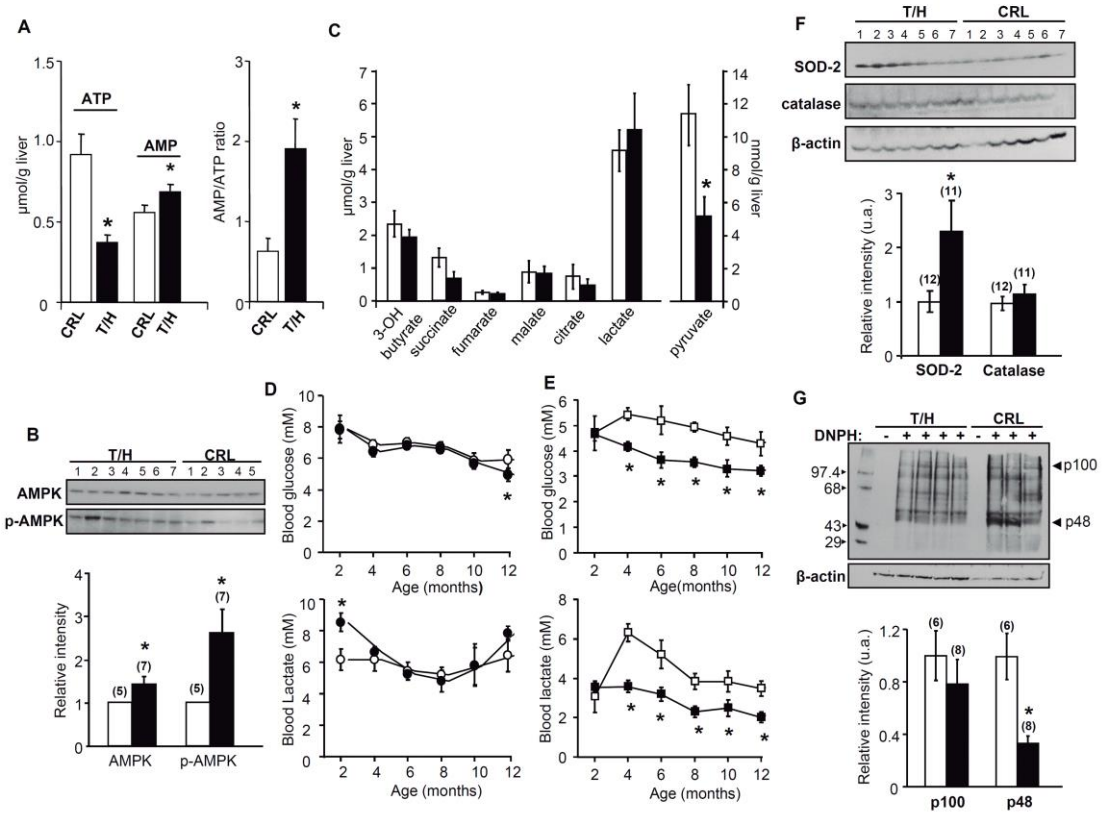

Figure S2, related to Fig. 1. Expression of hIF1 compromises the liver energy state. **(A)** Content of adenine nucleotides (ATP and AMP) and the AMP/ATP ratio in liver extracts of control (CRL, open bars) and T/H mice (closed bars). Histograms show the mean ± SEM of 12 mice per group. (**B)** Western blots show the hIF1-dependent phosphorylation of AMPK (p-AMPK) in liver extracts. Histograms show the mean ± SEM of 5 CRL and 7 T/H mice. (**C)** Liver organic acids. Histograms show the mean ± SEM of 4 CRL and 6 T/H mice. (**D** and **E**) Blood glucose and lactate concentrations in CRL (open dots and squares) and T/H (closed dots and squares) mice under fed (D) or fasted (E) conditions. The results shown are the mean ± SEM of 6 mice per group. (**F**) Expression of superoxide dismutase 2 (SOD2) and catalase in the liver of CRL and T/H mice. β-actin is shown as loading control. The histograms show the mean ± SEM of 12 and 11 mice for CRL and T/H mice, respectively. (**G**) Representative experiment showing the differential carbonylation of liver proteins in CRL and T/H mice. The

presence (+) or absence (-) of DNPH is indicated. Protein loading of the samples was verified by western blotting with anti β-actin. The migration of molecular mass markers is indicated to the left. Arrows (to the right) identify the migration of the two proteins used in quantification of protein carbonylation in the histograms. The results shown are the mean ± SEM of 6 CRL (open bars) and 8 T/H (closed bars) mice, respectively. (**A-G**) *****, $p<0.05$ when compared to control mice by Student's t test.

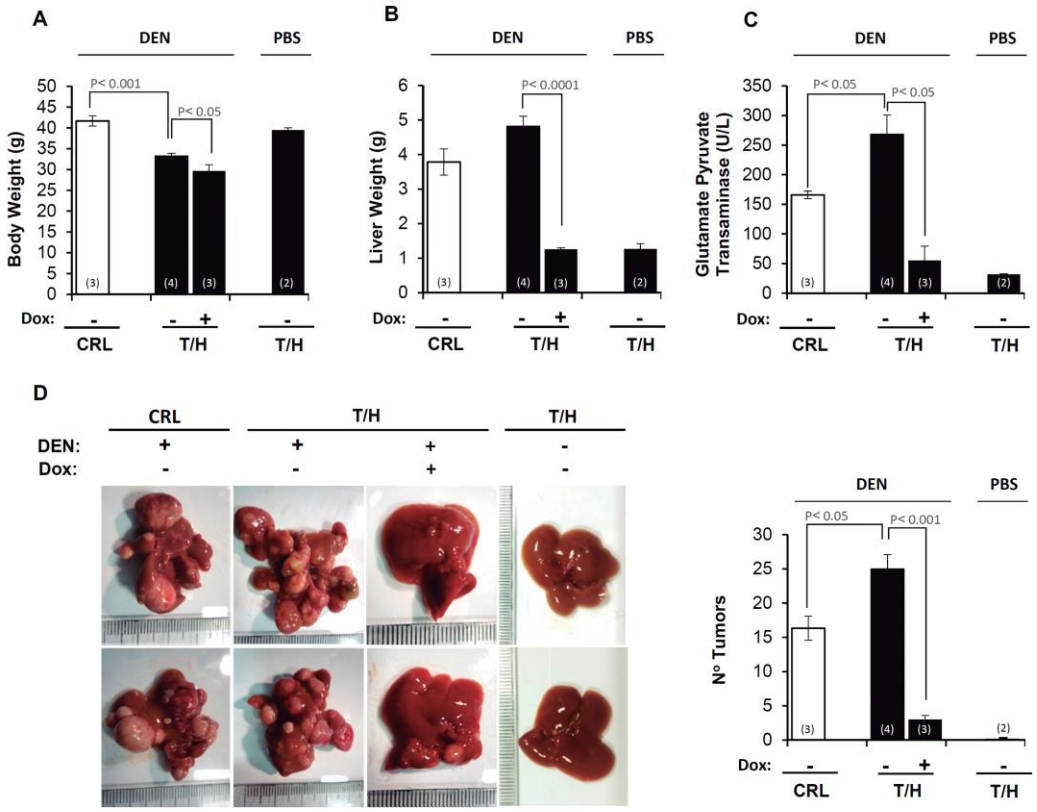

Figure S3, related to Fig. 3. The expression of hIF1 increased DEN-induced hepatocarcinogenesis in the single DEN-administration model. (A-C) Changes in body weight (**A**), liver weight (**B**) and blood GPT (**C**) in PBS or DEN-treated CRL (open bars) and hIF1 Tet-Off T/H (closed bars) mice, treated in presence (+) or absence (-) of Dox. **(D)** CRL and T/H livers of mice treated (+) or not treated (-) with DEN. The effect of Dox administration (+) or not (-) is also shown. The number of tumors in PBS or DEN-treated CRL (open bars) and T/H (closed bars) mouse livers treated (+) or not (-) with Dox. The number of mice is indicated in parenthesis. Results are means ± SEM. P values by Student's t test are indicated.

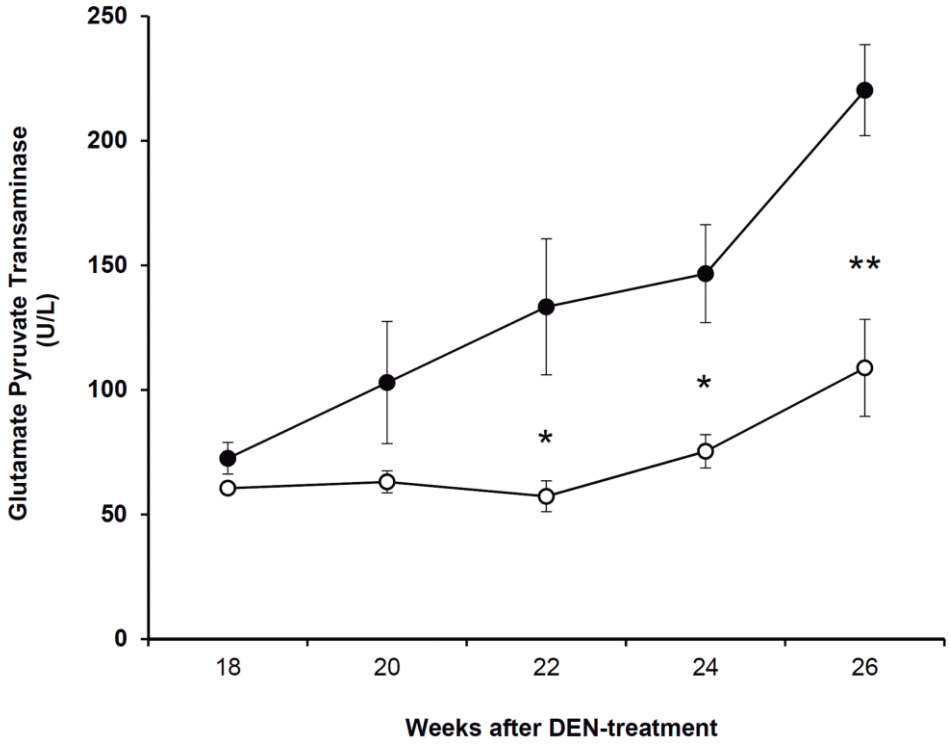

Figure S4, related to Fig.3. Progression of blood GPT levels during DEN-induced hepatocarcinogeneis. Blood glutamate/pyruvate transaminase activity (U/l) was determined in DEN-treated control (CRL, open circles) and hIF1 Tet-Off T/H (closed circles) mice. The results are means ± SEM of eleven animals per group. *, $p<0.05$ and **, $p<0.01$ when compared to control mice by Student's t test.

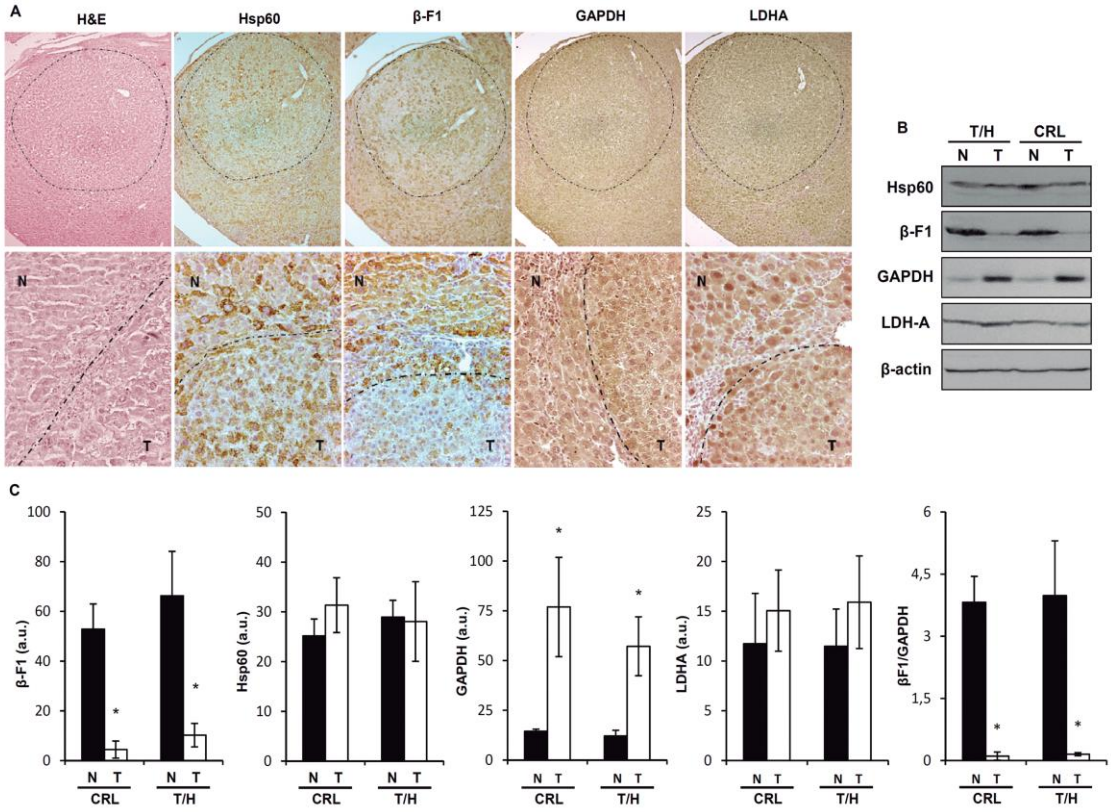

Figure S5, Related to Fig. 5. Repression of mitochondrial biogenesis in DEN-induced hepatocarcinogenesis (HCC). (A) Focal hepatic lesions in DEN-treated CRL mice identified by hematoxilin-eosin (H&E) and immunohistochemical staining with the antibodies against Hsp60, β-F1-ATPase (β-F1), GAPDH and LDHA in the same localized tumor area (upper panels, magnification 5x). The same study in normal (N, upper left) and tumor (T, lower right) areas at 20x magnification (lower panels). A dashed line marks the border between tumor and non-tumor areas**. (B)** Blots of Hsp60, β-F1-ATPase (β-F1), GAPDH, LDHA and β-actin (loading control) in normal (N) and tumor (T) tissue from CRL and T/H mice. (**C**) Histograms show the quantification of the proteins normalized to β-actin expression (arbitrary units, a.u.). The bioenergetic signature (β-F1-ATPase/GAPDH ratio) of the tissues is also shown. Results are means ± SEM for 7 animals. *P < 0.05 when compared with normal by Student's t test.

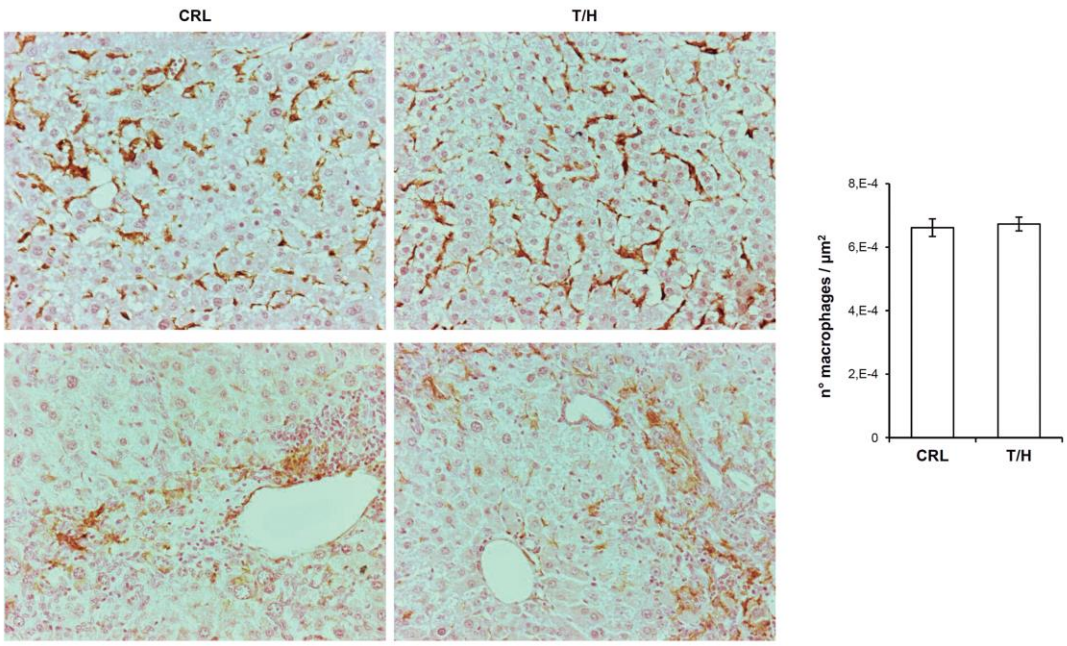

Figure S6, Related to Fig. 5. Macrophage infiltration in DEN-induced hepatocarcinogenesis (HCC). (A) Liver sections of DEN-treated CRL and hIF1 Tet-Off T/H mice were processed for immunohistochemistry to assess the rates of macrophage infiltration in HCC. F4/80 staining is shown in tumor (upper panels) and normal (lower panels) tissues. Magnification 20x. Histograms show the quantification of macrophage infiltration (number of macrophages/μm^2) in the tumor area from CRL and T/H animals. Bars are the mean ± SEM of 4 mice per group.

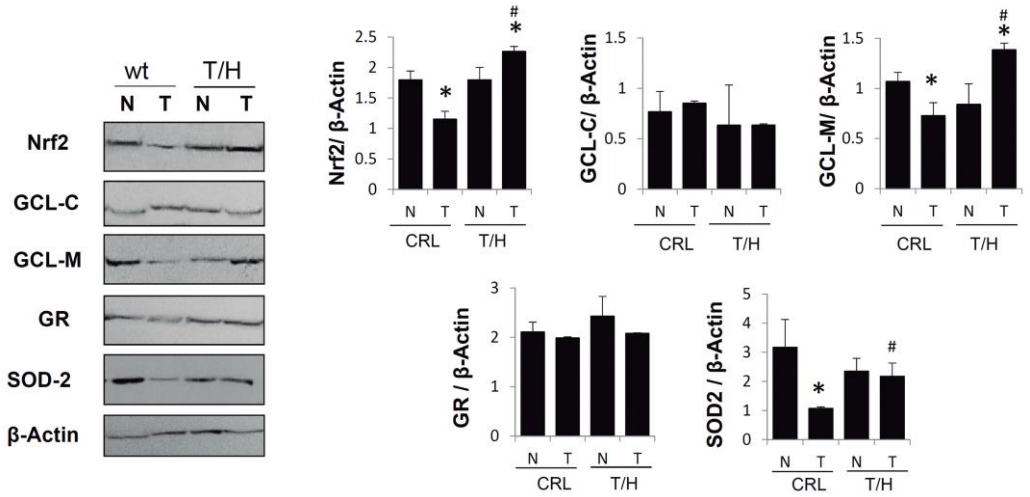

Figure S7, Related to Fig. 8. DEN treatment triggers an antioxidant response in the liver of hIF1 mice. Normal (N) and tumor (T) tissues from control (CRL) and Tet-Off T/H mice were analyzed after treatment with DEN. Blots of Nrf2, GCL-C, GCL-M, GR, SOD2 and β-Actin (loading control) are shown. Histograms show the quantification of the proteins normalized to the β-actin signal. The results are the mean ± S.E.M of 4 mice per group.*, $p<0.05$ when compared to normal tissue by Student's t test. #, $p<0.05$ when compared to tumor tissue in CRL by Student's t test.

Artículo #3

Formentini, L., Pereira, M.P., Sánchez-Cenizo, L., **Santacatterina, F.**, Lucas, J.J., Navarro, C., Martínez-Serrano, A., Cuezva, J.M. (2014). In vivo inhibition of the mitochondrial H+-ATP synthase in neurons promotes metabolic preconditioning. *EMBO J.* 1;33(7):762-7

Published online: February 12, 2014

Article

SOURCE DATA TRANSPARENT PROCESS

THE EMBO JOURNAL

In vivo inhibition of the mitochondrial H^+-ATP synthase in neurons promotes metabolic preconditioning

Laura Formentini[1,2,3], Marta P Pereira[1], Laura Sánchez-Cenizo[1,2,3], Fulvio Santacatterina[1,2,3], José J Lucas[1,4], Carmen Navarro[5], Alberto Martínez-Serrano[1] & José M Cuezva[1,2,3,*]

Abstract

A key transducer in energy conservation and signaling cell death is the mitochondrial H^+-ATP synthase. The expression of the ATPase inhibitory factor 1 (IF1) is a strategy used by cancer cells to inhibit the activity of the H^+-ATP synthase to generate a ROS signal that switches on cellular programs of survival. We have generated a mouse model expressing a mutant of human IF1 in brain neurons to assess the role of the H^+-ATP synthase in cell death *in vivo*. The expression of hIF1 inhibits the activity of oxidative phosphorylation and mediates the shift of neurons to an enhanced aerobic glycolysis. Metabolic reprogramming induces brain preconditioning affording protection against quinolinic acid-induced excitotoxicity. Mechanistically, preconditioning involves the activation of the Akt/p70S6K and PARP repair pathways and Bcl-xL protection from cell death. Overall, our findings provide the first *in vivo* evidence highlighting the H^+-ATP synthase as a target to prevent neuronal cell death.

Keywords brain preconditioning; energy metabolism; H^+-ATP synthase; inhibitory factor 1 (IF1); mitochondria

Subject Categories Autophagy & Cell Death; Metabolism; Neuroscience

DOI 10.1002/embj.201386392 | Received 24 July 2013 | Revised 8 January 2014 | Accepted 13 January 2014 | Published online 12 February 2014

EMBO Journal (2014) 33, 762–778

Introduction

The H^+-ATP synthase of the inner mitochondrial membrane is a master regulator of energy metabolism and cell fate. In oxidative phosphorylation (OXPHOS), the H^+-ATP synthase utilizes the H^+ electrochemical gradient generated by the respiratory chain to synthesize most of the ATP that is required to sustain cellular activities of the differentiated aerobic cell. Many findings corroborate the molecular and functional integration of OXPHOS (Dey & Moraes, 2000; Tomiyama *et al*, 2006) and specifically of the H^+-ATP synthase (Matsuyama *et al*, 1998; Shchepina *et al*, 2002; Santamaria *et al*, 2006; Alavian *et al*, 2011; Chen *et al*, 2011) with cell death. In fact, apoptosis has been shown to be strictly dependent upon subunits of the H^+-ATP synthase in yeast, mammals, and plants (Matsuyama *et al*, 1998; Gross *et al*, 2000; Chivasa *et al*, 2011). The point of no return in cell death is the permeabilization of the inner mitochondrial membrane to low molecular weight solutes, through opening of the so-called permeability transition pore (PTP) (Galluzzi *et al*, 2009; Di Lisa *et al*, 2011). Although the molecular composition of the PTP remains unknown, recent findings support that the high-conductance channel is composed by dimers of the H^+-ATP synthase (Giorgio *et al*, 2013), consistent with the finding that subunit c of the F0-channel of the H^+-ATP synthase is required for the activity of the PTP (Bonora *et al*, 2013). Cyclophilin D that regulates the activity of the PTP also interacts and regulates the activity of the H^+-ATP synthase (Giorgio *et al*, 2009).

Down-regulation of the H^+-ATP synthase is functionally linked to resistance to chemotherapy in cancer cells (Shin *et al*, 2005; Hernlund *et al*, 2009; Li *et al*, 2010; Sanchez-Arago *et al*, 2013a), consistent with the emerging role of the mitochondrial synthase in the execution of cell death. More recently, cancer cells have been shown to escape from death by inhibiting the activity of the H^+-ATP synthase by the overexpression of the ATPase inhibitory factor 1 (IF1) (Formentini *et al*, 2012; Faccenda *et al*, 2013; Sanchez-Arago *et al*, 2013b), which mimics the inhibitory effect of oligomycin (OL) in apoptosis (Matsuyama *et al*, 1998; Shchepina *et al*, 2002; Santamaria *et al*, 2006). IF1 is the physiological inhibitor of the mitochondrial H^+-ATP synthase (Gledhill *et al*, 2007). Mechanistically, cell survival results from rewiring of energy metabolism and nuclear reprogramming due to a reactive oxygen species (ROS) signal that

1 Departamento de Biología Molecular, Centro de Biología Molecular Severo Ochoa, Consejo Superior de Investigaciones Científicas-Universidad Autónoma de Madrid (CSIC-UAM), Madrid, Spain
2 Centro de Investigación Biomédica en Red de Enfermedades Raras (CIBERER), ISCIII, Madrid, Spain
3 Instituto de Investigación Hospital 12 de Octubre, Universidad Autónoma de Madrid, Madrid, Spain
4 Centro de Investigación Biomédica en Red de Enfermedades Neurodegenerativas (CIBERNED), ISCIII, Madrid, Spain
5 Departamento de Patología y Neuropatología, Instituto de Investigación Biomédica de Vigo (IBIV), Vigo, Spain
*Corresponding author. Tel: +34 91 196 4618; Fax: +34 91 196 4420; E-mail: jmcuezva@cbm.uam.es

is produced in mitochondria after the IF1-mediated inhibition of the H^+-ATP synthase (Formentini *et al*, 2012; Sanchez-Arago *et al*, 2013b).

We present a mouse model expressing a mutant of human IF1 (hIF1) in neurons under the control of a doxycyclin-regulated promoter. The purpose of this model was to inhibit by the most effective way the activity of the H^+-ATP synthase *in vivo*. Studies in total brain, isolated mitochondria, and primary neuronal cultures demonstrate that overexpression of hIF1 partially inhibits oxidative phosphorylation triggering an adaptive metabolic response that results in increased aerobic glycolysis. The IF1-mediated metabolic reprogramming results in brain preconditioning and involves a mild oxidative stress that protects neurons from excitotoxic damage, enhancing motor behavior. Overall, our findings provide the first demonstration that links the inhibition of the H^+-ATP synthase with protection from neuronal damage *in vivo*, highlighting the pivotal role that the engine of OXPHOS has a cell death regulator.

Results

A mouse model to inhibit the neuronal H^+-ATP synthase *in vivo*

To assess the role of OXPHOS in neurons, we generated a transgenic mouse (H^+) that integrates in its genome the mutant H49K of the human ATPase inhibitory factor 1 (hIF1) under a tetracycline-regulated promoter (TRE-H49K) (Fig 1A). The H49K mutant has a higher binding affinity for the β-catalytic subunit of the H^+-ATP synthase (Cabezon *et al*, 2000). Double transgenic Tet-Off mice (H^+/T^+) were generated by breeding H^+ animals with CamKII-tTA mice (T^+) that express the tTA transgene (Fig 1A) in neurons. Western blots (Fig 1A) and immunohistochemistry of coronal brain slices (Fig 1B, Supplementary Figs S1 and S2) revealed that only the H^+/T^+ genotype expresses hIF1 in mitochondria of neurons, resulting in approximately 3-fold increase in the total cellular content of IF1 (Fig 1A). The expression of hIF1 did not affect the expression of other mitochondrial proteins (Fig 1C and Supplementary Fig S3). However, the concentration of ATP was significantly diminished in the brain of H^+/T^+ mice when compared to controls (Fig 1D). These changes were accompanied by an increased concentration of AMP (Fig 1D) and the concurrent phosphorylation of the metabolic sensor AMPK (Fig 1E) in the brain of H^+/T^+ mice. Interestingly, a significant increase in the expression of the glycolytic enzymes GAPDH and LDH-A (Fig 1E) was observed in brain extracts of H^+/T^+ mice. Despite these differences, H^+/T^+ mice were born in the expected Mendelian ratios and were normal in appearance, home-cage behavior, reproduction, and longevity up to 1-year follow-up.

hIF1 inhibits the H^+-ATP synthase

The hydrolytic activity of the H^+-ATP synthase was significantly reduced in isolated brain mitochondria from H^+/T^+ mice when compared to controls (Fig 1F). Consistently, $TMRM^+$ staining after the administration of antimycin A revealed a minor capacity of mitochondria from H^+/T^+ mice to sustain the membrane potential ($\Delta\Psi m$) (Fig 1G). Likewise, oxygen consumption rates revealed that both State 3 (ADP-stimulated), uncoupled (FCCP-induced), and OL-sensitive respiration were significantly diminished when compared to controls (Fig 2A). The latter is consistent with the inhibition of the synthase activity of the ATP synthase by the expression of hIF1. No relevant differences were observed in $\Delta\Psi m$ in H^+/T^+ mice when compared to controls (Figs 1G and 2B). However, the addition of ADP triggered a larger $\Delta\Psi m$ depolarization in mitochondria of wild-type versus H^+/T^+ mice (Fig 2B), also consistent with the partial inhibition of the synthase activity of the H^+-ATP synthase by hIF1. A mild increase in the carbonylation of specific proteins (Fig 2C) and in the basal levels of catalase, SOD1, and SOD2 (Fig 2D) was observed in the brain of H^+/T^+ mice when compared to controls. However, no significant differences in GSH and GSH/GSSG ratio were observed (Fig 2E), showing that the oxidative stress induced by hIF1 expression is of mild intensity.

hIF1 inhibits cytochrome *c* oxidase activity

No relevant differences were noted in the content of native complexes I, II, III, and V in mitochondria between H^+/T^+ mice and controls (Fig 2F). Interestingly, mitochondria of H^+/T^+ mice showed no formation of supercomplex containing complex IV (Fig 2F). In fact, most of complex IV migrated as monomer (Fig 2F). Consistent with the role of supercomplexes in the rate of respiration (Acin-Perez *et al*, 2008; Lapuente-Brun *et al*, 2013), the enzymatic activity of complex IV was significantly diminished in mitochondria of H^+/T^+ mice (Fig 2G). No differences were noted in the activities of complex I and complexes II+III between both phenotypes (Fig 2G).

hIF1 promotes metabolic reprogramming and ROS signaling in cortical neurons

Only primary cultures of cortical neurons (Supplementary Fig S4) derived from H^+/T^+ embryos expressed hIF1 (Fig 3A–C). Expression of hIF1 resulted in a significant decrease in the cellular content of ATP (Fig 3D) and in the activity of the H^+-ATP synthase (Fig 3E). This effect was not observed in 4-d cultures (Fig 3E), when neurons are not yet expressing hIF1 (Fig 3B). The expression of hIF1 resulted in a significant increase in aerobic glycolysis as assessed by the rate of lactate production (Fig 3F). OL induced aerobic glycolysis only in neurons derived from control animals (Fig 3F), supporting that hIF1 is stimulating aerobic glycolysis to its maximum rate (Fig 3F). Analysis of the expression of PK-M2, LDH-A, and GAPDH confirmed the induction of glycolysis in H^+/T^+ neurons when compared to wild-type cultures (Fig 3G). Basal $TMRM^+$ fluorescence did not show significant differences between H^+/T^+ and controls (Fig 3H, Supplementary Figs S5 and S6), suggesting that there is no major difference in $\Delta\Psi m$. Consistent with the inhibition of both the synthase and hydrolase activity of the H^+-ATP synthase by hIF1, we observed that $\Delta\Psi m$ changes in response to OL were lower (Supplementary Fig S5), whereas those to antimycin A were higher (Supplementary Fig S6) in H^+/T^+ cultures than in control. The production of superoxide radical was enhanced in H^+/T^+ neurons when compared to wild type (Fig 3I). An increase in the carbonylation of specific neuronal proteins was observed (Fig 3J), consistent with a higher basal production of ROS in H^+/T^+ neurons and with data in brain homogenates (Fig 2C).

hIF1 mice are protected from quinolinic acid-induced brain damage

To assess the role of H^+-ATP synthase in cell death *in vivo*, 1-year-old control and hIF1-expressing mice received an injection of quinolinic acid into the left striatal region of the brain (Martinez-Serrano & Bjorklund, 1996; Schwarcz *et al*, 2012). Weight loss after injury (Fig 4A), spleen volume contraction (Fig 4B), and enlargement of the ipsilateral ventricle (Fig 4C), which are respective indexes of general impairment of animal health, monocyte recruitment, and tissue loss, suggest that hIF1-expressing mice are partially protected from excitotoxicity. Hematoxylin–eosin-stained brain sections also revealed a significant approximately 50% reduction in the lesion area in H^+/T^+ mice (Fig 4D). The reduced expression of the neuronal markers DARPP-32 (Fig 4E) and NeuN (Supplementary Fig S7) in the brain of controls further supports a higher neuronal protection in H^+/T^+ mice. Quantification of microglia (Fig 4E, Iba-1, red staining and Supplementary Fig S8) and phagocytes (Fig 4E, Ed-1, green staining and Supplementary Fig S8) revealed a significant increase in gliosis in control when compared to H^+/T^+ mice, suggesting that hIF1 protects neurons from damage and hence from the subsequent local inflammation.

Neurological evaluation indicates a better performance in hIF1 mice

No differences in locomotor performance were observed between control and H^+/T^+ mice before quinolinic acid administration (Supplementary Fig S9A–F). However, three locomotor tests showed that H^+/T^+ mice are partially protected from quinolinic acid-induced damage (Supplementary Fig S9 and Supplementary videos for control and hIF1-expressing mice). Paw usage contralateral to the brain lesion (right) was significantly diminished in control animals when compared to H^+/T^+ mice (Supplementary Fig S9A). No differences were noted in the use of the ipsilateral forelimb (left) (Supplementary Fig S9B). Gate analysis revealed that control mice showed an increased stride length of the contralateral forelimb (Supplementary Fig S9C) and in the coefficient of variation for base width of the hind limbs (Supplementary Fig S9D) when compared to H^+/T^+ mice in the "footprint" test (Carter *et al*, 1999). After lesion, all animals showed an increase in the number of paw slips in the grid test (Brooks & Dunnett, 2009) but as early as 4 days post-surgery H^+/T^+ mice were able to walk through the grid with a significantly lower number of paw slips (Supplementary Fig S9E). The motility index of H^+/T^+ mice was unaltered by lesion (Supplementary Fig S9F). However, control mice were less prone to explore than H^+/T^+ mice, suggesting a severe motor impairment (Supplementary Fig S9F) (Supplemental videos for control and hIF1-expressing mice). Overall, H^+/T^+ mice showed lower deviation from presurgical values than control animals.

hIF1 protects from quinolinic acid-induced cell death

Fluoro-Jade B-positive neurons both in the core and in penumbra region of the lesion were significantly augmented in control when compared to H^+/T^+ mice (Fig 5A). Analysis of apoptotic cell death by the determination of caspase 3 activation confirmed that hIF1 expressing neurons were protected from apoptosis in the penumbra (Fig 5B). Most of the toxic cascades stimulated by quinolinic acid implicate the formation of ROS (Schwarcz *et al*, 2012). Consistently, the GSH content in the damaged hemisphere was highly reduced when compared to the non-stressed tissue (compare Fig 5C versus Fig 2E). Remarkably, both the GSH content and the GSH/GSSG ratio were significantly higher in the affected hemisphere of hIF1-expressing mice than in controls (Fig 5C).

hIF1 signals the activation of neuroprotection pathways

Phosphorylation of Akt is part of the survival signaling pathway induced in cells confronted with mitochondrial respiration defects and/or mild oxidative stress (Leslie, 2006; Pelicano *et al*, 2006). Consistently, the phosphorylation of Akt was significantly augmented in both brain hemispheres of mice expressing hIF1 (Fig 5D). We also observed an enhanced phosphorylation of the pro-survival p70S6K in both brain hemispheres (Fig 5D) and enhanced expression of *c-fos* in the damaged area of H^+/T^+ mice (Fig 5E). Moreover, the content of IκBα, which is the negative regulator of NFκB transcription factor, was significantly diminished in the damaged hemisphere of H^+/T^+ mice (Fig 5D). Changes in IkBα expression were paralleled by opposite changes in the

Figure 1. Mice expressing hIF1 in neurons.

A PCR analysis for the H49K variant of hIF1 and tTA constructs in wild-type (wt), tTA (T^+), H49K (H^+) or double transgenic (H^+/T^+) mice is shown. Western blots reveal the expression of hIF1 and IF1 (12 kDa) in total brain extracts. hIF1 is only expressed in H^+/T^+ mice. β-actin expression is shown as a loading control.

B Immunohistochemistry (mitochondrial staining) for hIF1 and β-F1 ATPase (β-F1) in brain cortex of control (wt) and H^+/T^+ mice. Magnification 63×.

C Representative Western blots of the expression of hIF1, heat-shock protein 60 (HSP60), and mitochondrial complexes I (NADH9), II (SDH), III (core II), IV (COXI and COX IV), and V (β-F1) in total brain extracts of wt and H^+/T^+ mice. Two different samples per condition tested are shown.

D Content of adenine nucleotides in brain extracts of control (wt, closed bars) and H^+/T^+ mice (open bars).

E Western blots show the hIF1-dependent phosphorylation of AMPK (p-AMPK) and the concurrent increase in glycolytic proteins lactate dehydrogenase A (LDH-A) and glyceraldehyde-3-phosphate dehydrogenase (GAPDH) in brain extracts (see histograms to the right). Two different samples per condition tested are shown. β-F1 and HSP60 expressions are shown as loading controls.

F Hydrolytic activity of the H^+-ATP synthase in isolated mitochondria from brain of control (wt, black trace) and H^+/T^+ (gray trace) mice. Where indicated, 10 μM oligomycin (OL) was added.

G Variation in the membrane potential ($TMRM^+$ staining) of isolated mitochondria from control (black trace) and H^+/T^+ animals (gray trace) charged with 100 nM $TMRM^+$. The effect of 1 μM antimycin A in the presence of 10 mM ATP is shown.

Data information: In (D, E, and F), bars are the mean ± s.e.m. of six different samples; $*P < 0.05$ when compared to control by Students *t*-test. See also Supplementary Figs S1, S2, and S3.

Source data are available online for this figure.

expression of Bcl-xL, a downstream target of NFκB that is involved in preventing cell death (Fig 5D). In contrast, the expression of the anti-apoptotic Bcl-2 was not affected by hIF1 expression or by quinolinic acid administration (Fig 5D). Remarkably, the ATP and ADP content in the damaged area of the left hemisphere was much lower in H^+/T^+ mice (Fig 6A). In contrast, the AMP content was significantly increased (Fig 6A). The larger drop in ATP content of H^+/T^+ mice can be explained by the enforced hIF1-mediated inhibition of the synthase activity of the H^+-ATP synthase, but could also result from higher activation of ATP-consuming reactions

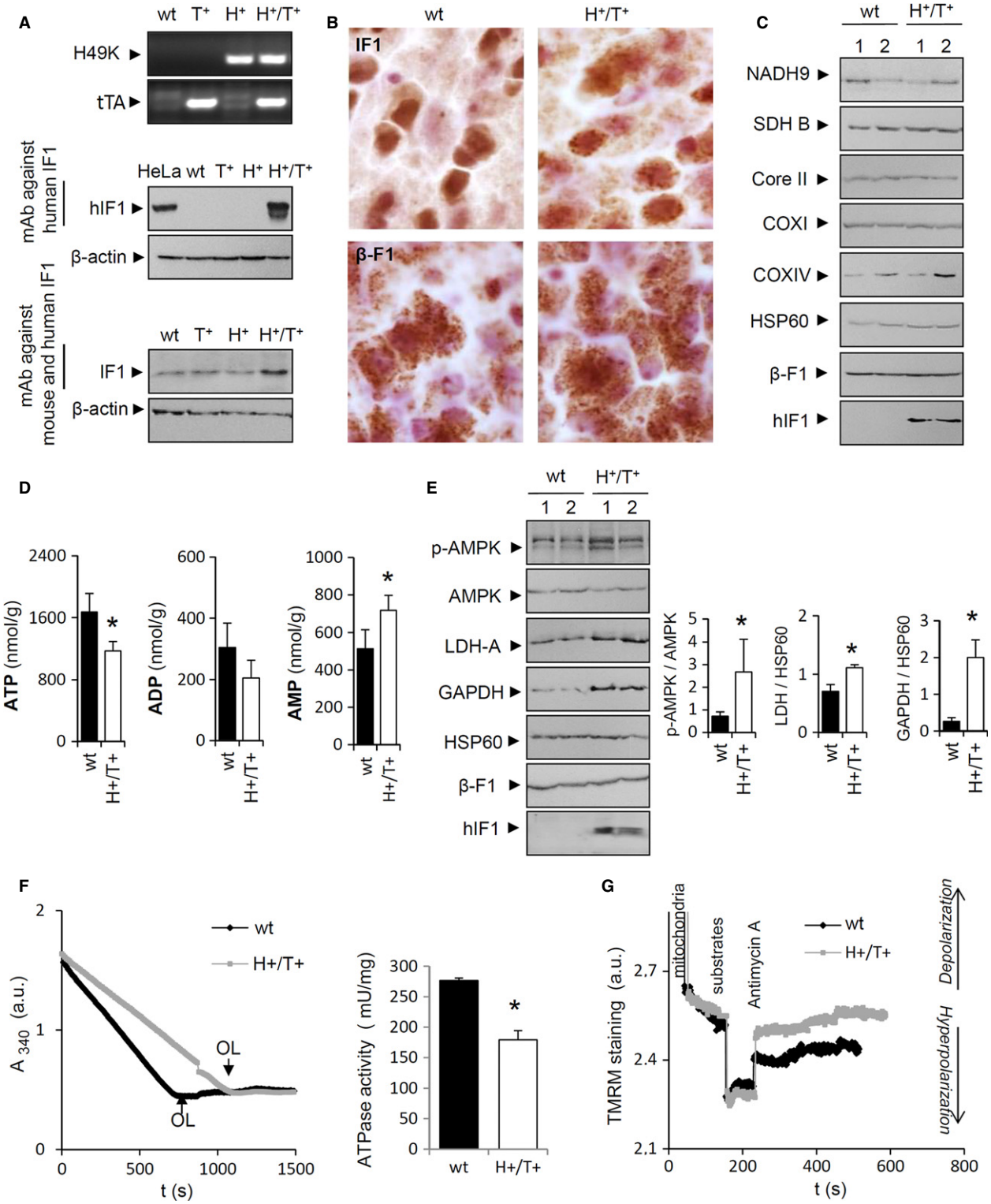

Published online: February 12, 2014
The EMBO Journal

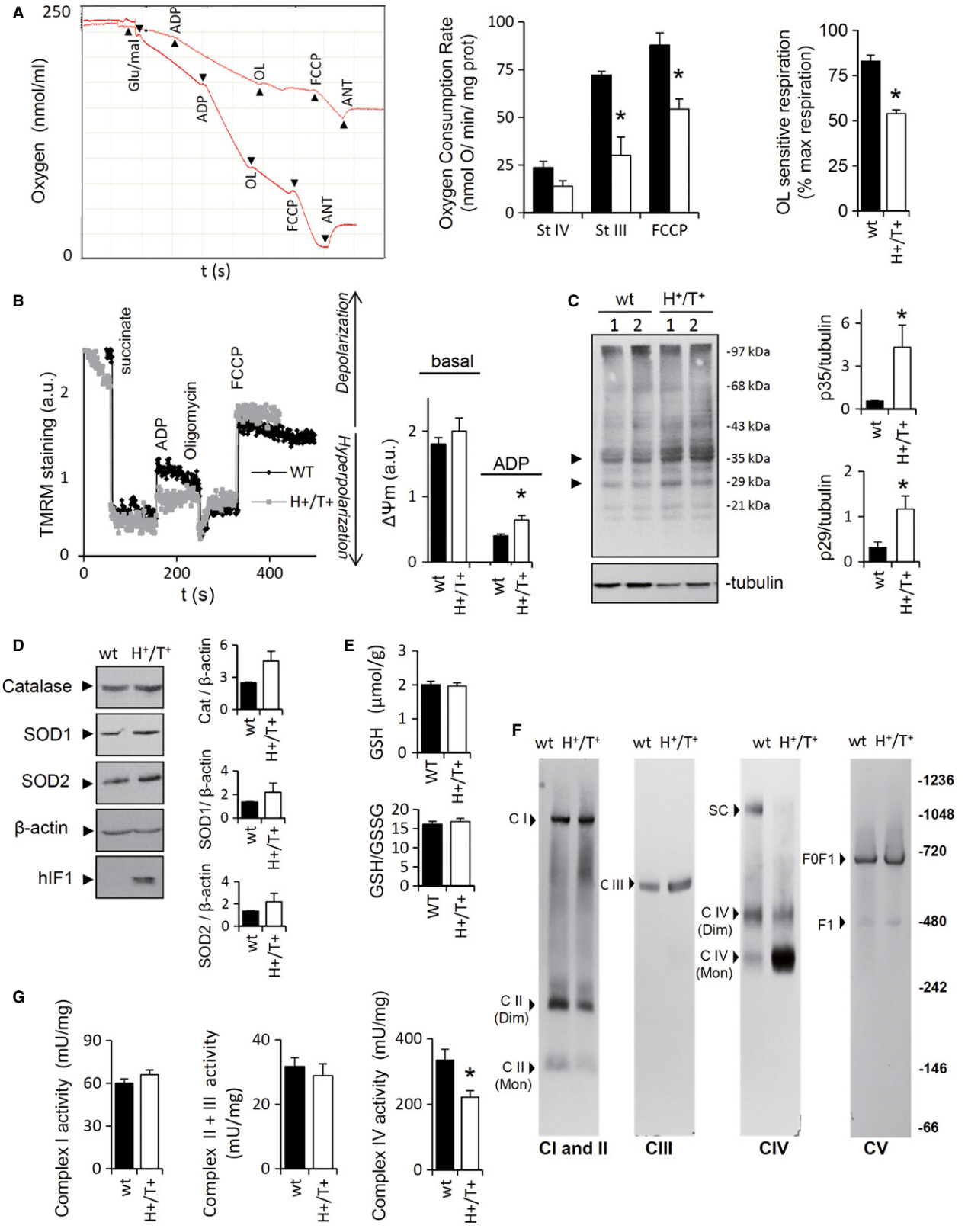

following the activation of repair mechanisms. This is consistent with a higher basal PARP activity in the brain of H^+/T^+ mice (Fig 6B), a difference that was magnified after hemispheric damage (Fig 6B).

ROS are involved in cell death

Consistent with the role of ROS in mediating neuronal excitotoxicity (Schwarcz *et al*, 2012), we observed that quenching ROS after

Figure 2. hIF1 impairs oxidative phosphorylation.

A Polarographic profiles of isolated mitochondria from control (lower trace) and H^+/T^+ animals (upper trace). The effect of 10 mM glutamate/malate, 0.5 mM ADP, 5 μM oligomycin (OL), 5 μM FCCP, and 1 μM antimycin A (Ant) is shown. Histograms reveal a reduction in State III (StIII) and uncoupled (FCCP) respiration in mitochondria of H^+/T^+ mice (open bars) when compared to controls (wt, closed bars). OL-sensitive ATP synthase activity is also shown as a percentage of maximal respiration.

B Variation in the membrane potential ($TMRM^+$ staining) of isolated mitochondria from control (black trace) and H^+/T^+ animals (gray trace) charged with 100 nM $TMRM^+$. The effect of 5 mM succinate, 1 mM ADP, 5 μM OL, and 5 μM FCCP 1 is shown. Histograms show a larger reduction in $\Delta\Psi m$ after ADP administration in controls (wt, closed bars) when compared to hIF1-expressing mice (H^+/T^+, open bars).

C Representative Western blot of the extent of carbonylation of total brain proteins. Two different samples per condition tested are shown. Tubulin was used as loading control. The migration of molecular mass markers is indicated to the right. Arrows (to the left) identify the migration of the two proteins used in the quantification of protein carbonylation (histograms).

D Representative Western blots of catalase (cat), superoxide dismutase 1 and 2 (SOD1 and SOD2) expression in control (wt, closed bars) and hIF1-expressing (H^+/T^+, open bars) mice.

E Cellular glutathione (GSH) and GSH/GSSG ratio in total brain.

F Blue-native immunoblot analysis of mitochondrial membrane proteins visualized with antibodies against mitochondrial complexes I (NADH9), II (SDH), III (core II), IV (COX IV), and V (β-F1-ATPase). The migration of monomers (Mon), dimers (Dim), supercomplex (SC), F1-ATPase (F1), H^+-ATP synthase (F0F1), and molecular mass markers is indicated.

G Enzymatic activity of mitochondrial complexes I, II+III, and IV in isolated brain mitochondria of control (wt, closed bars) and H^+/T^+ (open bars) mice.

Data information: Bars are the mean ± s.e.m. of three (A, B, D, G), four (C), or six (E, F) determinations; $*P < 0.05$ when compared to controls by Students *t*-test.

Source data are available online for this figure.

glutamate-induced cell death significantly arrested cell death in primary neuronal cultures of control mice (Fig 6C). The cell death response to glutamate was much less in neurons of hIF1-expressing mice (Fig 6C). In fact, cell death was essentially the same as that of control neurons treated with the antioxidant mito Q (Fig 6C), presumably because the hIF1-mediated activation of the pro-survival signaling pathways (Figs 5D and 6B) confers a more resistant phenotype against ROS-mediated cell death.

Bcl-xL participates in hIF1-mediated protection of neuronal death

Blue-native gels confirmed the interaction of Bcl-xL with the H^+-ATP synthase (Fig 6D), in agreement with recent findings (Alavian *et al*, 2011; Chen *et al*, 2011). However, and to our surprise, we found that Bcl-xL preferentially interacts with a native protein complex that migrates with complex I of the respiratory chain (Fig 6D). Remarkably, silencing of Bcl-xL in neurons restored the glutamate or hypoxia-driven cell death in preconditioned neurons of H^+/T^+ mice (Fig 6E), further supporting the role of the anti-apoptotic Bcl-xL in neuroprotection and eventually its cross-talk with the activity of the H^+-ATP synthase.

Discussion

Herein, we demonstrate that the expression of hIF1 partially inhibits the H^+-ATP synthase activity promoting rewiring of neuronal metabolism to an enhanced aerobic glycolysis. Inhibition of the H^+-ATP synthase activates pathways to prevent apoptotic cell death. In other words, expression of hIF1 induces a state of preconditioning that prevents neuronal death after excitotoxic damage as assessed both *in vivo* and in primary cultures. These findings provide the first *in vivo* account highlighting the relevance of rewiring energy metabolism in brain preconditioning, and stress the potential value of the H^+-ATP synthase as a target for therapeutic intervention. Moreover, the transgenic H^+ mouse developed offers a valuable tool to investigate the relevance of OXPHOS impairments in mammalian tissues *in vivo*. Until recently, IF1 was considered an inhibitor of the hydrolase activity of the ATP synthase that helps to preserve cellular ATP during hypoxia or ischemia (Gledhill *et al*, 2007; Faccenda *et al*, 2013). However, previous *in vitro* studies (Husain & Harris, 1983; Lippe *et al*, 1988) and more recent findings *in vivo* (Shen *et al*, 2009; Sanchez-Cenizo *et al*, 2010; Formentini *et al*, 2012; Sanchez-Arago *et al*, 2013b) have stressed the role of IF1 as an inhibitor of the synthase activity of the H^+-ATP synthase. The results in this study demonstrate the *in vivo* function of hIF1 as an inhibitor of the ATP synthase and of cell death.

Since we also observed a down-regulation of respiration and of the activity and assembly of complex IV, it can be argued that hIF1 exerts neuroprotection by its effect on the activity of the respiratory chain rather than on the ATP synthase. However, this explanation seems unlikely because the impairment of the respiratory chain is detrimental for cell survival. In fact, very recent findings (Cogliati *et al*, 2013) have highlighted that the disassembly of respiratory chain supercomplexes leads to an increase and not to a decrease in cell death, in agreement with our observation. Hence, we suggest that the effects of hIF1 on respiration result from feedback regulation of complex IV activity/assembly by the inhibition of the ATP synthase, although the mechanism involved deserves further investigation. However, we cannot rule out that hIF1 might be controlling the execution of cell death by regulating *cristae* remodeling (Cogliati *et al*, 2013; Faccenda *et al*, 2013) (Fig 7G). It is well established that dimers of the H^+-ATP synthase promote the high local curvature of the inner membrane at *cristae* ridges (Paumard *et al*, 2002; Davies *et al*, 2011, 2012). Recently, the genetic disruption of *cristae* shape morphology has been shown to favor apoptosis (Cogliati *et al*, 2013), providing a link between mitochondrial morphology and cell death. In this regard, it has been suggested that IF1 regulates the oligomeric state of the H^+-ATP synthase, increasing the density of *cristae* and the formation of dimeric ATP synthase complexes (Minauro-Sanmiguel *et al*, 2005; Garcia *et al*, 2006; Campanella *et al*, 2008; Bisetto *et al*, 2013). Although this suggestion has been questioned (Tomasetig *et al*, 2002; Wittig & Schagger, 2009; Fujikawa *et al*, 2012), it is possible that the overexpression of hIF1 might contribute to

Published online: February 12, 2014
The EMBO Journal

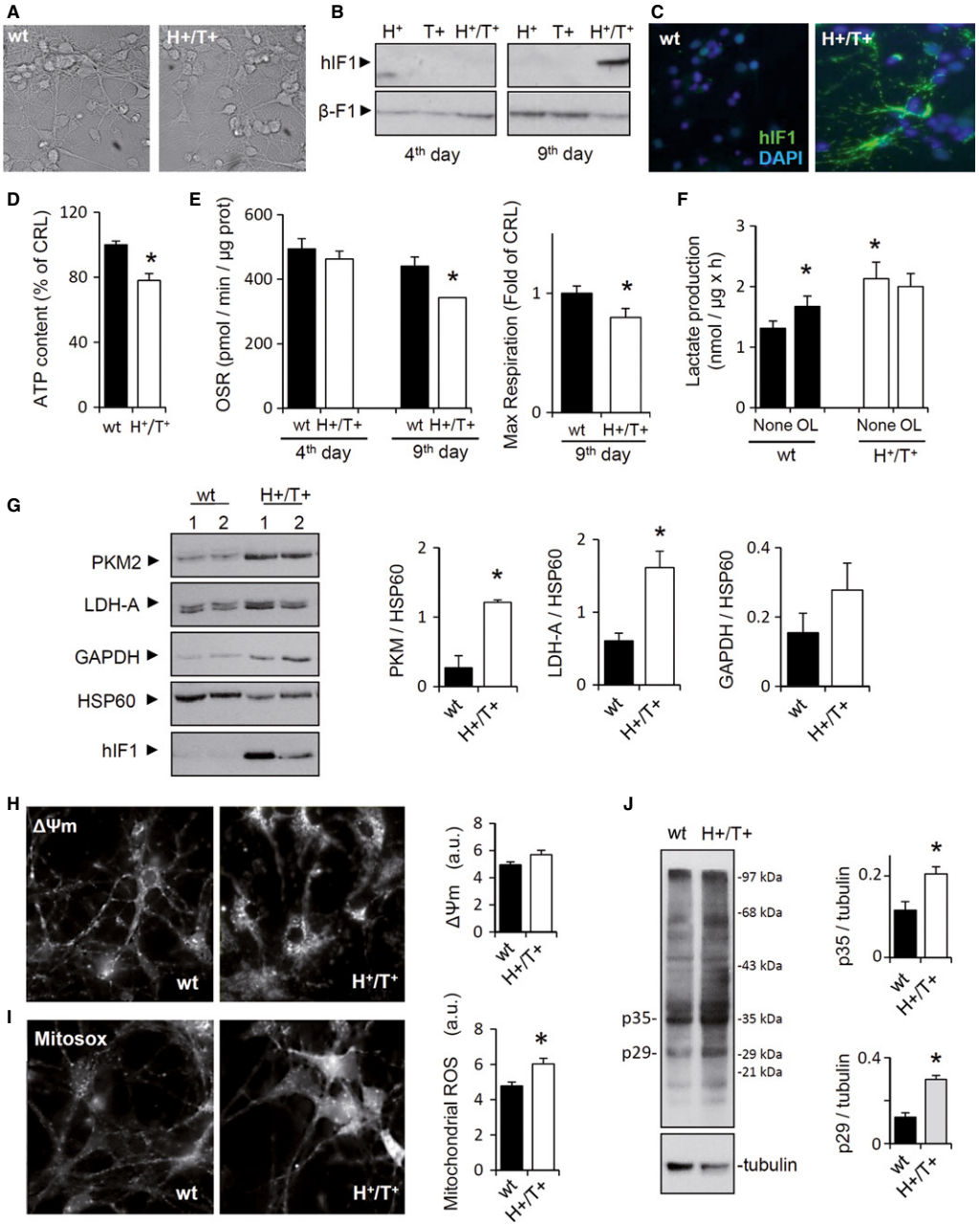

Figure 3. hIF1-induced metabolic reprogramming and ROS signaling in cortical neurons.

A–C *In vivo* phase-contrast images of 9-d cultures of cortical neurons obtained from control and H^+/T^+ embryos (A); magnification 40×. Representative Western blot (B) and immunocytochemistry (C) show the expression of hIF1 only in 9-d neurons of H^+/T^+ mice. β-F1-ATPase (β-F1) is used as a loading control. DAPI (4′,6-diamidino-2-phenylindole) staining is also shown. Magnification 40x.

D The cellular ATP content was determined in control (wt, closed bar) and H^+/T^+ (open bar) neuronal cultures.

E Shows the oligomycin-sensitive respiration (OSR) and maximal respiration in 4- and 9-day neuronal cultures from control (wt, closed bar) and H^+/T^+ (open bar) embryos.

F Rates of aerobic glycolysis (Lactate production) in the absence or presence of 5 µM oligomycin (OL).

G Representative Western blots of the expression of pyruvate kinase M2 (PKM2), lactate dehydrogenase A (LDH-A), glyceraldehyde-3-phosphate dehydrogenase (GAPDH), and heat-shock protein 60 (HSP60) in control (wt, closed bars) and hIF1-expressing (H^+/T^+, open bars) neurons.

H, I *In vivo* staining of $TMRM^+$ (H, $\Delta\Psi m$) or MitoSOX (I, ROS) charged mitochondria from 10-d primary cultures of cortical neurons. Magnification 40×.

J Representative experiment of carbonylation of proteins in primary neuronal cultures derived from control (wt) and H^+/T^+ mice. Tubulin is shown as a loading control. The migration of molecular mass markers is indicated to the right. Histograms show the quantification of p35 and p29 proteins.

Data information: The data shown are mean ± s.e.m. of three (D–F, H, and I) or four (G, J) cultures per condition. *$P < 0.05$ when compared to control by Students *t*-test. See also Supplementary Figs S4, S5, and S6.

Source data are available online for this figure.

Published online: February 12, 2014

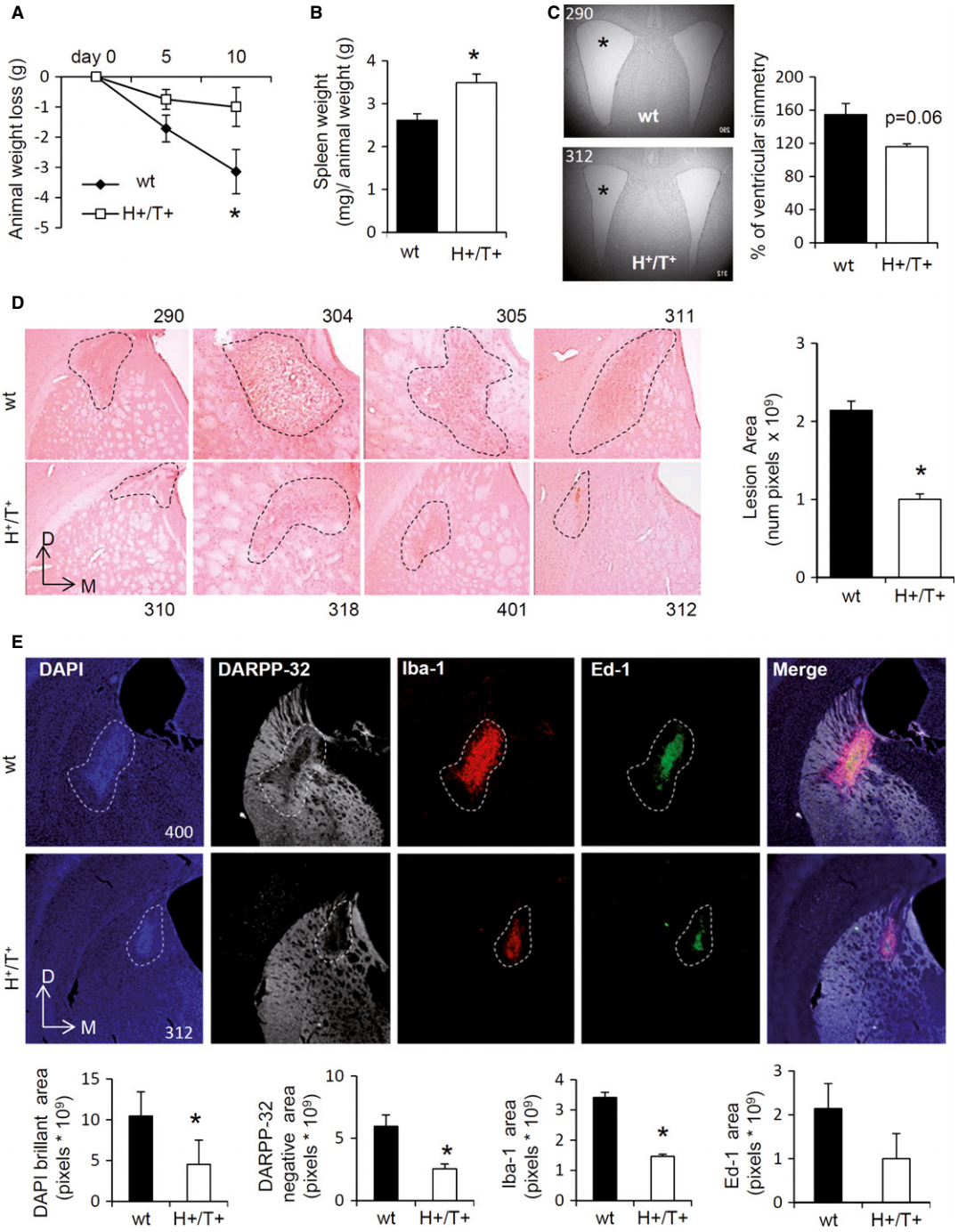

Figure 4. hIF1 protects from quinolinic acid-induced brain damage.

A, B Animal weight loss at the indicated time after surgery (A), and spleen weight at time of sacrifice (21st day) (B) in control (wt, closed squares and bar) and H^+/T^+ (open squares and bar) mice.

C Representative ventricular symmetry in sections of the brain from control (wt, closed bar) and H^+/T^+ (open bar) mice. Magnification 2.5×. The percentage increase in the ventricle area is shown.

D Brain sections stained with hematoxylin–eosin. Four different animals per condition tested are presented. The area of the lesion is indicated. Magnification 20×. Histograms show a reduction in the lesion area in H^+/T^+ mice (open bar) when compared to control (wt, closed bar) mice. Bars are the mean ± s.e.m. of five animals. D, dorsal; M, medial.

E Representative staining of nuclei (DAPI, blue), protein phosphatase 1 (DARPP-32, white), microglia (Iba-1, red), and macrophage/monocyte (Ed-1, green) by antibodies in the left hemisphere. Magnification 5×. Histograms show the quantification of fluorescence in controls (wt, closed bar) and H^+/T^+ (open bar) mice.

Data information: Bars are the mean ± s.e.m. of five (C–E) or ten (A, B) animals. Where indicated, numbers correspond to the identification code of the mouse. *$P < 0.05$ when compared to control by Students *t*-test. See also Supplementary Figs S7, S8, and S9 and Supplementary Videos.

stabilize *cristae* structure, hence upgrading, at the structural level, the threshold for cell death (Fig 7G).

Energy metabolism in neurons is highly dependent on OXPHOS. Unexpectedly, H^+/T^+ mice revealed no symptoms of neurological dysfunction. It is likely that the energy deficit triggered by a limited OXPHOS promotes the activation of the metabolic stress sensor AMPK (Mihaylova & Shaw, 2011) and the subsequent activation of aerobic glycolysis to partially compensate ATP provision in these neurons. It is really intriguing to find that tissues that have a very high energy demand, such as heart, liver, and kidney, are those that express higher levels of IF1 (Sanchez-Cenizo *et al*, 2010; Sanchez-Arago *et al*, 2013b). Mouse (Fig 7A) and human neurons of the brain and cerebellum (Fig 7B–F and Supplementary Fig S10) are not an exception showing a very high expression of IF1 when compared to astrocytes. Therefore, we suggest that the actual physiological function of IF1 in normal energy-demanding tissues is to ameliorate apoptosis geared by the activity of the H^+-ATP synthase under cellular stressful conditions. This hypothesis is supported by previous findings in different cancer cells (Sanchez-Cenizo *et al*, 2010; Formentini *et al*, 2012; Faccenda *et al*, 2013; Sanchez-Arago *et al*, 2013b). Obviously, this idea further supports that in addition to the well-characterized pH-regulated binding of IF1 to the H^+-ATP synthase under depolarization conditions (Cabezon *et al*, 2000), the activity of IF1 is regulated in these tissues by additional mechanisms that could involve the interaction of IF1 with other proteins (Lopez-Mediavilla *et al*, 1993) (Fig 7G) and/or tissue-specific post-translational modifications (Zhao *et al*, 2011).

Inhibition of the synthase activity of the H^+-ATP synthase by IF1 is known to promote a mild ROS signal (Formentini *et al*, 2012; Sanchez-Arago *et al*, 2013b), which is consistent with the observed inhibition of the H^+-ATP synthase, the enhanced production of ROS in neuronal cultures, and the increased carbonylation of brain and neuronal proteins in hIF1-expressing mice (Fig 7G). ROS are known activators of several of the pro-survival signaling pathways that we have shown to be activated in the brain of H^+/T^+ mice such as Akt/p70S6K (Datta *et al*, 1997; Harada *et al*, 2001) and NFκB (Ravati *et al*, 2001; Karin, 2006). The persistent mild oxidative stress in the brain of these animals could represent an additional mechanism involved in preconditioning (Iadecola & Anrather, 2011) by raising, at the functional level, the threshold at which a toxic insult will normally unlash the molecular events that trigger cell death (Fig 7G). Indeed, we have observed that quenching ROS largely inhibits glutamate-induced neuronal cell death only in non-preconditioned cultures. The finding that IF1 protects cancer cells from chemotherapy-induced apoptosis via ROS-mediated signaling (Formentini *et al*, 2012; Sanchez-Arago *et al*, 2013b) further supports this idea.

Importantly, our data show that hIF1-expressing neurons in the injured area are partially protected from cell death when compared to controls despite showing remarkably lower ATP and ADP concentrations. Hence, we suggest that either the set-point of ATP availability for triggering cell death has not been reached (Galluzzi *et al*, 2012) or that the flux at which ATP is being produced by the stimulation of aerobic glycolysis is enough to preserve cellular functions. An enhanced activity of ATP-consuming reactions such as the induction of protein synthesis revealed by the activation of p70S6K and of repair pathways by the activation of PARP in hIF1-expressing neurons might also contribute to the depletion of the phosphorylated nucleotides in these animals. Taken as a whole, our findings indicate that a sustained partial inhibition of OXPHOS mediates the activation of protein synthesis, the induction of repair mechanisms, and the prevention of apoptosis. Three behavioral locomotor tests confirm that hIF1-expressing mice show milder neurological impairment after injury.

Under conditions of cellular stress induced by different chemotherapeutic agents, the mitochondrial H^+-ATP synthase generates a high-intensity ROS signal that triggers apoptotic cell death (Johnson *et al*, 2005; Santamaria *et al*, 2006; Wondrak, 2009). Recent findings indicate that the H^+-ATP synthase forms part of the PTP (Bonora *et al*, 2013; Giorgio *et al*, 2013), stressing previous functional reports on the relevance of this complex of OXPHOS in cell death (Matsuyama *et al*, 1998; Shchepina *et al*, 2002; Santamaria *et al*, 2006) and the tangled circuitry of energy metabolism and apoptosis (Andersen & Kornbluth, 2013). Bcl-xL is the prevailing anti-apoptotic protein in the brain (Alavian *et al*, 2011; Michels *et al*, 2013). We suggest that the overexpression of Bcl-xL after induced excitotoxicity in the brain *in vivo* mediates the prevention of cell death, consistent with previous findings in cancer cells (Formentini *et al*, 2012; Sanchez-Arago *et al*, 2013b) and with the fact that the silencing of Bcl-xL reverted the protection afforded by IF1 overexpression. Moreover, Bcl-xL is also localized at the inner mitochondrial membrane where it interacts with the H^+-ATP synthase to enhance its activity by reducing futile ion cycling (Alavian *et al*, 2011; Chen *et al*, 2011). Herein, we have confirmed this interaction. We suggest that Bcl-xL might act as an additional

Figure 5. The inhibition of the H^+-ATP synthase protects neurons from apoptosis.

A Fluoro-Jade B staining in degenerating neurons in the core and penumbra of the striatal lesion. Three different images of animals identified by numbers are presented. Magnification 20×. Histograms show a reduction in the Fluoro-Jade B-positive area in H^+/T^+ (open bar) when compared to control (wt, closed bar) mice.

B Activated caspase 3 staining in the penumbra of the striatal lesion in control (wt, closed bars) and hIF1-expressing (H^+/T^+, open bars) mice. Magnification 20×. Histograms show a reduction in the apoptotic area in H^+/T^+ mice.

C Brain glutathione (GSH) content and GSH/GSSG ratio in the injured area of control (wt, closed bar) and H^+/T^+ (open bar) mice.

D Representative Western blots of the expression of protein kinase B (p-AKT, AKT), phospho p70 S6 kinase (p-P70S6), IkappaB alpha (IκBα), B-cell lymphoma-extra large (Bcl-xL), and B-cell lymphoma 2 (Bcl-2) in the right (R) and left (L) hemispheres of wt and H^+/T^+ mice. One control and two different H^+/T^+ animals are shown.

E DAPI (blue), c-Fos (green), and glial fibrillary acidic protein (GFAP, red) staining of brain slices of the left hemisphere after three weeks post-surgery. Magnification 5×. Histograms show the quantification of fluorescence in control (wt, closed bar) and H^+/T^+ (open bar) mice. D, dorsal; M, medial.

Data information: In (A–E), determinations were carried out at 21 day post-surgery. Bars are the mean ± s.e.m. of three (E), four (D), or five (A–C) animals. $*^{\#}P < 0.05$ when compared to the right or left hemisphere of controls, respectively.

Source data are available online for this figure.

regulator of the PTP, acting as the molecular bridge that links events at the inner and outer mitochondrial membranes. In fact, the silencing of Bcl-xL abrogates the pro-survival effect of the inhibition of the H^+-ATP synthase mediated by hIF1. Moreover, the finding that Bcl-xL also interacts with other complexes of the respiratory chain, presumably complex I, broadens the biological

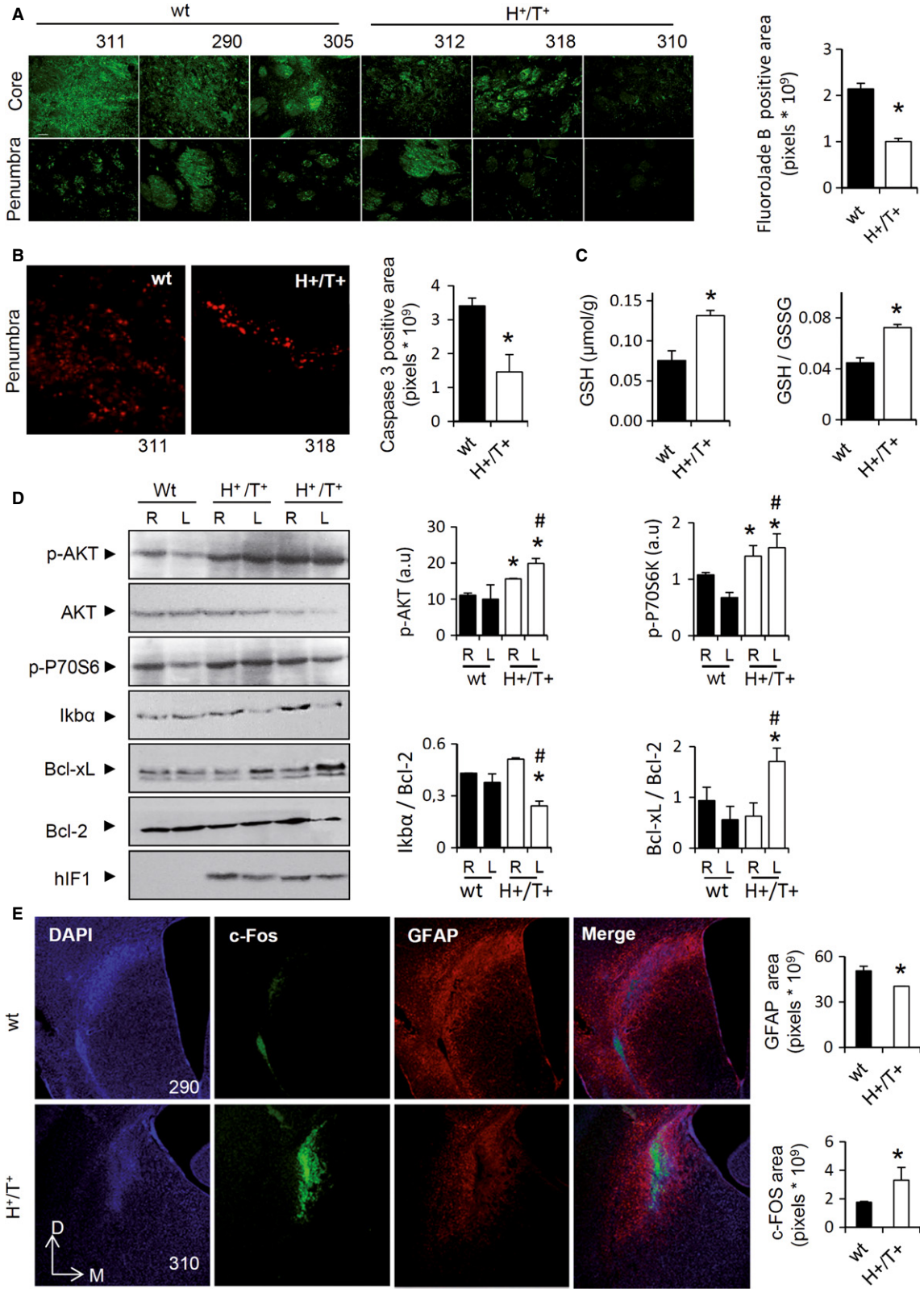

Published online: February 12, 2014
The EMBO Journal

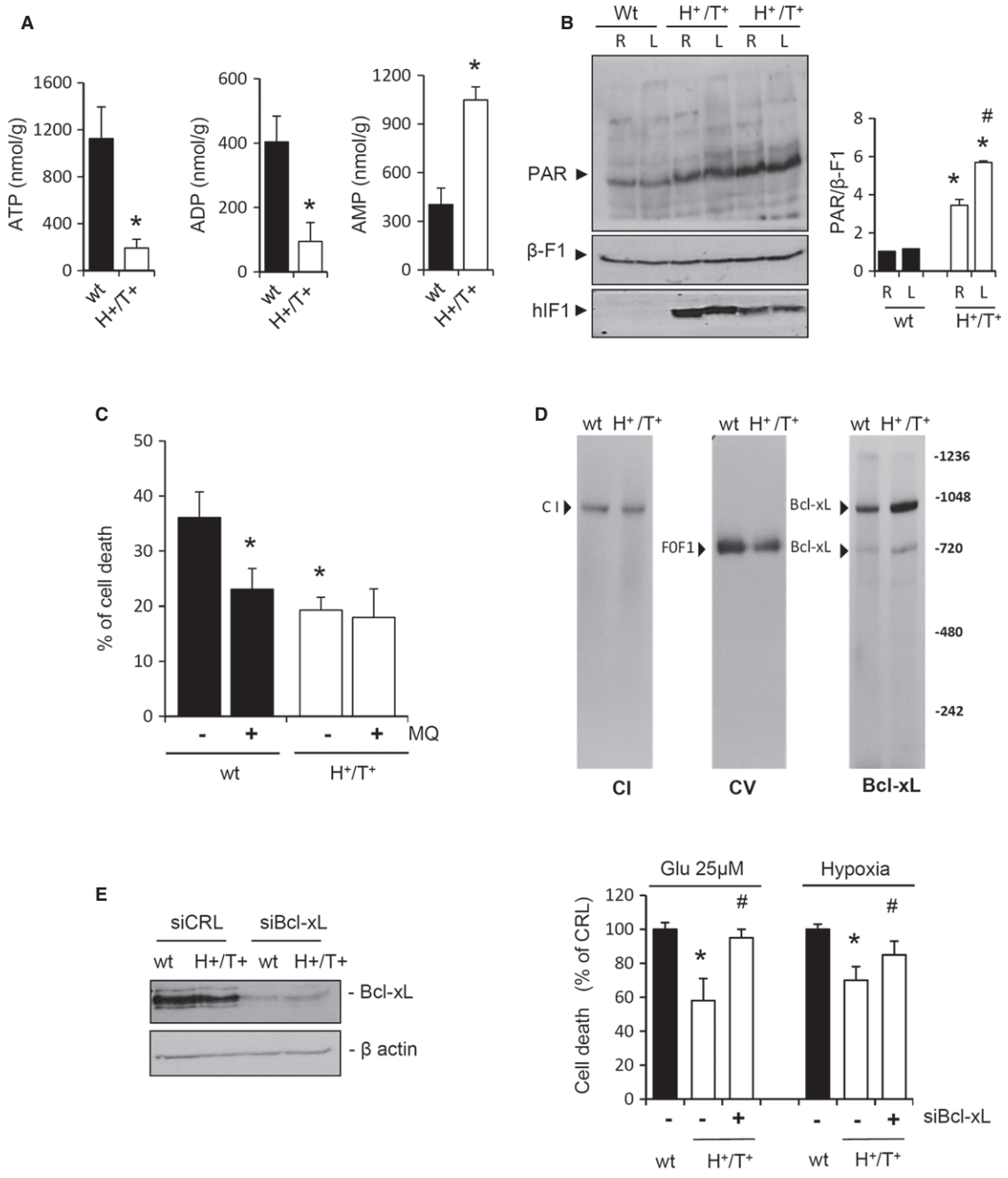

Figure 6. Bcl-xL is involved in hIF1-mediated protection of neurons.

A Content of adenine nucleotides in the injured area of the left hemisphere of control (wt, closed bars) and hIF1-expressing (H^+/T^+, open bars) mice. *$P < 0.05$ when compared to control (wt) by Student's *t*-test.

B Representative Western blots of the polymer poly-ADP-ribose (PAR), the product of poly-ADP-ribose polymerase-1 (PARP-1) activity, in right (R) and left (L) hemispheres of control (wt, closed bars) and H^+/T^+ (open bars) mice. One control and two H^+/T^+ mice are shown. β-F1-ATPase expression is shown as loading control. Histograms show the quantification of PAR/β-F1 ratio. * and #: $P < 0.05$ when compared to the right or left hemisphere of controls, respectively.

C Effect of ROS scavenging (20 nM mito Q, MQ) on glutamate-primed cell death in neurons derived from control (wt, closed bars) and H^+/T^+ (open bar) mice.

D Blue-native immunoblot analysis of Bcl-xL immunoreactivity associated with complexes of mitochondrial OXPHOS. The migration of complex I (CI, NADH9), F0F1-ATPase (CV, β-F1-ATPase), and Bcl-xL in control (wt) and H^+/T^+ mice is indicated. The migration of molecular mass markers is indicated to the right.

E Effect of glutamate and 1 h of hypoxia on cell death in primary cultures of cortical neurons derived from control (wt, closed bars) and H^+/T^+ (open bar) mice. The silencing of Bcl-xL (siBcl-xL) using β-actin as loading control is illustrated.

Data information: Bars are the mean ± s.e.m. of three (B, C, E) or five (A) experiments. * and #: $P < 0.05$ when compared to control (wt) or to silencing control (H^+/T^+, siCRL).

Source data are available online for this figure.

relevance of this anti-apoptotic protein in the regulation of mitochondrial physiology and cellular metabolism.

CryoEM studies of the macromolecular organization of the inner membrane reveal no interaction between complex I and the H^+-ATP synthase (Davies *et al*, 2011). However, cyclophilin D that favors PTP opening binds to and regulates the activity of the H^+-ATP synthase (Giorgio *et al*, 2009) and affects modulation of PTP by rotenone (Li *et al*, 2012). These findings suggest that the metabolic and/or the structural preconditioning mediated by hIF1 increases the threshold of PTP opening by preventing the channel formation capacity of the H^+-ATP synthase (Giorgio *et al*, 2013) (Fig 7G). Overall, our data provide the first *in vivo* demonstration that the activity of the H^+-ATP synthase is necessary for the efficient execution of cell death. Hence, the H^+-ATP synthase not only functions as the power plant of the cell but also as a pivotal regulator of cell death.

Materials and Methods

Transgenic animals

The pCMV-SPORT6-H49K plasmid (Sanchez-Cenizo *et al*, 2010) containing the H49K mutant version of human IF1 was PCR-amplified and the PCR product assembled into the pTRE2hyg vector (Clontech Laboratories Inc.) into the BamHI and NotI restriction sites. The TRE2hyg-H49K plasmid was digested with SexAI/BsrBI (New England Biolabs), and the 2.5-Kb DNA fragment of interest was purified with Elu-Quik kit (Shleicher & Schuell). Transgenic mice (TRE-H49K-25, H^+) were obtained by pronuclear microinjection of the construct by the Servicio de Trangenesis of the CNB/CBMSO (UAM, Madrid, Spain), using standard protocols. Integration of the construct was confirmed by PCR (forward, 5′-CAC AGAGTAGAGAACAACTG-3′; reverse, 5′-GTTAGTAGCACA CAGACAAA-3′). The Bl6-Tg(Camk2a-tTa)1Mmay/J mice (T^+) expressing the transactivator tTA in neurons (Mayford *et al*, 1996) were used. The Tet-Off double transgenic animals (H^+/T^+) were obtained by breeding H^+ and T^+ mice. Animals were maintained on the C57/Bl6 genetic background. To turn off the expression of hIF1, double transgenic mice were administered doxycyclin (2 mg/ml) in the drinking water for 15 days. Animal experiments were carried out after approval of the Institutional Review Board (Ethical Committee of the UAM, CEI-24-571) in compliance with animal policies and ethical guidelines of the European Community.

Brain mitochondria

Adult mice brain mitochondria were prepared after the permeabilization of synaptosomes with 100 μM digitonine. The purity of mitochondrial preparations was assessed by Western blotting. Oxygen consumption rates in isolated mitochondria (200 μg protein) were determined in a Clark-type electrode. Glutamate plus malate (10 mM) were used as respiratory substrates in the presence or absence of 0.5 mM ADP, 6 μM OL, 5 μM FCCP, and 1 μM antimycin A. The composition of the respiration buffer is 75 mM mannitol, 25 mM sucrose, 20 mM Tris–HCl, 5 mM phosphate, 0.3 mM EGTA, 0.5 mM EDTA, 100 mM KCl, 0.1% BSA, pH 7.4.

For the determination of the mitochondrial membrane potential, approximately 100 μg of mitochondria were charged with 100 nM $TMRM^+$ (Life Technologies). Changes in fluorescence were recorded using an Aminco-Bowman Series 2 Luminescence Spectrometer after the addition of the following compounds (final concentration): 10 mM succinate, 1 mM ADP, 6 μM OL, 5 μM FCCP, 2 μM rotenone, and 1 μM antimycin A.

Primary cultures of cortical neurons

Cerebral cortices were dissected from fetal mice at 16–17 days of gestation in neurobasal medium (NB) using the Papain Dissociation System kit (Worthington). Disrupted cortices were resuspended in NB supplemented with 10% HS and 2 mM glutamine. After 4–5 days in culture, non-neuronal cell division was halted by the addition of 3 mM cytosine arabinoside for 24 h. Neurons were identified evaluating their morphology and positive immunoreactivity to Neu-N antibody (Chemicon International Inc.; 1:1,000) and studied at 9–11 days of culture. Lack of staining with an anti-glial fibrillary acidic protein GFAP (Dako Cytomation; 1:1,000) revealed the absence of astrocytes in cell cultures.

The rates of lactate production and of oxygen consumption (XF24 Extracellular Flux Analyzer, Seahorse Bioscience) were determined (Sanchez-Cenizo *et al*, 2010). The final concentration and order of injected substances was 6 μM OL, 0.75 mM dinitrophenol (DNP), 1 μM rotenone, and 1 μM antimycin A.

For the determination of the $\Delta\Psi_m$ and ROS levels, 100 nM $TMRM^+$ or 2.5 μM MitoSOX™ (Life Technologies) was, respectively, used in "redistribution mode" (Duchen *et al*, 2003). The fluorescence was analyzed by confocal microscopy using a Biorad Radiance 2000 Zeiss Axiovert S100TV using red (590/617 nm) excitation/emission wavelengths and quantified using ImageJ software. Fluorescence intensity was quantified by removing background signal and measuring the mean fluorescence intensity in the pixels containing mitochondria in approximately the same number of cells and at least in 15 different fields per condition tested. Six micromolar OL, 2 μM rotenone, 1 μM antimycin A, and 5 μM FCCP were used.

Neuron transfection was done using Effectene Transfection Reagent (Qiagen) with control or Bcl-xL plasmid (Switchgear Genomics Inc.). For the determination of cell death, neurons were treated with 25 μM glutamate (Sigma-Aldrich) for 5 min or deprived of oxygen for 1 h (1% O_2) in a Hypoxic Workstation H35 (Don Whitley Scientific). Neurons were incubated for 24 h in the absence or presence of 20 nM Mito Q and then processed by confocal microscopy *in vivo* at 37°C and 5% CO_2 using an Axioskop2-plus vertical microscope (Zeiss) coupled to a ccd color camera. Propidium iodide (2 μM) and calcein (1 μM) were utilized to determine cell death and viability, respectively. The number of cells was quantified in 20 fields per treatment using ImageJ software.

Adenine nucleotides

Adenine nucleotides were extracted from frozen brain powder with a 6% perchloric acid solution. Determination of ATP, ADP, and AMP in frozen brain powder was carried out by standard enzymatic procedures. The ATP concentration in primary cultures was

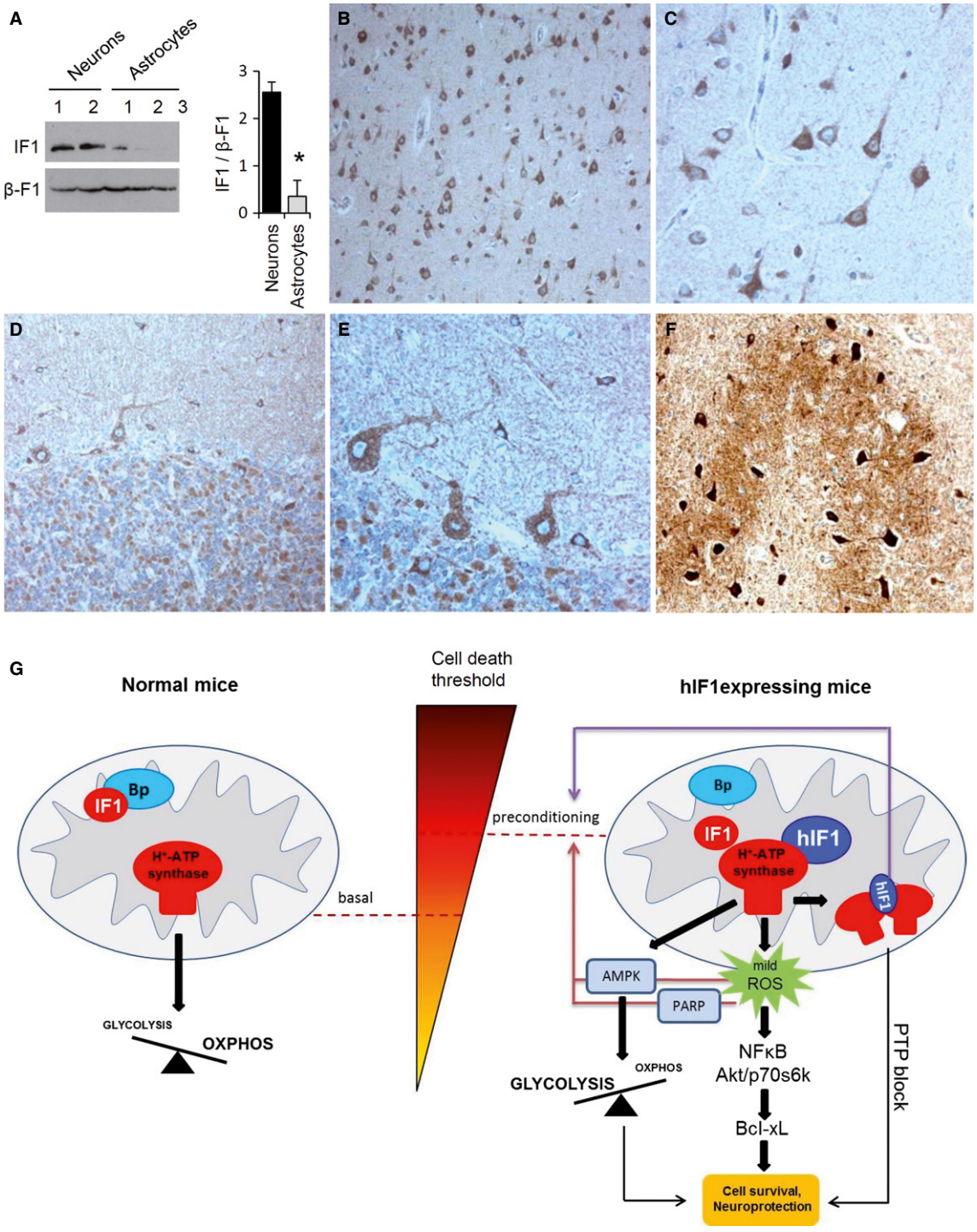

determined using the ATP Bioluminescence Assay Kit CLS II (Roche).

Protein electrophoresis, Western blotting, and protein carbonylation

Protein samples from brain and cellular extracts were fractionated on SDS–PAGE. Details of the antibodies used in Western blots are provided in Supplementary Information. For the determination of protein carbonylation, the Oxyblot Oxidized Protein Detection kit (Chemicon International Inc.) was used.

Blue-native (BN) PAGE

Protein extracts (250 μg) from control or H^+/T^+ mice brain mitochondria were solubilized in BN-loading buffer. 1 g of n-dodecyl

Figure 7. IF1 expression in human brain.

A Western blots of the expression of IF1 in fractionated proteins from mouse neurons and astrocytes using the commercial anti-mouse IF1. β-F1-ATPase (β-F1) expression is shown as a loading control. Histograms show the quantification of the IF1/β-F1 ratio. The data shown are the mean ± s.e.m. of 3–4 preparations. *$P < 0.05$ when compared to neuronal expression by Student's *t*-test.

B, C Immunocytochemistry of hIF1 in human cerebral cortex. Note IF1 immunolabeling in cortical neurons of the parieto-occipital cortex and the negative labeling of astrocytes. Magnification 20× (B) and 63× (C).

D–F Immunocytochemistry for IF1 in human cerebellar sections. Positive immunolabeling for hIF1 in Purkinje cells, granular neurons, and Golgi type II neurons (D, E), and strong hIF1 immunolabeling in neurons of the cerebellar dentate nucleus (F). Magnifications: 20× (D), 63× (E), and 20× (F).

G The schematic illustrates the role of overexpression of hIF1 in preconditioning of the brain. In normal mice, the IF1 present is non-functional as relevant repressor of the synthetic activity of the H^+-ATP synthase either by its binding to a putative receptor (Bp) and/or because of covalent modifications of the protein. The overexpression of hIF1 with higher affinity for β-F1-ATPase partially interferes with OXPHOS and promotes an enhanced glycolysis and a mild ROS signal that activates in the nucleus pathways of survival and repair enhancing the threshold level required to execute cell death. In addition, hIF1 overexpression might affect the dimerization of the H^+-ATP synthase that is involved in PTP formation. The metabolic (red arrows) and structural (violet arrow) pathways of brain preconditioning are highlighted. Upon administration of a death stimuli hIF1 inhibits more effectively the synthase activity of the H^+-ATP synthase than endogenous IF1. By a mechanism that remains to be discovered, IF1 prevents PTP opening and extensive neuronal cell death. See also Supplementary Fig S10.

Source data are available online for this figure.

β-D-maltoside/g protein was added to the samples and protein complexes were fractionated in BN gels after the addition of 2.5 μl of the Coomassie dye suspension. Electrophoresis was performed in "deep blue" cathode buffer B at constant voltage of 70 V until one-third of the whole electrophoresis run. Buffer B was then exchanged with the buffer "light blue." Electrophoresis was performed for other 12 h at 70 V and then 3 h at 200 V. BN-loading buffer: 50 mM NaCl, 1 mM EDTA, 5 mM 6-aminocaproic acid, 2% PMSF, 50 mM imidazole/HCl pH 7.0. BN gels: acrylamide/bisacrylamide ratio ranging from 3% to 13% w/v, 0.5 M 6-aminocaproic acid, and 25 mM imidazole. Coomassie dye suspension (5% SBG dye in 500 mM aminocaproic acid). Anode buffer: 25 mM imidazole, pH 7.0. "Deep blue" cathode buffer B: 50 mM tricine, 7.5 mM imidazole, 0.02% Serva Blue G (SBG), pH 7.0. "Light blue" cathode buffer B/10: the cathode buffer B with a ten times lower dye concentration (0.002% SBG).

Determination of enzyme activities

Brain mitochondria resuspended in respiration buffer containing 1% Triton X-100 were used for the spectrophotometric determination of complexes I, II+III, IV, and V activities as described (Barrientos *et al*, 2009).

Glutathione determination

The brain GSH and GSSG concentrations were determined using the Glutathione Assay Kit (BioVision Inc.).

Animal surgery and histology

One-year-old control ($n = 10$) and H^+/T^+ ($n = 10$) male mice were used for surgery. To induce excitotoxic damage, all animals received a single 0.5 μl dose of 20 nmol of quinolinic acid by stereotaxical injection into the left striatum. Coordinates (mm) AP (anteroposterior from bregma) = +0.25, ML = 2.75, D-V (vertical from dura) = −2.5 at a speed of 1 μl/min. The right hemisphere did not receive any surgery and served as histological control. Twenty days after the lesion, mice were sacrificed, transcardially perfused with 3% paraformaldehyde, and cryoprotected with 30% sucrose. Sections (30 μm thick) were taken in the coronal plane, stained with hematoxylin–eosin, and processed for immunohistochemistry.

Evaluation of animal behavior

Animal behavior was evaluated by footprint, grid, and cylinder tests in a blinded way before surgery and every 3 days post-surgery until day of sacrifice (21th day). Gait abnormalities were detected by analysis of motor coordination and synchrony using the "footprint" test (Carter *et al*, 1999). Briefly, fore and hind paws were dipped into water-soluble ink of different colors and animals were left free to walk over absorbent paper in a straight line. Analysis included measurement of stride length, width of the base of support for the hind limbs, and paw angle (fore and hind). Gait variability was studied using the coefficient of variation (CV) calculated from the equation 100 × standard deviation/mean value. For the grid test: Mice were left free to walk across a horizontal grid (size: 20 × 30 cm, 10 mm wire mesh). The number of ipsilateral and contralateral paw slips through the grid was counted and the motility index was calculated from the equation: percentage of the time spent moving/(number of foot faults + number of stops) (Brooks & Dunnett, 2009). For the cylinder test: Mice were placed in a perspex cylinder (9-cm diameter, 15-cm tall) for 5 min and recorded with a video camera. Paw usage was studied by measuring the number of forelimb wall contacts made with each paw when rearing (Brooks & Dunnett, 2009). Data are presented as number of contacts per minute for left, right, and both forepaws simultaneously.

Immunofluorescence/confocal microscopy and immunohistochemistry

Free-floating brain slices were incubated with blocking buffer (3% BSA and 0.1% Triton X-100 in PBS) for 1 h at RT and then incubated overnight at 4°C with the primary antibodies specified.

The primary antibodies used were: anti-NeuN (1:100) and Fluoro-Jade B (0.001%) from Millipore Bioscience Research Reagents; anti-GFAP (1:1,000) from Dako Cytomation; anti-Iba-1 (1:500) from Wako; anti-Ed-1 (1:100) and anti-c-fos (1:100) from Santa Cruz Biotechnology, Inc.; anti-DARP-32 (1:500) from Chemicon International Inc.; and anti-caspase-3 (1:100) from Cell Signaling Technology Inc. Secondary Cy-3/Cy-5/Cy-2-conjugated antibodies were used (Millipore Bioscience Research Reagents). Cellular fluorescence was analyzed by confocal microscopy using a Biorad Radiance 2000 Zeiss Axiovert S100TV using green (498/516 nm), red (590/617 nm), or blue (642/661 nm) excitation/emission wave

lengths. The area and intensity of fluorescence were quantified by ImageJ software.

Mice brain slices were incubated in 3% H_2O_2 in methanol for 10 min at room temperature to block the endogenous peroxidase activity. Antigens were retrieved by incubation in Dako Retrieval Solution (Dako Cytomation) for 2 min at 98°C. The anti-IF1 (1:200) and anti-β-F1-ATPase (1:20,000) were used for immunohistochemistry using the peroxidase-based EnVisionTM FLEX Mini kit High pH (Dako Cytomation). Specimens were then incubated with diaminobenzidine chromogenic substrate (Dako Cytomation) for 5 min at room temperature. To assess the expression of IF1 in human brain, 3-μm paraffin sections obtained from post-mortem CNS specimens from a patient with no neurological disease were processed for immunocytochemistry. Sections were automatically deparaffinized and immunostained with an Autostainer Link instrument from Dako (Carpinteria). Antigenic retrieval was performed at low pH, incubated with anti-IF1 at 1/100 dilution for 30 min, and visualized with EnVision Flex system from Dako (Carpinteria). Sections were observed with a Leica DMRE light microscope.

Statistical analysis

Statistical analyses were performed using a two-tailed Student's *t*-test. ANOVA with post hoc Dunnett's test was used for multiple comparisons to the control, using the SPSS 17.0 software package. The results shown are means ± s.e.m. A $P < 0.05$ was considered statistically significant.

Supplementary information for this article is available online: http://emboj.embopress.org

Acknowledgements
We thank Michael P. Murphy (Medical Research Council, UK) for kindly supplying mitoQ. The authors acknowledge the technical support provided by M. Chamorro, C. Nuñez de Arenas, E. Casas, C. Cuevas, and Z. Ortega. LF is supported by "Fundación de la Asociación Española Contra el Cáncer" (AECC). This work was supported by grants from the MEC (BFU2010-18903), CIBERER and by Comunidad de Madrid (S2011/BMD-2402) to JMC; MINECO (PLE2009-0101 and SAF2010-17167), TerCel (RD12/0019/0013), and Neurostem-CM (S2010-BMD-2336) to AMS and ISCIII Grant PI 10/02628 to CN, Spain. The CBMSO receives an institutional grant from Fundación Ramón Areces.

Author contributions
LF and JMC designed research; LF, MPP, LSC, FS, JJL, and CN performed research; LF, MPP, CN, AMS, and JMC analyzed data; LF and JMC wrote the paper.

Conflict of interest
The authors declare no conflict of interest.

References

Acin-Perez R, Fernandez-Silva P, Peleato ML, Perez-Martos A, Enriquez JA (2008) Respiratory active mitochondrial supercomplexes. *Mol Cell* 32: 529 – 539

Alavian KN, Li H, Collis L, Bonanni L, Zeng L, Sacchetti S, Lazrove E, Nabili P, Flaherty B, Graham M, Chen Y, Messerli SM, Mariggio MA, Rahner C, McNay E, Shore GC, Smith PJ, Hardwick JM, Jonas EA (2011) Bcl-x(L) regulates metabolic efficiency of neurons through interaction with the mitochondrial F(1)F(O) ATP synthase. *Nat Cell Biol* 13: 1224 – 1233

Andersen JL, Kornbluth S (2013) The tangled circuitry of metabolism and apoptosis. *Mol Cell* 49: 399 – 410

Barrientos A, Fontanesi F, Diaz F (2009) Evaluation of the mitochondrial respiratory chain and oxidative phosphorylation system using polarography and spectrophotometric enzyme assays. *Curr Protoc Hum Genet* 19: Unit19 13

Bisetto E, Comelli M, Salzano AM, Picotti P, Scaloni A, Lippe G, Mavelli I (2013) Proteomic analysis of F1F0-ATP synthase super-assembly in mitochondria of cardiomyoblasts undergoing differentiation to the cardiac lineage. *Biochim Biophys Acta* 1827: 807 – 816

Bonora M, Bononi A, De Marchi E, Giorgi C, Lebiedzinska M, Marchi S, Patergnani S, Rimessi A, Suski JM, Wojtala A, Wieckowski MR, Kroemer G, Galluzzi L, Pinton P (2013) Role of the c subunit of the FO ATP synthase in mitochondrial permeability transition. *Cell Cycle* 12: 674 – 683

Brooks SP, Dunnett SB (2009) Tests to assess motor phenotype in mice: a users guide. *Nat Rev Neurosci* 10: 519 – 529

Cabezon E, Butler PJ, Runswick MJ, Walker JE (2000) Modulation of the oligomerization state of the bovine F1-ATPase inhibitor protein, IF1, by pH. *J Biol Chem* 275: 25460 – 25464

Campanella M, Casswell E, Chong S, Farah Z, Wieckowski MR, Abramov AY, Tinker A, Duchen MR (2008) Regulation of mitochondrial structure and function by the F1Fo-ATPase inhibitor protein, IF1. *Cell Metab* 8: 13 – 25

Carter RJ, Lione LA, Humby T, Mangiarini L, Mahal A, Bates GP, Dunnett SB, Morton AJ (1999) Characterization of progressive motor deficits in mice transgenic for the human Huntingtons disease mutation. *J Neurosci* 19: 3248 – 3257

Chen YB, Aon MA, Hsu YT, Soane L, Teng X, McCaffery JM, Cheng WC, Qi B, Li H, Alavian KN, Dayhoff-Brannigan M, Zou S, Pineda FJ, O'Rourke B, Ko YH, Pedersen PL, Kaczmarek LK, Jonas EA, Hardwick JM (2011) Bcl-xL regulates mitochondrial energetics by stabilizing the inner membrane potential. *J Cell Biol* 195: 263 – 276

Chivasa S, Tome DF, Hamilton JM, Slabas AR (2011) Proteomic analysis of extracellular ATP-regulated proteins identifies ATP synthase beta-subunit as a novel plant cell death regulator. *Mol Cell Proteomics* 10: M110 003905

Cogliati S, Frezza C, Soriano ME, Varanita T, Quintana-Cabrera R, Corrado M, Cipolat S, Costa V, Casarin A, Gomes LC, Perales-Clemente E, Salviati L, Fernandez-Silva P, Enriquez JA, Scorrano L (2013) Mitochondrial cristae shape determines respiratory chain supercomplexes assembly and respiratory efficiency. *Cell* 155: 160 – 171

Datta SR, Dudek H, Tao X, Masters S, Fu H, Gotoh Y, Greenberg ME (1997) Akt phosphorylation of BAD couples survival signals to the cell-intrinsic death machinery. *Cell* 91: 231 – 241

Davies KM, Anselmi C, Wittig I, Faraldo-Gomez JD, Kuhlbrandt W (2012) Structure of the yeast F1Fo-ATP synthase dimer and its role in shaping the mitochondrial cristae. *Proc Natl Acad Sci USA* 109: 13602 – 13607

Davies KM, Strauss M, Daum B, Kief JH, Osiewacz HD, Rycovska A, Zickermann V, Kuhlbrandt W (2011) Macromolecular organization of ATP synthase and complex I in whole mitochondria. *Proc Natl Acad Sci USA* 108: 14121 – 14126

Dey R, Moraes CT (2000) Lack of oxidative phosphorylation and low mitochondrial membrane potential decrease susceptibility to apoptosis

and do not modulate the protective effect of Bcl-x(L) in osteosarcoma cells. *J Biol Chem* 275: 7087 – 7094

Di Lisa F, Carpi A, Giorgio V, Bernardi P (2011) The mitochondrial permeability transition pore and cyclophilin D in cardioprotection. *Biochim Biophys Acta* 1813: 1316 – 1322

Duchen MR, Surin A, Jacobson J (2003) Imaging mitochondrial function in intact cells. *Methods Enzymol* 361: 353 – 389

Faccenda D, Tan CH, Seraphim A, Duchen MR, Campanella M (2013) IF1 limits the apoptotic-signalling cascade by preventing mitochondrial remodelling. *Cell Death Differ* 20: 686 – 697

Formentini L, Sánchez-Aragó M, Sánchez-Cenizo L, Cuezva JM (2012) The mitochondrial ATPase Inhibitory Factor 1 (IF1) triggers a ROS-mediated retrograde pro-survival and proliferative response. *Mol Cell* 45: 731 – 742

Fujikawa M, Imamura H, Nakamura J, Yoshida M (2012) Assessing the actual contribution of IF1, an inhibitor of mitochondrial FoF1, to ATP homeostasis, cell growth, mitochondrial morphology and cell viability. *J Biol Chem* 287: 18781 – 18787

Galluzzi L, Blomgren K, Kroemer G (2009) Mitochondrial membrane permeabilization in neuronal injury. *Nat Rev Neurosci* 10: 481 – 494

Galluzzi L, Kepp O, Kroemer G (2012) Mitochondria: master regulators of danger signalling. *Nat Rev Mol Cell Biol* 13: 780 – 788

Garcia JJ, Morales-Rios E, Cortes-Hernandez P, Rodriguez-Zavala JS (2006) The inhibitor protein (IF1) promotes dimerization of the mitochondrial F1F0-ATP synthase. *Biochemistry* 45: 12695 – 12703

Giorgio V, Bisetto E, Soriano ME, Dabbeni-Sala F, Basso E, Petronilli V, Forte MA, Bernardi P, Lippe G (2009) Cyclophilin D modulates mitochondrial F0F1-ATP synthase by interacting with the lateral stalk of the complex. *J Biol Chem* 284: 33982 – 33988

Giorgio V, von Stockum S, Antoniel M, Fabbro A, Fogolari F, Forte M, Glick GD, Petronilli V, Zoratti M, Szabo I, Lippe G, Bernardi P (2013) Dimers of mitochondrial ATP synthase form the permeability transition pore. *Proc Natl Acad Sci USA* 110: 5887 – 5892

Gledhill JR, Montgomery MG, Leslie AG, Walker JE (2007) How the regulatory protein, IF(1), inhibits F(1)-ATPase from bovine mitochondria. *Proc Natl Acad Sci USA* 104: 15671 – 15676

Gross A, Pilcher K, Blachly-Dyson E, Basso E, Jockel J, Bassik MC, Korsmeyer SJ, Forte M (2000) Biochemical and genetic analysis of the mitochondrial response of yeast to BAX and BCL-X(L). *Mol Cell Biol* 20: 3125 – 3136

Harada H, Andersen JS, Mann M, Terada N, Korsmeyer SJ (2001) p70S6 kinase signals cell survival as well as growth, inactivating the pro-apoptotic molecule BAD. *Proc Natl Acad Sci USA* 98: 9666 – 9670

Hernlund E, Hjerpe E, Avall-Lundqvist E, Shoshan M (2009) Ovarian carcinoma cells with low levels of beta-F1-ATPase are sensitive to combined platinum and 2-deoxy-D-glucose treatment. *Mol Cancer Ther* 8: 1916 – 1923

Husain I, Harris DA (1983) ATP synthesis and hydrolysis in submitochondrial particles subjected to an acid-base transition. Effects of the ATPase inhibitor protein. *FEBS Lett* 160: 110 – 114

Iadecola C, Anrather J (2011) Stroke research at a crossroad: asking the brain for directions. *Nat Neurosci* 14: 1363 – 1368

Johnson KM, Chen X, Boitano A, Swenson L, Opipari AW Jr, Glick GD (2005) Identification and validation of the mitochondrial F1F0-ATPase as the molecular target of the immunomodulatory benzodiazepine Bz-423. *Chem Biol* 12: 485 – 496

Karin M (2006) Nuclear factor-kappaB in cancer development and progression. *Nature* 441: 431 – 436

Lapuente-Brun E, Moreno-Loshuertos R, Acin-Perez R, Latorre-Pellicer A, Colas C, Balsa E, Perales-Clemente E, Quiros PM, Calvo E, Rodriguez-Hernandez MA, Navas P, Cruz R, Carracedo A, Lopez-Otin C, Perez-Martos A, Fernandez-Silva P, Fernandez-Vizarra E, Enriquez JA (2013) Supercomplex assembly determines electron flux in the mitochondrial electron transport chain. *Science* 340: 1567 – 1570

Leslie NR (2006) The redox regulation of PI 3-kinase-dependent signaling. *Antioxid Redox Signal* 8: 1765 – 1774

Li B, Chauvin C, De Paulis D, De Oliveira F, Gharib A, Vial G, Lablanche S, Leverve X, Bernardi P, Ovize M, Fontaine E (2012) Inhibition of complex I regulates the mitochondrial permeability transition through a phosphate-sensitive inhibitory site masked by cyclophilin D. *Biochim Biophys Acta* 1817: 1628 – 1634

Li RJ, Zhang GS, Chen YH, Zhu JF, Lu QJ, Gong FJ, Kuang WY (2010) Down-regulation of mitochondrial ATPase by hypermethylation mechanism in chronic myeloid leukemia is associated with multidrug resistance. *Ann Oncol* 7: 1506 – 1514

Lippe G, Sorgato MC, Harris DA (1988) Kinetics of the release of the mitochondrial inhibitor protein. Correlation with synthesis and hydrolysis of ATP. *Biochim Biophys Acta* 933: 1 – 11.

Lopez-Mediavilla C, Vigny H, Godinot C (1993) Docking the mitochondrial inhibitor protein IF1 to a membrane receptor different from the F1-ATPase beta subunit. *Eur J Biochem* 215: 487 – 496

Martinez-Serrano A, Bjorklund A (1996) Protection of the neostriatum against excitotoxic damage by neurotrophin-producing, genetically modified neural stem cells. *J Neurosci* 16: 4604 – 4616

Matsuyama S, Xu Q, Velours J, Reed JC (1998) The Mitochondrial F0F1-ATPase proton pump is required for function of the proapoptotic protein Bax in yeast and mammalian cells. *Mol Cell* 1: 327 – 336

Mayford M, Bach ME, Huang YY, Wang L, Hawkins RD, Kandel ER (1996) Control of memory formation through regulated expression of a CaMKII transgene. *Science* 274: 1678 – 1683

Michels J, Kepp O, Senovilla L, Lissa D, Castedo M, Kroemer G, Galluzzi L (2013) Functions of BCL-X L at the interface between cell death and metabolism. *Int J Cell Biol* 2013: 705294

Mihaylova MM, Shaw RJ (2011) The AMPK signalling pathway coordinates cell growth, autophagy and metabolism. *Nat Cell Biol* 13: 1016 – 1023

Minauro-Sanmiguel F, Wilkens S, Garcia JJ (2005) Structure of dimeric mitochondrial ATP synthase: novel F0 bridging features and the structural basis of mitochondrial cristae biogenesis. *Proc Natl Acad Sci USA* 102: 12356 – 12358

Paumard P, Vaillier J, Coulary B, Schaeffer J, Soubannier V, Mueller DM, Brethes D, di Rago JP, Velours J (2002) The ATP synthase is involved in generating mitochondrial cristae morphology. *EMBO J* 21: 221 – 230

Pelicano H, Xu RH, Du M, Feng L, Sasaki R, Carew JS, Hu Y, Ramdas L, Hu L, Keating MJ, Zhang W, Plunkett W, Huang P (2006) Mitochondrial respiration defects in cancer cells cause activation of Akt survival pathway through a redox-mediated mechanism. *J Cell Biol* 175: 913 – 923

Ravati A, Ahlemeyer B, Becker A, Klumpp S, Krieglstein J (2001) Preconditioning-induced neuroprotection is mediated by reactive oxygen species and activation of the transcription factor nuclear factor-kappaB. *J Neurochem* 78: 909 – 919

Sanchez-Arago M, Formentini L, Cuezva JM (2013a) Mitochondria-Mediated Energy Adaption in Cancer: the H(+)-ATP Synthase-Geared Switch of Metabolism in Human Tumors. *Antioxid Redox Signal* 19: 285 – 298

Sanchez-Arago M, Formentini L, Martinez-Reyes I, Garcia-Bermudez J, Santacatterina F, Sanchez-Cenizo L, Willers IM, Aldea M, Najera L, Juarranz A, Lopez EC, Clofent J, Navarro C, Espinosa E, Cuezva JM (2013b) Expression, regulation and clinical relevance of the ATPase inhibitory factor 1 in human cancers. *Oncogenesis* 2: e46

Sanchez-Cenizo L, Formentini L, Aldea M, Ortega AD, Garcia-Huerta P, Sanchez-Arago M, Cuezva JM (2010) Up-regulation of the ATPase inhibitory factor 1 (IF1) of the mitochondrial H+-ATP synthase in human tumors mediates the metabolic shift of cancer cells to a Warburg phenotype. *J Biol Chem* 285: 25308 – 25313

Santamaria G, Martinez-Diez M, Fabregat I, Cuezva JM (2006) Efficient execution of cell death in non-glycolytic cells requires the generation of ROS controlled by the activity of mitochondrial H + -ATP synthase. *Carcinogenesis* 27: 925 – 935

Schwarcz R, Bruno JP, Muchowski PJ, Wu HQ (2012) Kynurenines in the mammalian brain: when physiology meets pathology. *Nat Rev Neurosci* 13: 465 – 477

Shchepina LA, Pletjushkina OY, Avetisyan AV, Bakeeva LE, Fetisova EK, Izyumov DS, Saprunova VB, Vyssokikh MY, Chernyak BV, Skulachev VP (2002) Oligomycin, inhibitor of the F0 part of H + -ATP-synthase, suppresses the TNF-induced apoptosis. *Oncogene* 21: 8149 – 8157

Shen L, Zhi L, Hu W, Wu MX (2009) IEX-1 targets mitochondrial F1Fo-ATPase inhibitor for degradation. *Cell Death Differ* 16: 603 – 612

Shin YK, Yoo BC, Chang HJ, Jeon E, Hong SH, Jung MS, Lim SJ, Park JG (2005) Down-regulation of mitochondrial F1F0-ATP synthase in human colon cancer cells with induced 5-fluorouracil resistance. *Cancer Res* 65: 3162 – 3170

Tomasetig L, Di Pancrazio F, Harris DA, Mavelli I, Lippe G (2002) Dimerization of F0F1ATP synthase from bovine heart is independent from the binding of the inhibitor protein IF1. *Biochim Biophys Acta* 1556: 133 – 141

Tomiyama A, Serizawa S, Tachibana K, Sakurada K, Samejima H, Kuchino Y, Kitanaka C (2006) Critical role for mitochondrial oxidative phosphorylation in the activation of tumor suppressors Bax and Bak. *J Natl Cancer Inst* 98: 1462 – 1473

Wittig I, Schagger H (2009) Supramolecular organization of ATP synthase and respiratory chain in mitochondrial membranes. *Biochim Biophys Acta* 1787: 672 – 680

Wondrak GT (2009) Redox-directed cancer therapeutics: molecular mechanisms and opportunities. *Antioxid Redox Signal* 11: 3013 – 3069

Zhao X, Leon IR, Bak S, Mogensen M, Wrzesinski K, Hojlund K, Jensen ON (2011) Phosphoproteome analysis of functional mitochondria isolated from resting human muscle reveals extensive phosphorylation of inner membrane protein complexes and enzymes. *Mol Cell Proteomics* 10: M110.000299

Supplementary Information.

Supplementary Figures.

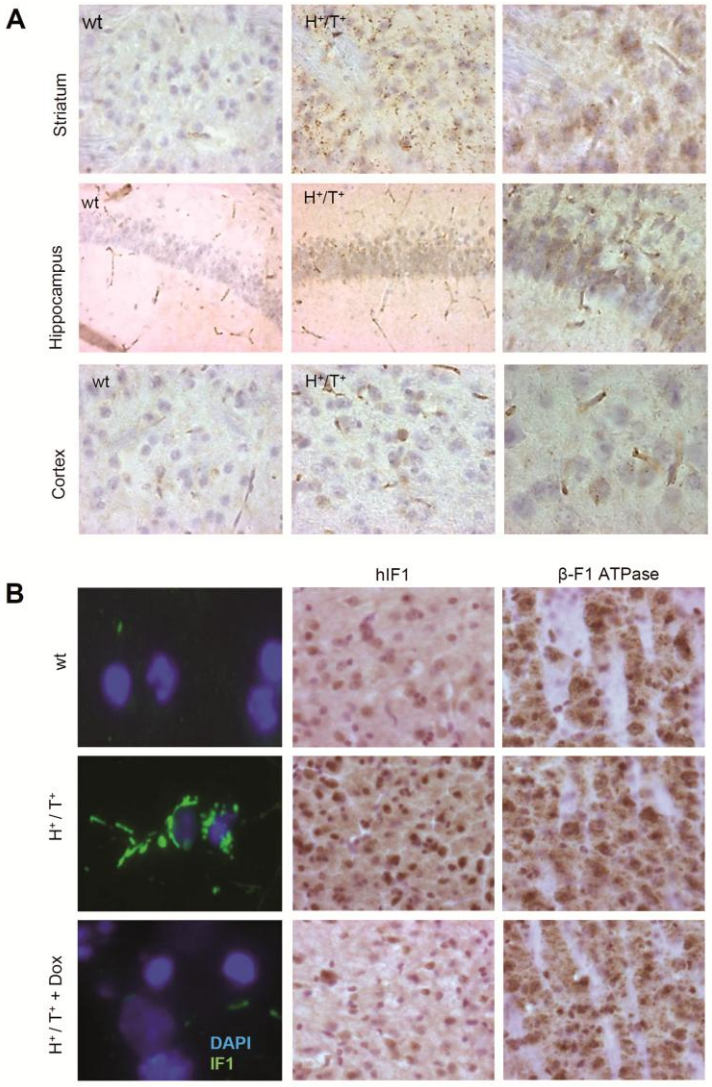

Figure S1. (**A**) Immunohistochemistry of hIF1 in brain striatum, hippocampus and cortex of control (wt) and hIF1 expressing (H^+/T^+) mice. Magnification 40x (first and second columns) and 63x (third column). (**B**) Immunofluorescence (first column) and immunohistochemistry of hIF1 and β-F1-ATPase in the brain of control (wt) and hIF1 expressing (H^+/T^+) mice. Note that the oral administration of doxycycline abrogates the expression of hIF1 in H^+/T^+ mice. Magnification 63x (first column) and 40x (second and third columns).

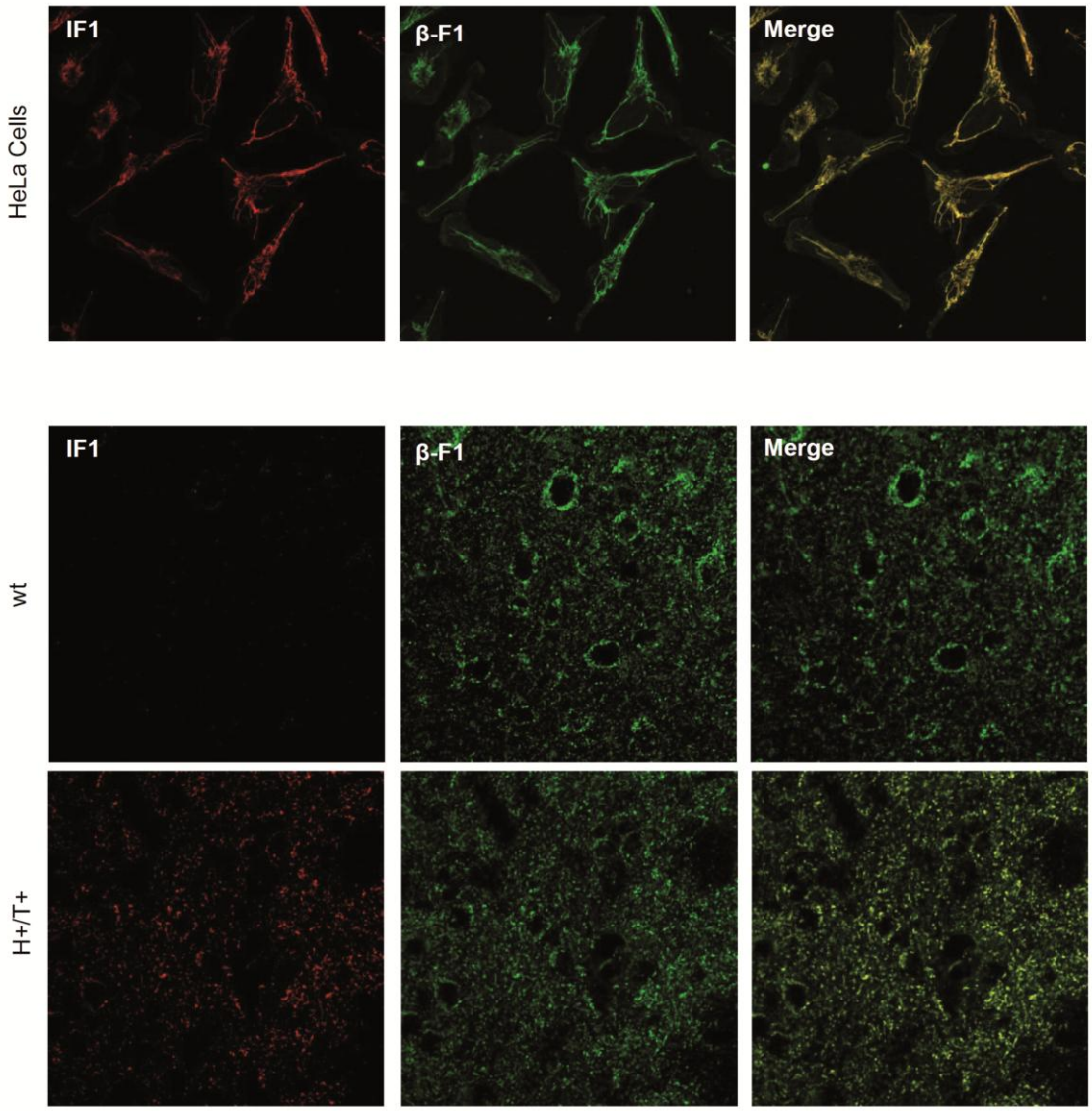

Figure S2. hIF1 is localized in mitochondria. Upper panels, HeLa cells were transfected with the pCMV-SPOR6-H49K plasmid and processed for immunofluorescene microscopy for hIF1 (red) and β-F1-ATPase (β-F1, green). Immunohistochemistry for hIF1 (red) and β-F1-ATPase (β-F1, green) in brain cortex of control (wt, middle panel) and H^+/T^+ (lower panel) mice. Magnification 40x (upper panel) and 20x (middle and lower panel). Note that hIF1 is only expressed in neurons of H^+/T^+ mice whereas β-F1-ATPase is present in glia and neurons of both phenotypes.

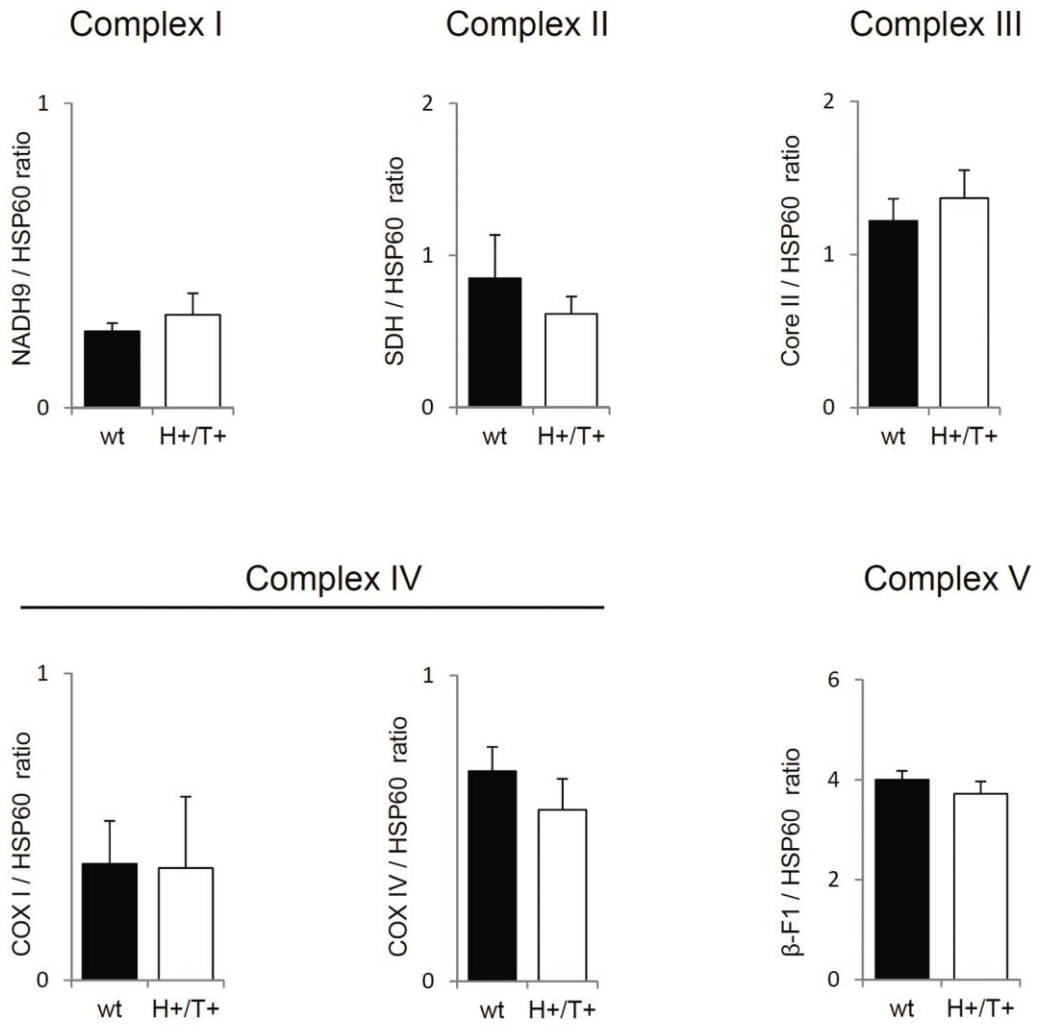

Figure S3. Quantification of the expression of OXPHOS proteins. Fractionated proteins were blotted against heat-shock protein 60 (HSP60), and mitochondrial complexes I (NADH9), II (SDH), III (Core II), IV (COXI and COX IV) and V (β-F1) in total brain extracts of wt and H+/T+ mice as shown in Fig. 1C. The data shown are mean ± SEM of 3 experiments assayed in duplicate.

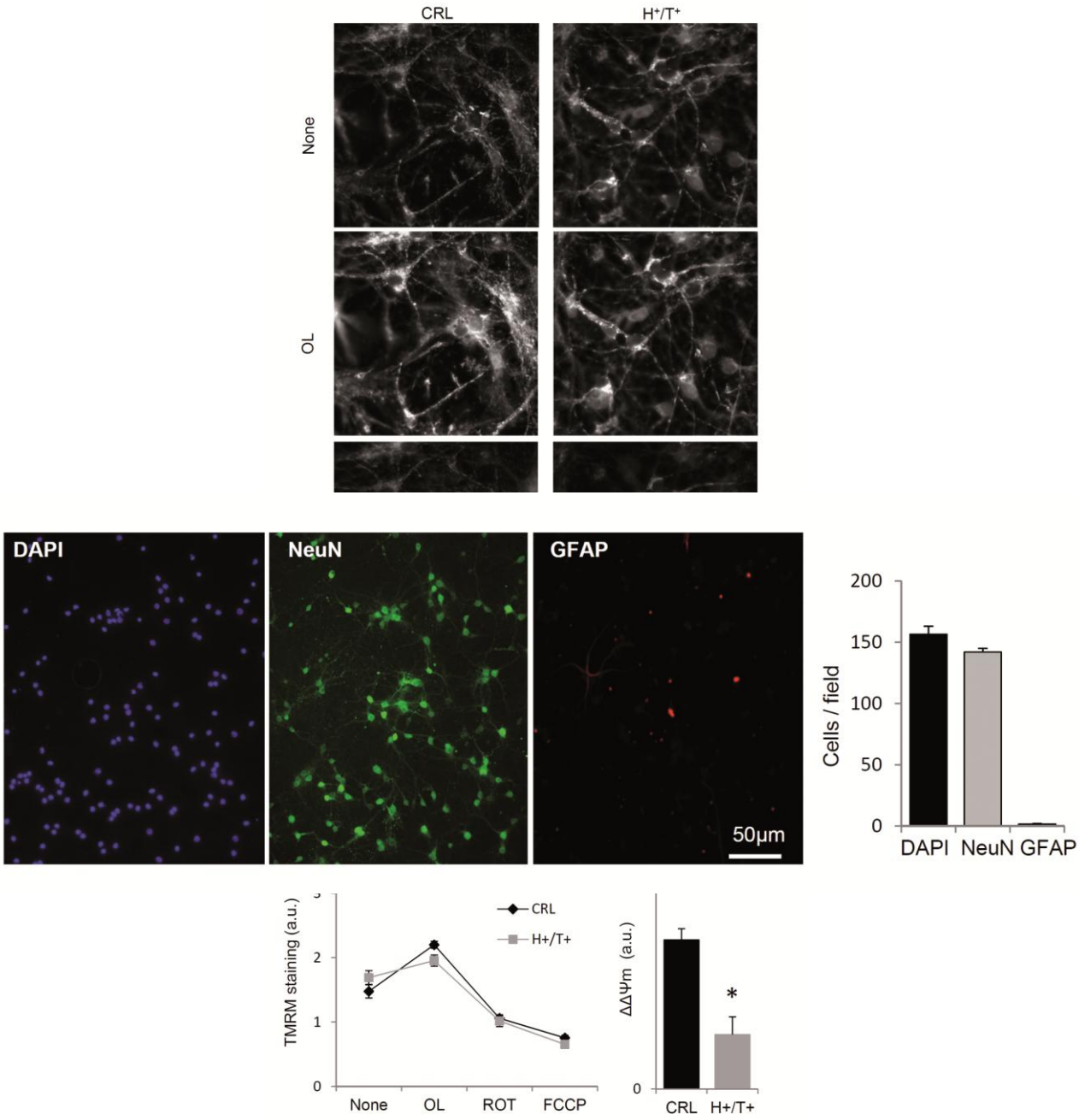

Figure S4. Nine days after seeding, the cultures revealed that they were mainly composed of neurons. Immunocytochemistry for the neuronal marker NeuN (green) and the astrocyte marker GFAP (red) in primary cultures of cortical neurons. The nuclei were stained with DAPI (blue). Histograms show the quantification of the number of each cell type per field. Magnification 10x. The data shown are mean ± SEM of 7 fields.

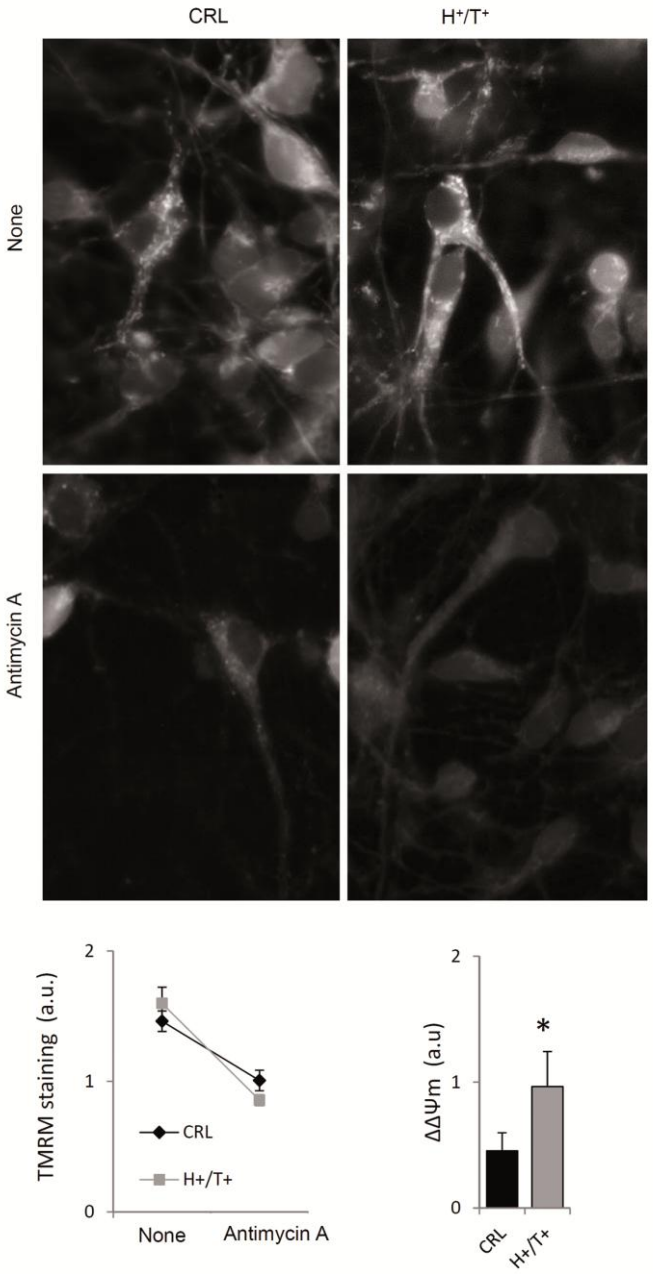

Figure S6. *In vivo* staining of $TMRM^+$ charged mitochondria from 9-10d primary cultures of cortical neurons derived from control (CRL) and H^+/T^+ embryos. Images and graph represent the sequential cytofluorometric measurements of mitochondrial membrane potential (TMRM staining, ΔΨm) in basal condition (None) and after the addition of 1µM antimycin A. Histograms show the quantification of ΔΨm differences between basal condition and antimycin treated cells. Magnification 40x. The data shown are mean ± SEM of 15 fields per condition. *, $p<0.05$ when compared to control by Student's t test.

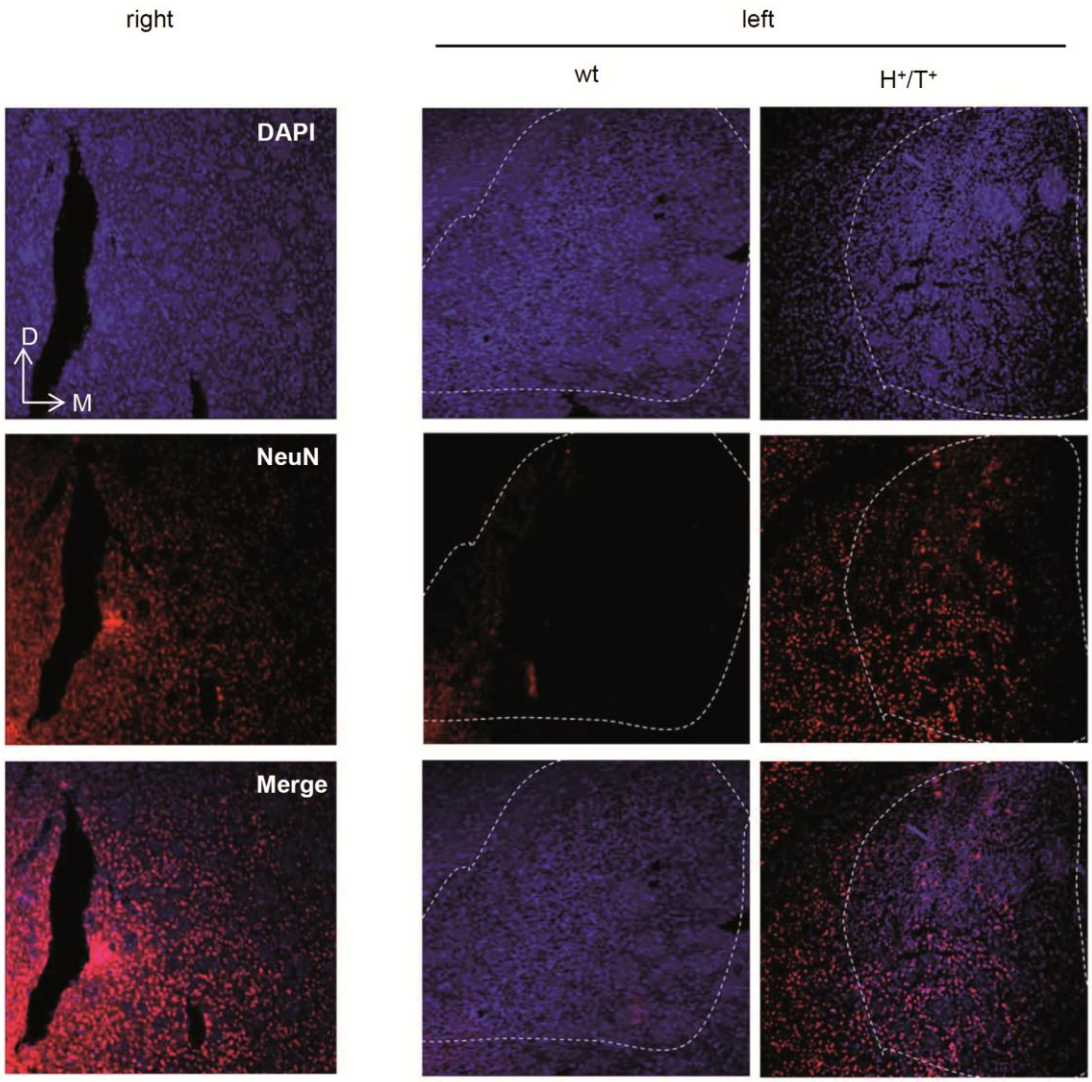

Figure S7. Immunohistochemistry for the neuronal marker NeuN (red) in right (non-damaged) and left (damaged) brain hemispheres of control (wt) and hIF1 expressing (H^+/T^+) mice. The nuclei have been stained with DAPI (blue). Magnification 10x. Note that at 20 days after surgery the striatum has already started to degenerate and the left hemisphere of control mice showed no NeuN expression in the focus of the lesion. In contrast, visible NeuN-staining was observed in H^+/T^+ mice indicating the partial protection from cell death exerted by hIF1. D, dorsal; M, medial.

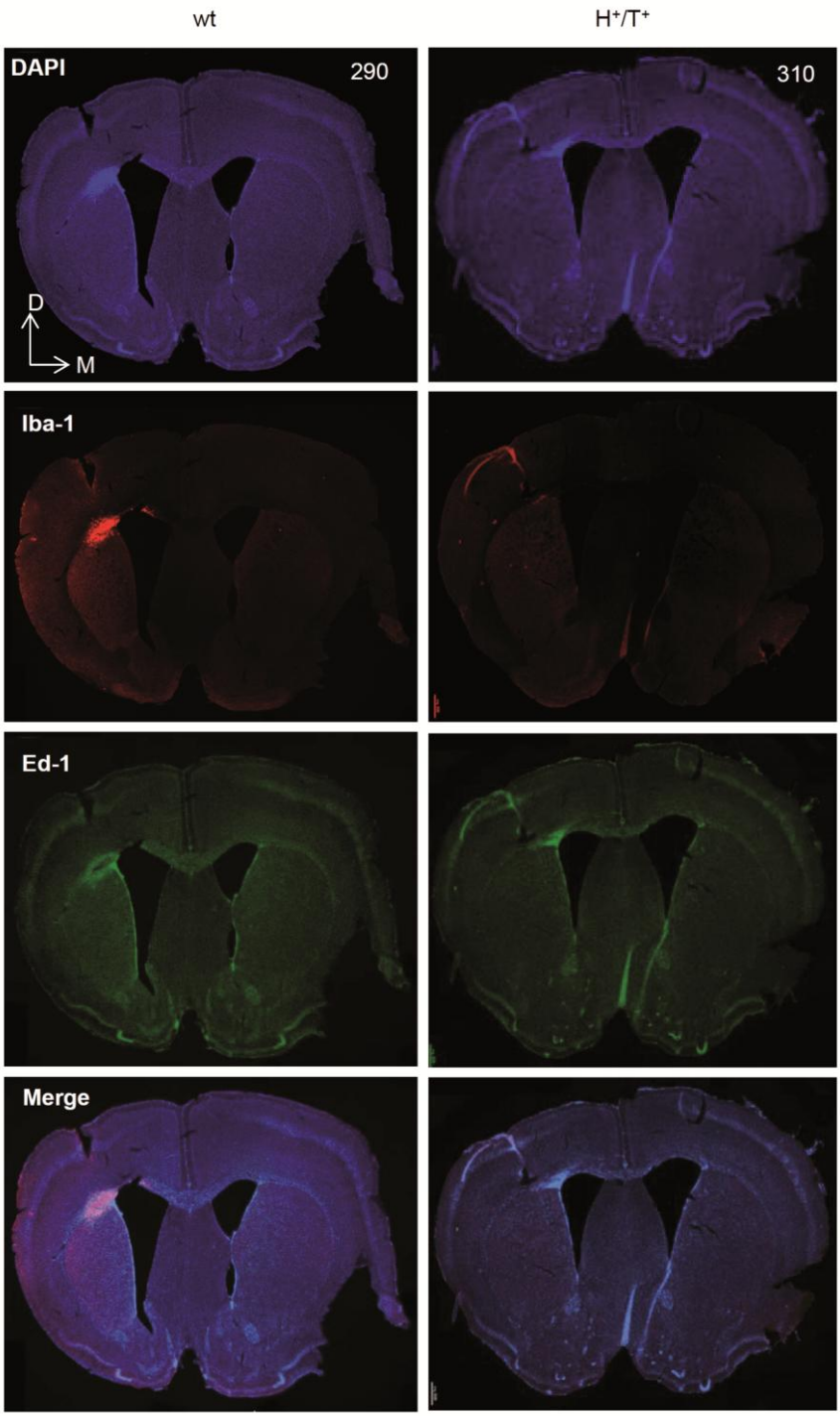

Figure S8. Representative staining of DAPI (nucleus, blue), Iba-1 (microglia, red) and Ed-1 (macrophage, green) antibodies in coronal slices of the brain in control (wt) and H^+/T^+ mice three weeks after surgery. Magnification 2.5x. Note the minor recruitment of inflamatory cells in the brain of hIF1 expressing mice.

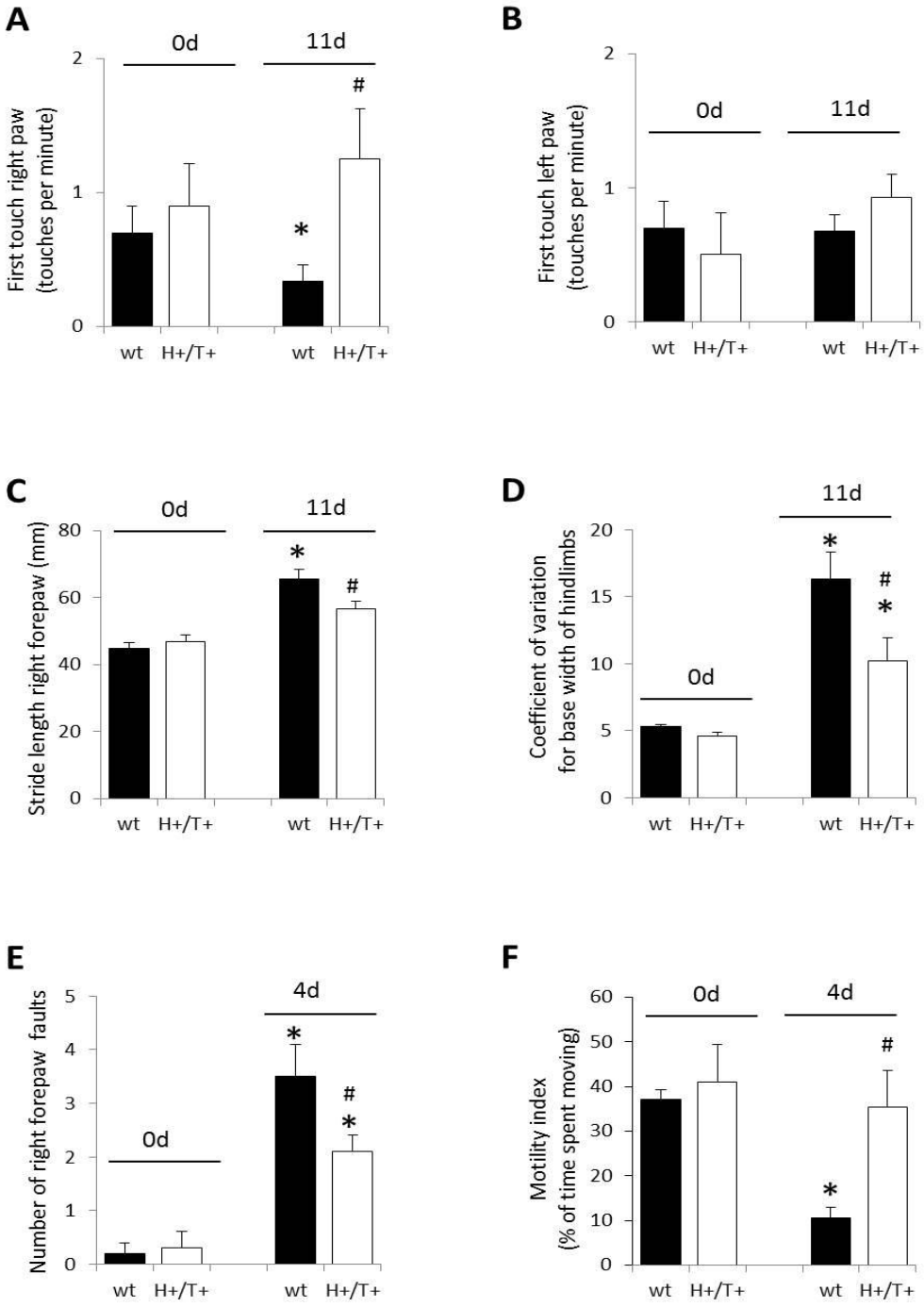

Figure S9. Locomotor evaluation indicates better performance in hIF1 expressing mice. Neurological evaluation in control (wt, closed bars) and hIF1 expressing (H^+/T^+, open bars) mice is shown. Cylinder test (**A** and **B**), foot print analysis (**C** and **D**) and grid test (**E** and **F**) before (0 d) and after four or eleven days (4 d, 11 d) post-surgery. Bars are the mean ± SEM. of ten animals. (**A**) Represents the number of the "first touch" per minute using the right paw, which is contralateral to the brain lesion while (**B**) shows

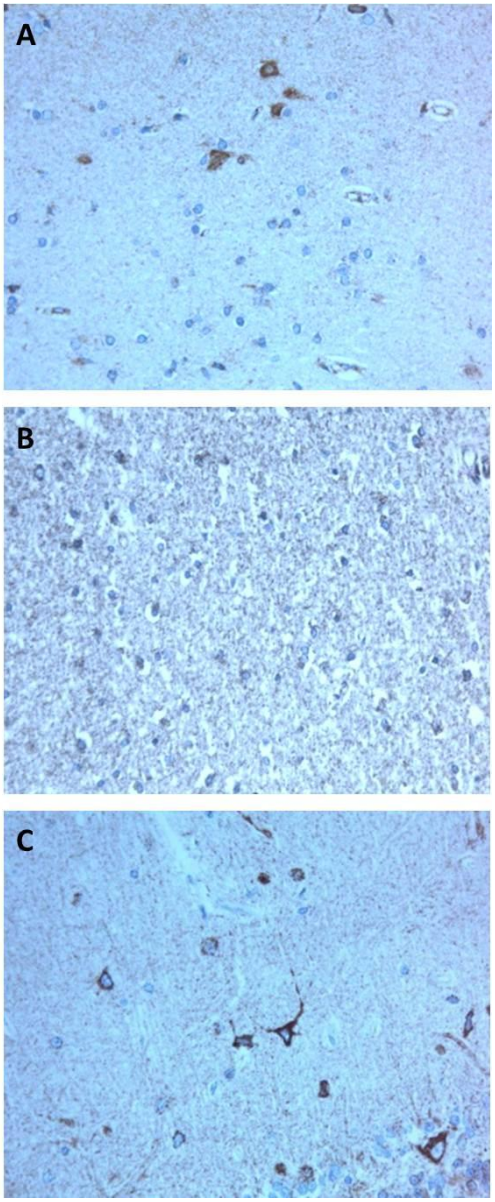

Figure S10. Immunocytochemistry of hIF1 in human cerebral cortex (**A, B**) and cerebellum (**C**) sections. (**A**) Cortico-subcortical area showing positive neurons and negative astrocytes. (**B**) White matter. Negative immunolabelling for astrocytes and oligodendrocytes. (**C**) Positive immunostaining in basket cells of the molecular layer. Magnification 63x. Other hIF1 positive neuronal types are: neurons from the diencephalic, thalamic, hypothalamic and mesencephalic nuclei, lateral and medial corpus geniculatum, motor and sensitive brain-stem nuclei, inferior olives, Clarke columns and motor and sensitive neurons from the spinal cord (data no shown).

Supplementary Materials and Methods.

Western Blot and Protein carbonylation antibodies. The primary monoclonal antibodies developed in our lab and used in this study were: anti-HSP60 (1:5,000), anti-NADH-9 (1:1,000), anti-β-F1-ATPase (1:20,000), anti-LDH-A (1:1,000), anti-GAPDH (1:20,000) and anti-PKM2 (1:1,000) (Acebo et al., 2009). The monoclonal antibody specifically recognizing the human (Sanchez-Cenizo et al., 2010) and mouse (Molecular Probes) IF1 proteins were used at 1:200 dilution. Other antibodies used were: anti-β-actin (1:20,000), anti-tubulin (1:5,000) and anti-catalase (1:5,000) from Sigma-Aldrich; anti-SDH (1:1000) from Life Technologies; anti-Complex III subunit Core 2 (1:1,000), anti-COXI (1:1,000), anti-COXIV (1:1,000) and anti-SOD1 (1:1,000) from Abcam; anti-SOD2 (1:5,000) from Santa Cruz Biotechnology, Inc.; anti-PAR (1:1000) from Enzo Life Science Inc.; anti-IκBα (1:1,000), anti-Akt (1:1,000), anti-p-Akt (1:1,000), anti-p-p70S6K (1:1,000), anti-Bcl-xL (1:1,000) and anti-Bcl-2 (1:1,000) from Cell Signaling Technology Inc. Peroxidase-conjugated anti-mouse, anti-goat or anti-rabbit IgGs (Nordic Immunology; 1:3,000) were used as secondary antibodies.

For the determination of protein carbonylation, dinitrophenylhydrazine (DNPH) derivatization was carried out on 20 μg of proteins derived from brain or neuronal extracts. Samples were fractionated on SDS–12% PAGE. The antibodies used were rabbit anti-DNP (1:150) and goat anti-rabbit IgGs (1:300). The blots were revealed using the ECL® reagent (Amersham Pharmacia Biotech). The intensity of the bands was quantified using a Kodak DC120 digital camera and the Kodak 1D Analysis Software.

Supplementary References.

Acebo, P., Giner, D., Calvo, P., Blanco-Rivero, A., Ortega, A.D., Fernandez, P.L., Roncador, G., Fernandez-Malave, E., Chamorro, M., and Cuezva, J.M. (2009) Cancer abolishes the tissue type-specific differences in the phenotype of energetic metabolism. *Transl Oncol* **2**: 138-145.

Sanchez-Cenizo L, Formentini L, Aldea M, Ortega AD, Garcia-Huerta P, Sanchez-Arago M, Cuezva JM (2010) Up-regulation of the ATPase inhibitory factor 1 (IF1) of the mitochondrial H+-ATP synthase in human tumors mediates the metabolic shift of cancer cells to a Warburg phenotype. J Biol Chem 285: 25308-25313

Supplementary Videos 1, 2, 3 and 4. Grid test in control mice 9, 290, 304 and 305 at 11 days post-surgery.

Supplementary Videos 5, 6, 7 and 8. Grid test in hIF1 expressing mice 296, 312, 345 and 346 at 11 days post-surgery.

Artículo #4

Sánchez-Aragó, M., García-Bermúdez, J., Martínez-Reyes, I., **Santacatterina, F.**, Cuezva, J.M. (2013). Degradation of IF1 controls energy metabolism during osteogenic differentiation of stem cells. *EMBO Rep.* 14(7):638-44

EMBO reports

SOURCE DATA TRANSPARENT PROCESS

scientific report

Degradation of IF1 controls energy metabolism during osteogenic differentiation of stem cells

María Sánchez-Aragó, Javier García-Bermúdez, Inmaculada Martínez-Reyes, Fulvio Santacatterina & José M. Cuezva[+]

Departamento de Biología Molecular, Centro de Biología Molecular Servero Ochoa, CSIC-UAM, Centro de Investigación Biomédica en Red de Enfermedades Raras (CIBERER), Centro de Investigación Hospital 12 de Octubre, ISCIII, Universidad Autónoma de Madrid, Madrid, Spain

Differentiation of human mesenchymal stem cells (hMSCs) requires the rewiring of energy metabolism. Herein, we demonstrate that the ATPase inhibitory factor 1 (IF1) is expressed in hMSCs and in prostate and colon stem cells but is not expressed in the differentiated cells. IF1 inhibits oxidative phosphorylation and regulates the activity of aerobic glycolysis in hMSCs. Silencing of IF1 in hMSCs mimics the metabolic changes observed in osteocytes and accelerates cellular differentiation. Activation of IF1 degradation acts as the switch that regulates energy metabolism during differentiation. We conclude that IF1 is a stemness marker important for maintaining the quiescence state.

Keywords: ATPase inhibitory factor 1; cellular differentiation; H^+-ATP synthase; mitochondria; protein degradation

EMBO *reports* (2013) **14,** 638–644. doi:10.1038/embor.2013.72

INTRODUCTION

A master regulator of energy metabolism in aerobic differentiated cells is the mitochondrial H^+-ATP synthase, the engine of oxidative phosphorylation (OXPHOS) that catalyses the synthesis of ATP using as driving force the proton gradient generated by the respiratory chain. The ATPase inhibitory factor 1 (IF1) [1] is the physiological inhibitor of the H^+-ATP synthase that is highly overexpressed in the mitochondria of cancer cells [2]. Overexpression of IF1 results in the inhibition of the ATP synthetic activity of the enzyme, the switch to an increased aerobic glycolysis [2] and the ROS-mediated signalling of several features of the oncogenic phenotype [3]. These findings supported a role for IF1 as a master regulator of energy metabolism and retrograde nuclear signalling in cancer.

Adult human mesenchymal stem cells (hMSCs) are characterized by their multi-lineage differentiation potential (pluripotency) and their self-renewal capacity [4]. Recently, the study of energy metabolism of stem cells has received attention because of its implication in nuclear reprogramming. Undifferentiated pluripotent stem cells have a low activity of mitochondrial OXPHOS and preferentially use aerobic glycolysis as a major source of energy supply [4]. In contrast, differentiated cells depend more heavily on OXPHOS [5,6]. Interestingly, stemness factor-mediated nuclear reprogramming of somatic cells induces the downregulation of OXPHOS concurrently with the activation of glycolysis [7]. However, the mechanism and signalling molecule that gears the stem cell decision to change its energy metabolism and hence to cause onset of proliferation or differentiation programs are unknown.

Here we demonstrate that the enhanced bioenergetic activity of mitochondria on osteogenic induction is not supported by proliferation of the organelles but by the bioenergetic differentiation of pre-existing mitochondria. We show that IF1 is expressed in hMSCs and in stem cell niches of CD44-positive cells of the human prostate and colon but is not expressed in differentiated osteocytes. Remarkably, IF1 promotes aerobic glycolysis in hMSCs and its expression is stringently regulated by degradation during osteogenic induction. Our findings support a functional role for IF1 in the regulation of stem cell fate decisions.

Departamento de Biología Molecular, Centro de Biología Molecular Servero Ochoa, CSIC-UAM, Centro de Biología Molecular Severo Ochoa, CSIC-UAM, Centro de Investigación Biomédica en Red de Enfermedades Raras (CIBERER), Centro de Investigación Hospital 12 de Octubre, ISCIII, Universidad Autónoma de Madrid 28049 Madrid, Spain

[+]Corresponding author: Tel: +34 91 1964618; Fax: +34 91 1964420; E-mail: jmcuezva@cbm.uam.es

Received 26 December 2012; revised 24 April 2013; accepted 10 May 2013; published online 31 May 2013

RESULTS

Onset of OXPHOS upon osteogenic differentiation

Osteogenesis from hMSCs promoted a large change in cellular morphology (Fig 1A) with concurrent upregulation of the osteogenic marker osteopontin (Fig 1B) and downregulation of the stem cell marker CD44 (Fig 1B). Hence, the osteopontin/CD44 ratio, an index of osteogenic differentiation, was significantly increased in osteocytes when compared to hMSCs (Fig 1B).

Basal rates of aerobic glycolysis were not significantly different between hMSCs and osteocytes (Fig 1C). Inhibition of OXPHOS

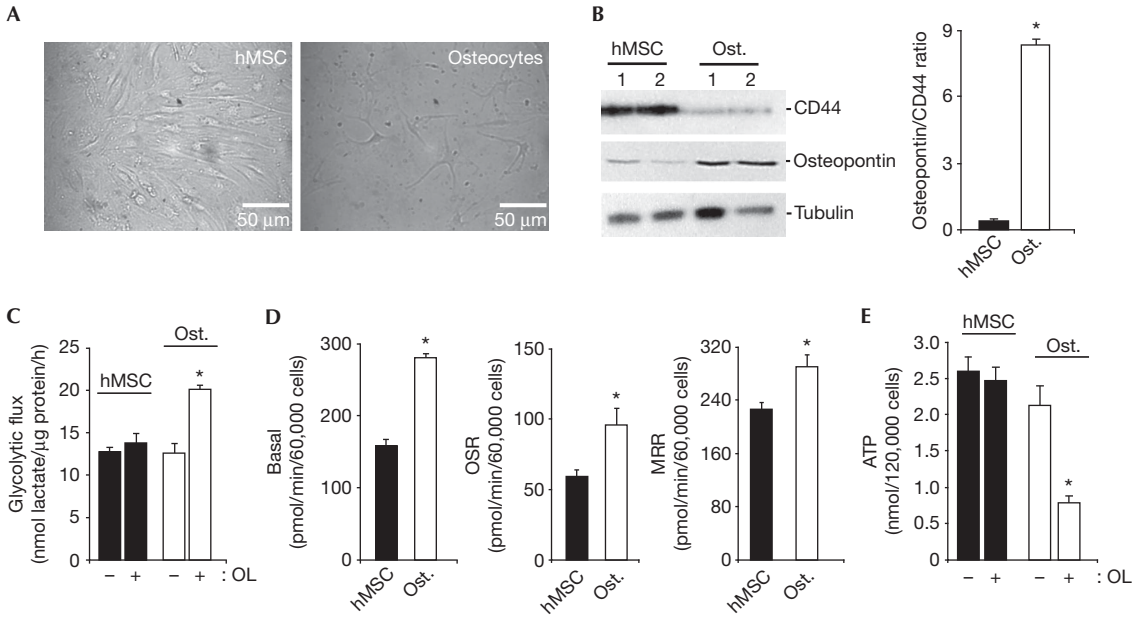

Fig 1 | Metabolic reprogramming of stem cells upon osteogenic differentiation. hMSCs were grown in the osteogenic induction media to promote differentiation. (**A**) Representative images of hMSCs and osteocytes. (**B**) Western blots of the expression of CD44, osteopontin and tubulin in two different preparations of hMSCs and Ost. The histograms show the calculated osteopontin/CD44 ratio. Bars are the mean ± s.e.m. of four different samples. *$P<0.05$ when compared to hMSCs. (**C**) hMSCs and osteocytes were processed for the determination of the rates of aerobic glycolysis in the absence (−) or presence (+) of 6 µM OL. Bars are the mean ± s.e.m. of 6–10 independent determinations. *$P<0.05$ when compared to OL-untreated cells. (**D**) The rates of basal respiration were determined in hMSCs and osteocytes. OSR and MRR were also measured after the addition of 6 µM OL and 0.75 mM DNP, respectively. Bars represent the mean ± s.e.m. of three independent experiments. *$P<0.05$ when compared to hMSCs. (**E**) Cellular ATP concentrations were determined in the absence (−) or presence (+) of 6 µM OL. Bars are the mean ± s.e.m. of three different experiments. *$P<0.05$ when compared to OL-untreated cells. DNP, 2,4-dinitrophenol; hMSCs, human mesenchymal stem cells; MRR, maximum respiratory rates; OL, oligomycin; OSR, oligomycin-sensitive respiration; Ost., osteocytes.

with oligomycin (OL) did not affect the rates of aerobic glycolysis in hMSCs (Fig 1C) but promoted an increase in glycolysis in osteocytes (Fig 1C). Consistently, osteocytes showed a significant increase in basal, OL sensitive and maximum uncoupled respiratory rates (Fig 1D). Basal cellular ATP concentrations were not significantly different between hMSCs and osteocytes (Fig 1E). However, OL only promoted a significant decrease in ATP content in osteocytes (Fig 1E). The drop in ATP levels in response to OL treatment in osteocytes could not be attributed to an enhanced cell death (supplementary Fig S1 online), but could be considered as a result of a higher dependence of this cellular type on OXPHOS.

Osteogenesis triggers mitochondrial differentiation

Cellular differentiation triggered a significant increase in the expression of nicotinamide adenine dinucleotide dehydrogenase subunit 9 from complex I, succinate dehydrogenase B from complex II, core 2 from complex III, cytochrome c oxidase subunits I and II from complex IV, and the α- and β-F1-ATPase subunits of the H^+-ATP synthase from complex V of OXPHOS (Fig 2A; supplementary Fig S2A online). A concurrent decrease in the expression of the glycolytic proteins glyceraldehyde-3-phosphate dehydrogenase, pyruvate kinase isoform M2 (PK-M2) and lactate dehydrogenase A was observed (Fig 2A; supplementary Fig S2A online). Hence, the overall mitochondrial capacity of the cell (β-F1-ATPase/glyceraldehyde-3-phosphate dehydrogenase ratio) [8] (see supplementary Information online) was significantly augmented in osteocytes (supplementary Fig S2A online). Other mitochondrial proteins such as nicotinamide adenine dinucleotide Fe-S protein 3 from complex I, cytochrome oxidase subunit IV from complex IV, hydroxyacyl-CoA dehydrogenase of β-oxidation, porin (VDAC, voltage-dependent anion channel) and the structural mitochondrial protein Hsp60 revealed no relevant changes during osteogenic induction (Fig 2A; supplementary Fig S2A online). Analysis of OXPHOS complexes in blue native gels revealed no relevant differences in their assembly between hMSCs and osteocytes (supplementary Fig S2B online), supporting that their assembly is not limiting OXPHOS in hMSCs.

In contrast with recent findings [6], we observed that osteogenic induction occurred in the absence of relevant changes in mitochondrial DNA (mtDNA) copy number (Fig 2B) as well as in mitochondrial mass as assessed by the cardiolipin content of the cell (Fig 2C). Analysis of mitochondrial morphology and abundance using MitoTracker Red revealed large differences in organelle shape (Fig 2D) and the absence of differences in mitochondrial content (the histogram in Fig 2D). Mitochondria in hMSCs were predominantly punctiform, whereas the thread-like morphology was more abundant in osteocytes (Fig 2D), in agreement with previous findings in pluripotent stem cells [9]. High-resolution electron microscopy further confirmed no significant differences in the number of mitochondria per cell

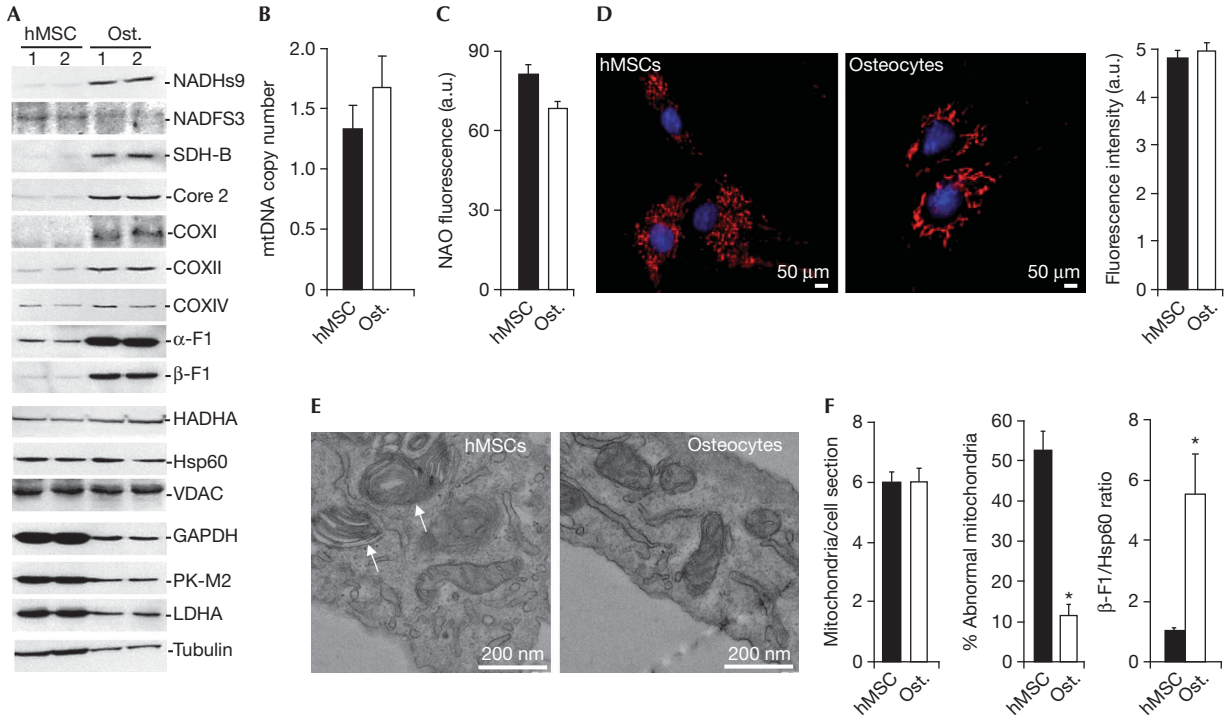

Fig 2 | Differentiation of mitochondria upon osteogenic induction. (**A**) Representative western blots of the expression of mitochondrial proteins (NADHs9, NDUFS3, SDH-B, Core 2, COXI, COXII, COXIV, α-F1-ATPase, β-F1-ATPase, HADHA, Hsp60 and VDAC), glycolytic enzymes (GAPDH, PK-M2 and LDHA) and tubulin in two different preparations of hMSCs and osteocytes. (**B**) hMSCs and osteocytes were processed for the determination of the relative mtDNA copy number (12S/β-F1-ATPase ratio). Bars represent the mean ± s.e.m. of seven independent determinations. (**C**) The mitochondrial mass was determined by the content of cardiolipin as assessed by NAO fluorescence. Bars are the mean ± s.e.m. of six independent determinations. *$P<0.05$ when compared to hMSCs. (**D**) Fluorescence microscopy of hMSC and osteocytes stained with MitoTracker Red and Hoechst. Images show a partially fragmented mitochondrial network in hMSCs when compared to the thread-like morphology of mitochondria observed in osteocytes. The histogram shows the quantification of the MitoTracker signal in hMSCs and osteocytes. The results shown are the mean ± s.e.m. of 45–60 different cells. (**E**) Representative electron microscopy images of mitochondria in hMSCs and osteocytes. Onion-like mitochondria (white arrows) are observed in hMSCs. The histograms show the quantification of the number of mitochondria per cell section and the percentage of abnormal organelles in ultrathin sections of hMSCs and osteocytes, respectively. The results shown are the mean ± s.e.m. of 45–50 different cells. *$P<0.05$ when compared to hMSCs. (**F**) The histogram shows the mean ± s.e.m. of the calculated β-F1-ATPase/Hsp60 ratio in hMSCs and osteocytes in four different samples. *$P<0.05$ when compared to hMSCs. a.u., arbitrary units; COX, cytochrome oxidase; GAPDH, Glyceraldehyde 3-phosphate dehydrogenase; hMSCs, human mesenchymal stem cells; LDH-A, lactate dehydrogenase A; NADHs9, nicotinamide adenine dinucleotide subunit 9; OL, oligomycin; OSR, oligomycin-sensitive respiration; Ost., osteocytes; PK-M2, pyruvate kinase isoform M2.

section between osteocytes and hMSCs (Fig 2E). However, hMSCs contained a high percentage of mitochondria with abnormal structure when compared to mitochondria in osteocytes (Fig 2E). These results indicate that osteogenic induction promotes the bioenergetic differentiation of mitochondria rather than organelle proliferation, as supported by the increase in the β-F1-ATPase/Hsp60 ratio [8] (see supplementary Information online) observed in osteocytes when compared to hMSCs (Fig 2F).

We observed no relevant differences in the expression of β-F1-ATPase messenger RNA (mRNA) between hMSCs and osteocytes (supplementary Fig S3A online), suggesting that the expression of β-F1-ATPase (Fig 2A) is controlled at the level of mRNA translation during differentiation, which is in agreement with similar findings in development and in oncogenesis [10]. miR-127-5p targets the 3′ untranslated region of β-F1-ATPase mRNA and inhibits its translation [11]. However, both hMSCs and osteocytes do not express significant levels of miR-127-5p (supplementary Fig S3B online), indicating that it is not involved in repressing the bioenergetic differentiation of mitochondria in hMSCs.

IF1 regulates energy metabolism of stem cells

Western blot analysis revealed that osteocytes do not express IF1 when compared to hMSCs (Fig 3A). Short interfering RNA-mediated silencing of IF1 in hMSCs resulted in a significant reduction in the rates of aerobic glycolysis (Fig 3B). In this situation, OL treatment promoted a significant increase in lactate production (Fig 3B). Consistently, downregulation of IF1 in hMSCs promoted an increase in the activity of the mitochondrial H^+-ATP synthase (Fig 3C). Although basal cellular ATP concentrations were not affected by IF1 downregulation (Fig 3D), a significant drop in cellular ATP content occurred in the presence of OL in IF1-silenced hMSCs (Fig 3D). These results suggest that IF1 is part of the switch that controls energy metabolism on osteogenic

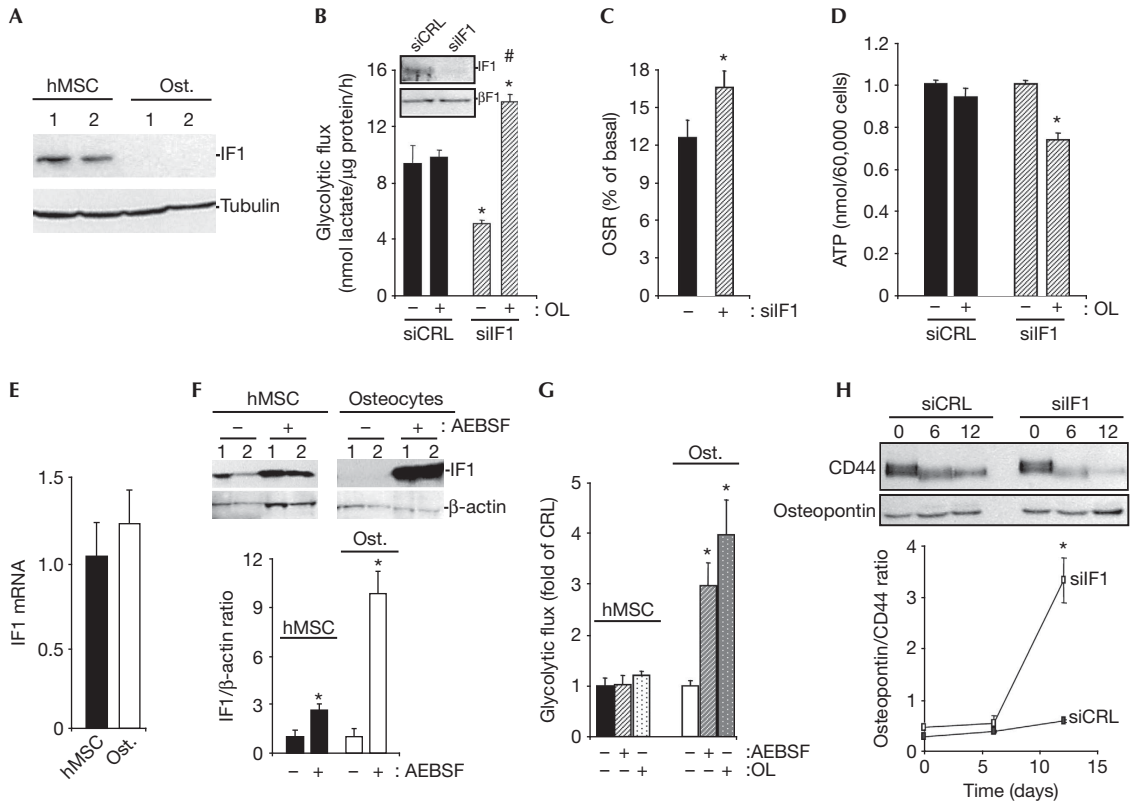

Fig 3 | IF1 degradation mediates metabolic reprogramming of stem cells during osteogenic differentiation. (**A**) Representative blots of IF1 and tubulin in two different preparations of hMSCs and osteocytes. Osteogenic induction is accompanied by repression of IF1 expression. (**B–D,H**) hMSCs were transfected with control (siCRL, closed bars) or siIF1 siRNA (siIF1, hatched bars) to regulate the expression of IF1. (**B**) Rates of aerobic glycolysis in the absence (−) or presence (+) of 6 μM OL. Bars are the mean ± s.e.m. of six independent determinations. * and $^{\#}P<0.05$ when compared to siCRL or siIF1 untreated cells, respectively. (**C**) The rates of OSR were determined after addition of 6 μM OL. Data are shown as percentage of the basal respiration. Bars are the mean ± s.e.m. of eight independent determinations. $^{*}P<0.05$ when compared to siCRL. (**D**) Cellular ATP concentrations were determined in the absence (−) or presence (+) of 6 μM OL. Bars are the mean ± s.e.m. of 12 independent determinations. $^{*}P<0.05$ when compared to OL-untreated cells. (**E**) IF1 mRNA expression was assessed by RT–qPCR in hMSCs and osteocytes. Bars are the mean ± s.e.m. of six independent determinations. (**F**) hMSCs and osteocytes were treated 24 h with (+) or without (−) 400 μM of the serine-protease inhibitor AEBSF to block the activity of mitochondrial proteases, and the expression of IF1 and β-actin (loading control) analysed by western blot in two different preparations. Plots are the mean ± s.e.m. of the calculated IF1/β-actin ratio in four different experiments. $^{*}P<0.05$ when compared to untreated (−) cells. (**G**) The rates of aerobic glycolysis in the absence (−) or presence (+) of 400 μM of AEBSF or 6 μM OL were determined in hMSCs and osteocytes. Bars are the mean ± s.e.m. of six independent determinations. $^{*}P<0.05$ when compared to untreated cells. (**H**) The expression of CD44 and osteopontin was analysed by western blot at the indicated times to assess the rate of differentiation after silencing of IF1. The plot represents the calculated osteopontin/CD44 ratio in siCRL and siIF1 cells. $^{*}P<0.05$ when compared to siCRL. AEBSF, 4-(2-Aminoethyl) benzenesulfonyl fluoride hydrochloride; CRL, control; hMSCs, human mesenchymal stem cells; IF1, inhibitory factor 1; mRNA, messenger RNA; OL, oligomycin; OSR, oligomycin-sensitive respiration; Ost., osteocyte; RT-qPCR, real-time quantitative polymerase chain reaction; siCRL, short interfering control; siIF1, short interfering IF1.

induction of hMSCs (Fig 1). The regulated expression of IF1 does not affect the proliferation rate of hMSCs (supplementary Fig S4 online), in contrast to data obtained in colon cancer cells [3] suggesting a cell-type specific variability in nuclear responses to IF1 signalling.

Regulation of IF1 expression in stem cells

hMSCs and osteocytes revealed no relevant differences in the cellular content of IF1 mRNA (Fig 3E). Twenty-four-hour treatment of hMSCs and osteocytes with AEBSF (a serine-protease inhibitor) promoted a large accumulation of IF1 in both cellular types (Fig 3F). However, the accumulation of IF1 in AEBSF-treated osteocytes exceeded by three-fold the accumulation observed in hMSCs, suggesting that normal differentiated cells degrade IF1 at a much faster rate than hMSCs. A short interfering RNA-based screen aimed at the identification of the protease involved in the degradation of IF1 in hMSCs (supplementary Fig S5A online), and HCT116 colon cancer cells (supplementary Fig S5B online) failed to provide a candidate responsible for the degradation of IF1 despite evidence of partial silencing of the seven proteases tested (supplementary Fig S5 online). Remarkably, whereas treatment of hMSCs with AEBSF

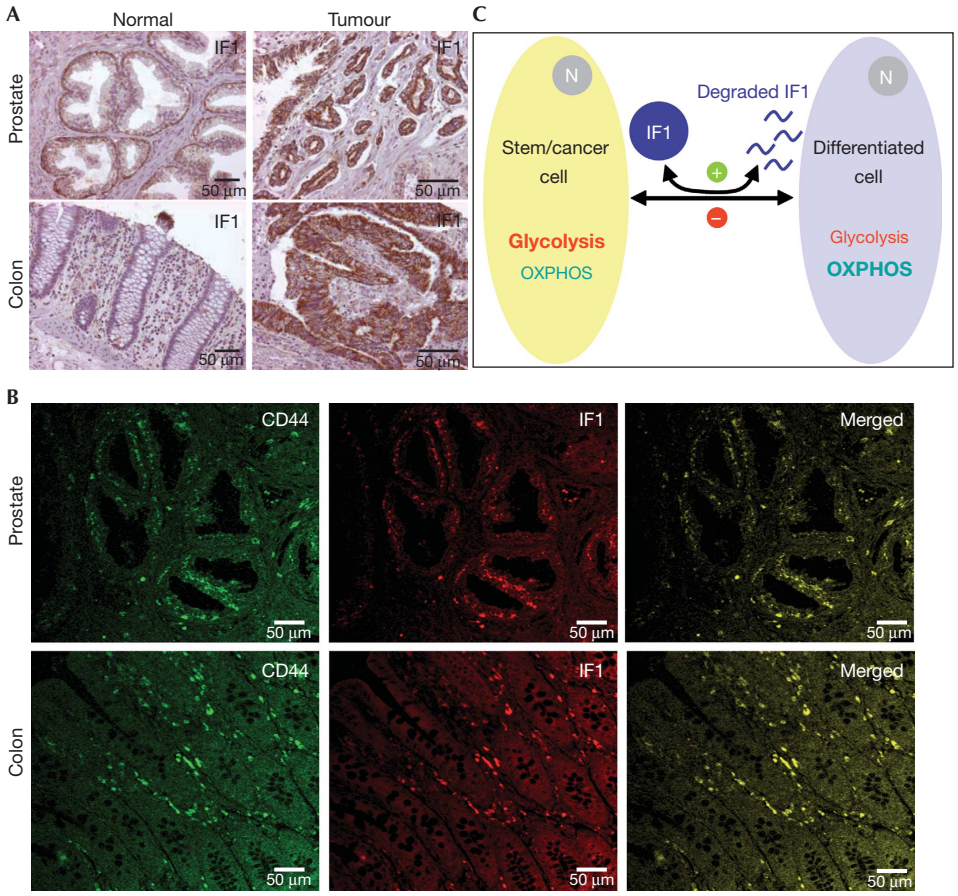

Fig 4 | IF1 is a stem cell marker. (**A**) Immunohistochemistry of IF1 expression in human normal and tumour prostate and colon tissues. Images are shown at × 20–40 magnification. (**B**) Double-immunofluorescence microscopy of normal human prostate and colon stained with CD44 antibody (green) and with monoclonal IF1 antibody (red). The merged images revealed the co-localization of IF1 in stem cell niches of both tissues. Images are shown at × 40 magnification. (**C**) Scheme of the proposed mechanism by which IF1 (dark blue) regulates metabolic rewiring upon cellular differentiation/dedifferentiation. Stem and cancer cells (dark yellow) show a high expression of IF1, which promotes the inhibition of OXPHOS favouring aerobic glycolysis. Differentiation triggers an enhanced degradation of IF1 (+, green) and the activation of OXPHOS in the differentiated cell (light blue). The relevance of glycolysis as ATP supplier is diminished in this situation. Dedifferentiation of somatic cells into cancer cells results in the accumulation of IF1, the inhibition of OXPHOS and the activation of aerobic glycolysis. The accumulation of IF1 in cancer cells might be regulated by inhibiting the degradation of the protein (−, red). IF1, inhibitory factor 1; OXPHOS, oxidative phosphorylation.

did not induce significant changes in the rates of aerobic glycolysis (Fig 3G); the same treatment in osteocytes triggered a large increase in the glycolytic flux (Fig 3G), comparable to that induced by treatment with OL (Fig 3G). Moreover, silencing of IF1 accelerated the rate of differentiation, as revealed by the osteopontin/CD44 ratio after 12 days of osteogenic induction (Fig 3H), suggesting a role for IF1 in signalling the repression of cellular differentiation.

IF1 is a marker of stem cells

Immunohistochemistry of IF1 revealed that it is expressed in basal epithelial cells of the prostate (Fig 4A) and in the Lieberkühn crypts of the colon (Fig 4A). A high expression of IF1 was also observed in prostate and colon carcinomas (Fig 4A). Double-immunofluorescence microscopy analysis for CD44 and IF1 in human prostate and colon showed the co-localization of both markers in basal epithelial cells and Lieberkühn crypts, respectively (Fig 4B), which are the sites where stem cells are located in these tissues [12,13].

DISCUSSION

Metabolic reprogramming during cellular differentiation [4–6] or in the dedifferentiation of somatic cells into iPSC [7] or cancer cells [3] is well established. Here we show that upon osteogenic differentiation of hMSCs, there is an upregulation of proteins of complex I, II, III, IV and V of OXPHOS. These changes result in an increase in the activity of the respiratory chain and of the H^+-ATP synthase, and a higher dependence of osteocytes on OXPHOS to provide the ATP needed to sustain cellular specialization. Despite the enhancement of OXPHOS and the partial downregulation of the cellular content of glycolytic enzymes in osteocytes, the differentiated cells still show similar rates of glycolysis as hMSCs, indicating that the higher energy requirements of osteocytes cannot be covered by OXPHOS alone. Moreover, the

maintenance of the glycolytic flux despite the diminished expression of glycolytic enzymes in osteocytes highlights the relevance of allosteric regulation of this metabolic pathway.

The mitochondrial phenotype of a given cell is the result of cell-type-specific programs that are regulated at both the transcriptional [14] and post-transcriptional [10] levels. Transcriptional programs usually result in the onset of mitochondrial proliferation [14], whereas post-transcriptional ones promote the rapid bioenergetic differentiation of the organelle in response to changing physiological cues (for a review, see Willers and Cuezva [10]). Our findings indicate that the enhanced activity of OXPHOS in osteocytes is not supported by an enhanced mitochondrial proliferation but by the bioenergetic differentiation of pre-existing stem cell mitochondria, in agreement with the findings upon pluripotent stem cell differentiation [9,15]. Consistently, the bioenergetic accomplishment of mitochondria during osteogenesis also seems to be regulated at the post-transcriptional level [10].

Rewiring of energy metabolism to aerobic glycolysis has been shown to foster nuclear reprogramming, both during oncogenesis [16] and in dedifferentiation to iPSC [7]. However, the molecule that orchestrates the metabolic switch during stem cell differentiation remains elusive. Here, we show that IF1 regulates the energy metabolism of hMSCs by inhibiting the activity of OXPHOS and promoting aerobic glycolysis, reproducing the effect of OL in cellular metabolism [2]. Kinetic evidence indicates that IF1 inhibits the ATP hydrolase activity of the H^+-ATP synthase [1]. However, it is likely that the binding of IF1 to the H^+-ATP synthase also depends on the mass–action ratio and hence, when IF1 is expressed, as it is the situation in hMSCs, it can also inhibit the synthase activity of the enzyme. Indeed, silencing of IF1 in hMSCs resulted in a drop in glycolysis and a concurrent increase in ATP synthase activity. Conversely, its overexpression in different cell types has been shown to increase glycolysis and to inhibit the ATP synthase activity, mimicking the metabolic effects triggered by the ATP synthase inhibitor OL [2,3]. Moreover, we document the expression of IF1 in hMSCs as well as in human prostate and colon stem cells, but not in osteocytes and other differentiated cells. Remarkably, disappearance of IF1 seems to be a prerequisite to facilitate the metabolic switch that accompanies cellular differentiation, emphasizing the prominent role that IF1 might play in the maintenance of stemness. However, other mechanisms might also operate, as it has been reported that human pluripotent stem cells have a low content of IF1 and their differentiation is triggered by repression of UCP2 [9].

Recent findings have stressed the relevance of post-translational modification of pluripotency-associated transcription factors in simultaneously maintaining pluripotency or inducing lineage-specific differentiation (for a review, see Cai *et al.* [17]). The results in this report add on the same idea by stressing the relevance of the degradation of IF1 in maintaining energy metabolism of the undifferentiated state of stem cells. The accumulation of IF1 in response to the inhibitor AEBSF indicates that the protein is degraded by a mitochondrial serine protease. The enhanced degradation of IF1 in osteocytes might thus result from the activation of any of these proteases as a surrogate process of the nuclear reprogramming that renders ongoing the differentiated state and/or because IF1 is experiencing a post-translational modification that makes it more susceptible to degradation. Our screening for the putative protease involved indicates that degradation of IF1 is more complex than originally anticipated and might involve an unexplored pathway for the degradation of mitochondrial proteins.

Cancer and stem cells show large phenotypic analogies regarding the molecular and functional activities of the proteins involved in glycolysis and in mitochondrial OXPHOS (Fig 4C). The expression of IF1 represents an additional phenotypic trait in common (Fig 4C). Deciphering the nuclear responses to the presence or absence of IF1 will certainly contribute to our understanding of stem cell fate decisions. Overall, we show that IF1 is a stem cell marker that regulates the energy metabolism of hMSCs. The regulated degradation of IF1 hinders self-renewal of stem cells to favour differentiation.

METHODS

Culture of hMSC. hMSCs were obtained from Lonza and cultured according to the manufacturer's instructions; for more details see Supporting Information online.

Aerobic glycolysis and oxygen consumption rates. The rates of aerobic glycolysis were determined by the enzymatic determination of lactate in the medium in the absence or presence of 6 μM OL [18]. The oxygen consumption rates were determined in a XF24 Extracellular Flux Analyzer (Seahorse Biosciences) [2].

Determination of ATP. Cells were incubated for 1 h in the presence or absence of 6 μM OL and cellular ATP concentrations were determined using the ATP Bioluminiscence Assay Kit CLS II (Roche).

Western blot analysis. Cellular lysates were processed for blotting as indicated [2]. Details of the antibodies used are provided in Supporting Information online.

Determination of mtDNA copy number. After cellular DNA extraction, the quantification of mtDNA (mtDNA/nDNA) was performed by qPCR using the LightCycler 2.0 real-time PCR system as described [19].

Electron microscopy. For ultrastructural studies, hMSCs and osteocytes were fixed with 2% glutaraldehyde in 0.1 M Sörensen phosphate buffer, pH 7.4, and processed for electron microscopy as detailed elsewhere [18].

Fluorescence microscopy. Cells were incubated for 45 min with 500 nM Mitotracker Red FM (Invitrogen) followed by staining with Hoechst (1 mg/ml) for 10 min at 37 °C. Cellular fluorescence was analysed in an Axiovert 200 (Zeiss) microscope using a CCD camera. The red fluorescence intensity of the cells was calculated using ImageJ.

Statistical analysis. Statistical analyses were performed using a two-tailed Student's *t* test. The results shown are the means ± s.e.m. $P<0.05$ was considered statistically significant.

Supplementary information is available at EMBO *reports* online (http://www.emboreports.org).

ACKNOWLEDGEMENTS

C. Núñez de Arenas and M. Chamorro are acknowledged for expert technical assistance. I.M.R., J.G.B. and F.S. were supported by pre-doctoral fellowships from Junta Ampliación Estudios-Consejo Superior de Investigaciones Científicas, Formación Personal Investigador-Ministerio Educación y Ciencia and Formación Personal Investigador-Universidad Autónoma de Madrid Spain, respectively. This work was supported by grants from the Ministerio de Educación y

Ciencia (BFU2010-18903), the Centro de Investigación Biomédica en Red de Enfermedades Raras (CIBERER), ISCIII and Comunidad de Madrid (S2011/BMD-2402), Spain. The Centro de Biología Molecular Severo Ochoa recieves an institutional grant from the Fundación Ramón Areces.

Author contributions: M.S.-A. and J.M.C. designed the research; M.S.-A., J.G.-B., I.M.-R. and F.S. performed the research; M.S.-A. and J.M.C. analysed the data; M.S.-A. and J.M.C. wrote the paper.

CONFLICT OF INTEREST

The authors declare that they have no conflict of interest.

REFERENCES

1. Gledhill JR, Montgomery MG, Leslie AG, Walker JE (2007) How the regulatory protein, IF(1), inhibits F(1)-ATPase from bovine mitochondria. *Proc Natl Acad Sci USA* **104:** 15671–15676
2. Sanchez-Cenizo L, Formentini L, Aldea M, Ortega AD, Garcia-Huerta P, Sanchez-Arago M, Cuezva JM (2010) Up-regulation of the ATPase inhibitory factor 1 (IF1) of the mitochondrial H + -ATP synthase in human tumors mediates the metabolic shift of cancer cells to a Warburg phenotype. *J Biol Chem* **285:** 25308–25313
3. Formentini L, Sánchez-Aragó M, Sánchez-Cenizo L, Cuezva JM (2012) The mitochondrial ATPase Inhibitory Factor 1 (IF1) triggers a ROS-mediated retrograde pro-survival and proliferative response. *Mol Cell* **45:** 731–742
4. Rehman J (2010) Empowering self-renewal and differentiation: the role of mitochondria in stem cells. *J Mol Med* **88:** 981–986
5. Tormos KV, Anso E, Hamanaka RB, Eisenbart J, Joseph J, Kalyanaraman B, Chandel NS (2011) Mitochondrial complex III ROS regulate adipocyte differentiation. *Cell Metab* **14:** 537–544
6. Chen CT, Shih YR, Kuo TK, Lee OK, Wei YH (2008) Coordinated changes of mitochondrial biogenesis and antioxidant enzymes during osteogenic differentiation of human mesenchymal stem cells. *Stem Cells* **26:** 960–968
7. Folmes CD, Nelson TJ, Martinez-Fernandez A, Arrell DK, Lindor JZ, Dzeja PP, Ikeda Y, Perez-Terzic C, Terzic A (2011) Somatic oxidative bioenergetics transitions into pluripotency-dependent glycolysis to facilitate nuclear reprogramming. *Cell Metab* **14:** 264–271
8. Cuezva JM *et al* (2002) The bioenergetic signature of cancer: a marker of tumor progression. *Cancer Res* **62:** 6674–6681
9. Zhang J *et al* (2011) UCP2 regulates energy metabolism and differentiation potential of human pluripotent stem cells. *EMBO J* **30:** 4860–4873
10. Willers IM, Cuezva JM (2011) Post-transcriptional regulation of the mitochondrial H(+)-ATP synthase: a key regulator of the metabolic phenotype in cancer. *Biochim Biophys Acta* **1807:** 543–551
11. Willers IM, Martínez-Reyes I, Martínez-Diez M, Cuezva J (2012) miR-127-5p targets the 3'UTR of human β-F1-ATPase mRNA and inhibits its translation. *Biochim Biophys Acta-Bioenergetics* **1817:** 838–848
12. Lawson DA, Xin L, Lukacs RU, Cheng D, Witte ON (2007) Isolation and functional characterization of murine prostate stem cells. *Proc Natl Acad Sci USA* **104:** 181–186
13. Olsen Hult LT, Kleiveland CR, Fosnes K, Jacobsen M, Lea T (2011) EP receptor expression in human intestinal epithelium and localization relative to the stem cell zone of the crypts. *PLoS One* **6:** e26816
14. Scarpulla RC (2008) Transcriptional paradigms in mammalian mitochondrial biogenesis and function. *Physiol Rev* **88:** 611–638
15. Birket MJ, Orr AL, Gerencser AA, Madden DT, Vitelli C, Swistowski A, Brand MD, Zeng X (2011) A reduction in ATP demand and mitochondrial activity with neural differentiation of human embryonic stem cells. *J Cell Sci* **124:** 348–358
16. Ramanathan A, Wang C, Schreiber SL (2005) Perturbational profiling of a cell-line model of tumorigenesis by using metabolic measurements. *Proc Natl Acad Sci USA* **102:** 5992–5997
17. Cai N, Li M, Qu J, Liu GH, Izpisua Belmonte JC (2012) Post-translational modulation of pluripotency. *J Mol Cell Biol* **4:** 262–265
18. Sanchez-Arago M, Chamorro M, Cuezva JM (2010) Selection of cancer cells with repressed mitochondria triggers colon cancer progression. *Carcinogenesis* **31:** 567–576
19. Martinez-Reyes I, Sanchez-Arago M, Cuezva JM (2012) AMPK and GCN2-ATF4 signal the repression of mitochondria in colon cancer cells. *Biochem J* **444:** 249–259

Supporting Information.

Degradation of IF1 controls energy metabolism during osteogenic differentiation of stem cells

María Sánchez-Aragó[1], Javier García-Bermúdez[1], Inmaculada Martínez-Reyes[1], Fulvio Santacatterina[1] and José M. Cuezva[1, *]

Supporting Results

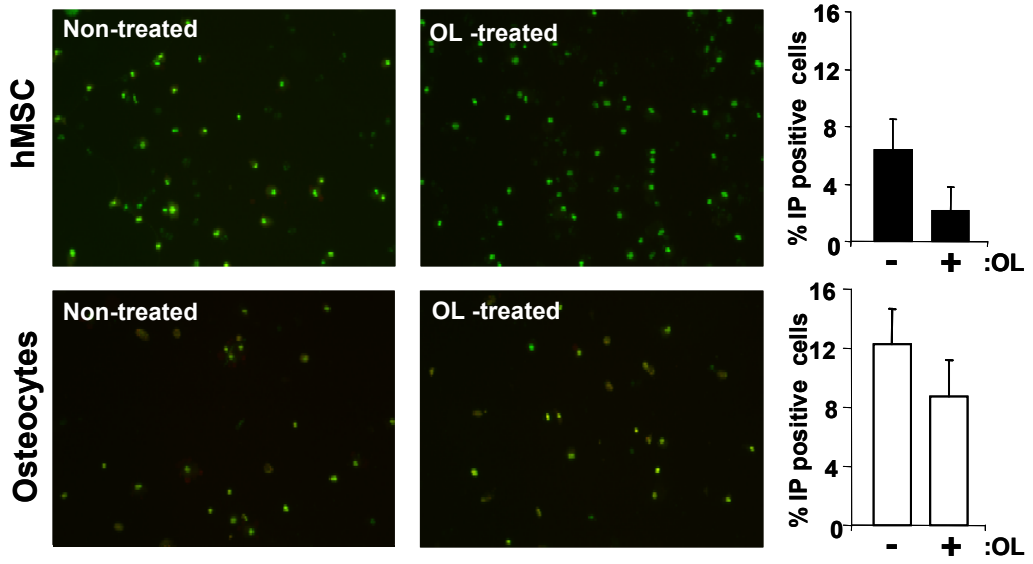

Figure S1. Oligomycin (OL) treatment has no effect on cell death in hMSCs and osteocytes. Cells were exposed to 6 μM OL or left untreated. Cells were double-stained with Hoechst 33342 (green) and propidium iodide (PI, red) and visualized using fluorescence microscopy at 20x magnification. The percentage of PI positive cells (dead cells) was determined by examination of 10 different fields taken at random. Histograms are the means ± S.E.M.

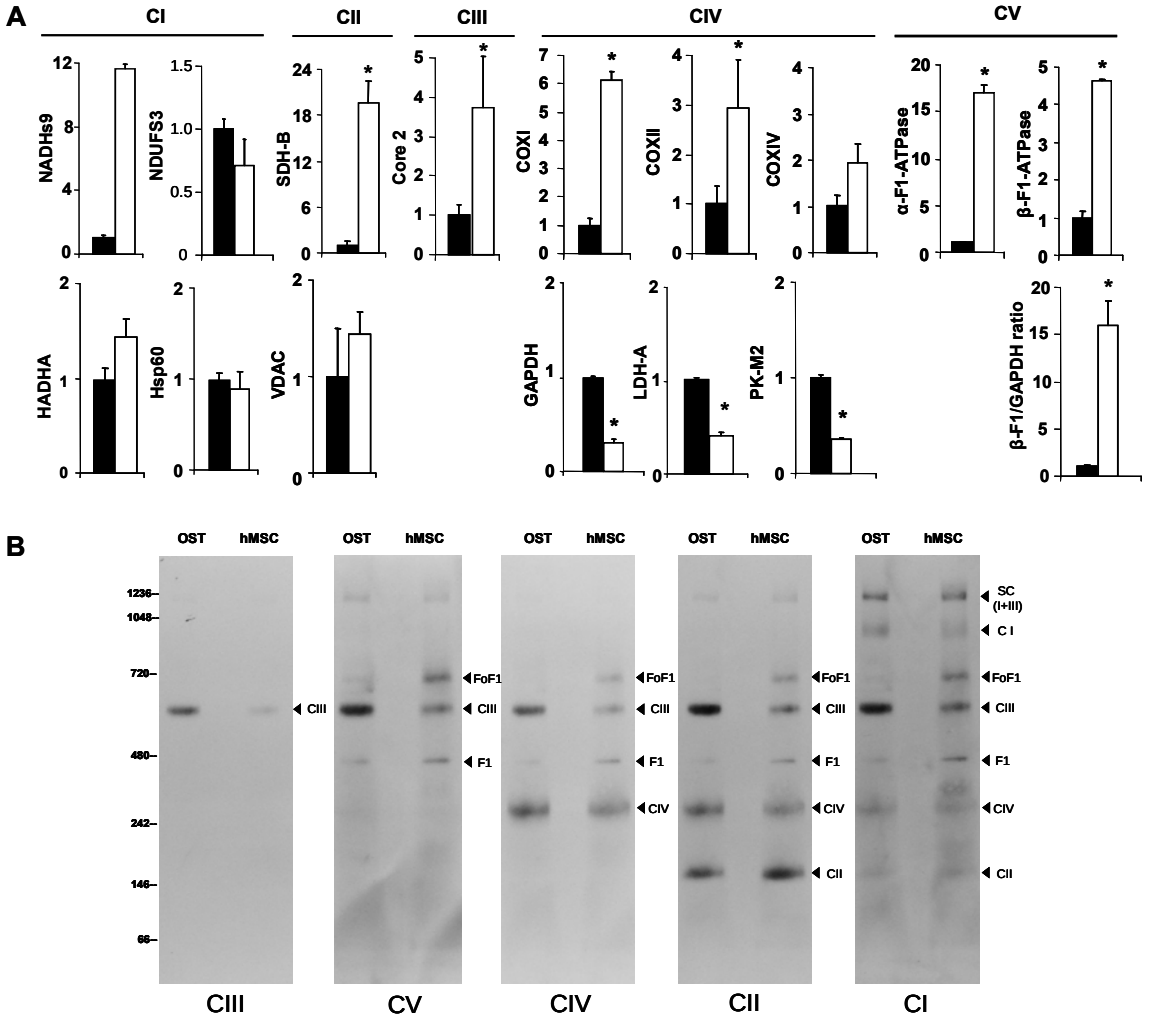

Figure S2. Differentiation of mitochondria upon osteogenic induction. A. Histograms show the quantification of the expression of mitochondrial (NADHs9, NDUFS3, SDH-B, Core 2, COXI, COXII, COXIV, α-F1-ATPase, β-F1-ATPase, HADHA, Hsp60 and VDAC) and glycolytic (GAPDH, LDH-A and PK-M2) enzymes in hMSCs (closed bars) and osteocytes (open bars) (for representative blots see Fig. 2A). The bioenergetic signature (β-F1/GAPDH ratio) in hMSCs and osteocytes is also shown. Data are expressed as fold change relative to the values in hMSCs. Bars represent the mean ± S.E.M. of four different preparations.*, $p<0.05$ when compared to hMSCs. **B.** Analysis of OXPHOS complexes by BN-PAGE in the presence of *n*-dodecyl β-D-maltoside from digitonin-enriched mitochondrial membranes from hMSC and osteocytes (OST). A representative experiment is shown. The membrane has been sequentially blotted with antibodies against complex III (CIII), complex V (F0F1), complex IV (CIV), complex II (CII) and complex I (CI). The migration of F1-ATPase (F1), supercomplex I+III (SC I+III) and of molecular mass markers (kDa) is also indicated.

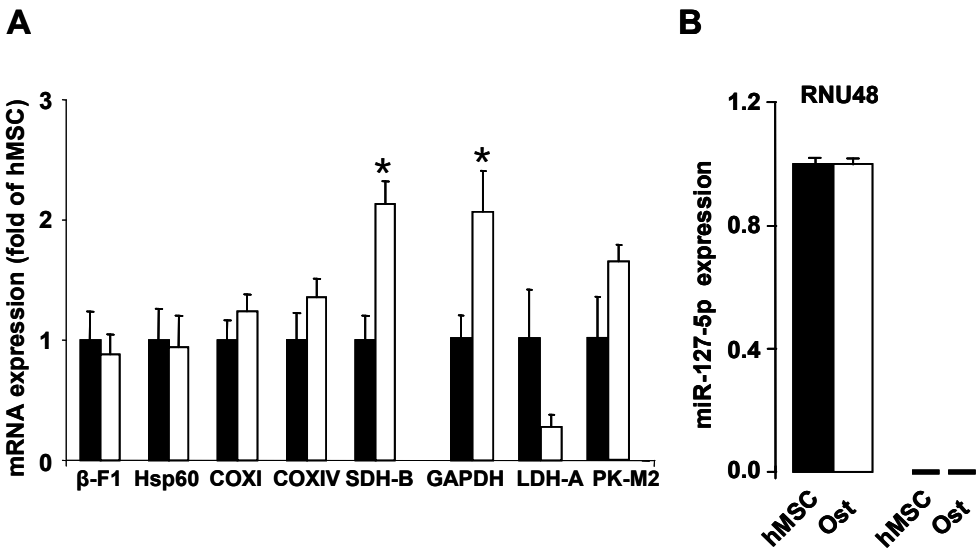

Figure S3. Post-transcriptional regulation of mitochondrial differentiation. Total RNA was extracted from hMSC (closed bars) and osteocytes (open bars). (**A**) Expression of representative mitochondrial (β-F1-ATPase, Hsp60, COXIV, COXI, and SDH-B) and glycolytic (GAPDH, LDH-A and PK-M2) mRNAs was assessed by RT-qPCR. Histograms show the mean ± S.E.M. of six different determinations. *, $p<0.05$ when compared to hMSCs. (**B**) Quantification of miR-127-5p by RT-qPCR in hMSCs and osteocytes. RNU48 values are shown to highlight the negligible expression of miR-127-5p in both undifferentiated and differentiated cells. Bars are the mean ± S.E.M. of 3 independent determinations.

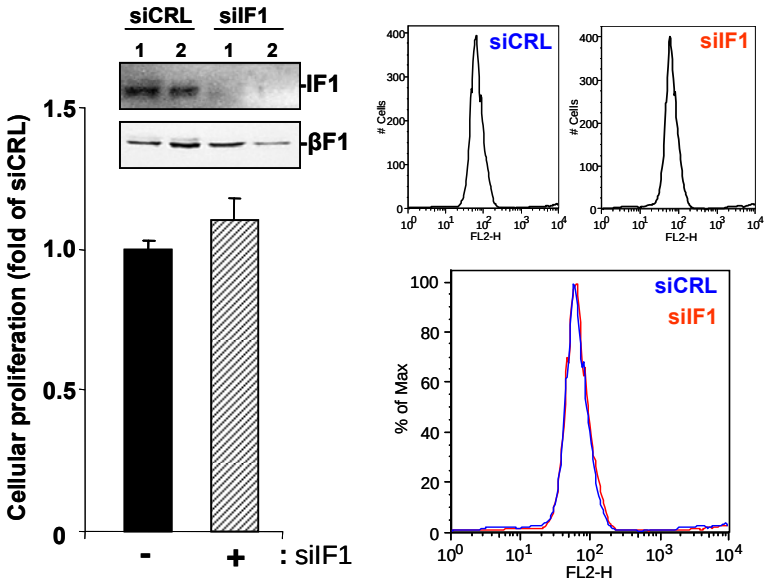

Figure S4. IF1 is not signaling cellular proliferation in hMSC. hMSCs were transfected with control (siCRL, closed bars) or siIF1 siRNA (siIF1, hatched bars) to regulate the expression of IF1. Cellular proliferation was assessed by the incorporation of EdU into cellular DNA. Blue (Control, siCRL) and red (siIF1) traces are shown. Bars are the mean ± S.E.M. of 6 independent determinations. Data are shown as fold change relative to the values in siCRL cells.

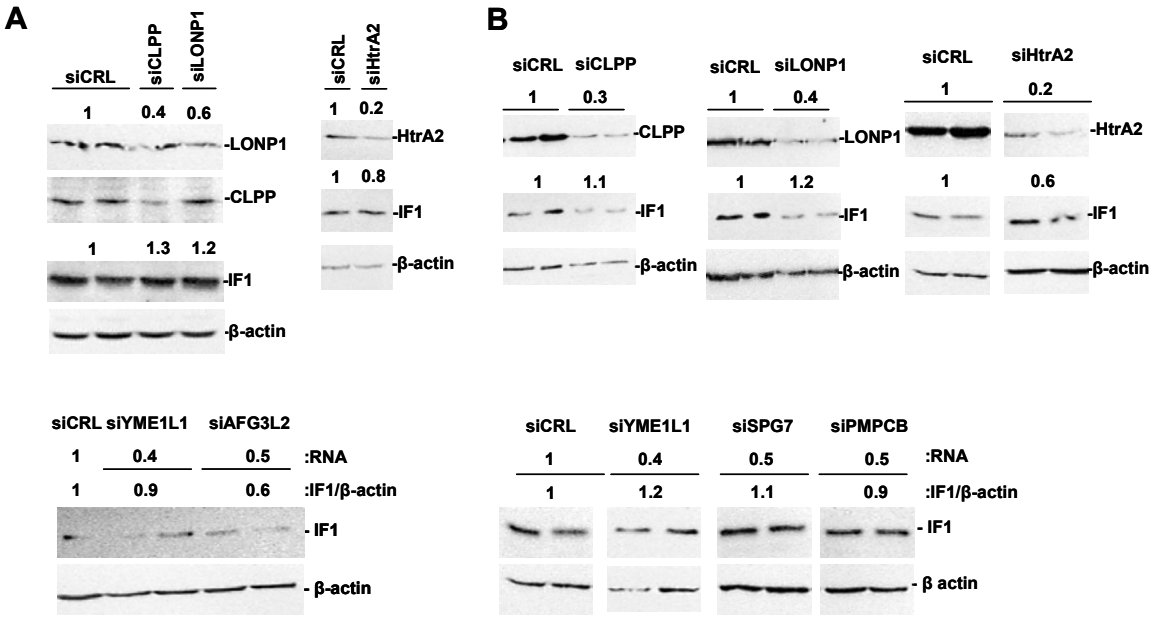

Figure S5. siRNA screening for the putative protease involved in the degradation of IF1. hMSCs **(A)** and HCT116 colon cancer cells **(B)** were transfected for 48 hours with 80-100 nM siCRL or with the specified siRNA for the following mitochondrial proteases: AFG3L2, CLPP, HtrA2, LONP1, PMPCB, SPG7 and YME1L1. Representative blots of IF1 and β-actin are shown. The calculated IF1/β-actin ratio is indicated on top of the blots. Silencing of CLPP, HtrA2 and LONP1 was verified by western blotting and the degree of silencing indicated on top of the blots. Silencing of AFG3L2, PMPCB, SPG7 and YME1L1 was verified by RT-qPCR and indicated.

Supporting Methods

Osteogenic induction and treatments. To induce osteogenic differentiation, hMSCs were incubated in the osteogenic media containing dexamethasone, ascorbate, Mesenchymal Cell Growth Supplement, L-glutamine, penicillin/streptomycin and β-glycerophosphate (Lonza). For inhibition of mitochondrial serine-proteases, hMSC and osteocytes were treated with 400μM of 4-(2-aminoethyl) benzenosulfonyl fluoride hydrochloride (AEBSF) for the indicated time.

Antibodies used: anti-CD44 (1:1,000) from Millipore; anti-β-F1-ATPase (1: 25,000) [1]; anti-IF1 (1:200) [2]; anti-PK-M2 (pyruvate kinase M2) (1:1000); anti-NADHs9 (NADH dehydrogenase subunit 9) (1:1,000); anti-GAPDH (1:20,000); anti-LDH-A (1:1,1000) [3]; anti-Hsp60 (Heat Shock Protein) (Stressgene SPA-807, 1:2,000); anti-SDH-B (succinate dehydrogenase subunit B) (1:500) and anti-COXIV (cytocrome c

oxidase subunit IV (1:250) from Invitrogen; anti-α-F1-ATPase (α-F1-ATPase) (1:1,000) from Molecular Probes; anti-osteopontin (1:1,000), anti-NDUFS3 of complex I (1:1,000), anti-Core 2 of complex III (1:500), anti-MTCO2 (cytocrome c oxidase subunit II) (1:500), anti-MTCO1 (cytocrome c oxidase subunit I) (1:100), anti-VDAC1 (porin) (1:500), anti-LONP1 antibody (1:250) and anti-CLPP (1:200) from Abcam; anti-Htra2/Omi (1:500) from Cell Signaling; anti-tubulin (1:5,000) and anti-β-actin (1:100,000) from Sigma. Peroxidase-conjugated anti-mouse and anti-rabbit IgGs (Nordic Immunonology, 1: 3,000) were used as secondary antibodies. The blots were developed using the ECL reagent. Quantification of the immunoreactive bands was accomplished using a Kodak DC120 Zoom digital camera and the Kodak 1D Image Analysis Software for Windows. The ratios β-F1-ATPase/Hsp60 and β-F1-ATPase/GAPDH were taken as respective indexes of the bioenergetic competence of the organelle (mitochondrial differentiation) and of the overall mitochondrial activity in the cell (that results from both mitochondrial proliferation and differentiation), and illustrate the two main pathways that restrain the bioenergetic activity of mitochondria in cancer cells [1, 4].

siRNA silencing. Transfections were performed using Lipofectamine and Plus Reagent (Invitrogen™). Suppression of IF1 (Qiagen S100908075) expression was exerted by small interfering RNA (siRNA). An inefficient siRNA sequence, Silencer® Select Negative Control #1 plasmid (Ambion/Applied Biosystems), was used as a control. Suppression of expression of mitocondrial proteases was exerted using the following Silencer Select siRNAs (Invitrogen): LONP1 (s17903), CLPP (s15686), HTRA2 (s653), AFG3L2 (s21516), SPG7 (s224671), PMPCB (s18239), YME1L1 (s21077). Silencer Negative Control siRNA #1 (AM4636) was used as control. Silencing was verified by western blotting (LONP1/CLPP/HTRA2) or by RT-qPCR (AFG3L2/SPG7/PMPCB/YME1L1). The forward (F) and reverse (R) primers used were: β-actin, F: 5'- CCAACCGCGAGAAGATGA-3', R: 5'-CCAGAGGCGTACAGGGATAG-3'; PMPCB, F: 5'-TGCCAGCTTGCTGTTTAATG-3', R: 5'-TTGCCTCTTTTATGGAAATGG-3'; YME1L1, F: 5'-CATGGTGGCAGGTGCTTAT-3', R: 5'-CTCCATCTCCCAGGCTCA-3'; SPG7, F: 5'-GTCCGGCTTCTCCAACAC-3', R: 5'-AGGGTAGCTGGTCAAGAGAGG-3'; AFG3L2, F: 5'-GAGGAAGAGGCAACTTTGGA-3', R: 5'AATGACGACATTTGTTGTTGTATTAAA-3'.

Immunohistochemistry. Formalin-fixed, paraffin-embedded normal and tumor 5 μm sections of human colon and prostate biopsies were used (Origene). Sections were deparaffined and the antigens retrieved by incubation in EDTA for 45 min at 155ºC. The monoclonal anti-IF1 (1:200) antibody was used as detailed [5]. Sections were counterstained with hematoxylin.

Immunofluorescence microscopy. For co-localization studies, deparaffinated normal human colon and prostate 5 μm tissue sections were used. The primary antibodies used were anti-CD44 (1:50) and anti-IF1 (1:50) [2]. Slides were incubated for 2h in the dark with anti-(rabbit) and anti-(mouse) IgGs conjugated to Alexa Fluor® 488 and 555, respectively. Cellular fluorescence was analyzed by confocal microscopy in a LSM510 META (Zeiss).

Gene expression analysis by RT-qPCR. Total RNA was extracted from cell cultures using TRIzol Reagent (Invitrogen) or RNAeasy Mini Kit (QIAgen). RNA was quantified with a Nanodrop ND-1000 spectrophotometer. RNA integrity was assessed with an Agilent 2100 Bioanalyzer. Reverse transcription (RT) reactions were performed using 1 μg of total RNA and the High Capacity Reverse Transcription Kit (Applied Biosystems) with random primers, following manufacturer's instructions. Real-time PCR was performed using Power Sybr Green PCR Master Mix with an ABIPRISM 7900HT instrument (Applied Biosystems). The expression level of indicated mRNAs was determined according to the ΔΔCt method using β-actin as internal control.

Assessment of cellular proliferation. The incorporation of 5-ethynyl-2´deoxy-uridine (EdU) into cellular DNA was determined using the Click-iT EdU Flow Cytometry Assay Kit (Molecular Probes) [5].

Cell death assays. Cells were harvested, washed with PBS and incubated in the dark for 5 min with Hoechst 33342 (1mg/mL) and propidium iodide (1mg/mL) solutions. After washing, samples were observed under a Leica DM-IRB fluorescence microscope (UV). The percentage of dead (red staining) cells was calculated from 10 different randomly selected fields for each condition assayed.

Blue native electrophoresis (BN)-PAGE. Enriched mitochondrial fractions were isolated from cell cultures using digitonin [6]. Protein extracts were solubilized in BN-loading buffer (1.5 M 6-aminocaproic acid, 50 mM Bis-Tris/HCl pH 7.0) in the presence of 2 μl PMSF/0.5 mM DMSO. *n*-dodecyl β-D-maltoside at the concentration of 3 g/g protein was added to the samples and incubated on ice for 10 min. Solubilized samples were centrifuged for 30 min at 30,000 rpm at 4ºC, and the supernatant was

combined with 2 µl of sample buffer (500 mM aminocaproic acid, 50 mM Bis-Tris/HCl pH 7.0, 0.5 mM EDTA, 5% Serva Blue G-250) prior to loading in 3-13% gradient gels [7].

Supporting References

1. Cuezva JM *et al* (2002) The bioenergetic signature of cancer: a marker of tumor progression. *Cancer Res* **62:** 6674-6681

2. Sanchez-Cenizo L, Formentini L, Aldea M, Ortega AD, Garcia-Huerta P, Sanchez-Arago M, Cuezva JM (2010) Up-regulation of the ATPase inhibitory factor 1 (IF1) of the mitochondrial H+-ATP synthase in human tumors mediates the metabolic shift of cancer cells to a Warburg phenotype. *J Biol Chem* **285:** 25308-25313

3. Acebo P *et al* (2009) Cancer abolishes the tissue type-specific differences in the phenotype of energetic metabolism. *Transl Oncol* **2:** 138-145

4. Cuezva JM, Ortega AD, Willers I, Sanchez-Cenizo L, Aldea M, Sanchez-Arago M (2009) The tumor suppressor function of mitochondria: translation into the clinics. *Biochim Biophys Acta* **1792:** 1145-1158

5. Formentini L, Sánchez-Aragó M, Sánchez-Cenizo L, Cuezva JM (2012) The mitochondrial ATPase Inhibitory Factor 1 (IF1) triggers a ROS-mediated retrograde pro-survival and proliferative response. *Mol Cell* **45:** 731-742

6. Calvaruso MA, Smeitink J, Nijtmans L (2008) Electrophoresis techniques to investigate defects in oxidative phosphorylation. *Methods* **46:** 281-287

7. Schägger H (2003) Membrane Protein Purification and Crystallization: A Practical Guide. Elsevier Science, USA.

Artículo #5

Santacatterina, F., Chamorro, M., de Arenas, C.N., Navarro, C., Martín, M.A., Cuezva, J.M., Sánchez-Aragó, M. (2015). Quantitative analysis of proteins of metabolism by reverse phase protein microarrays identifies potential biomarkers of rare neuromuscular diseases. *J Transl Med.* 18;13:65.

Santacatterina et al. Journal of Translational Medicine (2015) 13:65
DOI 10.1186/s12967-015-0424-1

JOURNAL OF TRANSLATIONAL MEDICINE

RESEARCH Open Access

Quantitative analysis of proteins of metabolism by reverse phase protein microarrays identifies potential biomarkers of rare neuromuscular diseases

Fulvio Santacatterina[1,2,3], Margarita Chamorro[1,2,3], Cristina Núñez de Arenas[1,2,3], Carmen Navarro[4], Miguel A Martín[2,3,5], José M Cuezva[1,2,3*] and María Sánchez-Aragó[1,2,3*]

Abstract

Background: Muscle diseases have been associated with changes in the expression of proteins involved in energy metabolism. To this aim we have developed a number of monoclonal antibodies against proteins of energy metabolism.

Methods: Herein, we have used Reverse Phase Protein Microarrays (RPMA), a high throughput technique, to investigate quantitative changes in protein expression with the aim of identifying potential biomarkers in rare neuromuscular diseases. A cohort of 73 muscle biopsies that included samples from patients diagnosed of Duchenne (DMD), Becker (BMD), symptomatic forms of DMD and BMD in female carriers (Xp21 Carriers), Limb Girdle Muscular Dystrophy Type 2C (LGMD2C), neuronal ceroid lipofuscinosis (NCL), glycogenosis type V (Mc Ardle disease), isolated mitochondrial complex I deficiency, intensive care unit myopathy and control donors were investigated. The nineteen proteins of energy metabolism studied included members of the mitochondrial oxidation of pyruvate, the tricarboxylic acid cycle, β-oxidation of fatty acids, electron transport and oxidative phosphorylation, glycogen metabolism, glycolysis and oxidative stress using highly specific antibodies.

Results: The results indicate that the phenotype of energy metabolism offers potential biomarkers that could be implemented to refine the understanding of the biological principles of rare diseases and, eventually, the management of these patients.

Conclusions: We suggest that some biomarkers of energy metabolism could be translated into the clinics to contribute to the improvement of the clinical handling of patients affected by rare diseases.

Keywords: Energy metabolism, Mitochondria, Biomarkers, Neuromuscular diseases, Rare diseases

Background

Genetic alterations that result in cellular dysfunction are usually accompanied by changes in the expression of proteins of energy metabolism. A good example in this regard is provided by the chromosomal abnormalities and multiple genetic mutations that promote cancer and that converge in the reprogramming of energy metabolism [1,2]. In fact, energy metabolism provides a valuable tool as biomarker of disease progression [3,4] and of the eventual response to therapy [5,6]. Most rare diseases have no cure and the living with the disease until the patient becomes diagnose, if at all, is a heavy burden for the patient and for their families. Hence, there is an urgent need to identify biomarkers that could aid in the diagnosis and/or follow up of these patients in order to increase the understanding of disease processes that could be further translated into potential therapeutic interventions.

Reverse Phase Protein Microarrays (RPMA) is a high-throughput technique that allows the quantification of a

* Correspondence: jmcuezva@cbm.csic.es; msanchez@cbm.csic.es
[1]Departamento de Biología Molecular, Centro de Biología Molecular, c/ Nicolás Cabrera 1, Universidad Autónoma de Madrid, 28049 Madrid, Spain
Full list of author information is available at the end of the article

given protein in minute amounts of sample from biological specimens [7,8]. The application of this technology allows the identification of new markers of diagnosis, the establishment of correlations between protein markers and the severity and progression of the disease and, eventually, of the response to a given treatment [7,8]. However, a bottle-neck in the application and development of RPMA is the availability of high-affinity and specific monoclonal antibodies that could be used in the unambiguous characterization of a particular phenotype, either because the antibodies have not been developed or they lack the required specificity [9,10]. As part of an ambitious project aimed at translating the "signature" of energy metabolism to bed-side application, we are producing specific monoclonal antibodies against enzymes of glycolysis and mitochondrial oxidative phosphorylation [11-13] to be applied in RPMA or any other technique, with the aim of facilitating patient management affected with different pathologies [4].

In the present investigation, we have produced additional antibodies against proteins of energy metabolism and applied RPMA technology to quantify and study the putative relevance of nineteen of these proteins as potential biomarkers in a cohort of seventy three muscle biopsies including control donors and patients affected of rare neuromuscular diseases such as Duchenne (DMD) and Becker (BMD) dystrophies, symptomatic forms of DMD and BMD in female carriers (Xp21 Carriers), Limb Girdle Muscular Dystrophy Type 2C (LGMD2C), neuronal ceroid lipofuscinosis (NCL), glycogen storage disease type V (Mc Ardle disease), isolated deficiency of mitochondrial respiratory chain complex I and intensive care unit myopathy. The results obtained indicate that enzymes of energy metabolism might offer relevant biomarkers that could aid the understanding of the biology of rare neuromuscular diseases and, eventually, the management of these patients.

Methods

Patients and protein extraction

A cohort of deltoid and quadriceps muscle biopsies of control donors (n = 20) and patients affected of neuromuscular diseases including Duchenne (DMD, n = 6), Becker (BMD, n = 6), symptomatic forms of DMD and BMD in female carriers (Xp21 Carriers, n = 4), Limb Girdle Muscular Dystrophy Type 2C (LGMD2C, n = 6), glycogenosis type V (McArdle disease, n = 7), deficit of mitochondrial Complex I (n = 12), neuronal ceroid lipofuscinosis (NCL, n = 6) and intensive care unit myopathy (n = 6) were processed. Frozen tissue sections obtained from surgical specimens were provided from Instituto de Investigación Biomédica de Vigo, Vigo and from Instituto de Investigación Hospital 12 de Octubre, Madrid, Spain. Routine histopathological study and appropriate molecular and clinical diagnosis of all the cases studied had been previously performed. The samples were obtained with informed consent following the Declaration of Helsinki and coded for anonymity to protect patient confidentiality. The Institutional Review Board approved the project. For protein extraction, the samples were homogenized in T-PER Tissue Protein Extraction Reagent (ThermoScientific, Inc. Madrid, Spain) containing protease inhibitors (protease Cocktail Tablets; Life Sciences, Madrid, Spain) in a 1:5 (w/v) ratio, and further freeze–thawed three times in liquid nitrogen [4]. The protein concentration was determined with the Bradford reagent (Bio-Rad, Inc. Madrid, Spain) using BSA as standard.

Cloning strategies, protein expression and purification

To obtain the recombinant proteins to be used for antibody production the cDNAs encoding human lactate dehydrogenase A (LDH-A; NP_005566), NADH-ubiquinone oxidoreductase α-subunit 9 (NADH-sub9; NM_005002), aconitase I (ACO1; NM_002197), glycerol-3-phosphate dehydrogenase 1 (GPD1; NM_005276) and citrate synthase (CS; NM_004077) were amplified by polymerase chain reaction as previously described [11]. The sequences of the forward (F) and reverse (R) primers used were as follows: LDH-A (F: 5′-GAGCTCATGGCAACTCTAAAGGATCA GC-3′; R: 5′- GCGGCCGCAAATTGCAGCTCCTTTTG GAT - 3′); NADH-sub9 (F: 5′-CGGGAGCTCATGGCGG CTGCCG-3′; R: 5′-ATAGTTTAGCGGCCGCTGAATGT TGACGGTCTTG-3′); ACO1 (F: 5′-GAGCTCATGCGTG TCATCCTGCAGGACTTT - 3′; R: 5′ GCGGCCGCGAT GGTTCCAGCAATTGCAT - 3′); GPD1 (F: 5′ CGGGAG CTCATGGCTAGCAAGAAAGTCT - 3′; R: 5′- ATAGTT TAGCGGCCGCCACATATGTTCTGGATGATT - 3′); and CS (F: 5' CGGAAGCTTATGGCTTTACTTACTG CG-3'; R: 5'-ATAGTTTACACGTGACCCACCCTGAC TTAGA-3'). Amplicons were first cloned into pGEM-T easy vector (Promega, Madison, WI) and after into pQE-Trisystem (for details see [11]). The resulting plasmids, pQE-LDH-A, pQE-NADH-sub9, pQE-ACO1, pQE-GPD1 and pQE-CS were used to transform Escherichia coli M15/pREP4 cells. It should be noted that pQE-ACO1 expresses a truncated version of ACO1. After induction of protein expression by adding IPTG (1 mM), the cells were resuspended in buffer A containing 100 mM NaH_2PO_4, 300 mM NaCl, pH 8.0 supplemented with lysozyme 1 mg/ml. The expressed proteins were purified using either Strep-Tactin or metal ion affinity chromatography Ni-NTA superflow resins (Qiagen, Hilden, Germany). The purity of the proteins was estimated by fractionation on SDS-PAGE (Additional file 1: Figure S1).

Antibody production

BALB/c mice were immunized by intraperitoneal injection with various dosages of the purified proteins (20 μg). Serum was obtained from mice and tested for reactivity

against the recombinant and native proteins by western blotting (Additional file 1: Figure S1). When a titer higher than 1000 was attained, hybridomas were produced by fusing spleen cells with myeloma SP2 or NS-1 cells with polyethylene glycol in HAT-RPMI 1640 medium according to standard hybridoma techniques [11-13]. Supernatants of the hybridomas were screened by indirect ELISA on polystyrene plates coated with the recombinant proteins (0–150 ng per well). Bound antibodies were detected using horseradish peroxidase–labeled goat antimouse antibodies (1:1000) (DAKO, Carpinteria, CA). After the final washing, 100 μl of OPD solution (Sigma, St. Louis, MO) was added, and the color reaction was developed for 15 minutes and stopped by the addition of 18 M H_2SO_4. Optical density at 490 nm was determined in a FluoStar Optima (BMG Labtech, Offenburg, Germany) apparatus. The positive colonies were cloned by limiting dilution. Mouse monoclonal antibodies were purified with Montage antibody purification kit (Millipore, Billerica, MA) according to the supplier's instructions. Highly specific monoclonal antibodies against NADHs9 15/22-5, Aco-I 13/18-1, GPD1 P5A1-1 and LDHA 4D3-A1 were obtained (Additional file 1: Figure S1). Specific polyclonal mouse antibodies against citrate synthase were used in the study (Additional file 1: Figure S1) because we failed in obtaining reliable hybridomas for this protein.

Printing and processing of reverse phase protein microarrays

Samples from patient biopsies were diluted in PBS (137 mM NaCl, 2.7 mM KCl, 10 mM Na2HPO4 and 1.8 mM KH2PO4 pH 7.4) to a final protein concentration of 1 μg/μl before printing. Serially diluted protein extracts (0–1 μg/μl) derived from HCT116 colocarcinoma cells were also prepared to asses printing quality and the linear response of protein recognition by the antibodies used. A solution of BSA (1 μg/μl) was also prepared for printing as internal negative control. Approximately, 1 nl volume of each sample was spotted in quadruplicate onto nitrocellulose-coated glass slides (FAST Slides, Schleicher & Schuell BioScience, Inc. Dassel, Germany) using a BioOdyssey Calligrapher MiniArrayer printer (Bio-Rad Laboratories, Inc., Madrid, Spain) equipped with a solid pin (MCP310S) at constant humidity of 45% and 10°C and 16°C for the plate and chamber, respectively. After printing, arrays were allowed to dry at room temperature for 16 hours and further blocked in PBS-T containing 5% skimmed milk. After, the arrays were incubated overnight at 4°C with the indicated concentrations of the following highly specific primary monoclonal antibodies (mAbs): anti-β-F1-ATPase (1:150), anti-Hsp60 (1:150), anti-GAPDH (1:250) and anti-PK (1:150) from [4], anti-IF1 (1:50) from [12], anti-α-F1-ATPase (1:250), anti-COXI (1:85) and anti-COXIV (1:50) from Molecular Probes (Madrid, Spain), anti-PDH (1:50) and anti-SDH (1:50) from Invitrogen (Madrid, Spain), anti-SOD2 (1:100), anti-PYGM (1:200), anti-β-actin (1:1000) from Sigma (Madrid, Spain), and the additional home-made anti-NADHs9 (1:1000), anti-LDH-A (1:2,500), anti-ACO1 (1:250) and anti-GPD1 (1:1000). The polyclonal mouse anti-CS (1:500) and rabbit anti-CPT1M (1:25) from Santa Cruz (Heidelberg, Germany) and anti-HADHA (1:1000) from Abcam (Cambridge, UK) were also used. Each array was incubated with each antibody independently. After incubation the arrays were washed with PBS-T and further incubated with a donkey anti-mouse or donkey anti-rabbit secondary antibody conjugated with alexa-488 (Invitrogen, Madrid, Spain). Microarrays were scanned using a Typhoon 9410 scanner (GE Healthcare, Inc. Madrid, Spain). The mean fluorescent intensity of the spots was quantified using FIJI software (N.I.H., USA) and converted into arbitrary units of expressed protein/ng of total protein in the tissue extract using the expression obtained in the linear plot of the HCT116 cell line as standard. The technical variance of the arrays calculated by the squared coefficient of variation (SCV $= \sigma^*100/ |x|$) was 8.6 ± 0.6.

Statistical analysis

Distribution of molecular markers was studied by using a two-tailed Student's *t* test. Analysis of variance (ANOVA) with post hoc Dunnett's test used for multiple comparisons to the control and analysis of variation in samples with box plot diagrams were performed using the PASW statistics 18 software package. For the expression profiles of metabolic markers data were reformatted by calculating the log(2) of the expression level in each sample relative to the mean expression level in normal samples. We used the Cluster Program from "Expression Profiler Clustering home page" at http://ep.ebi.ac.uk/EP/EPCLUST using the Euclidean distances and average linkage method (Weighted Group Average, WPGMA). The results shown are means ± S.E.M. A $p < 0.05$ was considered statistically significant.

Results

Validation of the antibodies used for RPMA

High affinity and specific monoclonal antibodies against proteins of energy metabolism are the rate-limiting tools required for the successful application of RPMA technology [14]. The metabolic pathways interrogated in this study included the degradation of glycogen (PYGM), glycolysis (GAPDH, PK, LDHA), the shuttling of cytosolic electrons to mitochondria (GPD1), mitochondrial decarboxylation of pyruvate (PDH), the mitochondrial import and oxidation of fatty acids (CPT1, HADHA), the Krebs cycle (CS), the electron transport chain (NADHs9,

SDHB, COX1), the ATP synthase as engine of oxidative phosphorylation (αF1, βF1, IF1), cytosolic (ACO1) and mitochondrial (SOD2) markers of oxidative stress. In addition, cellular (β-actin) and mitochondrial (Hsp60) structural markers were included to normalize changes in protein expression. The selection of target proteins was mostly based on the facts that they are abundant proteins in core pathways of energy provision. Hence, a first step of this study was to validate the specificity of the antibodies to be used in RPMA by western blotting using human muscle extracts (Figure 1). Both the antibodies commercially available or made in the lab were tested [11,12] (and see Additional file 1: Figure S1). The antibodies used in this study recognized one single protein band of the expected molecular weight in human muscle samples (Figure 1), validating their utilization for the purpose of quantification protein expression in RPMA techniques.

Protein expression in human muscle biopsies

A representative protein microarray illustrating the printing protocol of human muscle biopsies developed with antibodies against the glycolytic LDH-A is shown in Figure 2A. Arrays developed with other antibodies are shown below (Figure 2A). Protein extracts from muscle biopsies of control (green boxed in Figure 2A) and different neuromuscular diseases (red boxed in Figure 2A) were prepared and spotted onto RPMA in quadruplicate from left to right (Figure 2A). Increasing amounts of BSA (black boxed in Figure 2A) were spotted in the array as a control of the background of the assay. The arrays also contained increasing protein amounts of cellular extracts derived from HCT116 cells (blue boxed in Figure 2A). The HCT116 extracts revealed a linear increase in fluorescent intensity as the amount of protein increased in the spot (Figure 2B), providing the standard curve of the assay (see also Additional file 2: Figure S2).

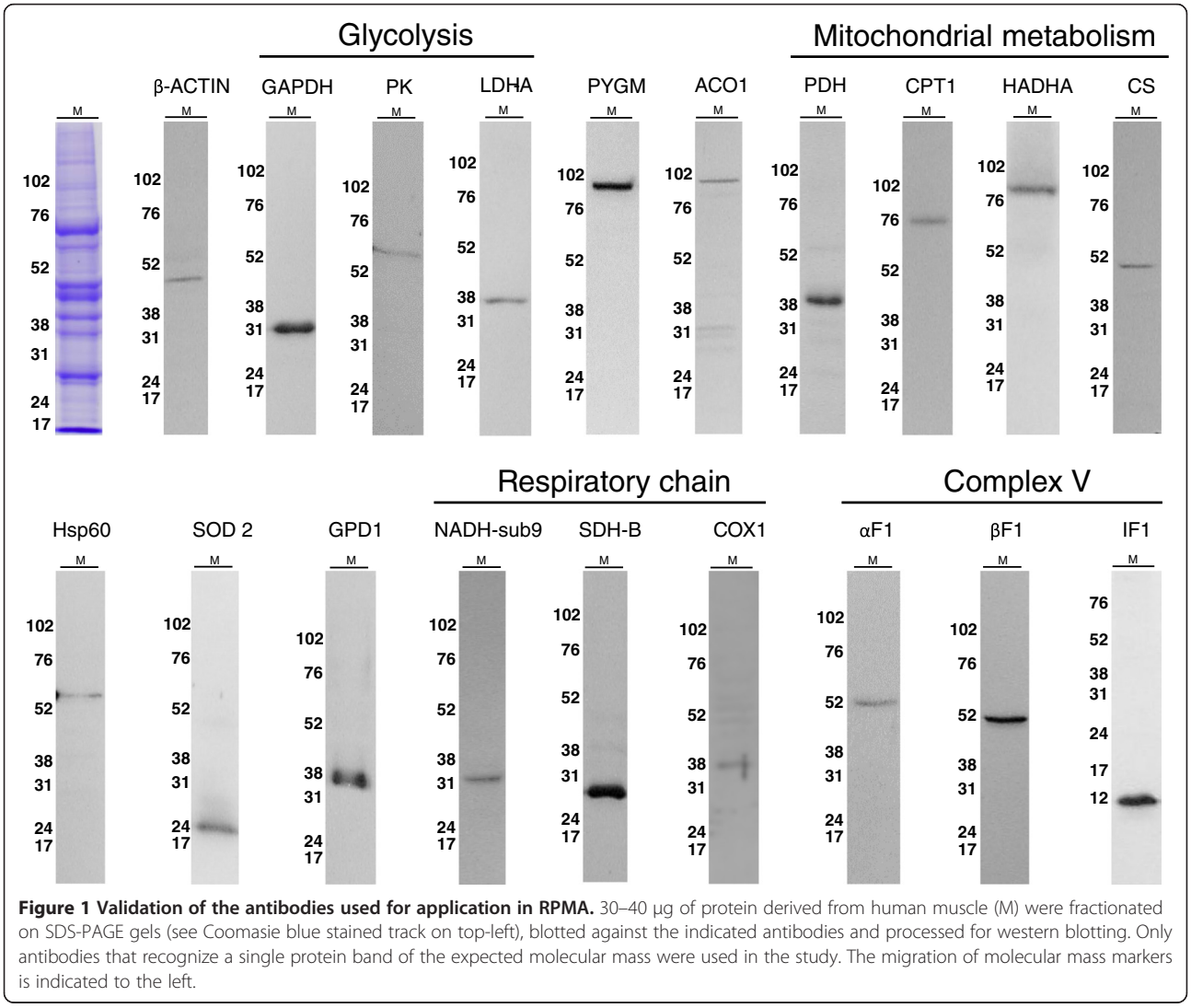

Figure 1 Validation of the antibodies used for application in RPMA. 30–40 μg of protein derived from human muscle (M) were fractionated on SDS-PAGE gels (see Coomasie blue stained track on top-left), blotted against the indicated antibodies and processed for western blotting. Only antibodies that recognize a single protein band of the expected molecular mass were used in the study. The migration of molecular mass markers is indicated to the left.

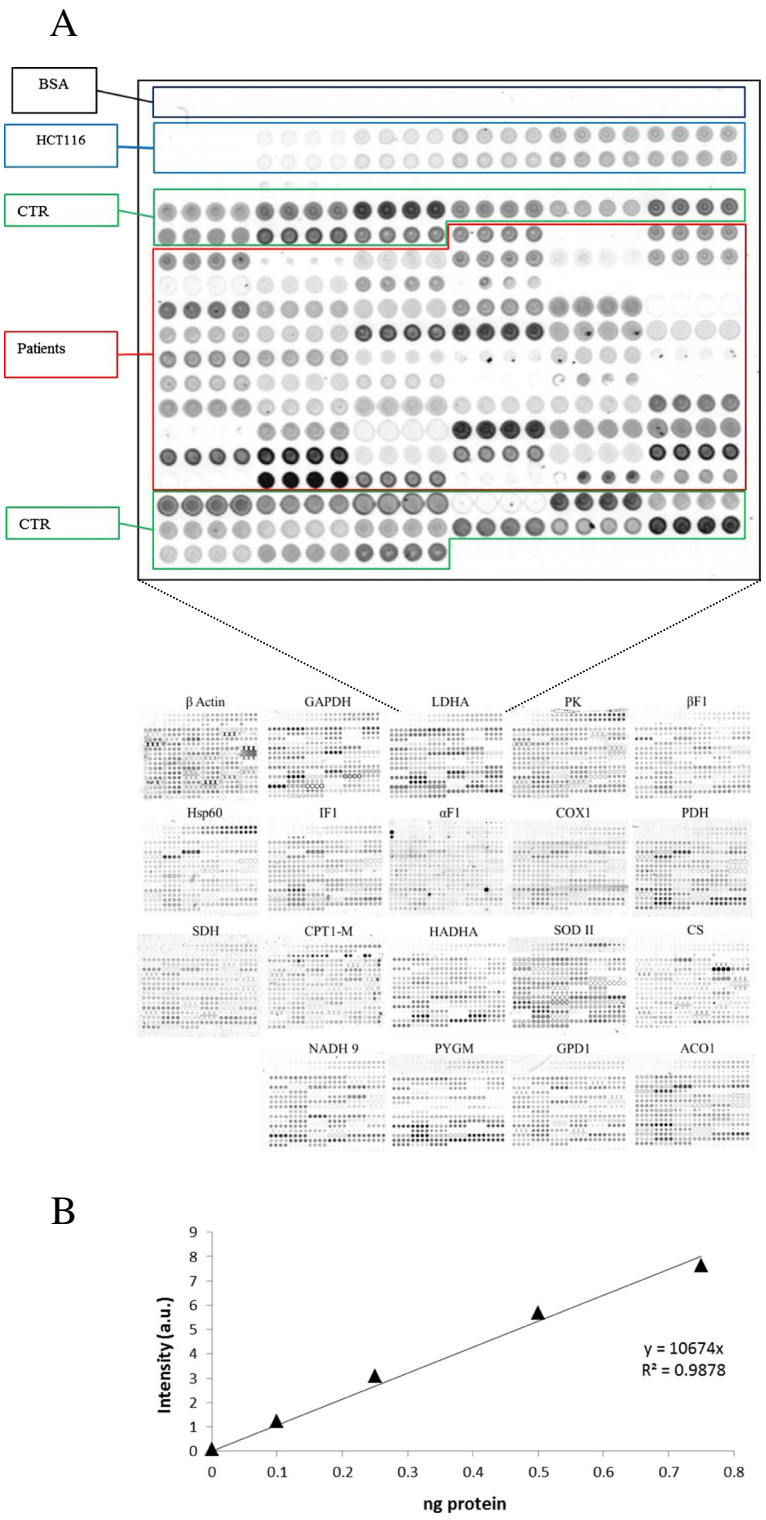

Figure 2 Printing of RPMA. A, Scheme of RPMA printing processed for anti-LDH-A is shown magnified. One nl samples were spotted in quadruplicate. Black boxed: negative controls of BSA; Blue boxed: standard curves of HCT116 cells; Green boxed: tissue samples from control donors; Red boxed: tissue samples from patients. Below are shown representative RPMAs processed with other antibodies. **B**, The plot illustrates the linear correlation that exists between the fluorescence intensity (arbitrary units, a.u.) and the amount of LDH-A protein in HCT116 cell lysates. Protein concentrations in the biopsies were calculated according to the fluorescence intensity obtained in the linear plot of HCT116 cells. For other details see Additional file 2: Figure S2.

The arrays illustrated the specific recognition of the corresponding antigen in minute amounts of printed protein of HCT116 extracts as well as in the biopsies (Figure 2A). As expected, no fluorescent signal was observed in BSA containing spots (Figure 2A), which provides the background of the technique by non-specific absorption of labeled antibodies to the proteins spotted. The quantification of the expression of each marker in control (n =20) and patient (n =53) biopsies was calculated by interpolating the fluorescent intensity signal obtained in the sample in the linear plot of HCT116 cells (Figure 2A and Additional file 2: Figure S2) and expressed as fold of control. Array duplicates show that the results obtained are highly reproducible validating the robustness of the technique for quantitative purposes (see Additional file 3: Figure S3).

The analysis of protein expression comparing patient's samples to their respective controls taking into consideration the muscle type of origin (deltoid or quadriceps; see printing scheme of the arrays on Figure 2) provided no significant differences. Hence, and for the sake of simplicity, we decided to present the data of controls all together (Table 1). The results in Table 1 and Additional file 4: Figure S4 summarizes the expression of nineteen proteins involved in different cellular activities and of the ratios derived from them, in different myopathies

Table 1 Relative expression of proteins of energy metabolism in muscle biopsies of neuromuscular diseases

		Rare Diseases							
		Metabolic		Muscular Dystrophies				Neurodegenerative	Intesive-Care Unit myopathy
	Controls	Mitochondrial Complex I	Glycogenosis type V	DMD	BMD	C. Xp21	LGMD 2C	NCL	ICU
Mitochondrial Markers									
PDH E1α	1.0 ± 0.1	1.3 ± 0.1	0.6 ± 0.1	1.3 ± 0.2	1.3 ± 0.4	0.7 ± 0.1	0.8 ± 0.1	0.7 ± 0.1	0.6 ± 0.1
SDH	1.0 ± 0.1	1.4 ± 0.1 **	0.9 ± 0.1	1.4 ± 0.2 *	1.1 ± 0.2	0.9 ± 0.2	0.6 ± 0.1 *	1.0 ± 0.2	0.8 ± 0.1
CS	1.0 ± 0.1	1.5 ± 0.2 *	0.8 ± 0.1	1.1 ± 0.3	0.8 ± 0.1	1.4 ± 0.4	0.5 ± 0.2	1.1 ± 0.3	1.2 ± 0.1
Hsp60	1.0 ± 0.1	1.3 ± 0.1	0.8 ± 0.1	1.7 ± 0.2 **	1.2 ± 0.2	0.9 ± 0.2	1.3 ± 0.3	0.9 ± 0.2	0.8 ± 0.1
CPT1-M	1.0 ± 0.1	0.9 ± 0.1	1.0 ± 0.1	1.2 ± 0.2	0.7 ± 0.0 *	0.9 ± 0.0	0.7 ± 0.2	1.0 ± 0.1	1.0 ± 0.1
HADHA	1.0 ± 0.1	1.6 ± 0.2 *	1.1 ± 0.2	0.7 ± 0.1	0.7 ± 0.1	0.8 ± 0.2	0.8 ± 0.3	1.1 ± 0.2	1.4 ± 0.2
NADH-9	1.0 ± 0.1	1.8 ± 0.2 **	1.2 ± 0.1	0.9 ± 0.1	0.9 ± 0.2	1.0 ± 0.2	0.6 ± 0.2	1.0 ± 0.1	1.2 ± 0.2
COX-1	1.0 ± 0.1	1.2 ± 0.1	0.6 ± 0.1 *	1.5 ± 0.1 *	1.3 ± 0.3	0.9 ± 0.1	0.9 ± 0.2	0.8 ± 0.1	0.7 ± 0.1
α-F1	1.0 ± 0.1	1.1 ± 0.1	0.7 ± 0.2	1.4 ± 0.1 *	1.3 ± 0.5	0.8 ± 0.1	1.0 ± 0.2	1.1 ± 0.2	0.7 ± 0.1
β-F1	1.0 ± 0.1	1.3 ± 0.1 *	0.9 ± 0.1	1.2 ± 0.2	1.2 ± 0.1	1.2 ± 0.3	0.8 ± 0.1	0.8 ± 0.1	1.0 ± 0.1
IF1	1.0 ± 0.1	1.0 ± 0.1	0.7 ± 0.1	1.1 ± 0.2	1.1 ± 0.2	0.7 ± 0.1	0.8 ± 0.2	0.7 ± 0.1 *	0.6 ± 0.1 *
SOD2	1.0 ± 0.1	0.8 ± 0.1	1.0 ± 0.1	0.5 ± 0.1 *	0.5 ± 0.1 *	0.7 ± 0.2	0.8 ± 0.3	0.8 ± 0.1	1.0 ± 0.1
Cytoplasmic Markers									
β-Actin	1.0 ± 0.1	1.1 ± 0.1	1.3 ± 0.2	1.0 ± 0.1	1.1 ± 0.3	1.0 ± 0.1	0.8 ± 0.2	1.1 ± 0.1	1.2 ± 0.2
GAPDH	1.0 ± 0.1	0.6 ± 0.1 *	0.8 ± 0.1	0.4 ± 0.1 *	0.9 ± 0.3	0.6 ± 0.1	0.3 ± 0.1 *	0.6 ± 0.1	0.5 ± 0.1 *
PK	1.0 ± 0.1	1.0 ± 0.1	0.8 ± 0.1	0.8 ± 0.2	1.0 ± 0.2	0.8 ± 0.0	0.7 ± 0.1	0.6 ± 0.1 *	0.7 ± 0.1 *
LDH-A	1.0 ± 0.1	0.7 ± 0.1	0.6 ± 0.2	0.4 ± 0.1 *	0.6 ± 0.2	0.5 ± 0.0	0.3 ± 0.0 *	0.4 ± 0.1 *	0.4 ± 0.1 *
GPD1	1.0 ± 0.1	1.1 ± 0.1	0.9 ± 0.1	0.4 ± 0.1 **	0.7 ± 0.2	0.6 ± 0.1 *	0.6 ± 0.2 *	0.5 ± 0.1 *	0.7 ± 0.1
PYGM	1.0 ± 0.1	1.5 ± 0.2 *	0.0 ± 0.0 **	0.2 ± 0.1 **	0.7 ± 0.3	0.7 ± 0.1	0.5 ± 0.1 *	0.5 ± 0.1 *	0.4 ± 0.1 **
ACO1	1.0 ± 0.1	1.1 ± 0.1	0.9 ± 0.1	0.8 ± 0.1	1.1 ± 0.3	0.9 ± 0.2	0.7 ± 0.2	1.0 ± 0.1	0.7 ± 0.1
Ratios									
β-F1/GAPDH	1.0 ± 0.1	2.5 ± 0.3 **	1.1 ± 0.2	3.1 ± 0.8 **	2.2 ± 1.0 *	1.6 ± 0.4	2.9 ± 0.6 **	1.3 ± 0.3	1.7 ± 0.3 *
BEC Index	1.0 ± 0.1	2.1 ± 0.2 **	1.4 ± 0.2	1.6 ± 0.3 *	1.8 ± 0.5 *	1.9 ± 0.2 *	2.5 ± 0.5 **	1.9 ± 0.5 *	2.5 ± 0.5 **
β-F1/LDH-A	1.0 ± 0.1	2.2 ± 0.3 **	1.8 ± 0.5 *	3.5 ± 0.6 **	2.7 ± 0.8 **	1.9 ± 0.4 *	2.5 ± 0.5 **	1.8 ± 0.3 **	3.2 ± 0.7 **

The table summarizes the expression of nineteen proteins involved in different mitochondrial and cytoplasmic activities of metabolism and of the ratios derived from them in different muscle myopathies when compared to controls. Values are expressed as fold of control. The results shown are the mean values ± S.E.M. *, $p < 0.05$ and **, $p < 0.001$ when compared to controls.

when compared to controls. The box plot in Additional file 4: Figure S4 illustrate the individual variation of the expression of the markers in each group of the pathologies studied as well as the outliers. In general, only Complex I deficient patients and patients affected of Duchenne muscular dystrophy showed a significant increase in several mitochondrial markers involved in energy metabolism when compared to controls (Table 1 and Additional file 4: Figure S4). Paradoxically, NADH-dehydrogenase subunit 9 expression was significantly increased in Complex I deficient patients (Table 1 and Additional file 4: Figure S4). A significant reduction in SOD2 expression was also noted in Duchenne and Becker muscular dystrophies (Table 1 and Additional file 4: Figure S4). Similarly, expression of the inhibitor of the mitochondrial H^+-ATP synthase, IF1, was also significantly diminished in patients affected of intense care unit and NCL myopathies (Table 1 and Additional file 4: Figure S4). This finding is consistent with the recent observation that inhibition of IF1 ameliorates severe mitochondrial respiratory chain dysfunctions [15]. In general, mitochondrial markers showed slight variations when compared to controls in glycogenosis type V, Becker and symptomatic forms of DMD and BMD in female carrier muscular dystrophies, patients affected of intensive care unit myopathy and NCL (Table 1 and Additional file 4: Figure S4).

However, Complex I deficient patients and patients affected of Duchenne Muscular Dystrophy, Limb Girdle Muscular Dystrophy Type 2C (LGMD2C), Neuronal Ceroid Lipofuscinosis and patients affected of intensive care unit myopathy provided significant differences in the expression of several of the cytosolic biomarkers studied when compared to control donors (Table 1 and Additional file 4: Figure S4). A significant decrease in the expression of myophosphorylase and several of the glycolytic enzymes was observed in muscular dystrophies (Duchenne Muscular Dystrophy, Limb Girdle Muscular Dystrophy Type 2C (LGMD2C), Neuronal Ceroid Lipofuscinosis and patients affected of intensive care unit myopathy) (Table 1 and Additional file 4: Figure S4). Remarkably, whereas myophosphorylase expression was increased in Complex I deficient biopsies (Table 1 and Additional file 4: Figure S4) it was completely vanished in patients affected of Glycogenosis type V (Table 1 and Additional file 4: Figure S4), consistent with the lack of myophosphorylase activity in McArdle disease [16,17]. Based on the opposite expression that exists between glycolytic and bioenergetic markers of the mitochondria during development, differentiation and in cancer [18], we calculated the bioenergetic signature of the biopsies (BEC index = βF1/Hsp60/GAPDH ratio) [3] and different alternative ratios between the catalytic subunit of the H^+-ATP synthase (β-F1-ATPase) and the expression of GAPDH or LDH-A (Table 1 and Additional file 4: Figure S4) [19]. Remarkably, the normalized cellular content of β-F1-ATPase, as assessed by the β-F1/LDH-A ratio, was significantly augmented in all the diseases studied despite the expression of the two markers alone showed no major differences. These findings supported the β-F1-ATPase/LDH-A ratio as a bioenergetic signature of muscular affectation independent of the different genetic or epigenetics mechanisms involved in the onset of neuromuscular diseases (Table 1).

Enzymes of metabolism as biomarkers of rare diseases

Having observed significant differences in the expression of proteins of energy metabolism for a diverse set of rare neuromuscular diseases, we next questioned their potential as discriminatory biomarkers of disease. To this aim, we carried out unsupervised hierarchical clustering of the biopsies using the expression of 4–5 markers for aggregation purposes. This statistical method groups samples by similarity of expression in different groups or clusters [20]. To illustrate this point, the clustering of the 39 biopsies of control, deficit of Complex I activity and of the expression of myophosphorylase using the expression of NADH dehydrogenase subunit 9, myophosphorylase and the β-F1-ATPase/GAPDH ratio resulted in the distribution of the biopsies in three separate groups with a classification sensitivity of 95% and 100% for complex I and myophosphorylase deficiencies, respectively (Figure 3A). A classification specificity of 90% and 100% for controls was also observed (Figure 3A). Hierarchical clustering of 42 biopsies of control and the four muscular dystrophies studied (DMD, BMD, Xp21 and LGMD2C) using the expression of LDH-A, the BEC index and PYGM resulted in two clearly distinguished groups corresponding to controls and dystrophic patients with a classification sensitivity of 96% for the pathologic samples and a specificity of 83% for the controls (Figure 3B). The same type of analysis using 26 biopsies of control and patients affected of NCL according to the expression pattern of PYGM, GPD1 and β-F1/LDH-A ratio resulted in their distribution into two different groups, control donors and NCL patients, with a high sensitivity (100%) and specificity (85%) (Figure 3C).

Inter-individual variation of the expression of the biomarkers (Additional file 4: Figure S4) is usually a handicap for its translation because they not always qualify for clinical use. Table 2 provides a summary of the power to discriminate different neuromuscular dystrophies/myopathies by the combination of the value of the β-F1-ATPase/LDH-A ratio with the expression level of a third biomarker. It should be noted that these combinations have 100% sensitivity (Table 2) when the markers used have no outliers (Additional file 4: Figure S4) supporting their potential use in future prospective studies.

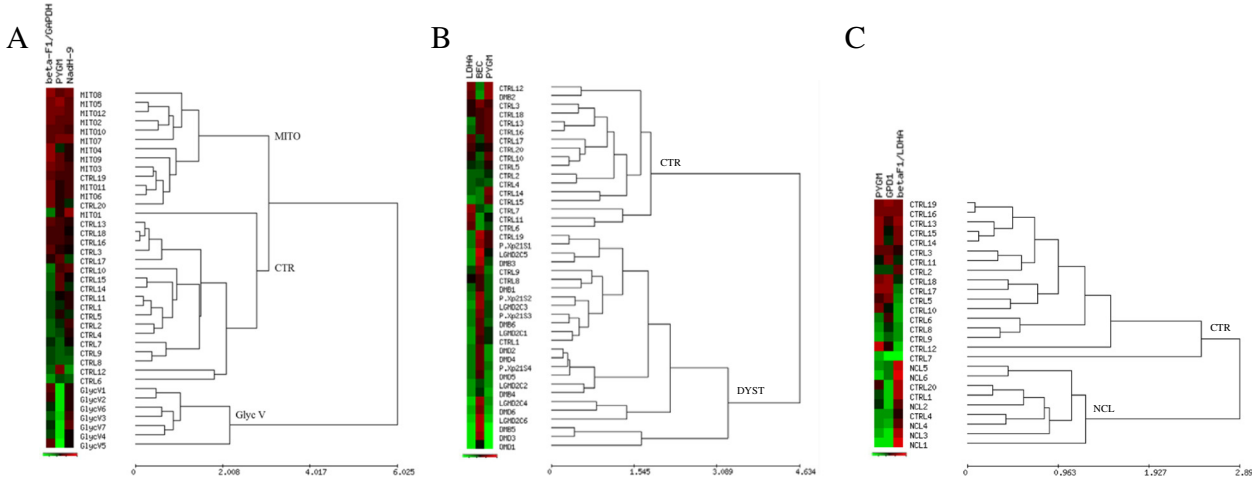

Figure 3 Hierarchical clustering analyses of the biopsies using enzymes of energy metabolism. Rows indicate type of sample, columns, proteins and derived ratios. Protein expression scores are shown normalized to the mean relative expression level in normal samples, according to a color scale (below panels): red indicates high; black, normal; and green, low expression. The dendogram (to the right of the matrix) represents overall similarities in expression profiles. The maximum and minimum values of the markers for each cluster are shown. **A**, Clustering of normal (CTR), isolated deficit of Complex I activity (MITO) and myophosphorylase (GlycV) biopsies using β-F1-ATPase/GAPDH ratio, PYGM and NADHs9 as biomarkers. **B**, Clustering of normal (CTR) and DMD, BMD, Xp21 and LGMD2C muscular dystrophies using LDH-A, BEC index and PYGM as biomarkers. **C**, Clustering of normal (CTR) and Neuronal Ceroid Lipofuscinosis (NCL) biopsies using PYGM, GPD1 and β-F1-ATPase/LDHA ratio as biomarkers.

Discussion

A large number of genes have been identified to be involved in different muscle-wasting neuromuscular disorders. However, knowledge of the pathophysiological mechanisms, markers of diagnosis and treatment of rare muscular diseases is scant or non-existent. Over the last two decades, remarkable progress has been made in the development of genetic-targeted therapeutic interventions for several muscular dystrophies [21]. More recently, next-generation sequencing (NGS) technologies have also been implemented for the identification of the genetic causes underlying neuromuscular diseases [22,23]. Much less studies have dealt with the analysis of the proteome of neuromuscular diseases despite having been demonstrated that the alterations in the expression of proteins of energy metabolism provides useful biomarkers in a complex genetic disorder such as cancer [5,6,19,24]. Within this context, RPMA offers a high-throughput technology for quantitative determination of the proteins that define the particular phenotype of a disease. RPMA allows the interrogation and identification of potential biomarkers, the establishment of correlations with patients' outcome [4] and eventually, the design of future rationale therapeutic approaches based on the biomarkers identified [7,24]. In this study we have developed five additional highly specific monoclonal antibodies against proteins of energy metabolism and interrogated a cohort of muscle biopsies of patients affected of neuromuscular diseases by applying the RPMA technology using nineteen different antibodies. The purpose was the identification of proteins that could inform of the activity of energy metabolism and could provide potential biomarkers for these diseases as an additional effort to stimulate its translation to bed-side application in this orphan field of investigation. Although we have not taken into account the age of patients [25], the specific type of muscle fibers and/or the presence of necrotic areas in the biopsies, which are known factors that influence protein expression [26,27], the low dispersion of the values obtained for each marker suggests that these are not main factors contributing to the differences reported.

Table 2 Potential diagnostic sensitivity of some metabolic biomarkers in neuromuscular dystrophies/myopathies

Disease	β-F1/LDH-A	AdditionalMarkers	Sensitivity
DMD	(2.9-4.1)	PYGM (0.1-0.3)	100%
BMD	(1.9-3.5)	GAPDH (0.6-1.2)	86%
NCL	(1.5-2.1)	GPD1 (0.4-0.6)	100%
LGMD-2C	(2.5-3.9)	SDH (0.5-0.7)	100%

The table summarizes the power to discriminate (sensitivity) the neuromuscular dystrophies/myopathies by the combination of the value of the β-F1-ATPase/LDH-A ratio with the expression level of a third biomarker. Sensitivity was calculated according to the classification rate of true positive samples following the formula: Sensitivity = True positives/(True positives + False positives).

Muscular dystrophies are a heterogeneous group of inherited disorders characterized by progressive muscle wasting and weakness [21,28,29]. Previous studies have suggested the potential relevance of the metabolic enzymes enolase and malate dehydrogenase as biomarkers of these disorders in animal models [30]. In this regard, we have extended the list of potential metabolic

biomarkers with our RPMA approach and, in agreement with findings in dystrophic dog muscle [30], we can confirm the down-regulation of the expression of most glycolytic proteins in human dystrophic muscle. In contrast to the findings in dystrophic dog muscle [30], we observed the up-regulation of mitochondrial proteins involved in oxidative phosphorylation in human dystrophic muscle. The analysis of mitochondrial function in a cardiotoxin-induced mouse model of muscular dystrophy [29] has revealed an impaired expression of mitochondrial proteins involved in the respiratory chain and oxidative phosphorylation (OXPHOS). These results contrast our findings in which it is observed, if any, a significant increase in several markers of the respiratory chain and OXPHOS (Table 1 and Additional file 4: Figure S4). These discrepancies might arise from differences between human and mouse muscle and/or from the experimental system and approaches used in these studies.

The most common and severely debilitating neuromuscular disorder, Duchenne muscular dystrophy, affects ~1 in 3,500 males and it is manifested by rapidly progressive proximal muscle wasting, respiratory insufficiency and cardiac failure that lead to premature death by the mid-20s [28]. The allelic disorder Becker muscular dystrophy is less common and milder, with relatively advanced survival age. Consistent with this, we have observed a lesser alteration of the expression of proteins of energy metabolism in biopsies of BMD patients (Table 1 and Additional file 4: Figure S4). Both diseases are caused by mutations in the dystrophin gene, one of the largest gene in the human genome, located on the X chromosome encoding a 427kD protein [28,31]. Dystrophin interacts with multiple proteins to assemble the dystrophin-associated protein complex (DAPC), a group of proteins that span the sarcolemma of the skeletal and cardiac muscle [21]. The core component of the DAPC is dystroglycan whose insufficient post-translational glycosylation is responsible for sarcoglycanopathies, a clinically heterogeneous group of congenital muscular dystrophies [28]. Within the DAPC, the subcomplex of integral proteins sarcoglycans and sarcospan provides additional mechanical support to the sarcolemma [32]. Mutations in genes encoding α, β, γ and δ subunits of the sarcoglycan complex cause sarcoglycanopathies, a subtype of recessively inherited limb-girdle muscular dystrophies (LGMDs) that also express a significant down-regulation of four cytoplasmic markers of energy metabolism, partially mimicking the findings observed in DMD (Table 1 and Additional file 4: Figure S4).

Different molecular mechanisms are responsible for the muscle wasting phenotypes [33]. However, it is noteworthy that the bioenergetic signature, as assessed by the β-F1-ATPase/LDH-A ratio, is always affected regardless of the muscular disease studied. The mechanisms promoting the global alteration of energy metabolism in the muscle of patients affected with a neuromuscular disease, best exemplified by the dramatic increase in the β-F1-ATPase/LDH-A ratio (Table 1), has remained largely unexplained. Perhaps, because it stems from the idea that only global gene expression analysis could be useful to delineate the pathophysiology of the disease. However, the situation is that genetic alterations that result in neuromuscular dystrophies vary from one specific disease to another but apparently act pleiotropically to regulate, either by genetic or epigenetic means (ICU patients), the signature of muscle energy metabolism.

Moreover, the quantification of the β-F1-ATPase/LDH-A ratio in addition to other proteins of energy metabolism provides a valuable fingerprint to discriminate between different myopathies (Table 2). Interestingly, the combination of the β-F1-ATPase/LDH-A ratio with the expression of myophosphorylase (PYGM) allows the discrimination of DMD patients with 100% of sensitivity (Table 2). Similarly, combination of this ratio with GPD1 expression discriminates patients affected of NCL with a classification sensitivity of 100% (Table 2). Moreover, the GAPDH and succinate dehydrogenase (SDH) in combination with the β-F1-ATPase/LDH-A ratio discriminate BMD (86% sensitivity) and LGMD-2C (100% sensitivity) diseases, respectively (Table 2). The metabolic markers that we have uncovered, alone or in combination with the detection of serum biomarkers [25,34,35] and/or other markers of energy metabolism that have been previously linked to muscular dystrophy in mdx models [30] and patients [35] could aid therapeutic clinical management of patients affected of these disorders.

Conclusions

Our study addresses the challenge of utilizing markers of energy metabolism to be used for translation in aiding the management of rare neuromuscular diseases patients. We demonstrate that the quantification of proteins of energy metabolism in a cohort of seventy three muscle biopsies of control donors and patients affected of different neuromuscular diseases offers sensitive and specific biomarkers that could be implemented to refine the understanding of the biological principles of rare diseases and, eventually, the management of these patients.

Additional files

Additional file 1: Figure S1. Characterization of the antibodies produced. Representative Western blot analysis showing the reactivity of the different antibodies produced against recombinant proteins and native proteins in different human cell lines (HCT116, HepG2 and 293 T) and human liver. The antibodies (0.4 μg/ml) exclusively recognized the recombinant (R; 50–100 ng of protein) and native protein (truncated Aconitase I, AcoI; Citrate synthase, CS; glycerol-3-phosphate dehydrogenase 1, GPD1; lactate dehydrogenase A, LDH-A and NADH-ubiquinone

oxidoreductase α-sub9, NADH-sub9). Note the lower electrophoretic mobility of the recombinant protein in most cases due to the tag used for purification.

Additional file 2: Figure S2. Linear correlation between the fluorescence intensity and the content of protein in HCT116 cells. Cell extracts (0–1 μg/μl) were spotted in the arrays (see Figure 2A). Significant linear correlations were obtained between the fluorescence intensity (arbitrary units, a.u) of the spots and the amount the protein interrogated in the arrays. Protein concentrations in the biopsies were calculated by interpolation in the respective linear plots.

Additional file 3: Figure S3. Validation of RPMA reproducibility. Histograms represent two different experiments (grey and red bars) of RPMA for GAPDH in different neuromuscular dystrophies/myopathies when compared to control donors, confirming that the results obtained with the RPMA approach are highly reproducible.

Additional file 4: Figure S4. Quantitative analysis of the expression of proteins of metabolism represented as box plots. The Y axis indicates the values of intensity (a.u) calculated by interpolation in the linear plot of HCT116 cells and normalized by the expression values of β-actin. The X axis represents patient groups. Box plots represent the lowest, lower quartile, median, upper quartile, and highest observations of each marker in the different groups of pathologies. ○, outlier values and #, extreme values. * and **, $p < 0.05$ and $p < 0.001$ when compared to controls, respectively.

Abbreviations

ACO1: Aconitase; α-F1-ATPase: α-subunit of the H^+-ATP synthase; BMD: Becker Muscular Dystrophy; β-F1-ATPase: β-subunit of the H^+-ATP synthase; COXI: Cytochrome c Oxidase subunit I; COXIV: Cytochrome c Oxidase subunit IV; CPTI: carnitine O-palmitoyl transferase I; CS: Citrate synthase; DMD: Duchenne Muscular Dystrophy; GAPDH: Glyceraldehyde-3-phosphate dehydrogenase; GPD1: glycerol-3-phosphate dehydrogenase 1; GlycV: Glycogenesis type V (Mc Ardle disease); HADHA: Hydroxyacyl-CoA dehydrogenase; Hsp60: Heat Shock Protein 60 kDa; IF1: Inhibitor Factor 1 of the H^+-ATP synthase; LDH-A: Lactate Dehydrogenase A; LGMD2C: Limb Girdle Muscular Dystrophy Type 2C; NADHs9: NADH dehydrogenase subunit 9; NCL: Neuronal Ceroid Lipofuscinosis; PDH: Pyruvate Dehydrogenase; PYGM: myophosphorylase; PK: Pyruvate Kinase; SDH: Succinate Dehydrogenase; SOD2: Superoxide Dismutase 2; Xp21 Carriers: symptomatic forms of DMD and BMD in female carriers.

Competing interests

FS, MSA and JMC as inventors, and the Universidad Autónoma de Madrid and CIBERER as Institutions, hold a Spanish patent application (ES2432653) on "*Un procedimiento y kit para el diagnóstico diferencial de una enfermedad que cursa con afectación muscular*". The rest of the authors in this contribution declare no competing interests.

Authors' contributions

F.S. designed the study, carried out analyses and interpretation of data, M.C and C.N-A carried out analyses, C.N and MA.M reviewed the manuscript for clinical content and contributed with samples, J.M.C. conceptualized and designed the study, carried out analyses and interpretation of data and drafted the manuscript, M.S-A. carried out interpretation of data and wrote the manuscript. All authors read and approved the final manuscript.

Acknowledgements

We thank Dr. Sébastien Tosi (Advanced Digital Microscopy - ADM, IRB Barcelona) for the development of the Image Analysis tool in ImageJ macro language and support of the publication fee by the CSIC Open Access Publication Support Initiative through its Unit of Information Resources for Research (URICI). FS was supported by a pre-doctoral fellowship from FPI-UAM Spain. This work was supported by grants from the Ministerio de Ciencia e Innovación (TREAT-CMT), Ministerio de Economía y Competitividad (SAF2013-41945-R), the Centro de Investigación Biomédica en Red de Enfermedades Raras (CIBERER), ISCIII, Madrid, Ministerio de Economía y Competitividad (FIS-ISCIII PI 12/01683 and PI 10/02628), and Comunidad de Madrid (S2011/BMD-2402), Spain. The CBMSO receives an institutional grant from Fundación Ramón Areces.

Author details

[1]Departamento de Biología Molecular, Centro de Biología Molecular, c/ Nicolás Cabrera 1, Universidad Autónoma de Madrid, 28049 Madrid, Spain. [2]Centro de Investigación Biomédica en Red de Enfermedades Raras (CIBERER), Madrid, Spain. [3]Instituto de Investigación Hospital 12 de Octubre, ISCIII, Madrid, Spain. [4]Instituto de Investigación Biomédico de Vigo (IBIV), Hospital Universitario de Vigo, Meixoeiro, 36200 Vigo, Spain. [5]Laboratorio de Enfermedades Mitocondriales y Neuromusculares, Hospital Universitario 12 de Octubre, 28041 Madrid, Spain.

Received: 30 October 2014 Accepted: 30 January 2015
Published online: 18 February 2015

References

1. Vander Heiden MG, Cantley LC, Thompson CB. Understanding the Warburg effect: the metabolic requirements of cell proliferation. Science. 2009;324:1029–33.
2. Willers IM, Cuezva JM. Post-transcriptional regulation of the mitochondrial H(+)-ATP synthase: A key regulator of the metabolic phenotype in cancer. Biochim Biophys Acta. 1807;2011:543–51.
3. Cuezva JM, Krajewska M, de Heredia ML, Krajewski S, Santamaria G, Kim H, et al. The bioenergetic signature of cancer: a marker of tumor progression. Cancer Res. 2002;62:6674–81.
4. Aldea M, Clofent J, Nunez De Arenas C, Chamorro M, Velasco M, Berrendero JR, et al. Reverse phase protein microarrays quantify and validate the bioenergetic signature as biomarker in colorectal cancer. Cancer Lett. 2011;311:210–8.
5. Sanchez-Arago M, Cuezva JM. The bioenergetic signature of isogenic colon cancer cells predicts the cell death response to treatment with 3-bromopyruvate, iodoacetate or 5-fluorouracil. J Transl Med. 2011;9:19.
6. Sanchez-Arago M, Formentini L, Cuezva JM. Mitochondria-mediated energy adaption in cancer: the H(+)-ATP synthase-geared switch of metabolism in human tumors. Antioxid Redox Signal. 2013;19:285–98.
7. Mueller C, Liotta LA, Espina V. Reverse phase protein microarrays advance to use in clinical trials. Mol Oncol. 2010;4:461–81.
8. Tibes R, Qiu Y, Lu Y, Hennessy B, Andreeff M, Mills GB, et al. Reverse phase protein array: validation of a novel proteomic technology and utility for analysis of primary leukemia specimens and hematopoietic stem cells. Mol Cancer Ther. 2006;5:2512–21.
9. Michaud GA, Salcius M, Zhou F, Bangham R, Bonin J, Guo H, et al. Analyzing antibody specificity with whole proteome microarrays. Nat Biotechnol. 2003;21:1509–12.
10. Strausberg RL, Simpson AJ, Old LJ, Riggins GJ. Oncogenomics and the development of new cancer therapies. Nature. 2004;429:469–74.
11. Acebo P, Giner D, Calvo P, Blanco-Rivero A, Ortega AD, Fernandez PL, et al. Cancer abolishes the tissue type-specific differences in the phenotype of energetic metabolism. Transl Oncol. 2009;2:138–45.
12. Sanchez-Cenizo L, Formentini L, Aldea M, Ortega AD, Garcia-Huerta P, Sanchez-Arago M, et al. Up-regulation of the ATPase inhibitory factor 1 (IF1) of the mitochondrial H + −ATP synthase in human tumors mediates the metabolic shift of cancer cells to a Warburg phenotype. J Biol Chem. 2010;285:25308–13.
13. Willers IM, Martínez-Reyes I, Martínez-Diez M, Cuezva JM. miR-127-5p targets the 3'UTR of human β-F1-ATPase mRNA and inhibits its translation. Biochim Biophys Acta-Bioenergetics. 1817;2012:838–48.
14. Liotta L, Petricoin E. Molecular profiling of human cancer. Nat Rev Genet. 2000;1:48–56.
15. Chen WW, Birsoy K, Mihaylova MM, Snitkin H, Stasinski I, Yucel B, et al. Inhibition of ATPIF1 ameliorates severe mitochondrial respiratory chain dysfunction in mammalian cells. Cell Rep. 2014;7:27–34.
16. Lucia A, Ruiz JR, Santalla A, Nogales-Gadea G, Rubio JC, Garcia-Consuegra I, et al. Genotypic and phenotypic features of McArdle disease: insights from the Spanish national registry. J Neurol Neurosurg Psychiatry. 2012;83:322–8.
17. Nogales-Gadea G, Consuegra-Garcia I, Rubio JC, Arenas J, Cuadros M, Camara Y, et al. A transcriptomic approach to search for novel phenotypic regulators in McArdle disease. PLoS One. 2012;7:e31718.
18. Cuezva JM, Sanchez-Arago M, Sala S, Blanco-Rivero A, Ortega AD. A message emerging from development: the repression of mitochondrial beta-F1-ATPase expression in cancer. J Bioenerg Biomembr. 2007;39:259–65.

19. Cuezva JM, Ortega AD, Willers I, Sanchez-Cenizo L, Aldea M, Sanchez-Arago M. The tumor suppressor function of mitochondria: translation into the clinics. Biochim Biophys Acta. 2009;1792:1145–58.
20. Balzano W, Del Sorbo MR. Genomic comparison using data mining techniques based on a possibilistic fuzzy sets model. Biosystems. 2007;88:343–9.
21. Rahimov F, Kunkel LM. The cell biology of disease: cellular and molecular mechanisms underlying muscular dystrophy. J Cell Biol. 2013;201:499–510.
22. Lemmers RJ, Tawil R, Petek LM, Balog J, Block GJ, Santen GW, et al. Digenic inheritance of an SMCHD1 mutation and an FSHD-permissive D4Z4 allele causes facioscapulohumeral muscular dystrophy type 2. Nat Genet. 2012;44:1370–4.
23. Manzini MC, Tambunan DE, Hill RS, Yu TW, Maynard TM, Heinzen EL, et al. Exome sequencing and functional validation in zebrafish identify GTDC2 mutations as a cause of Walker-Warburg syndrome. Am J Hum Genet. 2012;91:541–7.
24. Ledford H. Metabolic quirks yield tumour hope. Nature. 2014;508:158–9.
25. Hathout Y, Marathi RL, Rayavarapu S, Zhang A, Brown KJ, Seol H, et al. Discovery of serum protein biomarkers in the mdx mouse model and cross-species comparison to Duchenne muscular dystrophy patients. Hum Mol Genet. 2014;23(24):6458–69.
26. Brancaccio P, Lippi G, Maffulli N. Biochemical markers of muscular damage. Clin Chem Lab Med. 2010;48:757–67.
27. Shima K, Tashiro K, Hibi N, Tsukada Y, Hirai H. Carbonic anhydrase-III immunohistochemical localization in human skeletal muscle. Acta Neuropathol. 1983;59:237–9.
28. Emery AE. The muscular dystrophies. BMJ. 1998;317:991–5.
29. Ramadasan-Nair R, Gayathri N, Mishra S, Sunitha B, Mythri RB, Nalini A, et al. Mitochondrial alterations and oxidative stress in an acute transient mouse model of muscle degeneration: implications for muscular dystrophy and related muscle pathologies. J Biol Chem. 2014;289:485–509.
30. Guevel L, Lavoie JR, Perez-Iratxeta C, Rouger K, Dubreil L, Feron M, et al. Quantitative proteomic analysis of dystrophic dog muscle. J Proteome Res. 2011;10:2465–78.
31. Burghes AH, Logan C, Hu X, Belfall B, Worton RG, Ray PN. A cDNA clone from the Duchenne/Becker muscular dystrophy gene. Nature. 1987;328:434–7.
32. Yoshida M, Suzuki A, Yamamoto H, Noguchi S, Mizuno Y, Ozawa E. Dissociation of the complex of dystrophin and its associated proteins into several unique groups by n-octyl beta-D-glucoside. Eur J Biochem. 1994;222:1055–61.
33. Rahimov F, King OD, Leung DG, Bibat GM, Emerson Jr CP, Kunkel LM, et al. Transcriptional profiling in facioscapulohumeral muscular dystrophy to identify candidate biomarkers. Proc Natl Acad Sci U S A. 2012;109:16234–9.
34. Doran P, Donoghue P, O'Connell K, Gannon J, Ohlendieck K. Proteomic profiling of pathological and aged skeletal muscle fibres by peptide mass fingerprinting (Review). Int J Mol Med. 2007;19:547–64.
35. Nadarajah VD, van Putten M, Chaouch A, Garrood P, Straub V, Lochmuller H, et al. Serum matrix metalloproteinase-9 (MMP-9) as a biomarker for monitoring disease progression in Duchenne muscular dystrophy (DMD). Neuromuscul Disord. 2011;21:569–78.

S1

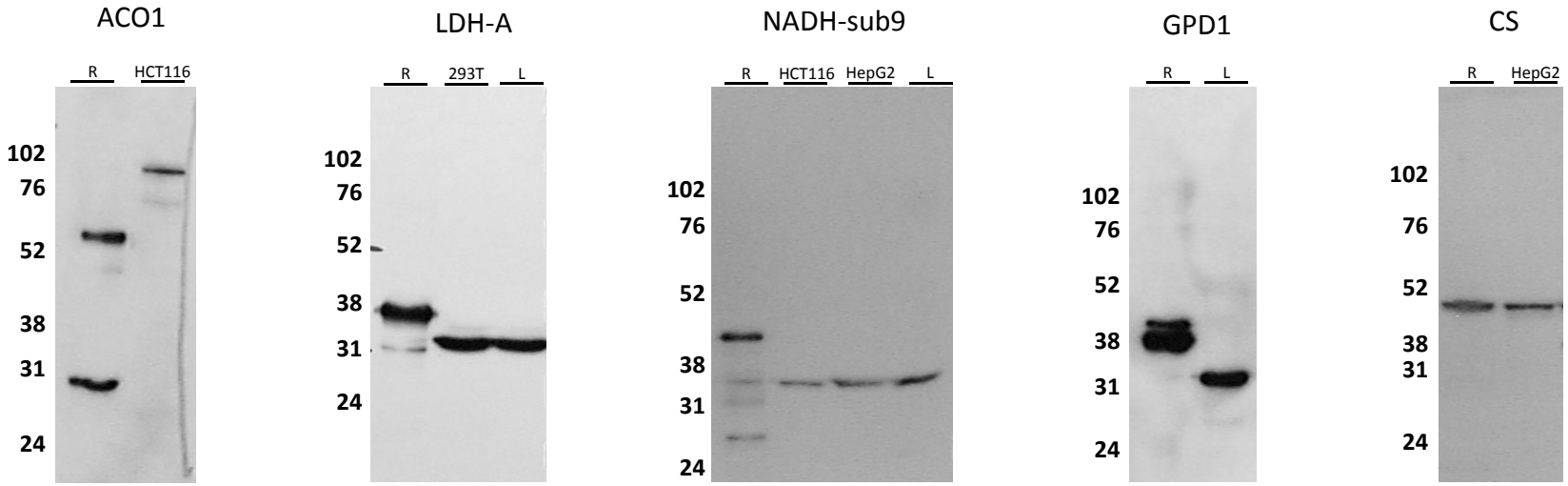
ACO1
R
HCT116
102
76
52
38
31
24
LDH-A
R
293T
L
102
76
52
38
31
24
NADH-sub9
R
HCT116
HepG2
L
102
76
52
38
31
24
GPD1
R
L
102
76
52
38
31
24
CS
R
HepG2
102
76
52
38
31
24

S2

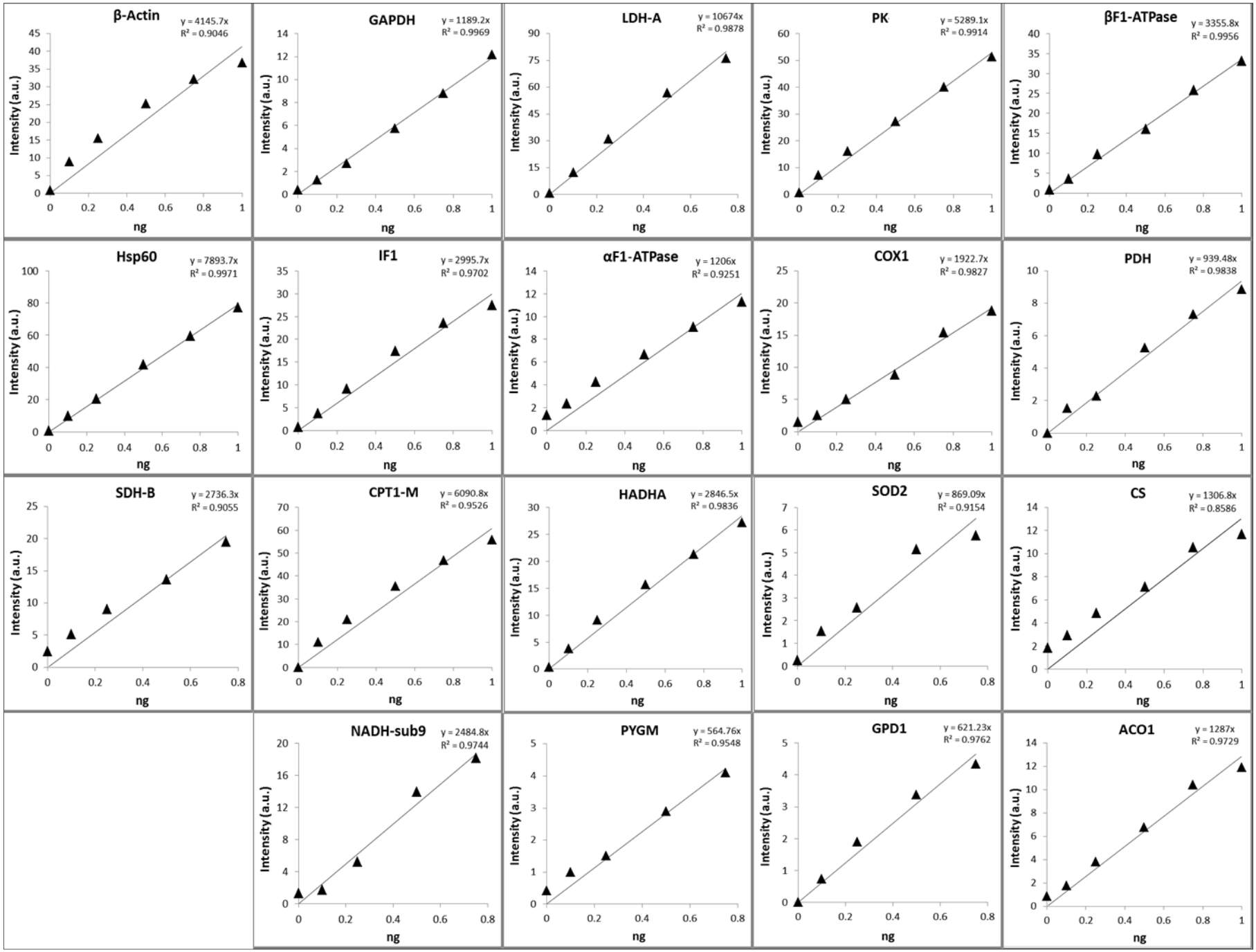
β-Actin
y = 4145.7x
R² = 0.9046
GAPDH
y = 1189.2x
R² = 0.9969
LDH-A
y = 10674x
R² = 0.9878
PK
y = 5289.1x
R² = 0.9914
βF1-ATPase
y = 3355.8x
R² = 0.9956
Hsp60
y = 7893.7x
R² = 0.9971
IF1
y = 2995.7x
R² = 0.9702
αF1-ATPase
y = 1206x
R² = 0.9251
COX1
y = 1922.7x
R² = 0.9827
PDH
y = 939.48x
R² = 0.9838
SDH-B
y = 2736.3x
R² = 0.9055
CPT1-M
y = 6090.8x
R² = 0.9526
HADHA
y = 2846.5x
R² = 0.9836
SOD2
y = 869.09x
R² = 0.9154
CS
y = 1306.8x
R² = 0.8586
NADH-sub9
y = 2484.8x
R² = 0.9744
PYGM
y = 564.76x
R² = 0.9548
GPD1
y = 621.23x
R² = 0.9762
ACO1
y = 1287x
R² = 0.9729
Intensity (a.u.)
ng

S3

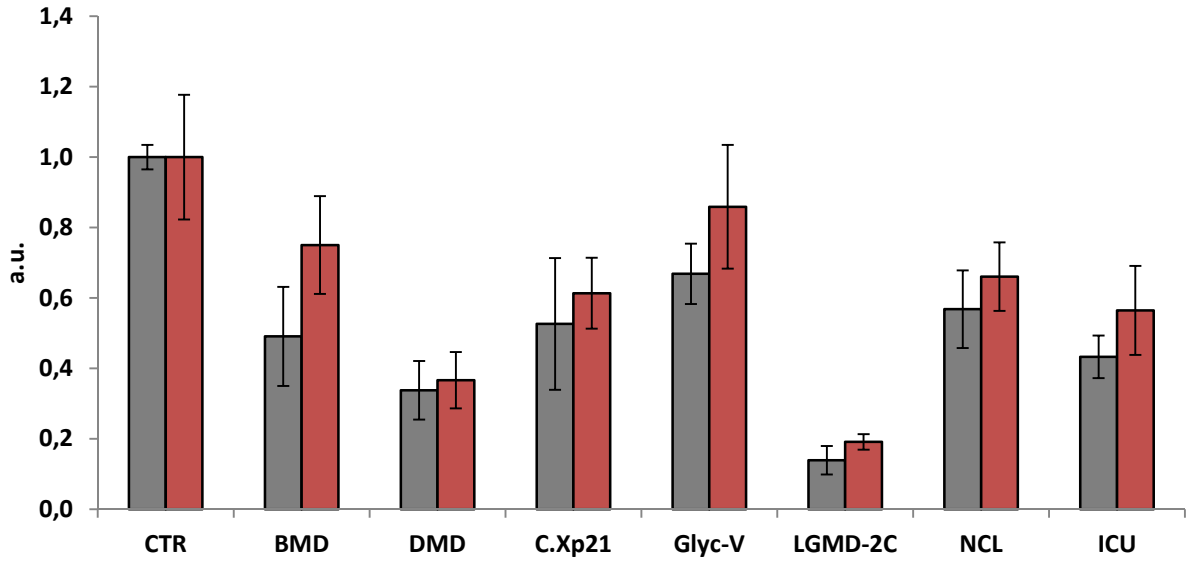

S4

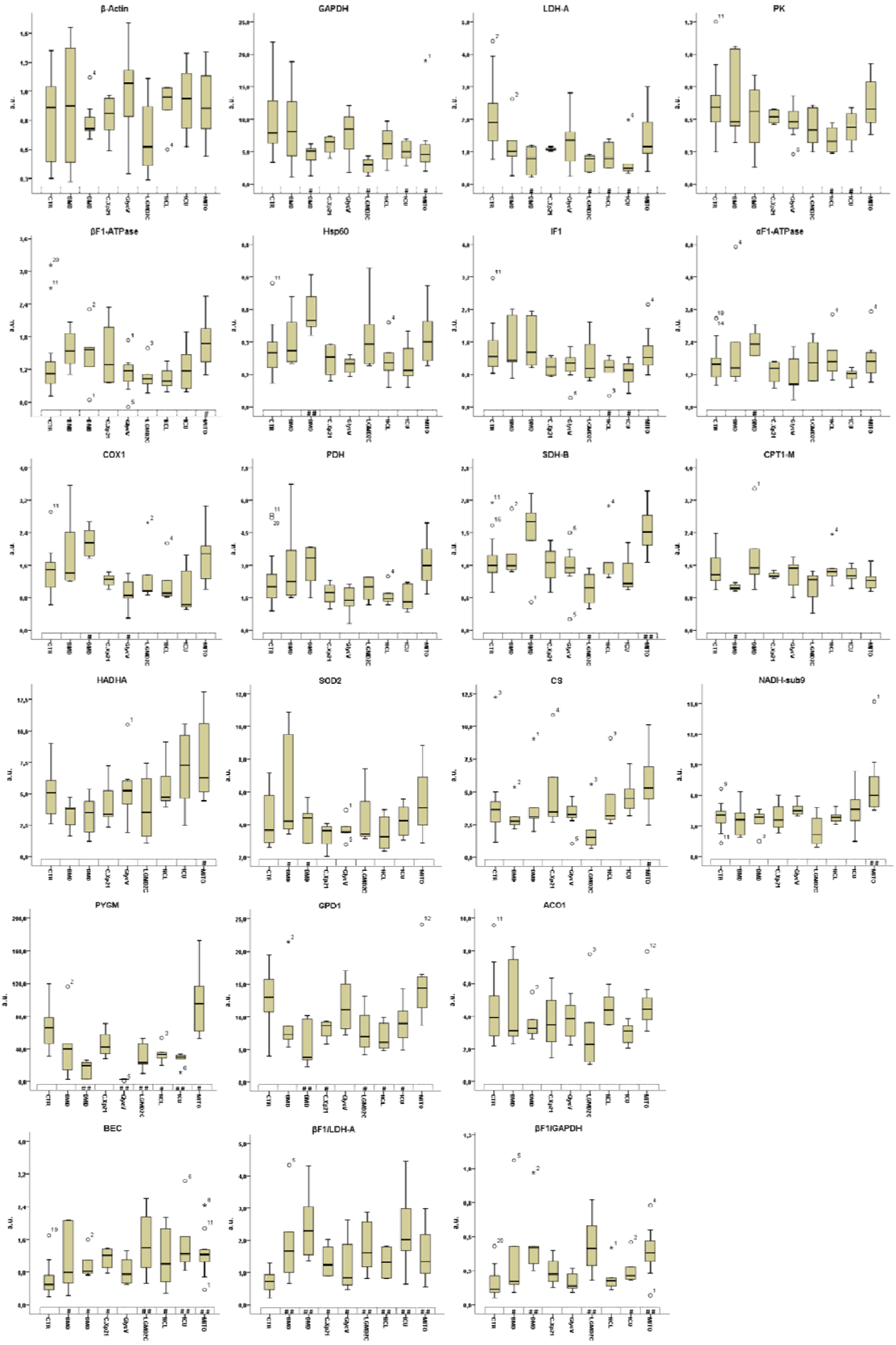
β-Actin
GAPDH
LDH-A
PK
βF1-ATPase
Hsp60
IF1
αF1-ATPase
COX1
PDH
SDH-B
CPT1-M
HADHA
SOD2
CS
NADH-sub9
PYGM
GPD1
ACO1
BEC
βF1/LDH-A
βF1/GAPDH
a.u.
CTR
HMD
HMD
CX-p21
OxyV
L-GMD3C
HCL
HCU
HMTO

Artículo #6

Santacatterina, F., Sánchez-Aragóa,M., de Arenas, C.N., Catalán, M., Garraboud, G., Cardellach, F., Cuezva, J.M. PKM2 and IF1 provide novel biomarkers of dermatomyositis: A metabolic link to oncogenesis.

PKM2 and IF1 provide novel biomarkers of dermatomyositis: A metabolic link to oncogenesis

Fulvio Santacatterina[a,b,c], María Sánchez-Aragó[a,b,c], Marc Catalán García[d,e], Glòria Garrabou[d,e], Francesc Cardellach[d,e] and José M. Cuezva[a,b,c,*].

[a]Departamento de Biología Molecular, Centro de Biología Molecular Severo Ochoa, CSIC-UAM, Universidad Autónoma de Madrid, 28049 Madrid, Spain, [b]Centro de Investigación Biomédica en Red de Enfermedades Raras (CIBERER), Madrid; [c]Instituto de Investigación Hospital 12 de Octubre, ISCIII, Madrid; [d]Muscle Research and Mitochondrial Function Laboratory, CELLEX- IDIBAPS, Faculty of Medicine-University of Barcelona, Internal Medicine Department-Hospital Clinic of Barcelona, Barcelona; [e]Centro de Investigación Biomédica en Red en Enfermedades Raras (CIBERER), Barcelona.

*, To whom correspondence should be addressed: Dr. J.M. Cuezva, Centro de Biología Molecular, c/ Nicolás Cabrera 1, Universidad Autónoma de Madrid, 28049 Madrid, Spain.
(Phone: 34911964618; Fax: 34911964420; E-mails: jmcuezva@cbm.csic.es)

Running Head: Biomarkers of inflammatory myopathies

Abbreviations: β-F1-ATPase: β-subunit of the H^+-ATP synthase; DM: Dermatomyositis; GAPDH: Glyceraldehyde-3-phosphate dehydrogenase; GPD1: Glycerol-3-phosphate dehydrogenase 1; Hsp60: Heat shock protein 60kDa; IBM: Inclusion Body Myositis; IF1: ATPase Inhibitory Factor 1; IM: Inflammatory Myopathy; LDH-A: Lactate dehydrogenase A; PYGM: Glycogen phosphorylase; PK: Pyruvate kinase; PKM2: Pyruvate kinase M2; PM: Polymyositis.

Abstract

Metabolic alterations usually involved in common human diseases regardless of the cause of origin. Herein, we have investigated the potential applicability that proteins of energy metabolism could provide as biomarkers of inflammatory myopathies (IMs). To this aim, we have interrogated a cohort of thirty-two muscle biopsies of the three major groups of IMs, polymyositis (PM), dermatomyositis (DM) and inclusion body myositis (IBM) and of control donors with a set of monoclonal antibodies against proteins of energy metabolism using Reverse Phase Protein Microarrays (RPPA), a high-throughput technique used for the identification of biomarkers. We report that the expression of the proteins is not significantly affected in the muscle of PM patients when compared to controls. However, and while the expression of β-actin is significantly increased in DM and IBM, the expression of proteins involved in glucose metabolism such as glycogen phosphorylase, glyceraldehyde-3-phosphate dehydrogenase, lactate dehydrogenase A and of glycerol phosphate dehydrogenase, which is involved in the shuttling of electrons to mitochondria display a significant reduction in muscle of IBM when compared to controls. In contrasts to these findings, the expression of the glycolytic pyruvate kinase isoform M2 (PKM2) and of the mitochondrial ATPase Inhibitor Factor 1 (IF1) and Hsp60 were significantly augmented in DM when compared to other IMs. PKM2 alone or in combination with other biomarkers allowed the discrimination of control and IMs with a very high (>95%) sensitivity and specificity. Unfortunately, plasma levels of PKM2 are not significantly altered in DM patients to allow its use as a non-invasive biomarker. However, we suggest that the pro-oncogenic metabolic phenotype afforded by the enhanced expression of PKM2 and IF1 might provide therapeutic targets to prevent the higher cancer incidence in DM patients.

Keywords: Inflammatory myopathies; Energy metabolism; Mitochondria; Biomarkers; Pyruvate kinase M2; ATPase Inhibitory Factor 1.

Introduction

Alteration of the expression of proteins of energy metabolism often accompanies the presentation of genetic disorders (1-3). The reprogramming of cellular metabolism that occurs in cancer is a good example in this regard (4, 5) providing valuable biomarkers of disease progression (1, 6) and of the response to therapy (7-9). Inflammatory myopathies (IMs) is a group of heterogeneous diseases characterized by muscle weakness and inflammatory infiltrates within the skeletal muscle. Due to their similar pathogenesis, polymyositis, dermatomyositis and the recently acknowledged, sporadic inclusion-body myositis (IBM) are the three major groups ascribed to IMs (10). A fourth and fifth subtypes termed necrotizing auto-immune myositis and overlap myositis are also being recognized within the group of IMs (11). IMs are considered rare diseases due to their low incidence, about of 2.1 to 7.7 new cases per every million inhabitants/year. IBM is the most common acquired myopathy in patients above 50 years (12-14). There are few biomarkers that could help the diagnosis and management of patients affected by IMs and an elevated serum activity of creatine kinase is a marker of patients affected by active forms of all subtypes of IMs (11).

Reverse Phase Protein Microarrays (RPPA) is a high-throughput quantitative technique adequate for multiplexed analysis of protein expression in minute amounts of sample in a large variety of biological specimens (15, 16). Over the last decade, RPPA technique has provided a precious tool in the discovery of biomarkers of disease which might become indispensable in the progress of diagnostic, prognostic and therapeutic fields. The Achilles heel for the development of a reliable RPPA platform, is the

availability of high-affinity and specific antibodies against the proteins investigated (17, 18). Herein, we have studied the putative relevance of proteins of energy metabolism as diagnostic biomarkers in inflammatory myopathies using RPPA. To this aim, we have studied the expression of enzymes of glucose metabolism and of oxidative phosphorylation in a cohort of thirty two muscle biopsies inclusive of control donors and patients affected with polymyositis (PM), dermatomyositis (DM) and inclusion body myositis (IBM) using validated monoclonal antibodies. The final purpose of the study is to translate the "signature" of energy metabolism to bed-side application of patients affected with IMs.

Materials and Methods

Patients and protein extraction. A cohort of thirty two muscle biopsies of control donors (n=6) and patients affected of IMs including polymyositis (PM, n=4), dermatomyositis (DM, n=13) and inclusion body myositis (IBM, n=9) were processed. A cohort of forty plasma samples of control donors (n=10) and patients affected of IMs including PM (n=5), DM (n=9) and IBM (n=16) were also collected. Frozen tissue sections obtained from surgical specimens and plasma samples were provided by the Internal Medicine Department-Hospital Clinic of Barcelona. Routine histopathological study and molecular and clinical diagnosis of all the cases studied had been previously performed. The samples were obtained with informed consent following the Declaration of Helsinki and coded for anonymity to protect patient confidentiality. The Institutional Review Board approved the project. For protein extraction, the samples were homogenized in T-PER Tissue Protein Extraction Reagent (ThermoScientific, Inc.) containing protease inhibitors (Roche) in a 1:5 (w/v) ratio, and further freeze–thawed

three times in liquid nitrogen (6). The protein concentration was determined with the Bradford reagent (Bio-Rad, Inc) using BSA as standard.

Protein electrophoresis and western blotting. Protein samples from muscle biopsies were fractionated on SDS–9% PAGE and blotted with anti-β-F1-ATPase (1:1000), anti-Hsp60 (1:1000), anti-GAPDH (1:1000) and anti-PKM2 (1:1000) from (19), anti-IF1 (1:500) from (20), anti-LDH-A (1:1000), anti-GPD1 (1:1000) from (2), anti-PYGM (Abcam, ab88078; 1:1000) and anti-β-actin (Sigma-Aldrich, A1978; 1:1000). Peroxidase-conjugated anti-mouse IgGs (Nordic Immunology; 1:3000) were used as secondary antibodies. The blots were revealed using the ECL® reagent (Amersham Pharmacia Biotech). The intensity of the bands was quantified using a Kodak DC120 digital camera and the Kodak 1D Analysis Software.

Printing and processing of reverse phase protein microarrays. Samples from muscle biopsies were diluted in PBS to a final protein concentration of 1 μg/μl before printing. Serially diluted protein extracts (0–1μg/μl) derived from HCT116 colocarcinoma cells were also prepared to assess printing quality and the linear response of protein recognition by the antibodies used. A standard curve of BSA (0-1 μg/μl) and mouse IgGs (0-1 ng/ml) were also prepared for printing as internal negative and positive controls, respectively. Plasma samples were diluted 1:20 (v/v) in PBS before printing. A Standard curve (0-1 ng/ml) of the PKM2 recombinant protein (r-PKM2) was printed to correlate the mean fluorescent intensity of the samples to the quantity of the protein. Approximately, 1 nl volume of each sample was spotted in triplicate onto nitrocellulose-coated glass slides (FAST Slides, Scheleicher & Schuell BioScience, Inc.) using a BioOdyssey Calligrapher MiniArrayer printer (Bio-Rad Laboratories, Inc.) equipped with a solid pin (MCP310S) at constant humidity (RH 45%) and temperature (16ºC).

After printing, arrays were allowed to dry and further blocked in PBS-T containing 5% skimmed milk. An additional blocking step with goat anti-human whole serum IgGs (Sigma-Aldrich, I1011; 1:100) was necessary to prevent the cross reaction of the secondary antibody with plasma IgGs. After, the arrays were incubated overnight at 4ºC with the indicated concentrations of the following primary monoclonal antibodies: anti-β-F1-ATPase (1:150), anti-Hsp60 (1:150), anti-GAPDH (1:250) and anti-PKM2 (1:150), anti-IF1 (1:150), anti-LDH-A (1:200), anti-GPD1 (1:1000), anti-PYGM (1:200) and anti-β-actin (1:1000). After incubation, the arrays were washed with PBS-T and further incubated with a donkey anti-mouse secondary antibody conjugated with alexa-555 (Invitrogen, Madrid, Spain) or, in the case of arrays of plasma samples, incubated with goat anti-mouse highly cross-adsorbed antibody conjugated with CF™647 (Sigma-Aldrich, SAB4600183; 1:500). To evaluate the unspecific binding of the secondary antibody to non-masked human IgGs in plasma samples, a pad was incubated directly with the secondary antibody as negative control of the RPPA analysis. Spotted samples in one of the pads were fixed with XFCF buffer (10% acetic acid, 30% ethanol) for 1h, stained with 0.0001% Fast Green FCF (Sigma-Aldrich, F7252) in XFCF for 5 minutes and washed 5 times with XFCF in order to quantify the total protein amount of each spot. Microarrays were scanned using a Typhoon 9410 scanner (GE Healthcare, Inc.). The mean fluorescent intensity of the spots was quantified using GenePix® Pro 7 software system and converted into arbitrary units of expressed protein/ng of protein in the sample using the expression obtained in the standard curve of the HCT116 cell line and normalized to the protein amount in the sample obtained from the FCF stained pad. Representative technical variances of the PKM2 arrays calculated by the squared coefficient of variation ($SCV = \sigma*100/|x|$) were 2.7 ± 0.4 for muscle samples and 3.2 ± 0.4 for plasma samples.

Indirect ELISA. Plasma samples (50 µl) from IBM (n= 8), DM (n= 9) patients and a control group (n= 8) were absorbed in F96 IMMUNO PLATE (NUNC, 442404) for 1h at 37ºC. A standard curve (0-4 µg/ml) of the recombinant PKM2 (r-PKM2) (19) was also adsorbed. After blocking and extensive washing, 50 µl of a solution containing mouse anti-PKM2 (1:150) were added to each well and incubated at 37ºC for 1h. Wells were washed with PBS-T, and after 50 µl of horseradish peroxidase-labeled goat anti-mouse IgG (1:1000) (Bio-Rad Laboratories, 172-1011) added. Color development was achieved by addition of 200 µl of the peroxidase substrate solution (Bio-Rad Laboratories, Inc., 172-1064). Reaction was stopped by addition of 100 µl/well of 2% oxalic acid. The absorbance at 415 nm was measured with a FLUOstar OMEGA Microplate Reader (BMG LABTECH).

Statistical analysis. Distribution of molecular markers was studied by using a two-tailed Student's t test. Analysis of variance (ANOVA) with post hoc Dunnett's test was used for multiple comparisons to the control. Inter-individual variation of the expression of protein levels in muscle biopsies were shown in box plots graphs, using the PASW statistics 18 software package. For the expression profiles of metabolic markers data were reformatted by calculating the log2 of the expression level in each sample relative to the mean expression level in normal samples. We used the Cluster Program from "Expression Profiler Clustering home page" at http://ep.ebi.ac.uk/EP/EPCLUST by the Average Linkage (Weighted Pair Group Method Average WPGMA) clustering based on the Euclidean distance function as proximity measure. The results shown are means ± S.E.M. A $p < 0.05$ was considered statistically significant.

Results

To explore the potential applicability of a signature of metabolism in the diagnosis of IMs we selected representative proteins from glycogenolysis (Glycogen phosphorilase, PYGM), glycolysis (glyceraldehyde-3-phosphate dehydrogenase, GAPDH, pyruvate kinase M2, PKM2 and lactate dehydrogenase A, LDHA), oxidative phosphorylation (β-subunit of the H^+-ATP synthase, β-F1-ATPase and ATPase Inhibitory Factor 1, IF1), and electron shuttling of glycolytic NADH to mitochondria (glycerol-phosphate dehydrogenase 1, GPD1). In addition, β-actin and heat shock protein 60kDa (Hsp60) were also studied as structural markers of the cell and mitochondria, respectively. The major limitation of quantitative RPPA is the availability of specific monoclonal antibodies (mAbs) against the proteins being studied. Fig. 1 shows that the mAbs used in this study only recognized a single protein band at the expected molecular weight in human muscle extracts validating their utilization in RPPA techniques (2, 19, 20)

A representative protein microarray illustrating the printing protocol of human muscle biopsies developed with antibodies against the glycolytic PKM2 is shown in Fig. 2A. Microarrays developed with the other antibodies are shown below (Fig. 2A). Protein extracts from muscle biopsies of control (green boxed in Fig. 2A), PM, DM and IBM (yellow, red and blue boxed in Fig. 2A, respectively) were prepared and spotted onto RPPA in triplicate from left to right (Fig. 2A). Increasing amounts of BSA and murine IgGs (black and brown boxed in Fig. 2A, respectively) were spotted in the array as control of the background of the assay and positive control of antibody recognition, respectively. Increasing protein amounts of cellular extracts derived from HCT116 cells were also spotted (magenta boxed in Fig. 2A). The HCT116 extracts revealed a linear increase in fluorescent intensity as the amount of protein increases (Fig. 2B), providing

the linear plot of the assay (Fig. 2B, see also Supplementary Fig. S1). The arrays illustrate the specific recognition of the corresponding antigen in minute amounts of printed protein of HCT116 extracts as well as in the biopsies (Fig. 2A). As expected BSA did not show any fluorescent signal, confirming the absence of non-specific binding of the primary and secondary antibodies onto the spotted proteins (Fig. 2A). In contrast, a linear increase in signal was observed in murine IgGs (Fig. 2A), confirming that the secondary antibody works properly. The quantification of the expression of each marker in control (n =6) and patient (n =26) biopsies was calculated by interpolating the fluorescent intensity signal obtained in the sample in the standard curve of HCT116 cells (Fig. 2B and Supplementary Fig. S1). The box plots in Figure 3 displays the results of protein expression in PM, DM and IBM when compared to controls revealing the inter-individual variation within each group.

Interestingly, only DM and IBM patients showed significant alterations of the expression level of the studied markers when compared to controls (Fig. 3). Muscle biopsies from patients affected with DM showed an increase in the expression of Hsp60 and β-actin concurrent with a similar increase in the expression of PKM2 and the mitochondrial ATPase inhibitor factor IF1 (Fig. 3). These changes occurred in the absence of relevant changes for the expression of other markers and with a significant reduction in PYGM expression (Fig. 3). In contrast, biopsies from IBM patients showed a significant reduction in the expression of the cytoplasmic GAPDH, LDH-A, PYGM, GPD1 and mitochondrial Hsp60 (Fig. 3). Concurrently, a significant increase in β-actin and IF1 expression (Fig. 3) was observed in IBM. Overall, and from the point of view of a potential biomarker to distinguish between DM from normal biopsies and the rest of the other IMs stands the sharp increase in PKM2 expression (Fig. 3). In the same

line, the down-regulation of glycolytic markers distinguishes IBM from control biopsies and other IMs (Fig. 3).

Representative western blot analysis of the three glycolytic markers investigated in RPPAs (Supplementary Fig. S2) confirmed the higher expression of PKM2 in DM samples and the downregulation of both GAPDH and LDH-A in IBM biopsies when compared to control or PM samples. Interestingly, PKM2 expression in DM was as high as in the HCT116 carcinoma cell line (Supplementary Fig. S2). A helpful biomarker that informs of the relative activity of energy provision pathways during development, differentiation and in cancer is the bioenergetic signature (6, 8, 21). The bioenergetic signature is calculated by the ratio between the catalytic subunit of the H^+-ATP synthase (β-F1-ATPase) relative to the expression of a glycolytic enzyme (8). Remarkably, the β-F1/PKM2 ratio was significantly diminished in DM providing an excellent bioenergetic marker in order to discriminate this disorder from controls or any other IM (Fig. 4A, Table 1). Likewise, unsupervised hierarchical clustering of the biopsies using the expression of 1, 2 or 3 proteins for aggregation further illustrated the potential of metabolic biomarkers to discriminate normal biopsies from DM (Fig. 4B, Table 1) and from IBM (Fig. 4C, Table 1) with very high sensitivity and specificity (Fig. 4 and Table 1).

To further explore the potential bed-side translation of PKM2 as a discriminating biomarker of DM we investigated whether the inflammation and tissue remodeling that accompanies the disease could be reflected on the plasma levels of PKM2. To this aim we studied the expression of PKM2 in plasma samples of control and IM patients by ELISA and by a modified RPPA technique. Unfortunately, the results obtained revealed that IMs do not modify plasma PKM2 levels to a significant extent when compared to

controls (Supplementary Fig. S3) what limits the utilization of PKM2 as a non-invasive biomarker of DM.

Discussion

Diagnostic criteria of inflammatory myopathies relies on histophatologic and immunopathologic examination of muscle biopsies by an experienced laboratory (11, 22). The diagnosis for DM and IBM is hard but usually unambiguous. The diagnosis of PM is often assessed by exclusion criteria (10). RPPA is a widely adopted high-throughput technique that allows quantitative protein profiling of the cell or tissue sample that is especially indicated for the identification of biomarkers of diagnosis, prognosis and therapeutic response (6, 15, 23, 24). In fact, RPPA have been recently approved for implementation in clinical trials (15). Herein, we have interrogated a cohort of muscle biopsies from inflammatory myopathic patients using RPPA and nine validated mAbs against key proteins of energy metabolism to uncover new biomarkers that could help differential diagnosis of IMs. We report that the metabolic biomarkers studied are unable to distinguish control from PM biopsies. In contrast, both DM and IBM reveal significant diferences in the expression of proteins of energy metabolism when compared to controls. Althought age, type of muscle fibers and extent of celular damage in the biopsies are likely to affect protein expression the low dispersion of the values obtained for each marker suggests that these are not main factors contribuiting to the differences reported.

Consistent with previous reports (22) we observed an increased expression in β-actin in both DM and IBM. β-actin overexpression in IMs is the likely consequence of muscle fiber regeneration, a criteria for the classification of IMs (22) also supported by

their association with connective tissue disorders (25, 26). Contrary to the increased expression of β-actin, IBM biopsies revealed a diminished expression of the glycolytic markers GAPDH and LDHA when compared to controls. Consistently, the expression of GPD1, which forms part of the mitochondrial shuttle of the glycolytic generated NADH was also diminished in IBM. Moreover, the expression of PYGM, which is upstream of glycolysis, was also diminished in IBM biopsies. These findings suggest that muscle fibers of IBM might experience a partial repression of glycolytic metabolism when compared to controls.

In contrast to the findings in muscle of IBM, the biopsies of DM patients showed an enhanced expression of the mitochondrial protein Hsp60 and IF1 and a very large increase in the glycolytic PKM2. The βF1/LDHA ratio, which has been recently described as a potential biomarker of neuromuscular diseases (2), failed in the discrimination of IMs. However, the βF1/PKM2 ratio offered a reliable indicator to discriminate DM from any other IM or from control biopsies. In fact, the power of PKM2 as a biomarker in IMs is well demonstrated by the high specificity and sensitivity in the stratification of patients affected with DM when compared to controls or any other group of patients affected with IMs. Overall, we support that the increased expression of PKM2 in DM, confers to this protein a great value as biomarker for this particular type of IM what might benefit some patients by sparing an additional muscle biopsy (22). Unfortunately, PKM2 levels in plasma of DM patients did not provide a non-invasive biomarker of the disease.

It is generally agreed that cancer is more associated with DM than with PM (11) and a clear increase of cancer related mortality has been reported in DM patients when compared to PM patients (10, 27-29). A distinctive feature of cancer cells is the enhanced aerobic glycolysis (4, 8). Pyruvate kinase (PK) is the enzyme that catalyzes

the final step in glycolysis, converting phosphoenolpyruvate (PEP) to pyruvate (30). Four different isoforms of pyruvate kinase exist: type-R and type-L are generated by alternative splicing of the *PKLR* gene and are expressed in erythrocytes and in liver, respectively (31). PKM1 is the isoform expressed in adult skeletal muscle while PKM2, which results from alternative splicing of the *PKM* gene is expressed exclusively in embryonic and proliferating tissues. Notably, PKM2 is the only isoform allosterically regulated due to its possibility to switch from a dimeric low-active form to a tetrameric very high active form (32-34). In addition, phosphorylation of S37 and Y105 in PKM2 prevents the binding of the PKM2 cofactor fructose-1,6-bisphosphate, thus inhibiting the active tetrameric form of PKM2 which promotes aerobic glycolysis and tumor growth (35) (Fig. 5). Moreover, PKM2 also has a "non-metabolic" role in tumorigenesis since its translocation into the nucleus regulates gene transcription of several pathways involved in metabolic reprograming, cell proliferation and cancer development (36-39) (Fig. 5).

Strikingly, and highly consistent with the increased cancer incidence observed in DM patients (10, 27-29), we found an elevated expression of the mitochondrial ATPase Inhibitory Factor 1 (IF1) in DM biopsies. In fact, IF1 is higly overexpressed in most prevalent human carcinomas (20, 40) in its active non-phosphorylated form (41). Overexpression of IF1 interferes with oxidative phosphorylation by inhibiting the H^+-ATP synthase and promoting aerobic glycolysis and signaling via reactive oxygen species (ROS) a pro-oncogenic phenotype (Fig. 5) that enhances by triggering proliferation, invasion and cell survival (20, 42, 43). More recently, the overexpression of IF1 in human hepatocellular carcinomas, bladder and gastric cancers, and in gliomas has provided a valuable biomarker of cancer prognosis (44-47). Mechanistically, the pro-oncogenic features of IF1 over-expression stem from its effects on favoring

proliferation, cell death resistence, EMT and angiogenesis (42-44, 48) Altogether, we suggest that the increased expression of PKM2 and IF1 cooperate to promote a metabolic phenotype in DM that is prone for the onset of oncogenesis (Fig 5). These findings might stimulate the investigation of further therapeutic approaches for the management of DM patients in order to prevent their higher incidence of cancer.

Acknowledgements

FS was supported by a pre-doctoral fellowship from FPI-UAM Spain. The work was supported by grants from the Ministerio de Economía y Competitividad (SAF 2013-41945-R), Fundación Ramón Areces (FRA), Centro de Investigación Biomédica en Red de Enfermedades Raras (CIBERER), ISCIII, and Comunidad de Madrid (S2011/BMD-2402), Spain. The CBMSO receives an institutional grant from FRA.

Competing financial interests

The authors declare no competing financial interests

Author's contributions

F.S. designed the study, carried out analyses, interpreted data and wrote the manuscript. M.S-A. interpreted data and drafted the manuscript. M.C.G., G.G. and F.G., recruit, studied and sampled patients. J.M.C. conceptualized and designed the study, interpreted data and wrote the manuscript. All authors read and approved the final manuscript.

Figure legends

Figure 1. Validation of the antibodies used in RPPA. Tissue extract (40 µg) derived from human muscle (M) were fractionated on SDS-PAGE gels, blotted against the indicated antibodies and processed for western blotting. Only antibodies that recognize a single protein band of the expected molecular mass were used in the study. The migration of molecular mass markers is indicated to the left.

Figure 2. Printing of RPPA. A, The scheme of printing of RPPA processed for antibody against PKM2 are shown magnified for details. One nl samples were spotted in triplicate. Black boxed: negative controls of BSA; Magenta boxed: standard curves of HCT116 cells; Brown boxed: positive controls of murine IgGs; Green boxed: samples from control donors; Yellow boxed: PM samples; Red boxed: DM samples; Blue boxed: IBM samples. Below are shown representative RPPAs processed with other antibodies. **B,** The plot illustrates the linear correlation that exists between the fluorescence intensity (arbitrary units, a.u.) and the amount of PKM2 in HCT116 cell lysates. Protein concentrations in the biopsies were calculated according to the fluorescence intensity obtained in the standard curve of HCT116 cells. For other details see Supplemental Fig. S1.

Figure 3. Expression values of proteins of energy metabolism and distribution in control and IMs groups. The Y axis indicates the values of intensity (a.u) calculated by interpolation in the linear plot of HCT116 cells. The X axis represent patient samples from PM, DM and IBM and the control (CTR) group. Box plots represent the lowest, lower quartile, median, upper quartile and highest observations of each marker in the

different groups of pathologies. ○, outlier values and; *, extreme values. The boxed * and ** in the X-axis indicates a, $p<0.05$ and $p<0.001$ when compared to controls, respectively.

Figure 4. Hierarchical clustering analyses of the biopsies using enzymes of energy metabolism. Rows indicate type of sample; columns, proteins and derived ratios. Protein expression scores are shown normalized to the mean relative expression level in normal samples in panels A, B, and C, according to a color scale (below panels): red, high; black, normal; green, low expression. The dendogram (to the right of the matrix) represents overall similarities in expression profiles. The maximum and minimum values of the markers for each cluster are shown. **A,** Clustering of control (CTR), DM, PM and IBM biopsies using βF1/PKM2 ratio as biomarker. **B,** Clustering of CTR and DM biopsies using PKM2 expression as biomarker. **C,** Clustering of CTR and IBM biopsies using βF1/LDHA ratio and β-actin as biomarkers. **D,** Scheme showing the contribution of four biomarkers to discriminate CTR, DM and IBM biopsies attending to high (red) or low (green) expression levels. For the additional details see Table 1.

Figure 5. Metabolic reprograming in dermatomyositis.

The scheme highlights the primary flux of energy provision pathways in the muscle of Normal and Dermatomyositis (DM) patients. In Normal biopsies, most of the glucose taken up by the cell is oxidized in mitochondria to generate a high yield of ATP by oxidative phosphorylation. Mitochondrial activity also generates a little amount of reactive oxygen species (ROS) in the respiratory chain. In contrast, in muscle cells of DM patients, glucose is partially oxidized in the cytoplasm to generate metabolic intermediates by the blockage imposed on the glycolytic pathway by overexpression of

the less active PKM2 isoform. Moreover, the overexpression of the ATPase Inhibitory Factor 1 (IF1) in mitochondria also restrains pyruvate oxidation, limiting ATP availability and enhances the production of reactive oxygen species (ROS). Diversion of the glycolytic flux by blockade of glycolysis and oxidative phosphorylation provides the metabolic intermediates that become precursors for the biosynthesis of the macromolecules required for cellular proliferation. PKM2 on its "non-metabolic" attributes translocates into the nucleus and activates the transcription of several genes involved in cancer development (36-39). Likewise, the IF1-mediated inhibition of the H^+-ATP synthase generates a ROS signal that activates in the nucleus of the cell programs involved with proliferation, cell death resistance, angiogenesis and invasion (40, 42-47). Thus, the concurrent increase of PKM2 and IF1 expression in the muscle of DM patients leads to metabolic rewiring and ROS signaling that are hallmarks of the oncogenic phenotype.

Table 1. Potential diagnostic sensitivity of some biomarkers in inflammatory myopathies.

The table summarizes the power to discriminate (sensitivity) the indicate myopathies by the value of the indicated markers. Sensitivity was calculated accordingly to the classification rate of the positive samples following the formula: Sensitivity = true positives / (true positives + false positives). Specificity = trues negatives / (true negatives + false positives).

Diseases		Markers			Sensitivity	Specificity
Controls	***all***	Actin	PKM2	βF1/Hsp60	96%	100%
	DM	PK-M2			100%	100%
	IBM	Actin	βF1/LDHA		100%	100%
DM	***all***	βF1/PKM2			95%	100%
	CTR				100%	100%
	PM				100%	100%
	IBM				90%	100%

Supplemental Material

Supplemental Figure S1. Linear correlation between the fluorescence intensity and the content of native proteins. HCT116 cell line extracts (0–1 μg/μl) were spotted in the arrays (see Figure 2A). Significant linear correlations were obtained between the fluorescence intensity (arbitrary units, a.u.) of the spots and the amount of the protein interrogated in the arrays. Protein concentrations in the biopsies were calculated by interpolation in the respective linear plots.

Supplemental Figure S2. Overexpression of PKM2 in DM. A, Tissue extracts (30 μg) derived from two randomly selected muscle biopsies of control donors (CTR), polymyositis (PM), dermatomyositis (DM) and inclusion body myositis (IBM) and of the HCT116 cell line were fractionated on SDS-PAGE and blotted against anti-PKM2, anti-GAPDH and anti-LDH-A. Electrophoresis of the protein is indicated to the left of each blot. **B,** Histograms show the expression of the proteins (a.u.) when compared to the expression in HCT116 cells.

Supplemental Figure S3. Plasma levels of PKM2 by ELISA and RPPA. A, Determination of PKM2 by ELISA in plasma samples of DM, IBM and CRL patients. **B,** Upper panel, scheme of printing of the plasma samples from CRL, IBM, DM and PM patients. One nl of 1:20 diluted samples were spotted in quadruplicate. Black boxed: negative controls of BSA; Orange boxed: standard curves of HCT116 cells; Magenta boxed: positive controls of murine IgGs; Deep green boxed: standard curve of PKM2 recombinant protein; Blue boxed: samples from control donors (CTR); Light green boxed: samples from IBM patients; Red boxed: samples from DM patients;

Yellow boxed: sample from PM patients. Lower panel, parallel array processed with goat anti-mouse IgGs CF647 as negative control. Please note the lack of cross-reactivity against the human plasma IgGs. **C,** The histogram shows the plasma levels of PKM2 quantified by RPPA assay. The results shown are means ± S.E.M.

References

1. Cuezva JM, Krajewska M, de Heredia ML, Krajewski S, Santamaria G, Kim H, et al. The bioenergetic signature of cancer: A marker of tumor progression. Cancer Res 2002;62:6674-81.
2. Santacatterina F, Chamorro M, Nuñez de Arenas C, Navarro C, Martin MA, Cuezva JM, Sánchez-Aragó M. Quantitative analysis of proteins of metabolism by reverse phase protein microarrays identifies potential biomarkers of rare neuromuscular diseases. J Trans Med 2015;13:65.
3. Boccuto L, Chen CF, Pittman AR, Skinner CD, McCartney HJ, Jones K, et al. Decreased tryptophan metabolism in patients with autism spectrum disorders. Mol Autism 2013;4:16.
4. Vander Heiden MG, Cantley LC, Thompson CB. Understanding the warburg effect: The metabolic requirements of cell proliferation. Science 2009;324:1029-33.
5. Willers IM, Cuezva JM. Post-transcriptional regulation of the mitochondrial h(+)-atp synthase: A key regulator of the metabolic phenotype in cancer. Biochimica et biophysica acta 2011;1807:543-51.
6. Aldea M, Clofent J, Nunez de Arenas C, Chamorro M, Velasco M, Berrendero JR, et al. Reverse phase protein microarrays quantify and validate the bioenergetic signature as biomarker in colorectal cancer. Cancer Lett 2011;311:210-8.
7. Sanchez-Arago M, Cuezva JM. The bioenergetic signature of isogenic colon cancer cells predicts the cell death response to treatment with 3-bromopyruvate, iodoacetate or 5-fluorouracil. J Transl Med 2011;9:19.
8. Cuezva JM, Ortega AD, Willers I, Sanchez-Cenizo L, Aldea M, Sanchez-Arago M. The tumor suppressor function of mitochondria: Translation into the clinics. Biochimica et biophysica acta 2009;1792:1145-58.
9. Pelicano H, Martin DS, Xu RH, Huang P. Glycolysis inhibition for anticancer treatment. Oncogene 2006;25:4633-46.
10. Dalakas MC, Hohlfeld R. Polymyositis and dermatomyositis. Lancet 2003;362:971-82.
11. Dalakas MC. Inflammatory muscle diseases. N Engl J Med 2015;372:1734-47.
12. Bohan A, Peter JB. Polymyositis and dermatomyositis (first of two parts). N Engl J Med 1975;292:344-7.
13. Mastaglia FL, Phillips BA. Idiopathic inflammatory myopathies: Epidemiology, classification, and diagnostic criteria. Rheum Dis Clin North Am 2002;28:723-41.
14. Catalan M, Selva-O'Callaghan A, Grau JM. Diagnosis and classification of sporadic inclusion body myositis (sibm). Autoimmun Rev 2014;13:363-6.
15. Mueller C, Liotta LA, Espina V. Reverse phase protein microarrays advance to use in clinical trials. Mol Oncol 2010;4:461-81.
16. Tibes R, Qiu Y, Lu Y, Hennessy B, Andreeff M, Mills GB, Kornblau SM. Reverse phase protein array: Validation of a novel proteomic technology and utility for analysis of primary leukemia specimens and hematopoietic stem cells. Molecular cancer therapeutics 2006;5:2512-21.
17. Michaud GA, Salcius M, Zhou F, Bangham R, Bonin J, Guo H, et al. Analyzing antibody specificity with whole proteome microarrays. Nat Biotechnol 2003;21:1509-12.

18. Strausberg RL, Simpson AJ, Old LJ, Riggins GJ. Oncogenomics and the development of new cancer therapies. Nature 2004;429:469-74.

19. Acebo P, Giner D, Calvo P, Blanco-Rivero A, Ortega AD, Fernandez PL, et al. Cancer abolishes the tissue type-specific differences in the phenotype of energetic metabolism. Transl Oncol 2009;2:138-45.

20. Sanchez-Cenizo L, Formentini L, Aldea M, Ortega AD, Garcia-Huerta P, Sanchez-Arago M, Cuezva JM. Up-regulation of the atpase inhibitory factor 1 (if1) of the mitochondrial h+-atp synthase in human tumors mediates the metabolic shift of cancer cells to a warburg phenotype. The Journal of biological chemistry 2010;285:25308-13.

21. Yizhak K, Le Devedec SE, Rogkoti VM, Baenke F, de Boer VC, Frezza C, et al. A computational study of the warburg effect identifies metabolic targets inhibiting cancer migration. Mol Syst Biol 2014;10:744.

22. Selva O'Callaghan A, Trallero Araguas E. [inflammatory myopathies. Dermatomyositis, polymyositis, and inclusion body myositis]. Reumatol Clin 2008;4:197-206.

23. Ledford H. Metabolic quirks yield tumour hope. Nature 2014;508:158-9.

24. Sereni MI, Pierobon M, Angioli R, Petricoin EF, 3rd, Frederick MJ. Reverse phase protein microarrays and their utility in drug development. Methods Mol Biol 2013;986:187-214.

25. Dalakas MC. Polymyositis, dermatomyositis and inclusion-body myositis. N Engl J Med 1991;325:1487-98.

26. van der Kooi AJ, de Visser M. Idiopathic inflammatory myopathies. Handb Clin Neurol 2014;119:495-512.

27. Sigurgeirsson B, Lindelof B, Edhag O, Allander E. Risk of cancer in patients with dermatomyositis or polymyositis. A population-based study. N Engl J Med 1992;326:363-7.

28. Hill CL, Zhang Y, Sigurgeirsson B, Pukkala E, Mellemkjaer L, Airio A, et al. Frequency of specific cancer types in dermatomyositis and polymyositis: A population-based study. Lancet 2001;357:96-100.

29. Chen YJ, Wu CY, Huang YL, Wang CB, Shen JL, Chang YT. Cancer risks of dermatomyositis and polymyositis: A nationwide cohort study in taiwan. Arthritis Res Ther 2010;12:R70.

30. Robinson JL, Rose IA. The proton transfer reactions of muscle pyruvate kinase. The Journal of biological chemistry 1972;247:1096-105.

31. Tsutsumi H, Tani K, Fujii H, Miwa S. Expression of l- and m-type pyruvate kinase in human tissues. Genomics 1988;2:86-9.

32. Mazurek S. Pyruvate kinase type m2: A key regulator of the metabolic budget system in tumor cells. Int J Biochem Cell Biol 2011;43:969-80.

33. Anastasiou D, Yu Y, Israelsen WJ, Jiang JK, Boxer MB, Hong BS, et al. Pyruvate kinase m2 activators promote tetramer formation and suppress tumorigenesis. Nature chemical biology 2012;8:839-47.

34. DeLaBarre B, Hurov J, Cianchetta G, Murray S, Dang L. Action at a distance: Allostery and the development of drugs to target cancer cell metabolism. Chemistry & biology 2014;21:1143-61.

35. Hitosugi T, Kang S, Vander Heiden MG, Chung TW, Elf S, Lythgoe K, et al. Tyrosine phosphorylation inhibits pkm2 to promote the warburg effect and tumor growth. Sci Signal 2009;2:ra73.

36. Iqbal MA, Gupta V, Gopinath P, Mazurek S, Bamezai RN. Pyruvate kinase m2 and cancer: An updated assessment. FEBS letters 2014;588:2685-92.

37. Wang HJ, Hsieh YJ, Cheng WC, Lin CP, Lin YS, Yang SF, et al. Jmjd5 regulates pkm2 nuclear translocation and reprograms hif-1alpha-mediated glucose metabolism. Proceedings of the National Academy of Sciences of the United States of America 2014;111:279-84.

38. Luo W, Hu H, Chang R, Zhong J, Knabel M, O'Meally R, et al. Pyruvate kinase m2 is a phd3-stimulated coactivator for hypoxia-inducible factor 1. Cell 2011;145:732-44.

39. Yang W, Xia Y, Ji H, Zheng Y, Liang J, Huang W, et al. Nuclear pkm2 regulates beta-catenin transactivation upon egfr activation. Nature 2011;480:118-22.

40. Sanchez-Arago M, Formentini L, Martinez-Reyes I, Garcia-Bermudez J, Santacatterina F, Sanchez-Cenizo L, et al. Expression, regulation and clinical relevance of the atpase inhibitory factor 1 in human cancers. Oncogenesis 2013;2:e46.

41. Garcia-Bermudez J, Sanchez-Arago M, Soldevilla B, Del Arco A, Nuevo-Tapioles C, Cuezva JM. Pka phosphorylates the atpase inhibitory factor 1 and inactivates its capacity to bind and inhibit the mitochondrial h-atp synthase. Cell Rep 2015;12:2143-55.

42. Formentini L, Sánchez-Aragó M, Sánchez-Cenizo L, Cuezva JM. The mitochondrial atpase inhibitory factor 1 (if1) triggers a ros-mediated retrograde pro-survival and proliferative response. Mol Cell 2012;45:731-42.

43. Santacatterina F, Sanchez-Cenizo L, Formentini L, Mobasher MA, Casas E, Rueda CB, et al. Down-regulation of oxidative phosphorylation in the liver by expression of the atpase inhibitory factor 1 induces a tumor-promoter metabolic state. Oncotarget 2015.

44. Song R, Song H, Liang Y, Yin D, Zhang H, Zheng T, et al. Reciprocal activation between atpase inhibitory factor 1 and nf-kappab drives hepatocellular carcinoma angiogenesis and metastasis. Hepatology 2014;60:1659-73.

45. Wei S, Fukuhara H, Kawada C, Kurabayashi A, Furihata M, Ogura S, et al. Silencing of atpase inhibitory factor 1 inhibits cell growth via cell cycle arrest in bladder cancer. Pathobiology : journal of immunopathology, molecular and cellular biology 2015;82:224-32.

46. Yin T, Lu L, Xiong Z, Wei S, Cui D. Atpase inhibitory factor 1 is a prognostic marker and contributes to proliferation and invasion of human gastric cancer cells. Biomedicine & pharmacotherapy = Biomedecine & pharmacotherapie 2015;70:90-6.

47. Wu J, Shan Q, Li P, Wu Y, Xie J, Wang X. Atpase inhibitory factor 1 is a potential prognostic marker for the migration and invasion of glioma. Oncology letters 2015;10:2075-80.

48. Garcia-Bermudez J, Cuezva JM. The atpase inhibitory factor 1 (if1): A master regulator of energy metabolism and of cell survival. Biochimica et biophysica acta 2016.

Figure 1

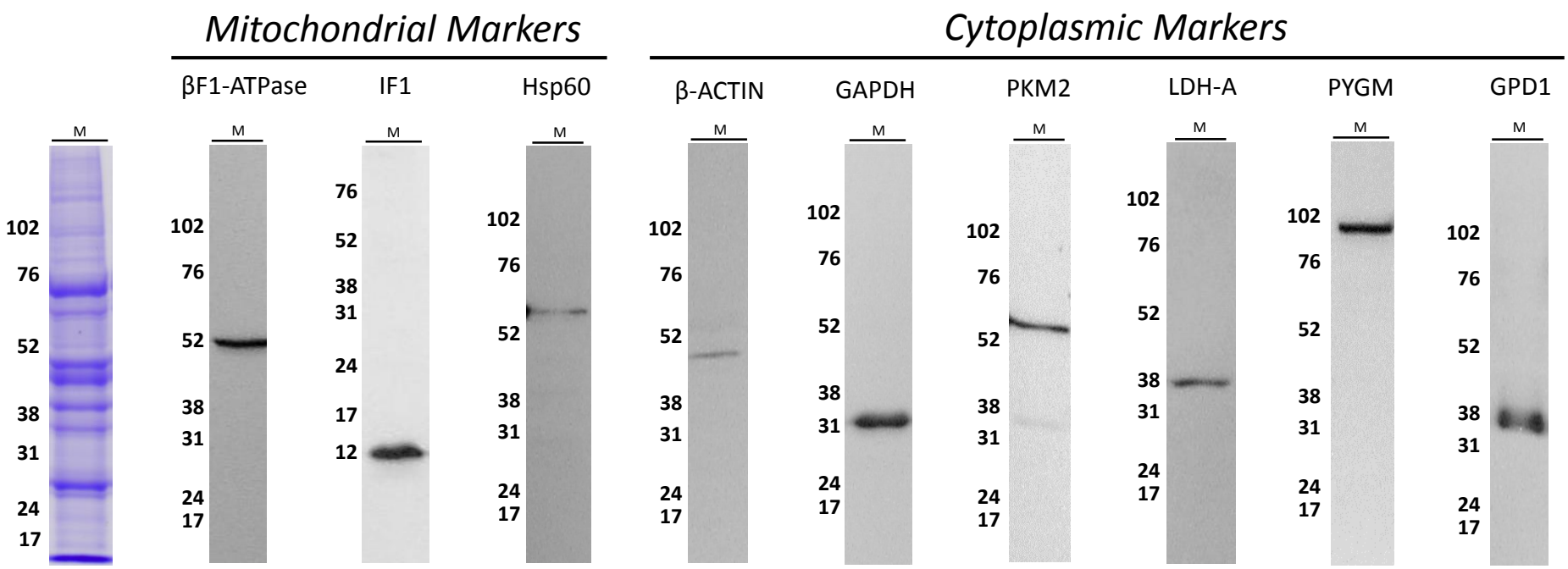
Mitochondrial Markers
Cytoplasmic Markers
βF1-ATPase
IF1
Hsp60
β-ACTIN
GAPDH
PKM2
LDH-A
PYGM
GPD1
M
102
76
52
38
31
24
17
12

Figure 2

A

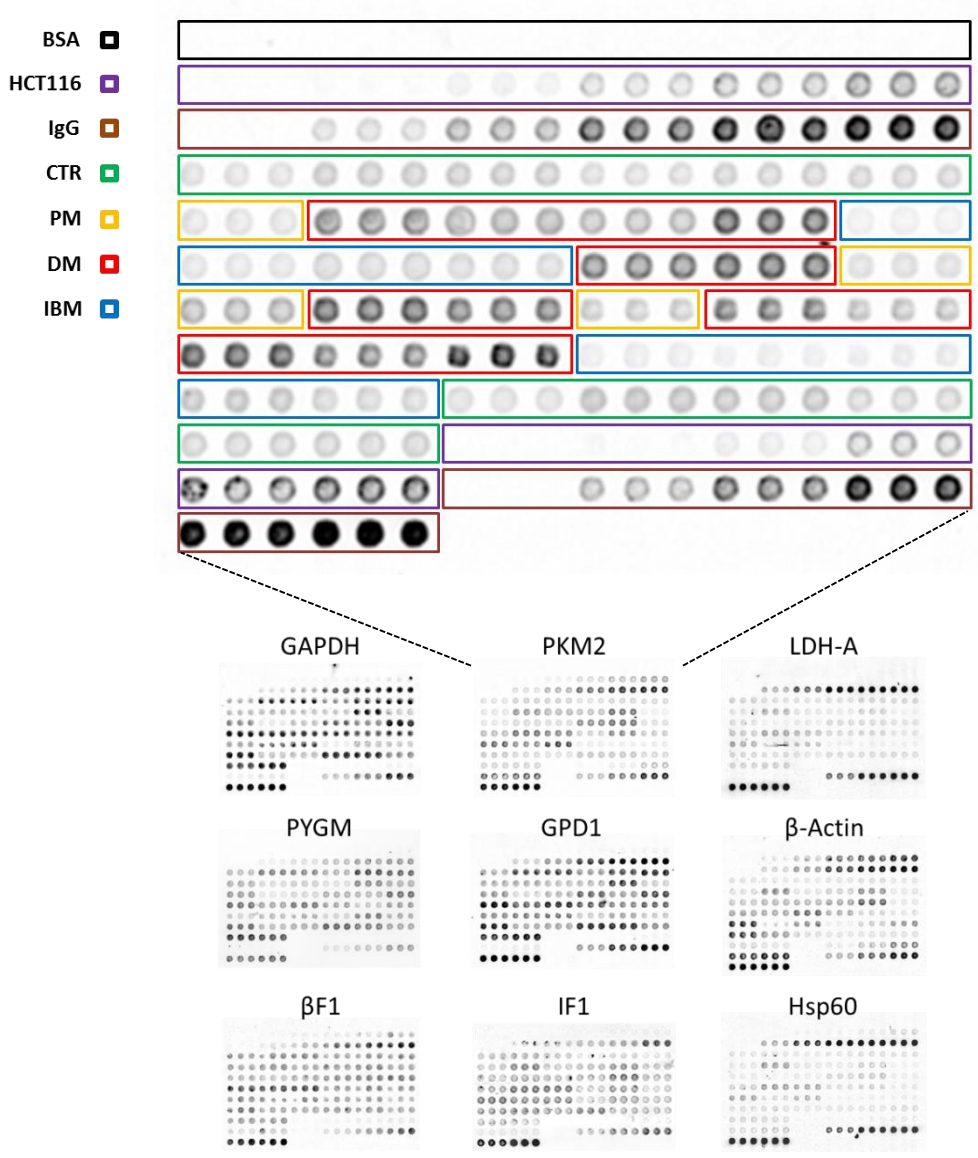
BSA
HCT116
IgG
CTR
PM
DM
IBM
GAPDH
PKM2
LDH-A
PYGM
GPD1
β-Actin
βF1
IF1
Hsp60

B

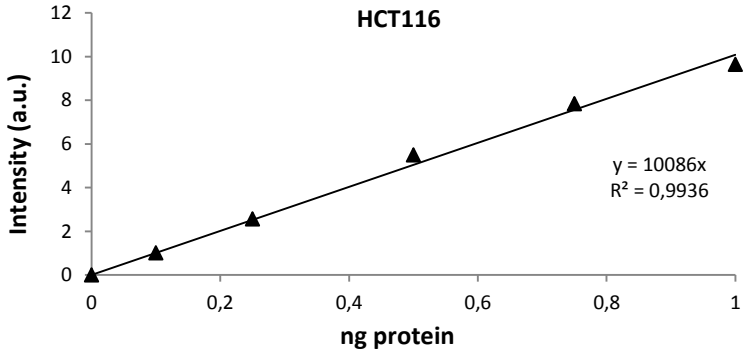
HCT116
Intensity (a.u.)
ng protein
y = 10086x
R² = 0,9936
0
2
4
6
8
10
12
0
0,2
0,4
0,6
0,8
1

Figure 3

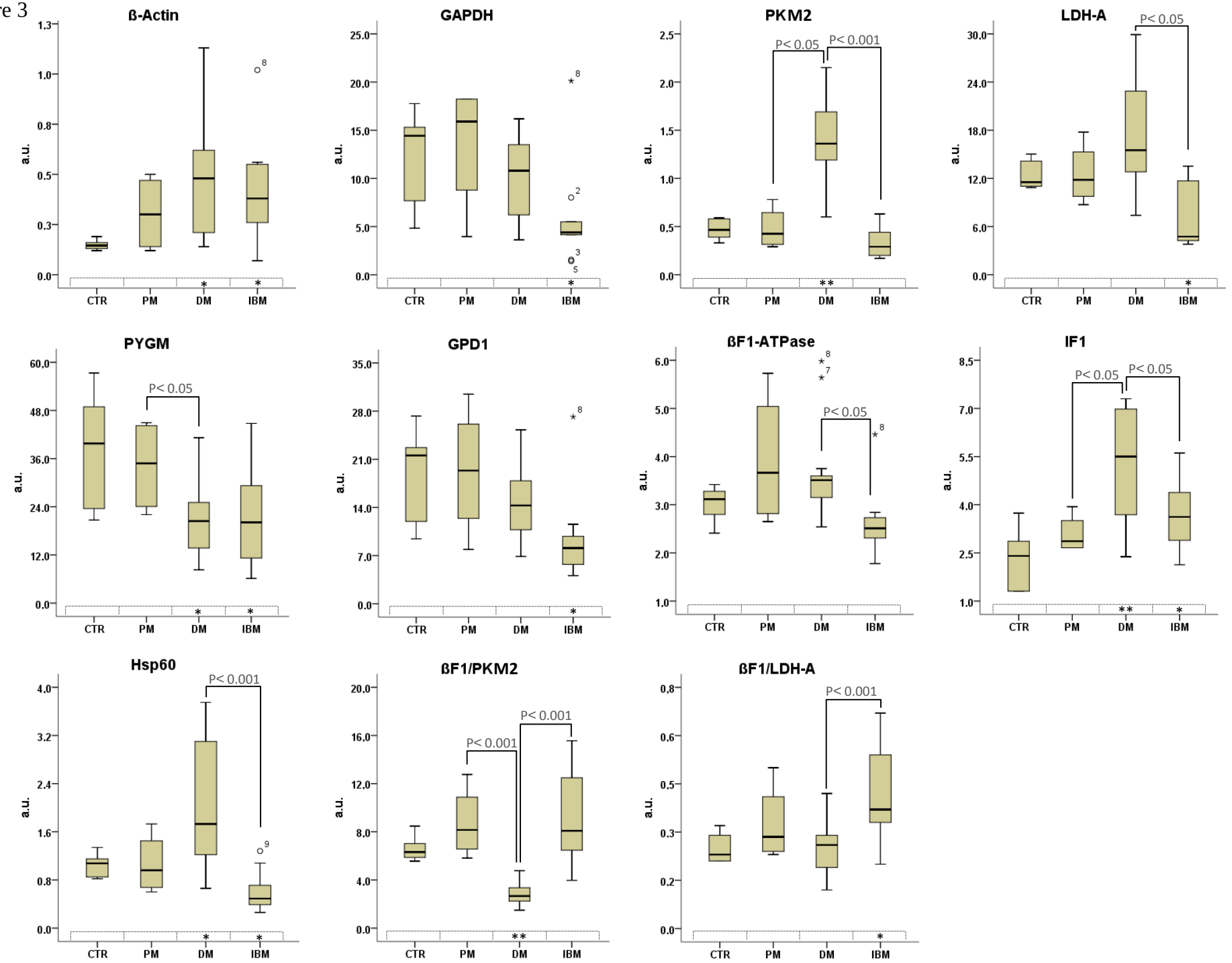
ß-Actin
GAPDH
PKM2
LDH-A
PYGM
GPD1
ßF1-ATPase
IF1
Hsp60
ßF1/PKM2
ßF1/LDH-A
a.u.
CTR
PM
DM
IBM
P< 0.05
P< 0.001

Figure 4

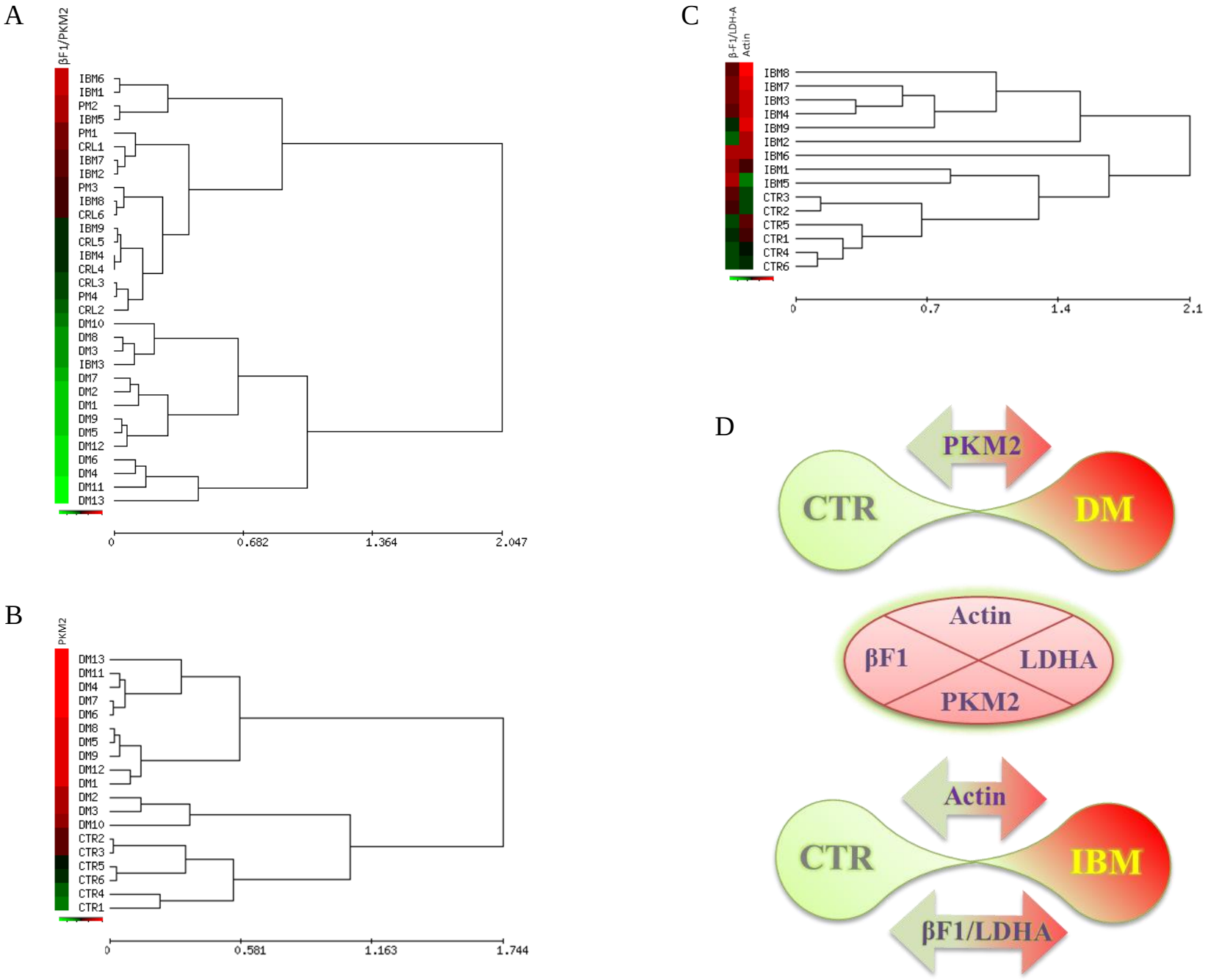
A
βF1/PKM2
IBM6
IBM1
PM2
IBM5
PM1
CRL1
IBM7
IBM2
PM3
IBM8
CRL6
IBM9
CRL5
IBM4
CRL4
CRL3
PM4
CRL2
DM10
DM8
DM3
IBM3
DM7
DM2
DM1
DM9
DM5
DM12
DM6
DM4
DM11
DM13
0
0.682
1.364
2.047
B
PKM2
DM13
DM11
DM4
DM7
DM6
DM8
DM5
DM9
DM12
DM1
DM2
DM3
DM10
CTR2
CTR3
CTR5
CTR6
CTR4
CTR1
0
0.581
1.163
1.744
C
β-F1/LDH-A
Actin
IBM8
IBM7
IBM3
IBM4
IBM9
IBM2
IBM6
IBM1
IBM5
CTR3
CTR2
CTR5
CTR1
CTR4
CTR6
0
0.7
1.4
2.1
D
PKM2
CTR
DM
Actin
βF1
LDHA
PKM2
Actin
CTR
IBM
βF1/LDHA

Figure 5

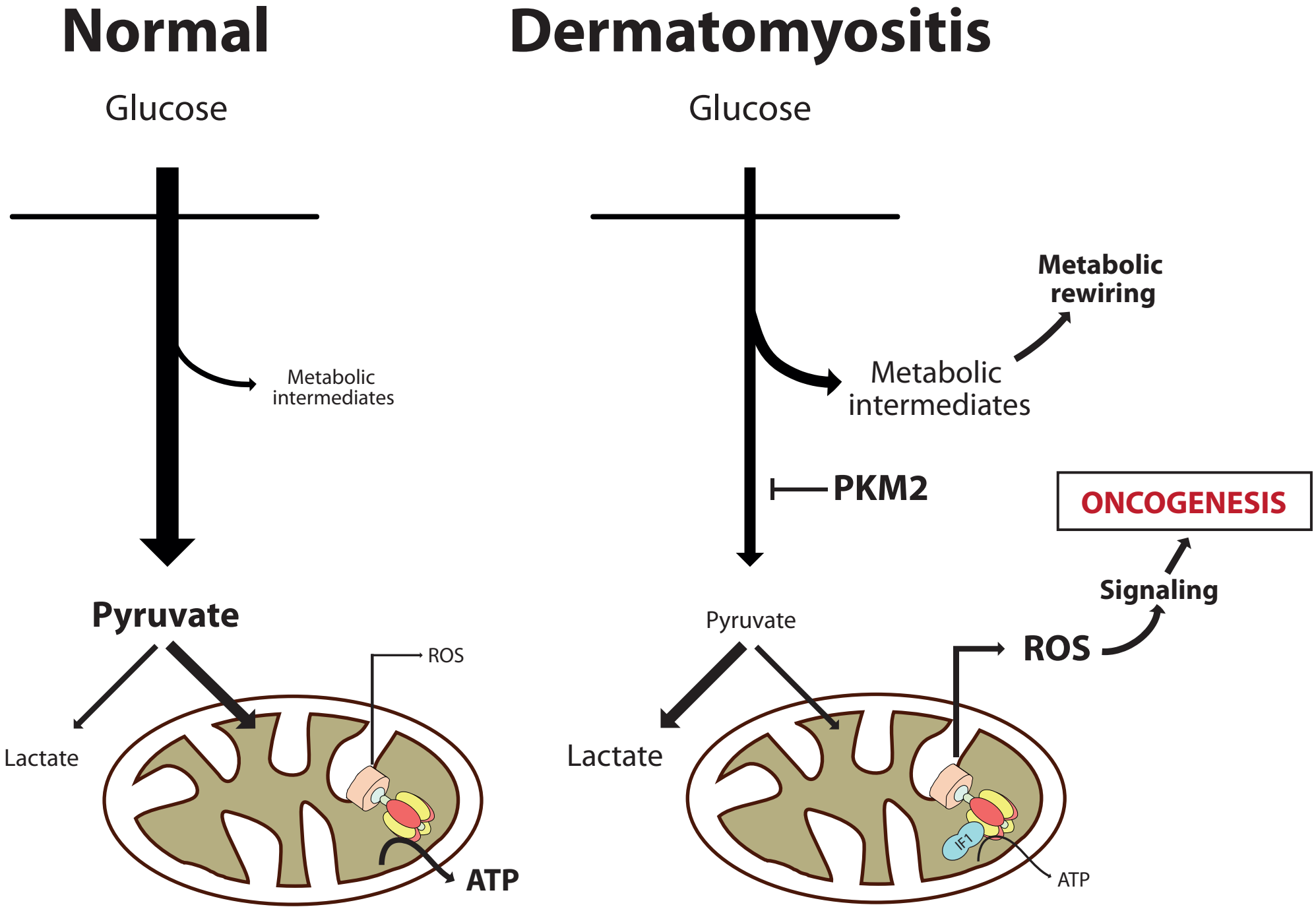
Normal
Dermatomyositis
Glucose
Glucose
Metabolic intermediates
Metabolic rewiring
Metabolic intermediates
PKM2
ONCOGENESIS
Signaling
Pyruvate
Pyruvate
ROS
ROS
Lactate
Lactate
IF1
ATP
ATP

Figure S1

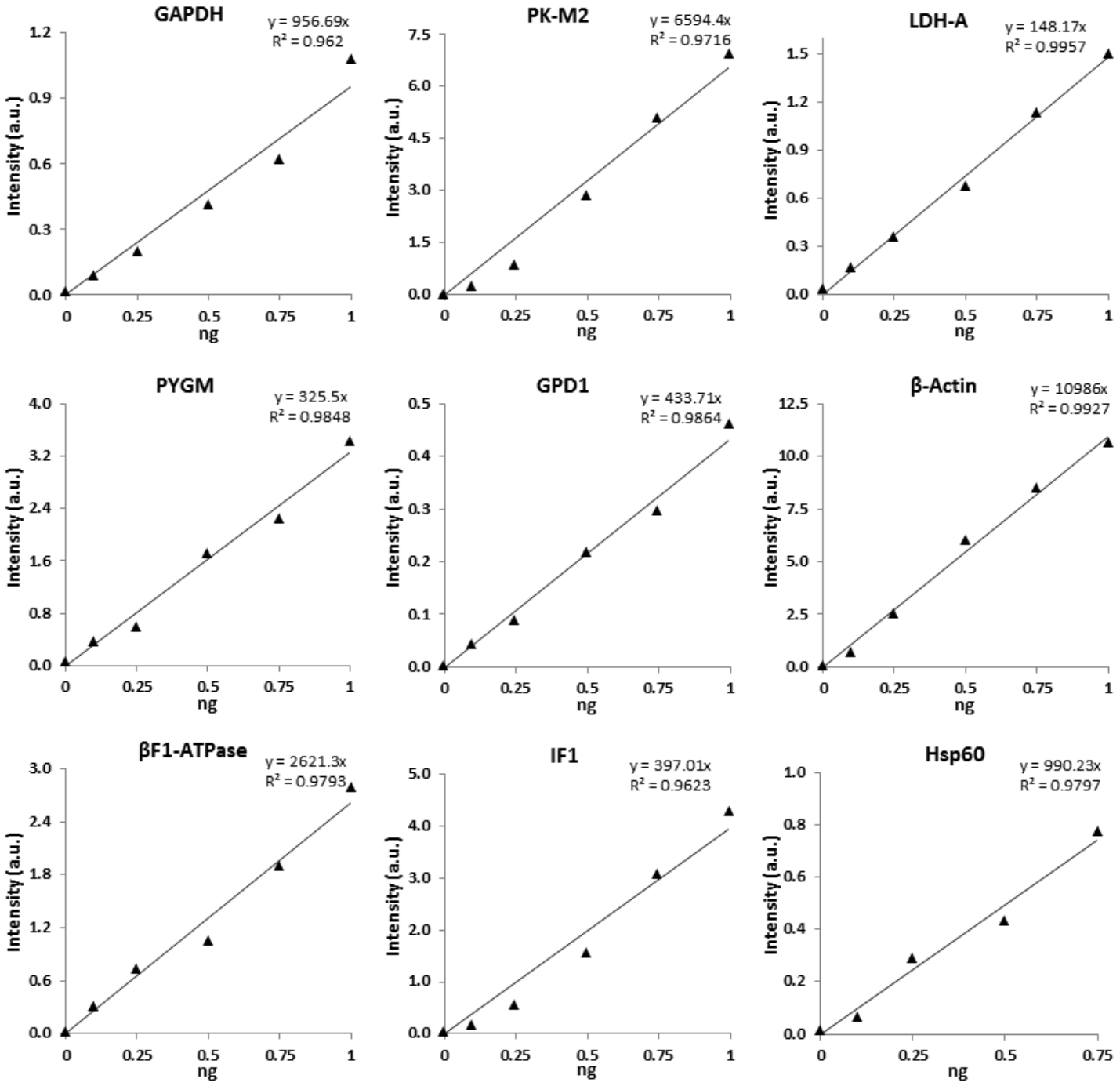
GAPDH
y = 956.69x
R² = 0.962
PK-M2
y = 6594.4x
R² = 0.9716
LDH-A
y = 148.17x
R² = 0.9957
PYGM
y = 325.5x
R² = 0.9848
GPD1
y = 433.71x
R² = 0.9864
β-Actin
y = 10986x
R² = 0.9927
βF1-ATPase
y = 2621.3x
R² = 0.9793
IF1
y = 397.01x
R² = 0.9623
Hsp60
y = 990.23x
R² = 0.9797
Intensity (a.u.)
ng

Figure S2

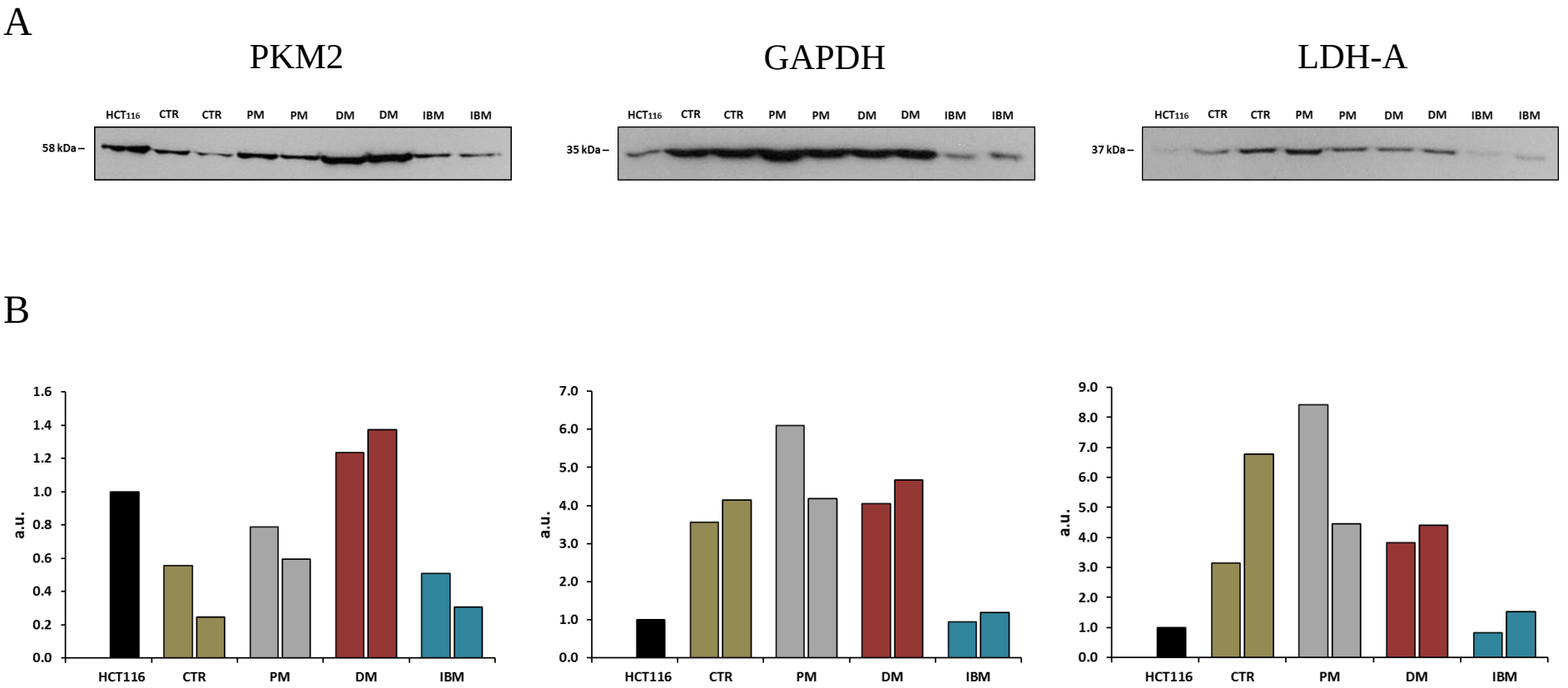
A
PKM2
GAPDH
LDH-A
HCT116 CTR CTR PM PM DM DM IBM IBM
58 kDa –
35 kDa –
37 kDa –
B
a.u.
HCT116
CTR
PM
DM
IBM

Figure S3

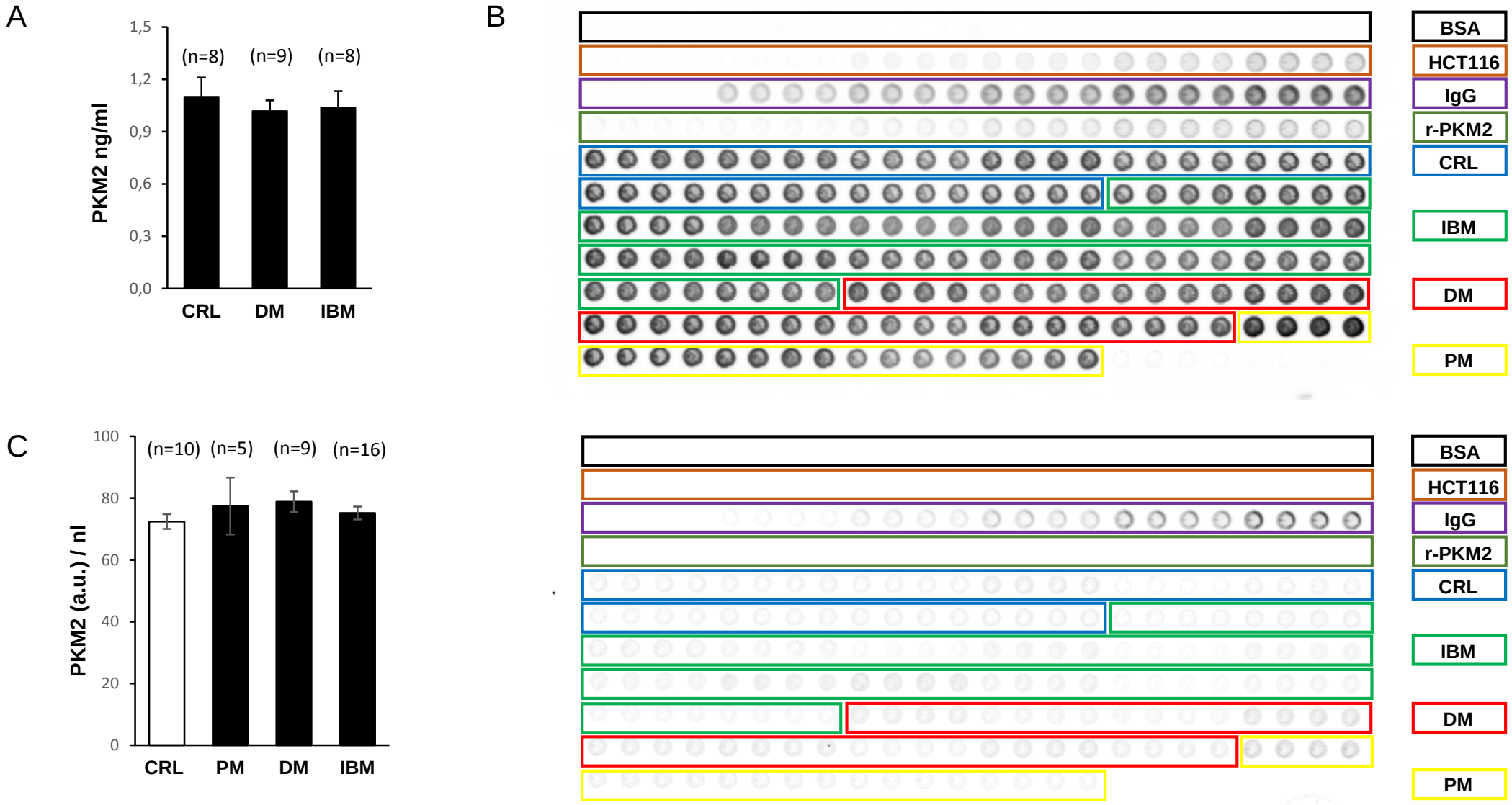
A
1,5
1,2
0,9
0,6
0,3
0,0
PKM2 ng/ml
(n=8)
(n=9)
(n=8)
CRL
DM
IBM
B
BSA
HCT116
IgG
r-PKM2
CRL
IBM
DM
PM
C
100
80
60
40
20
0
PKM2 (a.u.) / nl
(n=10)
(n=5)
(n=9)
(n=16)
CRL
PM
DM
IBM
BSA
HCT116
IgG
r-PKM2
CRL
IBM
DM
PM

DISCUSIÓN

2 Discusión

2.1 Adaptación metabólica por una OXPHOS reprimida

La desregulación del metabolismo energético, considerada previamente como un epifenómeno del cáncer, juega un papel esencial en la reprogramación oncogénica pudiendo controlar eventos genéticos y epigenéticos de las células. Debido al papel fundamental de IF1 como regulador del metabolismo, cada vez existen más estudios que van, paso a paso, determinando su importancia tanto en condiciones fisiológicas como en patología. Además de su papel como inhibidor de la actividad hidrolasa en condiciones de hipoxia (Cabezon *et al.*, 2003; Faccenda *et al.*, 2013; Galante *et al.*, 1981; Gledhill *et al.*, 2007; Pullman and Monroy, 1963), en los últimos años se ha demostrado la capacidad inhibitoria de IF1 o de su forma mutante H49K también con respecto a la actividad sintética de la ATP sintasa *in vitro* (Formentini *et al.*, 2012; Sanchez-Cenizo *et al.*, 2010) (**Artículo #1**; **Artículo #4**) como *in vivo* (Shen *et al.*, 2009) (**Artículo #2; Artículo 3#**). Además, hemos descrito cómo los niveles de expresión de este regulador del metabolismo energético varían significativamente entre diferentes tejidos humanos en relación a los requerimientos energéticos característicos de cada uno de ellos poniendo de manifiesto la paradoja de que tejidos con alta demanda energética tienen altos niveles de expresión del inhibidor (Sanchez-Cenizo *et al.*, 2010) (**Artículo #3**; **Artículo #1**, Fig. 1 y 2).

Concretamente, en el **Artículo #1** hemos visto cómo la expresión de IF1 está fuertemente inducida en algunos de los carcinomas humanos más prevalentes (colon, pulmón, mama y ovario), mientras que su expresión es mínima en los respectivos tejidos normales evaluada por western blot como por inmunohistoquímica (IHQ) (**Artículo #1**, Fig. 1 y 2). Sin embargo, la expresión de IF1 en tejido normal de estómago, endometrio y riñón no mostraba diferencias significativas en comparación con los respectivos tejidos tumorales (**Artículo #1**, Fig. 1 y 2), poniendo de manifiesto las diferencias tejido específicas en la regulación de la expresión de IF1 en cáncer. En este contexto, hemos demostrado que la acumulación de IF1 en carcinomas es independiente de la disponibilidad de mRNA y que la vida media tan corta de IF1 (~100min), representaría un mecanismo adicional de regulación de la expresión génica para adaptarse rápidamente a las fluctuaciones fisiopatológicas de la célula.

En nuestro grupo, se ha descrito cómo IF1 al bloquear la actividad de la ATP sintasa, promueve la activación de la glucolisis aerobia que está asociada a la proliferación (revisado en (Cuezva *et al.*, 2009)) y a su vez, produce una señal de ROS mitocondriales que activa una respuesta adaptativa encaminada a prevenir la muerte celular (Formentini *et al.*, 2012; Martinez-Reyes and Cuezva, 2014) (**Artículo #1**; **#2**; **#3**). A pesar de las diferencias en los niveles de expresión de IF1, la protección frente a muerte celular inducida por la señalización retrograda de ROS al núcleo, se manifestaba en todos los tipos celulares estudiados. Contrariamente, la estimulación de la proliferación que se observa en colon (Formentini *et al.*, 2012), no ocurre en carcinomas de mama, pulmón y ovario (**Artículo #1**). Estos resultados indican que existen programas de respuesta nuclear a la señalización por ROS que son comunes y otros específicos de cada tipo celular. Paradójicamente, la expresión de IF1 es

prácticamente paralela a su proteína diana, la β-F1 ATPasa, es decir, los niveles de expresión de IF1 son muy elevados en tejidos humanos con alta demanda energética como hígado, cerebro, corazón y riñón. Esta observación sugiere la existencia de mecanismos de regulación de la actividad del inhibidor no descritos hasta la fecha, además de la bien caracterizada regulación de su capacidad de unión a la ATP sintasa dependiente del pH mitocondrial (Cabezon *et al.*, 2000b). En efecto, IF1 puede estar sujeta a otros tipos de regulación mediados por la unión a otras proteínas (Lopez-Mediavilla *et al.*, 1993) y/o, por modificaciones covalentes por fosforilación como hemos descrito muy recientemente (Garcia-Bermudez *et al.*, 2015) (**Artículo #1**; **Artículo #4**).

La profunda reprogramación metabólica dirigida por IF1 o por su forma mutante H49K (Sanchez-Cenizo *et al.*, 2010), vista tanto en células cancerígenas y tumores humanos (Formentini *et al.*, 2012) (**Artículo #1**) como también en enfermedades con defectos en OXPHOS (Chen *et al.*, 2014), ha llevado a nuestro grupo a generar modelos de ratón que permiten estudiar el efecto de esta proteína en distintas situaciones fisiopatológicas. Así hemos generado el modelo de ratón transgénico que integra el gen de IF1 humano (hIF1), o de su forma mutante insensible al pH H49K (Cabezon *et al.*, 2000b; Schnizer *et al.*, 1996), bajo el control del elemento de respuesta a tetraciclina (TRE). El cruce con ratones transgénicos que expresan un transactivador tTA (Tet-Off) o rtTA-Advance (Tet-On) bajo el control de un promotor especifico de hígado (LAP), o de neurona (CAmK), da lugar a un ratón doble transgénico (T/H) que expresa nuestra proteína exclusivamente en hígado o en neurona de forma regulada por doxiciclina (Dox). El modelo de sobreexpresión de H49K en hígado y en cerebro nos ha valido para profundizar en la posible regulación de la actividad de la CTE por el complejo V así como para verificar en hígado el papel supresor de tumores que tiene la OXPHOS en hepatocarcinogénesis inducida.

En los modelos Tet-On y Tet-Off de hígado se demostró que los ratones que sobreexpresan el transgén no tenían alteraciones fenotípicas en el peso, longevidad y comportamiento, ni diferencias en la expresión de proteínas de los complejos OXPHOS tras un año de seguimiento (**Artículo #2**). A pesar de esto, la inhibición de la ATP sintasa mediada por H49K resultaba en una disminución de la respiración y de la fosforilación de ADP, como se demostró por análisis polarográfico en mitocondrias aisladas y por activación de AMPK, lo que compromete el desarrollo de la gluconeogénesis en hígado y propicia la hipoglucemia de los ratones tras el ayuno (**Artículo #2** Fig. 1). En el modelo de cerebro se verificó también que la sobreexpresión del transgén promueve la reprogramación metabólica a una activa glucolisis aerobia (**Artículo #3**).

Ha sido ampliamente descrito que la Dox posee la capacidad de inhibir la producción de proteínas mitocondriales (Onoda *et al.*, 2004; Son *et al.*, 2009) y promover la respuesta mitocondrial a proteínas no plegadas (UPRmt) (Jovaisaite *et al.*, 2014). En este estudio, con el propósito de descartar cualquiera implicación por parte de la Dox en la adaptación metabólica que pudiese venir mediada por la UPRmt, hemos elegido los modelos de ratón Tet-Off que expresan el transgén IF1-H49K en hígado o en neurona en ausencia de Dox. Como en el modelo Tet-On de hígado (**Artículo #2**, Fig. S1), en los

modelos Tet-Off se confirma el fenotipo de represión de OXPHOS mediada por H49K, que es independiente de la administración de Dox y por tanto de UPRmt (**Artículo #2**, Fig 1; **Artículo #3**, Fig. 1).

En ambos modelos experimentales se demostró la localización mitocondrial de hIF1 con la βF1 ATPasa por IHQ e IF (**Artículo #2**, Fig. 1B y S1D) y (**Artículo #3**, Fig. 1B y S1B). El perfil de expresión heterogénea de hIF1 en hígado es exclusivo de este órgano, puesto que en el modelo análogo de expresión de H49K en neuronas resultó homogénea (**Artículo #3**, Fig. 1B y S1B). Si la disminución de la respiración estimulada por ADP en ratones que sobreexpresan H49K podía ser debida a la inhibición de la ATP sintasa, la disminución de la respiración máxima que también observamos en ambos modelos nos hizo suponer que uno o más complejos de la CTE podían estar afectados (**Artículo #2**; **#3**). Efectivamente, en el estudio de los complejos respiratorios y de la actividad en geles nativos (BN-PAGE) del complejo I y IV en mitocondrias aisladas de hígado de ratones Tet-Off, vimos una disminución de la actividad del complejo IV y de sus supercomplejos, mientras que el complejo I no mostraba alteraciones (**Artículo #2**, Fig. 2B). Asimismo, la actividad hidrolítica sensible a oligomicina de la ATP sintasa, estudiada por actividad en geles nativos (CN-PAGE), resultaba fuertemente disminuida en ratones Tet-Off con respecto a los controles, demostrando que la inhibición de OXPHOS causada por la elevada expresión de H49K se produce tanto por la inhibición de la ATP sintasa como por una disminución de la tasa de respiración del complejo IV (**Artículo #2**, Fig. 2C).

Estos resultados apoyan el papel de los supercomplejos en la tasa de respiración (Acin-Perez *et al.*, 2008; Lapuente-Brun *et al.*, 2013), ya que se ve afectada la actividad de la citocromo c oxidasa de forma coincidente con la alteración en la capacidad de ensamblaje de los complejos respiratorios, como vimos por BN-PAGE en los dos modelos de hígado estudiados (**Artículo #2**, Fig. 2D). Se ha observado exactamente el mismo resultado en mitocondrias de neuronas, en el modelo análogo Tet-Off que sobreexpresa H49K, en el cual vimos cómo la mayoría de la subunidad COX IV migraba en forma de monómero, mientras que no observamos cambios en el ensamblaje de los demás complejos mitocondriales (**Artículo #3**, Fig. 2F). Esta pérdida en la formación de supercomplejo IV en neuronas, también se produce con una inhibición de la actividad de la citocromo c oxidasa. Se ha descrito que la citocromo oxidasa tiene regulada su actividad a diferentes niveles como son la regulación alostérica por ATP, fosforilaciones, inactivación mediada por ROS y modulación de su biogénesis y ensamblaje (Acin-Perez *et al.*, 2011; Arnold, 2012; Srinivasan and Avadhani, 2012). Aunque el mecanismo implicado deberá ser objeto de futuras investigaciones, especulamos que una señal moderada de ROS producida por el bloqueo parcial del consumo del gradiente de protones podría, por un mecanismo feed-back, regular la actividad y/o el ensamblaje del complejo IV. De esta manera, la actividad del complejo IV se ajustaría a la capacidad fosforilativa de la ATP sintasa, evitando la hiperpolarización de la membrana y el consecuente aumento en la producción de ROS que desencadenaría la muerte celular (Cogliati *et al.*, 2013).

Por otro lado, la disminución de la actividad del complejo V por la sobreexpresión de H49K se vio asociada a una agregación de este complejo en un supercomplejo (SC) y en el dímero de la ATP sintasa $(CV)_2$ (**Artículo #2**, Fig. 2D). El análisis por espectrofotometría de masas (RP-LC-MS/MS) de las tres bandas más altas en la figura 2D del artículo 2, revela que en la banda SC es el complejo I el componente predominante (**Artículo #2,** Tabla Suplementaria S1). Si bien la banda SC se ha detectado con el anticuerpo anti-βF1-ATPase no podemos afirmar que la co-localización sea debida a una agregación de varios de estos complejos, ya que el reconocimiento puede ser debido a la co-migración de dos elementos no agregados. En este sentido, un estudio por crio-microscopia electrónica ha sugerido que no hay interacción entre el complejo I y el V (Davies *et al.*, 2011). Además, estos resultados apuntan al debate abierto sobre la implicación de IF1 en la dimerización de la ATP sintasa, proporcionando la primera evidencia *in vivo* de que IF1 propicia este proceso (**Artículo #2**, Fig. 2D y Supplemental Table S1), y demostrando como IF1 ejerce su efecto inhibitorio tanto a nivel del monómero de la sintasa como en el dímero, agregaciones superiores y supercomplejos que contienen ATP sintasa (**Artículo #2**, Fig. 2C).

2.2 El fenotipo mitocondrial en la carcinogénesis.

Una extensa bibliografía describe la implicación del metabolismo en cáncer siendo la adquisición del metabolismo aberrante una característica común y necesaria de todos los tumores (Cuezva *et al.*, 2009; Hanahan, 2014; Hanahan and Weinberg, 2011; Sanchez-Arago *et al.*, 2013). Aunque hay muchas evidencias de que la reprogramación metabólica ocurre como consecuencia de la acción combinada de oncogenes y genes supresores de tumor, en algunas circunstancias, el metabolismo energético puede jugar un papel principal en la oncogénesis (Hirschey *et al.*, 2015). En este sentido, no se ha estudiado el papel que la inhibición parcial de OXPHOS puede jugar en la génesis y progresión de dicha patología. En esta tesis, aprovechando el modelo murino Tet-Off de hígado descrito, hemos caracterizado las repercusiones del fenotipo metabólico adquirido por una OXPHOS reprimida en la tumorogénesis *in vivo*.

Debemos mencionar que los ratones que expresan H49K no desarrollan tumores espontáneamente al menos tras un año de seguimiento. Para ello, hemos tratados los ratones que sobreexpresan H49K con un agente hepatocarcinogénico: la dietilnitrosoamina (DEN). Se ha llevado a cabo un experimento piloto, con una sola inyección de DEN, en un número reducido de animales. El estudio principal se ha efectuado con un protocolo de administración de DEN a largo plazo (Finnberg *et al.*, 2004) en 70 animales. En ambos estudios hemos obtenido resultados muy parecidos como se describe a continuación (**Artículo #2**, Fig. 3 y S3). A pesar de una diminución del peso corporal en todos los animales tratados con DEN, el peso del hígado al final del tratamiento era mayor con respecto a los animales tratados con PBS y a los tratados con DEN y Dox, especialmente aumentado en los ratones que expresan H49K (**Artículo #2**, Fig. 3A, 3B y S3B). Análogamente al peso del hígado, vimos un aumento en la actividad de la glutamato-piruvato transaminasa en la sangre aún más marcado durante

las últimas semanas de tratamiento en los mismos animales (**Artículo #2**, Fig. 3C, S3C y S4). Consistente con estos resultados el tratamiento con DEN, induce la producción de más tumores y de mayor tamaño en los ratones transgénicos con respecto a los controles, indicando un papel pro-oncogénico de IF1 (**Artículo #2**, Fig. 3D y S3D). El tratamiento con Dox, como era de esperar, inhibe la expresión de hIF1y revierte el fenotipo de los T/H y además confirma su efecto anticancerígeno (Onoda *et al.*, 2004), ya que tanto los ratones T/H como los controles tratados con DEN y Dox exhibían los niveles más bajos de tumores.

La reprogramación metabólica en cáncer hacia una activa glucolisis aerobia implica mecanismos diversos entre los que se encuentra la disminución de la expresión de ATP sintasa (Cuezva *et al.*, 2002; Willers and Cuezva, 2011). Una estrategia adicional para promover la proliferación es la inducción de IF1 (Sanchez-Cenizo *et al.*, 2010). En este contexto, IF1 promueve la adquisición de tres importantes características del fenotipo oncogénico, como son (i) el aumento de la proliferación, (ii) la evasión a muerte celular, y (iii) la reprogramación metabólica (Formentini *et al.*, 2012). En este estudio pudimos confirmar *in vivo* el papel oncogénico de IF1 propuesto en células de cáncer de colon, ya que vimos como su sobreexpresión en ratones T/H con respecto a los controles resultaba en un aumento significativo de la proliferación celular (**Artículo #2**, Fig. 4A) y en una menor tasa apoptótica, estudiada tanto por IHQ (**Artículo #2**, Fig. 4B) como por TUNEL (**Artículo #2**, Fig. 4C). Además, por ser la HCC inducida por DEN un ejemplo clásico de tumorogénesis causada por la inflamación, estudiamos también el reclutamiento de macrófagos sin encontrar diferencias entre controles y ratones T/H, sugiriendo que el nivel de IF1 no estaría implicado en este proceso (**Artículo #2**, Fig. S6).

En HCC humano se ha descrito una represión del programa de biogénesis mitocondrial (Cuezva *et al.*, 2002). Asimismo, en el HCC inducido por DEN, la progresión tumoral se ve acompañada por una represión de la biogénesis mitocondrial como pudimos evidenciar por la expresión de proteínas mitocondriales (**Artículo #2**, Fig.5A y S5). Además, por microscopía electrónica, vimos cómo el tejido tumoral estaba caracterizado por un menor contenido celular de mitocondrias y alteraciones en la estructura de las mismas (**Artículo #2**, Fig. 5C). Todo esto coincidía con una disminución significativa de los niveles de mtDNA y de la expresión del mRNA del factor de transcripción PGC1-α, responsable de la trascripción de proteínas mitocondriales codificadas en el nDNA, confirmando definitivamente una firme represión de la biogénesis mitocondrial en el tejido tumoral de los ratones T/H (**Artículo #2**, Fig. 5B y 5D). Consistentemente, el índice bioenergético celular BEC (razón βF1/GAPDH) está fuertemente disminuido en hepatocarcinoma ya sea de ratones controles o de ratones T/H (**Artículo #2**, Fig. S5), confirmando una vez más el valor del índice BEC como marcador tumoral (Cuezva *et al.*, 2004; Cuezva *et al.*, 2002; Chen *et al.*, 2002).

Cabe destacar que la expresión de H49K en áreas tumorales del hígado de los ratones T/H es prácticamente nula (**Artículo #2**, Fig. 5A). Esto se explicaría con la pérdida del fenotipo celular especializado del hepatocito que regresa a un estado menos diferenciado cuanto más alto es el grado del tumor y su capacidad de proliferación e invasión. En este contexto, las células menos diferenciadas

podrían haber perdido la capacidad de expresar el transactivador (tTA), ya que este se encuentra bajo el control de un promotor específico de células diferenciadas (el LAP en nuestro modelo de hígado). Además, nuestro anticuerpo monoclonal contra IF1 humano no reconoce el IF1 endógeno de ratón (Sanchez-Cenizo *et al.*, 2010) (**Artículo #3**, Fig. 1A), por tanto, la falta de expresión de H49K documentada en los tumores más avanzados no excluye que haya un aumento de expresión de IF1 endógeno relacionado con el estado avanzado del hepatocarcinoma (Song *et al.*, 2014). El HCC inducido por DEN cursa con la misma represión del programa de biogénesis mitocondrial e inducción del fenotipo glucolítico descrita en HCC humano (Cuezva *et al.*, 2002) y cabe destacar que no observamos diferencias entre los tumores generados en controles y animales transgénicos.

Muy recientemente, confirmando nuestro trabajo previo (**Artículo #1**), otros autores también han descrito que se produce la sobreexpresión de IF1 en tejidos tumorales de hígado (Song *et al.*, 2014) , vejiga (Wei *et al.*, 2015), estomago (Yin *et al.*, 2015) y en gliomas (Wu *et al.*, 2015). En hepatocarcinoma humano se ha descrito un vínculo entre IF1 y NFκB, esta vez mediante la vía no canónica de activación de NFκB. La activación de este factor de trascripción además de promover la expresión de IF1 promueve la activación de la invasión y metástasis por estimular la angiogénesis y la transición epitelio-mesénquima (EMT) (Song *et al.*, 2014).

No menos relevante es el valor de marcador pronóstico atribuido a IF1. Si bien en hígado, vejiga, estómago y gliomas se ha descrito la correlación de un alto nivel de IF1 con un peor pronóstico de supervivencia y recurrencia de la enfermedad (Song *et al.*, 2014; Wei *et al.*, 2015; Wu *et al.*, 2015; Yin *et al.*, 2015), nuestro estudio indica que paradójicamente en cáncer de colon y de mama, la alta expresión de IF1 es un marcador de buena prognosis (**Artículo #1**, Fig. 8). La expresión de IF1 está sujeta a una variación tejido específica que probablemente reside en la diferente demanda energética de los respectivos tejidos, siendo elevada en hígado, riñón, estómago y endometrio, y casi nula en colon, pulmón y mama (**Artículo #1**, Fig. 1 y 2). Sin embargo, el diferente comportamiento de IF1 en los distintos cánceres, podría ser debido a la susceptibilidad de los diferentes tipos celulares a formas particulares de estrés o a la posibilidad de ser fácilmente detectadas por el sistema inmune (Hanahan and Weinberg, 2011). En cualquier caso, son necesarios estudios adicionales para aclarar la supervivencia de los pacientes.

También hemos descrito cómo IF1 está implicado en la diferenciación celular (**Artículo #4**). Las células madre mesenquimales (hMSC) están caracterizadas por presentar una actividad mínima de OXPHOS y por utilizar, preferencialmente, la glucolisis aerobia como vía para el aprovisionamiento energético. Los niveles de IF1 disminuyen drásticamente durante la diferenciación osteocítica y además su silenciamiento acelera el proceso de diferenciación de las de hMSC hacia la adquisición del fenotipo ostecítico (**Artículo #4**). La reprogramación metabólica del osteocito diferenciado consta de un aumento de la biogénesis y expansión de la red mitocondrial. Sin embargo, a pesar del fuerte aumento de expresión de proteínas claves de la CTE en osteocitos diferenciados, el análisis de ensamblaje observado por BN-PAGE no revelaba diferencias relevantes entre hMSC y osteocitos

(**Artículo #4**, Fig. S2). En su papel como inhibidor de la ATP sintasa y por su elevado contenido en hMSC, IF1, contribuye a mantener el estado de pluripotencia y, por tanto, hemos sugerido que IF1 es un marcador de mantenimiento del estado de quiescencia en células madre. De acuerdo con esta función, un estudio reciente ha descrito que los niveles de IF1 aumentan en la desdiferenciación de células MEFs a IPs, también relacionado con la adquisición de un fenotipo más glucolítico (Vazquez-Martin *et al.*, 2013). Por el contrario, otro estudio sugiere que IF1 podría favorecer la diferenciación cardiomiogénica al incrementar el ensamblaje de la ATP sintasa (Bisetto *et al.*, 2013).

2.3 Inhibición de la apoptosis mediada por IF1

Se ha sugerido que la desorganización de las crestas mitocondriales, notoriamente formadas por dimerización y sucesiva oligomerización de la ATP sintasa (Davies *et al.*, 2012a; Davies *et al.*, 2012b; Davies *et al.*, 2011; Paumard *et al.*, 2002; Vonck and Schafer, 2009), favorece la apoptosis (Cogliati *et al.*, 2013). Por otro lado, IF1 ha sido descrito como responsable de la formación de dímeros y por tanto, regulador del estado oligomérico de la ATP sintasa y de la densidad y estabilidad de las crestas (Bisetto *et al.*, 2013; Cabezon *et al.*, 2000a; Campanella *et al.*, 2008; Garcia *et al.*, 2006; Minauro-Sanmiguel *et al.*, 2005). A raíz de este papel, se ha propuesto a IF1 como responsable de la protección frente a muerte celular (Cogliati *et al.*, 2013; Faccenda *et al.*, 2013) (**Artículo #2 y #3**). Muy recientemente se ha sugerido una función aún más central para la ATP sintasa en la ejecución de la muerte celular, ya que podría ser su estructura en forma de dímeros la que formara parte esencial del llamado poro de permeabilidad transicional (PTP) (Bernardi, 2013; Bonora *et al.*, 2013; Carraro *et al.*, 2014; Giorgio *et al.*, 2013). Aunque existen estudios dispares sobre la tendencia de IF1 a formar dímeros de ATP sintasa (Fujikawa *et al.*, 2012; Tomasetig *et al.*, 2002; Wittig and Schagger, 2009), nosotros hemos observado como la sobreexpresión de H49K tanto en ratones Tet-On como en Tet-Off incrementa la agregación de la ATP sintasa en lo que probablemente representa el dímero del complejo V (CV_2) (**Artículo #2**, Fig. 2D). Algunos autores han descrito que la ciclofilina D interacciona con la subunidad OSCP de la ATP sintasa y que tiene un papel en la regulación de la síntesis de ATP (Giorgio *et al.*, 2009). Además de este papel, también le atribuyen la capacidad de favorecer la apertura del PTP (Giorgio *et al.*, 2013) y de modular, según su expresión tejido-especifica, la sensibilidad del PTP a la rotenona y a la CsA por un mecanismo aún no conocido (Li *et al.*, 2012). Por todo ello, hemos sugerido que el efecto del pre-condicionamiento metabólico mediado por IF1 pueda ser debido a su capacidad de formar dímeros de ATP sintasa, que darían lugar a la formación del PTP (**Artículo #3**). Sin embargo, ya que no hemos observado diferencias entre ratones T/H expresando H49K y controles concluimos que el dímero de la ATP sintasa y/o la inhibición de la muerte celular mediada por IF1 podrían ser fenómenos independientes al de la apertura del PTP y/o de la estabilidad de las crestas mitocondriales (**Artículo #2**).

IF1, en cuanto inhibidor de OXPHOS, es protagonista de la estimulación de la glucolisis (Sanchez-Cenizo *et al.*, 2010) (**Artículo #1**) y de la proliferación del cáncer (Formentini *et al.*, 2012; Song *et*

al., 2014) (**Artículo #1**). La reprogramación metabólica mediada por H49K en hígado ha triplicado el efecto cancerígeno de la DEN, debido al efecto combinado de una elevada tasa proliferativa y de una disminución de la apoptosis en los tumores. En el mismo escenario metabólico surgen las lesiones hepáticas crónicas (Nishikawa *et al.*, 2014), en las cuales ya se había sugerido la participación de ROS en el estado inflamatorio crónico (Black *et al.*, 2004) y su implicación en la resistencia a la apoptosis (Raval *et al.*, 2006).

Los ROS mitocondriales son conocidos como activadores de muchas rutas bioquímicas (Ristow, 2014). El tratamiento con agentes quimioterapéuticos induce, por medio de la ATP sintasa, una elevada señal de ROS mitocondriales que desencadena la muerte apoptótica (Johnson *et al.*, 2005; Santamaria *et al.*, 2006; Wondrak, 2009). Sin embargo, una inhibición parcial de la ATP sintasa mediada por IF1 genera una señal leve de ROS que protege frente a muerte inducida por estaurosporina en las células tumorales (Formentini *et al.*, 2012) (**Artículo #1**). Más aún, la protección también se observa en respuesta a ácido quinolínico (**Artículo #3**) y en hepatocitos a paracetamol (APAP) (**Artículo #2**) dos agentes que promueven el estrés oxidativo. En concreto, la acción de IF1 y la sucesiva generación de ROS inducen un estado de pre-condicionamiento que eleva el umbral en el que un insulto tóxico desencadena la cascada de eventos que llevan a la muerte celular (**Artículo #2**, Fig. 9B y **#3**, Fig. 7G) (Figura 10).

La inhibición parcial de la ATP sintasa por IF1 genera un aumento de la razón AMP/ATP con la consiguiente activación del sensor metabólico AMPK que, induciendo un aumento de la glucolisis aerobia, compensa parcialmente la provisión de ATP (Mihaylova and Shaw, 2011), al igual que lo observado tanto en hígado (**Artículo #2**, Fig. S2A y S2B) como en neuronas (**Artículo #3**, Fig. 1D y 1E) (Figura 10). La activación de AMPK parece ser un camino común para ambos modelos. En neuronas, tras el insulto por ácido quinolínico (Schwarcz *et al.*, 2012), la prevención de muerte está asociada a la activación de la ruta PI3K/Akt (**Artículo #3**, Fig. 5D y 7G) (Figura 10).

El estrés oxidativo producido por la sobredosis de APAP tras 8h de tratamiento produce lesiones hepáticas centrilobulares que se ven mucho más reducidas en los ratones T/H adultos (**Artículo #2**, Fig. 6A, 6B y 6C). La capacidad de mitigar el estrés oxidativo de los ratones T/H reside en el mantenimiento de los niveles de expresión del factor de transcripción nuclear Nrf2, un regulador de la expresión de proteínas antioxidantes, del equilibrio redox y del proceso apoptótico (Morales-Gonzalez *et al.*, 2015) (**Artículo #2**, Fig. 8C) (Figura 10). Los ratones que expresan H49K se distinguen de los controles por una elevada expresión de proteínas dianas de Nrf2 como son SOD-2, HO-1 y GR o a la limitada degradación de otras como GCL-C y GCL-M (**Artículo #2**, Fig. 8). De acuerdo con un mejor equilibrio redox, los niveles basales de oxidación de las proteínas hepáticas son menos pronunciados en los modelos que expresan H49K (**Artículo #2**, Fig. 6D y Fig. S2G).

Los ROS son activadores de muchas vías de señalización dirigidas a sustentar la supervivencia celular. En este sentido, los ROS pueden modificar el estado de reducción de la tioredoxina, un regulador de la activación de AMPK (Shao *et al.*, 2014) y de p38MAPK (Dolado *et al.*, 2007), lo que

juega un papel importante en la adaptación al estrés, inhibición de la apoptosis e inducción de la proliferación (Cairns *et al.*, 2011; Formentini *et al.*, 2012) (**Artículo #2** Fig. 9A). Apoyando nuestros resultados, un estudio muy reciente ha descrito la influencia de ROS sobre la tioredoxina, lo que provoca un fuerte estado invasivo de las células cancerígenas de mama (Bhatia *et al.*, 2015).

Cabe destacar que la vía canónica de NFκB, un regulador crucial de la supervivencia celular (Karin, 2006; Ravati *et al.*, 2001), parece estar involucrada en la mayor supervivencia de hepatocitos y neuronas *in vivo* (**Artículo #2** y **#3**), así como en cáncer de colon y pulmón (Formentini *et al.*, 2012) (**Artículo #1**) (Figura 10). En estos tejidos, el mecanismo que genera una OXPHOS parcialmente inhibida por IF1, produce una respuesta nuclear mediada por ROS que promueve la degradación del inhibidor de NFκB, IKBα, y la acumulación de la proteína antiapoptotica Bcl-xL, diana de NFκB (**Artículo #1**, **#2**, **#3**) (Figura 10).

Todo ello indica la especial relevancia de la ATP sintasa y de su regulación en la biología de la célula, reforzando su valor como eventual diana para la intervención terapéutica.

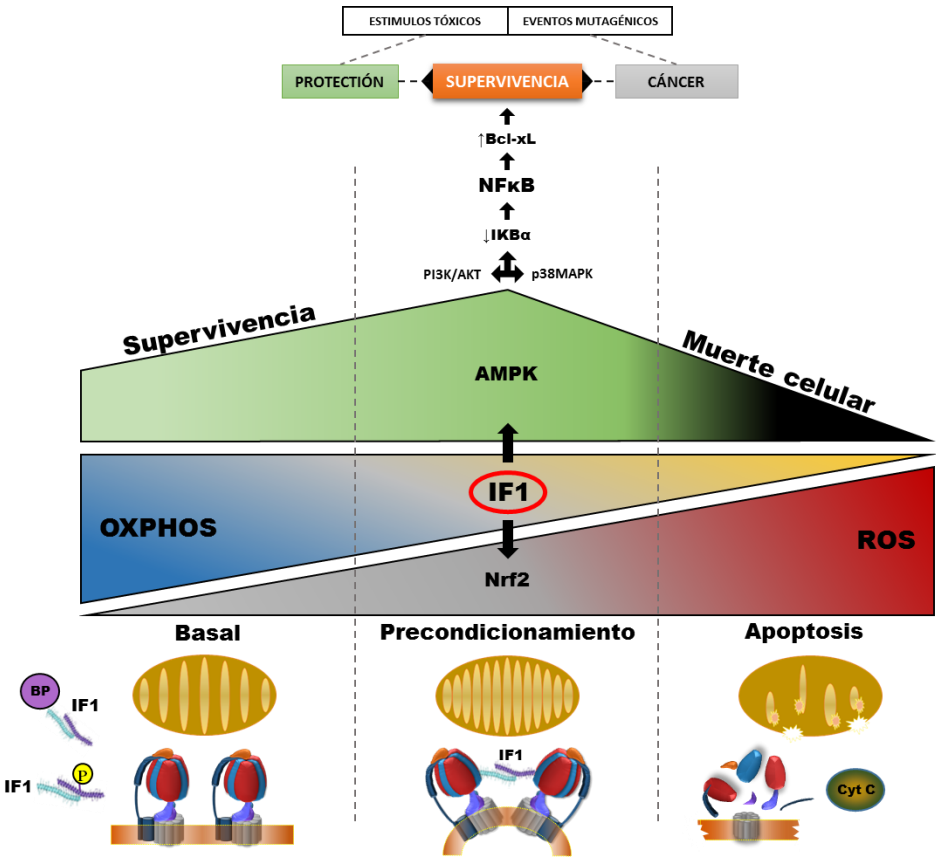

Figura 10. Señalización de IF1. El esquema describe el papel de IF1 en el precondicionamiento del hepatocito así como de la neurona. (Izquierda), En condiciones basales IF1 no es funcional debido a la unión a un receptor putativo (Bp) o a modificaciones covalentes como la fosforilación. (Centro), La inhibición parcial de la OXPHOS mediada por la sobrexpresión de IF1 en su estado activo favorece la dimerización e inhibición de la ATP sintasa generando, por tanto, un leve aumento de ROS. Los niveles de ROS se mantienen bajos por la activación de Nrf2 y por el desensamblaje del CIV, señalizando al núcleo la activación de un estado de precondicionamiento que activa las defensas contra estímulos perjudiciales (mitohormesis) y favorece la supervivencia. El incremento de ROS y la disminución de los niveles de ATP por inhibición de la ATP sintasa favorecen la activación del sensor metabólico AMPK. Esta activación, aunque sea por diferentes rutas tanto en hepatocitos (p38MAPK) como en neuronas (PI3K/Akt), promueve la activación del factor de transcripción NFκB y a la acumulación de la proteína antiapoptotica Bcl-xL determinando una mayor adaptación adaptación al estrés, resistencia a la apoptosis y estimulación de la proliferación. (Derecha), Por el contrario, elevados niveles de ROS producen alteraciones genéticas que promueven la progresión de la patología.

2.4 Biomarcadores metabólicos en enfermedades raras neuromusculares

Aunque se han identificado un gran número de genes implicados en enfermedades neuromusculares, el conocimiento de los mecanismos patofisiológicos, la disponibilidad de marcadores diagnósticos y de tratamientos terapéuticos son escasos o inexistentes. En las dos últimas décadas se han hecho progresos sustanciales en el campo de la terapia génica para el tratamiento de algunas distrofias musculares (Rahimov 2013) y, más recientemente, se han implementados nuevas tecnología de secuenciación (NGS: *next-generation sequencing*) para identificar los factores genéticos de enfermedades neuromusculares (Lemmers 2012; Manzini 2012). Sin embargo, en muy pocos estudios se ha analizado el proteoma de las enfermedades neuromusculares y de las miopatías inflamatorias (IMs), aunque está ampliamente demostrado que las alteraciones en la expresión de proteínas del metabolismo energético proporcionan biomarcadores útiles para trastornos adquiridos e incluso trastornos genéticos complejos como el cáncer (Cuezva *et al.*, 2009; Ledford, 2014; Sanchez-Arago and Cuezva, 2011; Sanchez-Arago *et al.*, 2013). En este contexto, los microarrays de proteínas de fase reversa (RPPA: *Reverse Phase Protein Microarray*) son una técnica de alto rendimiento ampliamente adoptada que permite cuantificar el perfil proteómico de células, tejidos y casi todo tipo de muestras biológicas y, por tanto, es especialmente indicada para la identificación de biomarcadores de diagnóstico, pronóstico y de respuesta a tratamiento terapéutico (Aldea *et al.*, 2011; Ledford, 2014; Mueller *et al.*, 2010; Sereni *et al.*, 2013). De hecho, los RPPAs han sido recientemente aprobados para su uso en ensayos clínicos (Mueller *et al.*, 2010).

El primer estudio de esta tesis aplicando nuestra plataforma RPPA se ha basado en el análisis de la expresión de 18 proteínas del metabolismo y la β-actina, en una cohorte de 73 biopsias musculares procedentes de pacientes con enfermedades raras y un grupo control, con el objetivo de identificar potenciales biomarcadores que nos informen sobre la actividad del metabolismo en estas enfermedades para su eventual traslación a la clínica. En concreto, las enfermedades estudiadas incluyen un grupo de enfermedades neuromusculares, cuatro de las cuales son distrofias (DMD, BMD, P. Xp21, LGMD-2C), dos metabólicas, glucogenosis de tipo V (Glyc-V) y una miopatía metabólica con defectos del complejo I (MITO), una enfermedad neurodegenerativa (lipofuscinosis neuronal ceroide, NCL) y por último un grupo de pacientes hospitalizados en la unidad de cuidado intensivo (ICU) por su debilidad y pérdida del tono muscular. El primer paso del estudio ha sido la validación de todos los anticuerpos utilizados, siendo el requisito mínimo de validación la identificación específica de la proteína diana por *Western blot* en el extracto proteico del tejido a analizar (biopsias musculares humanas). Para poder analizar la expresión por RPPA es esencial que el anticuerpo sólo reconozca la proteína de interés (**Artículo #5**, Fig. 1 y S1).

Las distrofias musculares son un grupo heterogéneo de trastornos hereditarios caracterizados por la pérdida progresiva del tono muscular y debilidad (Emery, 1998; Rahimov and Kunkel, 2013; Ramadasan-Nair *et al.*, 2014). Estudios previos en modelos animales han sugerido la potencial relevancia de algunas enzimas metabólicas como la enolasa y la malato deshidrogenasa, como

biomarcadores de estos trastornos (Guevel *et al.*, 2011). En este sentido, hemos ampliado la lista de biomarcadores a través de nuestra plataforma RPPA y hemos confirmado en pacientes, la disminución de la expresión de enzimas glucolíticas que se había descrito previamente en el modelo distrófico de perro (Guevel *et al.*, 2011) (**Artículo #5**, Tabla 1 y Fig. S4). Sin embargo, contrariamente a lo descrito en este modelo animal (Guevel *et al.*, 2011), en DMD hemos observado un aumento en la expresión de algunas proteínas implicadas en la OXPHOS, así como de Hsp60, lo que sugiere que hay una actividad y biogénesis mitocondrial sostenida (**Artículo #5**, Tabla 1 y Fig. S4). En otro estudio también se ha descrito una disminución en la expresión de proteínas de la CTE y OXPHOS en un modelo de ratón de distrofia muscular inducido por una cardiotoxina (Ramadasan-Nair *et al.*, 2014). Sin embargo, la discordancia con nuestros resultados podría ser debida a las diferencias entre humanos y modelos animales y/o al sistema experimental y la aproximación utilizada en estos estudios.

Cabe destacar que las alteraciones de los niveles de expresión de las enzimas, tanto glucolíticas como mitocondriales, eran más preponderantes en DMD con respecto a la BMD, sugiriendo, como era de esperar, que el fenotipo metabólico sufre una alteración mayor como efecto pleiotrópico conforme a la importancia del trastorno genético (**Artículo #5**, Tabla 1 y Fig. S4). Otro resultado destacable del análisis por RPPA es el valor de la firma bioenergética, definida como la relación de la expresión de βF1-ATPasa/LDH-A, que está alterada en todas las enfermedades estudiadas, de manera que puede considerarse un denominador común que revela la alteración metabólica global en enfermedades neuromusculares (**Artículo #5**, Tabla 1 y Fig. S4). Por tanto, las diferentes alteraciones genéticas que dan lugar a las distintas enfermedades neuromusculares podrían actuar pleiotrópicamente para regular, ya sea debido a la genética o a la epigenética (pacientes ICU), la huella del metabolismo energético muscular.

Patología	β-F1/LDHA	Marcadores adicionales	Sensibilidad
DMD	(2.9-4.1)	PYGM (0.1-0.3)	100%
BMD	(1.9-3.5)	GAPDH (0.6-1.2)	86%
NCL	(1.5-2.1)	GPD1 (0.4-0.6)	100%
LGMD-2C	(2.5-3.9)	SDH (0.5-0.7)	100%

Tabla 1. Potencial sensibilidad diagnostica de los biomarcadores metabólicos en miopatías neuromusculares y neurodegenerativas. La tabla resume el poder discriminatorio (sensibilidad) en miopatías distróficas (DMD, BMD, LGMD-2C) y neurodegenerativas (NCL), de la razón β-F1-ATPase/LDH-A en combinación con el valor de expresión de un tercer marcador.

La cuantificación de la razón βF1-ATPasa/LDH-A en combinación con otras proteínas proporciona un eficiente marcador para discriminar entre diferentes patologías (Tabla 1). En concreto, la combinación entre los valores de la razón βF1-ATPasa/LDH-A con los valores de expresión de la miofosforilasa (PYGM) permite discriminar los pacientes afectados por DMD con una sensibilidad del 100% (Tabla 1). Asimismo, la combinación entre esta relación y la expresión de GPD1 permite discriminar pacientes afectados por NCL con una sensibilidad del 100% (Tabla 1). La expresión de

GAPDH y succinato deshidrogenasa (SDH) en combinación con la razón βF1-ATPasa/LDH-A permite discriminar las enfermedades BMD (sensibilidad 86%) y LGMD-2C (sensibilidad 100%) (Tabla 1). Como era de esperar, la expresión de la PYGM en pacientes afectados por la enfermedad de Mc Ardle es casi nula, puesto que la enfermedad se caracteriza por la deficiencia en la glucógeno fosforilasa muscular, lo que confirma la fiabilidad de la técnica (**Artículo #5**, Fig. 3A, S4) (Tabla1). En su conjunto, los marcadores destacados en este estudio, solos o en combinación con marcadores plasmáticos (Doran *et al.*, 2007; Hathout *et al.*, 2014; Nadarajah *et al.*, 2011) y/o con otros marcadores el metabolismo energético descritos en otros estudios (Guevel *et al.*, 2011; Nadarajah *et al.*, 2011), podrían ayudar al manejo clínico y terapéutico de los pacientes afectados por estas patologías.

2.5 Biomarcadores metabólicos en Miopatías Inflamatorias.

Una segunda aproximación en el marco de esta tesis doctoral se ha basado en un análisis de una menor densidad de datos, analizando una cohorte de 32 biopsias musculares de pacientes afectados por los tres principales grupos de Miopatías Inflamatorias (IMs): la Polimiositis (PM), la Dermatomiositis (DM), la Miositis esporádica con cuerpos de inclusión (sIBM) y un grupo control de individuos sanos (**Artículo #6**). El análisis por RPPA de la expresión de nueve proteínas del metabolismo en IMs no ha proporcionado marcadores capaces de discriminar los pacientes del subgrupo PM del grupo control. Por el contrario, hemos encontrado diferencias significativas en la expresión de proteínas del metabolismo energético en DM y sIBM en comparación con el grupo control. Como en estudios previos (Selva O'Callaghan and Trallero Araguas, 2008), hemos observado un aumento en la expresión de β-actina en DM y sIBM y, aunque no estadísticamente significativa, también en el subgrupo PM (**Artículo #6**, Fig. 3). Efectivamente, la mayor expresión de β-actina en IMs parece ser una consecuencia de la regeneración de las fibras musculares, parámetro que se aplica como criterio de clasificación (Selva O'Callaghan and Trallero Araguas, 2008), apoyando la conocida asociación de las IMs con los trastornos del tejido conectivo (CTDs) (Dalakas, 1991; van der Kooi and de Visser, 2014). Contrariamente a la elevada expresión de β-actina, las biopsias de sIBM presentan una menor expresión de proteínas glucolíticas como GAPDH y LDH-A (**Artículo #6**, Fig. 3 y S3) y de GPD1, que forma parte del sistema lanzadera para transferir equivalentes de reducción del citosol a la mitocondria, en comparación con los controles (**Artículo #6**, Fig. 3).

Además, la expresión de PYGM, cuya reacción enzimática proporciona sustrato a la glucolisis, también está disminuida (**Artículo #6**, Fig. 3). Todo ello sugiere que las fibras musculares de pacientes afectados por sIBM se caracterizan por una represión parcial del metabolismo glucolítico en comparación con las fibras normales de los controles.

Contrariamente a los resultados obtenidos en sIBM, las biopsias de pacientes afectados por DM muestran una expresión aumentada de las proteínas mitocondriales Hsp60 e IF1 (**Artículo #6**, Fig. 3) y sobretodo un aumento muy significativo en la expresión de PKM2 (**Artículo #6**, Fig. 3 y S3). Cabe destacar que la razón βF1-ATPasa/LDH-A, que habíamos indicado como potencial marcador de

enfermedades neuromusculares y en concreto de todas las distrofias estudiadas (**Artículo #5**), está alterado sólo en las biopsias del subgrupo de pacientes con sIBM (**Artículo #6**, Fig. 3), lo que podría asignarle el valor de marcador metabólico restringido al grupo de las distrofias musculares. Por contra, la razón βF1-ATPasa/PKM2 proporciona un marcador fiable a la hora de discriminar el subgrupo de pacientes con DM de cualquier otra IM (**Artículo #6**, Fig. 4 y Tabla 1). De hecho, el potencial de PKM2 como biomarcador en IMs se demuestra por la alta especificidad y sensibilidad en la estratificación de los pacientes afectados por DM en comparación con los controles (**Artículo #6**, Fig. 4A y 4B). Por tanto, sugerimos que la traslación de este biomarcador a la clínica podría ahorrar una biopsia adicional a menudo requerida para el diagnóstico de algunos pacientes (Selva O'Callaghan and Trallero Araguas, 2008). Este resultado nos ha llevado a determinar si la elevada expresión de PKM2 en las biopsias se refleja también en el suero de pacientes con DM. Por ello, optimizamos la plataforma RPPA para la búsqueda de biomarcadores en plasma, con objeto de proporcionar biomarcadores del metabolismo energético no-invasivos (**Artículo #6**, Fig. S3). Desafortunadamente, tras el análisis de una cohorte de 40 muestras de plasma de pacientes afectados por IMs, no encontramos diferencias en los niveles de PKM2 (**Artículo #6**, Fig. S3).

En ambos estudios (**Artículos #5 y #6**) no hemos tenido en cuenta la edad, el tipo de fibras musculares (deltoides y/o cuádriceps) y el grado de daño tisular, factores que pueden modificar la expresión de las proteínas (Brancaccio *et al.*, 2010; Shima *et al.*, 1983). Sin embargo, la baja dispersión de los valores obtenidos para cada marcador indica que estos factores no parecen incidir de forma significativa a las diferencias descritas. Además, duplicados del RPPA (**Artículo #5**, Fig. S6), así como la validación de los resultados por *Western blot* (**Artículo #6**, Fig. S2), demuestran que los resultados obtenidos en ambos estudios son altamente reproducibles, validando, por tanto, la solidez de la técnica para fines cuantitativos.

Muchos estudios han asociado la DM y la PM con el cáncer (Dalakas, 2015). Aunque la estimación del riesgo es muy variable (6 - 60%), una observación unánime es que el cáncer está más relacionado con la DM que con la PM. Además, la tasa de mortalidad del cáncer es mayor en pacientes con DM al compararla con los pacientes diagnosticados con PM (Dalakas and Hohlfeld, 2003; Sigurgeirsson *et al.*, 1992). En este sentido, también cabe tener en cuenta la posibilidad de errores diagnósticos, tanto de los casos de DM como de PM, que pueden alterar la estimación del riesgo de cáncer en pacientes con PM (Hill *et al.*, 2001).

Se han descrito varios mecanismos que promueven el fenotipo Warburg de los tumores lo que propicia una marcada glucolisis aerobia (Cuezva *et al.*, 2009; Vander Heiden *et al.*, 2009). La enzima PKM2, producto del *splicing* alternativo del gen *PKM* y que se expresa exclusivamente en tejidos embrionarios y proliferativos, es una isoforma regulada alostéricamente debido a su capacidad de pasar de una forma tetramérica de alta actividad a una dimérica con una actividad 50 veces menor y responsable de favorecer la proliferación tumoral por propiciar la acumulación de intermediarios del ciclo glucolítico (Hitosugi *et al.*, 2009) (**Artículo #6**, Fig. 5). Además, se ha descrito un papel "no-

metabólico" de la PKM2 en la tumorigénesis. Parece que en su forma dimérica esta enzima pueda translocarse al núcleo y actuar como co-activador de factores transcripcionales regulando la transcripción de genes implicados en varias rutas de reprogramación metabólica, proliferación celular y desarrollo del cáncer (Iqbal *et al.*, 2014; Luo *et al.*, 2011; Wang *et al.*, 2014; Yang *et al.*, 2011) (Ver introducción 1.4.2.) (**Artículo #6**, Fig. 5). Sorprendentemente, y en consistencia con la elevada incidencia de cáncer observada en pacientes con DM (Chen *et al.*, 2010; Dalakas and Hohlfeld, 2003; Hill *et al.*, 2001; Sigurgeirsson *et al.*, 1992), también hemos observado una elevada expresión de IF1 en las biopsias de estos pacientes. La sobreexpresión de IF1 ya descrita en los tumores humanos más prevalentes (Sanchez-Cenizo *et al.*, 2010) (**Artículo #1**), promueve la glucolisis aerobia y desempeña un papel pro-oncogénico, a través de la señalización por ROS, estimulando la proliferación celular, invasión y resistencia a la apoptosis (Formentini *et al.*, 2012; Sanchez-Cenizo *et al.*, 2010) (**Artículos #1-4)** (**Artículo#6**, Fig. 5) así como transición epitelio-mesénquima y angiogénesis (Song *et al.*, 2014). Aunque sea por mecanismos diferentes, sugerimos que ambos factores pro-oncogénicos, IF1 y PKM2, cooperan para promover un fenotipo metabólico especialmente proclive a la oncogénesis en DM (**Artículo #6**, Fig. 5).

No excluimos que algunos tipos de células específicas del sistema inmunológico (Johansson *et al.*, 2008), presentes en el tejido por el contexto de la inflamación (Corrado *et al.*, 2016), proporcionen factores de crecimiento que sostengan la proliferación, resistencia a apoptosis, invasión, angiogénesis, metástasis o que inhiban la respuesta inmune anti-tumoral (Biswas and Mantovani, 2010; Murdoch *et al.*, 2008).

CONCLUSIONES

Conclusiones

1. La expresión de IF1 en tejidos humanos es muy variable siendo máxima en aquellos que tienen mayor demanda energética. La expresión de IF1 se ve muy incrementada en algunos carcinomas humanos aportando, paradójicamente, un marcador de buena prognosis en carcinomas de colon.

2. La sobreexpresión del dominante activo de IF1 humano H49K en hígado, así como en neuronas de ratones transgénicos, ha demostrado que esta proteína inhibe tanto el complejo V como el complejo IV de la respiración. La sobreexpresión de IF1 fomenta la dimerización/oligomerización del complejo V y su inhibición, desencadenando la desestabilización de la organización supramolecular del complejo IV.

3. La inhibición de la fosforilación oxidativa mediada por el dominante activo de IF1 en el hígado de ratones transgénicos genera un fenotipo susceptible a la trasformación oncogénica inducida por dietilnitrosoamina. Este fenotipo, se debe a un aumento de la proliferación y a una mayor prevención de la muerte celular desencadenados, muy probablemente, por el precondicionamiento metabólico frente al estrés oxidativo. El modelo de hepatocarcinogénesis inducida por dietilnitrosoamina en ratones reproduce el perfil fenotípico de represión de la biogénesis mitocondrial descrito en el hepatocarcinoma humano.

4. En el proceso de diferenciación de células madres mesenquimales (hMSC) a osteocitos, la inducción de la expresión de las proteínas de la OXPHOS no se acompaña de cambios significativos en la organización estructural de los respectivos complejos en las membranas mitocondriales.

5. Se han descubierto nuevos biomarcadores metabólicos en músculo que pueden ayudar al diagnóstico y manejo clínico de pacientes afectados por distrofia muscular tipo Duchenne y Becker, gamma-sarcoglicanopatia y Lipofuscinosis neuronal ceroide. La combinación de sólo tres marcadores facilita el diagnóstico diferencial de estas patologías con elevada sensibilidad.

6. Se ha desarrollado una plataforma de array de proteínas de fase reversa que permite la traslación de algunas proteínas del metabolismo como biomarcadores de la patología. Se ha procedido a la protección de la propiedad intelectual.

7. Se han descubierto nuevos biomarcadores metabólicos de utilidad para el diagnóstico diferencial de pacientes afectados por Miopatias Inflamatorias (IMs). Se destaca el poder discriminatorio del marcador PKM2 en Dermatomiositis. Además, la elevada expresión de dos factores pro-oncogénicos como PKM2 e IF1, proporciona eventuales marcadores para el pronóstico del riesgo de cáncer en Dermatomiositis.

BIBLIOGRAFÍA

Bibliografía

Acin-Perez, R., and Enriquez, J.A. (2014). The function of the respiratory supercomplexes: the plasticity model. *Biochim Biophys Acta* 1837, 444-450.

Acin-Perez, R., Fernandez-Silva, P., Peleato, M.L., Perez-Martos, A., and Enriquez, J.A. (2008). Respiratory active mitochondrial supercomplexes. *Mol Cell* 32, 529-539.

Acin-Perez, R., Gatti, D.L., Bai, Y., and Manfredi, G. (2011). Protein phosphorylation and prevention of cytochrome oxidase inhibition by ATP: coupled mechanisms of energy metabolism regulation. *Cell Metab* 13, 712-719.

Acin-Perez, R., Salazar, E., Kamenetsky, M., Buck, J., Levin, L.R., and Manfredi, G. (2009). Cyclic AMP produced inside mitochondria regulates oxidative phosphorylation. *Cell Metab* 9, 265-276.

Ackermann, U., and Geering, K. (1990). Mutual dependence of Na,K-ATPase alpha- and beta-subunits for correct posttranslational processing and intracellular transport. *FEBS Lett* 269, 105-108.

Adachi, K., Oiwa, K., Nishizaka, T., Furuike, S., Noji, H., Itoh, H., Yoshida, M., and Kinosita, K., Jr. (2007). Coupling of rotation and catalysis in F(1)-ATPase revealed by single-molecule imaging and manipulation. *Cell* 130, 309-321.

Alavian, K.N., Beutner, G., Lazrove, E., Sacchetti, S., Park, H.A., Licznerski, P., Li, H., Nabili, P., Hockensmith, K., Graham, M., Porter, G.A., Jr., and Jonas, E.A. (2014). An uncoupling channel within the c-subunit ring of the F1FO ATP synthase is the mitochondrial permeability transition pore. *Proc Natl Acad Sci U S A* 111, 10580-10585.

Alavian, K.N., Li, H., Collis, L., Bonanni, L., Zeng, L., Sacchetti, S., Lazrove, E., Nabili, P., Flaherty, B., Graham, M., Chen, Y., Messerli, S.M., Mariggio, M.A., Rahner, C., McNay, E., Shore, G.C., Smith, P.J., Hardwick, J.M., and Jonas, E.A. (2011). Bcl-x(L) regulates metabolic efficiency of neurons through interaction with the mitochondrial F(1)F(O) ATP synthase. *Nat Cell Biol* 13, 1224-1233.

Alberts, B., Bray, D., Hopkin, K., Johnson, A., Lewis, J., Raff, M., Roberts, K., and Walter, P. (2013). *Essential Cell Biology, Fourth Edition* (Taylor & Francis Group).

Aldea, M., Clofent, J., Nunez de Arenas, C., Chamorro, M., Velasco, M., Berrendero, J.R., Navarro, C., and Cuezva, J.M. (2011). Reverse phase protein microarrays quantify and validate the bioenergetic signature as biomarker in colorectal cancer. *Cancer Lett* 311, 210-218.

Anastasiou, D., Yu, Y., Israelsen, W.J., Jiang, J.K., Boxer, M.B., Hong, B.S., Tempel, W., Dimov, S., Shen, M., Jha, A., Yang, H., Mattaini, K.R., Metallo, C.M., Fiske, B.P., Courtney, K.D., Malstrom, S., Khan, T.M., Kung, C., Skoumbourdis, A.P., Veith, H., Southall, N., Walsh, M.J., Brimacombe, K.R., Leister, W., Lunt, S.Y., Johnson,

Z.R., Yen, K.E., Kunii, K., Davidson, S.M., Christofk, H.R., Austin, C.P., Inglese, J., Harris, M.H., Asara, J.M., Stephanopoulos, G., Salituro, F.G., Jin, S., Dang, L., Auld, D.S., Park, H.W., Cantley, L.C., Thomas, C.J., and Vander Heiden, M.G. (2012). Pyruvate kinase M2 activators promote tetramer formation and suppress tumorigenesis. *Nat Chem Biol* 8, 839-847.

Anderson, S., Bankier, A.T., Barrell, B.G., de Bruijn, M.H., Coulson, A.R., Drouin, J., Eperon, I.C., Nierlich, D.P., Roe, B.A., Sanger, F., Schreier, P.H., Smith, A.J., Staden, R., and Young, I.G. (1981). Sequence and organization of the human mitochondrial genome. *Nature* 290, 457-465.

Angenendt, P., Glokler, J., Murphy, D., Lehrach, H., and Cahill, D.J. (2002). Toward optimized antibody microarrays: a comparison of current microarray support materials. *Anal Biochem* 309, 253-260.

Angenendt, P., Glokler, J., Sobek, J., Lehrach, H., and Cahill, D.J. (2003). Next generation of protein microarray support materials: evaluation for protein and antibody microarray applications. *J Chromatogr A* 1009, 97-104.

Arnold, I., Pfeiffer, K., Neupert, W., Stuart, R.A., and Schagger, H. (1998). Yeast mitochondrial F1F0-ATP synthase exists as a dimer: identification of three dimer-specific subunits. *EMBO J* 17, 7170-7178.

Arnold, S. (2012). The power of life--cytochrome c oxidase takes center stage in metabolic control, cell signalling and survival. *Mitochondrion* 12, 46-56.

Arselin, G., Giraud, M.F., Dautant, A., Vaillier, J., Brethes, D., Coulary-Salin, B., Schaeffer, J., and Velours, J. (2003). The GxxxG motif of the transmembrane domain of subunit e is involved in the dimerization/oligomerization of the yeast ATP synthase complex in the mitochondrial membrane. *Eur J Biochem* 270, 1875-1884.

Bar-Even, A., Flamholz, A., Noor, E., and Milo, R. (2012). Rethinking glycolysis: on the biochemical logic of metabolic pathways. *Nat Chem Biol* 8, 509-517.

Barbosa, I.A., Machado, N.G., Skildum, A.J., Scott, P.M., and Oliveira, P.J. (2012). Mitochondrial remodeling in cancer metabolism and survival: Potential for new therapies. *Biochim Biophys Acta* 1826, 238-254.

Barbot, M., Jans, D.C., Schulz, C., Denkert, N., Kroppen, B., Hoppert, M., Jakobs, S., and Meinecke, M. (2015). Mic10 oligomerizes to bend mitochondrial inner membranes at cristae junctions. *Cell Metab* 21, 756-763.

Bason, J.V., Montgomery, M.G., Leslie, A.G., and Walker, J.E. (2014). Pathway of binding of the intrinsically disordered mitochondrial inhibitor protein to F1-ATPase. *Proc Natl Acad Sci U S A* 111, 11305-11310.

Belogrudov, G.I. (2009). Recent advances in structure-functional studies of mitochondrial factor B. *J Bioenerg Biomembr* 41, 137-143.

Bender, T., and Martinou, J.C. (2013). Where killers meet--permeabilization of the outer mitochondrial membrane during apoptosis. *Cold Spring Harb Perspect Biol* 5, a011106.

Bernardi, P. (2013). The mitochondrial permeability transition pore: a mystery solved? *Front Physiol* 4, 95.

Bernardi, P., Scorrano, L., Colonna, R., Petronilli, V., and Di Lisa, F. (1999). Mitochondria and cell death. Mechanistic aspects and methodological issues. *Eur J Biochem* 264, 687-701.

Bhatia, M., McGrath, K.L., Di Trapani, G., Charoentong, P., Shah, F., King, M.M., Clarke, F.M., and Tonissen, K.F. (2015). The thioredoxin system in breast cancer cell invasion and migration. *Redox Biol* 8, 68-78.

Bi, X., Lin, Q., Foo, T.W., Joshi, S., You, T., Shen, H.M., Ong, C.N., Cheah, P.Y., Eu, K.W., and Hew, C.L. (2006). Proteomic analysis of colorectal cancer reveals alterations in metabolic pathways: mechanism of tumorigenesis. *Mol Cell Proteomics* 5, 1119-1130.

Bianchi, C., Genova, M.L., Parenti Castelli, G., and Lenaz, G. (2004). The mitochondrial respiratory chain is partially organized in a supercomplex assembly: kinetic evidence using flux control analysis. *J Biol Chem* 279, 36562-36569.

Bisetto, E., Comelli, M., Salzano, A.M., Picotti, P., Scaloni, A., Lippe, G., and Mavelli, I. (2013). Proteomic analysis of F1F0-ATP synthase super-assembly in mitochondria of cardiomyoblasts undergoing differentiation to the cardiac lineage. *Biochim Biophys Acta* 1827, 807-816.

Biswas, S.K., and Mantovani, A. (2010). Macrophage plasticity and interaction with lymphocyte subsets: cancer as a paradigm. *Nat Immunol* 11, 889-896.

Black, D., Bird, M.A., Samson, C.M., Lyman, S., Lange, P.A., Schrum, L.W., Qian, T., Lemasters, J.J., Brenner, D.A., Rippe, R.A., and Behrns, K.E. (2004). Primary cirrhotic hepatocytes resist TGFbeta-induced apoptosis through a ROS-dependent mechanism. *J Hepatol* 40, 942-951.

Boekema, E.J., and Braun, H.P. (2007). Supramolecular structure of the mitochondrial oxidative phosphorylation system. *J Biol Chem* 282, 1-4.

Bonnet, S., Archer, S.L., Allalunis-Turner, J., Haromy, A., Beaulieu, C., Thompson, R., Lee, C.T., Lopaschuk, G.D., Puttagunta, L., Bonnet, S., Harry, G., Hashimoto, K., Porter, C.J., Andrade, M.A., Thebaud, B., and Michelakis, E.D. (2007). A mitochondria-K+ channel axis is suppressed in cancer and its normalization promotes apoptosis and inhibits cancer growth. *Cancer Cell* 11, 37-51.

Bonora, M., Bononi, A., De Marchi, E., Giorgi, C., Lebiedzinska, M., Marchi, S., Patergnani, S., Rimessi, A., Suski, J.M., Wojtala, A., Wieckowski, M.R., Kroemer, G., Galluzzi, L., and Pinton, P. (2013). Role of the c subunit of the FO ATP synthase in mitochondrial permeability transition. *Cell Cycle* 12, 674-683.

Boumans, H., Grivell, L.A., and Berden, J.A. (1998). The respiratory chain in yeast behaves as a single functional unit. *J Biol Chem* 273, 4872-4877.

Brancaccio, P., Lippi, G., and Maffulli, N. (2010). Biochemical markers of muscular damage. *Clin Chem Lab Med* 48, 757-767.

Brown, T.A., Tkachuk, A.N., Shtengel, G., Kopek, B.G., Bogenhagen, D.F., Hess, H.F., and Clayton, D.A. (2011). Superresolution fluorescence imaging of mitochondrial nucleoids reveals their spatial range, limits, and membrane interaction. *Mol Cell Biol* 31, 4994-5010.

Bultema, J.B., Braun, H.P., Boekema, E.J., and Kouril, R. (2009). Megacomplex organization of the oxidative phosphorylation system by structural analysis of respiratory supercomplexes from potato. *Biochim Biophys Acta* 1787, 60-67.

Burghes, A.H., Logan, C., Hu, X., Belfall, B., Worton, R.G., and Ray, P.N. (1987). A cDNA clone from the Duchenne/Becker muscular dystrophy gene. *Nature* 328, 434-437.

Bustos, D.M., and Velours, J. (2005). The modification of the conserved GXXXG motif of the membrane-spanning segment of subunit g destabilizes the supramolecular species of yeast ATP synthase. *J Biol Chem* 280, 29004-29010.

Buzhynskyy, N., Sens, P., Prima, V., Sturgis, J.N., and Scheuring, S. (2007). Rows of ATP synthase dimers in native mitochondrial inner membranes. *Biophys J* 93, 2870-2876.

Cabezon, E., Arechaga, I., Jonathan, P., Butler, G., and Walker, J.E. (2000a). Dimerization of bovine F1-ATPase by binding the inhibitor protein, IF1. *J Biol Chem* 275, 28353-28355.

Cabezon, E., Butler, P.J., Runswick, M.J., Carbajo, R.J., and Walker, J.E. (2002). Homologous and heterologous inhibitory effects of ATPase inhibitor proteins on F-ATPases. *J Biol Chem* 277, 41334-41341.

Cabezon, E., Butler, P.J., Runswick, M.J., and Walker, J.E. (2000b). Modulation of the oligomerization state of the bovine F1-ATPase inhibitor protein, IF1, by pH. *J Biol Chem* 275, 25460-25464.

Cabezon, E., Montgomery, M.G., Leslie, A.G., and Walker, J.E. (2003). The structure of bovine F1-ATPase in complex with its regulatory protein IF1. *Nat Struct Biol* 10, 744-750.

Cabezon, E., Runswick, M.J., Leslie, A.G., and Walker, J.E. (2001). The structure of bovine IF(1), the regulatory subunit of mitochondrial F-ATPase. *Embo J* 20, 6990-6996.

Cairns, R.A., Harris, I.S., and Mak, T.W. (2011). Regulation of cancer cell metabolism. *Nat Rev Cancer* 11, 85-95.

Calvo, S.E., and Mootha, V.K. (2010). The mitochondrial proteome and human disease. *Annu Rev Genomics Hum Genet* 11, 25-44.

Campanella, M., Casswell, E., Chong, S., Farah, Z., Wieckowski, M.R., Abramov, A.Y., Tinker, A., and Duchen, M.R. (2008). Regulation of mitochondrial structure and function by the F1Fo-ATPase inhibitor protein, IF1. *Cell Metab* 8, 13-25.

Carraro, M., Giorgio, V., Sileikyte, J., Sartori, G., Forte, M., Lippe, G., Zoratti, M., Szabo, I., and Bernardi, P. (2014). Channel formation by yeast F-ATP synthase and the role of dimerization in the mitochondrial permeability transition. *J Biol Chem* 289, 15980-15985.

Catalan, M., Selva-O'Callaghan, A., and Grau, J.M. (2014). Diagnosis and classification of sporadic inclusion body myositis (sIBM). *Autoimmun Rev* 13, 363-366.

Cintron, N.M., and Pedersen, P.L. (1979). A protein inhibitor of the mitochondrial adenosine triphosphatase complex of rat liver. Purification and characterization. *J Biol Chem* 254, 3439-3443.

Clem, B.F., O'Neal, J., Tapolsky, G., Clem, A.L., Imbert-Fernandez, Y., Kerr, D.A., 2nd, Klarer, A.C., Redman, R., Miller, D.M., Trent, J.O., Telang, S., and Chesney, J. (2013). Targeting 6-phosphofructo-2-kinase (PFKFB3) as a therapeutic strategy against cancer. *Mol Cancer Ther* 12, 1461-1470.

Cogliati, S., Enriquez, J.A., and Scorrano, L. (2016). Mitochondrial Cristae: Where Beauty Meets Functionality. *Trends Biochem Sci* 41, 261-273.

Cogliati, S., Frezza, C., Soriano, M.E., Varanita, T., Quintana-Cabrera, R., Corrado, M., Cipolat, S., Costa, V., Casarin, A., Gomes, L.C., Perales-Clemente, E., Salviati, L., Fernandez-Silva, P., Enriquez, J.A., and Scorrano, L. (2013). Mitochondrial cristae shape determines respiratory chain supercomplexes assembly and respiratory efficiency. *Cell* 155, 160-171.

Contessi, S., Comelli, M., Cmet, S., Lippe, G., and Mavelli, I. (2007). IF(1) distribution in HepG2 cells in relation to ecto-F(0)F (1)ATPsynthase and calmodulin. *J Bioenerg Biomembr* 39, 291-300.

Contessi, S., Haraux, F., Mavelli, I., and Lippe, G. (2005). Identification of a conserved calmodulin-binding motif in the sequence of F0F1 ATPsynthase inhibitor protein. *J Bioenerg Biomembr* 37, 317-326.

Contessi, S., Metelli, G., Mavelli, I., and Lippe, G. (2004). Diazoxide affects the IF1 inhibitor protein binding to F1 sector of beef heart F0F1ATPsynthase. *Biochem Pharmacol* 67, 1843-1851.

Cori, G.T., and Larner, J. (1951). Action of amylo-1,6-glucosidase and phosphorylase on glycogen and amylopectin. *J Biol Chem* 188, 17-29.

Corrado, M., Scorrano, L., and Campello, S. (2016). Changing perspective on oncometabolites: from metabolic signature of cancer to tumorigenic and immunosuppressive agents. *Oncotarget*.

Cortes-Cros, M., Hemmerlin, C., Ferretti, S., Zhang, J., Gounarides, J.S., Yin, H., Muller, A., Haberkorn, A., Chene, P., Sellers, W.R., and Hofmann, F. (2013). M2 isoform of pyruvate kinase is dispensable for tumor maintenance and growth. *Proc Natl Acad Sci U S A* 110, 489-494.

Crompton, M., and Costi, A. (1988). Kinetic evidence for a heart mitochondrial pore activated by Ca2+, inorganic phosphate and oxidative stress. A potential mechanism for mitochondrial dysfunction during cellular Ca2+ overload. *Eur J Biochem* 178, 489-501.

Crompton, M., Costi, A., and Hayat, L. (1987). Evidence for the presence of a reversible Ca2+-dependent pore activated by oxidative stress in heart mitochondria. *Biochem J* 245, 915-918.

Cuezva, J.M., Chen, G., Alonso, A.M., Isidoro, A., Misek, D.E., Hanash, S.M., and Beer, D.G. (2004). The bioenergetic signature of lung adenocarcinomas is a molecular marker of cancer diagnosis and prognosis. *Carcinogenesis* 25, 1157-1163.

Cuezva, J.M., Krajewska, M., de Heredia, M.L., Krajewski, S., Santamaria, G., Kim, H., Zapata, J.M., Marusawa, H., Chamorro, M., and Reed, J.C. (2002). The bioenergetic signature of cancer: a marker of tumor progression. *Cancer Res* 62, 6674-6681.

Cuezva, J.M., Ortega, A.D., Willers, I., Sanchez-Cenizo, L., Aldea, M., and Sanchez-Arago, M. (2009). The tumor suppressor function of mitochondria: translation into the clinics. *Biochim Biophys Acta* 1792, 1145-1158.

Cuezva, J.M., Sanchez-Arago, M., Sala, S., Blanco-Rivero, A., and Ortega, A.D. (2007). A message emerging from development: the repression of mitochondrial beta-F1-ATPase expression in cancer. *J Bioenerg Biomembr* 39, 259-265.

Currie, E., Schulze, A., Zechner, R., Walther, T.C., and Farese, R.V., Jr. (2013). Cellular Fatty Acid metabolism and cancer. *Cell Metab* 18, 153-161.

Czabotar, P.E., Lessene, G., Strasser, A., and Adams, J.M. (2014). Control of apoptosis by the BCL-2 protein family: implications for physiology and therapy. *Nat Rev Mol Cell Biol* 15, 49-63.

Chance, B., and Williams, G.R. (1955). A method for the localization of sites for oxidative phosphorylation. *Nature* 176, 250-254.

Chen, C., Ko, Y., Delannoy, M., Ludtke, S.J., Chiu, W., and Pedersen, P.L. (2004a). Mitochondrial ATP synthasome: three-dimensional structure by electron microscopy of the ATP synthase in complex formation with carriers for Pi and ADP/ATP. *J Biol Chem* 279, 31761-31768.

Chen, G., Gharib, T.G., Huang, C.C., Thomas, D.G., Shedden, K.A., Taylor, J.M., Kardia, S.L., Misek, D.E., Giordano, T.J., Iannettoni, M.D., Orringer, M.B., Hanash, S.M., and Beer, D.G. (2002). Proteomic analysis of lung adenocarcinoma: identification of a highly expressed set of proteins in tumors. *Clin Cancer Res* 8, 2298-2305.

Chen, G., Gharib, T.G., Wang, H., Huang, C.C., Kuick, R., Thomas, D.G., Shedden, K.A., Misek, D.E., Taylor, J.M., Giordano, T.J., Kardia, S.L., Iannettoni, M.D., Yee, J., Hogg, P.J., Orringer, M.B., Hanash, S.M., and Beer, D.G. (2003). Protein profiles associated with survival in lung adenocarcinoma. *Proc Natl Acad Sci U S A* 100, 13537-13542.

Chen, J., Kahne, T., Rocken, C., Gotze, T., Yu, J., Sung, J.J., Chen, M., Hu, P., Malfertheiner, P., and Ebert, M.P. (2004b). Proteome analysis of gastric cancer metastasis by two-dimensional gel electrophoresis and matrix assisted laser desorption/ionization-mass spectrometry for identification of metastasis-related proteins. *J Proteome Res* 3, 1009-1016.

Chen, W.W., Birsoy, K., Mihaylova, M.M., Snitkin, H., Stasinski, I., Yucel, B., Bayraktar, E.C., Carette, J.E., Clish, C.B., Brummelkamp, T.R., Sabatini, D.D., and Sabatini, D.M. (2014). Inhibition of ATPIF1 ameliorates severe mitochondrial respiratory chain dysfunction in mammalian cells. *Cell Rep* 7, 27-34.

Chen, Y.J., Wu, C.Y., Huang, Y.L., Wang, C.B., Shen, J.L., and Chang, Y.T. (2010). Cancer risks of dermatomyositis and polymyositis: a nationwide cohort study in Taiwan. *Arthritis Res Ther* 12, R70.

Chen, Z., and McKnight, S.L. (2007). A conserved DNA damage response pathway responsible for coupling the cell division cycle to the circadian and metabolic cycles. *Cell Cycle* 6, 2906-2912.

Chimeo, C., Fernandez-Gimenez, A.V., Campanella, M., Mendez-Romero, O., and Muhlia-Almazan, A. (2015). The shrimp mitochondrial FoF1-ATPase inhibitory factor 1 (IF1). *J Bioenerg Biomembr* 47, 383-393.

Chin, R.M., Fu, X., Pai, M.Y., Vergnes, L., Hwang, H., Deng, G., Diep, S., Lomenick, B., Meli, V.S., Monsalve, G.C., Hu, E., Whelan, S.A., Wang, J.X., Jung, G., Solis, G.M., Fazlollahi, F., Kaweeteerawat, C., Quach, A., Nili, M., Krall, A.S., Godwin, H.A., Chang, H.R., Faull, K.F., Guo, F., Jiang, M., Trauger, S.A., Saghatelian, A., Braas, D., Christofk, H.R., Clarke, C.F., Teitell, M.A., Petrascheck, M., Reue, K., Jung, M.E., Frand, A.R., and Huang, J. (2014). The metabolite alpha-ketoglutarate extends lifespan by inhibiting ATP synthase and TOR. *Nature* 510, 397-401.

Chinopoulos, C. (2011). Mitochondrial consumption of cytosolic ATP: not so fast. *FEBS Lett* 585, 1255-1259.

Choi, C., Ganji, S.K., DeBerardinis, R.J., Hatanpaa, K.J., Rakheja, D., Kovacs, Z., Yang, X.L., Mashimo, T., Raisanen, J.M., Marin-Valencia, I., Pascual, J.M., Madden, C.J., Mickey, B.E., Malloy, C.R., Bachoo, R.M., and Maher, E.A. (2012). 2-hydroxyglutarate detection by magnetic resonance spectroscopy in IDH-mutated patients with gliomas. *Nat Med* 18, 624-629.

Christofk, H.R., Vander Heiden, M.G., Harris, M.H., Ramanathan, A., Gerszten, R.E., Wei, R., Fleming, M.D., Schreiber, S.L., and Cantley, L.C. (2008). The M2 splice isoform of pyruvate kinase is important for cancer metabolism and tumour growth. *Nature* 452, 230-233.

D'Autreaux, B., and Toledano, M.B. (2007). ROS as signalling molecules: mechanisms that generate specificity in ROS homeostasis. *Nat Rev Mol Cell Biol* 8, 813-824.

D'Errico, I., Salvatore, L., Murzilli, S., Lo Sasso, G., Latorre, D., Martelli, N., Egorova, A.V., Polishuck, R., Madeyski-Bengtson, K., Lelliott, C., Vidal-Puig, A.J., Seibel, P., Villani, G., and Moschetta, A. (2011). Peroxisome proliferator-activated receptor-gamma coactivator 1-alpha (PGC1alpha) is a metabolic regulator of intestinal epithelial cell fate. *Proc Natl Acad Sci U S A* 108, 6603-6608.

Dalakas, M.C. (1991). Polymyositis, dermatomyositis and inclusion-body myositis. *N Engl J Med* 325, 1487-1498.

Dalakas, M.C. (2015). Inflammatory muscle diseases. *N Engl J Med* 372, 1734-1747.

Dalakas, M.C., and Hohlfeld, R. (2003). Polymyositis and dermatomyositis. *Lancet* 362, 971-982.

Dang, L., White, D.W., Gross, S., Bennett, B.D., Bittinger, M.A., Driggers, E.M., Fantin, V.R., Jang, H.G., Jin, S., Keenan, M.C., Marks, K.M., Prins, R.M., Ward, P.S., Yen, K.E., Liau, L.M., Rabinowitz, J.D., Cantley, L.C., Thompson, C.B., Vander Heiden, M.G., and Su, S.M. (2009). Cancer-associated IDH1 mutations produce 2-hydroxyglutarate. *Nature* 462, 739-744.

Daum, B., Walter, A., Horst, A., Osiewacz, H.D., and Kuhlbrandt, W. (2013). Age-dependent dissociation of ATP synthase dimers and loss of inner-membrane cristae in mitochondria. *Proc Natl Acad Sci U S A* 110, 15301-15306.

David, C.J., Chen, M., Assanah, M., Canoll, P., and Manley, J.L. (2010). HnRNP proteins controlled by c-Myc deregulate pyruvate kinase mRNA splicing in cancer. *Nature* 463, 364-368.

Davies, K.M., Anselmi, C., Wittig, I., Faraldo-Gomez, J.D., and Kuhlbrandt, W. (2012a). Structure of the yeast F1Fo-ATP synthase dimer and its role in shaping the mitochondrial cristae. *Proc Natl Acad Sci U S A* 109, 13602-13607.

Davies, K.M., Daum, B., Gold, V.A., Muhleip, A.W., Brandt, T., Blum, T.B., Mills, D.J., and Kuhlbrandt, W. (2014). Visualization of ATP synthase dimers in mitochondria by electron cryo-tomography. *J Vis Exp*, 51228.

Davies, K.M., Daum, B., Kuhlbrandt, W., Anselmi, C., and Faraldo-Gomez, J. (2012b). Structure of the mitochondrial ATP synthase and its role in shaping mitochondria cristae. *Microsc Microanal* 18 Suppl 2, 56-57.

Davies, K.M., Strauss, M., Daum, B., Kief, J.H., Osiewacz, H.D., Rycovska, A., Zickermann, V., and Kuhlbrandt, W. (2011). Macromolecular organization of ATP synthase and complex I in whole mitochondria. *Proc Natl Acad Sci U S A* 108, 14121-14126.

de Groof, A.J., te Lindert, M.M., van Dommelen, M.M., Wu, M., Willemse, M., Smift, A.L., Winer, M., Oerlemans, F., Pluk, H., Fransen, J.A., and Wieringa, B. (2009). Increased OXPHOS activity precedes rise in glycolytic rate in H-RasV12/E1A transformed fibroblasts that develop a Warburg phenotype. *Mol Cancer* 8, 54.

De los Rios Castillo, D., Zarco-Zavala, M., Olvera-Sanchez, S., Pardo, J.P., Juarez, O., Martinez, F., Mendoza-Hernandez, G., Garcia-Trejo, J.J., and Flores-Herrera, O. (2011). Atypical cristae morphology of human syncytiotrophoblast mitochondria: role for complex V. *J Biol Chem* 286, 23911-23919.

DeBerardinis, R.J., Lum, J.J., Hatzivassiliou, G., and Thompson, C.B. (2008). The biology of cancer: metabolic reprogramming fuels cell growth and proliferation. *Cell Metab* 7, 11-20.

DeBerardinis, R.J., Mancuso, A., Daikhin, E., Nissim, I., Yudkoff, M., Wehrli, S., and Thompson, C.B. (2007). Beyond aerobic glycolysis: transformed cells can engage in glutamine metabolism that exceeds the requirement for protein and nucleotide synthesis. *Proc Natl Acad Sci U S A* 104, 19345-19350.

DeLaBarre, B., Hurov, J., Cianchetta, G., Murray, S., and Dang, L. (2014). Action at a distance: allostery and the development of drugs to target cancer cell metabolism. *Chem Biol* 21, 1143-1161.

Desai, S., Ding, M., Wang, B., Lu, Z., Zhao, Q., Shaw, K., Yung, W.K., Weinstein, J.N., Tan, M., and Yao, J. (2014). Tissue-specific isoform switch and DNA hypomethylation of the pyruvate kinase PKM gene in human cancers. *Oncotarget* 5, 8202-8210.

Di Benedetto, G., Pendin, D., Greotti, E., Pizzo, P., and Pozzan, T. (2014). Ca2+ and cAMP cross-talk in mitochondria. *J Physiol* 592, 305-312.

Di Benedetto, G., Scalzotto, E., Mongillo, M., and Pozzan, T. (2013). Mitochondrial Ca(2)(+) uptake induces cyclic AMP generation in the matrix and modulates organelle ATP levels. *Cell Metab* 17, 965-975.

Di Lisa, F., Carpi, A., Giorgio, V., and Bernardi, P. (2011). The mitochondrial permeability transition pore and cyclophilin D in cardioprotection. *Biochim Biophys Acta* 1813, 1316-1322.

Di Pancrazio, F., Mavelli, I., Isola, M., Losano, G., Pagliaro, P., Harris, D.A., and Lippe, G. (2004). In vitro and in vivo studies of F(0)F(1)ATP synthase regulation by inhibitor protein IF(1) in goat heart. *Biochim Biophys Acta* 1659, 52-62.

Dienhart, M., Pfeiffer, K., Schagger, H., and Stuart, R.A. (2002). Formation of the yeast F1F0-ATP synthase dimeric complex does not require the ATPase inhibitor protein, Inh1. *J Biol Chem* 277, 39289-39295.

DiNardo, C.D., Propert, K.J., Loren, A.W., Paietta, E., Sun, Z., Levine, R.L., Straley, K.S., Yen, K., Patel, J.P., Agresta, S., Abdel-Wahab, O., Perl, A.E., Litzow, M.R., Rowe, J.M., Lazarus, H.M., Fernandez, H.F., Margolis, D.J., Tallman, M.S., Luger, S.M., and Carroll, M. (2013). Serum 2-hydroxyglutarate levels predict isocitrate dehydrogenase mutations and clinical outcome in acute myeloid leukemia. *Blood* 121, 4917-4924.

Dolado, I., Swat, A., Ajenjo, N., De Vita, G., Cuadrado, A., and Nebreda, A.R. (2007). p38alpha MAP kinase as a sensor of reactive oxygen species in tumorigenesis. *Cancer Cell* 11, 191-205.

Doran, P., Donoghue, P., O'Connell, K., Gannon, J., and Ohlendieck, K. (2007). Proteomic profiling of pathological and aged skeletal muscle fibres by peptide mass fingerprinting (Review). *Int J Mol Med* 19, 547-564.

Duchen, M.R., McGuinness, O., Brown, L.A., and Crompton, M. (1993). On the involvement of a cyclosporin A sensitive mitochondrial pore in myocardial reperfusion injury. *Cardiovasc Res* 27, 1790-1794.

Dudkina, N.V., Eubel, H., Keegstra, W., Boekema, E.J., and Braun, H.P. (2005). Structure of a mitochondrial supercomplex formed by respiratory-chain complexes I and III. *Proc Natl Acad Sci U S A* 102, 3225-3229.

Dudkina, N.V., Sunderhaus, S., Braun, H.P., and Boekema, E.J. (2006). Characterization of dimeric ATP synthase and cristae membrane ultrastructure from Saccharomyces and Polytomella mitochondria. *FEBS Lett* 580, 3427-3432.

Ekins, R.P. (1989). Multi-analyte immunoassay. *J Pharm Biomed Anal* 7, 155-168.

Ekins, R.P. (1998). Ligand assays: from electrophoresis to miniaturized microarrays. *Clin Chem* 44, 2015-2030.

Emery, A.E. (1998). The muscular dystrophies. *BMJ* 317, 991-995.

Enriquez, J.A. (2016). Supramolecular Organization of Respiratory Complexes. *Annu Rev Physiol* 78, 533-561.

Espina, V., Woodhouse, E.C., Wulfkuhle, J., Asmussen, H.D., Petricoin, E.F., 3rd, and Liotta, L.A. (2004). Protein microarray detection strategies: focus on direct detection technologies. *J Immunol Methods* 290, 121-133.

Faccenda, D., Tan, C.H., Seraphim, A., Duchen, M.R., and Campanella, M. (2013). IF1 limits the apoptotic-signalling cascade by preventing mitochondrial remodelling. *Cell Death Differ* 20, 686-697.

Fantin, V.R., St-Pierre, J., and Leder, P. (2006). Attenuation of LDH-A expression uncovers a link between glycolysis, mitochondrial physiology, and tumor maintenance. *Cancer Cell* 9, 425-434.

Feinberg, J.G. (1961). A 'microspot' test for antigens and antibodies. *Nature* 192, 985-986.

Feinberg, J.G. (1962). 'Microspot' test applied to cellulose acetate membranes. *Nature* 194, 307-308.

Feinberg, J.G., and Wheeler, A.W. (1963). Detection of auto-immune antibody and tissue antigens by the 'microspot' technique. *J Clin Pathol* 16, 282-284.

Finnberg, N., Stenius, U., and Hogberg, J. (2004). Heterozygous p53-deficient (+/-) mice develop fewer p53-negative preneoplastic focal liver lesions in response to treatment with diethylnitrosamine than do wild-type (+/+) mice. *Cancer Lett* 207, 149-155.

Formentini, L., Martinez-Reyes, I., and Cuezva, J.M. (2010). The mitochondrial bioenergetic capacity of carcinomas. *IUBMB Life* 62, 554-560.

Formentini, L., Sánchez-Aragó, M., Sánchez-Cenizo, L., and Cuezva, J.M. (2012). The mitochondrial ATPase Inhibitory Factor 1 (IF1) triggers a ROS-mediated retrograde pro-survival and proliferative response. *Mol. Cell* 45, 731-742.

Forner, F., Kumar, C., Luber, C.A., Fromme, T., Klingenspor, M., and Mann, M. (2009). Proteome differences between brown and white fat mitochondria reveal specialized metabolic functions. *Cell Metab* 10, 324-335.

Frezza, C., Cipolat, S., Martins de Brito, O., Micaroni, M., Beznoussenko, G.V., Rudka, T., Bartoli, D., Polishuck, R.S., Danial, N.N., De Strooper, B., and Scorrano, L. (2006). OPA1 controls apoptotic cristae remodeling independently from mitochondrial fusion. *Cell* 126, 177-189.

Fronzes, R., Weimann, T., Vaillier, J., Velours, J., and Brethes, D. (2006). The peripheral stalk participates in the yeast ATP synthase dimerization independently of e and g subunits. *Biochemistry* 45, 6715-6723.

Fujikawa, M., Imamura, H., Nakamura, J., and Yoshida, M. (2012). Assessing the actual contribution of IF1, an inhibitor of mitochondrial FoF1, to ATP homeostasis, cell growth, mitochondrial morphology and cell viability. *J Biol Chem* 287, 18781-18787.

Fukuda, R., Zhang, H., Kim, J.W., Shimoda, L., Dang, C.V., and Semenza, G.L. (2007). HIF-1 regulates cytochrome oxidase subunits to optimize efficiency of respiration in hypoxic cells. *Cell* 129, 111-122.

Fukumura, D., Xu, L., Chen, Y., Gohongi, T., Seed, B., and Jain, R.K. (2001). Hypoxia and acidosis independently up-regulate vascular endothelial growth factor transcription in brain tumors in vivo. *Cancer Res* 61, 6020-6024.

Funes, J.M., Quintero, M., Henderson, S., Martinez, D., Qureshi, U., Westwood, C., Clements, M.O., Bourboulia, D., Pedley, R.B., Moncada, S., and Boshoff, C. (2007). Transformation of human mesenchymal stem cells increases their dependency on oxidative phosphorylation for energy production. *Proc Natl Acad Sci U S A* 104, 6223-6228.

Galante, Y.M., Wong, S.Y., and Hatefi, Y. (1981). Mitochondrial adenosinetriphosphatase inhibitor protein: reversible interaction with complex V (ATP synthetase complex). *Biochemistry* 20, 2671-2678.

Galluzzi, L., Blomgren, K., and Kroemer, G. (2009). Mitochondrial membrane permeabilization in neuronal injury. *Nat Rev Neurosci* 10, 481-494.

Garcia-Bermudez, J., and Cuezva, J.M. (2016). The ATPase Inhibitory Factor 1 (IF1): A master regulator of energy metabolism and of cell survival. *Biochim Biophys Acta*.

Garcia-Bermudez, J., Sanchez-Arago, M., Soldevilla, B., Del Arco, A., Nuevo-Tapioles, C., and Cuezva, J.M. (2015). PKA Phosphorylates the ATPase Inhibitory Factor 1 and Inactivates Its Capacity to Bind and Inhibit the Mitochondrial H-ATP Synthase. *Cell Rep* 12, 2143-2155.

Garcia-Cao, I., Song, M.S., Hobbs, R.M., Laurent, G., Giorgi, C., de Boer, V.C., Anastasiou, D., Ito, K., Sasaki, A.T., Rameh, L., Carracedo, A., Vander Heiden, M.G., Cantley, L.C., Pinton, P., Haigis, M.C., and Pandolfi, P.P. (2012). Systemic elevation of PTEN induces a tumor-suppressive metabolic state. *Cell* 149, 49-62.

Garcia, J.J., Morales-Rios, E., Cortes-Hernandez, P., and Rodriguez-Zavala, J.S. (2006). The inhibitor protein (IF1) promotes dimerization of the mitochondrial F1F0-ATP synthase. *Biochemistry* 45, 12695-12703.

Gavin, P.D., Prescott, M., and Devenish, R.J. (2005). F1F0-ATP synthase complex interactions in vivo can occur in the absence of the dimer specific subunit e. *J Bioenerg Biomembr* 37, 55-66.

Genova, M.L., Baracca, A., Biondi, A., Casalena, G., Faccioli, M., Falasca, A.I., Formiggini, G., Sgarbi, G., Solaini, G., and Lenaz, G. (2008). Is supercomplex organization of the respiratory chain required for optimal electron transfer activity? *Biochim Biophys Acta* 1777, 740-746.

Geraets, R.D., Koh, S., Hastings, M.L., Kielian, T., Pearce, D.A., and Weimer, J.M. (2016). Moving towards effective therapeutic strategies for Neuronal Ceroid Lipofuscinosis. *Orphanet J Rare Dis* 11, 40.

Gillies, R.J., and Gatenby, R.A. (2007). Hypoxia and adaptive landscapes in the evolution of carcinogenesis. *Cancer Metastasis Rev* 26, 311-317.

Giorgio, V., Bisetto, E., Soriano, M.E., Dabbeni-Sala, F., Basso, E., Petronilli, V., Forte, M.A., Bernardi, P., and Lippe, G. (2009). Cyclophilin D modulates mitochondrial

F0F1-ATP synthase by interacting with the lateral stalk of the complex. *J Biol Chem* 284, 33982-33988.

Giorgio, V., von Stockum, S., Antoniel, M., Fabbro, A., Fogolari, F., Forte, M., Glick, G.D., Petronilli, V., Zoratti, M., Szabo, I., Lippe, G., and Bernardi, P. (2013). Dimers of mitochondrial ATP synthase form the permeability transition pore. *Proc Natl Acad Sci U S A* 110, 5887-5892.

Gledhill, J.R., Montgomery, M.G., Leslie, A.G., and Walker, J.E. (2007). How the regulatory protein, IF(1), inhibits F(1)-ATPase from bovine mitochondria. *Proc Natl Acad Sci U S A* 104, 15671-15676.

Gomes, L.C., Di Benedetto, G., and Scorrano, L. (2011). During autophagy mitochondria elongate, are spared from degradation and sustain cell viability. *Nat Cell Biol* 13, 589-598.

Gordon-Smith, D.J., Carbajo, R.J., Yang, J.C., Videler, H., Runswick, M.J., Walker, J.E., and Neuhaus, D. (2001). Solution structure of a C-terminal coiled-coil domain from bovine IF(1): the inhibitor protein of F(1) ATPase. *J Mol Biol* 308, 325-339.

Green, D.R., Galluzzi, L., and Kroemer, G. (2014). Cell biology. Metabolic control of cell death. *Science* 345, 1250256.

Grover, G.J., Atwal, K.S., Sleph, P.G., Wang, F.L., Monshizadegan, H., Monticello, T., and Green, D.W. (2004). Excessive ATP hydrolysis in ischemic myocardium by mitochondrial F1F0-ATPase: effect of selective pharmacological inhibition of mitochondrial ATPase hydrolase activity. *Am J Physiol Heart Circ Physiol* 287, H1747-1755.

Guevel, L., Lavoie, J.R., Perez-Iratxeta, C., Rouger, K., Dubreil, L., Feron, M., Talon, S., Brand, M., and Megeney, L.A. (2011). Quantitative proteomic analysis of dystrophic dog muscle. *J Proteome Res* 10, 2465-2478.

Gygi, S.P., Rochon, Y., Franza, B.R., and Aebersold, R. (1999). Correlation between protein and mRNA abundance in yeast. *Mol Cell Biol* 19, 1720-1730.

Hackenbrock, C.R., Chazotte, B., and Gupte, S.S. (1986). The random collision model and a critical assessment of diffusion and collision in mitochondrial electron transport. *J Bioenerg Biomembr* 18, 331-368.

Hamanaka, R.B., and Chandel, N.S. (2010). Mitochondrial reactive oxygen species regulate cellular signaling and dictate biological outcomes. *Trends Biochem Sci* 35, 505-513.

Hanahan, D. (2014). Rethinking the war on cancer. *Lancet* 383, 558-563.

Hanahan, D., and Weinberg, R.A. (2011). Hallmarks of cancer: the next generation. *Cell* 144, 646-674.

Harner, M., Korner, C., Walther, D., Mokranjac, D., Kaesmacher, J., Welsch, U., Griffith, J., Mann, M., Reggiori, F., and Neupert, W. (2011). The mitochondrial contact site complex, a determinant of mitochondrial architecture. *EMBO J* 30, 4356-4370.

Hashimoto, T., Negawa, Y., and Tagawa, K. (1981). Binding of intrinsic ATPase inhibitor to mitochondrial ATPase--stoichiometry of binding of nucleotides, inhibitor, and enzyme. *J Biochem* 90, 1151-1157.

Hashimoto, T., Yoshida, Y., and Tagawa, K. (1984). Purification and properties of factors in yeast mitochondria stabilizing the F1F0-ATPase-inhibitor complex. *J Biochem* 95, 131-136.

Hashimoto, T., Yoshida, Y., and Tagawa, K. (1990). Simultaneous bindings of ATPase inhibitor and 9K protein to F1F0-ATPase in the presence of 15K protein in yeast mitochondria. *J Biochem* 108, 17-20.

Hathout, Y., Marathi, R.L., Rayavarapu, S., Zhang, A., Brown, K.J., Seol, H., Gordish-Dressman, H., Cirak, S., Bello, L., Nagaraju, K., Partridge, T., Hoffman, E.P., Takeda, S., Mah, J.K., Henricson, E., and McDonald, C. (2014). Discovery of serum protein biomarkers in the mdx mouse model and cross-species comparison to Duchenne muscular dystrophy patients. *Hum Mol Genet*.

Hayashi, T., Rizzuto, R., Hajnoczky, G., and Su, T.P. (2009). MAM: more than just a housekeeper. *Trends Cell Biol* 19, 81-88.

He, Q.Y., Chen, J., Kung, H.F., Yuen, A.P., and Chiu, J.F. (2004). Identification of tumor-associated proteins in oral tongue squamous cell carcinoma by proteomics. *Proteomics* 4, 271-278.

Hekman, C., Tomich, J.M., and Hatefi, Y. (1991). Mitochondrial ATP synthase complex. Membrane topography and stoichiometry of the F0 subunits. *J. Biol. Chem.* 266, 13564-13571.

Hernlund, E., Hjerpe, E., Avall-Lundqvist, E., and Shoshan, M. (2009). Ovarian carcinoma cells with low levels of beta-F1-ATPase are sensitive to combined platinum and 2-deoxy-D-glucose treatment. *Mol Cancer Ther* 8, 1916-1923.

Hill, C.L., Zhang, Y., Sigurgeirsson, B., Pukkala, E., Mellemkjaer, L., Airio, A., Evans, S.R., and Felson, D.T. (2001). Frequency of specific cancer types in dermatomyositis and polymyositis: a population-based study. *Lancet* 357, 96-100.

Hirschey, M.D., DeBerardinis, R.J., Diehl, A.M., Drew, J.E., Frezza, C., Green, M.F., Jones, L.W., Ko, Y.H., Le, A., Lea, M.A., Locasale, J.W., Longo, V.D., Lyssiotis, C.A., McDonnell, E., Mehrmohamadi, M., Michelotti, G., Muralidhar, V., Murphy, M.P., Pedersen, P.L., Poore, B., Raffaghello, L., Rathmell, J.C., Sivanand, S., Vander Heiden, M.G., Wellen, K.E., and Target Validation, T. (2015). Dysregulated metabolism contributes to oncogenesis. *Semin Cancer Biol* 35 Suppl, S129-150.

Hitosugi, T., Kang, S., Vander Heiden, M.G., Chung, T.W., Elf, S., Lythgoe, K., Dong, S., Lonial, S., Wang, X., Chen, G.Z., Xie, J., Gu, T.L., Polakiewicz, R.D., Roesel, J.L., Boggon, T.J., Khuri, F.R., Gilliland, D.G., Cantley, L.C., Kaufman, J., and Chen, J. (2009). Tyrosine phosphorylation inhibits PKM2 to promote the Warburg effect and tumor growth. *Sci Signal* 2, ra73.

Hollenbeck, P.J., and Saxton, W.M. (2005). The axonal transport of mitochondria. *J Cell Sci* 118, 5411-5419.

Hsu, H.Y., Wittemann, S., Schneider, E.M., Weiss, M., and Joos, T.O. (2008). Suspension microarrays for the identification of the response patterns in hyperinflammatory diseases. *Med Eng Phys* 30, 976-983.

Hsu, P.P., and Sabatini, D.M. (2008). Cancer cell metabolism: Warburg and beyond. *Cell* 134, 703-707.

Huang, L.J., Chuang, I.C., Dong, H.P., and Yang, R.C. (2011). Hypoxia-inducible factor 1alpha regulates the expression of the mitochondrial ATPase inhibitor protein (IF1) in rat liver. *Shock* 36, 90-96.

Huang, R.P. (2003). Protein arrays, an excellent tool in biomedical research. *Front Biosci* 8, d559-576.

Hunter, D.R., and Haworth, R.A. (1979). The Ca2+-induced membrane transition in mitochondria. III. Transitional Ca2+ release. *Arch Biochem Biophys* 195, 468-477.

Ichikawa, N., Ando, C., and Fumino, M. (2006). Caenorhabditis elegans MAI-1 protein, which is similar to mitochondrial ATPase inhibitor (IF1), can inhibit yeast F0F1-ATPase but cannot be transported to yeast mitochondria. *J Bioenerg Biomembr* 38, 93-99.

Iqbal, M.A., Gupta, V., Gopinath, P., Mazurek, S., and Bamezai, R.N. (2014). Pyruvate kinase M2 and cancer: an updated assessment. *FEBS Lett* 588, 2685-2692.

Isidoro, A., Casado, E., Redondo, A., Acebo, P., Espinosa, E., Alonso, A.M., Cejas, P., Hardisson, D., Fresno Vara, J.A., Belda-Iniesta, C., Gonzalez-Baron, M., and Cuezva, J.M. (2005). Breast carcinomas fulfill the Warburg hypothesis and provide metabolic markers of cancer prognosis. *Carcinogenesis* 26, 2095-2104.

Izquierdo, J.M., Ricart, J., Ostronoff, L.K., Egea, G., and Cuezva, J.M. (1995). Changing patterns of transcriptional and post-transcriptional control of beta-F1-ATPase gene expression during mitochondrial biogenesis in liver. *J Biol Chem* 270, 10342-10350.

Jennings, R.B., Reimer, K.A., and Steenbergen, C. (1991). Effect of inhibition of the mitochondrial ATPase on net myocardial ATP in total ischemia. *J Mol Cell Cardiol* 23, 1383-1395.

Jiang, B.H., Jiang, G., Zheng, J.Z., Lu, Z., Hunter, T., and Vogt, P.K. (2001). Phosphatidylinositol 3-kinase signaling controls levels of hypoxia-inducible factor 1. *Cell Growth Differ* 12, 363-369.

Johansson, M., Denardo, D.G., and Coussens, L.M. (2008). Polarized immune responses differentially regulate cancer development. *Immunol Rev* 222, 145-154.

Johnson, K.M., Chen, X., Boitano, A., Swenson, L., Opipari, A.W., Jr., and Glick, G.D. (2005). Identification and validation of the mitochondrial F1F0-ATPase as the molecular target of the immunomodulatory benzodiazepine Bz-423. *Chem Biol* 12, 485-496.

Jovaisaite, V., Mouchiroud, L., and Auwerx, J. (2014). The mitochondrial unfolded protein response, a conserved stress response pathway with implications in health and disease. *J Exp Biol* 217, 137-143.

Karin, M. (2006). Nuclear factor-kappaB in cancer development and progression. *Nature* 441, 431-436.

Killian, J.K., Kim, S.Y., Miettinen, M., Smith, C., Merino, M., Tsokos, M., Quezado, M., Smith, W.I., Jr., Jahromi, M.S., Xekouki, P., Szarek, E., Walker, R.L., Lasota, J., Raffeld, M., Klotzle, B., Wang, Z., Jones, L., Zhu, Y., Wang, Y., Waterfall, J.J., O'Sullivan, M.J., Bibikova, M., Pacak, K., Stratakis, C., Janeway, K.A., Schiffman, J.D., Fan, J.B., Helman, L., and Meltzer, P.S. (2013). Succinate dehydrogenase mutation underlies global epigenomic divergence in gastrointestinal stromal tumor. *Cancer Discov* 3, 648-657.

Kim, H.S., Patel, K., Muldoon-Jacobs, K., Bisht, K.S., Aykin-Burns, N., Pennington, J.D., van der Meer, R., Nguyen, P., Savage, J., Owens, K.M., Vassilopoulos, A., Ozden, O., Park, S.H., Singh, K.K., Abdulkadir, S.A., Spitz, D.R., Deng, C.X., and Gius, D. (2010). SIRT3 is a mitochondria-localized tumor suppressor required for maintenance of mitochondrial integrity and metabolism during stress. *Cancer Cell* 17, 41-52.

Kim, J., Lee, J.H., and Iyer, V.R. (2008). Global identification of Myc target genes reveals its direct role in mitochondrial biogenesis and its E-box usage in vivo. *PLoS ONE* 3, e1798.

Kim, J.W., Gao, P., Liu, Y.C., Semenza, G.L., and Dang, C.V. (2007). Hypoxia-inducible factor 1 and dysregulated c-Myc cooperatively induce vascular endothelial growth factor and metabolic switches hexokinase 2 and pyruvate dehydrogenase kinase 1. *Mol Cell Biol* 27, 7381-7393.

Kim, J.W., Tchernyshyov, I., Semenza, G.L., and Dang, C.V. (2006). HIF-1-mediated expression of pyruvate dehydrogenase kinase: a metabolic switch required for cellular adaptation to hypoxia. *Cell Metab* 3, 177-185.

Klein, G., Lunardi, J., and Vignais, P.V. (1981). Effect of the natural ATPase inhibitor on the binding of adenine nucleotides and inorganic phosphate to mitochondrial F1-ATPase. *Biochim Biophys Acta* 636, 185-192.

Klein, G., Satre, M., Dianoux, A.C., and Vignais, P.V. (1980). Radiolabeling of natural adenosine triphosphatase inhibitor with phenyl (14C)isothiocyanate and study of its

interaction with mitochondrial adenosine triphosphatase. Localization of inhibitor binding sites and stoichiometry of binding. *Biochemistry* 19, 2919-2925.

Ko, Y.H., Delannoy, M., Hullihen, J., Chiu, W., and Pedersen, P.L. (2003). Mitochondrial ATP synthasome. Cristae-enriched membranes and a multiwell detergent screening assay yield dispersed single complexes containing the ATP synthase and carriers for Pi and ADP/ATP. *J Biol Chem* 278, 12305-12309.

Kodadek, T. (2001). Protein microarrays: prospects and problems. *Chem Biol* 8, 105-115.

Kominsky, D.J., Brownson, M.P., Updike, D.L., and Thorsness, P.E. (2002). Genetic and biochemical basis for viability of yeast lacking mitochondrial genomes. *Genetics* 162, 1595-1604.

Kondoh, H., Lleonart, M.E., Nakashima, Y., Yokode, M., Tanaka, M., Bernard, D., Gil, J., and Beach, D. (2007). A high glycolytic flux supports the proliferative potential of murine embryonic stem cells. *Antioxid Redox Signal* 9, 293-299.

Kononen, J., Bubendorf, L., Kallioniemi, A., Barlund, M., Schraml, P., Leighton, S., Torhorst, J., Mihatsch, M.J., Sauter, G., and Kallioniemi, O.P. (1998). Tissue microarrays for high-throughput molecular profiling of tumor specimens. *Nat Med* 4, 844-847.

Kontro, H., Cannino, G., Rustin, P., Dufour, E., and Kainulainen, H. (2015). DAPIT Over-Expression Modulates Glucose Metabolism and Cell Behaviour in HEK293T Cells. *PLoS One* 10, e0131990.

Kornmann, B., and Walter, P. (2010). ERMES-mediated ER-mitochondria contacts: molecular hubs for the regulation of mitochondrial biology. *J Cell Sci* 123, 1389-1393.

Krause, F., Reifschneider, N.H., Goto, S., and Dencher, N.A. (2005). Active oligomeric ATP synthases in mammalian mitochondria. *Biochem Biophys Res Commun* 329, 583-590.

Kroemer, G., and Pouyssegur, J. (2008). Tumor cell metabolism: cancer's Achilles' heel. *Cancer Cell* 13, 472-482.

Kusnezow, W., Jacob, A., Walijew, A., Diehl, F., and Hoheisel, J.D. (2003). Antibody microarrays: an evaluation of production parameters. *Proteomics* 3, 254-264.

Lagouge, M., Argmann, C., Gerhart-Hines, Z., Meziane, H., Lerin, C., Daussin, F., Messadeq, N., Milne, J., Lambert, P., Elliott, P., Geny, B., Laakso, M., Puigserver, P., and Auwerx, J. (2006). Resveratrol improves mitochondrial function and protects against metabolic disease by activating SIRT1 and PGC-1alpha. *Cell* 127, 1109-1122.

Lapuente-Brun, E., Moreno-Loshuertos, R., Acin-Perez, R., Latorre-Pellicer, A., Colas, C., Balsa, E., Perales-Clemente, E., Quiros, P.M., Calvo, E., Rodriguez-Hernandez, M.A., Navas, P., Cruz, R., Carracedo, A., Lopez-Otin, C., Perez-Martos, A., Fernandez-Silva, P., Fernandez-Vizarra, E., and Enriquez, J.A. (2013).

Supercomplex assembly determines electron flux in the mitochondrial electron transport chain. *Science* 340, 1567-1570.

Le, A., Cooper, C.R., Gouw, A.M., Dinavahi, R., Maitra, A., Deck, L.M., Royer, R.E., Vander Jagt, D.L., Semenza, G.L., and Dang, C.V. (2010). Inhibition of lactate dehydrogenase A induces oxidative stress and inhibits tumor progression. *Proc Natl Acad Sci U S A* 107, 2037-2042.

Lebo, R.V., Gorin, F., Fletterick, R.J., Kao, F.T., Cheung, M.C., Bruce, B.D., and Kan, Y.W. (1984). High-resolution chromosome sorting and DNA spot-blot analysis assign McArdle's syndrome to chromosome 11. *Science* 225, 57-59.

Ledford, H. (2014). Metabolic quirks yield tumour hope. *Nature* 508, 158-159.

Lefkimmiatis, K., and Zaccolo, M. (2014). cAMP signaling in subcellular compartments. *Pharmacol Ther* 143, 295-304.

Letouze, E., Martinelli, C., Loriot, C., Burnichon, N., Abermil, N., Ottolenghi, C., Janin, M., Menara, M., Nguyen, A.T., Benit, P., Buffet, A., Marcaillou, C., Bertherat, J., Amar, L., Rustin, P., De Reynies, A., Gimenez-Roqueplo, A.P., and Favier, J. (2013). SDH mutations establish a hypermethylator phenotype in paraganglioma. *Cancer Cell* 23, 739-752.

Leung, A.W., Varanyuwatana, P., and Halestrap, A.P. (2008). The mitochondrial phosphate carrier interacts with cyclophilin D and may play a key role in the permeability transition. *J Biol Chem* 283, 26312-26323.

Li, B., Chauvin, C., De Paulis, D., De Oliveira, F., Gharib, A., Vial, G., Lablanche, S., Leverve, X., Bernardi, P., Ovize, M., and Fontaine, E. (2012). Inhibition of complex I regulates the mitochondrial permeability transition through a phosphate-sensitive inhibitory site masked by cyclophilin D. *Biochim Biophys Acta* 1817, 1628-1634.

Li, Y., Liang, Q., Wen, Y.Q., Chen, L.L., Wang, L.T., Liu, Y.L., Luo, C.Q., Liang, H.Z., Li, M.T., and Li, Z. (2010). Comparative proteomics analysis of human osteosarcomas and benign tumor of bone. *Cancer Genet Cytogenet* 198, 97-106.

Liesa, M., and Shirihai, O.S. (2013). Mitochondrial dynamics in the regulation of nutrient utilization and energy expenditure. *Cell Metab* 17, 491-506.

Lin, P.C., Lin, J.K., Yang, S.H., Wang, H.S., Li, A.F., and Chang, S.C. (2008). Expression of beta-F1-ATPase and mitochondrial transcription factor A and the change in mitochondrial DNA content in colorectal cancer: clinical data analysis and evidence from an in vitro study. *Int J Colorectal Dis* 23, 1223-1232.

Liotta, L.A., and Kohn, E.C. (2003). Cancer's deadly signature. *Nat Genet* 33, 10-11.

Lopez-Mediavilla, C., Vigny, H., and Godinot, C. (1993). Docking the mitochondrial inhibitor protein IF1 to a membrane receptor different from the F1-ATPase beta subunit. *Eur J Biochem* 215, 487-496.

Lopez-Rios, F., Sanchez-Arago, M., Garcia-Garcia, E., Ortega, A.D., Berrendero, J.R., Pozo-Rodriguez, F., Lopez-Encuentra, A., Ballestin, C., and Cuezva, J.M. (2007). Loss of the mitochondrial bioenergetic capacity underlies the glucose avidity of carcinomas. *Cancer Res* 67, 9013-9017.

Lunt, S.Y., and Vander Heiden, M.G. (2011). Aerobic glycolysis: meeting the metabolic requirements of cell proliferation. *Annu Rev Cell Dev Biol* 27, 441-464.

Luo, W., Hu, H., Chang, R., Zhong, J., Knabel, M., O'Meally, R., Cole, R.N., Pandey, A., and Semenza, G.L. (2011). Pyruvate kinase M2 is a PHD3-stimulated coactivator for hypoxia-inducible factor 1. *Cell* 145, 732-744.

Lytovchenko, O., Naumenko, N., Oeljeklaus, S., Schmidt, B., von der Malsburg, K., Deckers, M., Warscheid, B., van der Laan, M., and Rehling, P. (2014). The INA complex facilitates assembly of the peripheral stalk of the mitochondrial F1Fo-ATP synthase. *EMBO J* 33, 1624-1638.

Mannella, C.A. (2000). Introduction: our changing views of mitochondria. *J Bioenerg Biomembr* 32, 1-4.

Mannella, C.A. (2006). Structure and dynamics of the mitochondrial inner membrane cristae. *Biochim Biophys Acta* 1763, 542-548.

Mao, H.Z., and Weber, J. (2007). Identification of the betaTP site in the x-ray structure of F1-ATPase as the high-affinity catalytic site. *Proc Natl Acad Sci U S A* 104, 18478-18483.

Martinez-Diez, M., Santamaria, G., Ortega, A.D., and Cuezva, J.M. (2006). Biogenesis and Dynamics of Mitochondria during the Cell Cycle: Significance of 3'UTRs. *PLoS ONE* 1, e107.

Martinez-Reyes, I., and Cuezva, J.M. (2014). The H(+)-ATP synthase: a gate to ROS-mediated cell death or cell survival. *Biochim Biophys Acta* 1837, 1099-1112.

Mastaglia, F.L., and Phillips, B.A. (2002). Idiopathic inflammatory myopathies: epidemiology, classification, and diagnostic criteria. *Rheum Dis Clin North Am* 28, 723-741.

Masuda, M., and Yamada, T. (2015). Signaling pathway profiling by reverse-phase protein array for personalized cancer medicine. *Biochim Biophys Acta* 1854, 651-657.

Mathupala, S.P., Ko, Y.H., and Pedersen, P.L. (2009). Hexokinase-2 bound to mitochondria: cancer's stygian link to the "Warburg Effect" and a pivotal target for effective therapy. *Semin Cancer Biol* 19, 17-24.

Matsuyama, S., Xu, Q., Velours, J., and Reed, J.C. (1998). The Mitochondrial F0F1-ATPase proton pump is required for function of the proapoptotic protein Bax in yeast and mammalian cells. *Mol Cell* 1, 327-336.

Mazurek, S. (2011). Pyruvate kinase type M2: a key regulator of the metabolic budget system in tumor cells. *Int J Biochem Cell Biol* 43, 969-980.

McGuinness, O., Yafei, N., Costi, A., and Crompton, M. (1990). The presence of two classes of high-affinity cyclosporin A binding sites in mitochondria. Evidence that the minor component is involved in the opening of an inner-membrane Ca(2+)-dependent pore. *Eur J Biochem* 194, 671-679.

Meikle, P.J., Hopwood, J.J., Clague, A.E., and Carey, W.F. (1999). Prevalence of lysosomal storage disorders. *JAMA* 281, 249-254.

Michelakis, E.D., Sutendra, G., Dromparis, P., Webster, L., Haromy, A., Niven, E., Maguire, C., Gammer, T.L., Mackey, J.R., Fulton, D., Abdulkarim, B., McMurtry, M.S., and Petruk, K.C. (2010). Metabolic modulation of glioblastoma with dichloroacetate. *Sci Transl Med* 2, 31-34.

Mihaylova, M.M., and Shaw, R.J. (2011). The AMPK signalling pathway coordinates cell growth, autophagy and metabolism. *Nat Cell Biol* 13, 1016-1023.

Miller, J.C., Zhou, H., Kwekel, J., Cavallo, R., Burke, J., Butler, E.B., Teh, B.S., and Haab, B.B. (2003). Antibody microarray profiling of human prostate cancer sera: antibody screening and identification of potential biomarkers. *Proteomics* 3, 56-63.

Minauro-Sanmiguel, F., Wilkens, S., and Garcia, J.J. (2005). Structure of dimeric mitochondrial ATP synthase: novel F0 bridging features and the structural basis of mitochondrial cristae biogenesis. *Proc Natl Acad Sci U S A* 102, 12356-12358.

Miranda-Goncalves, V., Honavar, M., Pinheiro, C., Martinho, O., Pires, M.M., Pinheiro, C., Cordeiro, M., Bebiano, G., Costa, P., Palmeirim, I., Reis, R.M., and Baltazar, F. (2013). Monocarboxylate transporters (MCTs) in gliomas: expression and exploitation as therapeutic targets. *Neuro Oncol* 15, 172-188.

Mitchell, P. (1961). Coupling of phosphorylation to electron and hydrogen transfer by a chemi-osmotic type of mechanism. *Nature* 191, 144-148.

Mittal, C.K., and Murad, F. (1977). Activation of guanylate cyclase by superoxide dismutase and hydroxyl radical: a physiological regulator of guanosine 3',5'-monophosphate formation. *Proc Natl Acad Sci U S A* 74, 4360-4364.

Mootha, V.K., Bunkenborg, J., Olsen, J.V., Hjerrild, M., Wisniewski, J.R., Stahl, E., Bolouri, M.S., Ray, H.N., Sihag, S., Kamal, M., Patterson, N., Lander, E.S., and Mann, M. (2003). Integrated analysis of protein composition, tissue diversity, and gene regulation in mouse mitochondria. *Cell* 115, 629-640.

Morales-Gonzalez, J.A., Madrigal-Santillan, E., Morales-Gonzalez, A., Bautista, M., Gayosso-Islas, E., and Sanchez-Moreno, C. (2015). What is Known Regarding the Participation of Factor Nrf-2 in Liver Regeneration? *Cells* 4, 169-177.

Mourier, A., Ruzzenente, B., Brandt, T., Kuhlbrandt, W., and Larsson, N.G. (2014). Loss of LRPPRC causes ATP synthase deficiency. *Hum Mol Genet* 23, 2580-2592.

Mueller, C., Liotta, L.A., and Espina, V. (2010). Reverse phase protein microarrays advance to use in clinical trials. *Mol Oncol* 4, 461-481.

Munn, E.A. (1974). The application of the negative staining technique to the study of membranes. *Methods Enzymol* 32, 20-35.

Murdoch, C., Muthana, M., Coffelt, S.B., and Lewis, C.E. (2008). The role of myeloid cells in the promotion of tumour angiogenesis. *Nat Rev Cancer* 8, 618-631.

Nadarajah, V.D., van Putten, M., Chaouch, A., Garrood, P., Straub, V., Lochmuller, H., Ginjaar, H.B., Aartsma-Rus, A.M., van Ommen, G.J., den Dunnen, J.T., and t Hoen, P.A. (2011). Serum matrix metalloproteinase-9 (MMP-9) as a biomarker for monitoring disease progression in Duchenne muscular dystrophy (DMD). *Neuromuscul Disord* 21, 569-578.

Nelson, D.L., and Cox, M.M. (2004). *Lehninger Principles of Biochemistry (4th edition).* , Fourth edn (W H Freeman & Co).

Nigro, V., and Savarese, M. (2014). Genetic basis of limb-girdle muscular dystrophies: the 2014 update. *Acta Myol* 33, 1-12.

Nishikawa, T., Bellance, N., Damm, A., Bing, H., Zhu, Z., Handa, K., Yovchev, M.I., Sehgal, V., Moss, T.J., Oertel, M., Ram, P.T., Pipinos, II, Soto-Gutierrez, A., Fox, I.J., and Nagrath, D. (2014). A switch in the source of ATP production and a loss in capacity to perform glycolysis are hallmarks of hepatocyte failure in advance liver disease. *J Hepatol* 60, 1203-1211.

Nishizuka, S.S., and Mills, G.B. (2016). New era of integrated cancer biomarker discovery using reverse-phase protein arrays. *Drug Metab Pharmacokinet* 31, 35-45.

Norling, B., Tourikas, C., Hamasur, B., and Glaser, E. (1990). Evidence for an endogenous ATPase inhibitor protein in plant mitochondria. Purification and characterization. *Eur J Biochem* 188, 247-252.

Ohsakaya, S., Fujikawa, M., Hisabori, T., and Yoshida, M. (2011). Knockdown of DAPIT (diabetes-associated protein in insulin-sensitive tissue) results in loss of ATP synthase in mitochondria. *J Biol Chem* 286, 20292-20296.

Olichon, A., Baricault, L., Gas, N., Guillou, E., Valette, A., Belenguer, P., and Lenaers, G. (2003). Loss of OPA1 perturbates the mitochondrial inner membrane structure and integrity, leading to cytochrome c release and apoptosis. *J Biol Chem* 278, 7743-7746.

Olson, K.A., Schell, J.C., and Rutter, J. (2016). Pyruvate and Metabolic Flexibility: Illuminating a Path Toward Selective Cancer Therapies. *Trends Biochem Sci* 41, 219-230.

Onoda, T., Ono, T., Dhar, D.K., Yamanoi, A., Fujii, T., and Nagasue, N. (2004). Doxycycline inhibits cell proliferation and invasive potential: combination therapy with

cyclooxygenase-2 inhibitor in human colorectal cancer cells. *J Lab Clin Med* 143, 207-216.

Orrenius, S., Gogvadze, V., and Zhivotovsky, B. (2007). Mitochondrial oxidative stress: implications for cell death. *Annu Rev Pharmacol Toxicol* 47, 143-183.

Ortega, A.D., Sanchez-Arago, M., Giner-Sanchez, D., Sanchez-Cenizo, L., Willers, I., and Cuezva, J.M. (2009). Glucose avidity of carcinomas. *Cancer Lett* 276, 125-135.

Osman, C., Voelker, D.R., and Langer, T. (2011). Making heads or tails of phospholipids in mitochondria. *J Cell Biol* 192, 7-16.

Osthus, R.C., Shim, H., Kim, S., Li, Q., Reddy, R., Mukherjee, M., Xu, Y., Wonsey, D., Lee, L.A., and Dang, C.V. (2000). Deregulation of glucose transporter 1 and glycolytic gene expression by c-Myc. *J Biol Chem* 275, 21797-21800.

Pagliarini, D.J., Calvo, S.E., Chang, B., Sheth, S.A., Vafai, S.B., Ong, S.E., Walford, G.A., Sugiana, C., Boneh, A., Chen, W.K., Hill, D.E., Vidal, M., Evans, J.G., Thorburn, D.R., Carr, S.A., and Mootha, V.K. (2008). A mitochondrial protein compendium elucidates complex I disease biology. *Cell* 134, 112-123.

Pagnozzi, D., Birolo, L., Leo, G., Contessi, S., Lippe, G., Pucci, P., and Mavelli, I. (2010). Stoichiometry and topology of the complex of the endogenous ATP synthase inhibitor protein IF(1) with calmodulin. *Biochemistry* 49, 7542-7552.

Paivarinne, H., and Kainulainen, H. (2001). DAPIT, a novel protein down-regulated in insulin-sensitive tissues in streptozotocin-induced diabetes. *Acta Diabetol* 38, 83-86.

Panchenko, M.V., and Vinogradov, A.D. (1985). Interaction between the mitochondrial ATP synthetase and ATPase inhibitor protein. Active/inactive slow pH-dependent transitions of the inhibitor protein. *FEBS Lett* 184, 226-230.

Papa, S., Zanotti, F., Cocco, T., Perrucci, C., Candita, C., and Minuto, M. (1996). Identification of functional domains and critical residues in the adenosinetriphosphatase inhibitor protein of mitochondrial F0F1 ATP synthase. *Eur J Biochem* 240, 461-467.

Patten, D.A., Wong, J., Khacho, M., Soubannier, V., Mailloux, R.J., Pilon-Larose, K., MacLaurin, J.G., Park, D.S., McBride, H.M., Trinkle-Mulcahy, L., Harper, M.E., Germain, M., and Slack, R.S. (2014). OPA1-dependent cristae modulation is essential for cellular adaptation to metabolic demand. *EMBO J* 33, 2676-2691.

Paumard, P., Vaillier, J., Coulary, B., Schaeffer, J., Soubannier, V., Mueller, D.M., Brethes, D., di Rago, J.P., and Velours, J. (2002). The ATP synthase is involved in generating mitochondrial cristae morphology. *EMBO J* 21, 221-230.

Pedersen, P.L., and Hullihen, J. (1984). Inhibitor peptide of mitochondrial proton adenosine triphosphatase. Neutralization of its inhibitory action by calmodulin. *J Biol Chem* 259, 15148-15153.

Pelicano, H., Xu, R.H., Du, M., Feng, L., Sasaki, R., Carew, J.S., Hu, Y., Ramdas, L., Hu, L., Keating, M.J., Zhang, W., Plunkett, W., and Huang, P. (2006). Mitochondrial respiration defects in cancer cells cause activation of Akt survival pathway through a redox-mediated mechanism. *J Cell Biol* 175, 913-923.

Perkins, G.A., and Frey, T.G. (2000). Recent structural insight into mitochondria gained by microscopy. *Micron* 31, 97-111.

Pfeiffer, K., Gohil, V., Stuart, R.A., Hunte, C., Brandt, U., Greenberg, M.L., and Schagger, H. (2003). Cardiolipin stabilizes respiratory chain supercomplexes. *J Biol Chem* 278, 52873-52880.

Plathow, C., and Weber, W.A. (2008). Tumor cell metabolism imaging. *J Nucl Med* 49 Suppl 2, 43S-63S.

Pullman, M.E., and Monroy, G.C. (1963). A Naturally Occurring Inhibitor of Mitochondrial Adenosine Triphosphatase. *J Biol Chem* 238, 3762-3769.

Quiros, P.M., Mottis, A., and Auwerx, J. (2016). Mitonuclear communication in homeostasis and stress. *Nat Rev Mol Cell Biol* 17, 213-226.

Rahimov, F., and Kunkel, L.M. (2013). The cell biology of disease: cellular and molecular mechanisms underlying muscular dystrophy. *J Cell Biol* 201, 499-510.

Rainbolt, T.K., Atanassova, N., Genereux, J.C., and Wiseman, R.L. (2013). Stress-regulated translational attenuation adapts mitochondrial protein import through Tim17A degradation. *Cell Metab* 18, 908-919.

Ramadasan-Nair, R., Gayathri, N., Mishra, S., Sunitha, B., Mythri, R.B., Nalini, A., Subbannayya, Y., Harsha, H.C., Kolthur-Seetharam, U., and Srinivas Bharath, M.M. (2014). Mitochondrial alterations and oxidative stress in an acute transient mouse model of muscle degeneration: implications for muscular dystrophy and related muscle pathologies. *J Biol Chem* 289, 485-509.

Rasola, A., and Bernardi, P. (2011). Mitochondrial permeability transition in Ca(2+)-dependent apoptosis and necrosis. *Cell Calcium* 50, 222-233.

Raval, J., Lyman, S., Nitta, T., Mohuczy, D., Lemasters, J.J., Kim, J.S., and Behrns, K.E. (2006). Basal reactive oxygen species determine the susceptibility to apoptosis in cirrhotic hepatocytes. *Free Radic Biol Med* 41, 1645-1654.

Ravati, A., Ahlemeyer, B., Becker, A., Klumpp, S., and Krieglstein, J. (2001). Preconditioning-induced neuroprotection is mediated by reactive oxygen species and activation of the transcription factor nuclear factor-kappaB. *J Neurochem* 78, 909-919.

Reddy, M.M., Fernandes, M.S., Deshpande, A., Weisberg, E., Inguilizian, H.V., Abdel-Wahab, O., Kung, A.L., Levine, R.L., Griffin, J.D., and Sattler, M. (2012). The JAK2V617F oncogene requires expression of inducible phosphofructokinase/fructose-bisphosphatase 3 for cell growth and increased metabolic activity. *Leukemia* 26, 481-489.

Rich, P.R. (1984). Electron and proton transfers through quinones and cytochrome bc complexes. *Biochim Biophys Acta* 768, 53-79.

Ristow, M. (2014). Unraveling the truth about antioxidants: mitohormesis explains ROS-induced health benefits. *Nat Med* 20, 709-711.

Rizzuto, R., De Stefani, D., Raffaello, A., and Mammucari, C. (2012). Mitochondria as sensors and regulators of calcium signalling. *Nat Rev Mol Cell Biol* 13, 566-578.

Robinson, M.M., McBryant, S.J., Tsukamoto, T., Rojas, C., Ferraris, D.V., Hamilton, S.K., Hansen, J.C., and Curthoys, N.P. (2007). Novel mechanism of inhibition of rat kidney-type glutaminase by bis-2-(5-phenylacetamido-1,2,4-thiadiazol-2-yl)ethyl sulfide (BPTES). *Biochem J* 406, 407-414.

Rohle, D., Popovici-Muller, J., Palaskas, N., Turcan, S., Grommes, C., Campos, C., Tsoi, J., Clark, O., Oldrini, B., Komisopoulou, E., Kunii, K., Pedraza, A., Schalm, S., Silverman, L., Miller, A., Wang, F., Yang, H., Chen, Y., Kernytsky, A., Rosenblum, M.K., Liu, W., Biller, S.A., Su, S.M., Brennan, C.W., Chan, T.A., Graeber, T.G., Yen, K.E., and Mellinghoff, I.K. (2013). An inhibitor of mutant IDH1 delays growth and promotes differentiation of glioma cells. *Science* 340, 626-630.

Rouslin, W., and Broge, C.W. (1996). Isoform-independent heart rate-related variation in cardiac myofibrillar Ca(2+)-activated Mg(2+)-ATPase activity. *Am J Physiol* 270, C1271-1276.

Rouslin, W., Frank, G.D., and Broge, C.W. (1995). Content and binding characteristics of the mitochondrial ATPase inhibitor, IF1, in the tissues of several slow and fast heart-rate homeothermic species and in two poikilotherms. *J Bioenerg Biomembr* 27, 117-125.

Rouslin, W., and Pullman, M.E. (1987). Protonic inhibition of the mitochondrial adenosine 5'-triphosphatase in ischemic cardiac muscle. Reversible binding of the ATPase inhibitor protein to the mitochondrial ATPase during ischemia. *J Mol Cell Cardiol* 19, 661-668.

Ruhle, T., and Leister, D. (2015). Assembly of F1F0-ATP synthases. *Biochim Biophys Acta* 1847, 849-860.

Sah, J.F., Kumar, C., and Mohanty, P. (1993). pH dependent conformational changes modulate functional activity of the mitochondrial ATPase inhibitor protein. *Biochem Biophys Res Commun* 194, 1521-1528.

Sanchez-Arago, M., and Cuezva, J.M. (2011). The bioenergetic signature of isogenic colon cancer cells predicts the cell death response to treatment with 3-bromopyruvate, iodoacetate or 5-fluorouracil. *J Transl Med* 9, 19.

Sanchez-Arago, M., Chamorro, M., and Cuezva, J.M. (2010). Selection of cancer cells with repressed mitochondria triggers colon cancer progression. *Carcinogenesis* 31, 567-576.

Sanchez-Arago, M., Formentini, L., and Cuezva, J.M. (2013). Mitochondria-mediated energy adaption in cancer: the H(+)-ATP synthase-geared switch of metabolism in human tumors. *Antioxid Redox Signal* 19, 285-298.

Sanchez-Cenizo, L., Formentini, L., Aldea, M., Ortega, A.D., Garcia-Huerta, P., Sanchez-Arago, M., and Cuezva, J.M. (2010). Up-regulation of the ATPase inhibitory factor 1 (IF1) of the mitochondrial H+-ATP synthase in human tumors mediates the metabolic shift of cancer cells to a Warburg phenotype. *J Biol Chem* 285, 25308-25313.

Santamaria, G., Martinez-Diez, M., Fabregat, I., and Cuezva, J.M. (2006). Efficient execution of cell death in non-glycolytic cells requires the generation of ROS controlled by the activity of mitochondrial H+-ATP synthase. *Carcinogenesis* 27, 925-935.

Satrustegui, J., Pardo, B., and Del Arco, A. (2007). Mitochondrial transporters as novel targets for intracellular calcium signaling. *Physiol Rev* 87, 29-67.

Schagger, H. (2001). Respiratory chain supercomplexes. *IUBMB Life* 52, 119-128.

Schagger, H., Cramer, W.A., and von Jagow, G. (1994). Analysis of molecular masses and oligomeric states of protein complexes by blue native electrophoresis and isolation of membrane protein complexes by two-dimensional native electrophoresis. *Anal Biochem* 217, 220-230.

Schagger, H., and Pfeiffer, K. (2000). Supercomplexes in the respiratory chains of yeast and mammalian mitochondria. *EMBO J* 19, 1777-1783.

Schell, J.C., Olson, K.A., Jiang, L., Hawkins, A.J., Van Vranken, J.G., Xie, J., Egnatchik, R.A., Earl, E.G., DeBerardinis, R.J., and Rutter, J. (2014). A role for the mitochondrial pyruvate carrier as a repressor of the Warburg effect and colon cancer cell growth. *Mol Cell* 56, 400-413.

Schena, M., Shalon, D., Davis, R.W., and Brown, P.O. (1995). Quantitative monitoring of gene expression patterns with a complementary DNA microarray. *Science* 270, 467-470.

Schmidt, O., Pfanner, N., and Meisinger, C. (2010). Mitochondrial protein import: from proteomics to functional mechanisms. *Nat Rev Mol Cell Biol* 11, 655-667.

Schnizer, R., Van Heeke, G., Amaturo, D., and Schuster, S.M. (1996). Histidine-49 is necessary for the pH-dependent transition between active and inactive states of the bovine F1-ATPase inhibitor protein. *Biochim Biophys Acta* 1292, 241-248.

Schwarcz, R., Bruno, J.P., Muchowski, P.J., and Wu, H.Q. (2012). Kynurenines in the mammalian brain: when physiology meets pathology. *Nat Rev Neurosci* 13, 465-477.

Sebens Muerkoster, S., Rausch, A.V., Isberner, A., Minkenberg, J., Blaszczuk, E., Witt, M., Folsch, U.R., Schmitz, F., Schafer, H., and Arlt, A. (2008). The apoptosis-inducing effect of gastrin on colorectal cancer cells relates to an increased IEX-1 expression mediating NF-kappa B inhibition. *Oncogene* 27, 1122-1134.

Selva O'Callaghan, A., and Trallero Araguas, E. (2008). [Inflammatory myopathies. Dermatomyositis, polymyositis, and inclusion body myositis]. *Reumatol Clin* 4, 197-206.

Semenza, G.L., Roth, P.H., Fang, H.M., and Wang, G.L. (1994). Transcriptional regulation of genes encoding glycolytic enzymes by hypoxia-inducible factor 1. *J Biol Chem* 269, 23757-23763.

Sereni, M.I., Pierobon, M., Angioli, R., Petricoin, E.F., 3rd, and Frederick, M.J. (2013). Reverse phase protein microarrays and their utility in drug development. *Methods Mol Biol* 986, 187-214.

Serrano, M., and Blasco, M.A. (2007). Cancer and ageing: convergent and divergent mechanisms. *Nat Rev Mol Cell Biol* 8, 715-722.

Seurynck-Servoss, S.L., White, A.M., Baird, C.L., Rodland, K.D., and Zangar, R.C. (2007). Evaluation of surface chemistries for antibody microarrays. *Anal Biochem* 371, 105-115.

Seyfried, T.N., Flores, R.E., Poff, A.M., and D'Agostino, D.P. (2014). Cancer as a metabolic disease: implications for novel therapeutics. *Carcinogenesis* 35, 515-527.

Shah, D.I., Takahashi-Makise, N., Cooney, J.D., Li, L., Schultz, I.J., Pierce, E.L., Narla, A., Seguin, A., Hattangadi, S.M., Medlock, A.E., Langer, N.B., Dailey, T.A., Hurst, S.N., Faccenda, D., Wiwczar, J.M., Heggers, S.K., Vogin, G., Chen, W., Chen, C., Campagna, D.R., Brugnara, C., Zhou, Y., Ebert, B.L., Danial, N.N., Fleming, M.D., Ward, D.M., Campanella, M., Dailey, H.A., Kaplan, J., and Paw, B.H. (2012). Mitochondrial Atpif1 regulates haem synthesis in developing erythroblasts. *Nature* 491, 608-612.

Shao, D., Oka, S., Liu, T., Zhai, P., Ago, T., Sciarretta, S., Li, H., and Sadoshima, J. (2014). A redox-dependent mechanism for regulation of AMPK activation by Thioredoxin1 during energy starvation. *Cell Metab* 19, 232-245.

Sheffer, M., Bacolod, M.D., Zuk, O., Giardina, S.F., Pincas, H., Barany, F., Paty, P.B., Gerald, W.L., Notterman, D.A., and Domany, E. (2009). Association of survival and disease progression with chromosomal instability: a genomic exploration of colorectal cancer. *Proc Natl Acad Sci U S A* 106, 7131-7136.

Shen, L., Zhi, L., Hu, W., and Wu, M.X. (2009). IEX-1 targets mitochondrial F1Fo-ATPase inhibitor for degradation. *Cell Death Differ* 16, 603-612.

Shima, K., Tashiro, K., Hibi, N., Tsukada, Y., and Hirai, H. (1983). Carbonic anhydrase-III immunohistochemical localization in human skeletal muscle. *Acta Neuropathol* 59, 237-239.

Shoubridge, E.A., and Wai, T. (2007). Mitochondrial DNA and the mammalian oocyte. *Curr Top Dev Biol* 77, 87-111.

Sigurgeirsson, B., Lindelof, B., Edhag, O., and Allander, E. (1992). Risk of cancer in patients with dermatomyositis or polymyositis. A population-based study. *N Engl J Med* 326, 363-367.

Son, K., Fujioka, S., Iida, T., Furukawa, K., Fujita, T., Yamada, H., Chiao, P.J., and Yanaga, K. (2009). Doxycycline induces apoptosis in PANC-1 pancreatic cancer cells. *Anticancer Res* 29, 3995-4003.

Song, R., Song, H., Liang, Y., Yin, D., Zhang, H., Zheng, T., Wang, J., Lu, Z., Song, X., Pei, T., Qin, Y., Li, Y., Xie, C., Sun, B., Shi, H., Li, S., Meng, X., Yang, G., Pan, S., Zhu, J., Qi, S., Jiang, H., Zhang, Z., and Liu, L. (2014). Reciprocal activation between ATPase inhibitory factor 1 and NF-kappaB drives hepatocellular carcinoma angiogenesis and metastasis. *Hepatology* 60, 1659-1673.

Song, Z., Chen, H., Fiket, M., Alexander, C., and Chan, D.C. (2007). OPA1 processing controls mitochondrial fusion and is regulated by mRNA splicing, membrane potential, and Yme1L. *J Cell Biol* 178, 749-755.

Speer, R., Wulfkuhle, J., Espina, V., Aurajo, R., Edmiston, K.H., Liotta, L.A., and Petricoin, E.F., 3rd (2007). Development of reverse phase protein microarrays for clinical applications and patient-tailored therapy. *Cancer Genomics Proteomics* 4, 157-164.

Srinivasan, S., and Avadhani, N.G. (2012). Cytochrome c oxidase dysfunction in oxidative stress. *Free Radic Biol Med* 53, 1252-1263.

Strauss, M., Hofhaus, G., Schroder, R.R., and Kuhlbrandt, W. (2008). Dimer ribbons of ATP synthase shape the inner mitochondrial membrane. *EMBO J* 27, 1154-1160.

Sydor, J.R., and Nock, S. (2003). Protein expression profiling arrays: tools for the multiplexed high-throughput analysis of proteins. *Proteome Sci* 1, 3.

Takuma, K., Kataoka, S., Ago, Y., and Matsuda, T. (2009). [Mitochondrial dysfunction and neuronal apoptosis: new molecular approach to prevent Alzheimer's disease]. *Nihon Yakurigaku Zasshi* 134, 180-183.

Templin, M.F., Stoll, D., Bachmann, J., and Joos, T.O. (2004). Protein microarrays and multiplexed sandwich immunoassays: what beats the beads? *Comb Chem High Throughput Screen* 7, 223-229.

Templin, M.F., Stoll, D., Schrenk, M., Traub, P.C., Vohringer, C.F., and Joos, T.O. (2002). Protein microarray technology. *Drug Discov Today* 7, 815-822.

Tennant, D.A., Duran, R.V., and Gottlieb, E. (2010). Targeting metabolic transformation for cancer therapy. *Nat Rev Cancer* 10, 267-277.

Thomas, D., Bron, P., Weimann, T., Dautant, A., Giraud, M.F., Paumard, P., Salin, B., Cavalier, A., Velours, J., and Brethes, D. (2008). Supramolecular organization of the yeast F1Fo-ATP synthase. *Biol Cell* 100, 591-601.

Thompson, C.B. (2009). Metabolic enzymes as oncogenes or tumor suppressors. *N Engl J Med* 360, 813-815.

Tomasetig, L., Di Pancrazio, F., Harris, D.A., Mavelli, I., and Lippe, G. (2002). Dimerization of F0F1ATP synthase from bovine heart is independent from the binding of the inhibitor protein IF1. *Biochim Biophys Acta* 1556, 133-141.

Twig, G., Hyde, B., and Shirihai, O. (2008). Mitochondrial fusion, fission and autophagy as a quality control axis: the bioenergetic view. *Biochim Biophys Acta* 1777, 1092-1097.

Unwin, R.D., Craven, R.A., Harnden, P., Hanrahan, S., Totty, N., Knowles, M., Eardley, I., Selby, P.J., and Banks, R.E. (2003). Proteomic changes in renal cancer and co-ordinate demonstration of both the glycolytic and mitochondrial aspects of the Warburg effect. *Proteomics* 3, 1620-1632.

Valko, M., Leibfritz, D., Moncol, J., Cronin, M.T., Mazur, M., and Telser, J. (2007). Free radicals and antioxidants in normal physiological functions and human disease. *Int J Biochem Cell Biol* 39, 44-84.

van der Kooi, A.J., and de Visser, M. (2014). Idiopathic inflammatory myopathies. *Handb Clin Neurol* 119, 495-512.

Vander Heiden, M.G., Cantley, L.C., and Thompson, C.B. (2009). Understanding the Warburg effect: the metabolic requirements of cell proliferation. *Science* 324, 1029-1033.

Vazquez-Martin, A., Corominas-Faja, B., Cufi, S., Vellon, L., Oliveras-Ferraros, C., Menendez, O.J., Joven, J., Lupu, R., and Menendez, J.A. (2013). The mitochondrial H(+)-ATP synthase and the lipogenic switch: new core components of metabolic reprogramming in induced pluripotent stem (iPS) cells. *Cell Cycle* 12, 207-218.

von Stockum, S., Giorgio, V., Trevisan, E., Lippe, G., Glick, G.D., Forte, M.A., Da-Re, C., Checchetto, V., Mazzotta, G., Costa, R., Szabo, I., and Bernardi, P. (2015). F-ATPase of Drosophila melanogaster forms 53-picosiemen (53-pS) channels responsible for mitochondrial Ca2+-induced Ca2+ release. *J Biol Chem* 290, 4537-4544.

Vonck, J., and Schafer, E. (2009). Supramolecular organization of protein complexes in the mitochondrial inner membrane. *Biochim Biophys Acta* 1793, 117-124.

Vuorinen, K., Ylitalo, K., Peuhkurinen, K., Raatikainen, P., Ala-Rami, A., and Hassinen, I.E. (1995). Mechanisms of ischemic preconditioning in rat myocardium. Roles of adenosine, cellular energy state, and mitochondrial F1F0-ATPase. *Circulation* 91, 2810-2818.

Walker, J.E. (2013). The ATP synthase: the understood, the uncertain and the unknown. *Biochem Soc Trans* 41, 1-16.

Wang, F., Travins, J., DeLaBarre, B., Penard-Lacronique, V., Schalm, S., Hansen, E., Straley, K., Kernytsky, A., Liu, W., Gliser, C., Yang, H., Gross, S., Artin, E., Saada, V., Mylonas, E., Quivoron, C., Popovici-Muller, J., Saunders, J.O., Salituro, F.G.,

Yan, S., Murray, S., Wei, W., Gao, Y., Dang, L., Dorsch, M., Agresta, S., Schenkein, D.P., Biller, S.A., Su, S.M., de Botton, S., and Yen, K.E. (2013). Targeted inhibition of mutant IDH2 in leukemia cells induces cellular differentiation. *Science* 340, 622-626.

Wang, H.J., Hsieh, Y.J., Cheng, W.C., Lin, C.P., Lin, Y.S., Yang, S.F., Chen, C.C., Izumiya, Y., Yu, J.S., Kung, H.J., and Wang, W.C. (2014). JMJD5 regulates PKM2 nuclear translocation and reprograms HIF-1alpha-mediated glucose metabolism. *Proc Natl Acad Sci U S A* 111, 279-284.

Wang, R.Y., Bodamer, O.A., Watson, M.S., Wilcox, W.R., and Diseases, A.W.G.o.D.C.o.L.S. (2011). Lysosomal storage diseases: diagnostic confirmation and management of presymptomatic individuals. *Genet Med* 13, 457-484.

Wang, Y., and Bogenhagen, D.F. (2006). Human mitochondrial DNA nucleoids are linked to protein folding machinery and metabolic enzymes at the mitochondrial inner membrane. *J Biol Chem* 281, 25791-25802.

Watt, I.N., Montgomery, M.G., Runswick, M.J., Leslie, A.G., and Walker, J.E. (2010). Bioenergetic cost of making an adenosine triphosphate molecule in animal mitochondria. *Proc Natl Acad Sci U S A* 107, 16823-16827.

Wei, S., Fukuhara, H., Kawada, C., Kurabayashi, A., Furihata, M., Ogura, S., Inoue, K., and Shuin, T. (2015). Silencing of ATPase Inhibitory Factor 1 Inhibits Cell Growth via Cell Cycle Arrest in Bladder Cancer. *Pathobiology* 82, 224-232.

Weimann, T., Vaillier, J., Salin, B., and Velours, J. (2008). The intermembrane space loop of subunit b (4) is a major determinant of the stability of yeast oligomeric ATP synthases. *Biochemistry* 47, 3556-3563.

Wilson, D.S., and Nock, S. (2003). Recent developments in protein microarray technology. *Angew Chem Int Ed Engl* 42, 494-500.

Willers, I.M., and Cuezva, J.M. (2011). Post-transcriptional regulation of the mitochondrial H(+)-ATP synthase: A key regulator of the metabolic phenotype in cancer. *Biochim Biophys Acta* 1807, 543-551.

Williams, R.E., and Mole, S.E. (2012). New nomenclature and classification scheme for the neuronal ceroid lipofuscinoses. *Neurology* 79, 183-191.

Wise, D.R., DeBerardinis, R.J., Mancuso, A., Sayed, N., Zhang, X.Y., Pfeiffer, H.K., Nissim, I., Daikhin, E., Yudkoff, M., McMahon, S.B., and Thompson, C.B. (2008). Myc regulates a transcriptional program that stimulates mitochondrial glutaminolysis and leads to glutamine addiction. *Proc Natl Acad Sci U S A* 105, 18782-18787.

Wittig, I., Braun, H.P., and Schagger, H. (2006). Blue native PAGE. *Nat Protoc* 1, 418-428.

Wittig, I., and Schagger, H. (2005). Advantages and limitations of clear-native PAGE. *Proteomics* 5, 4338-4346.

Wittig, I., and Schagger, H. (2008). Structural organization of mitochondrial ATP synthase. *Biochim Biophys Acta* 1777, 592-598.

Wittig, I., and Schagger, H. (2009). Supramolecular organization of ATP synthase and respiratory chain in mitochondrial membranes. *Biochim Biophys Acta* 1787, 672-680.

Wondrak, G.T. (2009). Redox-directed cancer therapeutics: molecular mechanisms and opportunities. *Antioxid Redox Signal* 11, 3013-3069.

Wouters, B.G., and Koritzinsky, M. (2008). Hypoxia signalling through mTOR and the unfolded protein response in cancer. *Nat Rev Cancer* 8, 851-864.

Wu, J., Shan, Q., Li, P., Wu, Y., Xie, J., and Wang, X. (2015). ATPase inhibitory factor 1 is a potential prognostic marker for the migration and invasion of glioma. *Oncol Lett* 10, 2075-2080.

Wu, M.X. (2003). Roles of the stress-induced gene IEX-1 in regulation of cell death and oncogenesis. *Apoptosis* 8, 11-18.

Xiao, M., Yang, H., Xu, W., Ma, S., Lin, H., Zhu, H., Liu, L., Liu, Y., Yang, C., Xu, Y., Zhao, S., Ye, D., Xiong, Y., and Guan, K.L. (2012). Inhibition of alpha-KG-dependent histone and DNA demethylases by fumarate and succinate that are accumulated in mutations of FH and SDH tumor suppressors. *Genes Dev* 26, 1326-1338.

Yalow, R.S., and Berson, S.A. (1960). Immunoassay of endogenous plasma insulin in man. *J Clin Invest* 39, 1157-1175.

Yang, C.S., Wang, X., Lu, G., and Picinich, S.C. (2009). Cancer prevention by tea: animal studies, molecular mechanisms and human relevance. *Nat Rev Cancer* 9, 429-439.

Yang, W., Xia, Y., Ji, H., Zheng, Y., Liang, J., Huang, W., Gao, X., Aldape, K., and Lu, Z. (2011). Nuclear PKM2 regulates beta-catenin transactivation upon EGFR activation. *Nature* 480, 118-122.

Yang, W., Zheng, Y., Xia, Y., Ji, H., Chen, X., Guo, F., Lyssiotis, C.A., Aldape, K., Cantley, L.C., and Lu, Z. (2012). ERK1/2-dependent phosphorylation and nuclear translocation of PKM2 promotes the Warburg effect. *Nat Cell Biol* 14, 1295-1304.

Yin, T., Lu, L., Xiong, Z., Wei, S., and Cui, D. (2015). ATPase inhibitory factor 1 is a prognostic marker and contributes to proliferation and invasion of human gastric cancer cells. *Biomed Pharmacother* 70, 90-96.

Yizhak, K., Le Devedec, S.E., Rogkoti, V.M., Baenke, F., de Boer, V.C., Frezza, C., Schulze, A., van de Water, B., and Ruppin, E. (2014). A computational study of the Warburg effect identifies metabolic targets inhibiting cancer migration. *Mol Syst Biol* 10, 744.

Yoshida, M., Muneyuki, E., and Hisabori, T. (2001). ATP synthase--a marvellous rotary engine of the cell. *Nat Rev Mol Cell Biol* 2, 669-677.

Yoshida, M., Suzuki, A., Yamamoto, H., Noguchi, S., Mizuno, Y., and Ozawa, E. (1994). Dissociation of the complex of dystrophin and its associated proteins into several unique groups by n-octyl beta-D-glucoside. *Eur J Biochem* 222, 1055-1061.

Yun, J., and Finkel, T. (2014). Mitohormesis. *Cell Metab* 19, 757-766.

Yuneva, M., Zamboni, N., Oefner, P., Sachidanandam, R., and Lazebnik, Y. (2007). Deficiency in glutamine but not glucose induces MYC-dependent apoptosis in human cells. *J Cell Biol* 178, 93-105.

Yunis, E.J., and Samaha, F.J. (1971). Inclusion body myositis. *Lab Invest* 25, 240-248.

Zanotti, F., Guerrieri, F., Che, Y.W., Scarfo, R., and Papa, S. (1987). Proton translocation by the H+-ATPase of mitochondria. Effect of modification by monofunctional reagents of thiol residues in F0 polypeptides. *Eur J Biochem* 164, 517-523.

Zanotti, F., Raho, G., Gaballo, A., and Papa, S. (2004). Inhibitory and anchoring domains in the ATPase inhibitor protein IF1 of bovine heart mitochondrial ATP synthase. *J Bioenerg Biomembr* 36, 447-457.

Zanotti, F., Raho, G., Vuolo, R., Gaballo, A., Papa, F., and Papa, S. (2000). Functional domains of the ATPase inhibitor protein from bovine heart mitochondria. *FEBS Lett* 482, 163-166.

Zhang, H., Gao, P., Fukuda, R., Kumar, G., Krishnamachary, B., Zeller, K.I., Dang, C.V., and Semenza, G.L. (2007). HIF-1 inhibits mitochondrial biogenesis and cellular respiration in VHL-deficient renal cell carcinoma by repression of C-MYC activity. *Cancer Cell* 11, 407-420.

Zhu, H., and Snyder, M. (2001). Protein arrays and microarrays. *Curr Opin Chem Biol* 5, 40-45.

Zick, M., Rabl, R., and Reichert, A.S. (2009). Cristae formation-linking ultrastructure and function of mitochondria. *Biochim Biophys Acta* 1793, 5-19.